Mission-Oriented Seismic Research Program

Annual Report

2006

M-OSRP

University of Houston

Sponsors and Advisory Board representatives

Corporate Sponsors

Amerada Hess ..... Scott Morton, Jacques Leveille
Anadarko ..... Roger Reagan
BP ..... Uwe Albertin
BHP ..... Mike Richardson
ChevronTexaco ..... Debbie Bones
ConocoPhillips ..... Douglas Foster, Robert Stolt
Devon Energy ..... Kenneth Beeney
ENI-Agip ..... Michele Buia
ExxonMobil ..... Peter Traynin
Geotrace Technologies ..... Jaime Stein
GX Technology ..... Nick Bernitsas, Robert Bloor
IBM ..... Tom McClure
Landmark ..... Dave Diller
Petrochina Company Limited ..... Jixiang Xu
Petrobras ..... Neiva Zago
PGS ..... Ruben Martinez
Saudi Aramco ..... Yi Luo
Shell ..... Jonathan Sheiman
Statoil ..... Lasse Amundsen
WesternGeco ..... Luis Canales

Federal Support

DOE Basic Energy Sciences ..... Nick Woodward
NSF CMG ..... Henry A. Warchall

M-OSRP Personnel

Faculty

Lasse Amundsen (Statoil) ..... Adjunct Professor (Physics)
Douglas J. Foster[1] (ConocoPhillips) ..... Adjunct Professor (Physics)
Kristopher A. Innanen ..... Assistant Professor (Physics)
Robert G. Keys (ExxonMobil) ..... Adjunct Professor (Physics)
Jacques Leveille (Amerada Hess) ..... Adjunct Professor (Physics)
Ken H. Matson (BP) ..... Adjunct Associate Professor (Physics)
Bogdan Nita (Assistant Professor, Montclair State U.) .... Adjunct Assistant Professor (Physics)
Jon Sheiman (Shell) ..... Adjunct Professor (Physics)
Robert H. Stolt (ConocoPhillips) ..... Adjunct Professor (Physics)
T. Hing Tan (Shell) ..... Adjunct Professor (Physics)
Arthur B. Weglein ..... Cullen Professor (Physics)
Daniel Whitmore (ConocoPhillips) ..... Adjunct Professor (Physics)

Ph.D. Students

Walter Kessinger ..... Geosciences
Jingfeng Zhang ..... Physics
Adrianna Citlali Ramirez ..... Physics
Shansong Jiang ..... Physics
Jose Eduardo Lira ..... Geosciences[2]
Xu Li ..... Physics
Zhiqiang Wang ..... Physics
Dan Fisher ..... Physics
Jim Mayhan ..... Physics

Recent Alumni

Haiyan Zhang ..... Physics
Fang Liu ..... Physics
Zhiqiang Guo ..... Geosciences
Francisco Miranda ..... Physics
Simon A. Shaw ..... Geosciences

Administrative Support

Jennifer Chin-Davis ..... Business Administrator
Nguyen Tran ..... Program Accountant
Jessica Maldonado ..... Program Coordinator
Joseph Ghobrial ..... Computer/IT Support
Jesse Weglein ..... Webmaster

[1]Chair, M-OSRP Advisory Board
[2]Petrobras, Brazil

Table of Contents

Introduction and Overview: MOSRP06

Executive Summary

Seismic processing algorithms are effective when their assumptions and prerequisites are satisfied, and when those assumptions are violated the result is the opposite of efficacy. There are many circumstances when the assumptions behind seismic methods are satisfied and also many significant instances when they are not. The latter is the source of seismic challenges, and connecting to and addressing those challenges defines relevant and differential research programs.

There are three different types of assumptions, and violating any one or more of these can cause seismic failure and erroneous and misleading predictions and dry hole drilling. The three distinct types of assumptions are: (1) acquisition—completeness, extent, sampling and fidelity and types of data collected and/or extrapolated/interpolated, (2) compute power: adequate compute capability for timely turn-around, and (3) algorithmic: innate algorithmic assumptions or limitations, and requirements, whose violations are not addressable by more complete acquisition and faster computers.

A comprehensive response to pressing seismic challenges begins with a frank and forthright problem definition and statement. There are cases where improved acquisition and faster computers will match the challenge, and other cases where an innate algorithmic challenge is the issue, and another type of response is required.

For example, there are 2D acoustic models where an adequate velocity cannot be determined for use by leading-edge imaging methods, and other very simple 2D models where given the exact overburden velocity model, we cannot find an adequate image beneath that perfectly provided overburden.

Combinations of lateral varying velocity and a range of reflector dip can readily produce the latter perfect velocity input imaging breakdown. These types of challenges, innate velocity and imaging algorithmic shortcomings, are present and remain with perfect and ideal acquisition and fully adequate computers. Many of our toughest sub-salt, sub-basalt and sub-karsted imaging challenges represent innate algorithmic breakdown.

There are two ways to address the violation of a requirement or assumption: (1) remove the violation by satisfying the assumption, and (2) avoid the violation by deriving a different method that doesnt make that assumption.

Both responses are reasonable. And within M-OSRP we adopt one or the other as indicated for the three different and distinct assumption types listed above. To illustrate: We can without much difficulty imagine, e.g., more complete 3D acquisition and faster and more effective computers, or methods of cross line extrapolation, and we are all aware of cases where added value was derived from those types of reasonable acquisition and extrapolation initiatives and computer advances.

The critical point here is that in marked contrast, for the innate algorithmic limitations and assumptions issue, we dont know of a single candidate concept, idea or method for satisfying the assumptions of current imaging that would allow the satisfaction of the separate, distinct and/or combined velocity and imaging demands, within the sphere of conventional velocity analysis and depth imaging thinking, that could even in principle accommodate the types of imaging challenges and plays we listed above, with e.g., high rugosity boundaries, in the overburden or at the target, and rapid heterogeneous lateral varying media.

Faced with the latter innate algorithmic assumptions reality, it is then reasonable to pursue a response to the innate algorithmic limitations of all current velocity model and imaging methods through the second route: derive a fundamentally new method for direct and accurate depth imaging that both in principle and practice doesnt make conventional imaging assumptions, that doesnt have an interest in or require the velocity model, nor any explicit nor implicit direct or indirect need for the velocity.

Since the inverse scattering series allows in principle for all seismic processing goals to be achieved directly and explicitly in terms of only measured data and water speed, it is natural to seek to extend our earlier work on removing free surface and internal multiples with absolutely no need or requirement or interest whatsoever in subsurface information, including velocity, to the tasks associated with primaries, depth imaging and non-linear AVO. Furthermore, those earlier developed multiple removal methods, while placing stringent demands on data acquisition, demonstrated their mettle, and efficacy and brought added value to the tool box of multiple removal methods under precisely the type of complex and ill-defined geologic subsurface conditions that are the current impenetrable and insurmountable obstacles for all our current leading-edge velocity analysis and imaging methods. You have to recognize the promise and the potential before you begin the hunt. That ultimate potential keeps you focused and on-track and on-target, as you reach partial objectives, and keeps you moving forward towards the prize. The idea is to provide the level of effectiveness for imaging and inverting primaries that we earlier brought to the removal of multiples. That capability and potential for primaries and multiples resides within one single set of equations (e.g., equation 5 of the strategy Abstract) .

Recognizing that that potential exists and resides within the inverse scattering series, equation (5), is one thing, locating and capturing that specific potential, for example, to attenuate or remove internal multiples or to depth image primaries within that over-all inverse scattering series machine, is another thing entirely.

To illustrate: Carvalho et al located the free surface multiple removal machinery and applied the algorithm to field data within 1.5 years; Araujo et al located the attenuation of internal multiples in 3 years, another 3-4 years to field data application.

The issues related to algorithm development for the removal of multiples were far from trivial, but the objective itself was fairly clear, eliminate the multiple and do not damage the primaries. Accurate depth imaging without the velocity is a more complex and complicated and subtle undertaking, and the capture of partial but significant capability has been completed (F. Liu et al) , further capture is underway, and all of these enterprises are far from trivial. But we are experienced hunters now, and that experience will serve us well. We have solicited data for our first field data test, and have received a positive response and good suggestions for synthetic and field data trials and we are going forward.

Foster, Matson, Shaw, Keys, Liu, H. Zhang, J. Zhang, Nita, Innanen, Ramirez, Otnes, Jiang et al., have pioneered the capture of direct velocity depth imaging capability within the series a capture which currently is partial, yet impressive and lightning fast and as we discussed in earlier communications that capture is being extended to model type generality and groomed for further synthetic and field data tests. That imaging task capture is also being extended to other currently elusive and imaging issues including diffractions. At the Annual Meeting we will describe the overall imaging project status and ongoing efforts and strategy and open issues and plans.

In the Annual Meeting presentations June 5th, 6th and 7th we decided to provide separate: (1) background/tutorial and (2) progress and plans presentations. There are basically two reasons to include tutorials: the major reason is to provide a framework and background for those looking for a way to grasp why what we are pursuing is possible, and then to examine how precisely these algorithms use the amplitude and phases in the recorded data, to achieve objectives that traditional mainstream thinking says requires e.g. velocity information.

The methods we are developing are direct generalizations of the free surface multiple removal methods, and we will link to that now acceptable methodology to show how more complicated tasks are achieved with similar data useage and input. The methods we progress are intrinsically complicated, and the thinking within the inverse scattering series brain is profound. Our goal is to make that inner logic and data flow and information and mathphysics essence accessible. The examples in our presentations are absent of pseudo differential operators, and Lebesgue integrals, and unnecessary abstraction, and generalized proofs in fractional and negative dimensions, and maximal number of superscripts and subscripts, often meant to dress up and obfuscate some old thinking in some new clothes.

Our philosophy is to illustrate the simplest incarnation of new thinking. If its a fundamental new wave concept you can show it with simple acoustic examples for those first trying to grasp what is going on. And if you know what you are doing you ought to be able to able to explain it in some way to an intelligent farmer.

Among highlights:

1. AVO framework, and unambiguous message concerning data requirements, the often reported observations of ambiguities with PP only data are not anecdotal but to be expected and additional data is not just appreciating the PP, PS, SP, SS etc data, as practical constraints. A message is communicated from the inverse scattering series based on first principles on data requirements needed for AVO. This we believe is an important message for those who practice or research AVO. AVO has fundamental theoretical open issues on the mechanical properties estimation side of things, and not only the bridge to rock and fluid properties, and probably deserves more attention, and not to be treated as only a tech service.

2. Interferometry as reheated Greens theorem (1828), but if are applying for a job I suggest you tell everyone you are progressing interferometry.

3. Flat common image gathers at the correct depth without damaging amplitudes as an automatic by-product of the direct velocity independent imaging algorithm.

4. Progress into inverse objectives in the anelastic world, towards Q compensation without Q, and separately, towards using the difference between the actual internal multiple and a predicted estimate to find an accumulated overburden transmission/Q factor.

5. And, most importantly, to recognize and congratulate Dr. Haiyan Zhang and Dr. Fang Liu for successfully completing their PhDs.

The inverse scattering series is an amazing and impressive beast in terms of how it figures out what it has to achieve and goes about its business. I suppose that its remarkable intelligence and purposefulness derives from the fact that it is a deterministic and direct inversion, without model matching, or optimization or objective functions, or searching or reference medium updating. It is unique as a prescriptive and consistent set of equations that respects the non-linear relationship between the change in any material property of a medium and the corresponding change in the wave-field.

Imagine a series where the individual terms first decide (for any given data set) whether the role and objective of that term is needed or called for prior to going into action. Two examples: (1) the term that first starts to attenuate internal multiples, first decides if you have internal multiples in your data, and if it concludes they are present it only then proceeds to predicting and removing those multiples, and (2) the depth imaging terms first determine if the chosen input velocity is adequate, and only if it decides that it isnt, that it then initiates action to remove the incorrect image and to create the correct one. The latter are examples of purposeful perturbation, very different from a sum of terms somehow wandering around model space towards and away from the answer.

I've always been and I remain impressed and frankly, more than somewhat in awe. I'm reminded of Richard Feynman's famous quote about quantum mechanics, he stated "I don't understand quantum mechanics, and those who claim they do, really don't!". We have mined the inverse scattering series for multiple removal and we are currently understanding and deciphering and capturing and testing how it responds to depth imaging and non-linear AVO challenges.

Our job within M-OSRP is to educate and mentor graduate students, while addressing the pressing innate seismic E & P algorithmic challenges. We fully understand and appreciate and are extremely grateful for the rare opportunity you provide us through our consortium partnership, to go after this fundamental high impact game-changing seismic capability.

The program is on track, and moving towards and achieving our goals. We look forward to seeing you at the Annual Meeting. Thanks.

Sincerely,

Art
Arthur B. Weglein

Acknowledgments

We are grateful to the sponsors of M-OSRP for supporting this research, as well as NSF-CMG (award DMS-0327778) and DOE Basic Energy Sciences (award DE-FG02-05ER15697).

Review of the deghosting algorithm derived from Green's Theorem

J. Zhang and A. B. Weglein

Abstract

In this paper, the derivation and testing of the Green's theorem deghosting algorithm are reviewed. In general, for towed streamer data, the source wavelet is necessary in order to perform deghosting, since the vertical derivative of the wavefield is not measured. However, through analyzing the Green's theorem deghosting algorithm, it is concluded that the scattered field can always be deghosted even without the source wavelet. Field data testing issues are also discussed.

1 Introduction

Deghosting is a seismic processing procedure to remove the up-going wave on the source side and the down-going wave on the receiver side. Ghosts produce an angle and frequency dependent seismic distortion and a notch in the frequency spectrum. Deghosting can improve the resolution and remove ghost notches in seismic data. All subsequent processing steps and objectives will benefit from effective deghosting. Furthermore, deghosting is a specific prerequisite of all inverse scattering series tasks, e.g., free surface multipel removal (Carvalho, 1992; Weglein et al., 1997), internal multiple attenuation (Araújo, 1994; Ramírez and Weglein, 2005), depth imaging without the velocity (Shaw and Weglein, 2003; Liu et al., 2004; Innanen and Weglein, 2003) and nonlinear inversion (Zhang and Weglein, 2005a, 2006a). For ocean bottom data, the deghosting is an important step since the ghost notch appears at a lower frequency and has had daunting challenges due to difficulty with stable and reliable dual sensor OBS measurements.

There is a extensive literature on deghosting (Schneider et al., 1964; Robertsson and Kragh, 2002). The deghosting algorithm derived from Green's/Extinction theorem has been presented and studied previously (Weglein et al., 2002; Zhang and Weglein, 2005b, 2006b). In this paper, we first review the derivation of the algorithm. At the same time, we will show that small changes on the derivation will enable us to obtain the wavelet estimation algorithm (Weglein and Secrest, 1990) and field prediction algorithm (Osen et al., 1998; Tan, 1999; Weglein et al., 2000). Moreover, through the analysis of the deghosting theory, we will discuss issues that arise when the algorithm is applied to field data.

2 Theory

The Green's Second identity (Green's theorem) is

$$\int_V \left(\psi(\mathbf{r}', \mathbf{r}_s, \omega)\nabla'^2\phi(\mathbf{r}', \mathbf{r}, \omega) - \phi(\mathbf{r}', \mathbf{r}, \omega)\nabla'^2\psi(\mathbf{r}', \mathbf{r}_s, \omega)\right) d\mathbf{r}'$$

$$= \oint_S \left[\psi(\mathbf{r}', \mathbf{r}_s, \omega)\nabla'\phi(\mathbf{r}', \mathbf{r}, \omega) - \phi(\mathbf{r}', \mathbf{r}, \omega)\nabla'\psi(\mathbf{r}', \mathbf{r}_s, \omega)\right] \cdot d\mathbf{S}', \tag{1}$$

where $\psi(\mathbf{r}', \mathbf{r}_s, \omega)$ and $\phi(\mathbf{r}', \mathbf{r}, \omega)$ are two arbitrary functions and the closed surface S enclosed volume V. In this paper, we will *always* associate $\psi(\mathbf{r}', \mathbf{r}_s, \omega)$ with the pressure wavefield in the actual medium $P(\mathbf{r}', \mathbf{r}_s, \omega)$ which is assumed to satisfy

$$\nabla'^2 P(\mathbf{r}', \mathbf{r}_s, \omega) + \frac{\omega^2}{c^2(\mathbf{r}')} P(\mathbf{r}', \mathbf{r}_s, \omega) = A(\omega)\delta(\mathbf{r}' - \mathbf{r}_s), \tag{2}$$

in the volume integral and where $A(\omega)$ is the source wavelet. This $P(\mathbf{r}', \mathbf{r}_s, \omega)$ at the receiver location will be the wavefield recorded by the hydrophone/geophone. Substituting $\frac{\omega^2}{c^2(\mathbf{r}')}$ with $k_0^2(1 - \alpha(\mathbf{r}'))$ where $k_0^2 = \frac{\omega^2}{c_0^2}$, Eq. 2 becomes

$$\nabla'^2 P(\mathbf{r}', \mathbf{r}_s, \omega) + k_0^2 P(\mathbf{r}', \mathbf{r}_s, \omega) = A(\omega)\delta(\mathbf{r}' - \mathbf{r}_s) + k_0^2\alpha(\mathbf{r}')P(\mathbf{r}', \mathbf{r}_s, \omega), \tag{3}$$

where $\alpha(\mathbf{r}')$ represents the difference between the actual medium and the reference medium, water. Throughout this paper, $\alpha(\mathbf{r}')$ is consistently regarded as consisting of two parts, $\alpha_{air}(\mathbf{r}')$ and $\alpha_{earth}(\mathbf{r}')$ which respectively denote the difference between air and water and earth and water. Thus, Eq. 3 becomes

$$\nabla'^2 P(\mathbf{r}', \mathbf{r}_s, \omega) + k_0^2 P(\mathbf{r}', \mathbf{r}_s, \omega) = A(\omega)\delta(\mathbf{r}' - \mathbf{r}_s) + k_0^2 \left(\alpha_{air}(\mathbf{r}') + \alpha_{earth}(\mathbf{r}')\right) P(\mathbf{r}', \mathbf{r}_s, \omega). \tag{4}$$

Next, the *arbitrary* function $\phi(\mathbf{r}', \mathbf{r}, \omega)$ and different volume V will be fully explored to obtain the algorithm needed.

2.1 Derivation of the deghosting algorithm (Weglein et al., 2002)

If we substitute $\phi(\mathbf{r}', \mathbf{r}, \omega)$ by the causal Green's function $G_0^+(\mathbf{r}', \mathbf{r}, \omega)$ in the whole space reference medium (water) which satisfies

$$\nabla'^2 G_0^+(\mathbf{r}', \mathbf{r}, \omega) + k_0^2 G_0^+(\mathbf{r}', \mathbf{r}, \omega) = \delta(\mathbf{r}' - \mathbf{r}), \tag{5}$$

then after substituting Eq. 5 and Eq. 4 into Eq. 1, we have

$$\begin{aligned}
&\int_V \Big(P(\mathbf{r}', \mathbf{r}_s, \omega)\nabla'^2 G_0^+(\mathbf{r}', \mathbf{r}, \omega) - G_0^+(\mathbf{r}', \mathbf{r}, \omega)\nabla'^2 P(\mathbf{r}', \mathbf{r}_s, \omega)\Big)\, d\mathbf{r}' \\
&= \int_V P(\mathbf{r}', \mathbf{r}_s, \omega)\Big(\delta(\mathbf{r}' - \mathbf{r}) - k_0^2 G_0^+(\mathbf{r}', \mathbf{r}, \omega)\Big) d\mathbf{r}' \\
&- \int_V G_0^+(\mathbf{r}', \mathbf{r}, \omega)\Big(A(\omega)\delta(\mathbf{r}' - \mathbf{r}_s) + k_0^2 \left(\alpha_{air}(\mathbf{r}') + \alpha_{earth}(\mathbf{r}')\right) P(\mathbf{r}', \mathbf{r}_s, \omega) - k_0^2 P(\mathbf{r}', \mathbf{r}_s, \omega)\Big)\, d\mathbf{r}' \\
&= \oint_S \left[P(\mathbf{r}', \mathbf{r}_s, \omega)\nabla' G_0^+(\mathbf{r}', \mathbf{r}, \omega) - G_0^+(\mathbf{r}', \mathbf{r}, \omega)\nabla' P(\mathbf{r}', \mathbf{r}_s, \omega)\right] \cdot d\mathbf{S}'.
\end{aligned} \tag{6}$$

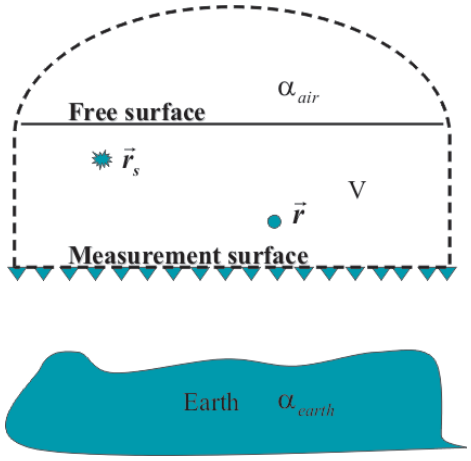

Figure 1: *First configuration for derivation of the deghosting algorithm.*

Now choosing the half space above the measurement surface as V, and puting $\mathbf{r}$ anywhere between the free surface and the measurement surface (inside of V) (Figure 1), Eq. 6 becomes

$$P(\mathbf{r},\mathbf{r}_s,\omega) - A(\omega)G_0^+(\mathbf{r},\mathbf{r}_s,\omega) - \int_V G_0^+(\mathbf{r}',\mathbf{r},\omega)k_0^2\alpha_{air}(\mathbf{r}')P(\mathbf{r}',\mathbf{r}_s,\omega)d\mathbf{r}' = \oint_S \left[P(\mathbf{r}',\mathbf{r}_s,\omega)\nabla' G_0^+(\mathbf{r}',\mathbf{r},\omega) - G_0^+(\mathbf{r}',\mathbf{r},\omega)\nabla' P(\mathbf{r}',\mathbf{r}_s,\omega)\right]\cdot d\mathbf{S}' \quad (7)$$

The physical meaning of Eq. 7 is analyzed as follows. The total wavefield at point $\mathbf{r}$ can be separated into three parts: (1) the direct wave which travels directly from the source to $\mathbf{r}$, (2) the field whose last motion is *downward* from the free surface and (3) the field whose last motion is *upward* from the earth. In Eq. 7 the term that contains the source wavelet is part (1) and the volume integration term is part (2). Therefore the whole LHS of Eq. 7 corresponds to part (3), the up-going (or the receiver side deghosted) wavefield at point $\mathbf{r}$. Thus we obtain the deghosting algorithm:

$$P^{deghosted}(\mathbf{r},\mathbf{r}_s,\omega) = \oint_S \left[P(\mathbf{r}',\mathbf{r}_s,\omega)\nabla' G_0^+(\mathbf{r}',\mathbf{r},\omega) - G_0^+(\mathbf{r}',\mathbf{r},\omega)\nabla' P(\mathbf{r}',\mathbf{r}_s,\omega)\right]\cdot d\mathbf{S}' \quad (8)$$

$$= \int_{m.s.} \left[P(\mathbf{r}',\mathbf{r}_s,\omega)\nabla' G_0^+(\mathbf{r}',\mathbf{r},\omega) - G_0^+(\mathbf{r}',\mathbf{r},\omega)\nabla' P(\mathbf{r}',\mathbf{r}_s,\omega)\right]\cdot d\mathbf{S}', \quad (9)$$

where in the last step the Sommerfeld Radiation condition eliminates the upper half space contribution at infinite distance and m.s. denotes the measurement surface. Using the reciprocity theorem, the same kind of Green's theorem argument on the output of Eq. 8 on the source side will eliminate the source side ghost.

Eq. 9 can be easily understood in if we use the idea of terms of Extinction theorem, which is an interpretation of the Green's theorem with causal Green's function. In optics, people use the name of Extinction theorem in order to emphasize one of the amazing properties of the surface integration term in Green's theorem: if causal $P(\mathbf{r}',\mathbf{r},\omega)$ and causal Green's function are used on the integration surface, then the surface integration term always produces the wavefield contributions

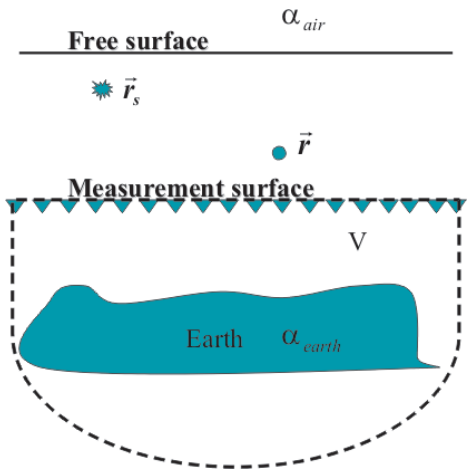

Figure 2: *Second configuration for derivation of the deghosting algorithm.*

due to sources inside (outside) of the volume V, if the output point $\mathbf{r}$ is outside (inside) of V, i.e., the outside (inside) source contributions have been extinguished/eliminated. Another interesting property of the surface integration term will be mentioned later in this paper.

To derive Eq. 9 using the Extinction theorem, we can choose the same the volume V and position $\mathbf{r}$ as above. Then, using Green's causal function and according to the above metioned property, the surface integration will eliminate wavefield contributions due to the source inside of V (which are the active source and the air) and only contributions due to source outside of V (which is the earth) will be kept. Since the wavefield due to the earth is up-going at $\mathbf{r}$, the surface integration term will produce the receiver side deghosted field.

Another way of using the Extinction theorem to derive Eq. 9 is to choose the volume V as the half space below the measurement surface (Figure 2), with the position of $\mathbf{r}$ (outside of V) and the causal Green's function being the same as above. Then the surface integration will only keep the contribution due to the source inside of V, which is the earth. Hence the integration provides the up-going, or receiver side deghosted wavefield.

2.2 Derivation of the wavelet estimation formula (Weglein and Secrest, 1990)

Substituting $\phi(\mathbf{r}', \mathbf{r}, \omega)$ by the Green's function $G_0^D(\mathbf{r}', \mathbf{r}, \omega)$ in whole space reference medium (water) which satisfies

$$\nabla'^2 G_0^D(\mathbf{r}', \mathbf{r}, \omega) + k_0^2 G_0^D(\mathbf{r}', \mathbf{r}, \omega) = \delta(\mathbf{r}' - \mathbf{r}) - \delta(\mathbf{r}' - \mathbf{r}_I), \tag{10}$$

where $\mathbf{r}_I$ is the mirror image of $\mathbf{r}$ with respect to the free surface, then after substituting Eq. 10 and Eq. 4 into Eq. 1, we have

$$\int_V \left(P(\mathbf{r}', \mathbf{r}_s, \omega) \nabla'^2 G_0^D(\mathbf{r}', \mathbf{r}, \omega) - G_0^D(\mathbf{r}', \mathbf{r}, \omega) \nabla'^2 P(\mathbf{r}', \mathbf{r}_s, \omega) \right) d\mathbf{r}'$$

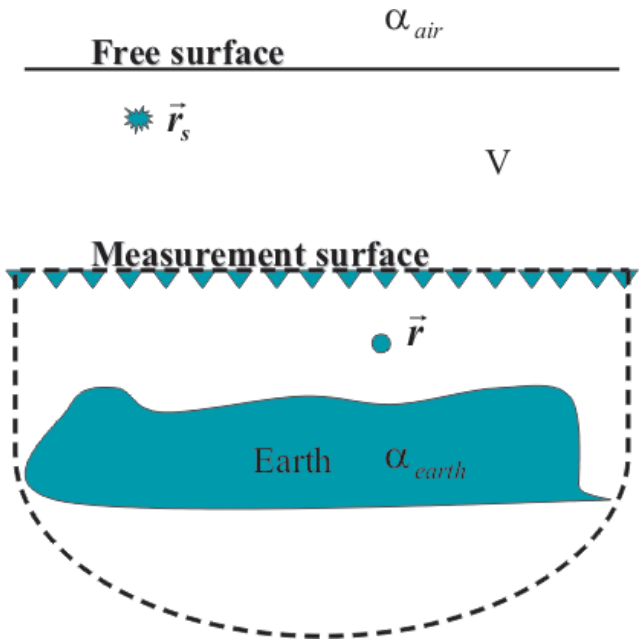

Figure 3: *First configuration for derivation of the wavelet estimation algorithm.*

$$
\begin{aligned}
&= \int_V P(\mathbf{r}', \mathbf{r}_s, \omega)\Big(\delta(\mathbf{r}' - \mathbf{r}) - \delta(\mathbf{r}' - \mathbf{r}_I) - k_0^2 G_0^D(\mathbf{r}', \mathbf{r}, \omega)\Big) d\mathbf{r}' \\
&- \int_V G_0^D(\mathbf{r}', \mathbf{r}, \omega)\Big(A(\omega)\delta(\mathbf{r}' - \mathbf{r}_s) + k_0^2\left(\alpha_{air}(\mathbf{r}') + \alpha_{earth}(\mathbf{r}')\right)P(\mathbf{r}', \mathbf{r}_s, \omega) - k_0^2 P(\mathbf{r}', \mathbf{r}_s, \omega)\Big)\, d\mathbf{r}' \\
&= \oint_S \left[P(\mathbf{r}', \mathbf{r}_s, \omega)\nabla' G_0^D(\mathbf{r}', \mathbf{r}, \omega) - G_0^D(\mathbf{r}', \mathbf{r}, \omega)\nabla' P(\mathbf{r}', \mathbf{r}_s, \omega)\right] \cdot d\mathbf{S}'. \qquad (11)
\end{aligned}
$$

Now, choosing the half space below the measurement surface as V, and choosing $\mathbf{r}$ at a point below the measurement surface (inside of V) (Figure 3), Eq. 11 becomes

$$
\begin{aligned}
P(\mathbf{r}, \mathbf{r}_s, \omega) - &\int_V G_0^D(\mathbf{r}', \mathbf{r}, \omega) k_0^2 \alpha_{earth}(\mathbf{r}') P(\mathbf{r}', \mathbf{r}_s, \omega) d\mathbf{r}' \\
&= \oint_S \left[P(\mathbf{r}', \mathbf{r}_s, \omega)\nabla' G_0^D(\mathbf{r}', \mathbf{r}, \omega) - G_0^D(\mathbf{r}', \mathbf{r}, \omega)\nabla' P(\mathbf{r}', \mathbf{r}_s, \omega)\right] \cdot d\mathbf{S}' \qquad (12)
\end{aligned}
$$

Again, the physical meaning of Eq. 12 is analyzed as follows. The total wavefield at point $\mathbf{r}$ can be separated into three parts: (1) the direct wave which travels directly from the source and the direct wave ghost, (2) the scattered field whose last travel step is from the earth, and (3) the scattered field whose last travel step is down from the free surface. Part (3) can also be regarded as the ghost of the part (2). It is not difficult to realize that in Eq. 12 the volume integration term is the sum of part (2) and (3). Then the whole LHS of Eq. 12 is part (1), the direct wave and its ghost at point $\mathbf{r}$. Thus, the wavelet estimation algorithm (Weglein and Secrest, 1990) is obtained:

$$
A(\omega) G_0^D(\mathbf{r}, \mathbf{r}_s, \omega) = \oint_S \left[P(\mathbf{r}', \mathbf{r}_s, \omega)\nabla' G_0^D(\mathbf{r}', \mathbf{r}, \omega) - G_0^D(\mathbf{r}', \mathbf{r}, \omega)\nabla' P(\mathbf{r}', \mathbf{r}_s, \omega)\right] \cdot d\mathbf{S}' \qquad (13)
$$

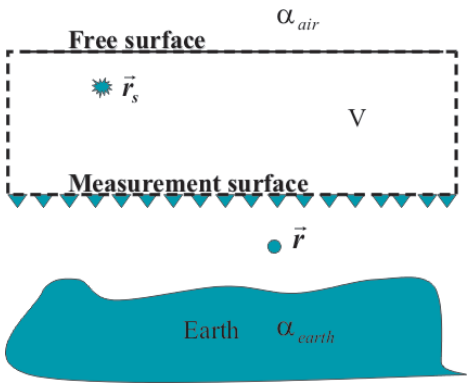

Figure 4: *Second configuration for derivation of the wavelet estimation algorithm.*

$$= \int_{m.s.} \left[P(\mathbf{r}', \mathbf{r}_s, \omega)\nabla' G_0^D(\mathbf{r}', \mathbf{r}, \omega) - G_0^D(\mathbf{r}', \mathbf{r}, \omega)\nabla' P(\mathbf{r}', \mathbf{r}_s, \omega)\right] \cdot d\mathbf{S}', \quad (14)$$

where at the last step, the properties of $P(\mathbf{r}', \mathbf{r}_s, \omega)$ and $G_0^D(\mathbf{r}', \mathbf{r}, \omega)$ at the free surface have been used.

Another way of deriving Eq. 14 is to start from Eq. 11, and choose the space between the free surface and measurement surface as volume V (Figure 4). Then we will directly obtain Eq. 14 since all sources are outside of V, except the active source $\delta(\mathbf{r}' - \mathbf{r}_s)$.

2.3 Derivation of the field prediction formula (Osen et al., 1998; Tan, 1999; Weglein et al., 2000)

If we substitute $\phi(\mathbf{r}', \mathbf{r}, \omega)$ by the Green's function $G_0^{DD}(\mathbf{r}', \mathbf{r}, \omega)$ in whole space reference medium (water) which satisfies

$$\nabla'^2 G_0^{DD}(\mathbf{r}', \mathbf{r}, \omega) + k_0^2 G_0^{DD}(\mathbf{r}', \mathbf{r}, \omega) = \delta(\mathbf{r}' - \mathbf{r}) + \sum_{i=1}^{\infty} a_i \delta(\mathbf{r}' - \mathbf{r}_i), \quad (15)$$

where $\mathbf{r}_i$, for $i = 1, 2, 3, \ldots$ is the position of one of the infinite number of mirror images of $\mathbf{r}$ with respect to the free surface and the measurement surface to assure the resulting G_0^{DD} vanishes at both surfaces, and coefficient a_i can be positive or negative 1, then after substituting Eq. 15 and Eq. 4 into Eq. 1, we have

$$\begin{aligned}
&\int_V \Big(P(\mathbf{r}', \mathbf{r}_s, \omega)\nabla'^2 G_0^{DD}(\mathbf{r}', \mathbf{r}, \omega) - G_0^{DD}(\mathbf{r}', \mathbf{r}, \omega)\nabla'^2 P(\mathbf{r}', \mathbf{r}_s, \omega)\Big)\, d\mathbf{r}' \\
&= \int_V P(\mathbf{r}', \mathbf{r}_s, \omega)\Big(\delta(\mathbf{r}' - \mathbf{r}) + \sum_{i=1}^{\infty} a_i \delta(\mathbf{r}' - \mathbf{r}_i) - k_0^2 G_0^{DD}(\mathbf{r}', \mathbf{r}, \omega)\Big) d\mathbf{r}' \\
&- \int_V G_0^{DD}(\mathbf{r}', \mathbf{r}, \omega)\Big(A(\omega)\delta(\mathbf{r}' - \mathbf{r}_s) + k_0^2 \left(\alpha_{air}(\mathbf{r}') + \alpha_{earth}(\mathbf{r}')\right) P(\mathbf{r}', \mathbf{r}_s, \omega) - k_0^2 P(\mathbf{r}', \mathbf{r}_s, \omega)\Big)\, d\mathbf{r}' \\
&= \oint_S \left[P(\mathbf{r}', \mathbf{r}_s, \omega)\nabla' G_0^{DD}(\mathbf{r}', \mathbf{r}, \omega) - G_0^{DD}(\mathbf{r}', \mathbf{r}, \omega)\nabla' P(\mathbf{r}', \mathbf{r}_s, \omega)\right] \cdot d\mathbf{S}'. \quad (16)
\end{aligned}$$

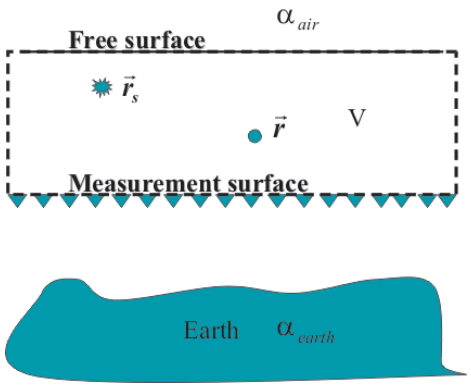

Figure 5: *Configuration for derivation of the field prediction algorithm.*

Now, choosing the space between the free surface and the measurement surface as V, and putting $\mathbf{r}$ anywhere inside of V (Figure 5), Eq. 16 becomes the field prediction equation (Osen et al., 1998; Tan, 1999; Weglein et al., 2000)

$$\begin{aligned} P(\mathbf{r},\mathbf{r}_s,\omega) =& A(\omega)G_0^{DD}(\mathbf{r},\mathbf{r}_s,\omega) \\ &+ \oint_S \left[P(\mathbf{r}',\mathbf{r}_s,\omega)\nabla' G_0^{DD}(\mathbf{r}',\mathbf{r},\omega) - G_0^{DD}(\mathbf{r}',\mathbf{r},\omega)\nabla' P(\mathbf{r}',\mathbf{r}_s,\omega)\right]\cdot d\mathbf{S}', \qquad (17) \\ =& A(\omega)G_0^{DD}(\mathbf{r},\mathbf{r}_s,\omega) + \int_{m.s.} P(\mathbf{r}',\mathbf{r}_s,\omega)\nabla' G_0^{DD}(\mathbf{r}',\mathbf{r},\omega)\cdot d\mathbf{S}', \qquad (18) \end{aligned}$$

where the last step used the properties of $P(\mathbf{r}',\mathbf{r}_s,\omega)$ and $G_0^{DD}(\mathbf{r}',\mathbf{r},\omega)$ on the surfaces. Osen et al. (1998) also regards the above equation as a wavelet estimation. The requirement is knowing the field $(P(\mathbf{r}',\mathbf{r}_s,\omega))$ on the measurement surface and one extra hydrophone measurement $(P(\mathbf{r},\mathbf{r}_s,\omega))$ at any position between the free surface and the measurement surface, then the only unknown variable in Eq. 18 is the source wavelet $A(\omega)$.

In this section, using Green's theorem, it has been demonstrated how to derive the algorithms for deghosting, wavelet estimation and field prediction. Collecting Eq. 8, Eq. 13 and Eq. 17, we will notice that the actual causal wavefield can always be obtained, although the volume V and the form of Green's function is very different. Actually, this is the other amazing property of the surface integration term that we want to mention. That is, as long as causal P on surface and volume integration has been used, the surface integration term will make sure the resulting wavefield $P(\mathbf{r},\mathbf{r}_s,\omega)$ will *always* be causal, regardless of what kind of Green's function has been used.

In the next section, some analysis of the deghosting algorithm will be given. It will be shown that the deghosting algorithm is closely related to the wavelet estimation and field prediction algorithm.

3 Analysis of the deghosting algorithm

The deghosting algorithm Eq. 9 can not be directly used since it requires both the wavefield $(P(\mathbf{r}',\mathbf{r}_s,\omega))$ and its vertical derivative while in practice, only the wavefield is available. This

difficulty can be easily overcome (at least theoretically) if the source wavelet is known, according to the wavelet estimation formula Eq. 14, in which the three functions P, $\frac{dP}{dz}$ and $A(\omega)$ form a triangle relationship. Any one of the functions can be calculated if the other two are known. For towed streamer data (Zhang and Weglein, 2005b), assuming the source wavelet is known and using the field prediction algorithm Eq. 18, the field and its vertical derivative are calculated at a pseudo-measurement surface which is a little bit higher than the actual measurement surface. Then Eq. 9 is used to perform deghosting. For ocean bottom data (Zhang and Weglein, 2006b), assuming the source wavelet is known, the vertical derivative of P is calculated using the wavelet estimation algorithm Eq. 14. Numerical tests for both cases are encouraging.

If the source wavelet is not known, usually we cannot perform deghosting using the field on the measurement surface only. However, we can always perform deghosting on the scattered field, even without source wavelet. This point has not been made clear before. Knowing the source wavelet will only help to get rid of the direct wave and its ghost. Knowing the wavelet or not has nothing to do with the deghosting of the scattered field. In the field prediction Eq. 18, the scattered field only exists in the surface integration term, which means as long as the total wavefield on the measurement surface is available, we will have all of the information needed for the scattered field. The contribution of knowing source wavelet in Eq. 18 will only help to calculate the terms containing $A(\omega)$, which only contributes to the prediction of direct wave and its ghost and has nothing to do with the scattered field. The consequence of deghosting without knowing source wavelet is that the scattered field will be deghosted well, while the direct wave and its ghost still exist in the final result. This property is appealing in the area that the scattered field does not interfere with the direct wave and its ghost.

When the deghosting algorithm is applied to the field data, there are several issues that need to be dealt with. When the field prediction procedure Eq. 18 is used, it assumes the data on the whole measurement surface is known. In practice, usually there are no hydrophones at very small offsets. Also, cross line distance usually is too large to be used directly. Data interpolation and extrapolation have to be performed in advance. Also, efficient numerical techniques have to be used in order to deal with the large amount of calculation when dealing with $3D$ data. For ocean bottom data, there are even more requirements for data interpolation and extrapolation since the receiver interval is usually much larger than the hydrophone interval on towed streamer.

4 Conclusions

As an important seismic processing step, deghosing has been studied extensively. In this paper, the Green's theorem deghosting algorithm derived from Green's theorem has been reviewed. The close relationship among deghosting, field prediction and wavelet estimation has been demonstrated. Deghosting usually requires the knowledge of the source wavelet. The scattered field can always be deghosted, even when the source wavelet is not known. Data interpolation and extrapolation is a prerequisite when the deghosting algorithm is applied to field data.

5 Acknowledgments

The support of M-OSRP sponsors and colleagures are greatly appreciated. This work has been partially funded by NSF-CMG award DMS-0327778 and DOE Basic Energy Sciences award DE-FG02-05ER15697. Jingfeng Zhang appreciates support as the 2006-2007 ConocoPhillips fellow.

References

Araújo, F. V. *Linear and non-linear methods derived from scattering theory: backscattered tomography and internal multiple attenuation*. PhD thesis, Universidade Federal da Bahia, 1994.

Carvalho, P. M. *Free-surface multiple reflection elimination method based on nonlinear inversion of seismic data*. PhD thesis, Universidade Federal da Bahia, 1992.

Innanen, K. A. and A. B. Weglein. "Simultaneous Imaging and Inversion with the Inverse Scattering Series." *Proceedings of the Eighth International Congress of the SBGf and Fifth Latin American Geophysical Conference*. . SBGf, 2003.

Liu, F., B. G. Nita, A. B. Weglein, and K. A. Innanen. "Inverse Scattering Series in the presence of lateral variations." *M-OSRP Annual Report* 3 (2004).

Osen, Are, Bruce G. Secrest, and Lasse Amundsen. "Wavelet estimation from marine pressure measurements." *Geophysics* 63 (November-December 1998): 2108–2119.

Ramírez, A. C. and A.B. Weglein. "An inverse scattering internal multiple elimination method: Beyond attenuation, a new algorithm and initial tests." *SEG Expanded Abstracts.* (2005): 2115–2118.

Robertsson, J.O.A. and E. Kragh. "Rough sea deghosting using a single streamer and a pressure gradient approximation." *Geophysics* 67 (2002): 2005–2011.

Schneider, W. A., K. L. Larner, J. P. Burg, and M. M. Backus. "A new data processing technique for the elimination of ghost arrivals on reflection seismograms." *Geophysics* 29 (1964): 783–805.

Shaw, S. A. and A. B. Weglein. "Imaging seismic reflection data at the correct depth without specifying an accurate velocity model: Initial examples of an inverse scattering subseries." *Frontiers of remote sensing information processing*. Ed. C. H. Chen. World Scientific Publishing Company, 2003. chapter 21, 469–484.

Tan, T.H. "Wavelet spectrum estimation." *Geophysics* 64 (November-December 1999): 1836–1846.

Weglein, A. B., F. A. Gasparotto, P. M. Carvalho, and R. H. Stolt. "An Inverse-Scattering Series Method for Attenuating Multiples in Seismic Reflection Data." *Geophysics* 62 (November-December 1997): 1975–1989.

Weglein, A. B., S. .A. Shaw, K. H. Matson, J. L. Sheiman, R. H. Solt, T. H. Tan, A. Osen, G. P. Correa, K. A. Innanen, Z. Guo, and J. Zhang. "New approaches to deghosting towed-streamer and ocean-bottem pressure measurements." *72nd Annual Internat. Mtg., Soc. Expl. Geophys., Expanded Abstracts*. . Soc. Expl. Geophys., 2002. 1016–1019.

Weglein, A. B., T. H. Tan, K. H. Matson, S. A. Shaw, and D. J. Foster. "Prediction of the wavefield anywhere above an ordinary towed streamer: Applications to source wavelet estimation, demultiple, and imaging." *70th Annual Internat. Mtg., Soc. Expl. Geophys., Expanded Abstracts*. . Soc. Expl. Geophys., 2000. 2413–2415.

Weglein, Arthur B. and Bruce G. Secrest. "Wavelet estimation for a multidimensional acoustic earth model." *Geophysics* 55 (July 1990): 902–913.

Zhang, H. and A. B. Weglein. "The inverse scattering series for tasks associated with primaries: depth imaging and direct non-linear inversion of 1D variable velocity and density acoustic media." *75th Annual Internat. Mtg., Soc. Expl. Geophys., Expanded Abstracts*. . Soc. Expl. Geophys., 2005. 1705–1708.

Zhang, H. and A. B. Weglein. "The inverse scattering series for tasks associated with primaries: direct non-linear inversion of 1D elastic media." *76th Annual Internat. Mtg., Soc. Expl. Geophys., Expanded Abstracts*. . Soc. Expl. Geophys., 2006. 2062–2066.

Zhang, J. and A. B. Weglein. "Extinction theorem deghosting method using towed streamer pressure data: Analysis of the receiver array effect on deghosting and subsequent free surface multiple removal." *75th Annual Internat. Mtg., Soc. Expl. Geophys., Expanded Abstracts*. . Soc. Expl. Geophys., 2005. 2095–2100.

Zhang, J. and A. B. Weglein. "Application of extinction theorem deghosting method on ocean bottom data." *76th Annual Internat. Mtg., Soc. Expl. Geophys., Expanded Abstracts*. . Soc. Expl. Geophys., 2006. 2694–2678.

Remarks on Green's Theorem for seismic interferometry

A. C. Ramírez and A. B. Weglein

Abstract

The foundations of interferometry and virtual source methods can be found in Green's theorem. This theorem, derived by George Green in 1828, gives exact equations that incorporate boundary conditions for wavefield retrieval. It has been applied to several seismic exploration problems ranging from deghosting and wavelet estimation, to complete removal of overburden and source signature effects in the measured data.

In this paper we study a unifying framework for a broad class of interferometry techniques using Green's theorem. This framework and foundation allows errors and artifacts that occur in certain compromised interferometry approaches to be anticipated and fully explained as a consequence of approximations made within Green's theorem. We also show the connection between virtual source and deconvolution techniques with designature/demultiple methods based on the same framework provided by George Green.

Introduction

In the last few years, a number of papers on seismic interferometry have shown methods to extract the Green's function between a pair of receivers by convolving, deconvolving or crosscorrelating data from a closed surface of sources (see for example Derode et al. (2003); Roux and Fink (2003); Wapenaar (2004); Weaver and Lobkis (2004); Bakulin and Calvert (2004); Schuster and Zhou (2006); Draganov et al. (2006); Snieder et al. (2006)). All of these methods are contained in the framework given by Green's theorem. Most of the current seismic interferometry methods require dual measurements (pressure field and its normal gradient) which are not always available. The lack of the normal derivative of the wavefield have encouraged the arrival of many algorithms using high frequency and one-way approximations to the normal field derivative. The approximations are compromises to the exact theory and, hence, produce artifacts.

Green's theorem relates a surface integral of two scalar functions u and ν, and their normal derivatives with a volume integral of the same functions and their Laplacians,

$$\int_V [u\nabla^2\nu - \nu\nabla^2 u]d\boldsymbol{x} = \int_S [u\boldsymbol{\nabla}\nu - \nu\boldsymbol{\nabla}u]\cdot\boldsymbol{n}d\boldsymbol{s}, \tag{1}$$

where $\boldsymbol{x}$ is a three dimensional vector (x_1, x_2, x_3) characterizing the volume V enclosed by the surface S, and $\boldsymbol{n}$ is the unit vector normal to this surface. Green's theorem has been extended to displacements by Betti (1872) and elastodynamic fields by Rayleigh (1873). The importance of this theorem lays in its generality. The functions u and ν can be any pair of scalar functions that have normal derivatives at the surface S and Laplacians in V.

The objective of this paper is to study and analyze different applications of Green's theorem to seismic exploration. For those different applications, there will be different choices of the volume and functions u and ν introduced to satisfy equation 1. These different choices are the foundation for applications dealing with seismic interferometry, wavelet estimation and wavefield deconvolution. They are all connected by the same framework and their differences rely on the specific functions and boundary conditions imposed upon Green's theorem as well as the approximations that some of these applications make to avoid certain requirements of the theory. The first function in equation 1, u, will be selected to be the pressure field P corresponding to recorded values of the pressure field in a marine seismic experiment. The second function ν will be selected depending on the application that we want to derive.

For the first application (seismic interferometry or wavefield retrieval), an anticausal Green's function satisfying the same Helmholtz operator as the pressure field is used as the second function ν in equation 1 (see for example Weaver and Lobkis (2004); Wapenaar (2004); Korneev and Bakulin (2006); Wapenaar and Fokkema (2006) and references within). The are two issues here. First, this Green's function requires knowledge of the medium that produced the pressure field. In general, that medium is unknown and the Green's function is replaced by the conjugate of a second pressure field produced by the same medium but by a different source. Seconds, this choice of functions in Green's theorem requires dual measurements (pressure data and its normal derivative). Since the normal derivative of the pressure field is not always measured, approximations are introduced into this form of seismic interferometry. The consequence of this is that the synthesized wavefield has errors and spurious events.

We next consider another form of seismic interferometry, direct wave seismic interferometry. This is found by selecting the function ν as a causal or anticausal reference Green's function satisfying the Helmholtz operator for two homogeneous half spaces separated by a zero pressure surface (such as the air-water surface in a marine experiment). Both choices will provide algorithms to retrieve the wavefield within a specified volume, requiring measurements of the pressure field and its normal derivative at the volume's surface. We will see that a high frequency approximation of the pressure field's normal derivative is more forgiving when an anticausal reference Green's function is used (Ramírez et al., 2007).

The choice of a causal reference Green's function, as the second function ν in equation 1 will also provide an algorithm for wavelet estimation that depends on dual measurements (Weglein and Secrest, 1990; Weglein and Devaney, 1992). A different choice for ν that removes the requirement of the wavefield's normal derivative is a Green's function that vanishes at two surfaces, which is going to be referred as Dirichlet Green's function (Osen et al., 1998; Tan, 1999). The two surfaces where the Dirichlet boundary conditions are imposed, in a marine experiment, are the air-water surface and the measurement surface. This choice of functions in Green's theorem gives a formalism for wavelet estimation that does not require the wavefield's normal derivative. With this choice of functions, another form of interferometry is also found. The latter requires only measured pressure data and it can be applied to surface seismic acquisitions (Weglein et al., 2000; Ramírez et al., 2007).

The last application is wavefield deconvolution, a theory applied to the removal of overburden effects (overburden refers to the medium above the receiver or measurement plane), *e.g.* removal of

free-surface multiples (events due to the existence of the air-water surface) and source effects (due to a source exploiting above the location of interest). For this purpose, the function ν is selected to be a Green's function produced by the same medium as the pressure field, but without the existence of a zero-pressure boundary condition at the free surface (Amundsen, 1999, 2001; Holvik and Amundsen, 2005). The algorithm derived with this choice will remove all the free-surface multiples and the source wavelet from the pressure field, and, it will retrieved the deconvolved wavefield at the receiver location (coincident source and receiver), effectively creating a source at the receiver location. A similar method for wavefield deconvolution, which requires the source wavelet, was derived by (Ziolkowski et al., 1998; Johnston and Ziolkowski, 1999).

We are going to start this analysis with a selection of a pressure field and a causal Green's function as u and ν in equation 1. First we are going to select a causal reference Green's function to obtain the general Weglein and Secrest (1990) result, which can also be derived from the Kirchhoff-Helmholtz integral representation (Weglein and Devaney, 1992; Osen et al., 1994). This selection will also allow us to obtain the equation for direct wave interferometry with correlations that requires dual measurements. The results will be analyzed and the next choice of functions and applications will be introduced.

1 Green's Theorem with a causal Green's function

In this section, two seismic applications, using Green's theorem, will be derived: wavelet estimation, and direct wave interferometry with correlations. Both methods are applied to a marine seismic experiment. An analysis and discussion of the results will be performed at the end of the section. This analysis will serve as motivation for the applications of Green's theorem discussed and derived in section 2.

In the following, we use Green's theorem to derive an integral representation of the pressure field P, which satisfies the inhomogeneous Helmholtz equation for a velocity distribution $c(\boldsymbol{x})$ and constant density

$$\left(\nabla^2 + \frac{\omega^2}{c^2(\boldsymbol{x})}\right) P(\boldsymbol{x}|\boldsymbol{x_a};\omega) = s(\boldsymbol{x},\omega), \tag{2}$$

where $s(\boldsymbol{x},\omega)$ is the source function.

The causal Green's function for the Helmholtz operator is given by

$$\left(\nabla^2 + \frac{\omega^2}{c_2^2(\boldsymbol{x})}\right) G^+(\boldsymbol{x}|\boldsymbol{x_b};\omega) = \delta(\boldsymbol{x}-\boldsymbol{x_b}), \tag{3}$$

where $\delta(\boldsymbol{x}-\boldsymbol{x_b})$ denotes the Dirac delta function centered at a position $\boldsymbol{x}=\boldsymbol{x_b}$ and the velocity distribution is given by $c_2(\boldsymbol{x})$. In general $c_2(\boldsymbol{x})$ has no relation to $c(\boldsymbol{x})$ in equation 2.

For simplicity, the source $s(\boldsymbol{x},\omega)$ in equation 2 is selected to be $A(\omega)\delta(\boldsymbol{x}-\boldsymbol{x_a})$, which represents an impulsive source at $x=x_a$ excited at $t=0$ with signature $A(t)$, producing the pressure field $P(\boldsymbol{x}|\boldsymbol{x_a};\omega)$.

Introducing $\frac{1}{c(\boldsymbol{x})^2} = \frac{1}{c_2(\boldsymbol{x}^2}\,(1-\alpha(\boldsymbol{x}))$ into equation 2, where α is the relative difference between the two media defined by equations 2 and 3 (Weglein and Secrest, 1990), we obtain

$$\nabla^2 P(\boldsymbol{x}|\boldsymbol{x_a};\omega) = -\frac{\omega^2}{c_2(\boldsymbol{x})^2} P(\boldsymbol{x}|\boldsymbol{x_a};\omega) + \frac{\omega^2}{c_2(\boldsymbol{x})^2}\alpha(\boldsymbol{x}) P(\boldsymbol{x}|\boldsymbol{x_a};\omega) + A(\omega)\delta(\boldsymbol{x}-\boldsymbol{x_a}). \tag{4}$$

Substituting the wavefield $P(\boldsymbol{x}|\boldsymbol{x_a};\omega)$ and the causal Green's function $G_0^+(\boldsymbol{x}|\boldsymbol{x_b};\omega)$ into equation 1 as u and ν, and using equations 3 and 4 in the volume integral, we obtain,

$$\begin{aligned}
&\int_V (P(\boldsymbol{x}|\boldsymbol{x_a};\omega)[-\frac{\omega^2}{c_2(\boldsymbol{x})^2} G_0^+(\boldsymbol{x}|\boldsymbol{x_b};\omega) + \delta(\boldsymbol{x}-\boldsymbol{x_b})] \\
&-G_0^+(\boldsymbol{x}|\boldsymbol{x_b};\omega)[-\frac{\omega^2}{c_2(\boldsymbol{x})^2} P(\boldsymbol{x}|\boldsymbol{x_a};\omega) + \frac{\omega^2}{c_2(\boldsymbol{x})^2}\alpha(\boldsymbol{x}) P(\boldsymbol{x}|\boldsymbol{x_a};\omega) + A(\omega)\delta(\boldsymbol{x}-\boldsymbol{x_a})])d\boldsymbol{x} \\
&\quad = \oint_S [P(\boldsymbol{x}|\boldsymbol{x_a};\omega)\boldsymbol{\nabla} G_0^+(\boldsymbol{x}|\boldsymbol{x_b};\omega) - G_0^+(\boldsymbol{x}|\boldsymbol{x_b};\omega)\boldsymbol{\nabla} P(\boldsymbol{x}|\boldsymbol{x_a};\omega)] \cdot \boldsymbol{n}\; d\boldsymbol{s}.
\end{aligned} \tag{5}$$

If, throughout the volume V, the medium parameters for the Green's function are chosen to be identical to the medium parameters satisfied by the pressure field P (*i.e.* $\alpha = 0$ within the volume), equation 5 simplifies to

$$\begin{aligned}
&\int_V \left(P(\boldsymbol{x}|\boldsymbol{x_a};\omega)\delta(\boldsymbol{x}-\boldsymbol{x_b}) - G^+(\boldsymbol{x}|\boldsymbol{x_b};\omega)A(\omega)\delta(\boldsymbol{x}-\boldsymbol{x_a})\right)\; d\boldsymbol{x} \\
&= \oint_S [P(\boldsymbol{x}|\boldsymbol{x_a};\omega)\boldsymbol{\nabla} G^+(\boldsymbol{x}|\boldsymbol{x_b};\omega) - G^+(\boldsymbol{x}|\boldsymbol{x_b};\omega)\boldsymbol{\nabla} P(\boldsymbol{x}|\boldsymbol{x_a};\omega)] \cdot \boldsymbol{n}\; d\boldsymbol{s},
\end{aligned} \tag{6}$$

which corresponds to the Kirchhoff-Helmholtz integral representation (see, e.g., Morse and Feshbach (1953); Weglein and Secrest (1990); Weglein and Devaney (1992)).

1.1 1^{st} Situation: The medium parameters for both fields are only equal at the boundary S and within the volume V

If the medium parameters for the pressure field and the Green's function are equal only throughout V,

$$c_2(\boldsymbol{x}) \begin{cases} = c(\boldsymbol{x}) & \text{within } V \\ \neq c(\boldsymbol{x}) & \text{outside } V, \end{cases} \tag{7}$$

the left hand side of equation 6 gives

$$l.h.s. = \begin{cases} P(\boldsymbol{x_b}|\boldsymbol{x_a};\omega) - A(\omega)G^+(\boldsymbol{x_a}|\boldsymbol{x_b};\omega) & \text{if both sources are strictly inside } S \\ P(\boldsymbol{x_b}|\boldsymbol{x_a};\omega) & \text{if only the observation point } \boldsymbol{x_b} \text{ lies within } V \\ -A(\omega)G^+(\boldsymbol{x_a}|\boldsymbol{x_b};\omega) & \text{if only the source } \boldsymbol{x_a} \text{ lies within } V, \end{cases} \tag{8}$$

The observation point is the position of the Green's function's source.

The **third case**,

$$-A(\omega)G^{+}(\boldsymbol{x_a}|\boldsymbol{x_b};\omega) = \oint_S [P(\boldsymbol{x}|\boldsymbol{x_a};\omega)\boldsymbol{\nabla} G^{+}(\boldsymbol{x}|\boldsymbol{x_b};\omega) - G^{+}(\boldsymbol{x}|\boldsymbol{x_b};\omega)\boldsymbol{\nabla} P(\boldsymbol{x}|\boldsymbol{x_a};\omega)] \cdot \boldsymbol{n}\ d\boldsymbol{s}, \qquad (9)$$

can be used to estimate the source wavelet in a marine seismic experiment (Weglein and Secrest, 1990; Weglein and Devaney, 1992). For this purpose, a convenient volume within the water column bounded by the measurement surface and the air-water interface, or free surface, is selected (see Figure 2). A reference Green's function, satisfying the properties of the medium within the volume and the Dirichlet boundary condition at the free-surface, is used.

Hence, the Green's function is chosen to propagate in a homogeneous half space bounded by a free-surface S_0 at depth $z = 0$. In order to impose the Dirichlet boundary condition at $z = 0$ required by the free-surface, the Helmholtz equation is expressed using a real source at $\boldsymbol{x_b} = (x_{1b}, x_{2b}, x_{3b})$ and an image source with negative amplitude at $-\boldsymbol{\chi_b} = (x_{1b}, x_{2b}, -x_{3b})$ (see Figure 1), where x_3 is the vertical direction and it is zero at the free surface. Thus,

$$\left(\nabla^2 + \frac{\omega^2}{c_0^2}\right) \mathcal{G}_0^{+}(\boldsymbol{x}|\boldsymbol{x_b};\omega) = \delta(\boldsymbol{x} - \boldsymbol{x_b}) - \delta(\boldsymbol{x} + \boldsymbol{\chi_b}). \qquad (10)$$

is the reference Green's function that is used in equation 9 to derive a method for source signature estimation in a marine experiment.

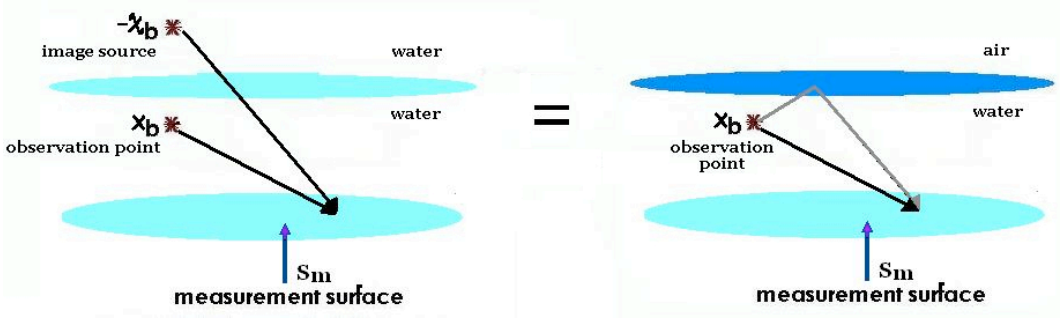

Figure 1: Green's function for an experiment with a free surface. On the left hand side, the method of images is illustrated. The right hand side shows the actual reference Green's function for a source and receiver below the zero pressure surface.

The causal Green's function $\mathcal{G}_0^{+}$ includes the wave that propagates directly from the real source to the receiver, $\mathcal{G}_0^{d+}$, and the wave that propagates directly from the image source to the receiver, $\mathcal{G}_0^{d'+}$,

$$\mathcal{G}_0^{+}(\boldsymbol{x}|\boldsymbol{x_b};\omega) = \mathcal{G}_0^{d+}(\boldsymbol{x}|\boldsymbol{x_b};\omega) - \mathcal{G}_0^{d'+}(\boldsymbol{x}|-\boldsymbol{\chi_b};\omega). \qquad (11)$$

In this experiment, both P and $\mathcal{G}_0^{+}$ vanish at the free-surface. Therefore, the upper boundary of V gives zero contribution to the integral. If we let the measurement surface approach infinity, then,

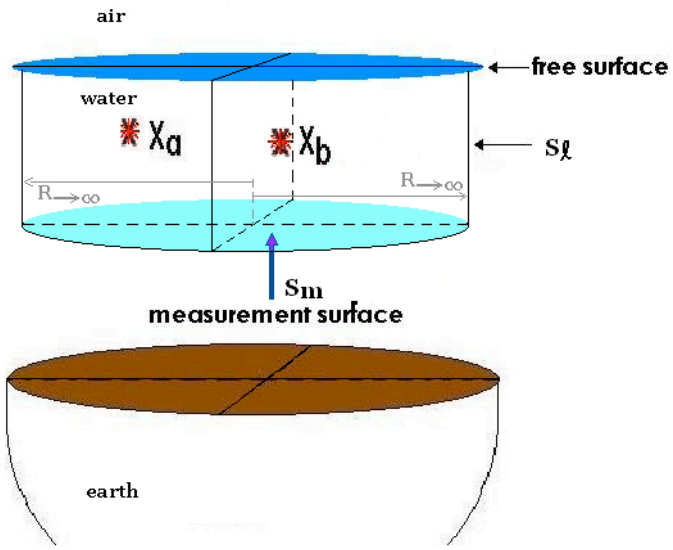

Figure 2: The cylindrical volume shown is bounded by the free surface and the measurement surface. The lateral surface of the cylinder is assumed to be at infinity.

only the measurement surface (S_m in Figure 2) will contribute to the surface integral, the lateral surface contribution S_l will vanish according to the Sommerfeld radiation condition (Sommerfeld, 1954). Selecting the actual source for the pressure field to be inside the volume V and the observation point (real source for the Green's function described by equation 10) to be outside the medium, below the measurement surface, equation 9 becomes

$$-A(\omega)\mathcal{G}_0^+(\boldsymbol{x_a}|\boldsymbol{x_b};\omega) = \int_{S_m} [P(\boldsymbol{x}|\boldsymbol{x_a};\omega)\boldsymbol{\nabla}\mathcal{G}_0^+(\boldsymbol{x}|\boldsymbol{x_b};\omega) - \mathcal{G}_0^+(\boldsymbol{x}|\boldsymbol{x_b};\omega)\boldsymbol{\nabla}P(\boldsymbol{x}|\boldsymbol{x_a};\omega)] \cdot \boldsymbol{n}\ d\boldsymbol{s}. \quad (12)$$

This equation reproduces the result first obtained by Weglein and Secrest (1990). Equation 9 is used to estimate the source wavelet in a marine experiment (the method has been extended to include a source array and to accommodate a land (elastic) experiment (Weglein and Secrest, 1990; Weglein and Devaney, 1992)). This technique relies on dual measurements (pressure field and its normal derivative) and the direct wave $\mathcal{G}_0^+$. The surface integral effectively filters the scattered wavefield from the integral.

Using the Green's function in equation 10 and, allowing the observation point and the actual source to be inside the medium, a formalism for seismic interferometry is obtained. It is given by the **first case** in equation 8,

$$P(\boldsymbol{x_b}|\boldsymbol{x_a};\omega) - A(\omega)\mathcal{G}_0^+(\boldsymbol{x_a}|\boldsymbol{x_b};\omega) = \int_{S_m} [P(\boldsymbol{x}|\boldsymbol{x_a};\omega)\boldsymbol{\nabla}\mathcal{G}_0^+(\boldsymbol{x}|\boldsymbol{x_b};\omega) - \mathcal{G}_0^+(\boldsymbol{x}|\boldsymbol{x_b};\omega)\boldsymbol{\nabla}P(\boldsymbol{x}|\boldsymbol{x_a};\omega)] \cdot \boldsymbol{n}\ d\boldsymbol{s}. \quad (13)$$

Using the principle of source-receiver reciprocity and the fact that the scattered field $P_s(\boldsymbol{x_a}|\boldsymbol{x_b};\omega) = P(\boldsymbol{x_a}|\boldsymbol{x_b};\omega) - A(\omega)\mathcal{G}_0^+(\boldsymbol{x_a}|\boldsymbol{x_b};\omega)$, we obtain

$$P_s(\boldsymbol{x_a}|\boldsymbol{x_b};\omega) = \int_{S_m} [P(\boldsymbol{x}|\boldsymbol{x_a};\omega)\boldsymbol{\nabla}\mathcal{G}_0^+(\boldsymbol{x}|\boldsymbol{x_b};\omega) - \mathcal{G}_0^+(\boldsymbol{x}|\boldsymbol{x_b};\omega)\boldsymbol{\nabla}P(\boldsymbol{x}|\boldsymbol{x_a};\omega)], \cdot \boldsymbol{n}\ d\boldsymbol{s}. \quad (14)$$

which is a very desired output in seismic exploration. It retrieves the total wavefield in new locations and removes the direct wave $A(\omega)\mathcal{G}_0^+(\boldsymbol{x_a}|\boldsymbol{x_b};\omega)$. The output is the scattered field. With both sources inside the volume, the surface integral effectively filters the reference field and retrieves the scattered field between the sources (as if one source was a receiver: virtual receiver). The retrieved scattered field is the total wavefield due to all sources being outside the volume. The "filtering" effect provided by the surface integral in Green's theorem in this kind of application is also known as extinction theorem. The application of the extinction theorem, will screen the scattered field if the observation point is outside V and, will screen the reference field for all actual sources inside the volume if the observation point lies inside V.

The **second case** in equation 8, places the actual source outside and the observation point inside V. The result is the total wavefield between the source outside and the observation point inside the medium,

$$P(\boldsymbol{x_b}|\boldsymbol{x_a};\omega) = \int_{S_m} [P(\boldsymbol{x}|\boldsymbol{x_a};\omega)\boldsymbol{\nabla}\mathcal{G}_0^+(\boldsymbol{x}|\boldsymbol{x_b};\omega) - \mathcal{G}_0^+(\boldsymbol{x}|\boldsymbol{x_b};\omega)\boldsymbol{\nabla}P(\boldsymbol{x}|\boldsymbol{x_a};\omega)] \cdot \boldsymbol{n}\ d\boldsymbol{s}. \tag{15}$$

Green's theorem retrieves the total wavefield due to all sources outside the volume, as explained in the previous paragraph. The **first** and **second case** are both good relations to retrieve the wavefield between two sources as if one of them was a receiver.

Equation 14 has both, the source and the virtual receiver, inside the volume and equation 15 has either the source or the virtual receiver inside V and the other point outside. Both equation retrieve the wavefield due to sources outside V. In terms of seismic interferometry, this would be direct wave seismic interferometry using correlations.

1.2 2^{nd} Situation: The medium parameters for both fields are equal everywhere

If the medium parameters for equations 2 and 3 are identical not only throughout the volume enclosed by S, but everywhere,

$$c(\boldsymbol{x}) \equiv c_2(\boldsymbol{x}), \quad (\forall \boldsymbol{x} \text{ in } R^3), \tag{16}$$

then, we use the pressure field P and the Green's function in equation 3 in Green's theorem. Since the medium parametes are set to be equal, $\alpha = 0$ everywhere and equation 5 reduces to equation 6.

The left hand side of equation 6 becomes

$$l.h.s. = \begin{cases} 0 & \text{if both sources are strictly inside } S \\ P(\boldsymbol{x_a}|\boldsymbol{x_b};\omega) & \text{if only the observation point } \boldsymbol{x_b} \text{ lies within } V \\ -P(\boldsymbol{x_a}|\boldsymbol{x_b};\omega) & \text{if only the source } \boldsymbol{x_a} \text{ lies within } V, \end{cases} \tag{17}$$

where the principle of source-receiver reciprocity has been used.

The **first case** in equation 17 constitutes a functional relationship between P and its normal gradient on S,

$$0 = \oint_S [P(\boldsymbol{x}|\boldsymbol{x_a};\omega)\boldsymbol{\nabla}G^+(\boldsymbol{x}|\boldsymbol{x_b};\omega) - G^+(\boldsymbol{x}|\boldsymbol{x_b};\omega)\boldsymbol{\nabla}P(\boldsymbol{x}|\boldsymbol{x_a};\omega)] \cdot \boldsymbol{n}\ d\boldsymbol{s}, \tag{18}$$

meaning that the pressure field and its normal derivative cannot be prescribed independently (Amundsen, 1994; Visser et al., 1998). This functional relation was used by Amundsen (1994) to develop an inverse wavefield extrapolation that allowed reconstruction of the wavefield within the subsurface by extrapolating the field from the measurement surface through each one of the different earth layers and applying boundary conditions at each interface before continuing extrapolation through the next layer. The medium between the different interfaces must be known (a smoothly varying approximation of the medium can be used) and dual measurements of the pressure field are also necessary. In general, imaging with Green's theorem requires knowledge of the medium. Another example of inverse wavefield extrapolation using the framework of green's theorem is given by the work of Schneider (1978).

The results in the **second** and **third case** in equation 17 are equivalent to the corresponding results in the previous subsection. The only difference is that $A(\omega)G^{+}(\boldsymbol{x_a}|\boldsymbol{x_b};\omega)$ is now equivalent to the total pressure field $P(\boldsymbol{x}|\boldsymbol{x_a};\omega)$ not the reference pressure field.

1.3 Analysis

Using Green's theorem, we derived formalisms that can be applied to wavelet estimation, seismic interferometry and inverse wavefield extrapolation. All of these applications require the availability of the pressure field and its normal derivative.

The more desired method for seismic interferometry or wavefield retrieval is the one that considers both sources located within the medium. Therefore, causal direct wave interferometry, as described by equation 14, seems to be the more convenient result. It can be readily applied to applications such as wavefield extrapolation, interpolation, and regularization in a surface seismic experiment. Using direct wave interferometry with correlations (or a causal Green's function) provides a method to extrapolate data into a regular grid of coincident sources and receivers in a 3D experiment by using an analytic Green's function $\mathcal{G}_0^{+}(\boldsymbol{x}|\boldsymbol{x_b};\omega)$ calculated for the actual receiver positions $\boldsymbol{x}$ and placing the observation point at the desired output locations. It is an exact method. Accordingly, it requires measurements of the pressure field and its normal derivative at the surface.

In general, for surface seismic experiments, the normal derivative is not measured and an estimate is not always available. To overcome this situation, an asymptotic approximation to the pressure field's normal derivative could be used,

$$\boldsymbol{\nabla} P(\boldsymbol{x}|\boldsymbol{x_a};\omega)] \cdot \boldsymbol{n} \approx ikP(\boldsymbol{x}|\boldsymbol{x_a};\omega) \tag{19}$$

where $k = \frac{\omega}{c_0}$. However, this is a very poor approximation for this particular situation. It is a high frequency and one-way wave approximation taken at a location where two-way waves exist. Asymptotic approximations, although often useful, are never equivalent to the original form. In fact, using this approximation in equation 14, we find a zero result

$$0 = \int_{S_m} [P(\boldsymbol{x}|\boldsymbol{x_a};\omega)\boldsymbol{\nabla}\mathcal{G}_0^{+}(\boldsymbol{x}|\boldsymbol{x_b};\omega) - \mathcal{G}_0^{+}(\boldsymbol{x}|\boldsymbol{x_b};\omega)ikP(\boldsymbol{x}|\boldsymbol{x_a};\omega)] \cdot \boldsymbol{n}\ d\boldsymbol{s}. \tag{20}$$

Hence, with the approximation in equation 19, the equation previously identified as direct wave interferometry (with correlations) is of no use. The fact that the left hand side of equation 14

vanishes, when the one-way wave approximation is used, can be shown by a simple 1D analytic example for 1D pressure data with a free surface, $p(z|z_a;\omega)$, and the a 1D reference Green's function $(g^+(z|z_b;\omega))$ satisfying equation 10. The 1D reference Green's function g^+ has the form:

$$g^+(z|z_b,\omega) = \frac{e^{ik|z-z_b|}}{2ik} - \frac{e^{ik(z+z_b)}}{2ik} \tag{21}$$

In 1D, the surface integral in equation 20 becomes an evaluation at the receiver location, $z = z_r$. Introducing $p(z|z_a;\omega)$ and $(g^+(z|z_b;\omega))$ on the right hand side of equation 20, gives

$$\begin{aligned}(p(z|z_a;\omega)\frac{d}{dz}g^+(z|z_b;\omega) - g^+(z|z_b;\omega)ikp(z|z_a;\omega))|_{z_r} =& ikp(z_r|z_a;\omega)g^+(z_r|z_b;\omega) \\ -\ & ikg^+(z_r|z_b;\omega)p(z_r|z_a;\omega) \ = \ 0. \end{aligned} \tag{22}$$

Numerical tests in 3D also confirm this result.

There are different ways of addressing this situation. The first (and more reliable) one is to provide all the ingredients required by Green's theorem by measuring the wavefield's normal derivative or, measuring the pressure field at a second surface parallel to the measurement surface and calculating the gradient between the fields. The second solution is to find a better approximation for the normal component of the particle velocity, we refer the interested reader to Amundsen et al. (1995); Guo et al. (2005) and references within. A third solution is to use an anticausal Green's function or pressure field in the calculations (Weaver and Lobkis, 2004; Wapenaar, 2004; Korneev and Bakulin, 2006; Draganov et al., 2006; Ramírez et al., 2007) as explained in the next chapter. Last, but not least, it is possible to use a different Green's function that annihilates the requirement of the wavefield's normal derivative, *i.e.* using a Green's function with Dirichlet boundary conditions at the free surface and at the measurement surface (Osen et al., 1998; Tan, 1999; Weglein et al., 2000; Ramírez et al., 2007) as explained in **section 3**.

2 Green's theorem with an anticausal Green's function

In this section, anticausal solutions for the Helmholtz operator will be used to derive standard seismic interferometry and direct wave interferometry with crosscorrelations. An analysis and discussion of these applications will be provided at the end of the section and certain limitations of this applications (due to assumptions that will be explained) will serve as motivation for section 3.

Equations 2, 3 and 10 can have a causal solution or an anticausal solution, with outgoing or ingoing boundary conditions, respectively. The anticausal Green's function $G^-(\boldsymbol{x}|\boldsymbol{x_b};\omega)$ is the complex conjugate of $G^+(\boldsymbol{x}|\boldsymbol{x_b};\omega)$, and $P^-(\boldsymbol{x}|\boldsymbol{x_b};\omega)$ is the complex conjugate of $P^+(\boldsymbol{x}|\boldsymbol{x_b};\omega)$. We define the anticausal Green's function by

$$G^-(\boldsymbol{x}|\boldsymbol{x_b};\omega) = \int_{-\infty}^{\infty} e^{-i\omega t}G^+(\boldsymbol{x}|\boldsymbol{x_b};-t)dt. \tag{23}$$

The anticausal Green's function for the Helmholtz operator is given by

$$\left(\nabla^2 + \frac{\omega^2}{c_2^2(\boldsymbol{x})}\right) G^-(\boldsymbol{x}|\boldsymbol{x_b};\omega) = \delta(\boldsymbol{x}-\boldsymbol{x_b}), \tag{24}$$

where $\delta(\boldsymbol{x}-\boldsymbol{x_b})$ denotes the Dirac delta function centered at a position $\boldsymbol{x}=\boldsymbol{x_b}$, the velocity distribution is given by $c_2(\boldsymbol{x})$. In general $c_2(\boldsymbol{x})$ has no relation to $c(\boldsymbol{x})$ in equation 2.

2.1 1^{st} Situation: The medium parameters for both fields are equal inside the volume V and different outside

Using an anticausal Green's function and the causal pressure field in Green's theorem, both corresponding to the same medium properties at the surface and throughout the volume V, Green's theorem becomes

$$\begin{aligned}&\int_V \left(P(\boldsymbol{x}|\boldsymbol{x_a};\omega)\delta(\boldsymbol{x}-\boldsymbol{x_b}) - G^-(\boldsymbol{x}|\boldsymbol{x_b};\omega)A(\omega)\delta(\boldsymbol{x}-\boldsymbol{x_a})\right)\, d\boldsymbol{x}\\ &= \oint_S [P(\boldsymbol{x}|\boldsymbol{x_a};\omega)\boldsymbol{\nabla}G^-(\boldsymbol{x}|\boldsymbol{x_b};\omega) - G^-(\boldsymbol{x}|\boldsymbol{x_b};\omega)\boldsymbol{\nabla}P(\boldsymbol{x}|\boldsymbol{x_a};\omega)]\cdot\boldsymbol{n}\, d\boldsymbol{s},\end{aligned} \tag{25}$$

where the left hand side gives

$$l.h.s. = \begin{cases} P(\boldsymbol{x_b}|\boldsymbol{x_a};\omega) - A(\omega)G^-(\boldsymbol{x_a}|\boldsymbol{x_b};\omega) & \text{if both sources are strictly inside } S\\ P(\boldsymbol{x_b}|\boldsymbol{x_a};\omega) & \text{if only the observation point } \boldsymbol{x_b} \text{ lies within } V\\ -A(\omega)G^-(\boldsymbol{x_a}|\boldsymbol{x_b};\omega) & \text{if only the source at } \boldsymbol{x_a} \text{ lies within } V. \end{cases} \tag{26}$$

For the current marine application of this result, a volume within the water column, bounded by the free-surface and the measurement surface, is selected. We assume that the medium parameters, at the closed boundary S and within the volume V (see Figure 2), producing the pressure field are equal to the ones where the Green's function propagates. Therefore, the surface integral in Green's theorem has no contribution from the upper boundary of V. Again, we let the measurement surface tend to infinity. Using causal wavefields, the contribution from the lateral surface S_l was assumed to vanish according to the Sommerfeld radiation condition (Sommerfeld, 1954). However, the anticausal waves have a contribution at infinity, so we will have a small error due to lack of measurements at this part of the surface. The measurement surface (S_m in Figure 2) will be the only contribution considered in the surface integral.

Plugging the anticausal version (or the complex conjugate) of the reference Green's function in equation 10 into the **first case** in equation 26, we find an equation for wavefield retrieval for source and receiver locations within V,

$$\begin{aligned}&P(\boldsymbol{x_a}|\boldsymbol{x_b};\omega) - A(\omega)\mathcal{G}_0^-(\boldsymbol{x_a}|\boldsymbol{x_b};\omega) =\\ &\int_{S_m} [P(\boldsymbol{x}|\boldsymbol{x_a};\omega)\boldsymbol{\nabla}\mathcal{G}_0^-(\boldsymbol{x}|\boldsymbol{x_b};\omega) - \mathcal{G}_0^-(\boldsymbol{x}|\boldsymbol{x_b};\omega)\boldsymbol{\nabla}P(\boldsymbol{x}|\boldsymbol{x_a};\omega)]\cdot\boldsymbol{n}\, d\boldsymbol{s},\end{aligned} \tag{27}$$

in agreement with the result derived by Ramírez et al. (2007). Introduce $P(\boldsymbol{x_a}|\boldsymbol{x_b};\omega) = P^0(\boldsymbol{x_a}|\boldsymbol{x_b};\omega) + P^s(\boldsymbol{x_a}|\boldsymbol{x_b};\omega)$, where $P^0 = A(\omega)\mathcal{G}_0^+(\boldsymbol{x_a}|\boldsymbol{x_b};\omega)$ is the reference field and P^s is the scattered field, and use it into equation 27.

The left hand side of equation 27, reduces to

$$P^s(\boldsymbol{x_a}|\boldsymbol{x_b};\omega) + A(\omega)\left[\mathcal{G}_0^+(\boldsymbol{x_a}|\boldsymbol{x_b};\omega) - \mathcal{G}_0^-(\boldsymbol{x_a}|\boldsymbol{x_b};\omega)\right]$$

$$= P^s(\boldsymbol{x_a}|\boldsymbol{x_b};\omega) + 2i\ A(\omega)\ \Im\left[\mathcal{G}_0^+(\boldsymbol{x_a}|\boldsymbol{x_b};\omega)\right], \tag{28}$$

where $\Im$ denotes imaginary part.

Thus, in equation 27, the total scattered field between sources at $\boldsymbol{x_a}$ and $\boldsymbol{x_b}$ is reconstructed (as if one source was a receiver), as well as the imaginary part of the direct wave. This result is less desirable than the one obtained with a causal Green's function. Using an anticausal Green's function the direct wave is not filtered by the surface integral. Using an anticausal reference Green's function, the surface integral only filters the real part of the direct wave. Let's remember the reason we decided to use an anticausal Green's function: when the normal particle velocity of a two-way wavefield is approximated by equation 19 and used in Green's theorem, the output of the surface integral with a causal Green's function vanishes. This does not happen with the anticausal Green's function. Therefore, for marine experiments, the approximation described by equation 19 was used in equation 28, to obtain

$$\begin{aligned} P(\boldsymbol{x_a}|\boldsymbol{x_b};\omega) \approx \oint_S [&P(\boldsymbol{x}|\boldsymbol{x_a};\omega)\boldsymbol{\nabla}\mathcal{G}_0^-(\boldsymbol{x}|\boldsymbol{x_b};\omega) \\ &- ikP(\boldsymbol{x}|\boldsymbol{x_a};\omega)\mathcal{G}_0^-(\boldsymbol{x}|\boldsymbol{x_b};\omega)] \cdot \boldsymbol{n}\ d\boldsymbol{s}, \end{aligned} \tag{29}$$

or

$$\begin{aligned} P^s(\boldsymbol{x_a}|\boldsymbol{x_b};\omega) + 2i\ A(\omega)\ \Im\left[\mathcal{G}_0^+(\boldsymbol{x_a}|\boldsymbol{x_b};\omega)\right] \approx \oint_S [&P(\boldsymbol{x}|\boldsymbol{x_a};\omega)\boldsymbol{\nabla}\mathcal{G}_0^-(\boldsymbol{x}|\boldsymbol{x_b};\omega) \\ &- ikP(\boldsymbol{x}|\boldsymbol{x_a};\omega)\mathcal{G}_0^-(\boldsymbol{x}|\boldsymbol{x_b};\omega)] \cdot \boldsymbol{n}\ d\boldsymbol{s}. \end{aligned} \tag{30}$$

The output is approximately equal to the scattered field and the imaginary part of the direct wave. This result is very accurate compared to other seismic interferometry methods, when applied to surface seismic experiment. This result was tested for data extrapolation and regularization by Ramírez et al. (2007) with encouraging results in 1D and 2D acoustic synthetics (calculated using finite difference code and the reflectivity method) as well as 3D synthetics for a marine experiment with an elastic earth (calculated using finite difference code).

2.2 2^{nd} Situation: The medium parameters for both fields are equal everywhere

The medium parameters for equations 2 and 3 are chosen to be identical everywhere. Using the pressure field P and the anticausal Green's function in equation 24 in Green's theorem and, using the principle of source-receiver reciprocity, the left hand side of equation 25 becomes

$$l.h.s. = \begin{cases} 2i\Im P(\boldsymbol{x_a}|\boldsymbol{x_b};\omega) & \text{if both sources are strictly inside } S \\ P(\boldsymbol{x_b}|\boldsymbol{x_a};\omega) & \text{if only observation point } \boldsymbol{x_b} \text{ lies within } V \\ -P^-(\boldsymbol{x_a}|\boldsymbol{x_b};\omega) = A(\omega)G^-(\boldsymbol{x_a}|\boldsymbol{x_b};\omega) & \text{if only the source at } \boldsymbol{x_a} \text{ lies within } V. \end{cases} \tag{31}$$

where the selected volume is bounded by the free-surface and the measurement surface. Since the medium parameters are equal everywhere, the results in equation 31 are not restricted to the water column.

The configuration leading the result for the **first case** in 31 is used as the starting point for common approaches to seismic interferometry. In these approaches, the normal derivatives are approximated with a far-field and one-way wave approximation shown in equation 19. After a simple mathematical manipulation, the wavefield retrieval equation (Wapenaar, 2004; Wapenaar and Fokkema, 2006) in ω space is obtained

$$2i\Im\left[P(\boldsymbol{x_b}|\boldsymbol{x_a};\omega)\right] \approx \int_{S_m} -2ik\ P(\boldsymbol{x}|\boldsymbol{x_a};\omega)G^{-}(\boldsymbol{x}|\boldsymbol{x_b};\omega)\ d\boldsymbol{x}. \tag{32}$$

The original equation derived by Wapenaar (2004) for seismic interferometry used the reciprocal experiment to the one presented in this work. In their derivation, two receivers inside the volume were surrounded by sources at S. Using source-receiver reciprocity, the standard interferometry equation is obtained

$$2i\Im\left[P(\boldsymbol{x_b}|\boldsymbol{x_a};\omega)\right] \approx \int_{S_m} -2ik\ P(\boldsymbol{x_a}|\boldsymbol{x};\omega)G^{-}(\boldsymbol{x_b}|\boldsymbol{x};\omega)\ d\boldsymbol{x}, \tag{33}$$

where $\boldsymbol{x}$ corresponds to source positions at the surface S_m, and, $\boldsymbol{x_a}$ and $\boldsymbol{x_b}$ are receiver positions. This equation requires the knowledge of the medium everywhere, since G^{-} satisfies the same medium properties as the actual field.

In general, the actual medium is unknown. Hence, G^{-} is substituted by the complex conjugate of a second pressure field $\overline{P}$, defining $P^{-} = conj(\overline{P})$. And the pressure field $\overline{P}$ is assumed to satisfy the same wave equation as P (equation 2). It is also assumed to be produced by the same source gather as P and measured at a different position within the volume, x_b.

To continue the analysis, and to be consistent with the rest of this paper, we retrieve the previous notation where $\boldsymbol{x_a}$ and $\boldsymbol{x_b}$ represent source locations and the surface integral is taken over receiver locations $\boldsymbol{x}$ at the measurement surface (refer to equation 32 and Figure 2). The source location in equation 2, $s(\boldsymbol{x},\omega)$, is set to explode at a different location, *i.e.* $s(\boldsymbol{x},\omega) = B(\omega)\delta(\boldsymbol{x}-\boldsymbol{x_b})$, where $B(\omega)$ is the source signature for P^{-}. Using these two pressure fields in Green's theorem multiplies the output by an extra source wavelet,

$$\begin{aligned}&\int_V \left(P(\boldsymbol{x}|\boldsymbol{x_a};\omega)B(\omega)\delta(\boldsymbol{x}-\boldsymbol{x_b}) - P^{-}(\boldsymbol{x}|\boldsymbol{x_b};\omega)A(\omega)\delta(\boldsymbol{x}-\boldsymbol{x_a})\right)\ d\boldsymbol{x}\\ &= \oint_S [P(\boldsymbol{x}|\boldsymbol{x_a};\omega)\boldsymbol{\nabla}P^{-}(\boldsymbol{x}|\boldsymbol{x_b};\omega) - P^{-}(\boldsymbol{x}|\boldsymbol{x_b};\omega)\boldsymbol{\nabla}P(\boldsymbol{x}|\boldsymbol{x_a};\omega)]\cdot\boldsymbol{n}\ d\boldsymbol{s},\end{aligned} \tag{34}$$

which becomes

$$2iB(\omega)\Im\left[P(\boldsymbol{x_b}|\boldsymbol{x_a};\omega)\right] \approx \int_{S_m} -2ik\ P(\boldsymbol{x}|\boldsymbol{x_a};t)P^{-}(\boldsymbol{x}|\boldsymbol{x_b};\omega)\ d\boldsymbol{x}, \tag{35}$$

after solving the volume integrals and approximating the normal derivatives. Since only the imaginary part of the field is reconstructed, a Hilbert transform is used to calculate the real part of the field.

The process of using two measured wavefields to construct new data instead of a measured wavefield and a Green's function introduces an extra factor of the source wavelet multiplied to the

reconstructed data. If we were able to calculate the anticausal Green's function, satisfying the same medium properties as the actual pressure field, we would not have an extra source signature (Wapenaar, 2004). This particular Green's function could be calculated by deconvolving the wavelet of the pressure field in a preprocessing step. However, the fact that this Green's function is not calculated analytically, constrains the reconstructed wavefield to locations where actual sources or receivers exist, and requires two approximations to the exact theory.

Equations 32 and 35 are a compromised form of Green's theorem and, hence, gives rise to spurious multiples. The normal derivative information required by Green's theorem, avoided by using far field approximations, would have combined nonlinearly to cancel the so-called spurious multiples by using differences in sign that identify opposite directions of the wavefield. The directionality information is part of the wavefield's normal derivative. The fact that equation 35 is compromising the theory has been discussed in Korneev and Bakulin (2006) in their derivation of the virtual source method.

2.3 Analysis

Using the anticausal Green's function, it is possible to find a formalism that allows an approximate retrieval of the Green's function between two sources (or receivers, using reciprocity principles) as if one of them was a receiver. Two methods were explained and both of them have compromises to the exact theory. The first one, anticausal direct wave interferometry (Ramírez et al., 2007), uses an analytic anticausal Green's function and only makes one approximation. The output of equation 30 is a close approximation to the total scattered field plus the imaginary part of the direct wave. The second one, standard seismic interferometry (Schuster, 2001; Derode et al., 2003; Roux and Fink, 2003; Wapenaar et al., 2002) uses the measured wavefield and its complex conjugate, making two approximations. The double compromise to the exact theory squares the output source signature and gives rise to the so called spurious multiples. In most surface seismic situations, the spurious multiple can damage the retrieved data significantly since their amplitudes are comparable to the ones for the reconstructed primaries.

The result provided by equation 35 is most commonly used for seismic interferometry and it is often used as the starting point for further analysis and applications. Some of this analysis, and further theoretical developments, aim to address the issues created by the compromises made to the exact theory and framework. However, it is necessary to understand that asymptotic analysis has, in fact two steps: (1) an asymptotic approximation (*e.g.*, a high frequency and one-way wave approximation) and (2) analysis, and conclusions reached from the result of the first step. The very reason for performing asymptotic approximation is to alter algorithms and their underlying assumptions, properties, and requirements. An approximation is not equivalent to the original form.

The analysis and new theory launched from seismic interferometry often ignored the fact that approximations were made. This theory aims to fix the weaknesses of interferometry, such as the extra power of the source wavelet and the spurious multiples. For example, Snieder et al. (2006), studies the appearance of spurious multiples and proposes types of sources and acquisition geometries that would help diminish it. Vasconcelos and Snieder (2006) derived a theory for

seismic interferometry that also deconvolves the source wavelet. We are not claiming that analyzing and using the result in standard seismic interferometry to develop new theory, understanding or applications is not a good path to follow, but there exists a danger of forgetting the assumptions and requirements of the original theory. In many situations, the new tools are effective and on target. For example, Otnes et al. (2006) derived a data-driven free surface demultiple algorithm for WVSP data. The method was derived by using seismic interferometry in a synthetic and a real WVSP experiment to effectively construct surface seismic data, which was convolved with the WVSP data to achieve its goal of removing the free-surface multiples without any subsurface information.

Another strategy taken was to understand that the errors in the synthesized wavefield were an effect of the assumptions applied to satisfy Green's theorem, as well as the functions used in its derivation. Hence, anticausal direct wave interferometry appears to be a better approximation for surface seismic experiments, where an analytic Green's function is available and fewer assumptions provide more accuracy. Furthermore, using an analytic reference Green's function, data can be extrapolated to positions where no receivers or sources were located and the synthesized data would have a single source signature. Thus, direct wave interferometry provides an improvement over traditional approaches. It is an improvement, but, the method still uses one approximation. Anticipating the consequences due to the compromises made, allows us to look at the original framework and attempt to find better ways to meet its requirements. If the vertical component of the pressure field is the weakness, then we can find ways to avoid that requirement. An example of this approach is accomplished by introducing another form of Green's theorem in which a two-surface Dirichlet boundary condition to the reference Green's function is imposed. This method does not need the normal component of the particle velocity.

3 Green's theorem with different boundary conditions imposed

In this section we introduce different boundary conditions imposed to the functions used in Green's theorem. It will be shown that, for the applications discussed in the previous sections, an improvement can be found in the framework given by Green's theorem.

3.1 Dirichlet boundary conditions: The medium parameters for both fields are equal inside the volume V and different at and below the measurement surface

A Green's function that vanishes on both the free and measurement surfaces eliminates the data requirement of the normal derivative in Green's theorem (Weglein and Devaney, 1992; Tan, 1992; Osen et al., 1998). This boundary condition can be fulfilled by the method of images or by adding a particular solution that contains the desired boundary conditions to the homogeneous solution for the Helmholtz equation (Morse and Feshbach, 1953).

The double-surface Dirichlet Green's function cannot be measured in a seismic experiment, since the actual medium only has one zero pressure surface. Thus, it needs to be analytically calculated. We

consider a homogeneous medium within the volume and the source point for the Green's function located inside V.

Let's use the configuration shown in Figure 2, where the selected volume lies entirely in a homogeneous medium and is bounded by the air-water surface and the measurement surface. These two surfaces are the ones on which the Dirichlet boundary conditions will be imposed for the Green's function calculation.

If we describe the two-surface Dirichlet Green's function $\mathcal{G}_0^D$ by the method of images, it will include the wave that propagates directly from the real source to the receiver and the wave that propagates directly from each image source to the receiver. Introducing P and $\mathcal{G}_0^D(\boldsymbol{x}|\boldsymbol{x_b};\omega)$ into equation 1 as u and ν, and assuming the medium parameters for both fields are equal within the volume V (where V is the volume in Figure 2), we obtain

$$\begin{aligned}&\int_V \left(P(\boldsymbol{x}|\boldsymbol{x_a};\omega)\delta(\boldsymbol{x}-\boldsymbol{x_b}) - G_0^D(\boldsymbol{x}|\boldsymbol{x_b};\omega)A(\omega)\delta(\boldsymbol{x}-\boldsymbol{x_a})\right)\, d\boldsymbol{x}\\ =&\int_{S_m} P(\boldsymbol{x}|\boldsymbol{x_a};\omega)\boldsymbol{\nabla}\mathcal{G}_0^D(\boldsymbol{x}|\boldsymbol{x_b};\omega)\cdot\boldsymbol{n}d\boldsymbol{s},\end{aligned} \tag{36}$$

where we have taken into account the boundary conditions. The left hand side gives

$$l.h.s. = \begin{cases} P(\boldsymbol{x_b}|\boldsymbol{x_a};\omega) - A(\omega)G_0^D(\boldsymbol{x_a}|\boldsymbol{x_b};\omega) & \text{if both sources are strictly inside } S \\ P(\boldsymbol{x_b}|\boldsymbol{x_a};\omega) & \text{if only the observation point } \boldsymbol{x_b} \text{ lies within } V. \end{cases} \tag{37}$$

The source for the Dirichlet Green's function must be inside the volume to satisfy the boundary conditions.

The **first case** in equation 37,

$$\begin{aligned}&P(\boldsymbol{x_a}|\boldsymbol{x_b};\omega) - A(\omega)\mathcal{G}_0^D(\boldsymbol{x_a}|\boldsymbol{x_b};\omega) =\\ &\int_{S_m} P(\boldsymbol{x}|\boldsymbol{x_a};\omega)\boldsymbol{\nabla}\mathcal{G}_0^D(\boldsymbol{x}|\boldsymbol{x_b};\omega)\cdot\boldsymbol{n}\; d\boldsymbol{s},\end{aligned} \tag{38}$$

shows a method to determine the wavefield above the measurement surface and below the free surface from measured pressure on a typical surface.

The algorithm described by equation 38 doesn't require the normal derivative of the pressure field. This method for seismic interferometry was proposed by Ramírez et al. (2007). However, it has an error of $-A(\omega)\mathcal{G}_0^D(\boldsymbol{x_a}|\boldsymbol{x_b};\omega)$, which, according to Tan (1992) and Weglein et al. (2000), for the typical surface seismic exploration source-receiver configurations and frequency content is small.

Equation 38 also has applications in source signature estimation (Osen et al., 1998; Tan, 1999). This result for wavelet estimation, as well as the analogous results in the previous sections using different Green's function, shows that when the receiver level is below the sources, there exists a triangle relationship between the pressure, its normal derivative, and the source wavelet. In order to theoretically calculate any one of these quantities, the other two must be known (Weglein

and Secrest, 1990; Amundsen, 2001). Green's theorem with a double Dirichlet Green's function apparently overcomes the need of a third quantity, the normal component of the particle velocity. However, it does not break the triangle relationship, since an extra pressure measurement at any point above the measurement surface and below the free-surface is needed. The extra measurement is, in general, not available and a possible solution is to introduce an approximation that alters equation 38 as described in Guo et al. (2005)

If an estimate of the wavelet is available, or obtainable, we can easily remove the error in equation 38 for seismic interferometry by adding a factor of $A(\omega)\mathcal{G}_0^D(\boldsymbol{x_a}|\boldsymbol{x_b};\omega)$. This will obtain an exact equation and the only limitation for a perfect output would be due to aperture limitations in the recorded pressure data. The rest of the ingredients required by Green's function would be fulfilled analytically.

When the wavelet is not available, and it is possible to separate the direct wave from the scattered field (*e.g.* in a deep water experiment), we can find an exact equation for reconstructing scattered field that does not need the source wavelet. It is given by the **second case** in equation 37. Substituting $P^s(\boldsymbol{x_a}|\boldsymbol{x_b};\omega)$, the scattered field, into Green's theorem (instead of the total wavefield), and using the two surface Dirichlet Green's function as the second function, will obtain

$$P^s(\boldsymbol{x_a}|\boldsymbol{x_b};\omega) = \int_{S_m} P^s(\boldsymbol{x}|\boldsymbol{x_a};\omega)\boldsymbol{\nabla}\mathcal{G}_0^D(\boldsymbol{x}|\boldsymbol{x_b};\omega)\cdot\boldsymbol{n}\ d\boldsymbol{s}. \tag{39}$$

This is possible because the scattered field obeys the wave equation without a source function,

$$\left(\nabla^2 + \frac{\omega^2}{c^2(\boldsymbol{x})}\right) P^s(\boldsymbol{x}|\boldsymbol{x_a};\omega) = 0. \tag{40}$$

Hence, only the observation point lies within the volume V. This form of Green's theorem does not require the normal derivative of the pressure field, nor the source signature. It only asks for the scattered field, or the pressure field due to sources outside the medium, and an analytic Green's function that vanishes at the measurement and air-water surface.

In this section, it was shown that certain choices of functions (and boundary conditions) used in Green's theorem, can help to avoid specific requirements and assumptions of other methods with similar purposes. An example of this requirement, is the pressure field's normal derivative required to satisfy the methods for wavefield retrieval and wavelet estimation discussed in sections 1 and 2. The wavefield's normal derivative was approximated two times for standard seismic interferometry and once for direct wave seismic interferometry. With a double Dirichlet boundary condition applied imposed upon the Green's function used in Green's theorem, a seismic interferometry method that only requires measurements of the pressure field at a surface within the water column, in a marine experiment, was retrieved. However, this is a very particular situation. There are circumstances when Green's function with a double Dirichlet boundary condition is not available (or it cannot be calculated analytically). Hence, it is not possible to overcome a requirement of the pressure field's normal derivative. An example of this situation is in the derivation of the virtual source method by Bakulin and Calvert (2004) and Korneev and Bakulin (2006) as well as in the derivation of wavefield deconvolution by (Amundsen, 2001), as explained in the following subsection.

3.2 Wavefield deconvolution and the virtual source method

In this section we discussed two methods to retrieve the wavefield between two receivers located at the water bottom or beneath the subsurface in a seismic experiment. These methods are wavefield deconvolution and the virtual source method. Both methods are based on Green's theorem and, in principle, both of them require dual measurements. In practice, the first method, wavefield deconvolution, is applied using both the pressure and its normal derivative measured in a seismic experiment (*e.g.* in OBC acquisitions). On the other hand, virtual source method is applied using only the pressure field, in clear analogy with other common seismic interferometry methods.

Besides the approximations and their effect on the retrieved wavefield, virtual source has another important difference with wavefield deconvolution: virtual source aims to retrieve the total wavefield between two receivers located beneath the subsurface while wavefield deconvolution retrieves the deconvolved wavefield for a coincident source-receiver experiment at the receiver location. Deconvolution refers to the removal of overburden effects and overburden refers to the medium above the receiver or measurement plane. In the following we are going to discuss the wavefield deconvolution method and then relate it to the virtual source method.

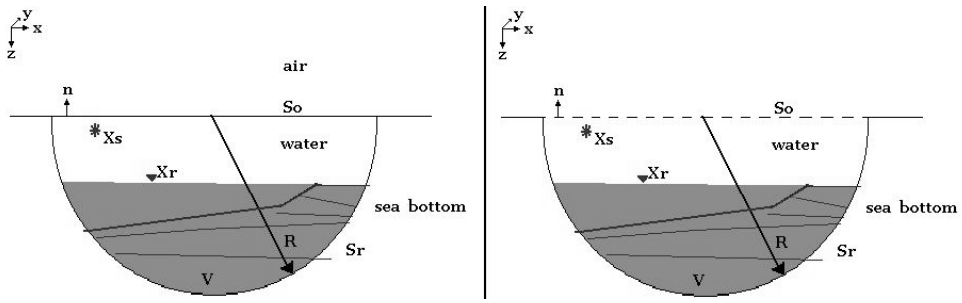

Figure 3: Volumes used in wavefield deconvolution.

In a marine experiment, there exist events that owe their existence to the presence of the air-water surface. These events are known a ghosts and free-surface multiples. In general, these events are removed from the data since they are not used for further processing. Imposing a specific selection of boundary conditions upon the pressure field and the Green's function we can find a formalism that eliminates the free-surface multiples and the wavelet from the pressure field (Amundsen, 2001; Holvik and Amundsen, 2005).

In wavefield deconvolution, two mediums are selected:

1) A medium corresponding to a physical seismic experiment in a marine setting (shown on the left hand side of Figure 3), it consists of the earth, a layer of water and a half space of air. The

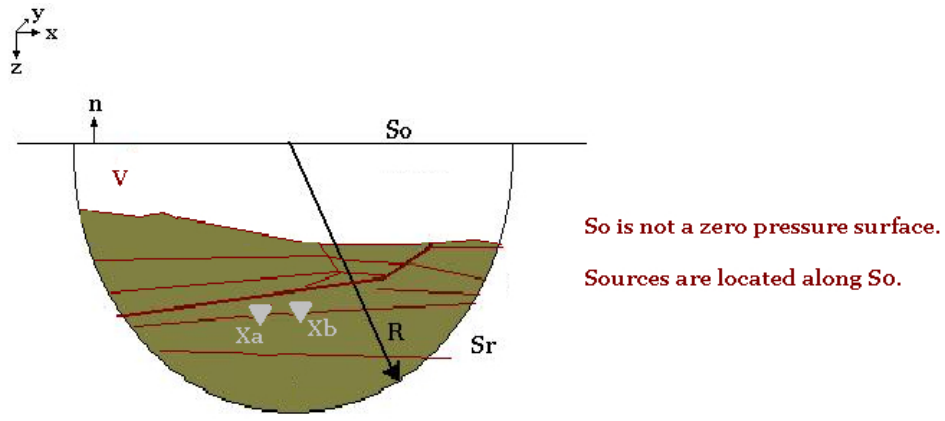

Figure 4: Volume used in the virtual source method.

position x_s denotes the location of the source (a source array could also be chosen) and x_r is the receiver location.

2) A medium corresponding to a hypothetical experiment (shown on the left hand side of Figure 3), it consists of the earth and a half space of water (no free-surface). The position x_s is the receiver location and x_r is the source location.

The pressure field P propagates in the first medium and a second pressure wavefield P' propagates in the second medium. Both pressure fields satisfy equation 2. A Dirichlet boundary condition is imposed to P. The volume selected to evaluate Green's theorem is shown in Figure 3. It is bounded by the surface S_0 (where the different boundary conditions are imposed) and the surface S_R which is assumed to be at infinity (it gives zero contribution to the surface integral in Green's theorem). Using the pressure fields P and P' as u and ν in Green's theorem, equation 1, gives

$$\begin{aligned}&\int_V \left(P(\boldsymbol{x_r}|\boldsymbol{x_s};\omega)A'(\omega)\delta(\boldsymbol{x}-\boldsymbol{x_s}) - P'(\boldsymbol{x_s}|\boldsymbol{x_r};\omega)A(\omega)\delta(\boldsymbol{x}-\boldsymbol{x_r})\right)\, d\boldsymbol{x}\\ &= \int_{S_0} [P(\boldsymbol{x}|\boldsymbol{x_s};\omega)\boldsymbol{\nabla}P'(\boldsymbol{x}|\boldsymbol{x_r};\omega) - P'(\boldsymbol{x}|\boldsymbol{x_r};\omega)\boldsymbol{\nabla}P(\boldsymbol{x}|\boldsymbol{x_s};\omega)]\cdot\boldsymbol{n}\, d\boldsymbol{s}.\end{aligned}$$

Evaluating the volume integral, we obtain an integral relation describing the relation between the experiments with and without a free-surface:

$$A'(\omega)P(\boldsymbol{x_r}|\boldsymbol{x_s};\omega) - A(\omega)P'(\boldsymbol{x_s}|\boldsymbol{x_r};\omega) = -\int_{S_0} P'(\boldsymbol{x}|\boldsymbol{x_r};\omega)\boldsymbol{\nabla}P(\boldsymbol{x}|\boldsymbol{x_s};\omega)\cdot\boldsymbol{n}\, d\boldsymbol{s}.$$

This integral equation has been derived and used for free-surface elimination by *e.g.* Fokkema and van den Berg (1993) and Amundsen (2001). In contrast to the previous solutions of Green's theorem derived in this work, the relation described by equation 41 is not a relation that can be readily applied to retrieve a useful result. The solution of the problem is the wavefield P' and it cannot retrieved from the previous equation unless more mathematical manipulations are done. There are

different mathematical manipulations that have been used to exploit equation 41 (the interested reader is referred to Fokkema and van den Berg (1993); Amundsen (1999, 2001) and references within). The method selected by Amundsen (2001), assumes that the pressure field is a sum of upgoing and downgoing waves,

$$P(\boldsymbol{x_r}|\boldsymbol{x_s};\omega) = u(\boldsymbol{x_r}|\boldsymbol{x_s};\omega) + d(\boldsymbol{x_r}|\boldsymbol{x_s};\omega) \tag{41}$$

and introduces the relations

$$u(\boldsymbol{k_r}, z_r|\boldsymbol{x_s};\omega) = \frac{1}{2}\left(P(\boldsymbol{k_r}, z_r|\boldsymbol{x_s};\omega) - \frac{\rho\omega}{kz}\boldsymbol{\nabla}P(\boldsymbol{k_r}, z_r|\boldsymbol{x_s};\omega)\cdot\boldsymbol{n}\right) \tag{42}$$

and,

$$d(\boldsymbol{k_r}, z_r|\boldsymbol{x_s};\omega) = \frac{1}{2}\left(P(\boldsymbol{k_r}, z_r|\boldsymbol{x_s};\omega) + \frac{\rho\omega}{kz}\boldsymbol{\nabla}P(\boldsymbol{k_r}, z_r|\boldsymbol{x_s};\omega)\cdot\boldsymbol{n}\right) \tag{43}$$

where u and d refer to upgoing and downgoing, respectively, $\boldsymbol{k_r}$ is the horizontal wavenumber conjugate to the variables (x_{1r}, x_{2r}), k_z is the vertical wavenumber conjugate to z, and $z_r = x_{3r}$ is the receiver depth. Equation 41 requires the normal derivative of the pressure field P at the free-surface. Amundsen (2001) redatumed the normal derivative of P in the wavenumber domain, to obtain its values at the free-surface, and introduced the relations in equations 42 and 43, to manipulate equation 41, and obtained a second integral equation:

$$A'(\omega)P(\boldsymbol{x_r}|\boldsymbol{x_s};\omega) = -\frac{1}{2\pi^2}\int_{-\infty}^{\infty}(ik_z)P'(-\boldsymbol{k}, z_r|\boldsymbol{x_r};\omega)d(\boldsymbol{k}, z_r|\boldsymbol{x_s};\omega)\cdot\boldsymbol{n}\ d\boldsymbol{s}.$$

where the integral is taken over the horizontal wavenumber $\boldsymbol{k}$. This result is a Fredholm integral equation of the first kind. This is an equation difficult to solve and in general it is ill-conditioned (Amundsen, 2001). However, when the medium is 1D (horizontally layered), a much simpler solution is found,

$$P'(-\boldsymbol{k}, z_r|\boldsymbol{\chi_s} = 0, z_r;\omega) = \frac{-A(\omega)}{2ik_z}\frac{P(-\boldsymbol{k}, z_r|\boldsymbol{\chi_s} = 0, z_r;\omega)}{d(-\boldsymbol{k}, z_r|\boldsymbol{\chi_s} = 0, z_s;\omega)}, \tag{44}$$

or,

$$P'_r(-\boldsymbol{k}, z_r|\boldsymbol{\chi_s} = 0, z_r;\omega) = \frac{-A(\omega)}{2ik_z}\frac{u(-\boldsymbol{k}, z_r|\boldsymbol{\chi_s} = 0, z_r;\omega)}{d(-\boldsymbol{k}, z_r|\boldsymbol{\chi_s} = 0, z_s;\omega)} \tag{45}$$

where $\boldsymbol{\chi_s}$ denotes the horizontal coordinates for the source position. It is set to zero because the medium is laterally invariant. P' is the wavefield corresponding to an hypothetical experiment without a free surface, and P'_r is the scattered field in that experiment. Hence, it is assumed that P' can be separated in a direct arrival P'_0 and a scattered field P'_r.

The right hand side of equation 45 contains a wavelet factor of $A(\omega)$. This wavelet can be selected to be different from the original. Furthermore, $A(\omega)$ can be set to be equal to unity, and the retrieved wavefield won't have any source signature, it will be the pressure wavefield due to an impulsive point source.

The final result retrieves a wavefield without overburden effects, and with coincident source and receiver positions. The wavefield retrieval is performed by deconvolving the total pressure field P with the downgoing part of P at the receiver location $\boldsymbol{x_r}$. It retrieves the wavefield for coincident source and receiver locations at $\boldsymbol{x_r}$. Hence, it effectively creates a virtual source at x_r. This method can be applied to image beneath complex structures when receivers are locating within th earth. In those cases the removal of free-surface multiples will be extended to the removal of all overburden effects in the retrieved wavefield. It is accurate when dual measurements exist at the receiver location. It has been extended for an elastic medium by Holvik and Amundsen (2005). A similar wavenumber domain scheme for wavefield deconvolution was derived by Ziolkowski et al. (1998). This method subtracts the direct wave from the pressure and its normal derivative prior to up-down decomposition. Hence, it requires dual measurements and benefits from the knowledge of the source wavelet. The authors explain that the knowledge of the source wavelet helps stabilizing the output (Johnston and Ziolkowski, 1999).

As discussed before, wavefield deconvolution has similarities with the virtual source method derived by Bakulin and Calvert (2004) and Korneev and Bakulin (2006), whose equation is given by a simplification of equation 35. To derive virtual source method, two pressure wavefields P and P^- are used as the functions u and ν in Green's theorem, equation 1. The medium parameters for both wavefields are assumed to be equal everywhere (see Section 2.2 and 2.3), and the selected volume is a halfspace in a seismic experiment, as shown in figure 4. The volume is bounded by a surface S_0 where the sources explode (which is not assumed to be a zero-pressure surface) and the surface S_r that is assumed to be at infinity. This surface does not vanishes when anticausal or time-reversed wavefields are used (in this case we are using the conjugate or time-reversed pressure field), but it is not possible to have sources or measurements along this surface, hence its contribution is ignored. Evaluating Green's theorem with this choice of functions and boundary conditions, gives

$$2iA(\omega)\Im\left[P(\boldsymbol{x_a}|\boldsymbol{x_b};\omega)\right] \approx \int_{S_0}\left[P(\boldsymbol{x_a}|\boldsymbol{x};\omega)\boldsymbol{\nabla}P^-(\boldsymbol{x_b}|\boldsymbol{x};\omega) - P^-(\boldsymbol{x_b}|\boldsymbol{x};\omega)\boldsymbol{\nabla}P(\boldsymbol{x_a}|\boldsymbol{x};\omega)\right]\cdot\boldsymbol{n}\ d\boldsymbol{s}, \quad (46)$$

where the sum is performed over source locations $\boldsymbol{x}$.

This equation is analogous to equation 34 derived in section 2.3. The difference are in the selected volume and surfaces taken into account, and the location of the receivers. In virtual source method, the receivers are assumed to be below a complex overburden.

$$2iB(\omega)\Im\left[P(\boldsymbol{x_b}|\boldsymbol{x_a};\omega)\right] \approx \int_{S_m} -2ik\ P(\boldsymbol{x}|\boldsymbol{x_a};t)P^-(\boldsymbol{x}|\boldsymbol{x_b};\omega)\ d\boldsymbol{x}. \quad (47)$$

As in the interferometry methods discussed in section 2, the wavefield's normal derivatives are assumed not to be available, and the previous equation is further approximated to wit

$$2iB(\omega)\Im\left[P(\boldsymbol{x_b}|\boldsymbol{x_a};\omega)\right] \approx \int_{S_m} P(\boldsymbol{x}|\boldsymbol{x_a};t)P^-(\boldsymbol{x}|\boldsymbol{x_b};\omega)\ d\boldsymbol{x}. \quad (48)$$

This equation is a compromise to Green's theorem, as explained by Korneev and Bakulin (2006). Hence, errors and artifacts are anticipated.

Using the virtual source method an approximate wavefield retrieval at the receiver level is achieved. In contrast to the more complete method (wavefield deconvolution), the overburden effects are not removed. In fact, an extra power of the source signature multiplies the retrieved wavefield. The advantage of the virtual source method is that it can be applied in the absence of the pressure field's normal derivative and an approximate wavefield is retrieved between two receivers located below a complex overburden. The synthesized wavefield will contain useful phase information.

3.3 Analysis

Most of the original, somewhat intuitive, interferometry methods were formulated to work on passive data (Schuster, 2001). The closed surface boundary was formed by sources (*i.e.* earthquakes or ambient fluctuations) far away from the receivers (Shapiro and Campillo, 2004; Sabra et al., 2005; Shapiro et al., 2005; Larose et al., 2006). Wavefield crosscorrelations were applied to pairs of receiver gathers and a noisy Green's function was retrieved from that passive data originally seen as noise. The theory that evolved from approximations to Green's theorem, to the representation theorem, or to the principle of time reversal came later to explain what was being reconstructed with crosscorrelations. (Derode et al., 2003; Roux and Fink, 2003; Wapenaar et al., 2002; Weaver and Lobkis, 2004; Draganov et al., 2006). New applications, analysis, and results were obtained along the way, *e.g.* the virtual source method (Bakulin and Calvert, 2004), VSP and WVSP applications (Schuster and Zhou, 2006; Otnes et al., 2006), connections with energy principles (Snieder et al., 2007), imaging, multiple removal, etc. As we explained in the analysis for the second section of this report, most of this work was performed using a compromised version of the framework provided by Green's theorem.

Having a framework, allows us to review it and anticipate that things are not going to be as accurate as we would like when we make compromises to the theory. This knowledge provides the opportunity to correct the weaknesses (when possible) of any approximate method by going back to first principles and attempting to better satisfy the framework instead of trying to create new theory to correct the compromised output. With this understanding, Weglein et al. (2000); Ramírez et al. (2007) proposed a method for seismic interferometry that overcomes the need for approximations. It requires only the pressure field at the measurement surface and it will be exact if we can input only the scattered field. Otherwise, an estimate of the wavelet would be necessary to decrease the occurrence of a small error in the synthesized wavefield.

Conclusions

Green's theorem is the theoretical basis that unifies a broad class of interferometry approaches. This mathematical relation was derived by George Green in 1828 and has been widely used during the past and present century in all kind of applications including almost any processing step in seismic exploration (*e.g.* wavelet estimation, wavefield retrieval, imaging, wavefield deconvolution, etc.). The attention given by the energy industry and the literature to methods dealing with wavefield retrieval, or seismic interferometry, and its applications to different seismic exploration

problems, has brought about a renewed interest in Green's theorem. The reason for this is that all the different approaches to what we call seismic interferometry can be derived from this single unifying framework: Green's theorem (and its extension for displacements by Betti (1872) and elastodynamic fields by Rayleigh (1873)).

Throughout this paper, Green's theorem was used to: 1) provide an overview of a broad set of seismic applications that recognize Green's theorem as the starting point of their theory and algorithms;
2) show that Green's theorem provides a platform and unifying principle for the field of seismic interferometry;
3) explain artifacts and spurious multiples (in certain interferometry approaches) as fully anticipated errors and as violations of the theory, rather than as some mystery or numerical manifestation that ought to be explained with physics; 4) provide a systematic approach to understanding, comparing and improving upon many current concepts, approximations and compromises.

4 Acknowledgments

We acknowledge and thank the sponsors and members of M-OSRP for the support of this research. This research was partially supported by the NSF-CMG award DMS-0327778 DOE Basic Energy Sciences award DE-FG02-05ER15697.
A. C. Ramírez appreciates the internship opportunity she had at Statoil during the fall of 2007, in which she was allowed to work on a seismic interferometry project. The author aknowledges useful and invaluable discussions with Ketil Hokstad and Einar Otnes. Lasse Amundsen, Ken Matson and Rodney Johnston are thanked for their insights on the wavefield deconvolution method.
Kris Innanen and Daniel Fisher are thanked for their help in editing this paper.

References

Amundsen, L. "The propagator matrix related to the Kirchhoff-Helmholtz integral in inverse wavefield extrapolation." *Geophysics* 59 (1994): 1902–1910.

Amundsen, L. "Elimination of free-surface related multiples without need of the source wavelet." *SEG Technical Program Expanded Abstracts* (1999): 1064–1067.

Amundsen, L. "Elimination of free-surface related multiples without need of the source wavelet." *Geophysics* 66 (2001): 327–341.

Amundsen, L., B. Secrest, and B. Arnsten. "Extraction of the normal component of the particle velocity from marine pressure data." *Geophysics* (1995).

Bakulin, A. and R. Calvert. "Virtual source: new method for imaging and 4d below complex overburden." *SEG Expanded Abstracts* (2004).

Betti, E. "Teoria dellelasticit a: Il Nuovo Cimento." *SEG Expanded Abstracts* (1872): Sezione 6, no. 78, 8797.

Derode, A., E. Larose, M. Tanter, J. de Rosny, a. Tourin, M. Campillo, and M. Fink. "Recovering the Green's function for a heterogeneous medium between two passive sensors? Application to acoustic waves." *Applied Physics Letter* 83 (2003): 3054–3056.

Draganov, D., K. A. Wapenaar, and J. Thorbecke. "Seismic interferometry: Reconstructing the earth's reflection response." *Geophysics* 71 (2006): S161–S170.

Fokkema, J. T. and P. M. van den Berg. "Seismic applications of acoustic reciprocity." *Elsevier Science Publ.* (1993).

Guo, Z., A. B. Weglein, and T. H. Tan. "Using pressure data on the cable to estimate the seismic wavelet." *SEG Technical Program Expanded Abstracts* (2005).

Holvik, E. and L. Amundsen. "Elimination of the overburden response from multicomponent source and receiver seismic data, with source designature and decomposition into PP-, PS-, SP-, and SS-wave responsesm." *Geophysics* 70 (2005): S43–S59.

Johnston, Rodney and Anton Ziolkowski. "Benefits of source signature measurements for multiple removal in streamer and OBC data." *SEG Technical Program Expanded Abstracts* 123 (1999): 1346–1349.

Korneev, V. and A. Bakulin. "On the fundamentals of the virtual source method." *Geophysics* 71 (2006): A13–A17.

Larose, E., L. Margerin, A. Derode, B. van Tiggelen, M. Campillo, N. Shapiro, A. Paul, L. Stehly, and M. Tanter. "Correlation of random wavefields: An interdisciplinary review." *Geophysics* 71 (2006): SI11–SI21.

Morse, P.M. and H. Feshbach. *Methods of Theoretical Physics*. International Series in Pure and Applied Physics. McGraw-Hill Book Co. (Div. of McGraw-Hill, Inc.), 1953.

Osen, A., L. Amundsen, and B.G. Secrest. "Source signature estimation in the seismic experiment." *64th Ann. Internat. Mtg., Soc. Expl. Geophys., Expanded Abstracts* (1994).

Osen, A., B.G. Secrest, L. Amundsen, and A. Reitan. "Wavelet estimation from marine pressure measurements." *Geophysics* 63 (1998): 2108–2119.

Otnes, E., K. Hokstad, G. Rønholt, and S.-K. Foss. "Data-driven surface related multiple elimination on walkaway VSP data." *Extended Abstracts of the 68th Annual International Meeting of the EAGE* (2006).

Ramírez, A. C., K. Hokstad, and E. Otnes. "Data driven regularization/extrapolation." *EAGE 69^{th} Conference & Exhibition London, UK* (2007).

Ramírez, A. C., A. B. Weglein, E. Otnes, and K. Hokstad. "The role of the direct wave and Greens Theorem in seismic interferometry and spurious multiples." *Submitted to SEG Technical Program Expanded Abstracts* (2007).

Rayleigh, Lord. "Some general theorems related to vibrations." *Proc. Lond. Math. Soc.* (1873).

Roux, P. and Fink. "Green's function estimation using secondary sources in a shallow water environment." *Journal of the Acoustic Society of America* 113 (2003): 1406–1416.

Sabra, K. G., P. Gerstoft, P. Roux, and W. A. Kuperman. "Extracting time-domain Green's function estimates from ambient seismic noise." *Geophysics Research Letters* 32 (2005).

Schneider, W. A. "Integral formulation for migration in two-dimensions and three-dimensions." *Geophysics* 43 (1978): 49–76.

Schuster, G. T. "Theory of daylight/interferometric imaging: tutorial." *Extended Abstracts of the 63rd Annual Meeting Conference and Exhibition, EAGE* A32 (2001).

Schuster, G. T. and M. Zhou. "A theoretical overview of model-based and correlation-based redatuming methods." *Geophysics* 4 (2006): SI103–SI110.

Shapiro, N. M. and M. Campillo. "Emergence of broadband Rayleigh waves from correlations of the ambient seismic noise." *Geophysics Research Letters* 31 (2004).

Shapiro, N. M., M. Campillo, L. Stehly, and M. H. Ritzwoller. "High-resolution surface-wave tomography from ambient seismic noise." *Science* 307 (2005): 1615–1618.

Snieder, R., K. Wapenaar, and K. Larner. "Spurious multiples in seismic interferometry of primaries." *Geophysics* 71 (2006): SI111–SI124.

Snieder, R., K. Wapenaar, and U. Wegler. "Unified Green's function retrieval by cross-correlation; connection with energy principles." *Physical review E* 75 (2007): 036103–1 – 036103–14.

Sommerfeld, A. *Optics*. Academic Press, 1954.

Tan, T. H. "Source signature estimation." *Presented at the Internat. Conf. and Expo. of Expl. and Development Geophys., Moscow, Russia.* (1992).

Tan, T. H. "Wavelet spectrum estimation." *Geophysics* 64 (1999): 1836–1846.

Vasconcelos, I. and R. Snieder. "Interferometric imaging by deconvolution: Theory and numerical examples." *SEG Technical Program Expanded Abstracts* (2006): 2416–2420.

Visser, T. D., P. S. Carney, and E. Wolf. "Remarks on boundary conditions for scalar scattering." *Physics letters A* 249 (1998): 243–247.

Wapenaar, K. "Retrieving the elastodynamic Green's function of an arbitrary inhomogeneous medium by cross correlation." *Phys. Rev. Lett.* 93(25) (2004): 254301–1 –254301–4.

Wapenaar, K., D. Draganov, J. Thorbecke, and J. Fokkema. "Theory of acoustic daylight imaging revisited." *72nd Annual International Meeting, SEG, Expanded Abstracts* (2002): 2269–2272.

Wapenaar, K. and J. Fokkema. "Green's function representations for seismic interferometry." *Geophysics* 71 (2006): SI33–SI46.

Weaver, R. L. and O. I. Lobkis. "Diffuse fields in open systems and the emergence of the Green's function." *Journal of the Acoustic Society of America* 116 (2004): 2731–2734.

Weglein, A. B. and A. J. Devaney. "The inverse source problem in the presence of external sources." *Proc. SPIE* 1767 (1992): 170176.

Weglein, A. B. and B.G. Secrest. "Wavelet estimation for a multidimensional acoustic or elastic earth." *Geophysics* 55 (1990): 1975–1989.

Weglein, A. B., T. H. Tan, S. A. Shaw, K. H. Matson, and D. J. Foster. "Prediction of the wavefield anywhere above an ordinary towed streamer: application to source waveform estimation, demultiple, deghosting, data reconstruction and imaging." *SEG Expanded Abstracts* (2000).

Ziolkowski, A.M., D.B. Taylor, and R.G.K. Johnston. "Multiple wavefields: separating incident from scattered, up from down, and primaries from multiples." *8th Ann. Internat. Mtg., Soc. Expl. Geophys., Expanded Abstracts* 6 (1998).

3D free-surface multiple elimination and summation in the cross-line conjugate domain

K. A. Innanen, S. T. Kaplan and A. B. Weglein

Abstract

3D free surface multiple elimination (3D-FSME), which acts in the k-ω domain, is wave-theoretically more complete than the x-ω domain surface-related multiple elimination (3D-SRME) algorithm; however, the latter has available to it strategies for managing inadequate cross-line sampling and aperture. To develop similar cross-line strategies within the context of 3D-FSME requires that (1) it be decomposed to isolate the cross-line component of the algorithm, and (2) the impact on this component of degraded sampling and aperture be both predictable and amenable to some form of compensation. We show that the first of these requirements is in place and discuss an investigative plan.

1 Introduction

The inverse scattering series free-surface multiple elimination (FSME) series (Carvalho, 1992; Weglein et al., 1997, 2003), which is calculated in k-ω space, differs in several ways from the DELPHI SRME algorithm (Verschuur et al., 1992a,b), which is calculated in x-ω space, primarily in the incorporation of the obliquity factor. In the x-ω domain, however, a variety of strategies exist (van Dedem and Verschuur, 2005; Matson and Abma, 2005; Hokstad and Sollie, 2006) for managing inadequate aperture and sampling in the cross-line dimension, a key part of practical implementation of this and the 3D FSME algorithm, the latter of which is in progress (Kaplan et al., 2005). With respect to cross-line data issues, two possible avenues are open for FSME. First, the algorithm could be inverse Fourier transformed into the x-ω domain, and the obliquity factor could be approximated and applied as a spatial filter. Second, we could examine the 3D FSME algorithm in k-ω space, its natural environs, and look for ways to isolate and manage the cross-line aperture/sampling issues therein. Both are reasonable approaches; here, we follow the second.

We present two main results, and some basic analysis. First, we re-cast the 3D algorithm to separate out in k-ω space the influence of the cross-line sampling/aperture from the influence of the other data dimensions. In effect, we express the 3D FSME algorithm as a set of applications of 2D FSME, that are summed together in a final step. Second, we characterize this last step by examining the multiple prediction just before performing the sum, analogous to the 3D "pre-summation gather" analysis done in the x-ω domain.

2 Isolation of the cross-line component of FSME

Let us begin by placing ourselves in a Cartesian coordinate system such that depth increases with positive z, the in-line (sail-line) dimension is x, and the cross-line direction is y. Furthermore, we assume that the goal is to compute the first term of the FSME series, which predicts the correct phase of all free-surface multiples and, provided all pre-requisites are in place, the correct amplitude. Deviations from these pre-requisites are addressed with adaptive subtraction methods (Abma et al., 2005; Kaplan and Innanen, 2006). In 3D, the deghosted data set with direct wave removed, is Fourier-transformed in the 4 lateral shot/receiver coordinates and over time. Calling this data $D(k_{xg}, k_{yg}, z_g, k_{xs}, k_{ys}, z_s, \omega)$, the multiple prediction is then M_{3D}, where

$$\begin{aligned} &M_{3D}(k_{xg},k_{yg}, z_g, k_{xs}, k_{ys}, z_s, \omega) \\ &\quad = \frac{A}{S(\omega)} \int\int dk'_x dk'_y q' e^{iq'(z_g+z_s)} \\ &\qquad \times D(k_{xg}, k_{yg}, z_g, k'_x, k'_y, z_s, \omega) D(k'_x, k'_y, z_g, k_{xs}, k_{ys}, z_s, \omega), \end{aligned} \tag{1}$$

and where

$$q' = \frac{\omega}{c_0}\sqrt{1 - \frac{k'^2_x c_0^2}{\omega^2} - \frac{k'^2_y c_0^2}{\omega^2}} \tag{2}$$

is the obliquity factor; A contains some constant integration factors and S is the source wavelet. Let us next re-express equation (1) such that the cross-line (y) activity is isolated. Consider first the 2D version of the algorithm (with variation in the in-line dimension only), in which the multiple prediction is M_{2D}:

$$\begin{aligned} &M_{2D}(k_{xg}, z_g, k_{xs}, z_s, \omega) \\ &= \frac{A'}{S(\omega)} \int dk'_x \tilde{q}' e^{i\tilde{q}'(z_g+z_s)} D(k_{xg}, z_g, k'_x, z_s, \omega) D(k'_x, z_g, k_{xs}, z_s, \omega), \end{aligned} \tag{3}$$

and where A' contains 2D integration factors, and the obliquity factor is slightly simpler:

$$\tilde{q}' = \frac{\omega}{c_0}\sqrt{1 - \frac{k'^2_x c_0^2}{\omega^2}}. \tag{4}$$

We note that within equation (1) are many instances of equation (3). In fact, if we define M^*_{2D} as a modified version of M_{2D}:

$$\begin{aligned} &M^*_{2D}(k_{xg}, k_{yg}, z_g, k_{xs}, k_{ys}, z_s, \omega | k'_y) \\ &\quad = \frac{A}{S(\omega)} \int dk'_x q' e^{iq'(z_g+z_s)} \\ &\quad \times D(k_{xg}, k_{yg}, z_g, k'_x, k'_y, z_s, \omega) D(k'_x, k'_y, z_g, k_{xs}, k_{ys}, z_s, \omega), \end{aligned} \tag{5}$$

i.e., a function that is built in exactly the same way as M_{2D}, but which involves three additional variables (and the 3D version of q'), then the 3D algorithm becomes

$$\begin{aligned} &M_{3D}(k_{xg}, k_{yg}, z_g, k_{xs}, k_{ys}, z_s, \omega) \\ &\qquad = \int dk'_y M^*_{2D}(k_{xg}, k_{yg}, z_g, k_{xs}, k_{ys}, z_s, \omega | k'_y). \end{aligned} \tag{6}$$

Two of the three extra variables are the cross-line wavenumbers of the prediction, k_{yg} and k_{ys}, and one of the three is the cross-line conjugate integration variable, k'_y. Equation (6) in processing terms is a straightforward stack across k'_y. The formulation effectively isolates the influence of cross-line sampling and aperture on the prediction process.

3 Cross-line gathers

If cross-line sampling and aperture are adequate, $M^*_{2D}(k'_y)$ is completely filled with prediction information, and the sum can be satisfactorily carried out. If the cross-line sampling and aperture are significantly compromised, the $M^*_{2D}(k'_y)$ spectrum will also be compromised. In either case, the influence of the cross-line spectrum on the prediction will be most apparent in the examination of

$$M^*_{2D}(k'_y, \omega)|_{k_{xg},k_{yg},k_{xs},k_{ys}}. \tag{7}$$

Equation (7) represents a k'_y-ω gather resulting from the fixture of all surface wavenumber coordinates.

4 Discussion

The main purpose here is to present a basic strategy for isolating and treating the cross-line component of a three-dimensional implementation of the k-ω domain free-surface multiple elimination algorithm; this dimension tends to be the one most compromised in terms of both sampling and aperture.

Sampling and aperture impact the pre-processing of the data, prior to application of the 3D FSME algorithm, since Fourier transforms must be taken over all coordinates; in fact, if it turns out to be optimal to do so, we may treat sampling/aperture as entirely pre-processing issues. That is, if we can entirely (somehow) correct the Fourier transforms for inadequate sampling and aperture, we will in principle have no more problems left to deal with and may expect impeccable FSME results. But data corrections in practice must be driven and tuned by what is to come next, so there is no avoiding the need to characterize 3D FSME in terms of acquisition and its current limitations.

As a case in point, sophisticated technology exists for performing Fourier transforms and/or reconstructions in aperture- and sampling-compromised settings (Sacchi and Ulrych, 1996; Zwartjes and Sacchi, 2007, e.g.). Often the methods rely on some level of prior information, for instance, the assumption that the spectrum that would be derived in aperture unlimited experiments are the sum of a limited set of monochromatic plane waves. By more completely understanding the response of 3D FSME to aperture and sampling issues, we might determine whether or not such assumptions are practically valid in a given case, and if so, under what circumstances. We continue to pursue these issues.

5 Acknowledgments

Kris Innanen and Art Weglein were supported by the DOE Basic Energy Sciences award DE-FG02-05ER15697; Art Weglein was supported by the NSF-CMG award DMS-0327778. The support of the M-OSRP sponsors is also gratefully acknowledged.

References

Abma, R., N. Kabir, K. H. Matson, S. Michell, S. A. Shaw, and B. McLain. "Comparisons of adaptive subtraction methods for multiple attenuation." *The Leading Edge* 24 (March 2005): 277–280.

Carvalho, P. M. *Free-surface multiple reflection elimination method based on nonlinear inversion of seismic data*. PhD thesis, Universidade Federal da Bahia, 1992.

Hokstad, K. and R. Sollie. "3D surface-related multiple elimination using parabolic sparse inversion." *Geophysics* 71 (2006): V145.

Kaplan, S. T. and K. A. Innanen. "Adaptive subtraction of free surface multiples through order-by-order prediction, matching filters and independent component analysis." *Submitted to Geophysics* (2006).

Kaplan, S. T., K. A. Innanen, and A. B. Weglein. "Updates to M-OSRP internal and free surface multiple coding projects." *Mission-Oriented Seismic Research Program (M-OSRP) Annual Report* (2005).

Matson, K. H. and R. Abma. "Fast 3D surface-related multiple elimination using azimuth moveout for multiples." *Proceedings of the 75th Annual Meeting of the Society of Exploration Geophysicists, Houston, TX.* . Soc. Expl. Geophys., 2005.

Sacchi, M. and T. J. Ulrych. "Estimation of the discrete Fourier transform, a linear inversion approach." *Geophysics* 61 (1996): 1128–1136.

van Dedem, E. J. and D. J. Verschuur. "3D surface-related multiple prediction: a sparse inversion approach." *Geophysics* 70 (2005): V31.

Verschuur, D. J., A. J. Berkhout, and C. P. A. Wapenaar. "Adaptive surface-related multiple elimination." *Geophysics* 57 (1992): 1166–1177.

Verschuur, D. J., A. J. Berkhout, and C. P. A. Wapenaar. "Adaptive surface-related mutiple elimination." *Geophysics* 57 (1992): 1166.

Weglein, A. B., F. V. Araújo, P. M. Carvalho, R. H. Stolt, K. H. Matson, R. T. Coates, D. Corrigan, D. J. Foster, S. A. Shaw, and H. Zhang. "Inverse Scattering Series and Seismic Exploration." *Inverse Problems* (2003): R27–R83.

Weglein, A. B., F. A. Gasparotto, P. M. Carvalho, and R. H. Stolt. "An Inverse-Scattering Series Method for Attenuating Multiples in Seismic Reflection Data." *Geophysics* 62 (November-December 1997): 1975–1989.

Zwartjes, P. and M. Sacchi. "Fourier reconstruction of nonuniformly sampled, aliased seismic data." *Geophysics* 72 (2007): V21–V32.

Estimating plane-wave transmission loss with the inverse scattering internal multiple attenuation algorithm: concept and an application to Q estimation

J. E. Lira, K. A. Innanen, A. B. Weglein and A. C. Ramirez

Abstract

The inverse scattering series internal multiple attenuation algorithm suppresses internal multiples to within an amplitude error that is determined by plane wave transmission losses down to, and across, the reflector acting as the multiple generator (the reflector at which the shallowest downward reflection of the multiple takes place). In this paper we propose that this be exploited to address the problem of estimating and removing overburden effects on reflected primaries, to the benefit of current leading edge imaging and inversion algorithms. We note that this is not inversion, but the calculation of a correction factor with no assumption about where the factor comes from, e.g., specific influences of rock mechanical properties. However, the approach can be used in a further, ad hoc scheme as a means to provide such a link. For instance, if an overburden is absorptive, the difference between the predicted and actual multiple spectra may be related to the integral of its Q profile. Furthermore, within a specific Q model, this estimation can be made insensitive to any scalar error in the multiple prediction arising from, e.g., numerical implementation. Early-stage synthetic examples provide evidence that extraction and calculation of the predicted and actual multiples' spectra, using straightforward FFT methods, stably provides estimates of the integrated Q profile. The average error in the estimation is approximately 5.5%. Research is ongoing on fundamental/analytic and practical/numerical aspects of this potential algorithm.

1 Introduction

The distinct inverse scattering subseries for removing multiples, depth imaging primaries and improving seismic resolution, all carry out their objectives without requiring the traditional subsurface velocity information or subsurface absorptive properties, respectively. A reasonable question that is frequently asked is: "Although we understand the fact that these algorithms don't require the velocity or Q model, could you nevertheless back out an estimated velocity or Q model after all is said and done, and after your velocity independent depth algorithm has found the depth image?" The answer is, you certainly can estimate bulk average properties. In this report that perennial question is raised and investigated regarding the issue of resolution and Q, and backing out a bulk Q estimate. And, the answer is affirmative.

A primary is a recorded seismic event with one upward reflection. These events are considered the source of subsurface information for structural mapping, parameter estimation, and, ultimately, petroleum delineation at the target. In all current leading-edge processing of primaries the ability to infer useful information at depth critically depends upon the ability to estimate and to remove the impact of the overburden on the character of the wave, during propagation from the source down to the reflector and from the reflector up to the receiver. The ability to effectively estimate (and

remove) the effects of the down and up propagation legs determines the level of realistic ambition in subsequent processing of primaries. In this paper we propose a new method to estimate overburden effects, turning a deficiency of the internal multiple attenuation into an asset—an indirect source of this important overburden information.

The inverse scattering series has provided a set of algorithms for the removal of all orders of free-surface and internal multiples (Weglein et al., 1997, 2003). Within the overall class of events referred to as internal multiples, events are further catalogued by order, meaning the number of downward reflections experienced. The algorithm of Araújo (1994) and Weglein et al. (1997) is a series for the attenuation of all orders of internal multiples, the first term of which attenuates the first-order event. It is to this first term that we direct our current attention. In practice, this component of the full algorithm has often been fully adequate; however, there are occasions when an elimination rather than attenuation algorithm would provide distinct added value. Ramírez and Weglein (2005a) have provided a closed-form *elimination* algorithm for the first-order internal multiple to fill this requirement. The key here is that the two above algorithms, attenuation and elimination, and the understood properties of the former (Weglein et al., 1997; Weglein and Matson, 1998; Ramírez and Weglein, 2005b), may be exploited to provide seismic information at depth. The value of this information and the applicability of this idea is of moment as the algorithm is refined (Nita and Weglein, 2004) and implemented in multiple dimensions for large data sets (Kaplan et al., 2005).

The amplitude discrepancy between the actual first-order internal multiple and the attenuator described above is a direct expression of plane wave amplitude loss down to a particular reflector. We propose that this be exploited to address the problem of estimating and removing overburden effects on reflected primaries, to the benefit of current leading edge imaging and inversion algorithms. The ambitious goal of separation and extraction of a well-located and accurate angle dependent reflection coefficient at depth is typically hindered by the experience of the primary wavefield as it propagates through an unknown overburden, which cloaks the event with spurious amplitude changes. Contemporary methodologies to counter these effects are generally inconsistent with wave theoretic processing, and rarely go forward without a well-tie. The information provided by the internal multiple algorithm is a direct, immediate correcting factor for the cloaked primary.

Practical motivation for use of this amplitude information is several-fold. First, the information is a by-product of an existing part of the wave-theoretic processing flow–the demultiple phase– and comes at no additional cost. Second, this occurs at a convenient point during processing, just prior to its likely use in primary processing/inversion. Third, it is consistent with wave-theoretic processing. Fourth, it is not restricted to a production setting, but is also applicable in reconnaissance and exploration settings. Fifth, in addition to its potential value for current high-bar imaging and inversion/AVO processing, it would act to make the non-linear inverse scattering target identification series (Zhang and Weglein, 2005) an exploration as well as production tool, again by eliminating the requirement for a well-tie.

In this paper we present a simple, early stage study and example of such information extraction. By our previous statements, if a medium or target overburden is characterized by non-negligible Q, which will tend to dominate transmission effects, the difference between the predicted and

actual spectra of the multiple event will bear interpretable information about the Q values in the overburden. We present basic theory and examples illustrating the use of internal multiple prediction as a means for Q estimation. In the first section we review the mathematical form of the internal multiple attenuation algorithm in 1D, its behavior in terms of the data sub-events, and the provenance of the amplitude error in the prediction. In the second section we review the influence of a well-known model for absorptive-dispersive wave propagation on the effective transmission coefficients present in reflection seismic data. In the third section, by generalizing the predicted internal multiple error to accommodate the above Q-type transmission coefficients, we demonstrate that the spectral ratio of the predicted and actual interbed multiples may be used to invert for the cumulative (integral) Q value down to and across the multiple generator. In the fourth section we carry this out on a layered medium model. We comment on the potential for extension of such methods to multiple dimensions and other avenues of research.

Determination of general attenuation vs. elimination properties

As a brief aside, let us comment on how the properties of the attenuation vs. elimination algorithms may be understood and thereafter exploited. It is known in principle (via the downward continuation/interface removal idea) that given complete medium information down to and across an interface acting as the downward reflector for a first-order internal multiple, that multiple may be precisely eliminated. This corresponds, then, to the information that would be required for brute transformation of the attenuated multiple into an eliminated multiple. Although the elimination series (Ramírez and Weglein, 2005a) does this task in the absence of such information, we then note that the brute division of the attenuated multiple by the actual multiple must correspond to the accumulation of the aforementioned overburden information.

2 IMA and predicted vs. actual amplitudes

The full multiple attenuation algorithm is a series of terms that attenuate sequentially higher orders of multiples in fully 3D pre-stack reflection data (Weglein et al., 2003). For the purposes of this paper, reducing the algorithm to its 1D form for normal incidence data with a plane wave source, and considering the first term only, we have the predicted multiple algorithm (Araújo, 1994):

$$\begin{aligned} b_{3IM}(k_z) = & \int_{-\infty}^{\infty} dz_1' b_1(z_1') e^{ik_z z_1'} \\ & \times \int_{-\infty}^{z_1'-\epsilon} dz_2' b_1(z_2') e^{-ik_z z_2'} \int_{z_2'+\epsilon}^{\infty} dz_3' b_1(z_3') e^{ik_z z_3'}, \end{aligned} \tag{1}$$

where ϵ is a small constant determined by the approximate length of the wavelet. In implementing the algorithm, our first job is to transform the data into the input term $b_1(z)$. This required form can be obtained (Weglein et al., 1997) by (*i*) taking the surface recorded data $D(t)$, Fourier transforming over time to produce $D(\omega)$; (*ii*) performing a change of variables to the pseudo-depth

conjugate variable $k_z = 2(\omega/c_0)$, where c_0 is waterspeed, and calling the data expressed in this variable $b_1(k_z)$; and (*iii*) performing an inverse Fourier transform over k_z to generate the pseudo-depth quantity $b_1(z)$. Each of these steps occurs entirely in terms of the measured data and a homogeneous background medium with wavespeed c_0.

The algorithm itself may then be applied. Using $b_1(z)$ as input, equation (1) searches for sub-events that obey the geometry dictated by the limits of the three integrals. Roughly speaking, the search proceeds as follows: via the outermost integral an event anywhere in $b_1(z)$, i.e., on $z = (-\infty, \infty)$, is sought. When an event is located, others are then sought at shallower pseudo-depths via the middle integral. Finally, if one or more shallower events are found a multiple is predicted by the final integral for any deeper event (including but not exclusive to the first). With the search over, eqn (1) essentially convolves the two deeper events, and then cross-correlates the result with the shallower event. This sums the travel-times of the deeper events and subtracts the travel-time of the shallower event, the correct time of the multiple is predicted (Figure 1). This second step, and hence the entire algorithm, also occurs entirely in terms of the data (via b_1) and the wavespeed c_0 (in the integral kernels).

Importantly for our current purposes, the predicted amplitudes are scaled by a factor that is related to the transmission coefficients of the interfaces above the *generator*, the reflector at which the downward reflection of the multiple takes place. See again Figure 1 and the Introduction. The discrepancy is a direct expression of *any* cumulative transmission losses above the generator. Hence, a correction of these losses could proceed with no assumptions made about their cause. Alternatively, if we are comfortable assuming a certain mechanism dominates the transmission loss, this information can also be used to derive specific estimates of overburden medium parameters, as well as thereafter providing corrections. Let us pursue this second route by assuming an absorptive/dispersive overburden.

3 Transmission coefficients in absorbing media

To do this, we must select an appropriate (quantitative) description of the influence of absorption on transmission above a multiple generator. *Intrinsic attenuation* describes amplitude and phase alterations in a wave due to friction. These alterations are modeled by a generalization of the (nominally real) wavefield phase velocity to a complex, frequency-dependent quantity, often parametrized in terms of Q, a measure of wave amplitude or energy lost per cycle. A reasonably well-accepted Q model (Aki and Richards, 2002; Kjartansson, 1979) alters the wavenumber describing propagation in a scalar medium, $k = \omega/c(z)$, to

$$K = \frac{\omega}{c(z)} \left[1 + \frac{F(\omega)}{Q(z)} \right], \tag{2}$$

where $F(\omega) = \frac{i}{2} - \frac{1}{\pi} \log(\omega/\omega_0)$. The reference frequency ω_0, at which the wave propagates with speed c, may be considered a parameter to be estimated, or assumed to be the largest frequency available to a given experiment. Notice that the model divides propagation up into three parts:

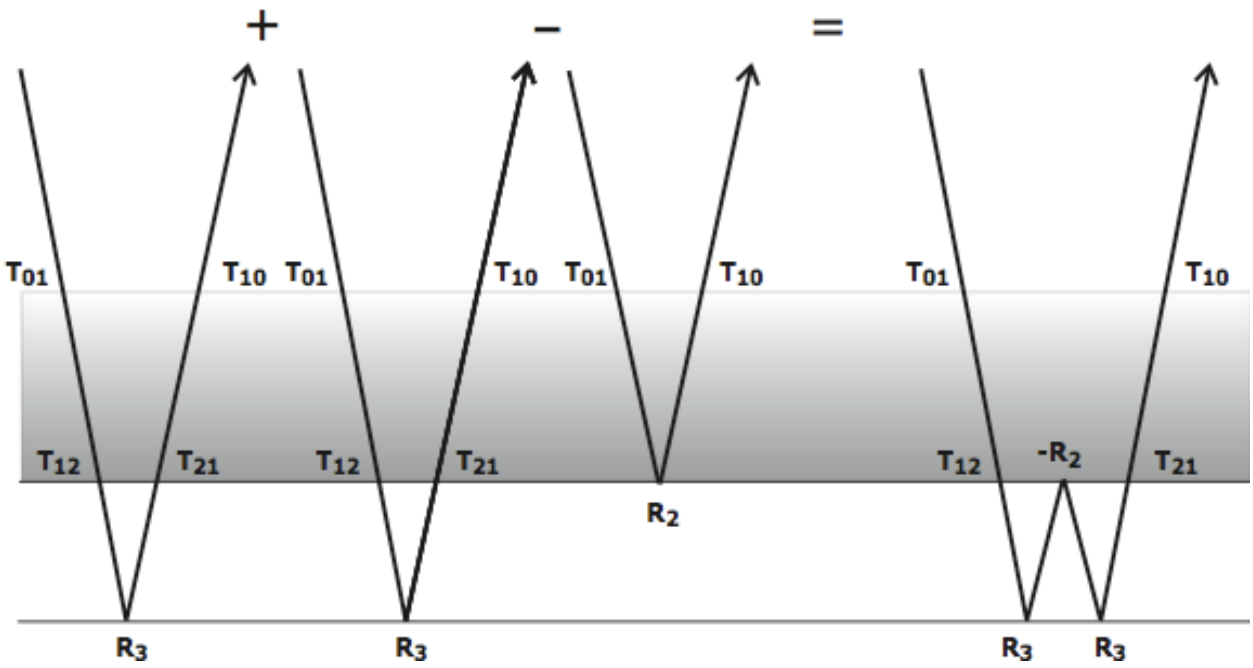

Figure 1: *Sub-events and amplitudes in the IMA algorithm.*

a propagation component, an attenuation component, and a dispersion component. Consider a plane wave of unit amplitude, normally-incident on a single layer (with interface depths z_1 and z_2) embedded in a homogeneous whole-space of wavespeed c_0, having departed from a source/receiver plane at depth $z = 0$ at $t = 0$. If the layer is acoustic with wavespeed c_1, amongst other components of the reflected field, the primary from the deeper interface (at z_2) may be written:

$$PR(\omega) = e^{i\frac{\omega}{c_0}z_1} T_{10} e^{i\frac{\omega}{c_1}(z_2-z_1)} R_2 e^{i\frac{\omega}{c_1}(z_2-z_1)} T_{01} e^{i\frac{\omega}{c_0}z_1}, \tag{3}$$

where $T_{10} = 2c_0/(c_0 + c_1)$ and $T_{01} = 2c_1/(c_0 + c_1)$, and R_2 is the reflection coefficient of the z_2 interface. If the layer is instead absorptive such that it obeys eqn (2), with parameters c_1 and Q_1, the primary may instead be written as

$$PR_Q(\omega) = e^{i\frac{\omega}{c_0}z_1} \mathcal{T}_{10} e^{i\frac{\omega}{c_1}(z_2-z_1)} R_2 e^{i\frac{\omega}{c_1}(z_2-z_1)} \mathcal{T}_{01} e^{i\frac{\omega}{c_0}z_1}, \tag{4}$$

where the transmission coefficients are generalized:

$$\mathcal{T}_{01} = \frac{2c_1[1 + F(\omega)/Q_1]^{-1}}{c_0 + c_1[1 + F(\omega)/Q_1]^{-1}} \exp\left[i\frac{\omega}{c_1}\frac{F(\omega)}{Q_1}(z_2 - z_1)\right], \tag{5}$$

and

$$\mathcal{T}_{10} = \frac{2c_0}{c_0 + c_1[1 + F(\omega)/Q_1]^{-1}} \exp\left[i\frac{\omega}{c_1}\frac{F(\omega)}{Q_1}(z_2 - z_1)\right]. \tag{6}$$

The transmission has been altered in two ways. First, the wave amplitude/phase is altered as it crosses the boundary at z_1 going down and coming up; this small but potentially informative filtering operation on the field also has an impact on reflection coefficients (Lam et al., 2004), in our case R_2. Much more important, however, are the new exponential terms, sensitive to the properties and extent of the absorbing medium above the reflection point; this operator decays the amplitudes in accordance with the attenuation law. Separating out the components of eqns (5)–(6) that do not contribute to this (dominant) exponential amplitude attenuation into a multiplicative factor W, the combined effective transmission coefficients due to the absorbing overburden may be expressed as

$$\mathcal{T}_{01}\mathcal{T}_{10}(z_2) = W \exp\left[-\omega \frac{1}{c_1 Q_1}(z_2 - z_1)\right]. \tag{7}$$

Generalizing to an arbitrary $c(z)$, $Q(z)$ profile above a reflector at depth z, and considering only the amplitude, we have

$$|\mathcal{T}_{01}\mathcal{T}_{10}(z)| \approx \exp\left[-\omega \int_0^z \frac{dz'}{c(z')Q(z')}\right]. \tag{8}$$

4 Estimating the integrated Q-profile

The internal multiple attenuation algorithm requires no knowledge of nor assumptions about the medium giving rise to the data (Weglein et al., 1997). What we are proposing is the use of the error in the algorithm in an *ad hoc* estimation scheme whose assumptions and requirements are independent of those of the algorithm. With that in mind, let us consider that a number of circumstances are in place. First, we have measured data above a reflector of interest; second, this reflector acts as the generator of an internal multiple; third, that the multiple is sufficiently separable within the data set (and the prediction) that its local spectrum may be estimated.

Weglein and Matson (1998) show analytically in a single layer acoustic case that the predicted internal multiple amplitude PRED and the actual internal multiple amplitude MULT are related by

$$\text{PRED} = T_{01}T_{10}\ \text{MULT}, \tag{9}$$

where the transmission coefficients are as defined in the previous section. To determine the transmission loss down to and across the generator requires the ratio of the predicted and actual multiples to be calculated, viz.

$$T_{01}T_{10} = \frac{\text{PRED}}{\text{MULT}}. \tag{10}$$

In the case of an attenuating overburden, the transmission down to and across a given reflector has been generalized and approximated in equation (8). That is, upon estimating the spectra of the

actual and predicted multiple, we surmise their ratio is related to Q by

$$\left|\frac{\mathrm{PRED}(\omega)}{\mathrm{MULT}(\omega)}\right| \approx \exp\left[-\omega \int_0^z \frac{dz'}{c(z')Q(z')}\right]. \tag{11}$$

This allows us access to the integrated effect of Q down to the generator. Calling

$$\mathrm{QC} \equiv \int_0^z \frac{dz'}{c(z')Q(z')}, \tag{12}$$

we have

$$\mathrm{QC} \approx -\frac{1}{\omega} \log\left|\frac{\mathrm{PRED}(\omega)}{\mathrm{MULT}(\omega)}\right|. \tag{13}$$

Notice that QC is independent of ω and hence may be estimated at any available frequency; or, all available frequencies may be used in (say) a least-squares estimation procedure. This situation is of course contingent on the particular Q model we have chosen.

Dealing with additional scalar error in the prediction

As a practical matter (that may occur when, e.g., using packaged FFT algorithms), when computing the internal multiple prediction, we may further wish to guard against the case in which the multiple prediction is modified by an unknown scalar factor, that is, in which the relation

$$A\left|\frac{\mathrm{PRED}(\omega)}{\mathrm{MULT}(\omega)}\right| \approx e^{-\omega \mathrm{QC}}, \tag{14}$$

with A unknown, holds. In the absence of attenuation there is no recourse, but the frequency-dependence (spectral shape) arising in the attenuation case provides an alternate route. Consider two frequencies in the spectrum, ω_1 and ω_2; since each provides a valid estimate of QC, we may calculate equation (14) with each, and divide, canceling out the scalar error and leaving

$$\left|\frac{\mathrm{PRED}(\omega_1)\mathrm{MULT}(\omega_2)}{\mathrm{MULT}(\omega_1)\mathrm{PRED}(\omega_2)}\right| \approx e^{-(\omega_1-\omega_2)\mathrm{QC}}, \tag{15}$$

which leads to a further slightly altered estimation

$$\mathrm{QC}(\omega_1,\omega_2) \approx -\frac{1}{\omega_1-\omega_2} \log\left|\frac{\mathrm{PRED}(\omega_1)\mathrm{MULT}(\omega_2)}{\mathrm{MULT}(\omega_1)\mathrm{PRED}(\omega_2)}\right|. \tag{16}$$

For further robustness, QC can be averaged thus over all available pairs of frequencies in the experiment.

5 Synthetic examples

In this section we present synthetic testing of the estimation procedure proposed in the previous section, using a layered medium with changing absorptive properties (Q). See Table 1.

Layer depths (m)	c (m/s)	Model Q_1	Q_2	Q_3	Q_4	Q_5	Q_6	Q_7	Q_8	Q_9	Q_{10}
000-300	1500	∞	∞	∞	∞	∞	∞	∞	∞	∞	∞
300-480	2200	300	200	150	100	80	75	60	50	30	20
480-855	2800	150	100	75	50	40	37.5	30	25	15	10
855-∞	3300	75	50	37.5	25	20	18.0	15	12.5	7.5	5

Table 1. *10 two-layer Earth models. First (left-most) column contains the depths of the layers; second contains the fixed layer velocities; the remaining columns contain the 10 sets of layer Q values used. Q_n is the name of the n'th model.*

The internal multiple algorithm of equation (1) is applied to these data, predicting the polarity-reversed internal multiple (an example data set is illustrated in Figure 2b for the case of Q=300). The spectra of the predicted and actual multiples are computed and compared (Figure 3a). Per the developments of the previous section, within the chosen Q model we may estimate QC (the integrated $Q(z)$, $c(z)$ profile down to the internal multiple generator) either with the absolute amplitudes of the spectra (Figure 3a), or with their relative shape (Figure 3b). The latter of these is here illustrated by shifting the actual spectrum such that the lowest frequency matches that of the predicted spectrum. We perform the same procedure for each one of the Q-models, using their relative shape and equation (7). Then we compare the estimated values with the values of QC_{int}.

The spectral shape approach involves choosing sets of frequency values to be used in pairs. To determine these, we first defined a frequency interval from which to choose such pairs that is consistent with seismic frequencies, from 12–86 Hz. Within this interval a set of 7 frequency pairs were tested (see Table 2).

Interval	Freq. 1	Freq. 2
Pair 1	12	16
Pair 2	12	20
Pair 3	20	27
Pair 4	27	47
Pair 5	47	66
Pair 6	66	86
Pair 7	12	86

Table 2. *Frequency pairs tested.*

Each of the 10 data sets were subjected to the estimation procedure for each frequency pair. The full results are tabulated in Appendix A; here we focus on some details. In particular, especially for lower Q (i.e., greater attenuation), we find that the estimated QC values are variable from pair

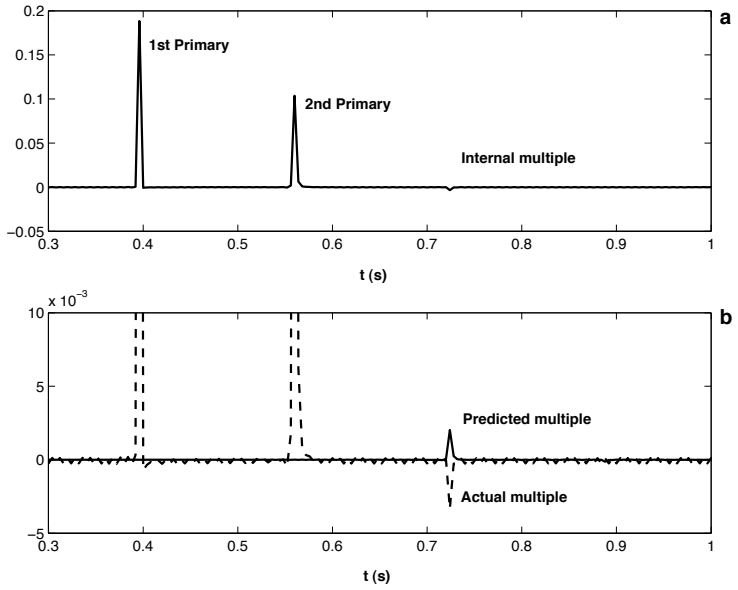

Figure 2: *Synthetic data. The requisite events in a normal incidence data set from a single absorptive layer are computed (***a***); the internal multiple is then predicted (***b***)and the predicted and actual events are compared.*

to pair (see the comparison between QC estimates for models 1 vs. 9, in Table 3). This is not an unexpected result. At high frequencies, the influence of Q is greatest, but because these frequencies have been preferentially suppressed, so has useable signal. Meanwhile, at low frequencies, where the signal is intact, Q has had no influence to be detected. Hence, we expect going in that some pairs of frequencies will be more amenable than others to providing stable, accurate estimation.

Pair	Model Q_9	Model Q_1
1	0.0004	0.0001
2	0.0029	0.0002
3	-0.0001	-0.0002
4	0.0002	0.0002
5	0.0041	0.0002
6	0.0008	0.0001
7	0.0022	0.0002

Table 3. *QC estimate for a model with large Q and a model with small Q at each of the 7 frequency pairs. See Table 1.*

Comparing the estimated to the known, exact values of QC, we find overall favorable results (see Appendix A), but that the best estimates are *always* found, for all models tested, with the frequency pair (12 Hz, 20 Hz) for each Q-models. Interestingly, all other (less accurate) estimates were too

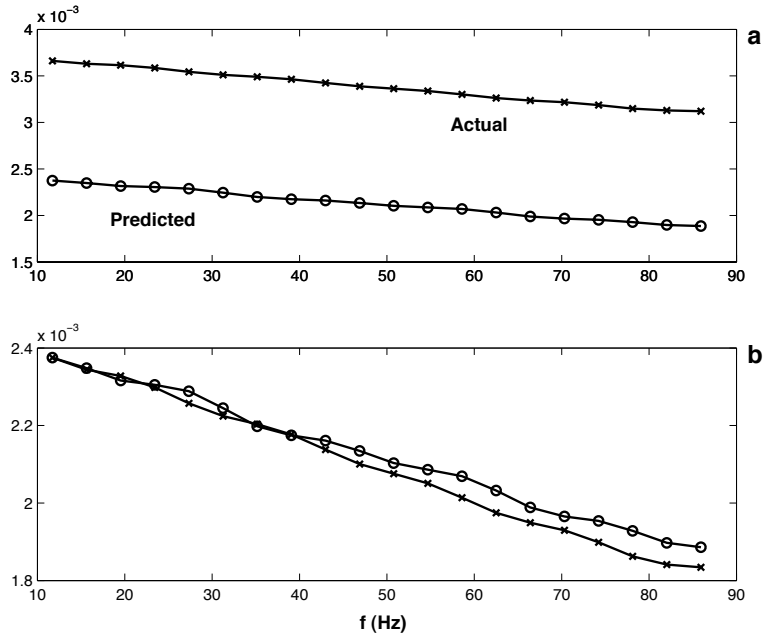

Figure 3: *Predicted vs. actual multiple spectra. The multiples may be compared in terms of (***a***) their absolute amplitudes, or (***b***) their relative spectral shape.*

small. Table 4 contains the actual and the predicted values of QC for the frequency pair (12 Hz, 20 Hz).

Model No.	Actual QC	QC-Est.
Q_{10}	0.0040	0.0043
Q_9	0.0029	0.0027
Q_8	0.0016	0.0016
Q_7	0.0014	0.0013
Q_6	0.0011	0.0010
Q_5	0.0010	0.0010
Q_4	0.0008	0.0008
Q_3	0.0005	0.0005
Q_2	0.0004	0.0004
Q_1	0.0003	0.0002

Table 4. *Estimated QC vs. actual QC for all 10 models using the frequency pair (12 Hz, 20 Hz).*

The integrated effect of Q down to the multiple generator interface was estimated and its values displayed on previous table. Strictly in order to better convey the accuracy of the prediction, let us use an assumed single layer (which we know to be the model) to estimate Q values from the integrated profiles, and compare them to the actual Q of each model. These are displayed in Table 5.

Model No.	Actual Q	Q-Est.
Q_1	20.00	19.07
Q_2	30.00	28.28
Q_3	50.00	51.25
Q_4	60.00	63.08
Q_5	75.00	82.00
Q_6	80.00	85.11
Q_7	100.00	102.50
Q_8	150.00	169.46
Q_9	200.00	205.00
Q_{10}	300.00	410.00

Table 5. *Estimated Q vs. actual Q for all 10 models using the frequency pair (12 Hz, 20 Hz).*

6 Conclusions

We have proposed that a discrepancy between a certain version of the inverse scattering series internal multiple attenuation algorithm be exploited to address the problem of estimating and removing overburden effects on reflected primaries. This includes, for instance, characterizing a Q profile down to and across an isolated internal multiple generator.

The results shown on table 4 encourage us to keep on working. Among several chosen pairs the best results were achieved between frequencies of 12 to 20 Hz for all models. The reason why it is the best interval is still not clear, we are investigating this at the moment. We intend to analyze these results for data with different frequency contents.

We anticipate that the information garnered from this specific application of the broad potential we are introducing, would be useful in two ways. First, it can be brought into a Q compensation operator and used to correct the primary in terms of resolution (as well as overall amplitude/phase). Second, within a further set of assumptions, it can be used to estimate the Q profile itself. As part of this ongoing study we further anticipate examination of a number of extensions of the methodology. First, to layered media with offset data, and beyond to multidimensional subsurface structure. Second, to more complete descriptions of the overburden in addition to acceptable Q models, e.g., elastic, for whom the transmission error has already been studied and characterized (Weglein et al., 2003).

The calculation of Q-values was used just to give a better idea of the accuracy of the procedure, since the main idea is to progress into a compensation operator without the need of finding the Q-values itself. The values displayed on table 5 show encouraging results for the procedure presented on this paper. We understand that there are several different kinds of models, with different features and properties, that we could have tested the procedure. But this is the beginning of a research and we intend to test and analyze the method for different models in the near future.

Finally, let us reiterate the broad beneficial aspects of the methodology we are developing: first, the information to be derived comes at no additional cost; second, it is derived at a convenient point during processing; third, it is consistent with wave-theoretic processing; fourth, it is applicable in reconnaissance and exploration as well as production settings; and fifth, it has the potential to transform the non-linear inverse scattering target identification series into an exploration tool, by eliminating the requirement for a well-tie.

7 Acknowledgments

Kris Innanen, Art Weglein, and Adriana Ramirez were supported by the DOE Basic Energy Sciences award DE-FG02-05ER15697; Art Weglein and Adriana Ramirez were supported by the NSF-CMG award DMS-0327778. The support of the M-OSRP sponsors is also gratefully acknowledged.

References

Aki, K. and P. G. Richards. *Quantitative Seismology.* 2nd edition. University Science Books, 2002.

Araújo, F. V. *Linear and non-linear methods derived from scattering theory: backscattered tomography and internal multiple attenuation.* PhD thesis, Universidade Federal da Bahia, 1994.

Kaplan, S. T., B. Robinson, and K. A. Innanen. "Optimizing internal multiple attenuation algorithms for large distributed computing systems." *Mission-Oriented Seismic Research Program (M-OSRP) Annual Report* (2005).

Kjartansson, E. "Constant-Q Wave Propagation and Attenuation." *Journal of Geophysical Research* 84 (1979): 4737–4748.

Lam, C. H., B. J. Kooij, and A. T. de Hoop. "Impulsive sound reflection from an absorptive and dispersive planar boundary." *J. Acoust. Soc. Am.* 116 (2004): 677–685.

Nita, B. G. and A. B. Weglein. "Imaging with tau=0 versus t=0: implications for the inverse scattering internal multiple attenuation algorithm." *Proceedings of the 74th Annual Meeting of the Society of Exploration Geophysicists, Denver, CO.* . Soc. Expl. Geophys., 2004.

Ramírez, A. C. and A.B. Weglein. "An inverse scattering internal multiple elimination method: Beyond attenuation, a new algorithm and initial tests." *SEG Expanded Abstracts.* (2005): 2115–2118.

Ramírez, A. C. and A.B. Weglein. "Progressing the analysis of the phase and amplitude prediction properties of the inverse scattering internal multiple attenuation algorithm.." *J. of Seismic Expl.* 13 (2005): 283–301.

Weglein, A. B. and K. H. Matson. "Inverse Scattering Internal Multiple Attenuation: An Analytic Example and Subevent interpretation." *SPIE Conference on Mathematical Methods in Geophysical Imaging.* 1998, 108–117.

Weglein, Arthur B., Fernanda V. Araújo, Paulo M. Carvalho, Robert H. Stolt, Kenneth H. Matson, Richard T. Coats, Dennis Corrigan, Douglas J. Foster, Simon A. Shaw, and Haiyan Zhang. "Inverse Scattering Series and Seismic Exploration." *Inverse Problems* (2003): R27–R83.

Weglein, Arthur B., Fernanda Araújo Gasparotto, Paulo M. Carvalho, and Robert H. Stolt. "An Inverse-Scattering Series Method for Attenuating Multiples in Seismic Reflection Data." *Geophysics* 62 (November-December 1997): 1975–1989.

Zhang, H. and A.B. Weglein. "The inverse scattering series for tasks associated with primaries: depth imaging and direct non-linear inversion of 1D variable velocity and density acoustic media." *SEG Technical Program Expanded Abstracts.* 2005, 1705–1708.

8 Appendix A

In this section we displayed the QC values generated from the Q-models presented in the main text. The following table shows the estimate values of QC_{int} for every Q-model and for all frequency intervals. The variability of the estimations decreases with the increase in Q values. The best estimates are shown in bold face.

Pair	Q_{10}	Q_9	Q_8	Q_7	Q_6	Q_5	Q_4	Q_3	Q_2	Q_1
1	-0.0002	0.0004	0.0006	0.0006	0.0005	0.0005	0.0004	0.0003	0.0002	0.0001
2	**0.0043**	**0.0029**	**0.0016**	**0.0013**	**0.0010**	**0.0010**	**0.0008**	**0.0005**	**0.0004**	**0.0002**
3	0.0016	-0.0001	-0.0004	-0.0004	-0.0004	-0.0004	-0.0004	-0.0003	-0.0002	-0.0002
4	0.0034	0.0002	0.0013	0.0010	0.0008	0.0007	0.0005	0.0003	0.0002	0.0002
5	0.0091	0.0041	0.0015	0.0011	0.0007	0.0007	0.0005	0.0003	0.0002	0.0002
6	-0.0008	0.0008	0.0002	0.0001	0.0000	0.0000	0.0000	0.0001	0.0001	0.0001
7	0.0037	0.0022	0.0009	0.0007	0.0005	0.0004	0.0003	0.0002	0.0002	0.0002

Table 3. *QC estimation values tabulated for all models and frequency pairs.*

Inverse scattering internal multiple elimination

A. C. Ramírez, A. B. Weglein and S. A. Shaw[1]
[1] *ConocoPhillips*

Abstract

The inverse scattering processing methods use nonlinear combinations of measured data and propagation in a reference medium. The method for multiple attenuation, based on the inverse scattering series, first separates free-surface multiples from primaries and internal multiples, and, subsequently, primaries from internal multiples. The separation is performed through task specific series in terms of measured data and propagation in reference medium. These series result in distinct algorithms for free-surface and internal multiple removal and neither requires a model of the subsurface reflectors that generate the multiples. The free-surface algorithm predicts free-surface multiples from data composed of primaries, internal, and free-surface multiples; the internal-multiple algorithm predicts internal multiples from data that consists of primaries and internal multiples.

Internal multiples are distinguished from primaries in the measured wavefield because primaries only experience one upward reflection in the subsurface while internal multiples experience at least one downward reflection (two upward reflections) in the subsurface. The first term in the subseries for internal multiple elimination is an attenuator. It predicts the correct travel time and an amplitude always less than the true internal multiples' amplitude. The leading and higher order terms in the elimination series corrects the amplitude predicted by the attenuator moving the algorithm towards an eliminator. The leading order terms in this series are identified as terms in a subseries with nonlinear self-interactions at the generating reflector. The location where the downward reflection of the first order internal multiple takes place is called the genarating reflector. Adding the leading order terms, we obtain a leading order closed form that eliminates all internal multiples generated at the first reflector and improves the attenuation of the remaining multiples. A second subseries improved the elimination of internal multiples generated at deeper reflectors. The main part of this second subseries is summed to find a higher order closed form that eliminates the internal multiples generated at the second reflector and further improves the reduction of all internal multiples.

1 Introduction

There has been a renewed interest in the elimination of internal multiples from measured seismic data in the literature and in the energy industry. This interest concerns on possible ways to extend and advance beyond current capability. To that end it is natural to pursue an examination of the ideas behind the wave theoretic inverse scattering internal multiple algorithm. This data driven method is derived from a formalism based on the inverse scattering series, where a piece of the third equation, that allowed for a *lower-higher-lower* diagram resembling the ray-form of

an internal multiple, was found to start a series that removes all internal multiples without any subsurface information (Weglein et al., 1981; Araújo, 1994; Weglein et al., 2003).

The first research efforts to attenuate internal multiples from marine seismic data without using any knowledge of the subsurface were done by Araújo et al. (1994) and Weglein et al. (1997). Attenuation refers to the amplitude reduction of certain event, or sets of events, in the seismic data. The algorithm derived by Araújo et al. (1994) and Weglein et al. (1997) is the first term in an infinite series that deals with internal multiple elimination. It is known as the attenuator. An analysis of the effectiveness of the attenuator shows that its travel time prediction is exact and the difference between elimination and attenuation resides in extra transmission coefficients in the prediction, when compared to the true multiple in the data(Weglein et al., 2003; Ramírez and Weglein, 2005b). The extra transmission coefficients correspond to coefficients down to, and including, the internal multiple's shallowest downward reflection. For example, an internal multiple having its shallowest downward reflection at the water bottom, in a marine experiment, has an error in its prediction related to the transmission coefficients at the water bottom. This error, or attenuation factor, is totally and completely independent of how many layers and how deep into the earth the multiple travels below the water bottom.

The first research efforts to address the complete removal of internal multiples from marine seismic data, without destroying primary reflections and without any subsurface information, were done by Ramírez and Weglein (2005a) (for the interested reader, a timetable with history highlights for the internal multiple is provided in Figure 1). Elimination refers to a complete removal of the amplitude of that event, or set of events, from the data. The overall purpose to develop a theory to eliminate internal multiples is to place internal multiples and free-surface multiples on the same footing (Carvalho, 1992; Weglein et al., 1997, 2003). The objective is to reach the same level of elimination effectiveness that the free-surface algorithm has, in which each single term completely removes all free-surface multiples of a certain order.

In seismic exploration, there are circumstances when: 1) internal multiple identification, or attenuation, is sufficient; and 2) when a residual, left from internal multiple attenuation, is a challenge and impediment for further processing. Depending on which of these circumstances are been faced (*e.g.* depending on the details of the geology and the level of ambition and demands of the processing and exploration objectives) an attenuator or an eliminator of internal multiples would be required. Among the circumstances when internal multiple elimination would provide value above that provided by an attenuator (for towed streamer marine data) are: 1) converted wave internal multiples; 2) proximal, or interfering, primaries and internal multiples at the target; 3) when there is a need to reduce the burden on adaptive subtraction to account for missing deterministic predictive capability. It is anticipated that internal multiple elimination will place greater demands on preprocessing steps such as data collection and wavelet estimation.

The methods presented here never move from not needing to need subsurface information when we progress from attenuate to eliminating internal multiples.

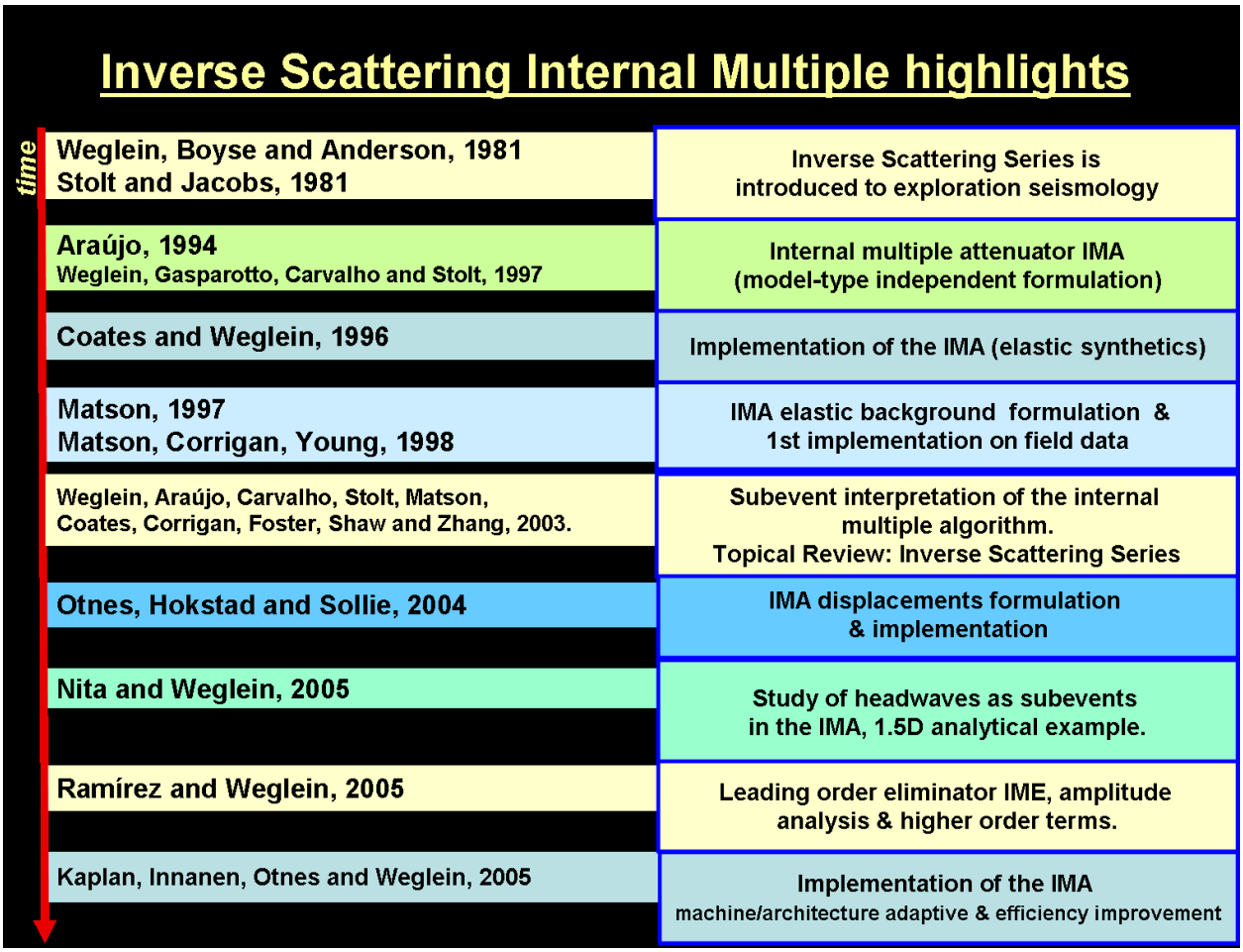

Figure 1: History highlights

Prerequisites for internal multiple elimination

The inverse scattering series task associated with internal multiple removal promises to accomplish its objective directly in terms of the measured data and reference propagation (Weglein et al., 2003). It never assumes that the reference medium is the actual. The reference medium is never moved or altered towards the actual. Inverse scattering internal multiple elimination is a wave equation demultiple approach that does not make assumptions about the earth below the receivers, nevertheless, it is subject to some constrains or prerequisites. It assumes that the data have been deghosted, there are no free-surface multiples and the source wavelet is known. For the most common practical implementations, the source wavelet is estimated during the multiple subtraction process by assuming that the source signature is the one that minimizes the energy in the demultipled wavefield. The energy minimizing adaptive subtraction, is often useful. However, it tends to fail precisely under the most complex circumstances where the underlying demultiple methods have their greatest strengths. For example, when interfering events and multiples of different orders

are proximal to primaries, adaptive subtraction will eliminate the primary along with the multiple. Hence, the internal multiple elimination have a high bar on the source signature estimation as well as deghosting and free-surface multiple elimination. If we are able to satisfy this high bar of prerequisite, then the internal multiple elimination method would have the opportunity to reach its potential. The work that Guo et al. (2005) and Zhang and Weglein (2006) have pioneered provide new robust methods for wavelet estimation and deghosting, respectively. These new methods, and further developments, will help to satisfy the prerequisites of the internal multiple algorithm.

Internal multiple elimination

The third term in the inverse scattering series: $(G_0V_1G_0V_1G_0V_1G_0)$ contains the leading order contribution for the removal series of 1^{st} order internal multiples (Weglein et al., 1997). This leading order term is the internal multiple attenuator Araújo et al. (1994).

To simplify the analysis of the attenuator, a medium that only varies in depth will be assumed. The $1D$ earth and normal incidence wave version (Weglein et al., 2003) of the first order internal multiple attenuator is

$$b_1(k) = D(\omega), \tag{1}$$

$$b_3^{IM_1}(k) = \int_{-\infty}^{\infty} dz_1 e^{ikz_1} b_1(z_1) \int_{-\infty}^{z_1-\epsilon} dz_2 e^{-ikz_2} b_1(z_2) \int_{z_2+\epsilon}^{\infty} dz_3 e^{ikz_3} b_1(z_3), \tag{2}$$

where $k = 2\frac{\omega}{c_0}$ is the vertical wave number, $D(\omega)$ is the temporal Fourier transform of the measured scattered field (data), ϵ is a small positive parameter chosen to insure that the relations $z_1 > z_2$ and $z_3 > z_2$ are satisfied, the pseudodepths z_1 and z_2 are defined with the reference velocity c_0 to be $z_i = \frac{c_0 t_i}{2}$, and the superscript IM_1 refers to the $1st$ order internal multiple elimination series.

The attenuator's prediction is performed by a nonlinear combination of three sets of data. This nonlinear combination predicts the exact travel time and an amplitude estimate of the true internal multiple in the data. The estimate is always less than the actual amplitude. The difference between the estimate and the true amplitude is the attenuation factor given by the formula (Ramírez and Weglein, 2005b)

$$(AF_{P.IM})_j = \begin{cases} T_{01}T_{10} & \text{for } j = 1 \\ \\ \Pi_{i=1}^{j-1} \left(T_{i\ i-1}^2 T_{i-1\ i}^2\right) T_{j\ j-1} T_{j-1\ j} & \text{for } 1 < j < J \end{cases} \tag{3}$$

where j represents the generating reflector, $T_{j-1\ j}$ and $T_{j\ j-1}$ are the transmission coefficients going down and up through the interface j, respectively, and J is the total number of interfaces in the model. The interfaces are numbered with integers, starting with the shallowest location. In a single layer medium, the first order internal multiple has an amplitude of $-T_{01}R_2R_1R_2T_{10}$ and $b_3^{IM_1}$ predicts a first order internal multiple with an amplitude of $T_{01}T_{10}R_2R_1R_2T_{10}T_{01}$. In agreement with equation (3), the predicted internal multiple is attenuated by a factor of $T_{01}T_{10}$ when compared to the true internal multiple. The attenuation factor, equation(3), is affected by

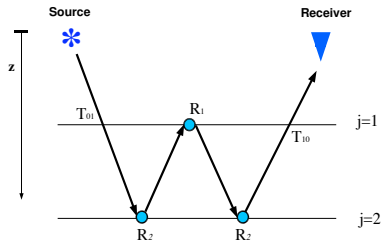

Figure 2: *First order internal multiple with downward reflection at $j = 1$.*

the history of the event down to and including only the depth of the generating reflector. It is a factor independent of the place where the two upward reflections occurred.

The first order internal multiple elimination series starts with $b_3^{IM_1}$. The multiples are predicted as traces in the same form as the effective data. The attenuation process is a simple addition $b_1 + b_3^{IM_1}$, since $b_3^{IM_1}$ contains internal multiples with opposite sign to the ones in the effective data. Each internal multiple predicted by $b_3^{IM_1}$, and generated at a certain j reflector, is attenuated by a factor of $(AF_{P.IM})_j$. The purpose of the higher order terms in the elimination series is to remove the effect of the attenuation factor. The higher order terms improve the effectiveness of the attenuator towards the objective of completely subtract the amplitude of multiples within the data. In order to achieve an elimination method, the inverse scattering subseries for internal multiple elimination must be able to predict the true amplitude for these events.

In the attenuator's prediction, the factor that multiplies the internal multiples generated at the first reflector, $(IM)_{j=1}$, is $T_{01}T_{10}$. Analytic analysis of this algorithm (Weglein et al., 2003; Ramírez and Weglein, 2005b) shows that this attenuation factor corresponds to the first term in the Taylor expansion of $(T_{01}T_{10})/(T_{01}T_{10}) = 1$,

$$\begin{aligned} T_{01}T_{10}\left(\frac{1}{T_{01}T_{10}}\right) &= T_{01}T_{10}\frac{1}{(1-R_1^2)} \\ &= T_{01}T_{10}\left(1 + R_1^2 + R_1^4 + R_1^6 + R_1^8 \cdots\right) \quad . \end{aligned} \tag{4}$$

Following the same analysis, it is found that the factor $(T_{01}T_{10})^2T_{12}T_{21}$ multiplying the prediction of internal multiples generated at the second reflector, $(IM)_{j=2}$, corresponds to the first term in the more complicated geometric series for:

$$\begin{aligned} \frac{(T_{01}T_{10})^2T_{12}T_{21}}{(T_{01}T_{10})^2T_{12}T_{21}} &= (T_{01}T_{10})^2T_{12}T_{21}\frac{1}{(1-R_1^2)^2(1-R_2^2)}, \\ &= (T_{01}T_{10})^2T_{12}T_{21}\left(1 + 2R_1^2 + R_2^2 + 3R_1^4 + 2R_2^2R_1^2 + \cdots\right). \end{aligned} \tag{5}$$

Each one of the terms in the Taylor expansions, equations (4) and (5), are calculated by higher order terms in the inverse scattering internal multiple elimination series. Identifying and adding these higher order terms builds a sum of amplitude corrections that improves the prediction and

subtraction of internal multiples from the data. The amplitude corrections are given by algorithms, found in the internal multiple elimination series $b_3^{IM_1} + b_5^{IM_1} + b_7^{IM_1} + \cdots$ (Ramírez and Weglein, 2005a), that only require measured values of the scattered field and the reference Green's function.

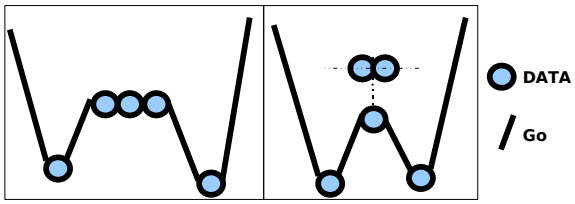

Figure 3: Diagrams for the fifth term in the internal multiple elimination series

The second term in the elimination series, ${b_5}^{IM_1}$, is fifth order in the data. It resides within the fifth term in the inverse series. It is the first step to move the attenuator towards an algorithm that eliminates 1^{st} order internal multiples. It is given by

$$\begin{aligned} b_5^{IM_1}(k) = & \int_{-\infty}^{\infty} dz e^{ikz} b_1(z) \\ & \times \int_{-\infty}^{z-\epsilon} dz' e^{-ikz'} \left[b_1(z')^3 + 2\, b_1(z') \int_{-\infty}^{z'-\epsilon} dz'''\, b_1(z''')^2 \right] \\ & \times \int_{z'+\epsilon}^{\infty} dz'' e^{ikz''} b_1(z''). \end{aligned} \tag{6}$$

and it can be separated in two parts (represented with the diagrams in Figure(3)),

$$\begin{aligned} b_{51}^{IM_1}(k) = & \int_{-\infty}^{\infty} dz e^{ikz} b_1(z) \\ & \times \int_{-\infty}^{z-\epsilon} dz' e^{-ikz'} b_1(z')^3 \int_{z'+\epsilon}^{\infty} dz'' e^{ikz''} b_1(z''), \end{aligned} \tag{7}$$

$$\begin{aligned} b_{52}^{IM_1}(k) = & \int_{-\infty}^{\infty} dz e^{ikz} b_1(z) \\ & \times \int_{-\infty}^{z-\epsilon} dz' e^{-ikz'} 2\, b_1(z') \int_{-\infty}^{z'-\epsilon} dz'''\, b_1(z''')^2 \int_{z'+\epsilon}^{\infty} dz'' e^{ikz''} b_1(z''). \end{aligned} \tag{8}$$

The diagram located on the left of Figure (3) corresponds to equation (7) and it belongs to a series that eliminates all 1^{st} order internal multiples that were downward reflected at the shallowest reflector. This term combines nonlinearly five sets of data. When added to the attenuator b_3 it provides extra amplitude information and the correct time of the internal multiples. The three hits in the diagram indicate triple self interaction at the generating reflector. Hence, the extra amplitude information given by the self-interacting data corresponds to powers of the reflection coefficient of each generating reflector, which is in agreement with the analysis in equations (4) and (5).

The analysis of the properties of this term, using its diagram representation and numerical examples, showed that it is the main contribution of $b_5^{IM_1}$ to the elimination of internal multiples (Ramírez and Weglein, 2005a). Its mathematical representation resembles the one of the attenuator, which is the leading order term of the series by itself. We can find the leading order terms by examining each term in the internal multiple elimination series and selecting the ones that only have data self-interactions at the generating reflector. The leading order terms are represented with the diagrams shown in Figure (4). The sum of these diagrams leads to the leading order closed form term

$$b_{LO}^{IM_1} = \int_{-\infty}^{\infty} dz e^{ikz} b_1(z) \times \int_{-\infty}^{z-\epsilon} dz' e^{-ikz'} \left(\frac{1}{1 - b_1(z')^2} \right) b_1(z') \int_{z'+\epsilon}^{\infty} dz'' e^{ikz''} b_1(z''). \quad (9)$$

This equation is the infinite sum of the main contributions in the inverse scattering internal multiple elimination series. It includes the first order term, the attenuator, and the main contribution from each subsequent term in the elimination series. The leading order eliminator, $b_{LO}^{IM_1}$, predicts all 1^{st} order internal multiples generated at the shallowest reflector without requiring a-priori information, nor a velocity model. The elimination step is performed in terms of the effective data, b_1, and the reference velocity contained in $k = \frac{2\omega}{c_0}$. Furthermore, the leading order eliminator helps to better attenuate all the internal multiples generated at deeper reflectors.

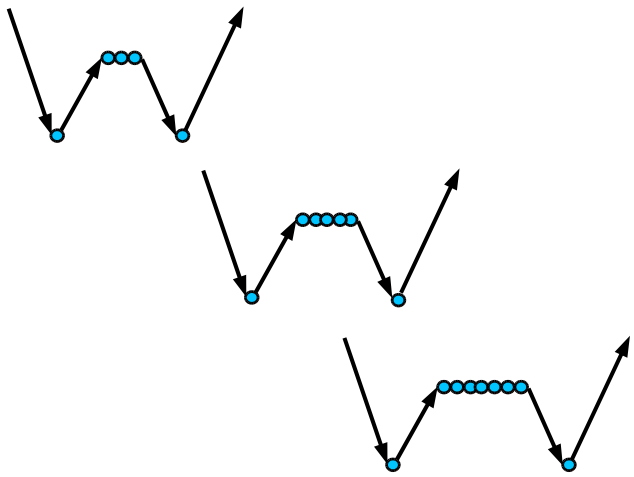

Figure 4: Leading order diagrams.

The diagram located on the right of Figure (3) represents equation (8). This equation contains $I = 2b_1(z') \int_{-\infty}^{z'-\epsilon} dz''' \, b_1(z''')^2$ in the middle integral. The term I, represented by the middle part of the diagram, has two self-interacting data within the overburden of the generating reflector. This double self interaction provides the series with second order corrections for any interface above the

generating reflector and, it only acts on internal multiples downward reflected at interfaces below the shallowest reflector. The internal multiples generated at the shallowest reflector are completely eliminated with the leading order closed form term in equation (9). The double self-interacting diagram further attenuates all 1^{st} order internal multiples generated at deeper reflectors[1]. The main part of these second subseries can be summed in a higher order closed form term,

$$b_{HO}^{IM_1} = \int_{-\infty}^{\infty} dz e^{ikz} b_1(z) \int_{-\infty}^{z-\epsilon} dz' e^{-ikz'} \frac{2G_1(z') \int_{-\infty}^{z'-\epsilon} dz''' \; J(z''')}{1 - \int_{-\infty}^{z'} dz''' \; J(z''')} \int_{z'+\epsilon}^{\infty} dz'' e^{ikz''} b_1(z''). \tag{10}$$

$$J(z''') = \frac{b_1(z''')^2}{1 - b_1(z''')^2} \tag{11}$$

$$G_1(z') = \frac{b_1(z')}{1 - b_1(z')^2} \tag{12}$$

The higher order eliminator, assumes that the action of the leading order eliminator has taken effect prior to its calculation. The leading order closed form added to the effective data eliminates all multiples generated at the first reflector. The only task left, in terms of internal multiples, is to finish correcting the amplitude of the deeper internal multiples and eliminate them. This is the task performed by the higher order eliminator, $b_{HO}^{IM_1}$.

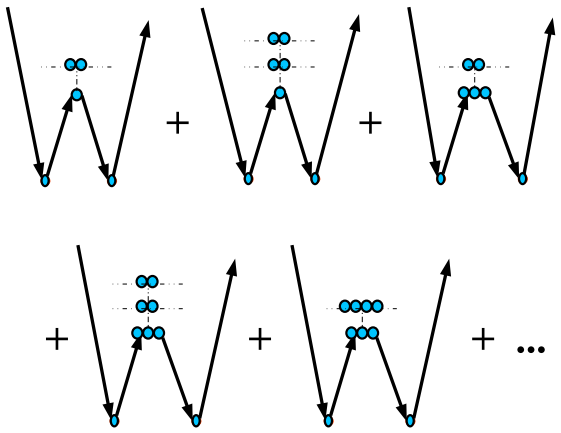

Figure 5: Higher order diagrams.

Some of the diagrams included in equation (10) are shown in Figure 5. Equation (10) is the infinite sum of the main terms in the higher order subseries of the internal multiple elimination series. The higher order eliminator includes diagrams that have extra data self-interactions above the generating reflector. The reason it is not including all the higher order terms is because, these terms in the inverse series for internal multiple elimination have different integer weights, which

[1]Where deeper refers to all reflector located below the shallowest one.

means that a specific higher order diagram is required to act more than once in the removal process. From the form of equation (10), the closed form only contains a weighting factor of 2 (please refer to the middle integral) in agreement to the weighting factor needed by equation 8. The first term included in the higher order closed form corresponds to equation 8, which is represented by the first diagram in Figure 5.

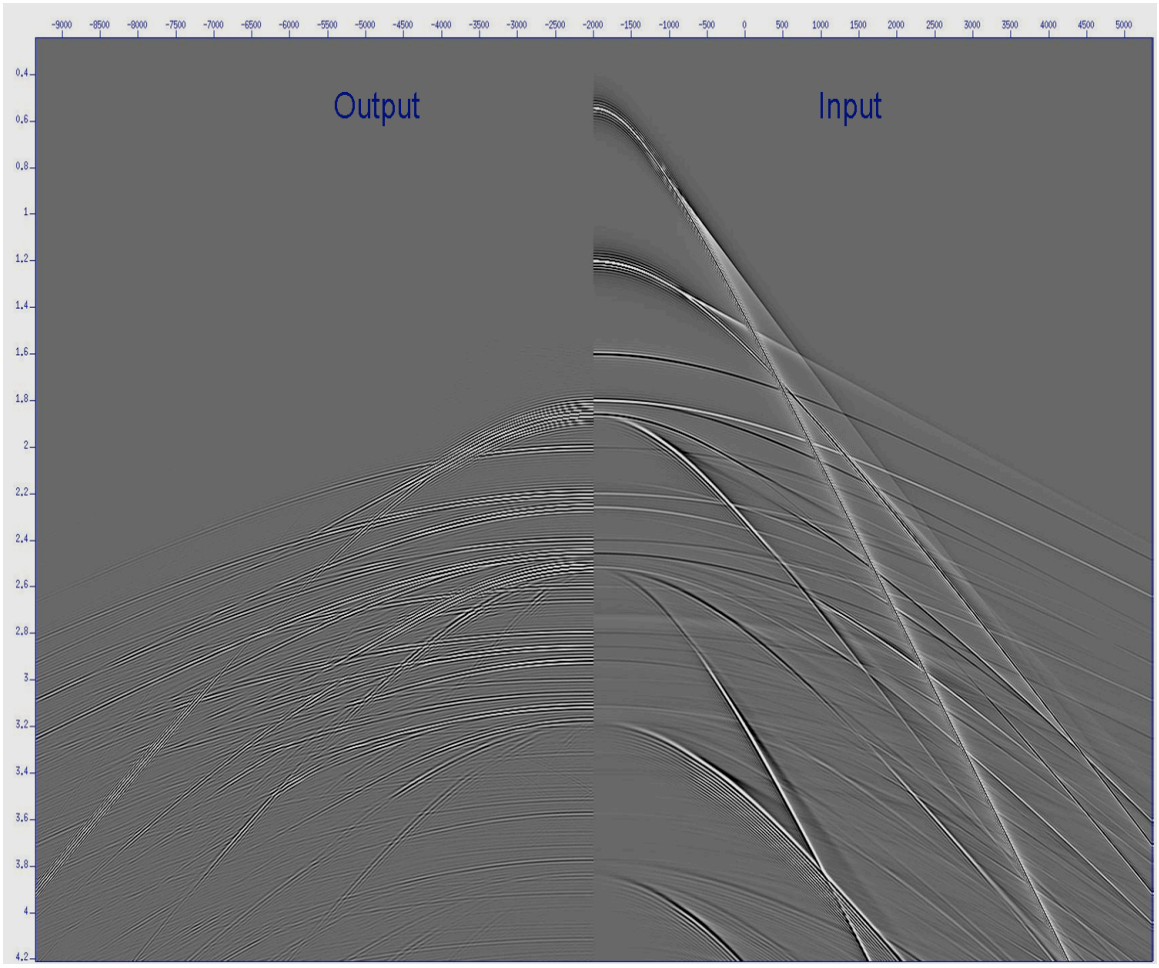

Figure 6: The left hand side shows the predicted internal multiples. The right hand side shows data containing primaries and internal multiples.

An elimination algorithm for internal multiples based on inverse scattering series has the potential of removing difficult internal multiples, leaving all primaries unaffected. Although the internal multiple amplitudes are reduced by the attenuator, $b_3^{IM_1}$, and substantially reduced (and a subset is eliminated) by the leading order closed form, $b_{LO}^{IM_1}$, there is in some cases an observable residual that can be further attenuated with the action of the higher order closed form, $b_{HO}^{IM_1}$. The higher order closed form term of the internal multiple elimination series complements the elimination of the amplitude of the remaining internal multiples by adding nonlinear contributions in terms of data and a reference Green's function. The combination of the leading order closed form with the

higher order closed form term gives an improved algorithm for the removal of internal multiples. A $1.5D$ numerical example of the internal multiple prediction with $b_{LO}^{IM_1}$ in a half space of water and a horizontally layered elastic medium representing the earth, is shown in Figure 6. The finite differences synthetic data, on the right of this figure, contains primaries and internal multiples due to an elastic halfspace. The traces on the right show the predicted internal multiples. Notice that all multiples were predicted at the exact time. The data were deconvolved with an statistical estimate of the wavelet. The wavelet used to model the data was not used in the internal multiple prediction. Hence, the predicted multiples have a different wavelet. The fact that the internal multiple elimination algorithm, with an acoustic background, predicts internal multiples propagated in an elastic Earth is a remarkable result of the model-type independent nature of the algorithm.

2 2D extension of the algorithm

In the theory presented in the previous section, no assumptions about the earth below the receivers are made, this characteristic makes it ideal for addressing one of the current challenges in exploration seismology: removing multiples, locating and identifying targets in highly complex medium. When the medium is complicated, an accurate velocity model that would allow modeling and subtraction of internal multiples is unobtainable. Hence, the extension to a multidimensional earth is a necessary step.

The attenuation algorithm for a $2D$ earth, presented in Araújo (1994); Weglein et al. (1997) and Weglein et al. (2003), is

$$b_1(k_g,k_s,q_g+q_s) = -2iq_sD(k_g,k_s,\omega), \tag{13}$$

$$\begin{aligned} b_3^{IM_1}(k_g,k_s,q_g+q_s) = \frac{1}{(2\pi)^2}\int_{-\infty}^{\infty} dk_1 e^{iq_1(x_s-x_g)}\int_{-\infty}^{\infty} dk_2 e^{iq_2(\epsilon_g-\epsilon_s)} \\ \times\int_{-\infty}^{\infty} dz_1 e^{i(q_g+q_1)z_1} b_1(k_g,-k_1,z_1) \\ \times\int_{-\infty}^{z_1-\epsilon_2} dz_2 e^{i(-q_1-q_2)z_2} b_1(k_1,-k_2,z_2) \\ \times\int_{z_2+\epsilon_1}^{\infty} dz_3 e^{i(q_2+q_s)z_3} b_1(k_2,-k_s,z_3), \end{aligned} \tag{14}$$

where ω represents the temporal frequency, c_0 is the acoustic velocity of water; k_g and k_s are the horizontal wave numbers corresponding to receiver and source coordinates: x_g and x_s, respectively; the 2-D wave vectors: $\mathbf{k}_g = (k_g, -q_g)$ and $\mathbf{k}_s = (k_s, q_s)$ are constrained by $|\mathbf{k}_g| = |\mathbf{k}_s| = \frac{\omega}{c_0}$; the vertical wave numbers are $q_g = sign(\omega)\sqrt{(\frac{\omega}{c_0})^2 - {k_g}^2}$ and $q_s = sgn(\omega)\sqrt{(\frac{\omega}{c_0})^2 - {k_s}^2}$, and ϵ_i is a small positive parameter chosen to insure that the relations $z_1 > z_2$ and $z_3 > z_2$ are satisfied.

In equations (13) and (14), the effective data $b_1(k_g,k_s,q_g+q_s)$ is defined as a source obliquity factor times the $2D$ measured values of the scattered field, D. The variable z is the Fourier conjugate to the sum of the vertical wave numbers, $k_z = -(q_g+q_s)$. The attenuation of multiples is performed by adding the attenuator, $b_3^{IM_1}$, to the effective data, b_1.

As we showed in $1D$, the second term in the 1^{st} order internal multiple elimination series can be separated in two equations. The 2D form, of the first equation is

$$\begin{aligned} b_{51}^{IM_1}(k_g,k_s,q_g+q_s) = \frac{1}{(2\pi)^2}\int_{-\infty}^{\infty} dk_1 e^{iq_1(x_s-x_g)} \int_{-\infty}^{\infty} dk_2 e^{iq_2(\epsilon_g-\epsilon_s)} \\ \times \int_{-\infty}^{\infty} dz_1 e^{i(q_g+q_1)z_1} b_1(k_g,-k_1,z_1) \\ \times \int_{-\infty}^{z_1-\epsilon_2} dz_2 e^{i(-q_1-q_2)z_2} \left[b_1(k_1,-k_2,z_2)\right]^3 \\ \times \int_{z_2+\epsilon_1}^{\infty} dz_3 e^{i(q_2+q_s)z_3} b_1(k_2,-k_s,z_3), \end{aligned} \tag{15}$$

which have the same diagrammatic representation as shown in Figure (3). Studying the higher order terms in the inverse scattering internal multiple elimination series in a multidimensional model type independent form, we find that the form of the terms with self-interacting data at the generating reflector conserves the properties and characteristics found in the simple $1D$ case. Analogous to the $1D$ case, the first term in the leading order elimination series is the attenuator, equation (18), and the second term is given by equation (15). The next terms in the leading order series have the form:

$$\begin{aligned} b_{51}^{IM_1}(k_g,k_s,q_g+q_s) = \sum_{N=0}^{\infty} \frac{1}{(2\pi)^2}\int_{-\infty}^{\infty} dk_1 e^{iq_1(x_s-x_g)} \int_{-\infty}^{\infty} dk_2 e^{iq_2(\epsilon_g-\epsilon_s)} \\ \times \int_{-\infty}^{\infty} dz_1 e^{i(q_g+q_1)z_1} b_1(k_g,-k_1,z_1) \\ \times \int_{-\infty}^{z_1-\epsilon_2} dz_2 e^{i(-q_1-q_2)z_2} \left[b_1(k_1,-k_2,z_2)\right]^{2N+1} \\ \times \int_{z_2+\epsilon_1}^{\infty} dz_3 e^{i(q_2+q_s)z_3} b_1(k_2,-k_s,z_3), \end{aligned} \tag{16}$$

We can add the leading order terms in the multidimensional case to a closed form, which is given by,

$$b_1(k_g,k_s,q_g+q_s) = -2iq_s D(k_g,k_s,\omega), \tag{17}$$

$$\begin{aligned} b_{LO}^{IM}(k_g,k_s,q_g+q_s) = \frac{1}{(2\pi)^2}\int_{-\infty}^{\infty} dk_1 e^{iq_1(x_s-x_g)} \int_{-\infty}^{\infty} dk_2 e^{iq_2(\epsilon_g-\epsilon_s)} \\ \times \int_{-\infty}^{\infty} dz_1 e^{i(q_g+q_1)z_1} b_1(k_g,-k_1,z_1) \\ \times \int_{-\infty}^{z_1-\epsilon_2} dz_2 e^{i(-q_1-q_2)z_2} \frac{b_1(k_1,-k_2,z_2)}{1-b_1(k_1,-k_2,z_2)^2} \\ \times \int_{z_2+\epsilon_1}^{\infty} dz_3 e^{i(q_2+q_s)z_3} b_1(k_2,-k_s,z_3), \end{aligned} \tag{18}$$

This is a $2D$ model type independent leading order elimination algorithm for internal multiples. The leading order eliminator is a data-driven algorithm written in terms of effective data b_1 (see

equation (17)). The leading order closed form, $b_{LO}^{IM_1}$, gives the main contribution towards eliminating internal multiples. It completely removes all 1^{st} order internal multiples generated at the first reflector and improves the attenuation of the remaining multiples. Leading order as an eliminator means it eliminates a class of internal multiples and further attenuates the rest. In a $2D$ medium, the multiples that have no cumulative transmission error (the ones with downward reflection at the shallowest reflector) are eliminated by the algorithm in equation (18), $b_1 + b_{LO}^{IM_1}$. The higher order closed form is being examined for a $2D$ extension. It is not always possible to generalize a $1D$ closed form to $2D$; an algorithm in $2D$ have more variables and different dependencies than the same algorithm in $1D$. However, we are studying the $2D$ expressions for the higher order terms in the elimination series. For a multidimensional world, the leading order eliminator provides the removal of all first order internal multiples generated at the first reflector and effectively attenuates the rest of the multiples.

There is an important subset of first order internal multiples that is now eliminated, and other internal multiples are reduced beyond attenuation. The former subset in practice can often be the most significant from a practical field viewpoint. The leading order elimination algorithm automatically eliminates those multiples that have their first reflection at the shallowest reflector, the water bottom, in marine exploration. The water bottom property is neither required nor determined for this eliminator algorithm, nor is information below the water bottom input to provide that ancillary benefit. The degree of the latter secondary benefit will vary but is always present. The fact that the new algorithm is not at all more expensive than the attenuator is worth noting. The sensitivity of the new algorithm for input wavelet is expected to be higher. In particular, an accurate estimation of the source wavelet will be needed to perform the division in the innermost integral. It will also allow convergence of the leading order closed form.

3 Internal multiples are predicted in terms of effective data

When the prerequisites of the internal multiple algorithm are satisfied, the predicted internal multiples can be attenuated/removed from the effective data b_1 by a simple addition $b_1 + b_3^{IM_1}$, for the attenuator, and $b_1 + b_{LO}^{IM}$, for the leading order eliminator. The output of this addition will be effective data with certain internal multiples removed and the rest attenuated. If instead of removing the internal multiples from effective data, one would like to remove them from measured data, then an extra obliquity factor is required as explained in the next lines.

The first inverse scattering equation,

$$D(k_g, k_s, \omega) = \frac{e^{-iq_g z_g}}{-2iq_g} V_1(k_g, k_{s,g} + q_s) \frac{e^{-iq_s z_s}}{-2iq_s}, \tag{19}$$

is used to define the effective data as

$$b_1(k_g, k_s, q_g + q_s) = -2iq_s D(k_g, k_s, \omega), \tag{20}$$

or

$$b_1(k_g, k_s, q_g + q_s) = \frac{e^{-iq_g z_g}}{-2iq_g} V_1(k_g, k_{s,g} + q_s) e^{-iq_s z_s}. \tag{21}$$

The internal multiple attenuation algorithm is found in the third inverse scattering equation, and is given by the algorithm in equation 14,

$$\begin{aligned} b_3^{IM_1}(k_g,k_s,q_g+q_s) = \frac{1}{(2\pi)^2}\int_{-\infty}^{\infty} dk_1 e^{iq_1(x_s-x_g)} \int_{-\infty}^{\infty} dk_2 e^{iq_2(\epsilon_g-\epsilon_s)} \\ \times \int_{-\infty}^{\infty} dz_1 e^{i(q_g+q_1)z_1} b_1(k_g,-k_1,z_1) \\ \times \int_{-\infty}^{z_1-\epsilon_2} dz_2 e^{i(-q_1-q_2)z_2} b_1(k_1,-k_2,z_2) \\ \times \int_{z_2+\epsilon_1}^{\infty} dz_3 e^{i(q_2+q_s)z_3} b_1(k_2,-k_s,z_3). \end{aligned} \tag{22}$$

The left hand side of this equation, $b_3^{IM_1}$, is effective data consisting of internal multiples only. Therefore, its relation with measured data is

$$b_3(k_g,k_s,q_g+q_s) = -2iq_s D^{IM}(k_g,k_s,\omega), \tag{23}$$

where D^{IM} represents data consisting of internal multiples. In other words, the output of the attenuator needs to be divided by a source obliquity factor of $-2iq_s$ in order to have a prediction in terms of measured data. By induction, this analysis can be extended for the higher order terms in the internal multiple elimination series and leading order closed form.

We can predict a dataset consisting of internal multiples only by the attenuator or the leading order closed form by a factor of $-2iq_s$, and then subtract the multiples directly from the recorded data $D - D_3^{IM}$ or $D - D_{LO}^{IM}$, where

$$\begin{aligned} D_3^{IM}(k_g,k_s,q_g+q_s) = \frac{1}{(2\pi)^2}\frac{1}{-2iq_s}\int_{-\infty}^{\infty} dk_1 e^{iq_1(x_s-x_g)} \int_{-\infty}^{\infty} dk_2 e^{iq_2(\epsilon_g-\epsilon_s)} \\ \times \int_{-\infty}^{\infty} dz_1 e^{i(q_g+q_1)z_1} b_1(k_g,-k_1,z_1) \\ \times \int_{-\infty}^{z_1-\epsilon_2} dz_2 e^{i(-q_1-q_2)z_2} b_1(k_1,-k_2,z_2) \\ \times \int_{z_2+\epsilon_1}^{\infty} dz_3 e^{i(q_2+q_s)z_3} b_1(k_2,-k_s,z_3). \end{aligned} \tag{24}$$

and

$$\begin{aligned} D_{LO}^{IM}(k_g,k_s,q_g+q_s) = \frac{1}{(2\pi)^2}\frac{1}{-2iq_s}\int_{-\infty}^{\infty} dk_1 e^{iq_1(x_s-x_g)} \int_{-\infty}^{\infty} dk_2 e^{iq_2(\epsilon_g-\epsilon_s)} \\ \times \int_{-\infty}^{\infty} dz_1 e^{i(q_g+q_1)z_1} b_1(k_g,-k_1,z_1) \\ \times \int_{-\infty}^{z_1-\epsilon_2} dz_2 e^{i(-q_1-q_2)z_2} \frac{b_1(k_1,-k_2,z_2)}{1-b_1(k_1,-k_2,z_2)^2} \\ \times \int_{z_2+\epsilon_1}^{\infty} dz_3 e^{i(q_2+q_s)z_3} b_1(k_2,-k_s,z_3), \end{aligned} \tag{25}$$

Conclusions

The first order term in the inverse scattering internal multiple series, known as the attenuator, provides an effective solution for many circumstances encountered in exploration seismology (Weglein et al., 2003). It predicts the correct arrival time and an estimate of the true amplitude of internal multiples in the data. There are circumstances when the attenuation, or identification, of internal multiples is not enough. An example of those possible circumstances (for towed streamer pressure measurements) is the possibility of either having a residual that is far from small (*e.g.* converted wave internal multiples) or where having a small residual interfering with a target primary, and the latter is itself small. In these cases, the attenuation is not enough and other algorithms need to be developed to extend the previous methods and advance beyond current capability. The internal multiple elimination series and closed forms aim to reduce residual internal multiples where the magnitude of the residual can be significant.

The higher order terms in the series add contributions to the attenuator to improve its effectiveness towards an elimination of internal multiples. The algorithm presented is based on inverse scattering, and it goes further in the removal of first order internal multiples. Two closed forms were obtained and used in examples. The first one, adds the leading order terms elimination subseries and it is an algorithm that completely eliminates all first order internal multiples generated at the first reflector. The second closed form adds the main contribution of the higher order terms. It shows a better estimate of the amplitudes, and provides an improvement towards the elimination of 1^{st} order internal multiples. In this theory, no assumptions about the earth below the receivers are made.

The extension to a multidimensional earth was achieved for the leading order closed form term. The leading order eliminator provides the removal of all first order internal multiples generated at the shallowest reflector and effectively attenuates the rest of the multiples. The extension to a multidimensional earth of the higher order terms as well as extensions of definitions is our current subject of study.

The output of the attenuator (Weglein et al., 1997), and the leading order eliminator, is a wavefield of internal multiples in terms of effective data. In order to have traces consisting of internal multiples in terms of data, the obliquity factor $-2iq_S$ needs to be deconvolved from the prediction.

Acknowledgments

We acknowledge and thank the sponsors and members of M-OSRP for the support of this research. This research was partially supported by the NSF-CMG award DMS-0327778 DOE Basic Energy Sciences award DE-FG02-05ER15697.
The third author thanks ConocoPhillips for permission to publish.
The first author appreciates the internship opportunity she had at ConocoPhillips and thanks the Subsurface Technology group for the excellent environment, support and encouragement of this research. Fernanda Araújo is thanked for useful discussions on internal multiple attenuation and elimination. Ken Matson is acknowledged for his help writing the history timetable.

References

Araújo, F. V. *Linear and non-linear methods derived from scattering theory: backscattering tomography and internal-multiple attenuation.* PhD thesis, Universidade Federal da Bahia, Brazil, 1994. in Portuguese.

Araújo, F. V., A. B. Weglein, P. M. Carvalho, , and R. H Stolt. "Inverse scattering series for multiple attenuation: An example with surface and internal multiples.." *SEG Expanded Abstracts, 1039-1041* (1994).

Carvalho, P. M. *Free-surface multiple reflection elimination method based on nonlinear inversion of seismic data: Ph.D. thesis*. PhD thesis, Universidad Federal da Bahía, Brazil, 1992.

Guo, Z., A. B. Weglein, and T. H. Tan. "Using pressure data on the cable to estimate the seismic wavelet." *SEG Technical Program Expanded Abstracts* (2005).

Ramírez, A. C. and A.B. Weglein. "An inverse scattering internal multiple elimination method: Beyond attenuation, a new algorithm and initial tests." *SEG Expanded Abstracts.* (2005): 2115–2118.

Ramírez, A. C. and A.B. Weglein. "Progressing the analysis of the phase and amplitude prediction properties of the inverse scattering internal multiple attenuation algorithm.." *J. of Seismic Expl.* 13 (2005): 283–301.

Weglein, A. B., F. V. Araujo, P. M. Carvalho, R. H. Stolt, K. H. Matson, R. T. Coates, D. Corrigan, D. J. Foster, S. A. Shaw, and H. Zhang. "Topical Review: Inverse scattering series and seismic exploration." *Inverse Problems* 19 (2003): 27–83.

Weglein, A. B., F. V. Araujo Gasparotto, P. M. Carvalho, and R. H. Stolt. "An inverse-scattering series method for attenuating multiples in seismic reflection data.." *Geophysics* 62 (1997): 1975–1989.

Weglein, A. B., W. E. Boyse, and J. E. Anderson. "Obtaining three-dimensional velocity information directly from reflection seismic data: an inverse scattering formalism." *Geophysics* 46 (1981): 1116–1120.

Zhang, J. and A. B. Weglein. "Application of extinction theorem deghosting method on ocean bottom data." 2006.

Imaging at depth without the velocity: M-OSRP goals, overall strategy and specific coordinated initiatives within that campaign

A. B. Weglein

In this note, we review the basic logic behind the imaging at depth strategy we are pursuing. That logic begins with the goal of addressing the innate algorithmic assumptions/limitations component of a comprehensive response to pressing seismic E & P challenges. In the Introduction we placed our program's goals within that broader landscape of overall issues related to seismic effectiveness.

Basically, we are recognizing and then seeking to capture the potential within the inverse scattering series to provide imaging algorithms that avoid the distinct limiting assumptions of both current velocity analysis and imaging methods and thus can provide useful and accurate images when current imaging methods have difficulty or fail. In short: to provide an accurate depth image under conditions of exploration interest where there is a target reflector but we currently have an erroneous or misplaced image or no image.

The purpose of this note is to provide a perspective of where we are in that campaign and what are the different activities currently being pursued within M-OSRP as we move forward and achieve those goals.

Several key points:

1. It is conceptually easier to understand finding the depth with the velocity than finding the depth without the velocity. The former is $d = vt$ and Green's theorem consistent, and the latter is counter-intuitive and strange. Furthermore, finding the depth with (and needing) the velocity is consistent with modeling (where all modeling methods—including forward scattering series modeling methods— require every single and precise detail of the medium, including velocity, to predict primaries and multiples) and perhaps most important it is consistant with linear inverse scattering, the basis of all migration-inversion and conventional migration theory (F-K, Kirchhoff, phase-shift, phase-screen, beam, reversed-time, split-step, CFP, CRS, Feedback Loop imaging, etc.). The need to have the velocity to determine the depth is also in agreement with both model matching and iterative linear inversion. The inverse scattering series (and the task specific subseries for depth imaging) stands alone on that point.

2. The inverse scattering series responds to the different issues that are required to be addressed to achieve inversion related tasks, that are automatically established and set in motion and called into play by the infrastructure of the L, L_0, and V operators. For example, as soon as the spatial dimension and number of acoustic, elastic, or anelastic parameters, number and types of reference velocities, and constant, slowly-varying or discontinuous reference media are defined, the inverse scattering series automatically, definitively, directly and purposefully responds to the tasks of inversion within each different context and infrastructure. The

tasks of, e.g., imaging with or without a velocity in a one parameter, one dimensional earth are fundamentally different than the issues faced in a multi-dimensional, multi-parameter subsurface. To illustrate: there are no diffractions in 1D and no diffractions to collapse, with or without the velocity. In a one dimensional earth, a single horizontal reflector beneath a known homogeneous overburden is not an imaging challenge. In a multidimensional earth a single high-rugosity reflector beneath a known homogeneous overburden is an imaging challenge. The latter issue gives rise to terms in the inverse scattering series and ultimately in a multi-D depth imaging algorithm that don't exist (nor are they needed) for a 1-D earth.

The above list of migration methods (in item 1) represents a huge set of experiences and investment in terms of intellectual capital, careers, and associated expertise, insights and issues to be addressed, all defined within that framework.

To provide a superseding (imaging) vision one must: (1) match current capability within the sphere of its assumptions and usefulness, and (2) demonstrate new predictive capability that moves outside the sphere of current assumptions and expands the range of accommodation and effectiveness. The inverse scattering series imaging capability has the potential of providing a superseding imaging vision. That potential and promise remains high; and in fact recent partial capture imaging algorithm results are more encouraging in terms of efficacy and efficiency, than we had ever anticipated.

Our central goal and objective is to examine the current effective but partial imaging capture, and a more complete capture (which we are pursuing), to test, evaluate and determine their ability to first match and then go beyond our current best velocity analysis and imaging capability. To date, we have focused our attention on developing imaging algorithms that are tested, where progress is measured in abolute terms. We plan to begin the real test: the evaluation of the inverse scattering series imaging capability in relative terms: i.e., how well do these new algorithms stack-up against our best current methods to determine the velocity and to use that velocity to provide depth images.

There is a set of imaging challenges, each with different types and degrees of velocity and/or imaging breakdown. We anticipate that different degrees of capture of imaging capability within the inverse scattering series will be needed to match these different velocity and/or imaging challenges.

With the standard notation used in forward and inverse scattering formulations we have

$$\overbrace{\underbrace{G_0}_{water}, V}^{Earth} \rightarrow \underbrace{D}_{Data} \longmapsto \ldots forward$$

$$\underbrace{G_0}_{water}, \underbrace{D}_{data} \rightarrow \underbrace{V}_{earth} \longmapsto \ldots, inverse$$

where G_0 is the water speed Green's function, G is the actual Green's function, V is the difference between earth properties and water, and the data, D, is the measured values of $(G - G_0)_m$.

The forward and inverse scattering series input and output

The forward and inverse scattering series respect and honor the non-linearity within the forward and inverse maps $G_0, V \rightarrow D$ and $G_0, D \rightarrow V$. Linear inverse scattering (first term only) with $V_1 \approx V$, and requires $G_0 \approx G$ for a reasonable estimate of V.

For those comfortable with Taylor series the forward series can be cast as:

$$\psi - \psi_0 = D(m) - D(m_0) = D'(m_0)\Delta m + \frac{D''(m_0)(\Delta m)^2}{2} + \ldots, \tag{1}$$

and the inverse series as ($D_0 = D(m_0)$)

$$V = m(D) - \underbrace{m(D_0)}_{m_0} = m'(D_0)D + \frac{m''(D_0)D^2}{2} + \ldots. \tag{2}$$

For those happier with the Lippman-Schwinger scattering equation:

$$\begin{aligned} G - G_0 &= G_0 V G \\ (1 - G_0 V)G &= G_0 \\ G &= \frac{G_0}{1 - G_0 V} \end{aligned} \tag{3}$$

The forward series is

$$G = G_0 + G_0 V G_0 + \ldots \tag{4}$$

and in Taylor series terms

$$D(m) = D(m_0) + D'(m_0)\Delta m + \cdots .$$

The forward scattered series is

$$G - G_0 = \frac{G_0 - (1 - G_0 V)G_0}{1 - G_0 V} = \frac{G_0 V G_0}{1 - G_0 V}, \tag{5}$$

then from Eq. 4,

$$\begin{aligned} \psi_s \equiv G - G_0 &= G_0 V G_0 + G_0 V G_0 V G_0 + \cdot \\ &= (\psi_s)_1 + (\psi_s)_2 + \cdots . \end{aligned} \tag{6}$$

In the inverse direction:

$$\begin{aligned} G - G_0 &= G_0 V G \\ \psi_s &= \frac{G_0 V G_0}{1 - G_0 V} \end{aligned} \tag{7}$$

$$
\begin{aligned}
(G-G_0)(1-G_0V) &= G_0VG_0 \\
\\
G-G_0 &= G_0V(G-G_0)+G_0VG_0 \\
&= G_0VG-G_0+G_0 \\
\frac{G-G_0}{G-G_0+G_0} &= G_0V \\
\frac{(G-G_0)G_0}{G-G_0+G_0} &= G_0VG_0 \\
\frac{G-G_0}{1+\frac{G-G_0}{G_0}} &= G_0VG_0 \\
G_0VG_0 &= G-G_0-\frac{(G-G_0)^2}{G_0}\ldots,
\end{aligned}
\tag{8}
$$

for the inverse problem relating V to $G-G_0$) on the measurement surface

$$
(G_0VG_0)_m = (G-G_0)_m - \left(\frac{(G-G_0)^2}{G_0}\right)_m + \ldots, \tag{9}
$$

where subscript m indicates the measurement surface.

The right hand side of equation 9 is a power series in $(G-G_0)_m$, i.e. the data, D.

The terms on the RHS of different orders contribute to V as the portion of V n-th order in the data, $(G-G_0)_m$. If V_n is the portion of V n-th order in the data and $V=\sum_{n=1}^{\infty}V_n$, then:

$$
\begin{aligned}
(G_0V_1G_0)_m &= (G-G_0)_m \\
(G_0V_2G_0)_m &= -\left(\frac{(G-G_0)^2}{G_0}\right) \\
&= -\frac{(G_0V_1G_0G_0V_1G_0)_m}{G_0} \\
(G_0V_2G_0)_m &= -(G_0V_1G_0V_1G_0)_m
\end{aligned}
\tag{10}
$$

The latter demonstration is merely a pedagogic device and a cartoon "derivation" that relates to the inverse series. To actually derive the inverse series requires a little more respect for operators. (Weglein et al., 1997, 2001; Shaw et al., 2002; Weglein et al., 2003).

The message is *don't truncate the series*: respect, honor it and understand it and the potential of a superseding imaging vision arrives. It is that simple. It's that simple but it's not that easy. Locating imaging only capability within the series is neither simple nor complete and arranging those (infinite upon infinite number of imaging) terms into reasonable algorithms is also a trick. That objective is partially achieved. Much has been achieved, and the current types of imaging capture will be extended to more general models (e.g., elastic) for use on field data; and simultaneously and

separately the imaging capture net within a model type will be broadened to include types of imaging ability beyond our current algorithms.

The current imaging capture is for a single parameter (velocity only) multi-dimensional acoustic earth. In addition, within that world only terms which retain a purpose in a $1D$ world have been captured, and leading order and higher order terms are collected but not all the orders (beyond higher order) within even that framework. The algorithm by Liu et al. (2006) is not in any way a repeated application of a $1D$ imaging formula at different mid-point locations assuming a quasi-local $1D$ earth. It is a full $2D$ imaging formula. It has a $1D$ analog, but it is not a patching together a several $1D$ imaging results. It is a closed form and lightning speed fast and part of our strategy is to generalize it to more than a single parameter to provide enough realism to allow the accommodation of amplitude and phase relations for field data application. In conventional imaging methods the location is determined by using the time (phase) information of primary events and the velocity model to locate structure. That's it. For imaging a reflector without the velocity the inverse scattering series algorithms use a communication that involves the amplitude and phase of a collection of primaries. The inverse scattering series velocity independent imaging series is a more subtle, and sophisticated and complicated undertaking and the event conversation towards imaging needs to be examined to assume that events from the real earth will have the appropriate conversation required in their world. That is being pursued from several different directions; one gleans lessons and patterns from examining imaging activity in models with two or three parameters and a second is coming from a diagram perspective.

While the current imaging capture and theory is being extended for field data readiness, other initiatives are being pursued to bring fully multi-dimensional issues, e.g., imaging breakdown with a perfect velocity, collapsing diffractions and beyond higher order terms into our imaging algorithms' grasp.

Why is the imaging capture so diffcult?

Stated succintly:

1. *One term* in the inverse series eliminates *one order of free surface multiple*;
2. One term in the inverse series attenuates one order of internal multiple; *an entire series* is required to *eliminate one order*, or any one individual internal multiple;
3. One term in the imaging series indicates that there is an imaging issue and an entire series is necessary to *partially* deal with an imaging problem (that series is called leading order imaging series); *a cascaded series* is necessary for further imaging capability, called higher order imaging series, and there are terms beyond what is being called higher order.

   Hence, when you locate a term, e.g., that is dealing with uniquely $2D$ issues such as collapsing diffractions, that is a good thing and a start but far from capturing a collapsing diffraction capability. The latter requires examing further terms and *patterns of terms* with that diffraction collapsing interest and to generalize (sometimes by guessing) what terms beyond what you can derive would look like and collecting them into an algorithm.

The algorithm will be an infinite series; and, more likely a cascaded infinite series and then you need to be able to compute it. Can you find a closed form, or a recursive form or are stuck with computing terms. If the latter is the case, then convergence, rate of convergence and use of a variable velocity background to speed up convergence might be indicated. That's why it is complicated and that's why all of that full multi-D imaging capture is yet to be achieved. Accurate depth imaging beneath a complex ill-defined medium or imaging a complex boundary is a complex and difficult problem. And complex equals complex: one simple sum (one term) of a complex highly demanding term (actual velocity and data) or a highly complex sum of a very undemanding set of terms (water speed and data).

The inverse scattering series prescribes the highly complex sum. Sometimes the highly complex sum reduces to a simple closed form. Then you have the collapse of a complex cascaded double infinite sum of a simple water speed migration ingredient into a very simple form in terms of the simple ingredient. That's amazing. That's the status of current imaging capture. In that current capture, the entire algorithm runs in 1.3 times the time for a single water speed FK migration. No velocity, no tomographic velocity analysis, no residual velocity analysis, no interpretation, no picking, no iterates with migration to different depths and marching down. With that Stolt FK migration speed and partial multi-D imaging capture, why wouldn't we want to extend Fang Liu's imaging algorithm to more realistic models to allow for field data tests?

In summary, we are: (1) going to extend to current imaging algorithm to be able to accommodate a minimally realistic earth model; (2) test these imaging algorithms with more complex synthetics and compare with best available methods that estimate the velocity and use conventional imaging; (3) collect a set of field data examples (for testing) with ever increasing imaging challenges, beginning with fault shallow zones; and (4) broaden the imaging capture.

References

Liu, F., Arthur B. Weglein, Kristopher A. Innanen, and Bogdan G. Nita. "Multi-dimensional seismic imaging using the inverse scattering series." *76th Annual Internat. Mtg., Soc. Expl. Geophys., Expanded Abstracts.* . Soc. Expl. Geophys., 2006. 937–940.

Shaw, Simon A., A. B. Weglein, K. H. Matson, and D. J. Foster. "Cooperation of the leading order terms in an inverse-scattering subseries for imaging: 1-D analysis and evaluation.." *SEG Technical Program Expanded Abstracts* (2002): 2277–2280.

Weglein, A. B., F. V. Araújo, P. M. Carvalho, R. H. Stolt, K. H. Matson, R. T. Coates, D. Corrigan, D. J. Foster, S. A. Shaw, and H. Zhang. "Inverse Scattering Series and Seismic Exploration." *Inverse Problems* (2003): R27–R83.

Weglein, A. B., D. J. Foster, K. H. Matson, S. A. Shaw, P. M. Carvalho, and D. Corrigan. "An inverse-scattering sub-series for predicting the spatial location of reflectors without the precise reference medium and wave velocity." *71st Annual Internat. Mtg., Soc. Expl. Geophys., Expanded Abstracts.* . Soc. Expl. Geophys., 2001. 2108–2111.

Weglein, A. B., F. A. Gasparotto, P. M. Carvalho, and R. H. Stolt. "An Inverse-Scattering Series Method for Attenuating Multiples in Seismic Reflection Data." *Geophysics* 62 (November-December 1997): 1975–1989.

A note: data requirements for inverse theory

A. B. Weglein

1. What does linear in the data mean?
2. Linear in what data?
3. Conservation of dimension (having enough degrees of freedom in your data to "solve" an equation) is not a sufficient condition to define "what data" and being able to solve an equation (in isolation) is not the same as finding a physically meaningful solution or even a linear estimate;
4. Solving an equation without the context and framework within which that equation resides, and ignoring the assumptions that lead to that equation is a dangerous path towards an inverse illusion;
5. Implications for data collection and target identification.

Scattering theory relates the perturbation (the difference between the reference and actual medium properties) to the scattered wave field (the difference between the reference medium's and the actual medium's wave field). It is therefore reasonable that in discussing scattering theory, we begin with the basic wave equations governing the wave propagation in the actual and reference medium, respectively,

$$LG = \delta, \tag{1}$$

$$L_0 G_0 = \delta, \tag{2}$$

where L and L_0 are respectively the differential operators that describe wave propagation in the actual and reference medium, and G and G_0 are the corresponding Green's operators. The δ on the right hand side of both equations is a Dirac delta operator and represents an impulsive source.

The perturbation is defined as $V = L_0 - L$. The Lippmann-Schwinger equation,

$$G = G_0 + G_0 V G, \tag{3}$$

relates G, G_0 and V (see, e.g., Taylor, 1972). Iterating this equation back into itself generates the forward scattering series

$$G = G_0 + G_0 V G_0 + G_0 V G_0 V G_0 + \cdots . \tag{4}$$

Then the scattered field $\psi_s \equiv G - G_0$ can be written as

$$\begin{aligned} \psi_s &= G_0 V G_0 + G_0 V G_0 V G_0 + \cdots \\ &= (\psi_s)_1 + (\psi_s)_2 + \cdots , \end{aligned} \tag{5}$$

where $(\psi_s)_n$ is the portion of ψ_s that is n^{th} order in V. The measured values of ψ_s are the data, D, where

$$D = (\psi_s)_{ms} = (\psi_s)_{\text{on the measurement surface}}.$$

In the inverse scattering series, expanding V as a series in orders of D,

$$V = V_1 + V_2 + V_3 + \cdots, \tag{6}$$

then substituting Eq. 6 into Eq. 5, and evaluating Eq. 5 on the measurement surface yields

$$D = [G_0(V_1 + V_2 + \cdots)G_0]_{ms} + [G_0(V_1 + V_2 + \cdots)G_0(V_1 + V_2 + \cdots)G_0]_{ms} + \cdots. \tag{7}$$

Setting terms of equal order in the data equal, leads to the equations that determine V_1, V_2, ... directly from D and G_0.

$$D = [G_0V_1G_0]_{ms}, \tag{8}$$

$$0 = [G_0V_2G_0]_{ms} + [G_0V_1G_0V_1G_0]_{ms}, \tag{9}$$

$$\begin{aligned} 0 =& [G_0V_3G_0]_{ms} + [G_0V_1G_0V_2G_0]_{ms} + [G_0V_2G_0V_1G_0]_{ms} \\ &+ [G_0V_1G_0V_1G_0V_1G_0]_{ms}, \end{aligned} \tag{10}$$

etc. Equations (8) $\sim$ (10) permit the sequential calculation of V_1, V_2, ..., and, hence, achieve full inversion for V (see Eq. 6) from the recorded data D and the reference wave field (i.e., the Green's operator of the reference medium) G_0. Therefore, the inverse scattering series is a multi-D inversion procedure that directly determines physical properties using only reflection data and reference medium information.

1 Acoustic case

In this section, we will consider a 1D acoustic two parameter earth model (e.g. bulk modulus and density or velocity and density). We start with the 3D acoustic wave equations in the actual and reference medium:

$$\left[\frac{\omega^2}{K(\mathbf{r})} + \nabla \cdot \frac{1}{\rho(\mathbf{r})}\nabla\right] G(\mathbf{r}, \mathbf{r}_s; \omega) = \delta(\mathbf{r} - \mathbf{r}_s), \tag{11}$$

$$\left[\frac{\omega^2}{K_0(\mathbf{r})} + \nabla \cdot \frac{1}{\rho_0(\mathbf{r})}\nabla\right] G_0(\mathbf{r}, \mathbf{r}_s; \omega) = \delta(\mathbf{r} - \mathbf{r}_s), \tag{12}$$

where $G(\mathbf{r}, \mathbf{r}_s; \omega)$ and $G_0(\mathbf{r}, \mathbf{r}_s; \omega)$ are respectively the free-space causal Green's functions that describe wave propagation in the actual and reference medium. $K = c^2\rho$, is P-wave bulk modulus, c is P-wave velocity and ρ is the density. The quantities with subscript "0" are for the reference medium, and those without the subscript are for the actual medium. The perturbation is

$$V = L_0 - L = \frac{\omega^2\alpha}{K_0} + \nabla \cdot \frac{\beta}{\rho_0}\nabla, \tag{13}$$

where $\alpha = 1 - \frac{K_0}{K}$ and $\beta = 1 - \frac{\rho_0}{\rho}$ are the two parameters we choose to do the inversion. Assuming both ρ_0 and c_0 are constants, Eq. 12 becomes

$$\left(\frac{\omega^2}{c_0^2} + \nabla^2\right) G_0(\mathbf{r}, \mathbf{r}_s; \omega) = \rho_0 \delta(\mathbf{r} - \mathbf{r}_s). \tag{14}$$

For the 1-D case, the perturbation V has the following form

$$V(z, \nabla) = \frac{\omega^2 \alpha(z)}{K_0} + \frac{1}{\rho_0}\beta(z)\frac{\partial^2}{\partial x^2} + \frac{1}{\rho_0}\frac{\partial}{\partial z}\beta(z)\frac{\partial}{\partial z}. \tag{15}$$

$V(z, \nabla)$, $\alpha(z)$ and $\beta(z)$ can be expanded respectively as

$$V(z, \nabla) = V_1(z, \nabla) + V_2(z, \nabla) + \cdots, \tag{16}$$

$$\alpha(z) = \alpha_1(z) + \alpha_2(z) + \cdots, \tag{17}$$

$$\beta(z) = \beta_1(z) + \beta_2(z) + \cdots. \tag{18}$$

Then we have

$$V_1(z, \nabla) = \frac{\omega^2 \alpha_1(z)}{K_0} + \frac{1}{\rho_0}\beta_1(z)\frac{\partial^2}{\partial x^2} + \frac{1}{\rho_0}\frac{\partial}{\partial z}\beta_1(z)\frac{\partial}{\partial z}, \tag{19}$$

$$V_2(z, \nabla) = \frac{\omega^2 \alpha_2(z)}{K_0} + \frac{1}{\rho_0}\beta_2(z)\frac{\partial^2}{\partial x^2} + \frac{1}{\rho_0}\frac{\partial}{\partial z}\beta_2(z)\frac{\partial}{\partial z}, \tag{20}$$

$$\vdots$$

Substituting Eq. 19 into Eq. 8, we can get the linear solution for α_1 and β_1 in the frequency domain

$$\widetilde{D}(q_g, \theta, z_g, z_s) = -\frac{\rho_0}{4} e^{-iq_g(z_s + z_g)} \left[\frac{1}{\cos^2\theta}\widetilde{\alpha_1}(-2q_g) + (1 - \tan^2\theta)\widetilde{\beta}_1(-2q_g)\right]. \tag{21}$$

Let $z_s = z_g = 0$,

$$D(z, \theta) = -\frac{\rho_0}{4}\Big(\frac{1}{\cos^2\theta}\alpha_1(z) + (1 - \tan^2\theta)\beta_1(z)\Big) \tag{22}$$

Let's consider the following logic. Eq. 22 is an exact equation for the linear estimates $\alpha_1(z)$ and $\beta_1(z)$, and choosing two (or more) values of θ will allow you to solve Eq. 22 for $\alpha_1(z)$ and $\beta_1(z)$.

For a single reflector model, the left hand side of Eq. 22 is the migration of the surface recorded data. The migration provides a step-function at the depth of the reflector whose angle dependent amplitude is the reflector's angle dependent reflection coefficient.

The right hand side of Eq. 22 can be rewritten as

$$-\frac{\rho_0}{4}\Big(\alpha_1(z) + \beta_1(z) + (\alpha_1(z) - \beta_1(z))\tan^2\theta\Big). \tag{23}$$

Separately, we know that the exact plane wave reflection coefficient is (e.g., Keys, 1989)

$$R(\theta) = \frac{(\rho_1/\rho_0)(c_1/c_0)\sqrt{1-\sin^2\theta} - \sqrt{1-(c_1^2/c_0^2)\sin^2\theta}}{(\rho_1/\rho_0)(c_1/c_0)\sqrt{1-\sin^2\theta} + \sqrt{1-(c_1^2/c_0^2)\sin^2\theta}}. \tag{24}$$

and we can find a Taylor series in R as a function of $\sin^2\theta$ or another Taylor series using

$$\sin^2\theta \quad = \tfrac{\tan^2\theta}{1+\tan^2\theta}.$$

This series is

$$\begin{aligned} R(\theta) =& R(\tan^2\theta) \\ =& R(\tan^2\theta = 0) + \Big(\frac{d\,R(\tan^2\theta)}{d(\tan^2\theta)}\Big)\Big|_{\tan^2\theta=0} \cdot \tan^2\theta \\ &+ \Big(\frac{d\,R(\tan^2\theta)}{d(\tan^2\theta)}\Big)\Big|_{\tan^2\theta=0} \cdot \tan^4\theta + \cdots \end{aligned} \tag{25}$$

Eq. 25 is exact and the amplitude of the step-function in Eq. 23 is

$$R(\tan^2\theta) = \alpha_1 + \beta_1 + (\alpha_1 - \beta_1)\tan^2\theta. \tag{26}$$

The first term in the inverse scattering series is (claimed to be) an exact equation for the linear estimate of α and β, α_1 and β_1, respectively.

How can you reconcile Eq. 26 being exact with Eq. 25 being exact?

Eq. 26 would seem to represent a truncated; and, therefore, approximate form of the Zoeppritz exact reflection coefficient (Eq. 25).

If we don't accept Eq. 26 as an approximation as being acceptable then we must alter either Eq. 25 or Eq.26, and we are not going to alter Zoeppritz Eq. 25.

We are forced to conclude that consistency between Eq. 25 and Eq. 26 requires that α_1 and β_1 must be functions of θ.

Let's see where that supposition then takes us from Eq. 26:

$$R(\tan^2\theta) = \alpha_1(\theta) + \beta_1(\theta) + [\alpha_1(\theta) - \beta_1(\theta)]\tan^2\theta; \tag{27}$$

and, if you choose two value of θ, say θ_1 and θ_2, then Eq. 27 will lead to two equations in four unknowns, $\alpha_1(\theta_1)$, $\alpha_1(\theta_2)$, $\beta_1(\theta_1)$ and $\beta_1(\theta_2)$. Not a positive moment.

What the problem is here is we have forgotten the basic meaning and starting point in defining α, β and α_1, β_1.

In an inverse scattering series expansion for a parameter in orders of the data it is critically important to assure that the data in terms of which you are expanding the parameter is sufficient

to determine that parameter. The data needed to determine a parameter is dependent upon what other parameters are (or are not) in your model; i.e., it depends on the context within which that parameter resides.

Now consider a two parameter world defined by $\alpha(z)$ and $\beta(z)$, and the expansions of α and β in orders of the data. In this case, if we suppose that α and β are expandable in terms of data at two different plane wave angles assuming that such a relationship between $D(z,\theta_1)$, $D(z,\theta_2)$ and α and β exists and is sufficient to determine α and β (not α_1 and β_1) then we can write the series for $\alpha(z)$ and $\beta(z)$ as follows:

$$\alpha(z) \quad = \quad \alpha_1(z, D(z,\theta_1), D(z,\theta_2)) + \alpha_2(z, D(z,\theta_1), D(z,\theta_2)) + \cdots$$

and in a compact notation

$$\alpha(z) \quad = \quad \alpha_1(z,\theta_1,\theta_2) + \alpha_2(z,\theta_1,\theta_2)) + \cdots$$

where α_1 is the portion of α linear in the data set $(D(z,\theta_1), D(z,\theta_2))$. Similarly,

$$\beta(z) = \beta_1(z,\theta_1,\theta_2) + \beta_2(z,\theta_1,\theta_2) + \cdots \tag{28}$$

If the model only allowed bulk modulus changes, but not density variation then the data required for solving for α would only consist of data at a single angle; and in that single parameter world

$$\alpha(z) = \alpha_1(z,\theta_1) + \alpha_2(z,\theta_1) + \ldots. \tag{29}$$

Now in the two parameter inverse problem, the data is

$$\begin{pmatrix} D(z,\theta_1) \\ D(z,\theta_2) \end{pmatrix}$$

and then $D = G_0 V_1 G_0$ is equal to

$$\begin{pmatrix} D(z,\theta_1) \\ D(z,\theta_2) \end{pmatrix} = \begin{pmatrix} (1+\tan^2\theta_1) & (1-\tan^2\theta_1) \\ (1+\tan^2\theta_2) & (1-\tan^2\theta_2) \end{pmatrix} \begin{pmatrix} \alpha_1(z,\theta_1,\theta_2) \\ \beta_1(z,\theta_1,\theta_2) \end{pmatrix} \tag{30}$$

and $\begin{pmatrix} \alpha_1(z,\theta_1,\theta_2) \\ \beta_1(z,\theta_1,\theta_2) \end{pmatrix}$ is linearly related to $\begin{pmatrix} D(z,\theta_1) \\ D(z,\theta_2) \end{pmatrix}$. α_1 and β_1 will depend upon which particular angles θ_1 and θ_2 were chosen, and that is anticipated and perfectly reasonable, since being a linear approximation in the data could(and should) be a different linear estimate depending on the data subset you are considering.

Eq. 30, a matrix equation, is the first term in the inverse series and determines α_1 and β_1, the linear estimate of α and β.

The lesson here is that the inverse problem doesn't start with $G_0 V_1 G_0 = D$ but with $V = V_1 + V_2 + V_3 + \ldots$ and the latter equation is driven by a view of what data set can determine the operator V.

This might seem like a somewhat useless academic exercise, since Eq. 30 is the equation you would have solved for α_1 and β_1 if you just ignored their θ dependence entirely. It is anything but that. There are at least two problems with that conclusion. The value of the above analysis is: (1) with α_1 and β_1 independent of θ, you have difficulty claiming or satisfying the important requirement that the first equation in the inverse series is exact; and (2) more importantly you can get into serious conceptual and practical problems in the elastic case if you don't have very clear grasp of the underlying inverse issues and relationships in the acoustic case.

2 Elastic case

The scattering theory and the inverse scattering series for the 1-D isotropic elastic earth is developed in Zhang and Weglein (2007)

2.1 Background for 2D elastic inversion

In this section we consider the inversion problem in two dimensions for an elastic medium. We start with the displacement space, and then, for convenience (Weglein and Stolt, 1992; Aki and Richards, 2002, e.g.), we change the basis and transform the equations to PS space. Finally, we do the elastic inversion in the PS domain.

2.2 In the displacement space

We begin with some basic equations in the displacement space (Matson, 1997):

$$L\mathbf{u} = \mathbf{f}, \tag{31}$$

$$L_0\mathbf{u} = \mathbf{f}, \tag{32}$$

$$LG = \delta, \tag{33}$$

$$L_0G_0 = \delta, \tag{34}$$

where L and L_0 are the differential operators that describe the wave propagation in the actual and reference medium, respectively, $\mathbf{u}$ and $\mathbf{f}$ are the corresponding displacement and source terms, respectively, and G and G_0 are the corresponding Green's operators for the actual and reference medium.

Following closely Weglein et al. (1997), Weglein et al. (2002) and Weglein et al. (2003), defining the perturbation $V = L_0 - L$, the Lippmann- Schwinger equation for the elastic media in the displacement space is

$$G = G_0 + G_0VG. \tag{35}$$

Iterating this equation back into itself generates the Born series

$$G = G_0 + G_0VG_0 + G_0VG_0VG_0 + \cdots . \tag{36}$$

We define the data D as the measured values of the scattered wave field. Then, on the measurement surface, we have

$$D = G_0 V G_0 + G_0 V G_0 V G_0 + \cdots . \tag{37}$$

Expanding V as a series in orders of D we have

$$V = V_1 + V_2 + V_3 + \cdots . \tag{38}$$

Substituting Eq. 38 into Eq. 37, evaluating Eq. 37, and setting terms of equal order in the data equal, the equations that determine V_1, V_2, ... from D and G_0 would be obtained.

$$D = G_0 V_1 G_0, \tag{39}$$

$$0 = G_0 V_2 G_0 + G_0 V_1 G_0 V_1 G_0, \tag{40}$$

$$\vdots$$

In the actual medium, the 2-D elastic wave equation is (Weglein and Stolt, 1992)

$$L\mathbf{u} \equiv \left[\rho\omega^2 \begin{pmatrix} 1 & 0 \\ 0 & 1 \end{pmatrix} + \begin{pmatrix} \partial_1\gamma\partial_1 + \partial_2\mu\partial_2 & \partial_1(\gamma - 2\mu)\partial_2 + \partial_2\mu\partial_1 \\ \partial_2(\gamma - 2\mu)\partial_1 + \partial_1\mu\partial_2 & \partial_2\gamma\partial_2 + \partial_1\mu\partial_1 \end{pmatrix}\right] \begin{bmatrix} u_1 \\ u_2 \end{bmatrix} = \mathbf{f}, \tag{41}$$

where

$\mathbf{u} = \begin{bmatrix} u_1 \\ u_2 \end{bmatrix}$ = displacement,

ρ = density,

γ = bulk modulus ($\equiv \rho\alpha^2$ where α = P-wave velocity),

μ = shear modulus ($\equiv \rho\beta^2$ where β = S-wave velocity),

ω = temporal frequency (angular), ∂_1 and ∂_2 denote the derivative over x and z, respectively, and $\mathbf{f}$ is the source term.

For constant $(\rho, \gamma, \mu) = (\rho_0, \gamma_0, \mu_0)$, $(\alpha, \beta) = (\alpha_0, \beta_0)$, the operator L becomes

$$L_0 \equiv \left[\rho_0\omega^2 \begin{pmatrix} 1 & 0 \\ 0 & 1 \end{pmatrix} + \begin{pmatrix} \gamma_0\partial_1^2 + \mu_0\partial_2^2 & (\gamma_0 - \mu_0)\partial_1\partial_2 \\ (\gamma_0 - \mu_0)\partial_1\partial_2 & \mu_0\partial_1^2 + \gamma_0\partial_2^2 \end{pmatrix}\right]. \tag{42}$$

Then,

$$\begin{aligned} V \equiv & L_0 - L \\ = & -\rho_0 \begin{bmatrix} a_\rho\omega^2 + \alpha_0^2\partial_1 a_\gamma\partial_1 + \beta_0^2\partial_2 a_\mu\partial_2 & \partial_1(\alpha_0^2 a_\gamma - 2\beta_0^2 a_\mu)\partial_2 + \beta_0^2\partial_2 a_\mu\partial_1 \\ \partial_2(\alpha_0^2 a_\gamma - 2\beta_0^2 a_\mu)\partial_1 + \beta_0^2\partial_1 a_\mu\partial_2 & a_\rho\omega^2 + \alpha_0^2\partial_2 a_\gamma\partial_2 + \beta_0^2\partial_1 a_\mu\partial_1 \end{bmatrix}, \end{aligned} \tag{43}$$

where $a_\rho \equiv \frac{\rho}{\rho_0} - 1$, $a_\gamma \equiv \frac{\gamma}{\gamma_0} - 1$ and $a_\mu \equiv \frac{\mu}{\mu_0} - 1$ are the three parameters we choose to do the elastic inversion. For a 1D earth (i.e. a_ρ, a_γ and a_μ are only functions of depth z), the expression above for V becomes

$$V = -\rho_0 \begin{bmatrix} a_\rho\omega^2 + \alpha_0^2 a_\gamma\partial_1^2 + \beta_0^2\partial_2 a_\mu\partial_2 & (\alpha_0^2 a_\gamma - 2\beta_0^2 a_\mu)\partial_1\partial_2 + \beta_0^2\partial_2 a_\mu\partial_1 \\ \partial_2(\alpha_0^2 a_\gamma - 2\beta_0^2 a_\mu)\partial_1 + \beta_0^2 a_\mu\partial_1\partial_2 & a_\rho\omega^2 + \alpha_0^2\partial_2 a_\gamma\partial_2 + \beta_0^2 a_\mu\partial_1^2 \end{bmatrix}. \tag{44}$$

2.3 Transforming to PS space

For convenience, we can change the basis from $\mathbf{u} = \begin{bmatrix} u_1 \\ u_2 \end{bmatrix}$ to $\begin{pmatrix} \phi^P \\ \phi^S \end{pmatrix}$ to allow L_0 to be diagonal,

$$\mathbf{\Phi} = \begin{pmatrix} \phi^P \\ \phi^S \end{pmatrix} = \begin{bmatrix} \gamma_0(\partial_1 u_1 + \partial_2 u_2) \\ \mu_0(\partial_1 u_2 - \partial_2 u_1) \end{bmatrix}, \tag{45}$$

also, we have

$$\begin{pmatrix} \phi^P \\ \phi^S \end{pmatrix} = \Gamma_0 \Pi \mathbf{u} = \begin{bmatrix} \gamma_0(\partial_1 u_1 + \partial_2 u_2) \\ \mu_0(\partial_1 u_2 - \partial_2 u_1) \end{bmatrix}, \tag{46}$$

where $\Pi = \begin{pmatrix} \partial_1 & \partial_2 \\ -\partial_2 & \partial_1 \end{pmatrix}$, $\Gamma_0 = \begin{pmatrix} \gamma_0 & 0 \\ 0 & \mu_0 \end{pmatrix}$. In the reference medium, the operator L_0 will transform in the new basis via a transformation

$$\hat{L}_0 \equiv \Pi L_0 \Pi^{-1} \Gamma_0^{-1} = \begin{pmatrix} \hat{L}_0^P & 0 \\ 0 & \hat{L}_0^S \end{pmatrix},$$

where $\hat{L}_0$ is L_0 transformed to PS space, $\Pi^{-1} = \begin{pmatrix} \partial_1 & -\partial_2 \\ \partial_2 & \partial_1 \end{pmatrix} \nabla^{-2}$ is the inverse matrix of Π, $\hat{L}_0^P = \omega^2/\alpha_0^2 + \nabla^2$, $\hat{L}_0^S = \omega^2/\beta_0^2 + \nabla^2$, and

$$\mathbf{F} = \Pi \mathbf{f} = \begin{pmatrix} F^P \\ F^S \end{pmatrix}. \tag{47}$$

Then, in PS domain, Eq. 32)becomes,

$$\begin{pmatrix} \hat{L}_0^P & 0 \\ 0 & \hat{L}_0^S \end{pmatrix} \begin{pmatrix} \phi^P \\ \phi^S \end{pmatrix} = \begin{pmatrix} F^P \\ F^S \end{pmatrix}. \tag{48}$$

Since $G_0 \equiv L_0^{-1}$, let $\hat{G}_0^P = \left(\hat{L}_0^P\right)^{-1}$ and $\hat{G}_0^S = \left(\hat{L}_0^S\right)^{-1}$, then the displacement G_0 in PS domain becomes

$$\hat{G}_0 = \Gamma_0 \Pi G_0 \Pi^{-1} = \begin{pmatrix} \hat{G}_0^P & 0 \\ 0 & \hat{G}_0^S \end{pmatrix}. \tag{49}$$

So, in the reference medium, after transforming from the displacement domain to PS domain, both L_0 and G_0 become diagonal.

Multiplying Eq. 35 from the left by the operator $\Gamma_0\Pi$ and from the right by the operator Π^{-1}, and using Eq. 49,

$$\begin{aligned} \Gamma_0 \Pi G \Pi^{-1} &= \hat{G}_0 + \hat{G}_0 \left(\Pi V \Pi^{-1} \Gamma_0^{-1}\right) \Gamma_0 \Pi G \Pi^{-1} \\ &= \hat{G}_0 + \hat{G}_0 \hat{V} \hat{G}, \end{aligned} \tag{50}$$

where the displacement Green's operator G is transformed to the PS domain as

$$\hat{G} = \Gamma_0 \Pi G \Pi^{-1} = \begin{pmatrix} \hat{G}^{PP} & \hat{G}^{PS} \\ \hat{G}^{SP} & \hat{G}^{SS} \end{pmatrix}. \tag{51}$$

The perturbation V in the PS domain becomes

$$\hat{V} = \Pi V \Pi^{-1} \Gamma_0^{-1} = \begin{pmatrix} \hat{V}^{PP} & \hat{V}^{PS} \\ \hat{V}^{SP} & \hat{V}^{SS} \end{pmatrix}, \tag{52}$$

where the left superscripts of the matrix elements represent the type of measurement and the right ones are the source type.

Similarly, applying the PS transformation to the entire inverse series gives

$$\hat{V} = \hat{V}_1 + \hat{V}_2 + \hat{V}_3 + \cdots . \tag{53}$$

It follows, from Eqs. 50 and 53 that

$$\hat{D} = \hat{G}_0 \hat{V}_1 \hat{G}_0, \tag{54}$$

$$\hat{G}_0 \hat{V}_2 \hat{G}_0 = -\hat{G}_0 \hat{V}_1 \hat{G}_0 \hat{V}_1 \hat{G}_0, \tag{55}$$

$$\vdots$$

where $\hat{D} = \begin{pmatrix} \hat{D}^{PP} & \hat{D}^{PS} \\ \hat{D}^{SP} & \hat{D}^{SS} \end{pmatrix}$ are the data in the PS domain.

In the displacement space we have, for Eq. 31,

$$\mathbf{u} = G\mathbf{f}. \tag{56}$$

Then, in the PS domain, Eq. 56 becomes

$$\mathbf{\Phi} = \hat{G}\mathbf{F}. \tag{57}$$

On the measurement surface, we have

$$\hat{G} = \hat{G}_0 + \hat{G}_0 \hat{V}_1 \hat{G}_0. \tag{58}$$

Substituting Eq. 58 into Eq. 57, and rewriting Eq. 57 in matrix form:

$$\begin{pmatrix} \phi^P \\ \phi^S \end{pmatrix} = \begin{pmatrix} \hat{G}_0^P & 0 \\ 0 & \hat{G}_0^S \end{pmatrix} \begin{pmatrix} F^P \\ F^S \end{pmatrix} + \begin{pmatrix} \hat{G}_0^P & 0 \\ 0 & \hat{G}_0^S \end{pmatrix} \begin{pmatrix} \hat{V}_1^{PP} & \hat{V}_1^{PS} \\ \hat{V}_1^{SP} & \hat{V}_1^{SS} \end{pmatrix} \begin{pmatrix} \hat{G}_0^P & 0 \\ 0 & \hat{G}_0^S \end{pmatrix} \begin{pmatrix} F^P \\ F^S \end{pmatrix}. \tag{59}$$

This can be written as the following two equations

$$\phi^P = \hat{G}_0^P F^P + \hat{G}_0^P \hat{V}_1^{PP} \hat{G}_0^P F^P + \hat{G}_0^P \hat{V}_1^{PS} \hat{G}_0^S F^S, \tag{60}$$

$$\phi^S = \hat{G}_0^S F^S + \hat{G}_0^S \hat{V}_1^{SP} \hat{G}_0^P F^P + \hat{G}_0^S \hat{V}_1^{SS} \hat{G}_0^S F^S. \tag{61}$$

We can see, from the two equations above, that for homogeneous media, (no perturbation, $\hat{V}_1 = 0$), there are only direct P and S waves and that the two kind of waves are separated. However, for inhomogeneous media, these two kinds of waves will be mixed together. If only the P wave is incident, $F^P = 1$, $F^S = 0$, then the two Eqs. 60 and 61 above are respectively reduced to

$$\phi^P = \hat{G}_0^P + \hat{G}_0^P \hat{V}_1^{PP} \hat{G}_0^P, \tag{62}$$

$$\phi^S = \hat{G}_0^S \hat{V}_1^{SP} \hat{G}_0^P. \tag{63}$$

Hence, in this case, there is only the direct P wave $\hat{G}_0^P$, and no direct wave S. But there are two kinds of scattered waves: one is the P-to-P wave $\hat{G}_0^P \hat{V}_1^{PP} \hat{G}_0^P$, and the other is the P-to-S wave $\hat{G}_0^S \hat{V}_1^{SP} \hat{G}_0^P$. For the acoustic case, only the P wave exists, and hence we only have one equation $\phi^P = \hat{G}_0^P + \hat{G}_0^P \hat{V}_1^{PP} \hat{G}_0^P$.

Similarly, if only the S wave is incident, $F^P = 0$, $F^S = 1$, and the two Eqs. 60 and 61 are, respectively, reduced to

$$\phi^P = \hat{G}_0^P \hat{V}_1^{PS} \hat{G}_0^S, \tag{64}$$

$$\phi^S = \hat{G}_0^S + \hat{G}_0^S \hat{V}_1^{SS} \hat{G}_0^S. \tag{65}$$

In this case, there is only the direct S wave $\hat{G}_0^S$, and no direct P wave. There are also two kinds of scattered waves: one is the S-to-P wave $\hat{G}_0^P \hat{V}_1^{PS} \hat{G}_0^S$, the other is the S-to-S wave $\hat{G}_0^S \hat{V}_1^{SS} \hat{G}_0^S$.

2.4 Linear inversion of a 1D elastic medium

Writing Eq. 54 in matrix form

$$\begin{pmatrix} \hat{D}^{PP} & \hat{D}^{PS} \\ \hat{D}^{SP} & \hat{D}^{SS} \end{pmatrix} = \begin{pmatrix} \hat{G}_0^P & 0 \\ 0 & \hat{G}_0^S \end{pmatrix} \begin{pmatrix} \hat{V}_1^{PP} & \hat{V}_1^{PS} \\ \hat{V}_1^{SP} & \hat{V}_1^{SS} \end{pmatrix} \begin{pmatrix} \hat{G}_0^P & 0 \\ 0 & \hat{G}_0^S \end{pmatrix}, \tag{66}$$

leads to four equations

$$\hat{D}^{PP} = \hat{G}_0^P \hat{V}_1^{PP} \hat{G}_0^P, \tag{67}$$

$$\hat{D}^{PS} = \hat{G}_0^P \hat{V}_1^{PS} \hat{G}_0^S, \tag{68}$$

$$\hat{D}^{SP} = \hat{G}_0^S \hat{V}_1^{SP} \hat{G}_0^P, \tag{69}$$

$$\hat{D}^{SS} = \hat{G}_0^S \hat{V}_1^{SS} \hat{G}_0^S. \tag{70}$$

For $z_s = z_g = 0$, in the $(k_s, z_s; k_g, z_g; \omega)$ domain, we get the following four equations relating the linear components of the three elastic parameters and the four data types:

$$\begin{aligned} \widetilde{D}^{PP}(k_g, 0; -k_g, 0; \omega) = &- \frac{1}{4}\left(1 - \frac{k_g^2}{\nu_g^2}\right) \widetilde{a}_\rho^{(1)}(-2\nu_g) - \frac{1}{4}\left(1 + \frac{k_g^2}{\nu_g^2}\right) \widetilde{a}_\gamma^{(1)}(-2\nu_g) \\ &+ \frac{2k_g^2\beta_0^2}{(\nu_g^2 + k_g^2)\alpha_0^2} \widetilde{a}_\mu^{(1)}(-2\nu_g), \end{aligned} \tag{71}$$

$$\widetilde{D}^{PS}(\nu_g, \eta_g) = -\frac{1}{4}\left(\frac{k_g}{\nu_g} + \frac{k_g}{\eta_g}\right) \widetilde{a}_\rho^{(1)}(-\nu_g - \eta_g) - \frac{\beta_0^2}{2\omega^2} k_g(\nu_g + \eta_g)\left(1 - \frac{k_g^2}{\nu_g \eta_g}\right) \widetilde{a}_\mu^{(1)}(-\nu_g - \eta_g), \tag{72}$$

$$\widetilde{D}^{SP}(\nu_g, \eta_g) = \frac{1}{4}\left(\frac{k_g}{\nu_g} + \frac{k_g}{\eta_g}\right) \widetilde{a}_\rho^{(1)}(-\nu_g - \eta_g) + \frac{\beta_0^2}{2\omega^2} k_g(\nu_g + \eta_g)\left(1 - \frac{k_g^2}{\nu_g \eta_g}\right) \widetilde{a}_\mu^{(1)}(-\nu_g - \eta_g), \tag{73}$$

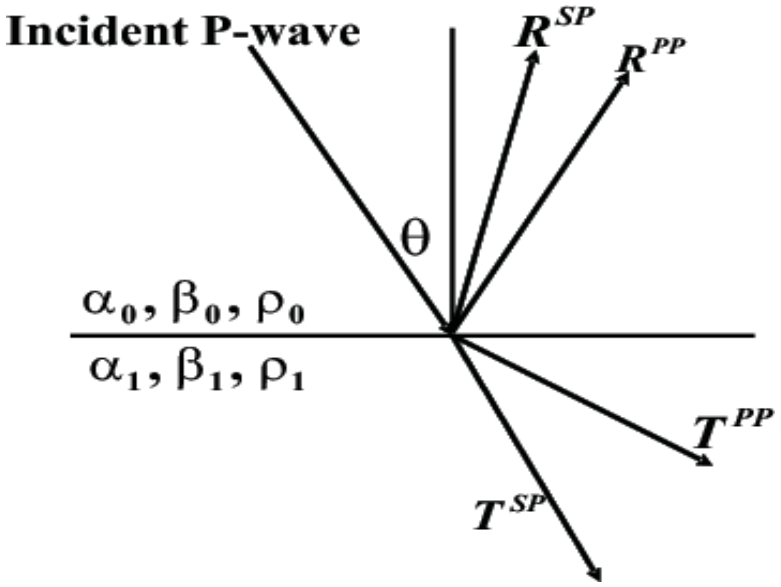

Figure 1: Response of incident compressional wave on a planar elastic interface. α_0, β_0 and ρ_0 are the compressional wave velocity, shear wave velocity and density of the upper layer, respectively; α_1, β_1 and ρ_1 denote the compressional wave velocity, shear wave velocity and density of the lower layer. R^{PP}, R^{SP}, T^{PP} and T^{SP} denote the coefficients of the reflected compressional wave, the reflected shear wave, the transmitted compressional waveand the transmitted shear wave, respectively (Foster et al., 1997).

$$\widetilde{D}^{SS}(k_g,\eta_g) = -\frac{1}{4}\left(1-\frac{k_g^2}{\eta_g^2}\right)\widetilde{a}_\rho^{(1)}(-2\eta_g) - \left[\frac{\eta_g^2+k_g^2}{4\eta_g^2} - \frac{2k_g^2}{\eta_g^2+k_g^2}\right]\widetilde{a}_\mu^{(1)}(-2\eta_g), \tag{74}$$

where

$$\nu_g^2 + k_g^2 = \frac{\omega^2}{\alpha_0^2},$$

$$\eta_g^2 + k_g^2 = \frac{\omega^2}{\beta_0^2}.$$

For the P-wave incidence case (see Fig. 1), using $k_g^2/\nu_g^2 = \tan^2\theta$ and $k_g^2/(\nu_g^2+k_g^2) = \sin^2\theta$, where θ is the P-wave incident angle, Eq. 71 becomes

$$\widetilde{D}^{PP}(\nu_g,\theta) = -\frac{1}{4}(1-\tan^2\theta)\widetilde{a}_\rho^{(1)}(-2\nu_g) - \frac{1}{4}(1+\tan^2\theta)\widetilde{a}_\gamma^{(1)}(-2\nu_g) + \frac{2\beta_0^2\sin^2\theta}{\alpha_0^2}\widetilde{a}_\mu^{(1)}(-2\nu_g). \tag{75}$$

In this case, when $\beta_0 = \beta_1 = 0$, Eq. 75 reduces to the acoustic two parameter case Eq. (7) in Zhang and Weglein (2005) for $z_g = z_s = 0$.

$$\widetilde{D}(q_g,\theta) = -\frac{\rho_0}{4}\left[\frac{1}{\cos^2\theta}\widetilde{\alpha_1}(-2q_g) + (1-\tan^2\theta)\widetilde{\beta}_1(-2q_g)\right], \tag{76}$$

2.5 Direct non-linear inversion of 1D elastic medium

Writing Eq. 55 in matrix form:

$$\begin{aligned}&\begin{pmatrix}\hat{G}_0^P & 0\\ 0 & \hat{G}_0^S\end{pmatrix}\begin{pmatrix}\hat{V}_2^{PP} & \hat{V}_2^{PS}\\ \hat{V}_2^{SP} & \hat{V}_2^{SS}\end{pmatrix}\begin{pmatrix}\hat{G}_0^P & 0\\ 0 & \hat{G}_0^S\end{pmatrix}\\ &= -\begin{pmatrix}\hat{G}_0^P & 0\\ 0 & \hat{G}_0^S\end{pmatrix}\begin{pmatrix}\hat{V}_1^{PP} & \hat{V}_1^{PS}\\ \hat{V}_1^{SP} & \hat{V}_1^{SS}\end{pmatrix}\begin{pmatrix}\hat{G}_0^P & 0\\ 0 & \hat{G}_0^S\end{pmatrix}\begin{pmatrix}\hat{V}_1^{PP} & \hat{V}_1^{PS}\\ \hat{V}_1^{SP} & \hat{V}_1^{SS}\end{pmatrix}\begin{pmatrix}\hat{G}_0^P & 0\\ 0 & \hat{G}_0^S\end{pmatrix},\end{aligned} \tag{77}$$

leads to four equations

$$\hat{G}_0^P\hat{V}_2^{PP}\hat{G}_0^P = -\hat{G}_0^P\hat{V}_1^{PP}\hat{G}_0^P\hat{V}_1^{PP}\hat{G}_0^P - \hat{G}_0^P\hat{V}_1^{PS}\hat{G}_0^S\hat{V}_1^{SP}\hat{G}_0^P, \tag{78}$$

$$\hat{G}_0^P\hat{V}_2^{PS}\hat{G}_0^S = -\hat{G}_0^P\hat{V}_1^{PP}\hat{G}_0^P\hat{V}_1^{PS}\hat{G}_0^S - \hat{G}_0^P\hat{V}_1^{PS}\hat{G}_0^S\hat{V}_1^{SS}\hat{G}_0^S, \tag{79}$$

$$\hat{G}_0^S\hat{V}_2^{SP}\hat{G}_0^P = -\hat{G}_0^S\hat{V}_1^{SP}\hat{G}_0^P\hat{V}_1^{PP}\hat{G}_0^P - \hat{G}_0^S\hat{V}_1^{SS}\hat{G}_0^S\hat{V}_1^{SP}\hat{G}_0^P, \tag{80}$$

$$\hat{G}_0^S\hat{V}_2^{SS}\hat{G}_0^S = -\hat{G}_0^S\hat{V}_1^{SP}\hat{G}_0^P\hat{V}_1^{PS}\hat{G}_0^S - \hat{G}_0^S\hat{V}_1^{SS}\hat{G}_0^S\hat{V}_1^{SS}\hat{G}_0^S. \tag{81}$$

Since $\hat{V}_1^{PP}$ relates to $\hat{D}^{PP}$, $\hat{V}_1^{PS}$ relates to $\hat{D}^{PS}$, and so on, the four components of the data will be coupled in the non-linear elastic inversion. We cannot perform the direct non-linear inversion without knowing all components of the data. As shown in Zhang and Weglein (2005) and this note, when the work on the two parameter acoustic case is extended to the present three parameter elastic case, it is not just simply adding one more parameter, but there are more issues involved. Even for the linear case, the linear solutions found in (71) $\sim$ (74) are much more complicated than those of the acoustic case. For instance, four different sets of linear parameter estimates are produced from each component of the data. Also, generally four distinct reflector mislocations arise from the two reference velocities (P-wave velocity and S-wave velocity).

The three parameters we are seeking to determine

- $a_\gamma \rightarrow$ relative change in bulk modulus,
- $a_\rho \rightarrow$ relative change in density,
- $a_\mu \rightarrow$ relative change in shear modulus,

are to be expanded as a series in the data. What data?

The answer is once again the data needed to determine those three quantities.

What H. Zhang's thesis has demonstrated for the first time is not only an explicit and direct set of equations for improving upon linear estimates of the changes in those elastic properties, but perhaps equally and maybe even more important, is for the first time the absolutely clear data requirements for determining a_γ, a_ρ and a_μ.

The data requirements are

$$D = \begin{pmatrix}\hat{D}^{PP} & \hat{D}^{PS}\\ \hat{D}^{SP} & \hat{D}^{SS}\end{pmatrix}, \tag{82}$$

for a $2D$ earth and generalize to a 3×3 matrix for a $3D$ earth with SH and SV shear waves.

The $2D$ message is delivered in Eq. 77 , Eq. 78-81 that the first non-linear contribution to a_γ, a_μ, a_ρ requires that data; and, hence the exact determination of those elastic quantities also require that data set.

$$\begin{pmatrix} V^{PP} & V^{PS} \\ V^{SP} & V^{SS} \end{pmatrix} = \begin{pmatrix} V_1^{PP} & V_1^{PS} \\ V_1^{SP} & V_1^{SS} \end{pmatrix} + \begin{pmatrix} V_2^{PP} & V_2^{PS} \\ V_2^{SP} & V_2^{SS} \end{pmatrix} + \cdots \tag{83}$$

The logic is as follows:
$\begin{pmatrix} a_\gamma \\ a_\mu \\ a_\rho \end{pmatrix}$ requires $\begin{pmatrix} \hat{D}^{PP} & \hat{D}^{PS} \\ \hat{D}^{SP} & \hat{D}^{SS} \end{pmatrix}$ since $\begin{pmatrix} a_\gamma^{(2)} \\ a_\mu^{(2)} \\ a_\rho^{(2)} \end{pmatrix}$ requires $\begin{pmatrix} \hat{D}^{PP} & \hat{D}^{PS} \\ \hat{D}^{SP} & \hat{D}^{SS} \end{pmatrix}$. Hence $\begin{pmatrix} a_\gamma^{(1)} \\ a_\mu^{(1)} \\ a_\rho^{(1)} \end{pmatrix}$ must mean linear in $\begin{pmatrix} \hat{D}^{PP} & \hat{D}^{PS} \\ \hat{D}^{SP} & \hat{D}^{SS} \end{pmatrix}$, i.e., linear in the data needed to determine $\begin{pmatrix} a_\gamma \\ a_\mu \\ a_\rho \end{pmatrix}$.

Inverting

$$\hat{D}^{PP} = G_0^P V_1^{PP} G_0^P$$

alone for $a_\gamma^{(1)}$, $a_\mu^{(1)}$ and $a_\rho^{(1)}$ while mathematically achievable is a challenged and incorrect linear relationship since what you determine from that procedure doesn't represent the linear estimate of those quantities in terms of a data that can actually determine those quantities.

Solving for $a_\gamma^{(1)}$, $a_\mu^{(1)}$ and $a_\rho^{(1)}$ from $\hat{D}^{PP}$ alone is an injured or challenged linear estimate.

The inverse scattering series and task specific subseries need to : (1) treat the linear term with respect and then (2) the higher order terms can carry out their purpose.

If you injure the linear estimate, the inverse scattering series cannot recover or compensate–it wants the linear estimate to be the linear estimate, and never expects it to be exact or close to exact, but it never expects it to be less than linear, as well. Let linear be linear.

The power and promise of the inverse scattering series derives from its deliberate and physically consistent and explicit nature. It recognizes that when you perturb anything in a medium the associated perturbation in the wavefield is always non-linearly related to that change.

The inverse implies that the medium perturbation is itself non-linearly related to the perturbation in the wavefield; including the change in the wavefield on the measurement surface.

$$\psi_s = (\psi_s)_1 + (\psi_s)_2 + (\psi_s)_3 + \dots \tag{84}$$
$$V = V_1 + V_2 + V_3 + \dots, \tag{85}$$

where $(\psi_s)_n$ is the portion of ψ_s nth order in V and where V_n is the portion of V n'th order in the measured values of ψ_s. That's it, Eq. 84 and 85. That is all you assume, and that is hard to argue against.

Beyond that point the process and procedure for determining $V_1, V_2, V_3, \ldots$ is out of your hands and away from your control. How you find V_1 from D is prescribed and what you do with V_1 to determine V_2 is also prescribed. That non-linear explicit and direct nature, and the steps to determine those terms $V_1, V_2, V_3, \ldots$ are not decision making opportunities for you. If *you* decide what to do with V_1 rather than have the non-linear relationship between data and V decide, then you step away from a single and defined physics into, e.g., the math world of iterative linear inversion or model matching. How do you formulate a multiple removal algorithm concept in iterative linear inverse or model matching scheme? The latter immediately aim to either improve or match the models properties with the subsurface. From the inverse scattering series perspective, the latter all or nothing strategy is: (1) missing the opportunity to achieve other useful but less daunting tasks, i.e., multiple removal and depth imaging; and (2) moving at the first step straight into the most challenging task: parameter estimation, with all of the pitfalls of insufficient modeltypes and bandwidth sensitivities.

For the inverse scattering series the decisions are not under your control or influence. It is away from you and it is carrying out its single-minded purpose. It has one physical model and a single *unchanged* separation of the earth into a reference medium and the perturbation and an all at once set of direct equations to solve.

Only that 100% physics consistent inverse formalism predicted that you required $\begin{pmatrix} \hat{D}^{PP} & \hat{D}^{PS} \\ \hat{D}^{SP} & \hat{D}^{SS} \end{pmatrix}$ to even linearly estimate elastic properties. Iterative linear tries to substitute a set of constantly changed problems with linear updates for a single entirely prescriptive, consistent and explicit non-linear physics. The latter is the inverse scattering series, the former has an attraction to linear inverses (and generalized inverses) which has no single physical theory and consistency. Linear inversion and generalized inverse theory are part of standard graduate training in geophysics; and, hence it's easy to understand trying to recast the actual non-linear problem into a set of iterative linear problems where the tools are familiar. The model matching schemes and iteratively linear inversion are reasonable and sometimes useful but they are more math than physics and have no way to provide the framework for inversion that staying consistent with the physics will provide. The table that follows represents an informal report card of different inverse methods:

	Count	Direct	Compute	Physics	Understandable/Accessible
Model matching	V	V	F	F	A
Iterative linear	H	V	C	C	A
Inverse scattering	H	H	A	A	F

where:

- $V \rightarrow$ Violates (or can violate);
- $H \rightarrow$ Honors (respects);
- $A =$ good;

- F = bad;
- C = forget about it.

The table shows a report card comparing model matching, iterative linear, and the inverse scattering series. There are times that *model matching* can be an effective tool even though on a scale of F to A it is F in terms of physics driven.

Modeling matching for the subtraction of $3D$ multiples earns it a F for compute requirements compared at A for ISS.

There is a unique and unambiguous data requirement message sent out from the inverse scattering series. Other methods and approaches that look at the inverse problem either linear or beyond linear, e.g., iterative linear or model matching have never and will never provide that clarity and definition. We can model-match D_{pp} or iteratively invert D_{pp} until the cows come home and you will find *ambiguities* and resolution challenges, and when those methods use more data they sometimes produce less ambiguity and better resolution, but we don't know why.

As a final remark it is interesting to note that the first and linear term of the elastic inverse problem was not only influenced by the non-linear term, it was in fact defined by that term. That data requirement message, along with the entire inverse series apparatus, results from the observation that the perturbed wavefield and the perturbation are non-linearly related. Honor and respect that fundamental non-linear relationship and a physics driven set of consistent, deliberate and purposeful algorithms and a clear platform and unambiguous framework (rather than anecdotal experiences) are the dividend and reward.

References

Aki, K. and P. G. Richards. *Quantitative Seismology.* 2nd edition. University Science Books, 2002.

Foster, D. J., R. G. Keys, and D. P. Schmitt. *Detecting subsurface hydrocarbons with elastic wavefields.* Springer-In Inverse Problems in Wave Progagation, Volume 90 of The IMA Volumes in Mathematics and its Applications, 1997.

Keys, R. G. "Polarity reversals in reflections from layered media." *Geophysics* 54 (1989): 900–905.

Matson, K. H. *An inverse-scattering series method for attenuating elastic multiples from multi-component land and ocean bottom seismic data.* PhD thesis, University of British Columbia, 1997.

Taylor, J. R. *Scattering theory: the quantum theory of nonrelativistic collisions.* John Wiley & Sons, Inc., 1972.

Weglein, A. B., F. V. Araújo, P. M. Carvalho, R. H. Stolt, K. H. Matson, R. T. Coates, D. Corrigan, D. J. Foster, S. A. Shaw, and H. Zhang. "Inverse Scattering Series and Seismic Exploration." *Inverse Problems* (2003): R27–R83.

Weglein, A. B., D. J. Foster, K. H. Matson, S. A. Shaw, P. M. Carvalho, and D. Corrigan. "Predicting the correct spatial location of reflectors without knowing or determining the precise medium and wave velocity: initial concept, algorithm and analytic and numerical example." *Journal of Seismic Exploration* 10 (2002): 367–382.

Weglein, A. B., F. A. Gasparotto, P. M. Carvalho, and R. H. Stolt. "An Inverse-Scattering Series Method for Attenuating Multiples in Seismic Reflection Data." *Geophysics* 62 (November-December 1997): 1975–1989.

Weglein, A. B. and R. H. Stolt. 1992 "Approaches on linear and non-linear migration-inversion.". Personal Communication.

Zhang, H. and A. B. Weglein. "The inverse scattering series for tasks associated with primaries: Depth imaging and direct non-linear inversion of 1D variable velocity and density acoustic media." *75th Annual Internat. Mtg., Soc. Expl. Geophys., Expanded Abstracts.* . Soc. Expl. Geophys., 2005. 1705–1708.

Zhang, Haiyan and Arthur B. Weglein. "Direct non-linear inversion of multi-parameter 1D elastic media using the inverse scattering series." *Geophysics* submitted (2007).

Direct non-linear inversion of 1D acoustic media using inverse scattering subseries

H. Zhang and A. B. Weglein

Abstract

A task specific multi-parameter [1] direct non-linear inversion subseries of the inverse scattering series is derived and tested for a velocity and density varying 1D acoustic media. Numerical test results indicate that one term beyond linear provides added values beyond standard practice. Imaging and inversion for two parameter media are much more complicated than that of the one parameter case. Three important messages (purposeful perturbation, leakage and special parameter for linear inversion) have been discussed by analyzing the two parameter non-linear result.

1 Introduction

The objective of seismic exploration is to determine the location (imaging) and mechanical properties (inversion) of hydrocarbon resources in the earth using recorded data. The recorded data have a non-linear relationship with the property changes across a reflector. Current inversion methods include: (1) the linear approximation (Clayton and Stolt, 1981; Weglein and Stolt, 1992, e.g.,) which is often useful, especially in the presence of small earth property changes across the boundary and/or small angle reflections, and (2) indirect model matching methods with global searching (Tarantola et al., 1984; Sen and Stoffa, 1995, e.g.,) which define an objective function assumed to be minimized when the best fitting model is obtained. The assumptions of the former methods (like the small contrast assumptions) are often violated in practice and can cause erroneous predictions; the latter category usually involves a significant and often daunting computation effort (especially in multi-D cases) and/or sometimes have reported erroneous or ambiguous results.

In this paper, a more comprehensive multi-parameter multi-dimensional direct non-linear inversion framework is developed based on the inverse scattering task-specific subseries (see, e.g., Weglein et al. (2003)). In order to provide more accurate and reliable target identification especially with large contrast, large angle target geometry, we isolated the inverse scattering subseries responsible for non-linear amplitude inversion of data.

The original inverse scattering series research aimed at separating imaging and inversion tasks on primaries was developed for a 1D acoustic one parameter case (constant density medium, only velocity variable in depth) and a plane wave at normal incidence (Weglein et al., 2002; Shaw et al., 2003). In this paper we move a step closer to seismic exploration relevance by extending that earlier work to a multi-parameter case — two parameter case (velocity and density vary vertically in depth) and allowing for point sources and receivers over a 1D acoustic medium. Clayton and Stolt (1981)

[1] More than one mechanical property changes across a reflector.

gave a two parameter *linear* inversion solution for *2D* acoustic media (velocity and density vary both vertically and laterally). In this paper, we use the same parameters but concentrate on *1D* acoustic media to derive the direct *non-linear* inversion solution. In the application of the direct *non-linear* inverse algorithm, we move one step each time (e.g., from one parameter 1D acoustic case to two parameter 1D acoustic case, or to one parameter 2D acoustic case, instead of 'jumping' directly to two parameter 2D acoustic case) so that we can solve the problem step by step and learn lessons from each step which would guide us to step further towards greater realism. For one parameter 1D and 2D acoustic media, some work on direct non-linear imaging with reference velocity is presented by Shaw (2005) and Liu et al. (2005). It has been shown in this paper that imaging and inversion for two parameter medium are much more complicated compared to one parameter case, although it seems like just simply adding one parameter. Examples of the new messages that come up are leakage, purposeful perturbation and the identification of the special parameter for inversion, and all of them will be discussed in the following.

For the direct non-linear inversion solution obtained in this paper, the tasks for imaging-only and inversion-only terms are separated. Tests with analytic data indicate significant added value for parameter predictions, beyond linear estimates, in terms of both the proximity to actual value and the increased range of angles over which the improved estimates are useful.

A closed form of the inversion terms for the one-interface case is also obtained. This closed form might be useful in predicting the precritical data using the postcritical data.

A special parameter Δc ($\Delta c = c - c_0$) (P-wave velocity change across an interface) is also found. Its Born inversion $(\Delta c)_1$ always has the right sign. That is, the sign of $(\Delta c)_1$ is always the same as that of Δc. In practice, it could be very useful to know whether the velocity increases or decreases across the interface. After changing parameters, from α (relative changes in P-wave bulk modulus) and β (relative changes in density) to velocity and β, another form of the non-linear solution is obtained. There is no leakage correction (please see details in the section on three important messages) in this solution. This new form clearly indicates that the imaging terms care only about velocity errors. The mislocation is due to the wrong velocity. This is suggestive of possible generalization to multi-D medium, and also of possible model-type independent imaging which only depends on velocity changes.

The following section is a brief introduction of the inverse scattering subseries. We then gave the derivation in detail and followed by the numerical tests. Last is a further discussion about the special parameters.

2 Inverse scattering subseries

Scattering theory relates the perturbation (the difference between the reference and actual medium properties) to the scattered wave field (the difference between the reference medium's and the actual medium's wave field). It is therefore reasonable that in discussing scattering theory, we begin with the basic wave equations governing the wave propagation in the actual and reference medium, respectively [2],

$$LG = \delta, \tag{1}$$

$$L_0 G_0 = \delta, \tag{2}$$

[2]In this introductory math development, we follow closely Weglein et al. (1997); Weglein et al. (2002); Weglein et al. (2003).

where L and L_0 are respectively the differential operators that describe wave propagation in the actual and reference medium, and G and G_0 are the corresponding Green's operators. The δ on the right hand side of both equations is a Dirac delta operator and represents an impulsive source.

The perturbation is defined as $V = L_0 - L$. The Lippmann-Schwinger equation,

$$G = G_0 + G_0 V G, \tag{3}$$

relates G, G_0 and V (see, e.g., (Taylor, 1972)). Iterating this equation back into itself generates the forward scattering series

$$G = G_0 + G_0 V G_0 + G_0 V G_0 V G_0 + \cdots . \tag{4}$$

Then the scattered field $\psi_s \equiv G - G_0$ can be written as

$$\begin{aligned} \psi_s &= G_0 V G_0 + G_0 V G_0 V G_0 + \cdots \\ &= (\psi_s)_1 + (\psi_s)_2 + \cdots , \end{aligned} \tag{5}$$

where $(\psi_s)_n$ is the portion of ψ_s that is n^{th} order in V. The measured values of ψ_s are the data, D, where

$$D = (\psi_s)_{ms} = (\psi_s)_{\text{on the measurement surface}}.$$

In the inverse scattering series, expanding V as a series in orders of D,

$$V = V_1 + V_2 + V_3 + \cdots , \tag{6}$$

then substituting Eq. (6) into Eq. (5), and evaluating Eq. (5) on the measurement surface yields

$$D = [G_0(V_1 + V_2 + \cdots)G_0]_{ms} + [G_0(V_1 + V_2 + \cdots)G_0(V_1 + V_2 + \cdots)G_0]_{ms} + \cdots . \tag{7}$$

Setting terms of equal order in the data equal, leads to the equations that determine V_1, V_2, ... directly from D and G_0.

$$D = [G_0 V_1 G_0]_{ms}, \tag{8}$$

$$0 = [G_0 V_2 G_0]_{ms} + [G_0 V_1 G_0 V_1 G_0]_{ms}, \tag{9}$$

$$\begin{aligned} 0 =& [G_0 V_3 G_0]_{ms} + [G_0 V_1 G_0 V_2 G_0]_{ms} + [G_0 V_2 G_0 V_1 G_0]_{ms} \\ &+ [G_0 V_1 G_0 V_1 G_0 V_1 G_0]_{ms}, \end{aligned} \tag{10}$$

etc. Equations (8) $\sim$ (10) permit the sequential calculation of V_1, V_2, ..., and, hence, achieve full inversion for V (see Eq. 6) from the recorded data D and the reference wave field (i.e., the Green's operator of the reference medium) G_0. Therefore, the inverse scattering series is a multi-D inversion procedure that directly determines physical properties using only reflection data and reference medium information.

3 Derivation of α_1, β_1 and α_2, β_2

In this section, we will consider a 1D acoustic two parameter earth model (e.g. bulk modulus and density or velocity and density). We start with the 3D acoustic wave equations in the actual and reference medium ((Clayton and Stolt, 1981); (Weglein et al., 1997))

$$\left[\frac{\omega^2}{K(\mathbf{r})} + \nabla \cdot \frac{1}{\rho(\mathbf{r})}\nabla\right] G(\mathbf{r}, \mathbf{r}_s; \omega) = \delta(\mathbf{r} - \mathbf{r}_s), \tag{11}$$

$$\left[\frac{\omega^2}{K_0(\mathbf{r})}+\nabla\cdot\frac{1}{\rho_0(\mathbf{r})}\nabla\right]G_0(\mathbf{r},\mathbf{r}_s;\omega)=\delta(\mathbf{r}-\mathbf{r}_s), \tag{12}$$

where $G(\mathbf{r},\mathbf{r}_s;\omega)$ and $G_0(\mathbf{r},\mathbf{r}_s;\omega)$ are respectively the free-space causal Green's functions that describe wave propagation in the actual and reference medium. $K=c^2\rho$, is P-wave bulk modulus, c is P-wave velocity and ρ is the density. The quantities with subscript "0" are for the reference medium, and those without the subscript are for the actual medium. The perturbation is

$$V=L_0-L=\frac{\omega^2\alpha}{K_0}+\nabla\cdot\frac{\beta}{\rho_0}\nabla, \tag{13}$$

where $\alpha=1-\frac{K_0}{K}$ and $\beta=1-\frac{\rho_0}{\rho}$ are the two parameters we choose to do the inversion. Assuming both ρ_0 and c_0 are constants, Eq. (12) becomes

$$\left(\frac{\omega^2}{c_0^2}+\nabla^2\right)G_0(\mathbf{r},\mathbf{r}_s;\omega)=\rho_0\delta(\mathbf{r}-\mathbf{r}_s). \tag{14}$$

For the 1-D case, the perturbation V has the following form

$$V(z,\nabla)=\frac{\omega^2\alpha(z)}{K_0}+\frac{1}{\rho_0}\beta(z)\frac{\partial^2}{\partial x^2}+\frac{1}{\rho_0}\frac{\partial}{\partial z}\beta(z)\frac{\partial}{\partial z}. \tag{15}$$

$V(z,\nabla)$, $\alpha(z)$ and $\beta(z)$ can be expanded respectively as

$$V(z,\nabla)=V_1(z,\nabla)+V_2(z,\nabla)+\cdots, \tag{16}$$

$$\alpha(z)=\alpha_1(z)+\alpha_2(z)+\cdots, \tag{17}$$

$$\beta(z)=\beta_1(z)+\beta_2(z)+\cdots. \tag{18}$$

Then we have

$$V_1(z,\nabla)=\frac{\omega^2\alpha_1(z)}{K_0}+\frac{1}{\rho_0}\beta_1(z)\frac{\partial^2}{\partial x^2}+\frac{1}{\rho_0}\frac{\partial}{\partial z}\beta_1(z)\frac{\partial}{\partial z}, \tag{19}$$

$$V_2(z,\nabla)=\frac{\omega^2\alpha_2(z)}{K_0}+\frac{1}{\rho_0}\beta_2(z)\frac{\partial^2}{\partial x^2}+\frac{1}{\rho_0}\frac{\partial}{\partial z}\beta_2(z)\frac{\partial}{\partial z}, \tag{20}$$

$$\vdots$$

Substituting Eq. (19) into Eq. (8), we can get the linear solution for α_1 and β_1 in the frequency domain

$$\widetilde{D}(q_g,\theta,z_g,z_s)=-\frac{\rho_0}{4}e^{-iq_g(z_s+z_g)}\left[\frac{1}{\cos^2\theta}\widetilde{\alpha_1}(-2q_g)+(1-\tan^2\theta)\widetilde{\beta}_1(-2q_g)\right], \tag{21}$$

where the subscripts s and g denote source and receiver quantities respectively, and q_g, θ and $k=\omega/c_0$ shown in Fig. 1, have the following relations (Matson, 1997)

$$q_g=q_s=k\cos\theta,$$
$$k_g=k_s=k\sin\theta.$$

Similarly, substituting Eq. (20) into Eq. (9), we can get the solution for $\alpha_2(z)$ and $\beta_2(z)$ as a function of $\alpha_1(z)$ and $\beta_1(z)$

$$\frac{1}{\cos^2\theta}\alpha_2(z)+(1-\tan^2\theta)\beta_2(z)=-\frac{1}{2\cos^4\theta}\alpha_1^2(z)-\frac{1}{2}(1+\tan^4\theta)\beta_1^2(z)+\frac{\tan^2\theta}{\cos^2\theta}\alpha_1(z)\beta_1(z)$$

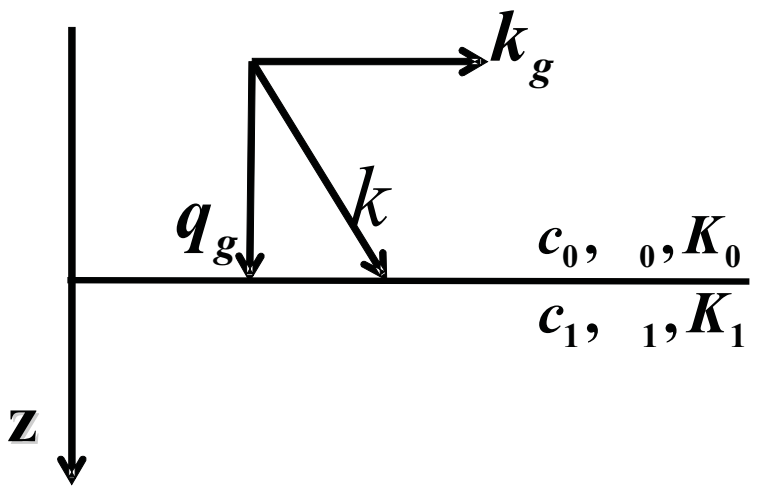

Figure 1: The relationship between q_g, k_g and θ.

$$- \frac{1}{2\cos^4\theta}\alpha_1'(z)\int_0^z dz'[\alpha_1(z') - \beta_1(z')]$$
$$+ \frac{1}{2}(\tan^4\theta - 1)\beta_1'(z)\int_0^z dz'[\alpha_1(z') - \beta_1(z')], \qquad (22)$$

where $\alpha_1'(z) = \frac{\mathrm{d}\alpha_1(\mathrm{z})}{\mathrm{dz}}$, $\beta_1'(z) = \frac{\mathrm{d}\beta_1(\mathrm{z})}{\mathrm{dz}}$.

The first two parameter direct non-linear inversion of 1D acoustic media for a 2D experiment has been obtained. As shown in Eq. (21) and Eq. (22), given two different angles θ, we can determine α_1, β_1 and then α_2, β_2. For a single-interface example, it can be shown that only the first three terms on the right hand side contribute to parameter predictions, while the last two terms perform imaging in depth since they will be zero after the integration across the interface (see the section on three important messages). Therefore, in this solution, the tasks for imaging-only and inversion-only terms are separated.

For the $\theta = 0$ and constant density case, Eq. (22) reduces to the non-linear solution for 1D one parameter normal incidence case (Shaw, 2005, e.g.,))

$$\alpha_2(z) = -\frac{1}{2}\left[\alpha_1^2(z) + \alpha_1'(z)\int_{-\infty}^z dz'\alpha_1(z')\right]. \qquad (23)$$

If another choice of free parameter other than θ (e.g., ω or k_h) is selected, then the functional form between the data and the first order perturbation Eq. (21) would change. Furthermore, the relationship between the first and second order perturbation Eq. (22) would, then, also be different, and new analysis would be required for the purpose of identifying specific task separated terms. Empirically, the choice of θ as free parameter (for a 1D medium) is particularly well suited for allowing a task separated identification of terms in the inverse series.

There are several important messages that exist in Eq. (21) and Eq. (22): (1) purposeful perturbation, (2) leakage, and (3) the special parameter for inversion. These three concepts will be discussed

later in this paper. In Eq. (21), it seems simple and straightforward to use data at two angles in order to obtain α_1 and β_1. This is what we do in this paper. However, by doing this, it requires a whole new understanding of the definition of "the data". That is part of the discoveries of on-going research activities by Weglein et al. (2007). The imaging algorithm given by Liu et al. (2005) has been generalized to the two parameter case by Weglein et al. (2007) based on the understanding of Eq. (22).

4 A special case: one-interface model

In this section, we derive a closed form for the inversion-only terms. From this closed form, we can easily get the same inversion terms as those in Eqs. (21) and (22). We also show some numerical tests using analytic data. From the numerical results, we see how the corresponding non-linear terms contribute to the parameter predictions such as the relative changes in the P-wave bulk modulus $\left(\alpha = \frac{\Delta K}{K}\right)$, density $\left(\beta = \frac{\Delta \rho}{\rho}\right)$, impedance $\left(\frac{\Delta I}{I}\right)$ and velocity $\left(\frac{\Delta c}{c}\right)$.

4.1 Closed form for the inversion terms

1. Incident angle not greater than critical angle, i.e. $\theta \leq \theta_c$

For a single interface example, the reflection coefficient has the following form (Keys, 1989)

$$R(\theta) = \frac{(\rho_1/\rho_0)(c_1/c_0)\sqrt{1-\sin^2\theta} - \sqrt{1-(c_1^2/c_0^2)\sin^2\theta}}{(\rho_1/\rho_0)(c_1/c_0)\sqrt{1-\sin^2\theta} + \sqrt{1-(c_1^2/c_0^2)\sin^2\theta}}. \tag{24}$$

After adding 1 on both sides of Eq. (24), we can get

$$1 + R(\theta) = \frac{2\cos\theta}{\cos\theta + (\rho_0/\rho_1)\sqrt{\left(c_0^2/c_1^2\right) - \sin^2\theta}}. \tag{25}$$

Then, using the definitions of $\alpha = 1 - \frac{K_0}{K_1} = 1 - \frac{\rho_0 c_0^2}{\rho_1 c_1^2}$ and $\beta = 1 - \frac{\rho_0}{\rho_1}$, Eq. (25) becomes

$$\frac{4R(\theta)}{(1+R(\theta))^2} = \frac{\alpha}{\cos^2\theta} + (1-\tan^2\theta)\beta - \frac{\alpha\beta}{\cos^2\theta} + \beta^2\tan^2\theta, \tag{26}$$

which is the closed form we derived for the one interface two parameter acoustic inversion-only terms.

2. Incident angle greater than critical angle, i.e. $\theta > \theta_c$

For $\theta > \theta_c$, Eq. (24) becomes

$$R(\theta) = \frac{(\rho_1/\rho_0)(c_1/c_0)\sqrt{1-\sin^2\theta} - i\sqrt{(c_1^2/c_0^2)\sin^2\theta - 1}}{(\rho_1/\rho_0)(c_1/c_0)\sqrt{1-\sin^2\theta} + i\sqrt{(c_1^2/c_0^2)\sin^2\theta - 1}}. \tag{27}$$

Then, Eq. (25) becomes

$$1 + R(\theta) = \frac{2\cos\theta}{\cos\theta + i\,(\rho_0/\rho_1)\sqrt{\sin^2\theta - \left(c_0^2/c_1^2\right)}}, \tag{28}$$

which leads to the same closed form as Eq. (26)

$$\frac{4R(\theta)}{(1+R(\theta))^2} = \frac{\alpha}{\cos^2\theta} + (1-\tan^2\theta)\beta - \frac{\alpha\beta}{\cos^2\theta} + \beta^2\tan^2\theta.$$

As we see, this closed form is valid for all incident angles.

In addition, for normal incidence ($\theta = 0$) and constant density ($\beta = 0$) media, the closed form Eq. (26) will be reduced to

$$\alpha = \frac{4R}{(1+R)^2}. \tag{29}$$

This represents the relationship between α and R for the one parameter 1D acoustic constant density medium and 1D normal incidence obtained by Innanen (2003). In this case, α becomes $1 - c_0^2/c_1^2$ and R becomes $(c_1 - c_0)\,/\,(c_1 + c_0)$.

3. Derivation of the inversion terms from the closed form

From the closed form Eq. (26), using Taylor expansion on the left hand side

$$\frac{1}{(1+R(\theta))^2} = \left[1 - R(\theta) + R^2(\theta) - \ldots\right]^2,$$

and setting the terms of equal order in the data equal, we have

$$\frac{\alpha_1}{\cos^2\theta} + (1-\tan^2\theta)\beta_1 = 4R(\theta), \tag{30}$$

$$\frac{\alpha_2}{\cos^2\theta} + (1-\tan^2\theta)\beta_2 = -\frac{1}{2}\frac{\alpha_1^2}{\cos^4\theta} - \frac{1}{2}(1+\tan^4\theta)\beta_1^2 + \frac{\tan^2\theta}{\cos^2\theta}\alpha_1\beta_1. \tag{31}$$

For a one-interface example (in Fig. 2), Eqs. (21) and (22) will respectively reduce to the same form as Eqs. (30) and (31), which is shown below.

Assume the interface surface is at depth $z = a$, and suppose $z_s = z_g = 0$. Using the analytic data

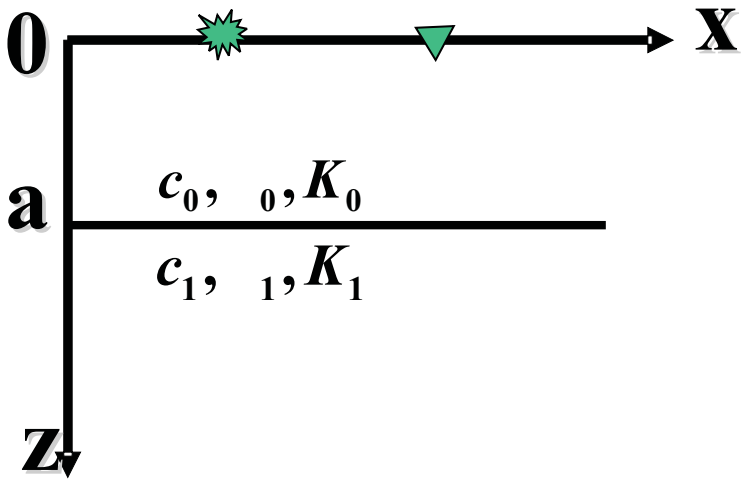

Figure 2: 1D one-interface acoustic model.

(Clayton and Stolt, 1981; Weglein et al., 1986),

$$\widetilde{D}(q_g,\theta)=\rho_0 R(\theta)\frac{e^{2iq_g a}}{4\pi i q_g}, \tag{32}$$

and substituting Eq. (32) into Eq. (21), after Fourier transformation over $2q_g$, for $z>a$ and fixed θ, we get

$$\frac{1}{\cos^2\theta}\alpha_1(z)+(1-\tan^2\theta)\beta_1(z)=4R(\theta)H(z-a). \tag{33}$$

Also, the non-linear solution Eq. (22) will reduce to

$$\begin{aligned}\frac{1}{\cos^2\theta}\alpha_2(z)+(1-\tan^2\theta)\beta_2(z)=&-\frac{1}{2\cos^4\theta}\alpha_1^2(z)-\frac{1}{2}(1+\tan^4\theta)\beta_1^2(z)\\&+\frac{\tan^2\theta}{\cos^2\theta}\alpha_1(z)\beta_1(z),\end{aligned} \tag{34}$$

The two equations Eqs. (33) and (34) agree with Eqs. (30) and (31), respectively.

4.2 Numerical tests

From Eq. (33), we choose two different angles to solve for α_1 and β_1

$$\beta_1(\theta_1,\theta_2)=4\frac{R(\theta_1)\cos^2\theta_1-R(\theta_2)\cos^2\theta_2}{\cos(2\theta_1)-\cos(2\theta_2)}, \tag{35}$$

$$\alpha_1(\theta_1,\theta_2)=\beta_1(\theta_1,\theta_2)+4\frac{R(\theta_1)-R(\theta_2)}{\tan^2\theta_1-\tan^2\theta_2}. \tag{36}$$

Similarly, from Eq. (34), given two different angles we can solve for α_2 and β_2 in terms of α_1 and β_1

$$\begin{aligned}\beta_2(\theta_1,\theta_2)=&\left[-\frac{1}{2}\alpha_1^2\left(\frac{1}{\cos^2\theta_1}-\frac{1}{\cos^2\theta_2}\right)+\alpha_1\beta_1\left(\tan^2\theta_1-\tan^2\theta_2\right)-\frac{1}{2}\beta_1^2\right.\\&\left.\times\left(\cos^2\theta_1-\cos^2\theta_2+\frac{\sin^4\theta_1}{\cos^2\theta_1}-\frac{\sin^4\theta_2}{\cos^2\theta_2}\right)\right]/\left[\cos(2\theta_1)-\cos(2\theta_2)\right],\end{aligned} \tag{37}$$

$$\begin{aligned}\alpha_2(\theta_1,\theta_2)=&\beta_2(\theta_1,\theta_2)+\left[-\frac{1}{2}\alpha_1^2\left(\frac{1}{\cos^4\theta_1}-\frac{1}{\cos^4\theta_2}\right)+\alpha_1\beta_1\left(\frac{\tan^2\theta_1}{\cos^2\theta_1}-\frac{\tan^2\theta_2}{\cos^2\theta_2}\right)\right.\\&\left.-\frac{1}{2}\beta_1^2\left(\tan^4\theta_1-\tan^4\theta_2\right)\right]/\left(\tan^2\theta_1-\tan^2\theta_2\right);\end{aligned} \tag{38}$$

where α_1 and β_1 in Eqs. (37) and (38) denote $\alpha_1(\theta_1,\theta_2)$ and $\beta_1(\theta_1,\theta_2)$, respectively.

For a specific model, $\rho_0=1.0g/cm^3$, $\rho_1=1.1g/cm^3$, $c_0=1500m/s$ and $c_1=1700m/s$, in the following figures we give the results for the relative changes in the P-wave bulk modulus $\left(\alpha=\frac{\Delta K}{K}\right)$, density $\left(\beta=\frac{\Delta\rho}{\rho}\right)$, impedance $\left(\frac{\Delta I}{I}\right)$ and velocity $\left(\frac{\Delta c}{c}\right)$ corresponding to different pairs of θ_1 and θ_2.

From Fig. 3, we can see that when we add α_2 to α_1, the result is much closer to the exact value of α. Furthermore, the result is better behaved; i.e., the plot surface becomes flatter, over a larger

range of precritical angles. Similarly, as shown in Fig. 4, the results of $\beta_1 + \beta_2$ are much better than those of β_1. In addition, the sign of β_1 is wrong at some angles, while, the results for $\beta_1 + \beta_2$ always have the right sign. So after including β_2, the sign of the density is corrected, which is very important in the earth identification, and also the results of $\frac{\Delta I}{I}$ (see Fig. 5) and $\frac{\Delta c}{c}$ (see Fig. 6) are much closer to their exact values respectively compared to the linear results.

Especially, the values of $\left(\frac{\Delta c}{c}\right)_1$ are always greater than zero, that is, the sign of $(\Delta c)_1$ is always positive, which is the same as that of the exact value Δc. We will further discuss this in the next section.

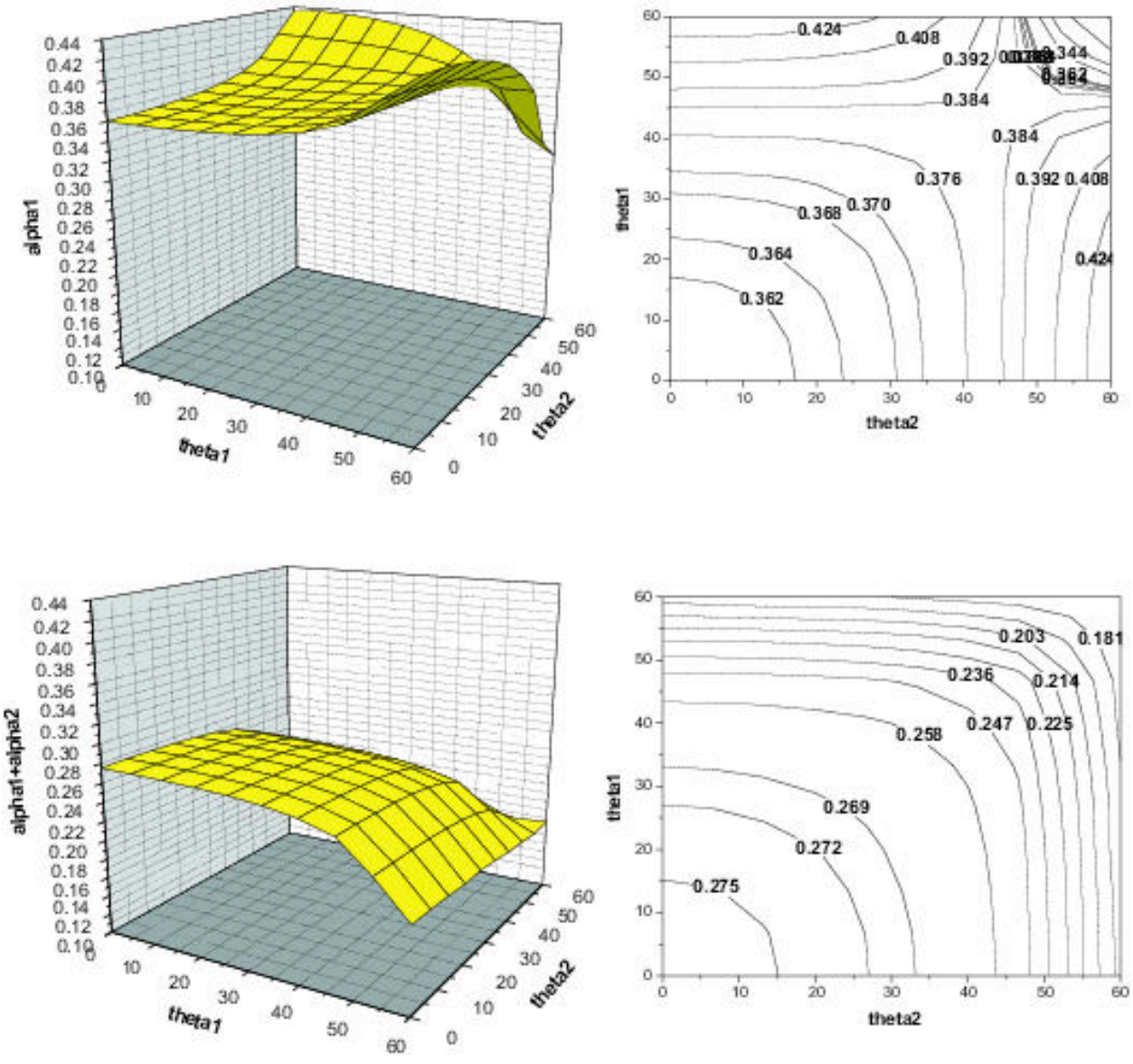

Figure 3: α_1 (top) and $\alpha_1 + \alpha_2$ (bottom) displayed as a function of two different angles. The graphs on the right are the corresponding contour plots of the graphs on the left. In this example, the exact value of α is 0.292.

5 Three important messages

As mentioned before, in general, since the relationship between data and target property changes is non-linear, linear inversion will produce errors in target property prediction. When one actual property change is zero, the linear prediction of the change can be non-zero. Also, when the actual change is positive, the predicted linear approximation can be negative. There is a special parameter for linear inversion of acoustic media, that never suffers the latter problem.

From Eq. (24) we can see that when $c_0 = c_1$, the reflection coefficient is independent of θ, then from the linear form Eq. (36), we have

$$\left(\frac{\Delta c}{c}\right)_1 = \frac{1}{2}(\alpha_1 - \beta_1) = 0 \text{ when } \Delta \mathrm{c} = 0,$$

i.e., when $\Delta c = 0$, $(\Delta c)_1 = 0$. This generalizes to $(\Delta c)_1 > 0$ when $\Delta c > 0$, or $(\Delta c)_1 < 0$ when $\Delta c < 0$, as well. This can be shown mathematically (See Appendix B for details).

Therefore, we can, first, get the right sign of the relative change in P-wave velocity from the linear inversion $(\Delta c)_1$, then, get more accurate values by including non-linear terms.

Another interesting point is that the image does not move when the velocity does not change across an interface, i.e., $c_0 = c_1$, since, in this situation, the integrands of imaging terms $\alpha_1 - \beta_1$ in Eq. (22) are zero. We can see this more explicitly when we change the two parameters α and β to $\frac{\Delta c}{c}$ and β. Using the two relationships below (See details in Appendix A)

$$\left(\frac{\Delta c}{c}\right)_1 = \frac{1}{2}(\alpha_1 - \beta_1),$$

and

$$\left(\frac{\Delta c}{c}\right)_2 = \frac{1}{2}\left[\frac{1}{4}(\alpha_1 + \beta_1)^2 - \beta_1^2 + (\alpha_2 - \beta_2)\right],$$

rewriting Eq. (22) as

$$\begin{aligned}\frac{1}{\cos^2\theta}\left(\frac{\Delta c}{c}\right)_2(z) + \beta_2(z) =& \frac{\cos^2\theta - 2}{2\cos^4\theta}\left(\frac{\Delta c}{c}\right)_1^2(z) - \frac{1}{2}\beta_1^2(z) \\ &- \frac{1}{\cos^4\theta}\left(\frac{\Delta c}{c}\right)_1'(z)\int_0^z dz'\left(\frac{\Delta c}{c}\right)_1 \\ &- \frac{1}{\cos^2\theta}\beta_1'(z)\int_0^z dz'\left(\frac{\Delta c}{c}\right)_1. \end{aligned} \tag{39}$$

This equation indicates two important concepts. One is leakage: there is no leakage correction at all in this expression. Here the leakage means that, if the actual value of α (relative changes in P-wave bulk modulus) is zero, its linear approximation α_1 could be non-zero since α and β are coupled together (like the coupled term $\alpha_1\beta_1$ in Eq. 22) and α_1 could get leakage values from β_1. While in Eq. (39), no such coupled term is present at all and thus, if the actual changes in the velocity are zero, then its linear inversion $\left(\frac{\Delta c}{c}\right)_1$ would be zero and there would be no leakage from β_1. This leakage issue or coupled term has no analogue in the 1D one parameter acoustic case (Eq. 23) since in this case we only have one parameter and there is no other parameter to leak

into. In other words, in the one parameter (velocity) case, each 'jump' in the amplitude of the data (primaries only) corresponds to each wrong location with a wrong amplitude for the parameter predicted in the linear inverse step; while in the two parameter case of this paper, each 'jump' in the data no longer has the simple one-to-one relationship with the amplitude and location of the two parameters.

The other concept is purposeful perturbation. The integrand $\left(\frac{\Delta c}{c}\right)_1$ of the imaging terms clearly tells that if we have the right velocity, the imaging terms will automatically be zero even without doing any integration; otherwise, if we do not have the right velocity, these imaging terms would be used to move the interface closer to the right location from the wrong location. The conclusion from this equation is that the depth imaging terms depend only on the velocity errors.

6 Conclusion

In this paper, we derive the first two parameter direct non-linear inversion solution for 1D acoustic media with 2D experiment. Numerical tests show that the terms beyond linearity in earth property identification subseries provide added value. Although the model we used in the numerical tests is simple (for some readers), Eqs. (21) and (22) also work for more complex models since the inverse scattering series is a direct inversion procedure which inverts data directly without knowing the specific properties of the target.

As shown above, adding one parameter in the wave equation makes the problem much more complicated than the one parameter case. Three important concepts (purposeful perturbation, leakage and special parameter for inversion) have been discussed on the linear and non-linear derivations. More discoveries are being obtained through on-going research.

The work presented in this paper is an important step for target identification towards more realism. The encouraging numerical results motivated us to move one step further — extension of our work to the elastic case (Boyse and Keller, 1986, e.g.,) using three parameters.

Acknowledgements

We thank all sponsors of M-OSRP and we are grateful that Robert Keys and Douglas Foster for valuable discussions.

Appendix A

In this appendix, we derive the expressions of $\left(\frac{\Delta c}{c}\right)_1$, $\left(\frac{\Delta c}{c}\right)_2$, $\left(\frac{\Delta I}{I}\right)_1$ and $\left(\frac{\Delta I}{I}\right)_2$ in terms of α_1, β_1 and α_2, β_2. Define $\Delta c = c - c_0$, $\Delta I = I - I_0$, $\Delta K = K - K_0$ and $\Delta\rho = \rho - \rho_0$.

Since $K = c^2\rho$, then we have

$$(c - \Delta c)^2 = \frac{K - \Delta K}{\rho - \Delta\rho}.$$

Divided by c^2, the equation above will become

$$2\left(\frac{\Delta c}{c}\right) - \left(\frac{\Delta c}{c}\right)^2 = \frac{\frac{\Delta K}{K} - \frac{\Delta\rho}{\rho}}{1 - \frac{\Delta\rho}{\rho}}.$$

Remember that $\alpha = \frac{\Delta K}{K}$ and $\beta = \frac{\Delta \rho}{\rho}$, the equation above can be rewritten as

$$2\left(\frac{\Delta c}{c}\right) - \left(\frac{\Delta c}{c}\right)^2 = \frac{\alpha - \beta}{1 - \beta}.$$

Then we have

$$2\left(\frac{\Delta c}{c}\right) - \left(\frac{\Delta c}{c}\right)^2 = (\alpha - \beta)(1 + \beta + \beta^2 + \cdots), \tag{40}$$

where the series expansion is valid for $|\beta| < 1$.

Similar to Eqs. (17) and (18), $\frac{\Delta c}{c}$ can be expanded as

$$\left(\frac{\Delta c}{c}\right) = \left(\frac{\Delta c}{c}\right)_1 + \left(\frac{\Delta c}{c}\right)_2 + \cdots. \tag{41}$$

Then substitute Eqs. (41), (17) and (18) into Eq. (40), and set those terms of equal order equal on both sides of Eq. (40), we can get

$$\left(\frac{\Delta c}{c}\right)_1 = \frac{1}{2}(\alpha_1 - \beta_1), \tag{42}$$

and

$$\left(\frac{\Delta c}{c}\right)_2 = \frac{1}{2}\left[\frac{1}{4}(\alpha_1 + \beta_1)^2 - \beta_1^2 + (\alpha_2 - \beta_2)\right]. \tag{43}$$

Similarly, using $I = c\rho$, we have

$$(I - \Delta I)^2 = (K - \Delta K)(\rho - \Delta \rho).$$

Divided by I^2, the equation above will become

$$2\left(\frac{\Delta I}{I}\right) - \left(\frac{\Delta I}{I}\right)^2 = \alpha + \beta - \alpha\beta. \tag{44}$$

Expanding $\frac{\Delta I}{I}$ as

$$\left(\frac{\Delta I}{I}\right) = \left(\frac{\Delta I}{I}\right)_1 + \left(\frac{\Delta I}{I}\right)_2 + \cdots, \tag{45}$$

and substitute Eqs. (45), (17) and (18) into Eq. (44), setting those terms of equal order equal on both sides of Eq. (44), we can get

$$\left(\frac{\Delta I}{I}\right)_1 = \frac{1}{2}(\alpha_1 + \beta_1), \tag{46}$$

and

$$\left(\frac{\Delta I}{I}\right)_2 = \frac{1}{2}\left[\frac{1}{4}(\alpha_1 - \beta_1)^2 + (\alpha_2 + \beta_2)\right]. \tag{47}$$

Appendix B

In this appendix, we show that $\left(\frac{\Delta c}{c}\right)_1$ has the same sign as Δc. For the single interface example, from Eqs. (36) and (42), we have

$$\left(\frac{\Delta c}{c}\right)_1 = 2\frac{R(\theta_1) - R(\theta_2)}{\tan^2\theta_1 - \tan^2\theta_2}.$$

The reflection coefficient is

$$R(\theta) = \frac{(\rho_1/\rho_0)(c_1/c_0)\sqrt{1-\sin^2\theta} - \sqrt{1-(c_1^2/c_0^2)\sin^2\theta}}{(\rho_1/\rho_0)(c_1/c_0)\sqrt{1-\sin^2\theta} + \sqrt{1-(c_1^2/c_0^2)\sin^2\theta}}.$$

Let

$$A(\theta) = (\rho_1/\rho_0)(c_1/c_0)\sqrt{1-\sin^2\theta},$$
$$B(\theta) = \sqrt{1-(c_1^2/c_0^2)\sin^2\theta}.$$

Then

$$R(\theta_1) - R(\theta_2) = 2\frac{A(\theta_1)B(\theta_2) - B(\theta_1)A(\theta_2)}{[A(\theta_1)+B(\theta_1)]\,[A(\theta_2)+B(\theta_2)]},$$

where the denominator is greater than zero. The numerator is

$$\begin{aligned}2\left[A(\theta_1)B(\theta_2) - B(\theta_1)A(\theta_2)\right] =& 2(\rho_1/\rho_0)(c_1/c_0)\left[\sqrt{1-\sin^2\theta_1}\sqrt{1-(c_1^2/c_0^2)\sin^2\theta_2}\right.\\ &\left.-\sqrt{1-\sin^2\theta_2}\sqrt{1-(c_1^2/c_0^2)\sin^2\theta_1}\right].\end{aligned}$$

Let

$$C = \sqrt{1-\sin^2\theta_1}\sqrt{1-(c_1^2/c_0^2)\sin^2\theta_2},$$
$$D = \sqrt{1-\sin^2\theta_2}\sqrt{1-(c_1^2/c_0^2)\sin^2\theta_1}.$$

Then,

$$C^2 - D^2 = \left(\frac{c_1^2}{c_0^2} - 1\right)(sin^2\theta_1 - sin^2\theta_2).$$

When $c_1 > c_0$ and $\theta_1 > \theta_2$, we have (Noticing that both C and D are positive.)

$$\left(\frac{c_1^2}{c_0^2} - 1\right)(sin^2\theta_1 - sin^2\theta_2) > 0,$$

so

$$R(\theta_1) - R(\theta_2) > 0;$$

Similarly, when $c_1 < c_0$ and $\theta_1 > \theta_2$, we have

$$\left(\frac{c_1^2}{c_0^2} - 1\right)(sin^2\theta_1 - sin^2\theta_2) < 0,$$

so

$$R(\theta_1) - R(\theta_2) < 0.$$

Remembering that $\left(\frac{\Delta c}{c}\right)_1 = 2\frac{R(\theta_1)-R(\theta_2)}{\tan^2\theta_1-\tan^2\theta_2}$. So for $c_1 > c_0$, $(\Delta c)_1 > 0$ and for $c_1 < c_0$, $(\Delta c)_1 < 0$.

References

Boyse, W. E. and J. B. Keller. "Inverse elastic scattering in three dimensions." *J. Acoust. Soc. Am.* 79 (1986): 215–218.

Clayton, R. W. and R. H. Stolt. "A Born-WKBJ inversion method for acoustic reflection data." *Geophysics* 46 (1981): 1559–1567.

Innanen, Kristopher. A. *Methods for the treatment of acoustic and absorptive/dispersive wave field measurements*. PhD thesis, University of British Columbia, 2003.

Keys, R. G. "Polarity reversals in reflections from layered media." *Geophysics* 54 (1989): 900–905.

Liu, F., A. B. Weglein K. A. Innanen, and B. G. Nita. "Extension of the non-linear depth imaging capability of the inverse scattering series to multidimensional media: strategies and numerical results." *9th Ann. Cong. SBGf, Expanded Abstracts*. . SBGf, 2005.

Matson, K. H. *An inverse-scattering series method for attenuating elastic multiples from multi-component land and ocean bottom seismic data*. PhD thesis, University of British Columbia, 1997.

Sen, M. and P. L. Stoffa. *Global Optimization Methods in Geophysical Inversion*. Amsterdam: Elsevier, 1995.

Shaw, S. A. *An inverse scattering series algorithm for depth imaging of reflection data from a layered acoustic medium with an unknown velocity model*. PhD thesis, University of Houston, 2005.

Shaw, S. A., A. B. Weglein, D. J. Foster, K. H. Matson, and R. G. Keys. "Isolation of a leading order depth imaging series and analysis of its convergence properties." *M-OSRP Annual Report* 2 (2003): 157–195.

Tarantola, A., A. Nercessian, and O. Gauthier. "Nonlinear Inversion of Seismic Reflection Data." *54rd Annual Internat. Mtg., Soc. Expl. Geophys., Expanded Abstracts*. . Soc. Expl. Geophys., 1984. 645–649.

Taylor, J. R. *Scattering theory: the quantum theory of nonrelativistic collisions*. John Wiley and Sons, Inc., 1972.

Weglein, A. B., F. V. Araújo, P. M. Carvalho, R. H. Stolt, K. H. Matson, R. T. Coates, D. Corrigan, D. J. Foster, S. A. Shaw, and H. Zhang. "Inverse scattering series and seismic exploration." *Inverse Problems* 19 (2003): R27–R83.

Weglein, A. B., D. J. Foster, K. H. Matson, S. A. Shaw, P. M. Carvalho, and D. Corrigan. "Predicting the correct spatial location of reflectors without knowing or determining the precise medium and wave velocity: initial concept, algorithm and analytic and numerical example." *Journal of Seismic Exploration* 10 (2002): 367–382.

Weglein, A. B., F. A. Gasparotto, P. M. Carvalho, and R. H. Stolt. "An inverse-scattering series method for attenuating multiples in seismic reflection data." *Geophysics* 62 (1997): 1975–1989.

Weglein, A. B. and R. H. Stolt. 1992 "Approaches on linear and non-linear migration-inversion.". Personal Communication.

Weglein, A. B., P. B. Violette, and T. H. Keho. "Using multiparameter Born theory to obtain certain exact multiparameter inversion goals." *Geophysics* 51 (1986): 1069–1074.

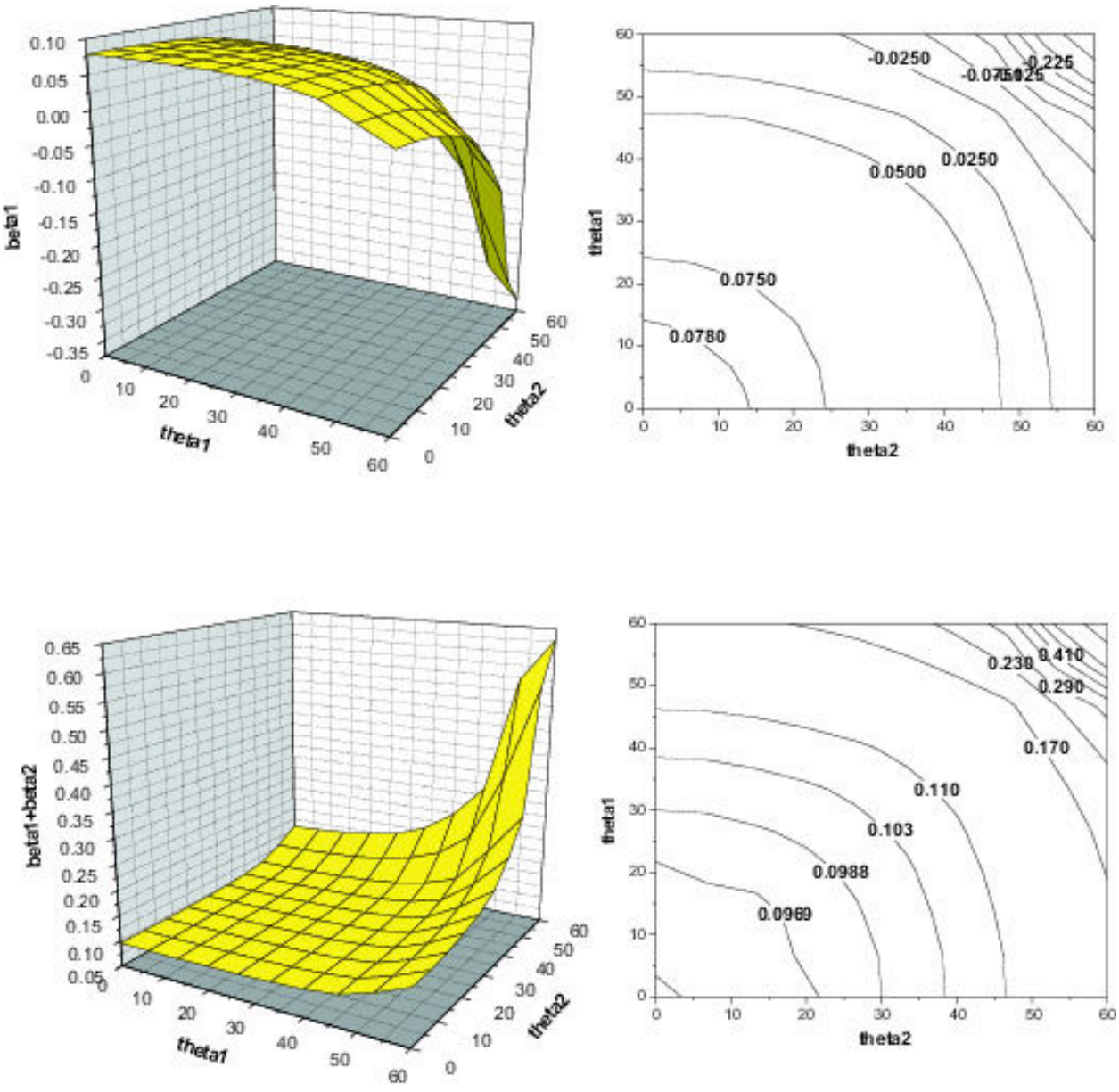

Figure 4: β_1 (top) and $\beta_1 + \beta_2$ (bottom). In this example, the exact value of β is 0.09.

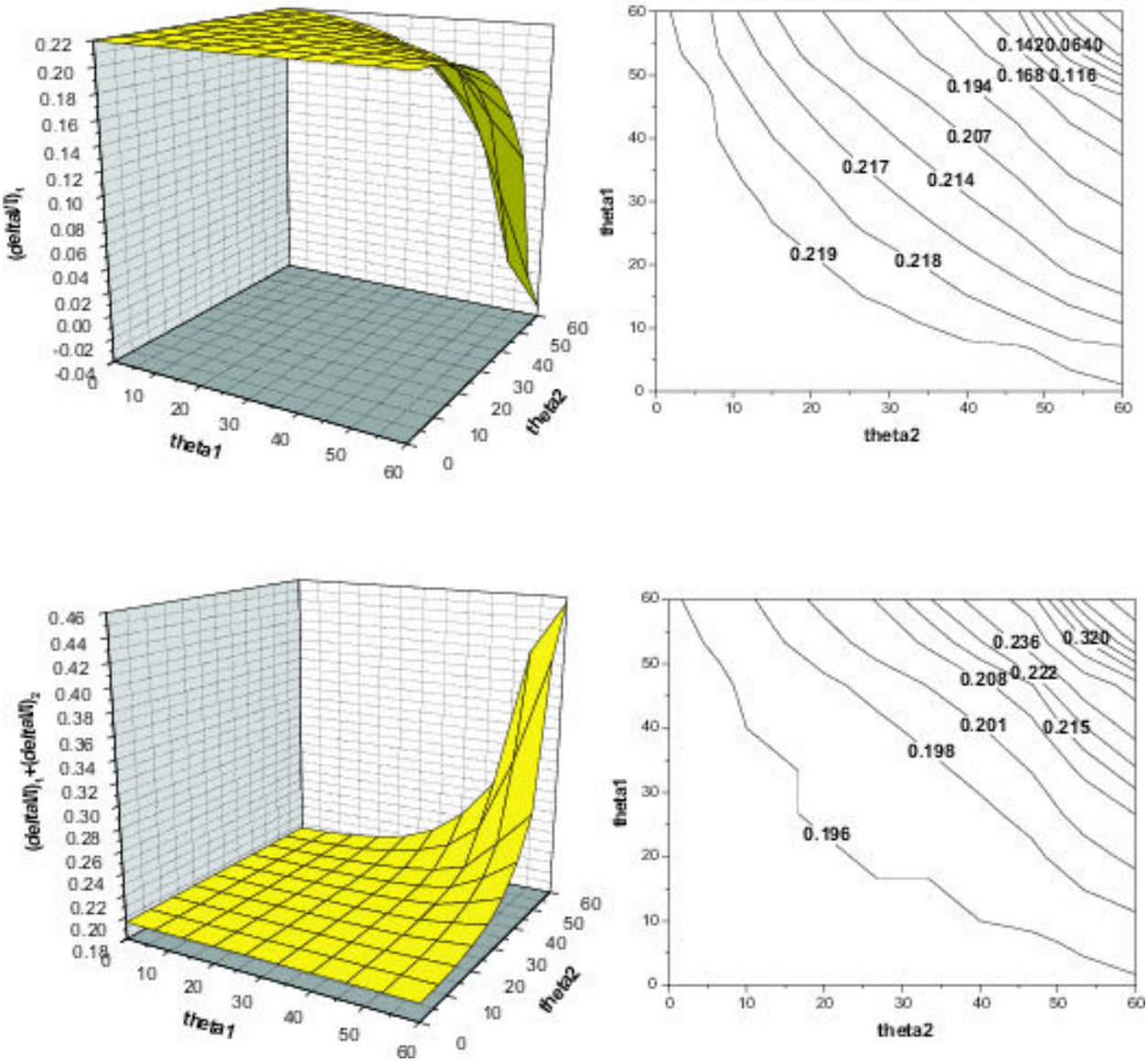

Figure 5: Linear approximation to relative change in impedance (see details in Appendix A) $\left(\frac{\Delta I}{I}\right)_1 = \frac{1}{2}(\alpha_1 + \beta_1)$ (top). Sum of linear and first non-linear terms $\left(\frac{\Delta I}{I}\right)_1 + \left(\frac{\Delta I}{I}\right)_2 = \left(\frac{\Delta I}{I}\right)_1 + \frac{1}{2}\left[\frac{1}{4}(\alpha_1 - \beta_1)^2 + (\alpha_2 + \beta_2)\right]$ (bottom). In this example, the exact value of $\frac{\Delta I}{I}$ is 0.198.

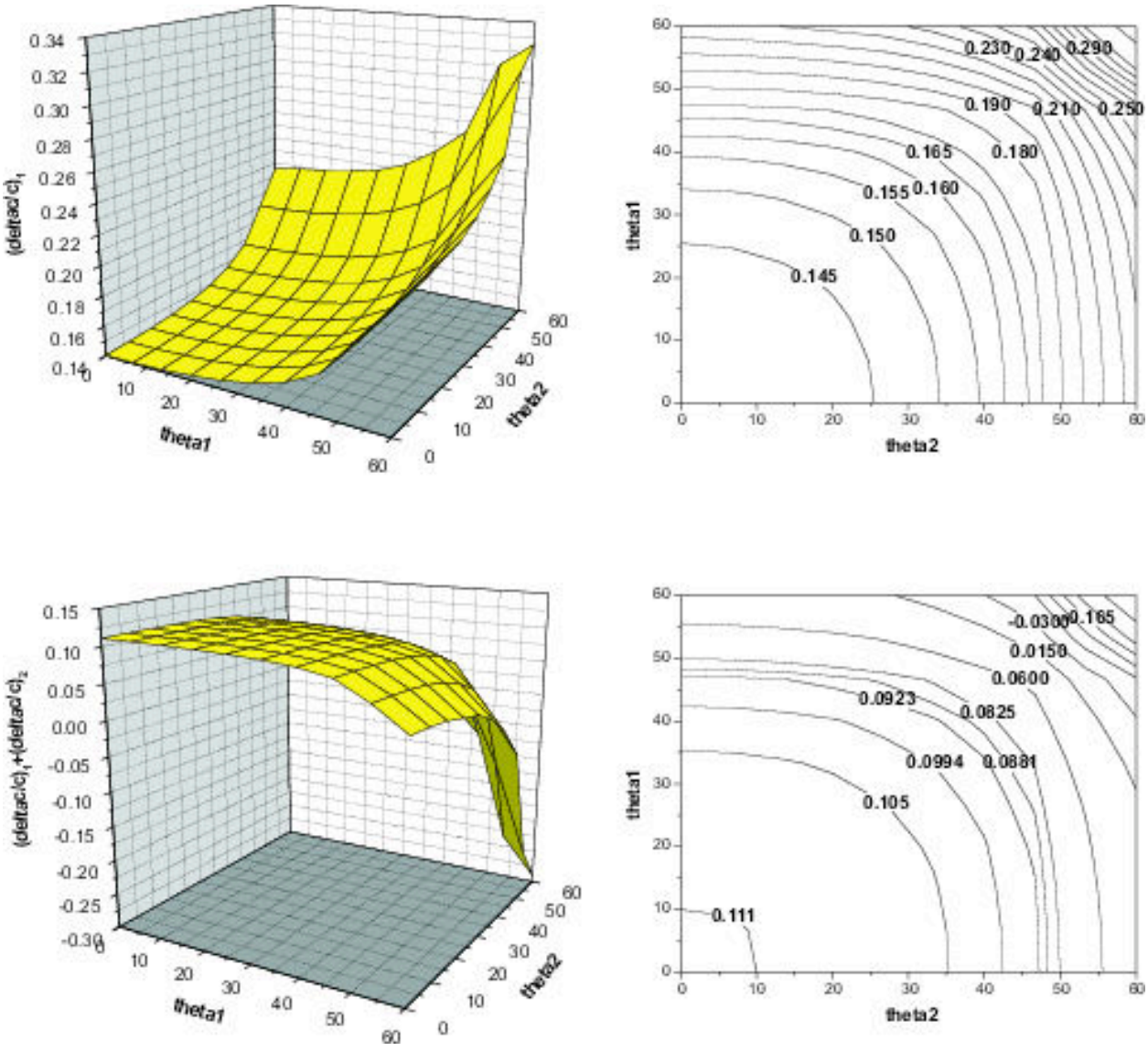

Figure 6: Linear approximation to relative change in velocity (see details in Appendix A) $\left(\frac{\Delta c}{c}\right)_1 = \frac{1}{2}(\alpha_1 - \beta_1)$ (top). Sum of linear and first non-linear terms $\left(\frac{\Delta c}{c}\right)_1 + \left(\frac{\Delta c}{c}\right)_2 = \left(\frac{\Delta c}{c}\right)_1 + \frac{1}{2}\left[\frac{1}{4}(\alpha_1 + \beta_1)^2 - \beta_1^2 + (\alpha_2 - \beta_2)\right]$ (bottom). In this example, the exact value of $\frac{\Delta c}{c}$ is 0.118.

Direct non-linear inversion of multi-parameter 1D elastic media using the inverse scattering series

H. Zhang and A. B. Weglein

Abstract

In this paper, we present the first non-linear direct target identification method and algorithm for 1D elastic media (P velocity, shear velocity and density vary in depth) from the inverse scattering series. The results clearly demonstrate that, in order to achieve full elastic inversion, all four components of data ($\hat{D}^{PP}$, $\hat{D}^{PS}$, $\hat{D}^{SP}$ and $\hat{D}^{SS}$) are needed. The terms for moving mislocated reflectors are separated from amplitude correction terms. Although in principle this direct inversion approach requires all four components of elastic data, synthetic tests indicate that consistent value-added results may be achieved given only $\hat{D}^{PP}$ measurements. We can reasonably infer that further value would derive from actually measuring $\hat{D}^{PP}$, $\hat{D}^{PS}$, $\hat{D}^{SP}$ and $\hat{D}^{SS}$ as the method requires. For the case that all four components of data are available, we give one consistent method to solve for all of the second terms (the first terms beyond linear). The method is direct with neither a model matching nor cost function minimization.

1 Introduction

The ultimate objective of inverse problems is to determine medium and target properties from measurements external to the object under investigation. At the very first moment of problem definition, there is an immediate requirement and unavoidable expectation, that the model type of the medium be specified. In that step of model type specification, the number and type of parameters and dimension of spatial variation of those parameters are given, and carefully prescribed, and in that way you provide the inverse problem with clarity and meaning. Among the different model types used in exploration seismology are, e.g., acoustic, elastic, heterogeneous, anisotropic, and anelastic, and perhaps most important, the dimension of variability of the properties associated with these model types. One would reasonably expect that the details of methods and algorithms for inversion objectives, and any tasks associated with achieving those ultimate objectives, would overall and each separately depend upon that starting assumption on model type. However, the ultimate objective of seismic inversion has never been achieved in a straight ahead single step manner directly from the seismic data, and that lack of success has not been due to a lack of computer power. The indirect model matching procedures have that computer power problem, especially in the applications to a multi-dimensional complex earth, where it is rare to have a reasonable proximal starting model. Those complex ill-defined geologic circumstances are the biggest impediments and challenges to current exploration and production seismic effectiveness.

The only direct multi-dimensional inversion procedure for seismic application, the inverse scattering series, does not require a proximal starting model and only assumes reference medium information. Of course, the whole inverse series has very limited application (Carvalho et al., 1992). What makes the inverse scattering series powerful is the so-called task isolated subseries which is a subset of the whole series that acts like only one task is performed for that subset (Weglein et al., 2003). All of these subseries act in a certain sequence so that the total seismic data can be processed accordingly. The order of processing is : (1) free-surface multiple removal, (2) internal multiple

removal, (3) depth imaging without velocity, and (4) inversion or target identification. Since the entire process requires only reflection data and reference medium information, it is reasonable to assume that these intermediate steps, i.e., all of the derived subseries which are associated with achieving that objective, would also be attainable with only the reference medium and reflection data and no subsurface medium information is required.

The free surface multiple removal and internal multiple attenuation subseries have been presented by (Carvalho, 1992; Araújo, 1994; Weglein et al., 1997; Matson, 1997). Those two multiple procedures are model type independent, i.e., they work for acoustic, elastic and anelastic medium. Taking internal multiples from attenuation to elimination is being studied (Ramírez and Weglein, 2005). The task specific subseries associated with primaries (i.e., for imaging and inversion) have been progressed too: (1) imaging without the velocity for one parameter 1D and then 2D acoustic media (Weglein et al., 2002; Shaw and Weglein, 2003; Shaw et al., 2003a; Shaw et al., 2003b; Shaw et al., 2004; Shaw and Weglein, 2004; Liu and Weglein, 2003; Liu et al., 2004; Liu et al., 2005), and (2) direct non-linear inversion for multi-parameter 1D acoustic and then elastic media (Zhang and Weglein, 2005). Furthermore, recent work (Innanen and Weglein, 2004; Innanen and Weglein, 2005) suggests that some well-known seismic processing tasks associated with resolution enhancement (i.e., "Q-compensation") can be accomplished within the task-separated inverse scattering series framework. In this paper, we focus on item (2) above.

Compared with model type independent multiple removal procedures, there is a full expectation that tasks and algorithms associated with primaries will have a closer interest in model type. For example, there is no way to even imagine that medium property identification can take place without reference to a specific model type. Tasks and issues associated with structural determination, without knowing the medium, are also vastly different depending on the dimension of variation number of velocities that are required for imaging. Hence, a staged approach and isolation of tasks philosophy is essential in this yet tougher neighborhood, and even more in demand for seeking insights and then practical algorithms for these more complicated and daunting objectives. We adopt the staged and isolation of issues approach for primaries. The isolated task achievement plan can often spin-off incomplete but useful intermediate objectives. The test and standard is not necessarily how complete the method is but rather how does it compare to, and improve upon, current best practice.

The stages within the strategy for primaries are as follows: (1) 1D earth, with one parameter, velocity as a function of depth, and a normal incidence wave, (2) 1D earth with one parameter subsurface and offset data, one shot record; (3) 2D earth with one parameter, velocity, varying in x and z, and a suite of shot records; (4) 1D acoustic earth with two parameters varying, velocity and density, one propagation velocity, and one shot record of PP data, and (5) 1D elastic earth, two elastic isotropic parameters and density, and two wave speeds, for P and S waves, and PP, PS, SP, and SS shot records data collected. This paper takes another step of direct non-linear inversion methodology, and task isolation and specifically for tasks associated with primaries, to the 1D elastic case, stage (5). The model is elastic and another paper in acoustic has been presented in Zhang and Weglein (2005). We take these steps and learn to navigate through this complexity and steer it towards useful and powerful algorithms.

However, more realism is more complicated with more issues involved. Following the task separation strategy, we ask the question what kind of tasks should we expect in this more complex, elastic, setting? In the acoustic case, for example, the acoustic medium only supports P-waves, and hence only one reference velocity (P-wave velocity) is involved. Therefore, when only one velocity is incorrect (i.e., poorly estimated), there exists only one "mislocation" for each parameter, and the

imaging terms only need to correct this one mislocation. When we extend our previous work on the two parameter acoustic case to the present three parameter elastic case, there will be four mislocations because of the two reference velocities (P wave velocity and S velocity). Our reasoning is that the elastic medium supports both P- and S-wave propagation, and hence two reference velocities (P-wave velocity and S-wave velocity) are involved. When both of these velocities are incorrect, generally, there exist four mislocations due to each of four different combinations [1] of the two wrong velocities. Therefore, in non-linear elastic imaging-inversion, the imaging terms need to correct the four mislocations arising from linear inversion of any single mechanical property, such that a single correct location for the corresponding actual change in that property is determined.

In this paper, the first non-linear inversion term for three parameter 1D elastic medium is presented. It is demonstrated that under the inverse scattering series inversion framework, all four components of the data are needed in order to perform full elastic inversion. For the case that we don't have all four components data and only PP data are available, encouraging inversion results have been obtained by constructing other components of data from PP data. This means that we could perform elastic inversion only using pressure measurements, i.e. towed streamer data. For the case that all four components of data are available, a consistent method is provided.

The paper has the following structure: the next section is a brief introduction to the inverse scattering series and then presents, respectively, the derivations and numerical tests for elastic non-linear inversion when only PP data is available. A full non-linear elastic inversion method is also provided. Finally we will present some concluding remarks.

2 Background for 2D elastic inversion

In this section we consider the inversion problem in two dimensions for an elastic medium. We start with the displacement space, and then, for convenience (see e.g., Weglein and Stolt, 1992; Aki and Richards, 2002), we change the basis and transform the equations to PS space. Finally, we do the elastic inversion in the PS domain.

2.1 In the displacement space

We begin with some basic equations in the displacement space (Matson, 1997):

$$L\mathbf{u} = \mathbf{f}, \tag{1}$$

$$L_0\mathbf{u} = \mathbf{f}, \tag{2}$$

$$LG = \delta, \tag{3}$$

$$L_0G_0 = \delta, \tag{4}$$

where L and L_0 are the differential operators that describe the wave propagation in the actual and reference medium, respectively, $\mathbf{u}$ and $\mathbf{f}$ are the corresponding displacement and source terms,

[1] The "four combinations" refers to PP, PS, SP and SS, where, for instance, PP means P-wave incidence, and P-wave reflection. Since P-waves non-normal incidence on an elastic interface can produce S-waves, or vice versa, which in those cases are known as converted waves (Aki and Richards, 2002), the elastic data generally contain four components: PP, PS, SP and SS.

respectively, and G and G_0 are the corresponding Green's operators for the actual and reference medium.

Following closely Weglein et al. (1997); Weglein et al. (2002) and Weglein et al. (2003), defining the perturbation $V = L_0 - L$, the Lippmann- Schwinger equation for the elastic media in the displacement space is

$$G = G_0 + G_0 V G. \tag{5}$$

Iterating this equation back into itself generates the Born series

$$G = G_0 + G_0 V G_0 + G_0 V G_0 V G_0 + \cdots . \tag{6}$$

We define the data D as the measured values of the scattered wave field. Then, on the measurement surface, we have

$$D = G_0 V G_0 + G_0 V G_0 V G_0 + \cdots . \tag{7}$$

Expanding V as a series in orders of D we have

$$V = V_1 + V_2 + V_3 + \cdots . \tag{8}$$

Substituting Eq. (8) into Eq. (7), evaluating Eq. (7), and setting terms of equal order in the data equal, the equations that determine V_1, V_2, ... from D and G_0 would be obtained.

$$D = G_0 V_1 G_0, \tag{9}$$

$$0 = G_0 V_2 G_0 + G_0 V_1 G_0 V_1 G_0, \tag{10}$$

$$\vdots$$

In the actual medium, the 2-D elastic wave equation is (Weglein and Stolt, 1992)

$$L\mathbf{u} \equiv \left[\rho\omega^2 \begin{pmatrix} 1 & 0 \\ 0 & 1 \end{pmatrix} + \begin{pmatrix} \partial_1\gamma\partial_1 + \partial_2\mu\partial_2 & \partial_1(\gamma - 2\mu)\partial_2 + \partial_2\mu\partial_1 \\ \partial_2(\gamma - 2\mu)\partial_1 + \partial_1\mu\partial_2 & \partial_2\gamma\partial_2 + \partial_1\mu\partial_1 \end{pmatrix}\right] \begin{bmatrix} u_1 \\ u_2 \end{bmatrix} = \mathbf{f}, \tag{11}$$

where

$\mathbf{u} = \begin{bmatrix} u_1 \\ u_2 \end{bmatrix}$ = displacement,

ρ = density,

γ = bulk modulus ($\equiv \rho\alpha^2$ where α = P-wave velocity),

μ = shear modulus ($\equiv \rho\beta^2$ where β = S-wave velocity),

ω = temporal frequency (angular), ∂_1 and ∂_2 denote the derivative over x and z, respectively, and $\mathbf{f}$ is the source term.

For constant $(\rho, \gamma, \mu) = (\rho_0, \gamma_0, \mu_0)$, $(\alpha, \beta) = (\alpha_0, \beta_0)$, the operator L becomes

$$L_0 \equiv \left[\rho_0\omega^2 \begin{pmatrix} 1 & 0 \\ 0 & 1 \end{pmatrix} + \begin{pmatrix} \gamma_0\partial_1^2 + \mu_0\partial_2^2 & (\gamma_0 - \mu_0)\partial_1\partial_2 \\ (\gamma_0 - \mu_0)\partial_1\partial_2 & \mu_0\partial_1^2 + \gamma_0\partial_2^2 \end{pmatrix}\right]. \tag{12}$$

Then,

$$V \equiv L_0 - L$$

$$= -\rho_0 \begin{bmatrix} a_\rho\omega^2 + \alpha_0^2\partial_1 a_\gamma \partial_1 + \beta_0^2\partial_2 a_\mu \partial_2 & \partial_1(\alpha_0^2 a_\gamma - 2\beta_0^2 a_\mu)\partial_2 + \beta_0^2\partial_2 a_\mu \partial_1 \\ \partial_2(\alpha_0^2 a_\gamma - 2\beta_0^2 a_\mu)\partial_1 + \beta_0^2\partial_1 a_\mu \partial_2 & a_\rho\omega^2 + \alpha_0^2\partial_2 a_\gamma \partial_2 + \beta_0^2\partial_1 a_\mu \partial_1 \end{bmatrix}, \quad (13)$$

where $a_\rho \equiv \frac{\rho}{\rho_0} - 1$, $a_\gamma \equiv \frac{\gamma}{\gamma_0} - 1$ and $a_\mu \equiv \frac{\mu}{\mu_0} - 1$ are the three parameters we choose to do the elastic inversion. For a 1D earth (i.e. a_ρ, a_γ and a_μ are only functions of depth z), the expression above for V becomes

$$V = -\rho_0 \begin{bmatrix} a_\rho\omega^2 + \alpha_0^2 a_\gamma \partial_1^2 + \beta_0^2\partial_2 a_\mu \partial_2 & (\alpha_0^2 a_\gamma - 2\beta_0^2 a_\mu)\partial_1\partial_2 + \beta_0^2\partial_2 a_\mu \partial_1 \\ \partial_2(\alpha_0^2 a_\gamma - 2\beta_0^2 a_\mu)\partial_1 + \beta_0^2 a_\mu \partial_1\partial_2 & a_\rho\omega^2 + \alpha_0^2\partial_2 a_\gamma \partial_2 + \beta_0^2 a_\mu \partial_1^2 \end{bmatrix}. \quad (14)$$

2.2 Transforming to PS space

For convenience, we can change the basis from $\mathbf{u} = \begin{bmatrix} u_1 \\ u_2 \end{bmatrix}$ to $\begin{pmatrix} \phi^P \\ \phi^S \end{pmatrix}$ to allow L_0 to be diagonal,

$$\mathbf{\Phi} = \begin{pmatrix} \phi^P \\ \phi^S \end{pmatrix} = \begin{bmatrix} \gamma_0(\partial_1 u_1 + \partial_2 u_2) \\ \mu_0(\partial_1 u_2 - \partial_2 u_1) \end{bmatrix}, \quad (15)$$

also, we have

$$\begin{pmatrix} \phi^P \\ \phi^S \end{pmatrix} = \Gamma_0 \Pi \mathbf{u} = \begin{bmatrix} \gamma_0(\partial_1 u_1 + \partial_2 u_2) \\ \mu_0(\partial_1 u_2 - \partial_2 u_1) \end{bmatrix}, \quad (16)$$

where $\Pi = \begin{pmatrix} \partial_1 & \partial_2 \\ -\partial_2 & \partial_1 \end{pmatrix}$, $\Gamma_0 = \begin{pmatrix} \gamma_0 & 0 \\ 0 & \mu_0 \end{pmatrix}$. In the reference medium, the operator L_0 will transform in the new basis via a transformation

$$\hat{L}_0 \equiv \Pi L_0 \Pi^{-1}\Gamma_0^{-1} = \begin{pmatrix} \hat{L}_0^P & 0 \\ 0 & \hat{L}_0^S \end{pmatrix},$$

where $\hat{L}_0$ is L_0 transformed to PS space, $\Pi^{-1} = \begin{pmatrix} \partial_1 & -\partial_2 \\ \partial_2 & \partial_1 \end{pmatrix} \nabla^{-2}$ is the inverse matrix of Π, $\hat{L}_0^P = \omega^2/\alpha_0^2 + \nabla^2$, $\hat{L}_0^S = \omega^2/\beta_0^2 + \nabla^2$, and

$$\mathbf{F} = \Pi \mathbf{f} = \begin{pmatrix} F^P \\ F^S \end{pmatrix}. \quad (17)$$

Then, in PS domain, Eq. (2) becomes,

$$\begin{pmatrix} \hat{L}_0^P & 0 \\ 0 & \hat{L}_0^S \end{pmatrix} \begin{pmatrix} \phi^P \\ \phi^S \end{pmatrix} = \begin{pmatrix} F^P \\ F^S \end{pmatrix}. \quad (18)$$

Since $G_0 \equiv L_0^{-1}$, let $\hat{G}_0^P = \left(\hat{L}_0^P\right)^{-1}$ and $\hat{G}_0^S = \left(\hat{L}_0^S\right)^{-1}$, then the displacement G_0 in PS domain becomes

$$\hat{G}_0 = \Gamma_0 \Pi G_0 \Pi^{-1} = \begin{pmatrix} \hat{G}_0^P & 0 \\ 0 & \hat{G}_0^S \end{pmatrix}. \quad (19)$$

So, in the reference medium, after transforming from the displacement domain to PS domain, both L_0 and G_0 become diagonal.

Multiplying Eq. (5) from the left by the operator $\Gamma_0\Pi$ and from the right by the operator Π^{-1}, and using Eq. (19),

$$\Gamma_0 \Pi G \Pi^{-1} = \hat{G}_0 + \hat{G}_0 \left(\Pi V \Pi^{-1}\Gamma_0^{-1}\right) \Gamma_0 \Pi G \Pi^{-1}$$

$$= \hat{G}_0 + \hat{G}_0 \hat{V} \hat{G}, \tag{20}$$

where the displacement Green's operator G is transformed to the PS domain as

$$\hat{G} = \Gamma_0 \Pi G \Pi^{-1} = \begin{pmatrix} \hat{G}^{PP} & \hat{G}^{PS} \\ \hat{G}^{SP} & \hat{G}^{SS} \end{pmatrix}. \tag{21}$$

The perturbation V in the PS domain becomes

$$\hat{V} = \Pi V \Pi^{-1} \Gamma_0^{-1} = \begin{pmatrix} \hat{V}^{PP} & \hat{V}^{PS} \\ \hat{V}^{SP} & \hat{V}^{SS} \end{pmatrix}, \tag{22}$$

where the left superscripts of the matrix elements represent the type of measurement and the right ones are the source type.

Similarly, applying the PS transformation to the entire inverse series gives

$$\hat{V} = \hat{V}_1 + \hat{V}_2 + \hat{V}_3 + \cdots. \tag{23}$$

It follows, from Eqs. (20) and (23) that

$$\hat{D} = \hat{G}_0 \hat{V}_1 \hat{G}_0, \tag{24}$$

$$\hat{G}_0 \hat{V}_2 \hat{G}_0 = -\hat{G}_0 \hat{V}_1 \hat{G}_0 \hat{V}_1 \hat{G}_0, \tag{25}$$

$$\vdots$$

where $\hat{D} = \begin{pmatrix} \hat{D}^{PP} & \hat{D}^{PS} \\ \hat{D}^{SP} & \hat{D}^{SS} \end{pmatrix}$ are the data in the PS domain.

In the displacement space we have, for Eq. (1),

$$\mathbf{u} = G\mathbf{f}. \tag{26}$$

Then, in the PS domain, Eq. (26) becomes

$$\mathbf{\Phi} = \hat{G}\mathbf{F}. \tag{27}$$

On the measurement surface, we have

$$\hat{G} = \hat{G}_0 + \hat{G}_0 \hat{V}_1 \hat{G}_0. \tag{28}$$

Substituting Eq. (28) into Eq. (27), and rewriting Eq. (27) in matrix form:

$$\begin{pmatrix} \phi^P \\ \phi^S \end{pmatrix} = \begin{pmatrix} \hat{G}_0^P & 0 \\ 0 & \hat{G}_0^S \end{pmatrix} \begin{pmatrix} F^P \\ F^S \end{pmatrix} + \begin{pmatrix} \hat{G}_0^P & 0 \\ 0 & \hat{G}_0^S \end{pmatrix} \begin{pmatrix} \hat{V}_1^{PP} & \hat{V}_1^{PS} \\ \hat{V}_1^{SP} & \hat{V}_1^{SS} \end{pmatrix} \begin{pmatrix} \hat{G}_0^P & 0 \\ 0 & \hat{G}_0^S \end{pmatrix} \begin{pmatrix} F^P \\ F^S \end{pmatrix}. \tag{29}$$

This can be written as the following two equations

$$\phi^P = \hat{G}_0^P F^P + \hat{G}_0^P \hat{V}_1^{PP} \hat{G}_0^P F^P + \hat{G}_0^P \hat{V}_1^{PS} \hat{G}_0^S F^S, \tag{30}$$

$$\phi^S = \hat{G}_0^S F^S + \hat{G}_0^S \hat{V}_1^{SP} \hat{G}_0^P F^P + \hat{G}_0^S \hat{V}_1^{SS} \hat{G}_0^S F^S. \tag{31}$$

We can see, from the two equations above, that for homogeneous media, (no perturbation, $\hat{V}_1 = 0$), there are only direct P and S waves and that the two kind of waves are separated. However, for

inhomogeneous media, these two kinds of waves will be mixed together. If only the P wave is incident, $F^P = 1$, $F^S = 0$, then the two Eqs. (30) and (31) above are respectively reduced to

$$\phi^P = \hat{G}_0^P + \hat{G}_0^P \hat{V}_1^{PP} \hat{G}_0^P, \tag{32}$$

$$\phi^S = \hat{G}_0^S \hat{V}_1^{SP} \hat{G}_0^P. \tag{33}$$

Hence, in this case, there is only the direct P wave $\hat{G}_0^P$, and no direct wave S. But there are two kinds of scattered waves: one is the P-to-P wave $\hat{G}_0^P \hat{V}_1^{PP} \hat{G}_0^P$, and the other is the P-to-S wave $\hat{G}_0^S \hat{V}_1^{SP} \hat{G}_0^P$. For the acoustic case, only the P wave exists, and hence we only have one equation $\phi^P = \hat{G}_0^P + \hat{G}_0^P \hat{V}_1^{PP} \hat{G}_0^P$.

Similarly, if only the S wave is incident, $F^P = 0$, $F^S = 1$, and the two Eqs. (30) and (31) are, respectively, reduced to

$$\phi^P = \hat{G}_0^P \hat{V}_1^{PS} \hat{G}_0^S, \tag{34}$$

$$\phi^S = \hat{G}_0^S + \hat{G}_0^S \hat{V}_1^{SS} \hat{G}_0^S. \tag{35}$$

In this case, there is only the direct S wave $\hat{G}_0^S$, and no direct P wave. There are also two kinds of scattered waves: one is the S-to-P wave $\hat{G}_0^P \hat{V}_1^{PS} \hat{G}_0^S$, the other is the S-to-S wave $\hat{G}_0^S \hat{V}_1^{SS} \hat{G}_0^S$.

3 Linear inversion of a 1D elastic medium

Writing Eq. (24) in matrix form

$$\begin{pmatrix} \hat{D}^{PP} & \hat{D}^{PS} \\ \hat{D}^{SP} & \hat{D}^{SS} \end{pmatrix} = \begin{pmatrix} \hat{G}_0^P & 0 \\ 0 & \hat{G}_0^S \end{pmatrix} \begin{pmatrix} \hat{V}_1^{PP} & \hat{V}_1^{PS} \\ \hat{V}_1^{SP} & \hat{V}_1^{SS} \end{pmatrix} \begin{pmatrix} \hat{G}_0^P & 0 \\ 0 & \hat{G}_0^S \end{pmatrix}, \tag{36}$$

leads to four equations

$$\hat{D}^{PP} = \hat{G}_0^P \hat{V}_1^{PP} \hat{G}_0^P, \tag{37}$$

$$\hat{D}^{PS} = \hat{G}_0^P \hat{V}_1^{PS} \hat{G}_0^S, \tag{38}$$

$$\hat{D}^{SP} = \hat{G}_0^S \hat{V}_1^{SP} \hat{G}_0^P, \tag{39}$$

$$\hat{D}^{SS} = \hat{G}_0^S \hat{V}_1^{SS} \hat{G}_0^S. \tag{40}$$

For $z_s = z_g = 0$, in the $(k_s, z_s; k_g, z_g; \omega)$ domain, we get the following four equations relating the linear components of the three elastic parameters and the four data types:

$$\begin{aligned} \widetilde{D}^{PP}(k_g, 0; -k_g, 0; \omega) = &-\frac{1}{4}\left(1 - \frac{k_g^2}{\nu_g^2}\right) \widetilde{a}_\rho^{(1)}(-2\nu_g) - \frac{1}{4}\left(1 + \frac{k_g^2}{\nu_g^2}\right) \widetilde{a}_\gamma^{(1)}(-2\nu_g) \\ &+ \frac{2k_g^2 \beta_0^2}{(\nu_g^2 + k_g^2)\alpha_0^2} \widetilde{a}_\mu^{(1)}(-2\nu_g), \end{aligned} \tag{41}$$

$$\widetilde{D}^{PS}(\nu_g, \eta_g) = -\frac{1}{4}\left(\frac{k_g}{\nu_g} + \frac{k_g}{\eta_g}\right) \widetilde{a}_\rho^{(1)}(-\nu_g - \eta_g) - \frac{\beta_0^2}{2\omega^2} k_g(\nu_g + \eta_g)\left(1 - \frac{k_g^2}{\nu_g \eta_g}\right) \widetilde{a}_\mu^{(1)}(-\nu_g - \eta_g), \tag{42}$$

$$\widetilde{D}^{SP}(\nu_g, \eta_g) = \frac{1}{4}\left(\frac{k_g}{\nu_g} + \frac{k_g}{\eta_g}\right) \widetilde{a}_\rho^{(1)}(-\nu_g - \eta_g) + \frac{\beta_0^2}{2\omega^2} k_g(\nu_g + \eta_g)\left(1 - \frac{k_g^2}{\nu_g \eta_g}\right) \widetilde{a}_\mu^{(1)}(-\nu_g - \eta_g), \tag{43}$$

$$\widetilde{D}^{SS}(k_g,\eta_g) = -\frac{1}{4}\left(1-\frac{k_g^2}{\eta_g^2}\right)\widetilde{a}_\rho^{(1)}(-2\eta_g) - \left[\frac{\eta_g^2+k_g^2}{4\eta_g^2} - \frac{2k_g^2}{\eta_g^2+k_g^2}\right]\widetilde{a}_\mu^{(1)}(-2\eta_g), \tag{44}$$

where

$$\nu_g^2 + k_g^2 = \frac{\omega^2}{\alpha_0^2},$$

$$\eta_g^2 + k_g^2 = \frac{\omega^2}{\beta_0^2}.$$

For the P-wave incidence case (see Fig. 1), using $k_g^2/\nu_g^2 = \tan^2\theta$ and $k_g^2/(\nu_g^2+k_g^2) = \sin^2\theta$, where θ is the P-wave incident angle, Eq. (41) becomes

$$\widetilde{D}^{PP}(\nu_g,\theta) = -\frac{1}{4}(1-\tan^2\theta)\widetilde{a}_\rho^{(1)}(-2\nu_g) - \frac{1}{4}(1+\tan^2\theta)\widetilde{a}_\gamma^{(1)}(-2\nu_g) + \frac{2\beta_0^2\sin^2\theta}{\alpha_0^2}\widetilde{a}_\mu^{(1)}(-2\nu_g). \tag{45}$$

In this case, when $\beta_0 = \beta_1 = 0$, Eq. (45) reduces to the acoustic two parameter case Eq. (7) in Zhang and Weglein (2005) for $z_g = z_s = 0$.

$$\widetilde{D}(q_g,\theta) = -\frac{\rho_0}{4}\left[\frac{1}{\cos^2\theta}\widetilde{\alpha_1}(-2q_g) + (1-\tan^2\theta)\widetilde{\beta}_1(-2q_g)\right], \tag{46}$$

In Eq. (45), it seems straightforward that using the data at three angles to obtain the linear inversion of a_ρ, a_γ and a_μ, and this is what we do in this paper. However, by doing this it requires a whole new understanding of the definition of "the data". This point has been discussed by Weglein et al. (2007).

4 Direct non-linear inversion of 1D elastic medium

Writing Eq. (25) in matrix form:

$$\begin{aligned}&\begin{pmatrix}\hat{G}_0^P & 0\\ 0 & \hat{G}_0^S\end{pmatrix}\begin{pmatrix}\hat{V}_2^{PP} & \hat{V}_2^{PS}\\ \hat{V}_2^{SP} & \hat{V}_2^{SS}\end{pmatrix}\begin{pmatrix}\hat{G}_0^P & 0\\ 0 & \hat{G}_0^S\end{pmatrix}\\ &= -\begin{pmatrix}\hat{G}_0^P & 0\\ 0 & \hat{G}_0^S\end{pmatrix}\begin{pmatrix}\hat{V}_1^{PP} & \hat{V}_1^{PS}\\ \hat{V}_1^{SP} & \hat{V}_1^{SS}\end{pmatrix}\begin{pmatrix}\hat{G}_0^P & 0\\ 0 & \hat{G}_0^S\end{pmatrix}\begin{pmatrix}\hat{V}_1^{PP} & \hat{V}_1^{PS}\\ \hat{V}_1^{SP} & \hat{V}_1^{SS}\end{pmatrix}\begin{pmatrix}\hat{G}_0^P & 0\\ 0 & \hat{G}_0^S\end{pmatrix},\end{aligned} \tag{47}$$

leads to four equations

$$\hat{G}_0^P\hat{V}_2^{PP}\hat{G}_0^P = -\hat{G}_0^P\hat{V}_1^{PP}\hat{G}_0^P\hat{V}_1^{PP}\hat{G}_0^P - \hat{G}_0^P\hat{V}_1^{PS}\hat{G}_0^S\hat{V}_1^{SP}\hat{G}_0^P, \tag{48}$$

$$\hat{G}_0^P\hat{V}_2^{PS}\hat{G}_0^S = -\hat{G}_0^P\hat{V}_1^{PP}\hat{G}_0^P\hat{V}_1^{PS}\hat{G}_0^S - \hat{G}_0^P\hat{V}_1^{PS}\hat{G}_0^S\hat{V}_1^{SS}\hat{G}_0^S, \tag{49}$$

$$\hat{G}_0^S\hat{V}_2^{SP}\hat{G}_0^P = -\hat{G}_0^S\hat{V}_1^{SP}\hat{G}_0^P\hat{V}_1^{PP}\hat{G}_0^P - \hat{G}_0^S\hat{V}_1^{SS}\hat{G}_0^S\hat{V}_1^{SP}\hat{G}_0^P, \tag{50}$$

$$\hat{G}_0^S\hat{V}_2^{SS}\hat{G}_0^S = -\hat{G}_0^S\hat{V}_1^{SP}\hat{G}_0^P\hat{V}_1^{PS}\hat{G}_0^S - \hat{G}_0^S\hat{V}_1^{SS}\hat{G}_0^S\hat{V}_1^{SS}\hat{G}_0^S. \tag{51}$$

Since $\hat{V}_1^{PP}$ relates to $\hat{D}^{PP}$, $\hat{V}_1^{PS}$ relates to $\hat{D}^{PS}$, and so on, the four components of the data will be coupled in the non-linear elastic inversion. We cannot perform the direct non-linear inversion without knowing all components of the data. As shown in Zhang and Weglein (2005) and this chapter, when the work on the two parameter acoustic case is extended to the present three parameter elastic case, it is not just simply adding one more parameter, but there are more issues involved. Even

for the linear case, the linear solutions found in (41) $\sim$ (44) are much more complicated than those of the acoustic case. For instance, four different sets of linear parameter estimates are produced from each component of the data. Also, generally four distinct reflector mislocations arise from the two reference velocities (P-wave velocity and S-wave velocity).

However, in some situations like the towed streamer case, we do not have all components of data available. A particular non-linear approach to be presented in the next section, has been chosen to side-step a portion of this complexity and address our typical lack of four components of elastic data: using $\hat{D}^{PP}$ as the fundamental data input, and perform a reduced form of non-linear elastic inversion, concurrently asking: what beyond-linear value does this simpler framework add? We will see from the numerical tests presented in the following section.

4.1 Only using $\hat{D}^{PP}$ — a particular non-linear approach and the numerical tests

When assuming only $\hat{D}^{PP}$ are available, first, we compute the linear solution for $a_\rho^{(1)}$, $a_\gamma^{(1)}$ and $a_\mu^{(1)}$ from Eq. (41). Then, substituting the solution into the other three equations (42), (43) and (44), we synthesize the other components of data — $\hat{D}^{PS}$, $\hat{D}^{SP}$ and $\hat{D}^{SS}$. Finally, using the given $\hat{D}^{PP}$ and the synthesized data, we perform the non-linear elastic inversion, getting the following second order (first term beyond linear) elastic inversion solution from Eq. (48),

$$
\begin{aligned}
&\left(1-\tan^2\theta\right)a_\rho^{(2)}(z)+\left(1+\tan^2\theta\right)a_\gamma^{(2)}(z)-8b^2\sin^2\theta a_\mu^{(2)}(z)\\
=&-\frac{1}{2}\left(\tan^4\theta-1\right)\left[a_\gamma^{(1)}(z)\right]^2+\frac{\tan^2\theta}{\cos^2\theta}a_\gamma^{(1)}(z)a_\rho^{(1)}(z)\\
&+\frac{1}{2}\left[\left(1-\tan^4\theta\right)-\frac{2}{C+1}\left(\frac{1}{C}\right)\left(\frac{\alpha_0^2}{\beta_0^2}-1\right)\frac{\tan^2\theta}{\cos^2\theta}\right]\left[a_\rho^{(1)}(z)\right]^2\\
&-4b^2\left[\tan^2\theta-\frac{2}{C+1}\left(\frac{1}{2C}\right)\left(\frac{\alpha_0^2}{\beta_0^2}-1\right)\tan^4\theta\right]a_\rho^{(1)}(z)a_\mu^{(1)}(z)\\
&+2b^4\left(\tan^2\theta-\frac{\alpha_0^2}{\beta_0^2}\right)\left[2\sin^2\theta-\frac{2}{C+1}\frac{1}{C}\left(\frac{\alpha_0^2}{\beta_0^2}-1\right)\tan^2\theta\right]\left[a_\mu^{(1)}(z)\right]^2\\
&-\frac{1}{2}\left(\frac{1}{\cos^4\theta}\right)a_\gamma^{(1)\prime}(z)\int_0^z dz'\left[a_\gamma^{(1)}\left(z'\right)-a_\rho^{(1)}\left(z'\right)\right]\\
&-\frac{1}{2}\left(1-\tan^4\theta\right)a_\rho^{(1)\prime}(z)\int_0^z dz'\left[a_\gamma^{(1)}\left(z'\right)-a_\rho^{(1)}\left(z'\right)\right]\\
&+4b^2\tan^2\theta a_\mu^{(1)\prime}(z)\int_0^z dz'\left[a_\gamma^{(1)}\left(z'\right)-a_\rho^{(1)}\left(z'\right)\right]\\
&+\frac{2}{C+1}\frac{1}{C}\left(\frac{\alpha_0^2}{\beta_0^2}-1\right)\tan^2\theta\left(\tan^2\theta-C\right)b^2\int_0^z dz' a_{\mu\ z}^{(1)}\left(\frac{(C-1)\,z'+2z}{(C+1)}\right)a_\rho^{(1)}\left(z'\right)\\
&-\frac{2}{C+1}\frac{2}{C}\left(\frac{\alpha_0^2}{\beta_0^2}-1\right)\tan^2\theta\left(\tan^2\theta-\frac{\alpha_0^2}{\beta_0^2}\right)b^4\int_0^z dz' a_{\mu\ z}^{(1)}\left(\frac{(C-1)\,z'+2z}{(C+1)}\right)a_\mu^{(1)}\left(z'\right)\\
&+\frac{2}{C+1}\frac{1}{C}\left(\frac{\alpha_0^2}{\beta_0^2}-1\right)\tan^2\theta\left(\tan^2\theta+C\right)b^2\int_0^z dz' a_\mu^{(1)}\left(z'\right)a_{\rho\ z}^{(1)}\left(\frac{(C-1)z'+2z}{(C+1)}\right)\\
&-\frac{2}{C+1}\frac{1}{2C}\left(\frac{\alpha_0^2}{\beta_0^2}-1\right)\tan^2\theta\left(\tan^2\theta+1\right)\int_0^z dz' a_\rho^{(1)}\left(z'\right)a_{\rho\ z}^{(1)}\left(\frac{(C-1)\,z'+2z}{(C+1)}\right),
\end{aligned}
\tag{52}
$$

where $a_\rho^{(1)}{}_z\left(\frac{(C-1)z'+2z}{(C+1)}\right) = d\left[a_\rho^{(1)}\left(\frac{(C-1)z'+2z}{(C+1)}\right)\right]/dz$, $b = \frac{\beta_0}{\alpha_0}$ and $C = \frac{\eta_g}{\nu_g} = \frac{\sqrt{1-b^2\sin^2\theta}}{b\sqrt{1-\sin^2\theta}}$.

The first five terms on the right side of Eq. (52) are inversion terms; i.e., they contribute to parameter predictions. The other terms on the right side of the equation are imaging terms. The arguments for the remarks above are the same as in the acoustic case in (Zhang and Weglein, 2005). For one interface model, there is no imaging task. The only task is inversion. In this case, all of the integration terms on the right side of Eq. (52) are zero, and only the first five terms can be non-zero. Thus, we conclude that the integration terms (which care about duration) are imaging terms, and the first five terms are inversion terms. Both the inversion and imaging terms (especially the imaging terms) become much more complicated after the extension of acoustic case (Zhang and Weglein, 2005) to elastic case. The integrand of the first three integral terms is the first order approximation of the relative change in P-wave velocity. The derivatives $a_\gamma^{(1)\prime}$, $a_\rho^{(1)\prime}$ and $a_\mu^{(1)\prime}$ in front of those integrals are acting to correct the wrong locations caused by the inaccurate reference P-wave velocity. The other four terms with integrals will be zero as $\beta_0 \to 0$ since in this case $C \to \infty$.

In the following, we test this approach numerically.

For a single interface 1D elastic medium case, as shown in Fig. 1, the reflection coefficient R^{PP} has the following form (Foster et al., 1997)

$$R^{PP} = \frac{N}{D}, \tag{53}$$

where

$$\begin{aligned} N =& -(1+2kx^2)^2 b\sqrt{1-c^2x^2}\sqrt{1-d^2x^2} - (1-a+2kx^2)^2 bcdx^2 \\ &+ (a-2kx^2)^2 cd\sqrt{1-x^2}\sqrt{1-b^2x^2} \\ &+ 4k^2x^2\sqrt{1-x^2}\sqrt{1-b^2x^2}\sqrt{1-c^2x^2}\sqrt{1-d^2x^2} - ad\sqrt{1-b^2x^2}\sqrt{1-c^2x^2} \\ &+ abc\sqrt{1-x^2}\sqrt{1-d^2x^2}, \end{aligned} \tag{54}$$

$$\begin{aligned} D =& (1+2kx^2)^2 b\sqrt{1-c^2x^2}\sqrt{1-d^2x^2} + (1-a+2kx^2)^2 bcdx^2 \\ &+ (a-2kx^2)^2 cd\sqrt{1-x^2}\sqrt{1-b^2x^2} \\ &+ 4k^2x^2\sqrt{1-x^2}\sqrt{1-b^2x^2}\sqrt{1-c^2x^2}\sqrt{1-d^2x^2} + ad\sqrt{1-b^2x^2}\sqrt{1-c^2x^2} \\ &+ abc\sqrt{1-x^2}\sqrt{1-d^2x^2}, \end{aligned} \tag{55}$$

where $a = \rho_1/\rho_0$, $b = \beta_0/\alpha_0$, $c = \alpha_1/\alpha_0$, $d = \beta_1/\alpha_0$, $k = ad^2 - b^2$ and $x = \sin\theta$, and the subscripts "0" and "1" denote the reference medium and actual medium respectively. Similar to the acoustic case, using the analytic data (Clayton and Stolt, 1981; Weglein et al., 1986)

$$\widetilde{D}^{PP}(\nu_g, \theta) = R^{PP}(\theta)\frac{e^{2i\nu_g a}}{4\pi i\nu_g}, \tag{56}$$

where a is the depth of the interface. Substituting Eq.(56) into Eq.(45), Fourier transforming Eq.(45) over $2\nu_g$, and fixing $z > a$ and θ, we have

$$(1-\tan^2\theta)a_\rho^{(1)}(z) + (1+\tan^2\theta)a_\gamma^{(1)}(z) - 8\frac{\beta_0^2}{\alpha_0^2}\sin^2\theta a_\mu^{(1)}(z) = 4R^{PP}(\theta)H(z-a). \tag{57}$$

In this section, we numerically test the direct inversion approach on the following four models:

Model 1: shale (0.20 porosity) over oil sand (0.10 porosity). $\rho_0 = 2.32g/cm^3$, $\rho_1 = 2.46g/cm^3$; $\alpha_0 = 2627m/s$, $\alpha_1 = 4423m/s$; $\beta_0 = 1245m/s$, $\beta_1 = 2939m/s$.

Model 2: shale over oil sand, 0.20 porosity. $\rho_0 = 2.32g/cm^3$, $\rho_1 = 2.27g/cm^3$; $\alpha_0 = 2627m/s$, $\alpha_1 = 3251m/s$; $\beta_0 = 1245m/s$, $\beta_1 = 2138m/s$.

Model 3: shale (0.20 porosity) over oil sand (0.30 porosity). $\rho_0 = 2.32g/cm^3$, $\rho_1 = 2.08g/cm^3$; $\alpha_0 = 2627m/s$, $\alpha_1 = 2330m/s$; $\beta_0 = 1245m/s$, $\beta_1 = 1488m/s$.

Model 4: oil sand over wet sand, 0.20 porosity. $\rho_0 = 2.27g/cm^3$, $\rho_1 = 2.32g/cm^3$; $\alpha_0 = 3251m/s$, $\alpha_1 = 3507m/s$; $\beta_0 = 2138m/s$, $\beta_1 = 2116m/s$.

To test and compare methods, the top of sand reflection was modeled for oil sands with porosities of 10, 20, and 30%. The three models used the same shale overburden. An oil/water contact model was also constructed for the 20% porosity sand.

The low porosity model (10%) represents a deep, consolidated reservoir sand. Pore fluids have little effect on the seismic response of the reservoir sand. It is difficult to distinguish oil sands from brine sands on the basis of seismic response. Impedance of the sand is higher than impedance of the shale.

The moderate porosity model (20%) represents deeper, compacted reservoirs. Pore fluids have a large impact on seismic response, but the fluid effect is less than that of the high porosity case. The overlying shale has high density compared to the reservoir sand, but the P-wave velocity of the oil sand exceeds that of the shale. As a result, impedance contrast is reduced, and shear wave information becomes more important for detecting the reservoir.

The high porosity model (30%) is typical of a weakly consolidated, shallow reservoir sand. Pore fluids have a large impact on the seismic response. Density, P-wave velocity, and the α/β ratio of the oil sand are lower than the density, P-wave velocity, and α/β ratio of the overlying shale. Consequently, there is a significant decrease in density and P-wave bulk modulus and an increase in shear modulus at the shale/oil sand interface.

The fourth model denotes an oil/water contact in a 20% porosity sand. At a fluid contact, both density and P-wave velocity increase in going from the oil zone into the wet zone. Because pore fluids have no affect on shear modulus, there is no change in shear modulus.

Using these four models, we can find the corresponding R^{PP} from Eq. (53). Then, choosing three different angles θ_1, θ_2 and θ_3, we can get the linear solutions for $a_\rho^{(1)}$, $a_\gamma^{(1)}$ and $a_\mu^{(1)}$ from Eq. (57) , and then get the solutions for $a_\rho^{(2)}$, $a_\gamma^{(2)}$ and $a_\mu^{(2)}$ from Eq. (52).

There are two plots in each figure. The left ones are the results for the first order, while the right ones are the results for the first order plus the second order. The red lines denote the corresponding actual values. In the figures, we illustrate the results corresponding to different sets of angles θ_1 and θ_2. The third angle θ_3 is fixed at zero.

The numerical results indicate that all the second order solutions provide improvements over the linear solutions for all of the four models. When the second term is added to linear order, the results become much closer to the corresponding exact values and the surfaces become flatter in a larger range of angles. But the degrees of those improvements are different for different models. How accurately $\hat{D}^{PP}$ effectively synthesize $\hat{D}^{PS}$ and $\hat{D}^{SP}$ (as shown in Figs. 14 $\sim$ 17) determined

the degree of benefit provided by the non-linear elastic approach. All of the "predicted" values in the figures are predicted using the linear results from $\hat{D}^{PP}$. And the "actual" values are calculated from the Zoeppritz' equations.

In principle, the elastic non-linear direct inversion in 2D requires all four components of data. However, in this section we introduce an approach which requires only $\hat{D}^{PP}$ and approximately synthesizes the other required components. Based on this approach, the first direct non-linear elastic inversion solution is derived. Value-added results are obtained from the non-linear inversion terms beyond linear. Although $\hat{D}^{PP}$ can itself provide useful non-linear direct inversion results, the implication of this research is that further value would derive from actually measuring $\hat{D}^{PP}$, $\hat{D}^{PS}$, $\hat{D}^{SP}$ and $\hat{D}^{SS}$, as the method requires. In the following section, we give a consistent method and solve all of the second order Eqs. (48), (49), (50) and (51) with all four components of data available.

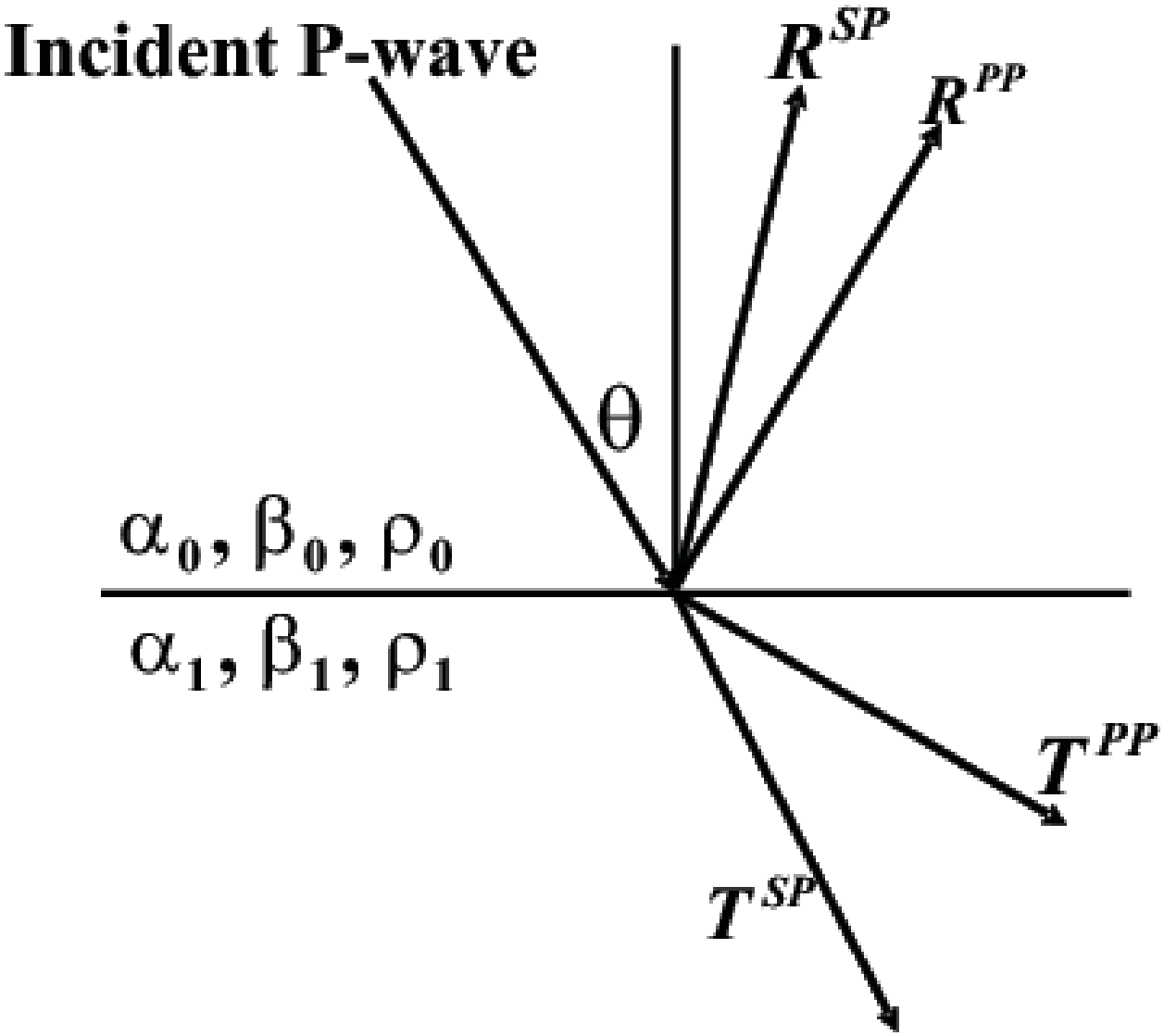

Figure 1: Response of incident compressional wave on a planar elastic interface. α_0, β_0 and ρ_0 are the compressional wave velocity, shear wave velocity and density of the upper layer, respectively; α_1, β_1 and ρ_1 denote the compressional wave velocity, shear wave velocity and density of the lower layer. R^{PP}, R^{SP}, T^{PP} and T^{SP} denote the coefficients of the reflected compressional wave, the reflected shear wave, the transmitted compressional wave and the transmitted shear wave, respectively. (Foster et al., 1997)

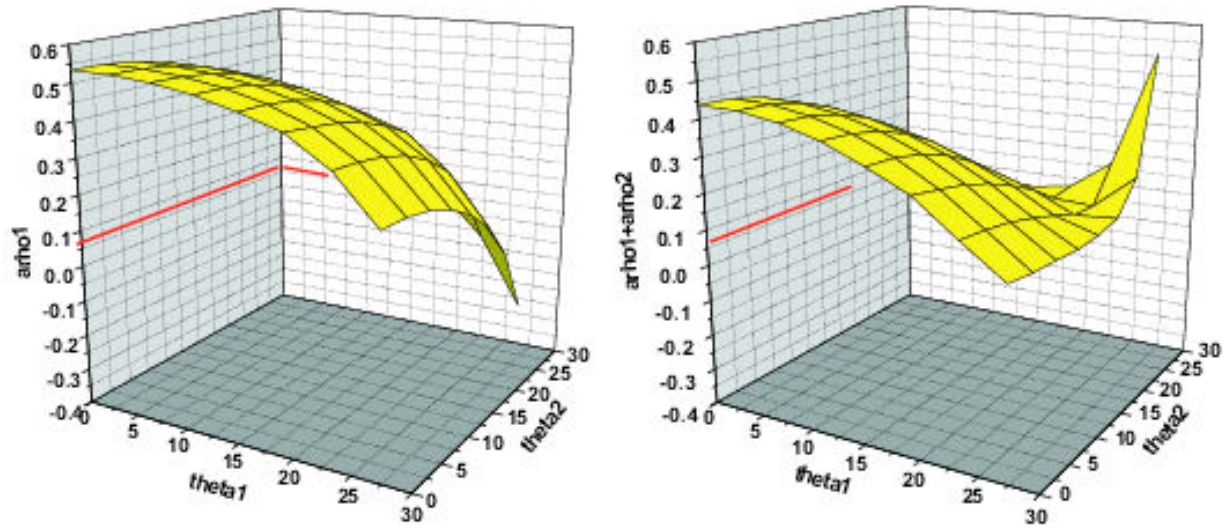

Figure 2: Model 1: shale (0.20 porosity) over oil sand (0.10 porosity). $\rho_0 = 2.32 g/cm^3, \rho_1 = 2.46 g/cm^3; \alpha_0 = 2627 m/s, \alpha_1 = 4423 m/s; \beta_0 = 1245 m/s, \beta_1 = 2939 m/s$. For this model, the exact value of a_ρ is 0.06. The linear approximation $a_\rho^{(1)}$ (left) and the sum of linear and first non-linear $a_\rho^{(1)} + a_\rho^{(2)}$ (right).

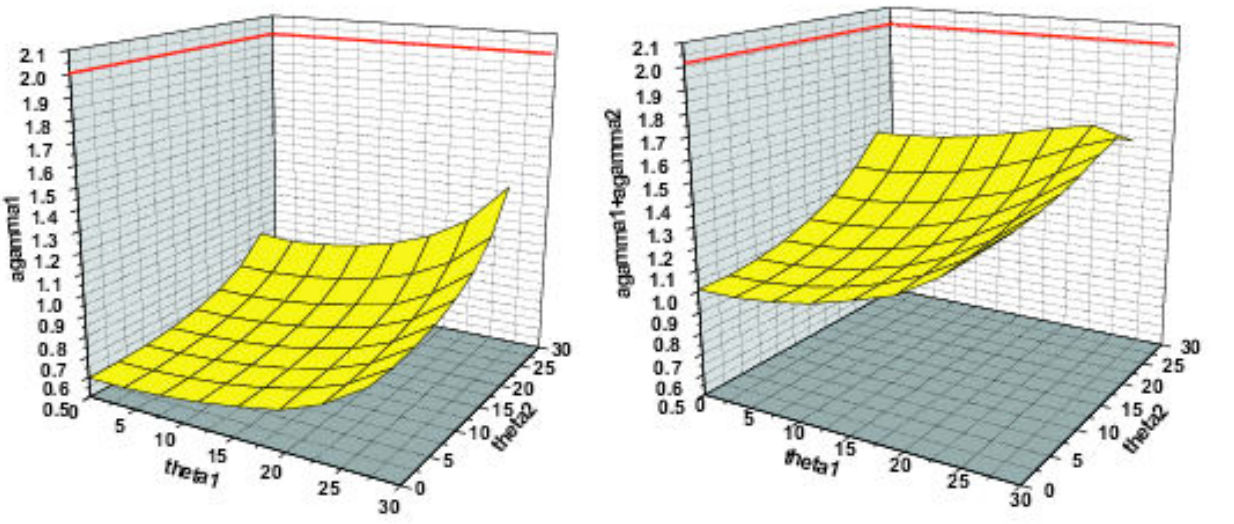

Figure 3: Model 1: shale (0.20 porosity) over oil sand (0.10 porosity). $\rho_0 = 2.32 g/cm^3, \rho_1 = 2.46 g/cm^3; \alpha_0 = 2627 m/s, \alpha_1 = 4423 m/s; \beta_0 = 1245 m/s, \beta_1 = 2939 m/s$. For this model, the exact value of a_γ is 2.01. The linear approximation $a_\gamma^{(1)}$ (left) and the sum of linear and first non-linear $a_\gamma^{(1)} + a_\gamma^{(2)}$ (right).

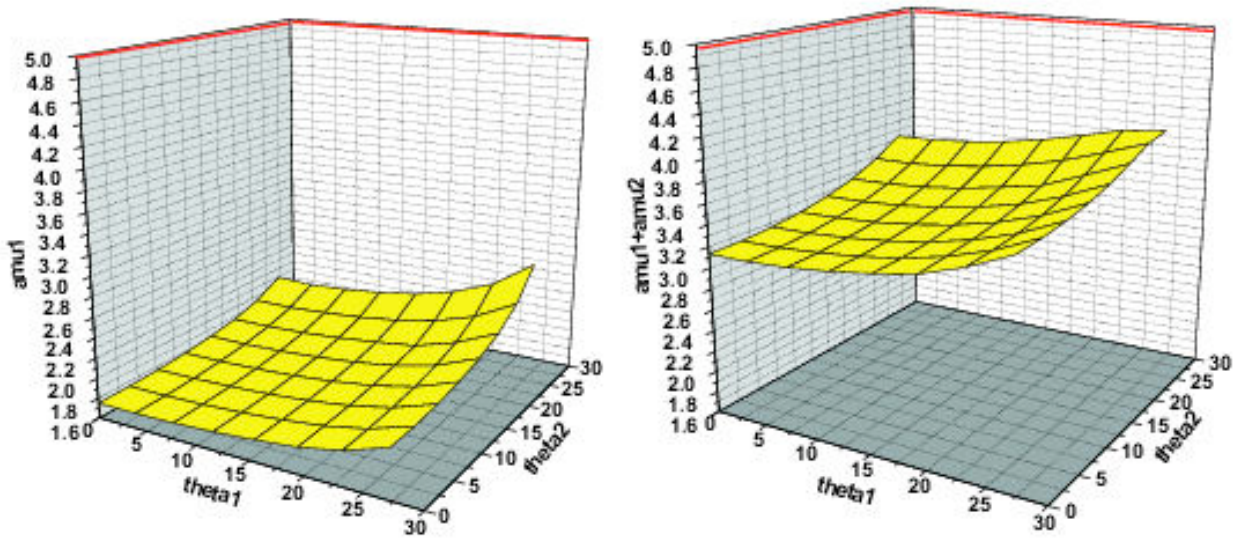

Figure 4: Model 1: shale (0.20 porosity) over oil sand (0.10 porosity). $\rho_0 = 2.32g/cm^3, \rho_1 = 2.46g/cm^3; \alpha_0 = 2627m/s, \alpha_1 = 4423m/s; \beta_0 = 1245m/s, \beta_1 = 2939m/s$. For this model, the exact value of a_μ is 4.91. The linear approximation $a_\mu^{(1)}$ (left) and the sum of linear and first non-linear $a_\mu^{(1)} + a_\mu^{(2)}$ (right).

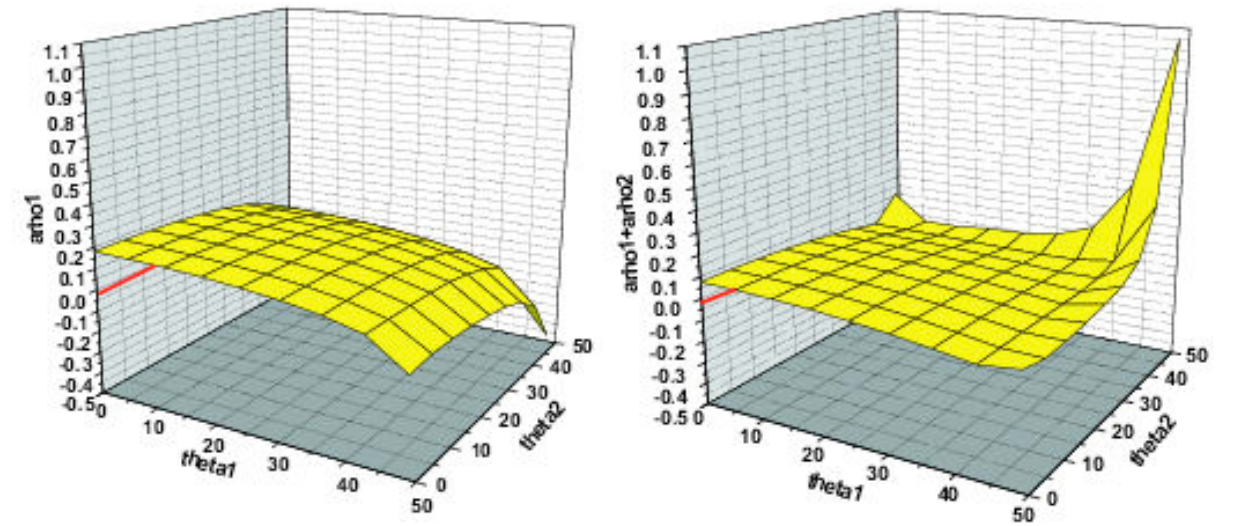

Figure 5: Model 2: shale over oil sand, 0.20 porosity. $\rho_0 = 2.32g/cm^3, \rho_1 = 2.27g/cm^3; \alpha_0 = 2627m/s, \alpha_1 = 3251m/s; \beta_0 = 1245m/s, \beta_1 = 2138m/s$. For this model, the exact value of a_ρ is -0.022. The linear approximation $a_\rho^{(1)}$ (left) and the sum of linear and first non-linear $a_\rho^{(1)} + a_\rho^{(2)}$ (right).

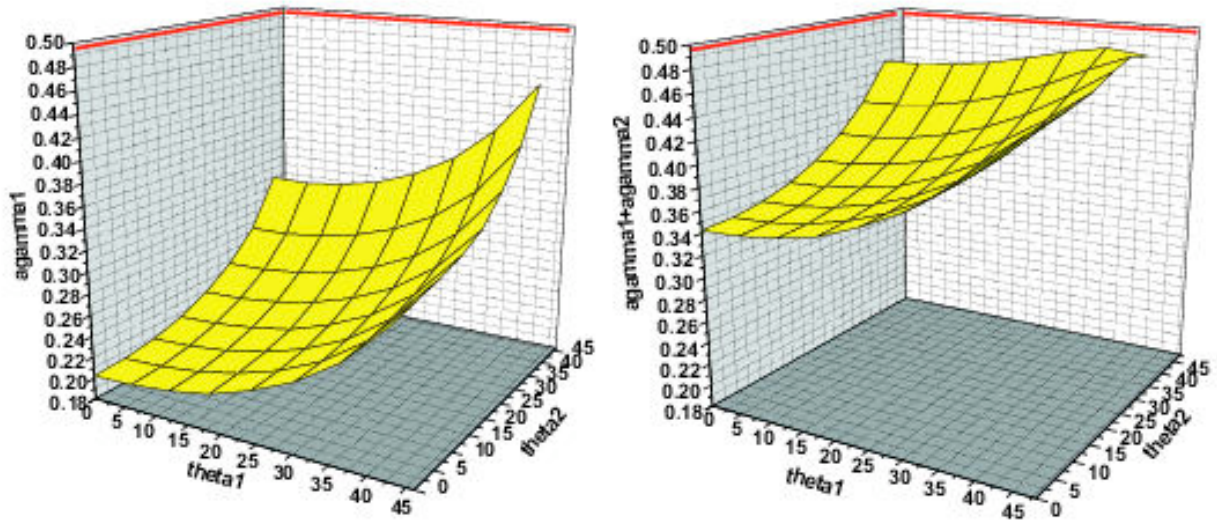

Figure 6: Model 2: shale over oil sand, 0.20 porosity. $\rho_0 = 2.32g/cm^3, \rho_1 = 2.27g/cm^3; \alpha_0 = 2627m/s, \alpha_1 = 3251m/s; \beta_0 = 1245m/s, \beta_1 = 2138m/s$. For this model, the exact value of a_γ is 0.498. The linear approximation $a_\gamma^{(1)}$ (left) and the sum of linear and first non-linear $a_\gamma^{(1)} + a_\gamma^{(2)}$ (right).

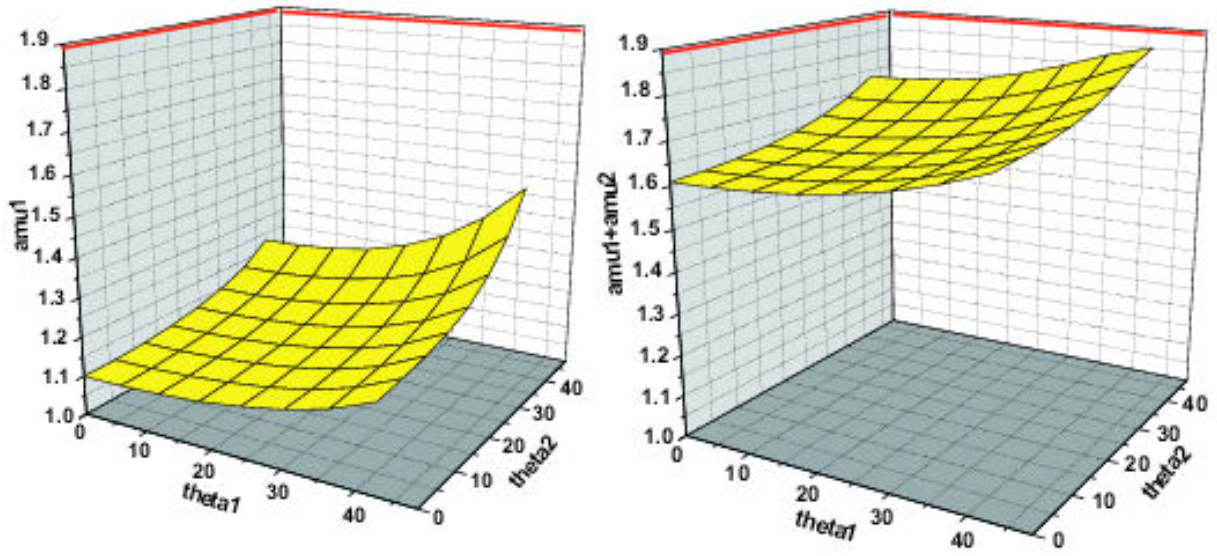

Figure 7: Model 2: shale over oil sand, 0.20 porosity. $\rho_0 = 2.32g/cm^3, \rho_1 = 2.27g/cm^3; \alpha_0 = 2627m/s, \alpha_1 = 3251m/s; \beta_0 = 1245m/s, \beta_1 = 2138m/s$. For this model, the exact value of a_μ is 1.89. The linear approximation $a_\mu^{(1)}$ (left) and the sum of linear and first non-linear $a_\mu^{(1)} + a_\mu^{(2)}$ (right).

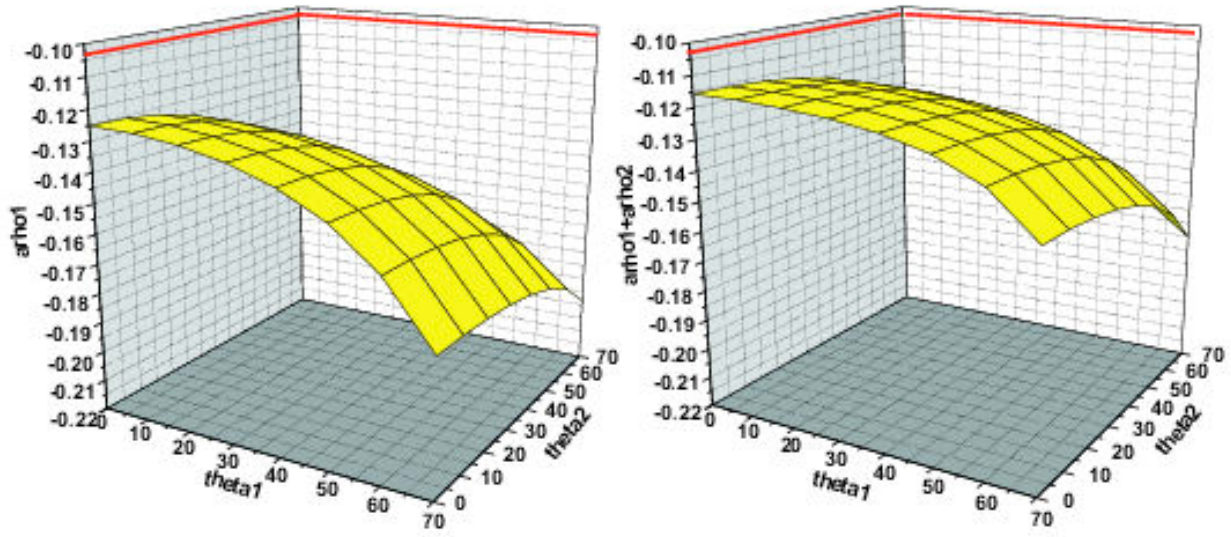

Figure 8: Model 3: shale (0.20 porosity) over oil sand (0.30 porosity). $\rho_0 = 2.32 g/cm^3, \rho_1 = 2.08 g/cm^3; \alpha_0 = 2627 m/s, \alpha_1 = 2330 m/s; \beta_0 = 1245 m/s, \beta_1 = 1488 m/s$. For this model, the exact value of a_ρ is -0.103. The linear approximation $a_\rho^{(1)}$ (left) and the sum of linear and first non-linear $a_\rho^{(1)} + a_\rho^{(2)}$ (right).

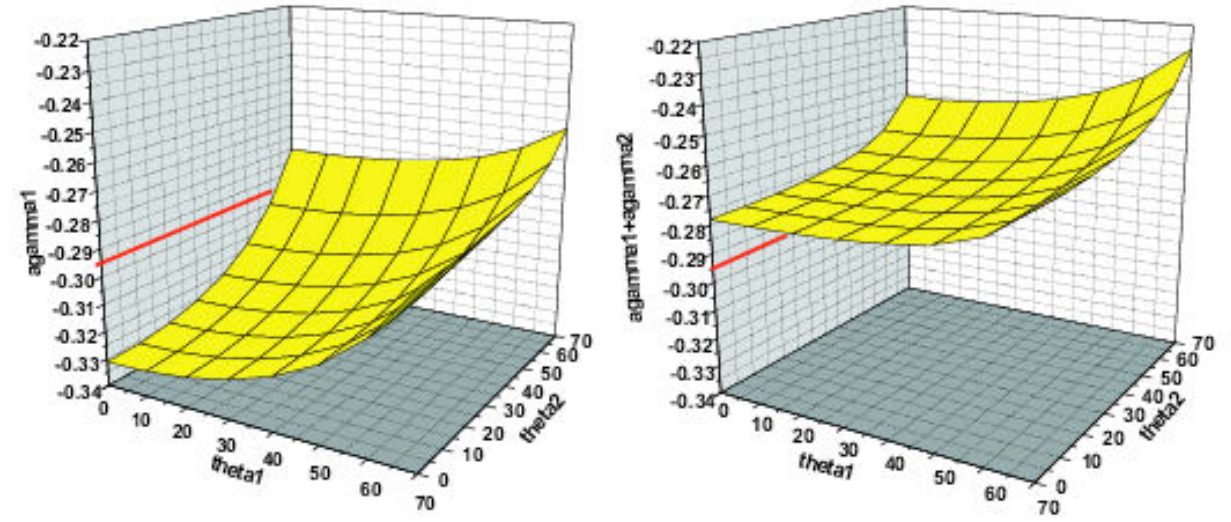

Figure 9: Model 3: shale (0.20 porosity) over oil sand (0.30 porosity). $\rho_0 = 2.32 g/cm^3, \rho_1 = 2.08 g/cm^3; \alpha_0 = 2627 m/s, \alpha_1 = 2330 m/s; \beta_0 = 1245 m/s, \beta_1 = 1488 m/s$. For this model, the exact value of a_γ is -0.295. The linear approximation $a_\gamma^{(1)}$ (left) and the sum of linear and first non-linear $a_\gamma^{(1)} + a_\gamma^{(2)}$ (right).

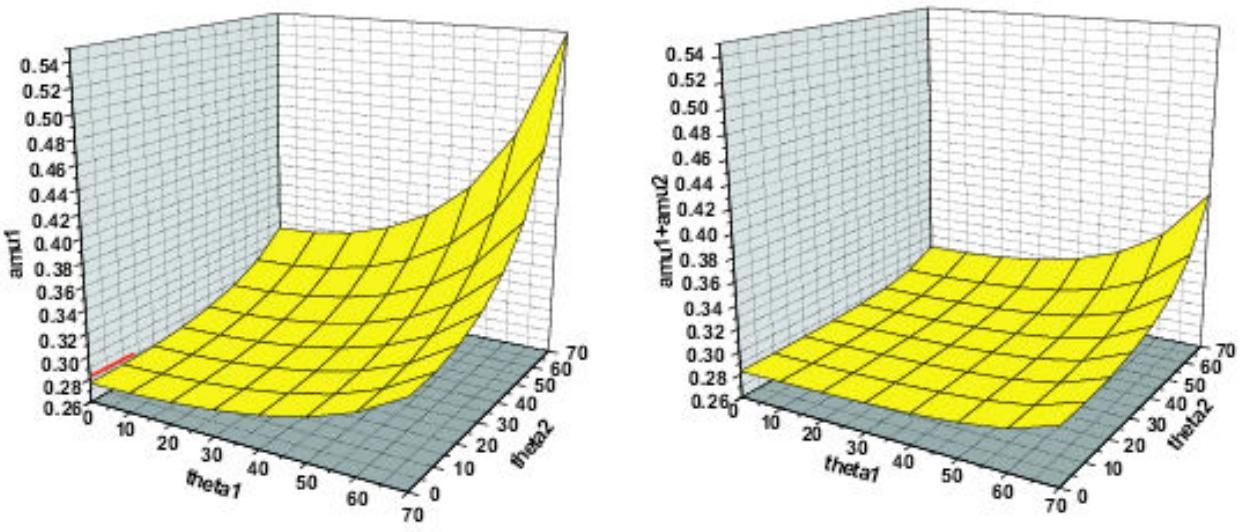

Figure 10: Model 3: shale (0.20 porosity) over oil sand (0.30 porosity). $\rho_0 = 2.32g/cm^3, \rho_1 = 2.08g/cm^3; \alpha_0 = 2627m/s, \alpha_1 = 2330m/s; \beta_0 = 1245m/s, \beta_1 = 1488m/s$. For this model, the exact value of a_μ is 0.281. The linear approximation $a_\mu^{(1)}$ (left) and the sum of linear and first non-linear $a_\mu^{(1)} + a_\mu^{(2)}$ (right).

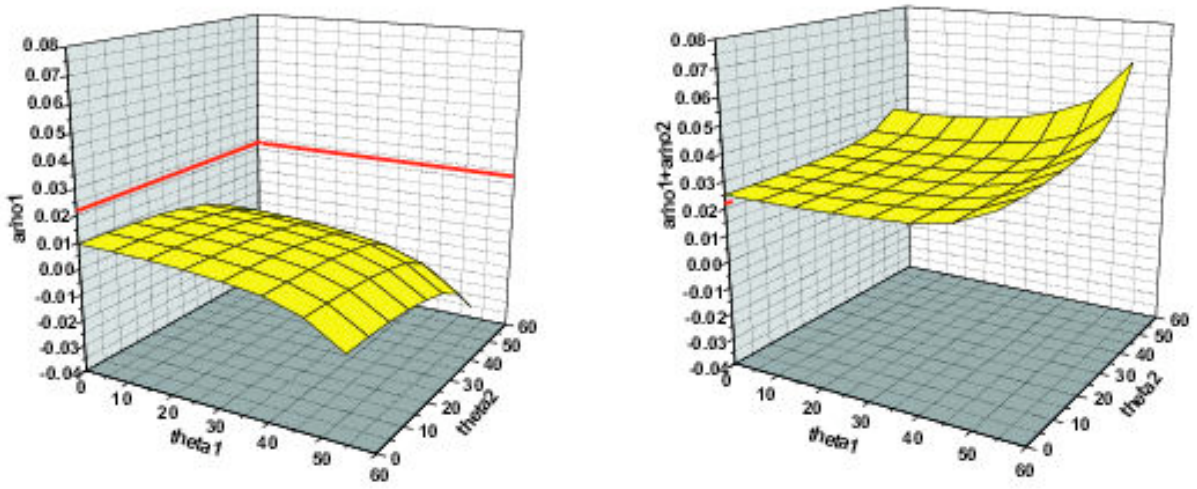

Figure 11: Model 4: oil sand over wet sand, 0.20 porosity. $\rho_0 = 2.27g/cm^3, \rho_1 = 2.32g/cm^3; \alpha_0 = 3251m/s, \alpha_1 = 3507m/s; \beta_0 = 2138m/s, \beta_1 = 2116m/s$. For this model, the exact value of a_ρ is 0.022. The linear approximation $a_\rho^{(1)}$ (left) and the sum of linear and first non-linear $a_\rho^{(1)} + a_\rho^{(2)}$ (right).

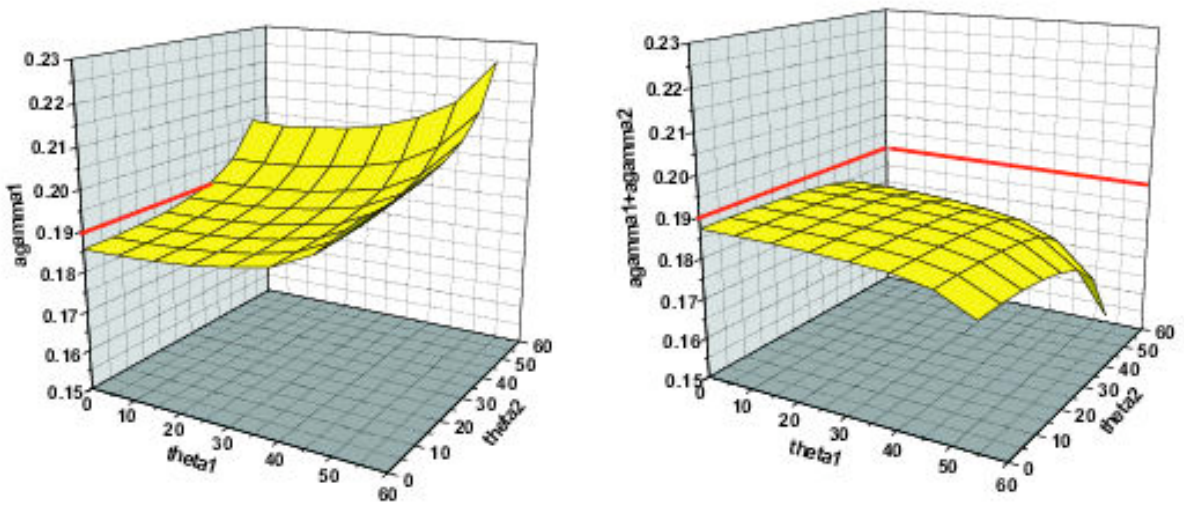

Figure 12: Model 4: oil sand over wet sand, 0.20 porosity. $\rho_0 = 2.27g/cm^3, \rho_1 = 2.32g/cm^3; \alpha_0 = 3251m/s, \alpha_1 = 3507m/s; \beta_0 = 2138m/s, \beta_1 = 2116m/s$. For this model, the exact value of a_γ is 0.19. The linear approximation $a_\gamma^{(1)}$ (left) and the sum of linear and first non-linear $a_\gamma^{(1)} + a_\gamma^{(2)}$ (right).

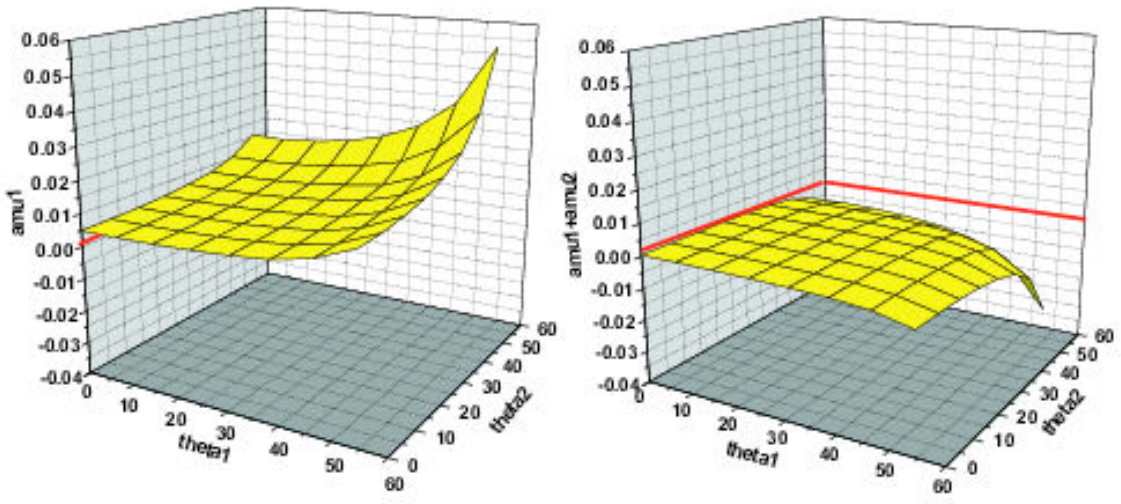

Figure 13: Model 4: oil sand over wet sand, 0.20 porosity. $\rho_0 = 2.27g/cm^3, \rho_1 = 2.32g/cm^3; \alpha_0 = 3251m/s, \alpha_1 = 3507m/s; \beta_0 = 2138m/s, \beta_1 = 2116m/s$. For this model, the exact value of a_μ is 0.001. The linear approximation $a_\mu^{(1)}$ (left) and the sum of linear and first non-linear $a_\mu^{(1)} + a_\mu^{(2)}$ (right).

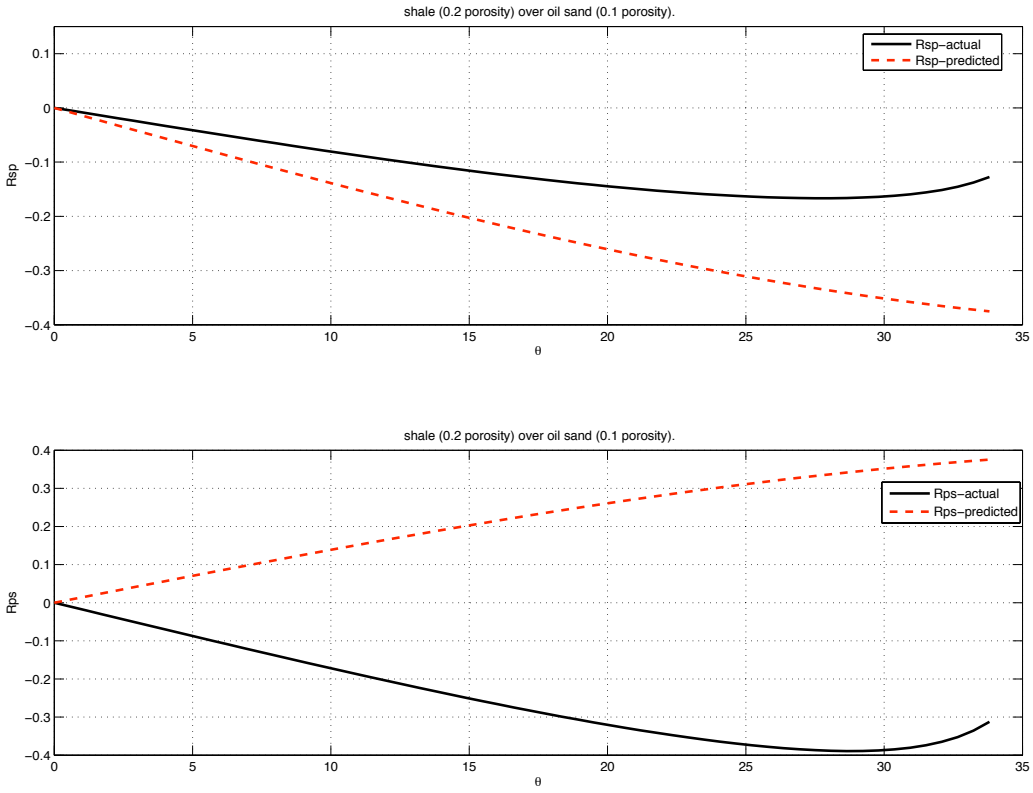

Figure 14: The comparison between the synthesized values and the actual values of Rsp (top) and Rps (bottom) for Model 1: shale (0.20 porosity) over oil sand (0.10 porosity). $\rho_0 = 2.32g/cm^3, \rho_1 = 2.46g/cm^3; \alpha_0 = 2627m/s, \alpha_1 = 4423m/s; \beta_0 = 1245m/s, \beta_1 = 2939m/s$.

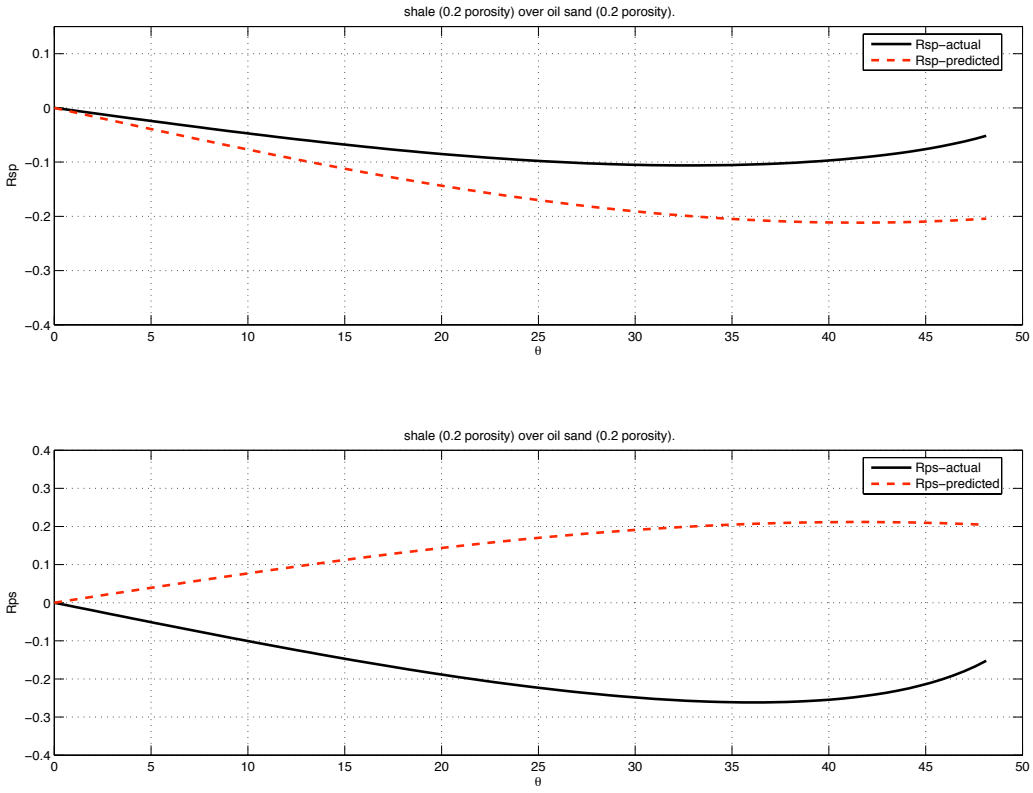

Figure 15: The comparison between the synthesized values and the actual values of Rsp (top) and Rps (bottom) for Model 2: shale over oil sand, 0.20 porosity. $\rho_0 = 2.32g/cm^3, \rho_1 = 2.27g/cm^3; \alpha_0 = 2627m/s, \alpha_1 = 3251m/s; \beta_0 = 1245m/s, \beta_1 = 2138m/s.$

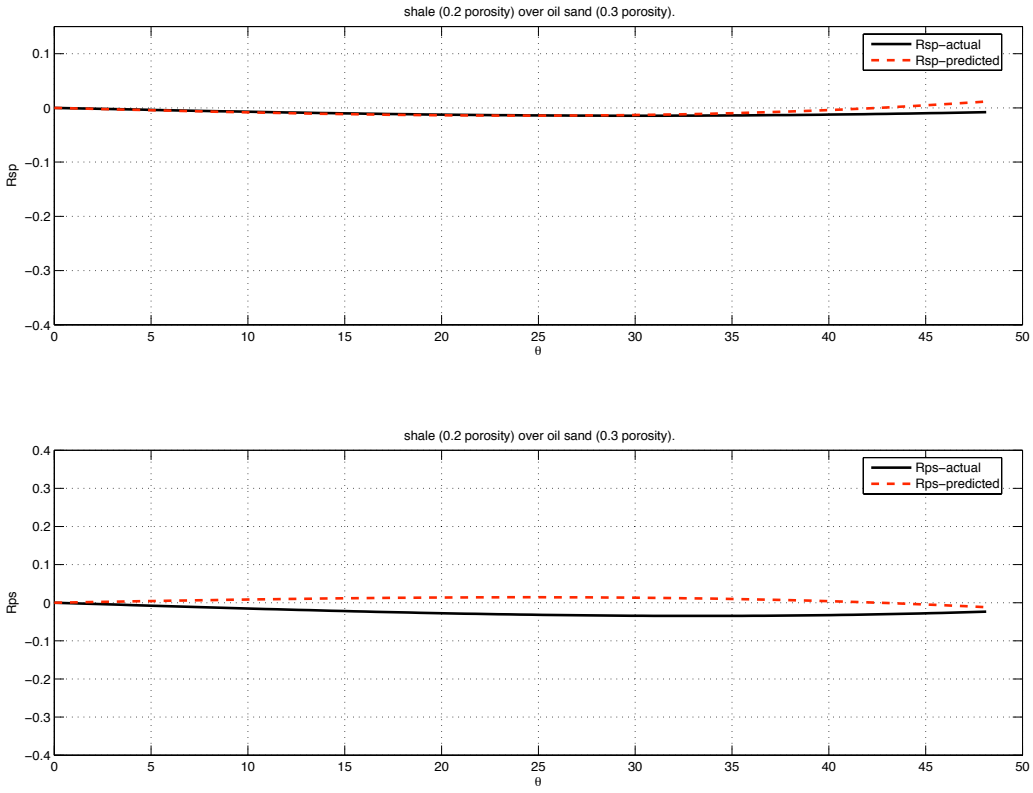

Figure 16: The comparison between the synthesized values and the actual values of Rsp (top) and Rps (bottom) for Model 3: shale (0.20 porosity) over oil sand (0.30 porosity). $\rho_0 = 2.32g/cm^3, \rho_1 = 2.08g/cm^3; \alpha_0 = 2627m/s, \alpha_1 = 2330m/s; \beta_0 = 1245m/s, \beta_1 = 1488m/s$.

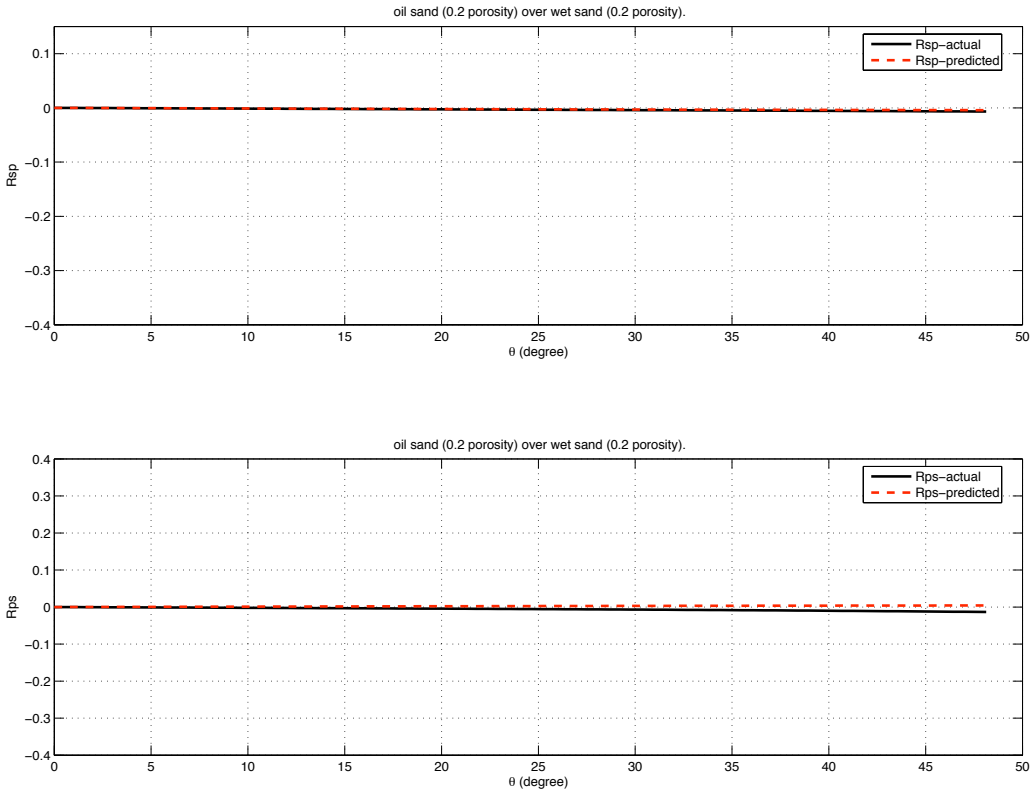

Figure 17: The comparison between the synthesized values and the actual values of Rsp (top) and Rps (bottom) for Model 4: oil sand over wet sand, 0.20 porosity. $\rho_0 = 2.27g/cm^3, \rho_1 = 2.32g/cm^3; \alpha_0 = 3251m/s, \alpha_1 = 3507m/s; \beta_0 = 2138m/s, \beta_1 = 2116m/s$.

4.2 Using all four components of data — full direct non-linear elastic inversion

Using four components of data, one consistent method to solve for the second terms is, first, using the linear solutions as shown in Eqs. (41), (42), (43) and (44), we can get the linear solution for $a_\rho^{(1)}$, $a_\gamma^{(1)}$ and $a_\mu^{(1)}$ in terms of $\hat{D}^{PP}, \hat{D}^{PS}, \hat{D}^{SP}$and $\hat{D}^{SS}$ through the following way

$$\begin{pmatrix} a_\rho^{(1)} \\ a_\gamma^{(1)} \\ a_\mu^{(1)} \end{pmatrix} = (O^T O)^{-1} O^T \begin{pmatrix} \hat{D}^{PP} \\ \hat{D}^{PS} \\ \hat{D}^{SP} \\ \hat{D}^{SS} \end{pmatrix}, \tag{58}$$

where the matrix O is

$$\begin{pmatrix} -\frac{1}{4}\left(1-\frac{k_g^{PP\,2}}{\nu_g^{PP\,2}}\right) & -\frac{1}{4}\left(1+\frac{k_g^{PP\,2}}{\nu_g^{PP\,2}}\right) & \frac{2\beta_0^2 k_g^{PP\,2}}{\alpha_0^2\left(\nu_g^{PP\,2}+k_g^{PP\,2}\right)} \\ -\frac{1}{4}\left(\frac{k_g^{PS}}{\nu_g^{PS}}+\frac{k_g^{PS}}{\eta_g^{PS}}\right) & 0 & -\frac{\beta_0^2}{2\omega^2}k_g^{PS}\left(\nu_g^{PS}+\eta_g^{PS}\right)\left(1-\frac{k_g^{PS\,2}}{\nu_g^{PS}\eta_g^{PS}}\right) \\ \frac{1}{4}\left(\frac{k_g^{SP}}{\nu_g^{SP}}+\frac{k_g^{SP}}{\eta_g^{SP}}\right) & 0 & \frac{\beta_0^2}{2\omega^2}k_g^{SP}\left(\nu_g^{SP}+\eta_g^{SP}\right)\left(1-\frac{k_g^{SP\,2}}{\nu_g^{SP}\eta_g^{SP}}\right) \\ -\frac{1}{4}\left(1-\frac{k_g^{SS\,2}}{\eta_g^{SS\,2}}\right) & 0 & -\left[\frac{k_g^{SS\,2}+\eta_g^{SS\,2}}{4\eta_g^{SS\,2}}-\frac{2k_g^{SS\,2}}{k_g^{SS\,2}+\eta_g^{SS\,2}}\right] \end{pmatrix}, \tag{59}$$

and O^T is the transpose of matrix O, the superscript -1 denotes the inverse of the matrix $O^T O$.

Let the arguments of $a_\rho^{(1)}$ and $a_\mu^{(1)}$ in Eqs. (41), (42), (43) and (44) equal, we need

$$-2\nu_g^{PP} = -\nu_g^{PS} - \eta_g^{PS} = -\nu_g^{SP} - \eta_g^{SP} = -2\eta_g^{SS},$$

which leads to (please see details in Appendix A)

$$\begin{aligned} 2\frac{\omega}{\alpha_0}\cos\theta^{PP} &= \frac{\omega}{\alpha_0}\sqrt{1-\frac{\alpha_0^2}{\beta_0^2}\sin^2\theta^{PS}} + \frac{\omega}{\beta_0}\cos\theta^{PS} = \frac{\omega}{\alpha_0}\cos\theta^{SP} + \frac{\omega}{\beta_0}\sqrt{1-\frac{\beta_0^2}{\alpha_0^2}\sin^2\theta^{SP}} \\ &= 2\frac{\omega}{\beta_0}\cos\theta^{SS}. \end{aligned}$$

From the expression above, given θ^{PP}, as shown in Fig. 18, we can find the corresponding angles θ^{PS}, θ^{SP} and θ^{SS} which appear in matrix O

$$\begin{aligned} \theta^{PS} &= \cos^{-1}\left[\frac{4b^2\cos^2\theta^{PP}+1-b^2}{4b\cos\theta^{PP}}\right], \\ \theta^{SP} &= \cos^{-1}\left[\frac{4b^2\cos^2\theta^{PP}-1+b^2}{4b^2\cos\theta^{PP}}\right], \\ \theta^{SS} &= \cos^{-1}\left(b\cos\theta^{PP}\right), \end{aligned}$$

where $b = \frac{\beta_0}{\alpha_0}$.

Then, through the similar way, we can get the solution for $a_\rho^{(2)}$, $a_\gamma^{(2)}$ and $a_\mu^{(2)}$ in terms of $a_\rho^{(1)}$, $a_\gamma^{(1)}$ and $a_\mu^{(1)}$

$$\begin{pmatrix} a_\rho^{(2)} \\ a_\gamma^{(2)} \\ a_\mu^{(2)} \end{pmatrix} = (O^T O)^{-1} O^T Q, \tag{60}$$

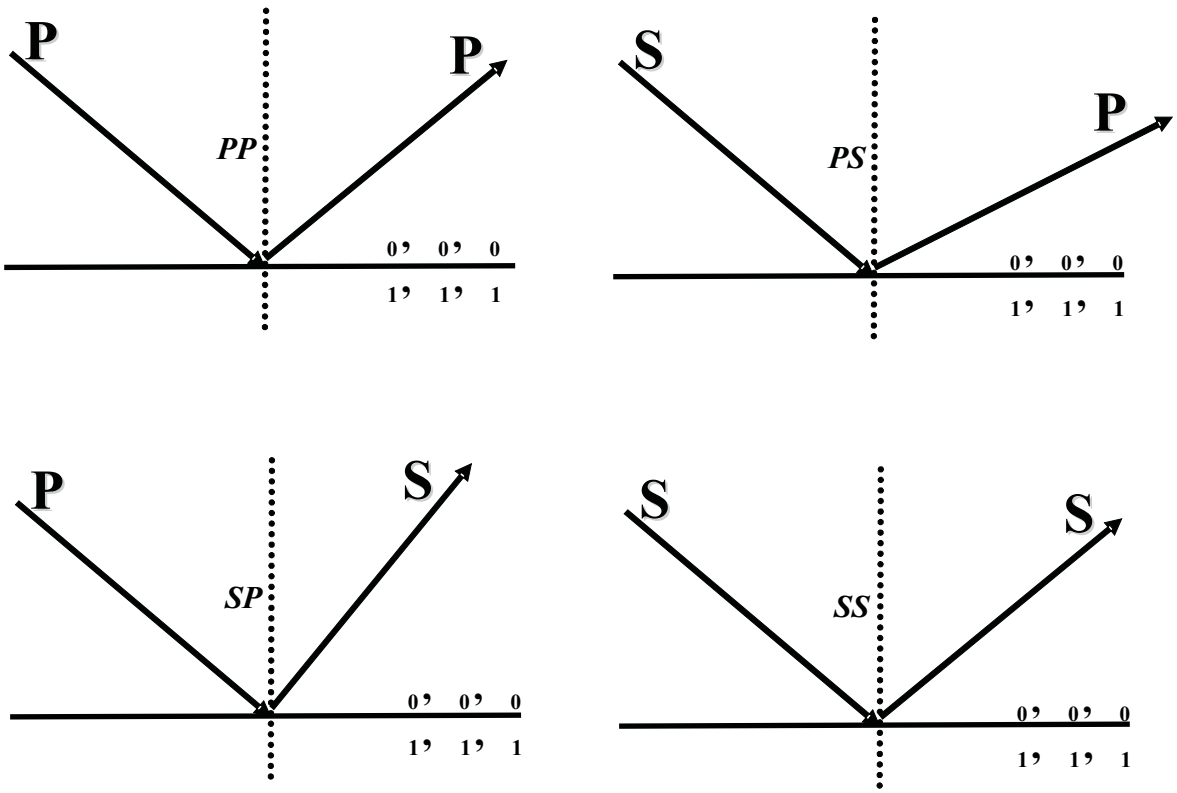

Figure 18: Different incident angles.

where the matrix Q is in terms of $a_\rho^{(1)}$, $a_\gamma^{(1)}$ and $a_\mu^{(1)}$.

Based on this idea, we get the following non-linear solutions for Eqs. (48), (49), (50) and (51) respectively.

The form of the solution for Eq. (48), i.e.,

$$\hat{G}_0^P \hat{V}_2^{PP} \hat{G}_0^P = -\hat{G}_0^P \hat{V}_1^{PP} \hat{G}_0^P \hat{V}_1^{PP} \hat{G}_0^P - \hat{G}_0^P \hat{V}_1^{PS} \hat{G}_0^S \hat{V}_1^{SP} \hat{G}_0^P,$$

is the same as Eq. (52). In the $(k_s, z_s; k_g, z_g; \omega)$ domain, we get the the other three solutions respectively, for Eqs. (49), (50) and (51).

The solution for Eq. (49), i.e.,

$$\hat{G}_0^P \hat{V}_2^{PS} \hat{G}_0^S = -\hat{G}_0^P \hat{V}_1^{PP} \hat{G}_0^P \hat{V}_1^{PS} \hat{G}_0^S - \hat{G}_0^P \hat{V}_1^{PS} \hat{G}_0^S \hat{V}_1^{SS} \hat{G}_0^S,$$

is

$$\begin{aligned} &-\frac{1}{4}\left(\frac{k_g}{\nu_g}+\frac{k_g}{\eta_g}\right) a_\rho^{(2)}(z) - \frac{\beta_0^2}{2\omega^2} k_g \left(\nu_g+\eta_g\right)\left(1-\frac{k_g^2}{\nu_g\eta_g}\right) a_\mu^{(2)}(z) \\ =&-\left[\left(\frac{1}{2}+\frac{1}{C+1}\right)\frac{1}{\eta_g\nu_g^2}\left(\frac{\beta_0^4}{\alpha_0^4} C k_g^3 - 3\frac{\beta_0^2}{\alpha_0^2} C k_g^5 \frac{\beta_0^2}{\omega^2} - k_g^3\nu_g^2\frac{\beta_0^2}{\omega^2} + 2k_g^5\nu_g^2\frac{\beta_0^4}{\omega^4} + 2Ck_g^7\frac{\beta_0^4}{\omega^4}\right)\right. \end{aligned}$$

$$
+\left(\frac{1}{2}-\frac{1}{C+1}\right)\frac{1}{\eta_g\nu_g^2}\left(\frac{\beta_0^2}{\alpha_0^2}Ck_g^3\nu_g^2\frac{\beta_0^2}{\omega^2}+2\frac{\beta_0^2}{\alpha_0^2}k_g^5\frac{\beta_0^2}{\omega^2}-2Ck_g^5\nu_g^2\frac{\beta_0^4}{\omega^4}-\frac{\beta_0^2}{\alpha_0^2}k_g^3+k_g^5\frac{\beta_0^2}{\omega^2}-2k_g^7\frac{\beta_0^4}{\omega^4}\right)
$$

$$
+\left(\frac{1}{2C}+\frac{1}{C+1}\right)\frac{1}{4\eta_g^2\nu_g}\left(6k_g^3-12k_g^5\frac{\beta_0^2}{\omega^2}-k_g\frac{\omega^2}{\beta_0^2}+8k_g^7\frac{\beta_0^4}{\omega^4}+8C^3\nu_g^2k_g^5\frac{\beta_0^4}{\omega^4}\right.
$$

$$
\left.-4\frac{\beta_0^2}{\alpha_0^2}C^3\nu_g^2k_g^3\frac{\beta_0^2}{\omega^2}\right)
$$

$$
-\left(\frac{1}{2C}-\frac{1}{C+1}\right)\frac{1}{4\eta_g\nu_g^2}\left(4\frac{\beta_0^2}{\alpha_0^2}k_g^3-8k_g^5\frac{\beta_0^2}{\omega^2}-k_g\frac{\omega^2}{\alpha_0^2}+2k_g^3-4C\nu_g^2k_g^3\frac{\beta_0^2}{\omega^2}+8C\nu_g^2k_g^5\frac{\beta_0^4}{\omega^4}\right.
$$

$$
\left.-4\frac{\beta_0^2}{\alpha_0^2}k_g^5\frac{\beta_0^2}{\omega^2}+8k_g^7\frac{\beta_0^4}{\omega^4}\right)-\frac{\beta_0^2}{\alpha_0^2}\frac{k_g^3}{\nu_g}\frac{\beta_0^2}{\omega^2}+\frac{k_g}{2\eta_g}\left(2k_g^2\frac{\beta_0^2}{\omega^2}-1\right)\Bigg]a_\mu^{(1)}(z)a_\mu^{(1)}(z)
$$

$$
-\left[\left(\frac{1}{2}+\frac{1}{C+1}\right)\frac{k_g}{8\eta_g\nu_g^2}\left(Ck_g^2+\nu_g^2\right)-\left(\frac{1}{2}-\frac{1}{C+1}\right)\frac{k_g}{8\eta_g\nu_g^2}\left(k_g^2+C\nu_g^2\right)\right.
$$

$$
\left.+\left(\frac{1}{2C}+\frac{1}{C+1}\right)\frac{k_g}{8\eta_g^2\nu_g}\left(C^3\nu_g^2+k_g^2\right)-\left(\frac{1}{2C}-\frac{1}{C+1}\right)\frac{k_g}{8\eta_g\nu_g^2}\left(k_g^2+C\nu_g^2\right)\right]a_\rho^{(1)}(z)a_\rho^{(1)}(z)
$$

$$
-\left[\left(\frac{1}{2}+\frac{1}{C+1}\right)\frac{\beta_0^2}{\alpha_0^2}\frac{1}{4\nu_g^3}k_g\left(k_g^2-\nu_g^2\right)+\left(\frac{1}{2}-\frac{1}{C+1}\right)\frac{1}{4\eta_g\nu_g^2}\left(k_g\frac{\omega^2}{\alpha_0^2}-2\frac{\beta_0^2}{\alpha_0^2}k_g^3\right)+\frac{\beta_0^2}{\alpha_0^2}\frac{k_g}{2\nu_g}\right]
$$

$$
\times a_\mu^{(1)}(z)a_\gamma^{(1)}(z)
$$

$$
+\left[\left(\frac{1}{2}+\frac{1}{C+1}\right)\frac{k_g\left(k_g^2+\nu_g^2\right)}{8\nu_g^3}-\left(\frac{1}{2}-\frac{1}{C+1}\right)\frac{k_g\left(k_g^2+\nu_g^2\right)}{8\eta_g\nu_g^2}\right]a_\rho^{(1)}(z)a_\gamma^{(1)}(z)
$$

$$
-\left[\left(\frac{1}{2}+\frac{1}{C+1}\right)\frac{1}{4\eta_g\nu_g^2}\left(3\frac{\beta_0^2}{\alpha_0^2}Ck_g^3+\nu_g^2k_g-4Ck_g^5\frac{\beta_0^2}{\omega^2}-4k_g^3\nu_g^2\frac{\beta_0^2}{\omega^2}\right)\right.
$$

$$
-\left(\frac{1}{2}-\frac{1}{C+1}\right)\frac{1}{4\eta_g\nu_g^2}\left(\frac{\beta_0^2}{\alpha_0^2}C\nu_g^2k_g+k_g^3-4k_g^5\frac{\beta_0^2}{\omega^2}-4Ck_g^3\nu_g^2\frac{\beta_0^2}{\omega^2}+2\frac{\beta_0^2}{\alpha_0^2}k_g^3\right)
$$

$$
+\left(\frac{1}{2C}+\frac{1}{C+1}\right)\frac{1}{4\eta_g^2\nu_g}\left(k_g^3-2k_g^5\frac{\beta_0^2}{\omega^2}+\frac{\beta_0^2}{\alpha_0^2}C^3\nu_g^2k_g-4C^3\nu_g^2k_g^3\frac{\beta_0^2}{\omega^2}-\frac{1}{2}k_g\frac{\omega^2}{\beta_0^2}\right.
$$

$$
\left.+2C^2\nu_g^2k_g^3\frac{\beta_0^2}{\omega^2}\right)
$$

$$
-\left(\frac{1}{2C}-\frac{1}{C+1}\right)\frac{1}{4\eta_g\nu_g^2}\left(C\nu_g^2k_g-2C\nu_g^2k_g^3\frac{\beta_0^2}{\omega^2}+\frac{\beta_0^2}{\alpha_0^2}k_g^3-2k_g^5\frac{\beta_0^2}{\omega^2}+2C^2\nu_g^2k_g^3\frac{\beta_0^2}{\omega^2}\right.
$$

$$
\left.\left.-2C\nu_g^2k_g^3\frac{\beta_0^2}{\omega^2}-\frac{1}{2}k_g\frac{\omega^2}{\beta_0^2}\right)\right]\times a_\rho^{(1)}(z)a_\mu^{(1)}(z)
$$

$$
-\frac{1}{\eta_g\nu_g^2}\left(\frac{\beta_0^4}{\alpha_0^4}Ck_g^3-3\frac{\beta_0^2}{\alpha_0^2}Ck_g^5\frac{\beta_0^2}{\omega^2}-k_g^3\nu_g^2\frac{\beta_0^2}{\omega^2}+2k_g^5\nu_g^2\frac{\beta_0^4}{\omega^4}+2Ck_g^7\frac{\beta_0^4}{\omega^4}\right)
$$

$$
\times\left[\frac{1}{2}\int_0^z dz' a_\mu^{(1)}{}_z\left(\frac{(C+1)z-(C-1)z'}{2}\right)a_\mu^{(1)}\left(z'\right)+\frac{1}{C+1}a_\mu^{(1)'}(z)\int_0^z dz' a_\mu^{(1)}(z')\right]
$$

$$
-\frac{1}{\eta_g\nu_g^2}\left(\frac{\beta_0^2}{\alpha_0^2}Ck_g^3\nu_g^2\frac{\beta_0^2}{\omega^2}+2\frac{\beta_0^2}{\alpha_0^2}k_g^5\frac{\beta_0^2}{\omega^2}-2Ck_g^5\nu_g^2\frac{\beta_0^4}{\omega^4}-\frac{\beta_0^2}{\alpha_0^2}k_g^3+k_g^5\frac{\beta_0^2}{\omega^2}-2k_g^7\frac{\beta_0^4}{\omega^4}\right)
$$

$$
\times\left[\frac{1}{2}\int_0^z dz' a_\mu^{(1)}{}_z\left(\frac{(C+1)z-(C-1)z'}{2}\right)a_\mu^{(1)}\left(z'\right)-\frac{1}{C+1}a_\mu^{(1)'}(z)\int_0^z dz' a_\mu^{(1)}(z')\right]
$$

$$
\begin{aligned}
&- \frac{1}{4\eta_g^2\nu_g}\left(6k_g^3 - 12k_g^5\frac{\beta_0^2}{\omega^2} - k_g\frac{\omega^2}{\beta_0^2} + 8k_g^7\frac{\beta_0^4}{\omega^4} + 8C^3\nu_g^2k_g^5\frac{\beta_0^4}{\omega^4} - 4\frac{\beta_0^2}{\alpha_0^2}C^3\nu_g^2k_g^3\frac{\beta_0^2}{\omega^2}\right)\\
&\times\left[\frac{1}{2C}\int_0^z dz' a_\mu^{(1)}{}_z\left(\frac{(C+1)z+(C-1)\,z'}{2C}\right)a_\mu^{(1)}\left(z'\right) + \frac{1}{C+1}a_\mu^{(1)'}(z)\int_0^z dz' a_\mu^{(1)}(z')\right]\\
&+ \frac{1}{4\eta_g\nu_g^2}\left(4\frac{\beta_0^2}{\alpha_0^2}k_g^3 - 8k_g^5\frac{\beta_0^2}{\omega^2} - k_g\frac{\omega^2}{\alpha_0^2} + 2k_g^3 - 4C\nu_g^2k_g^3\frac{\beta_0^2}{\omega^2} + 8C\nu_g^2k_g^5\frac{\beta_0^4}{\omega^4} - 4\frac{\beta_0^2}{\alpha_0^2}k_g^5\frac{\beta_0^2}{\omega^2} + 8k_g^7\frac{\beta_0^4}{\omega^4}\right)\\
&\times\left[\frac{1}{2C}\int_0^z dz' a_\mu^{(1)}{}_z\left(\frac{(C+1)z+(C-1)\,z'}{2C}\right)a_\mu^{(1)}\left(z'\right) - \frac{1}{C+1}a_\mu^{(1)'}(z)\int_0^z dz' a_\mu^{(1)}(z')\right]\\
&- \frac{k_g\left(Ck_g^2+\nu_g^2\right)}{8\eta_g\nu_g^2}\left[\frac{1}{2}\int_0^z dz' a_\rho^{(1)}{}_z\left(\frac{(C+1)z-(C-1)\,z'}{2}\right)a_\rho^{(1)}\left(z'\right)\right.\\
&\left.+\frac{1}{C+1}a_\rho^{(1)'}(z)\int_0^z dz' a_\rho^{(1)}(z')\right]\\
&+ \frac{k_g\left(k_g^2+C\nu_g^2\right)}{8\eta_g\nu_g^2}\left[\frac{1}{2}\int_0^z dz' a_\rho^{(1)}{}_z\left(\frac{(C+1)z-(C-1)\,z'}{2}\right)a_\rho^{(1)}\left(z'\right)\right.\\
&\left.-\frac{1}{C+1}a_\rho^{(1)'}(z)\int_0^z dz' a_\rho^{(1)}(z')\right]\\
&- \frac{C^3k_g\nu_g^2+k_g^3}{8\eta_g^2\nu_g}\left[\frac{1}{2C}\int_0^z dz' a_\rho^{(1)}{}_z\left(\frac{(C+1)z+(C-1)\,z'}{2C}\right)a_\rho^{(1)}\left(z'\right)\right.\\
&\left.+\frac{1}{C+1}a_\rho^{(1)'}(z)\int_0^z dz' a_\rho^{(1)}(z')\right]\\
&+ \frac{k_g\left(k_g^2+C\nu_g^2\right)}{8\eta_g\nu_g^2}\left[\frac{1}{2C}\int_0^z dz' a_\rho^{(1)}{}_z\left(\frac{(C+1)z+(C-1)\,z'}{2C}\right)a_\rho^{(1)}\left(z'\right)\right.\\
&\left.-\frac{1}{C+1}a_\rho^{(1)'}(z)\int_0^z dz' a_\rho^{(1)}(z')\right]\\
&- \frac{\beta_0^2}{\alpha_0^2}\frac{k_g\left(k_g^2-\nu_g^2\right)}{4\nu_g^3}\left[\frac{1}{2}\int_0^z dz' a_\gamma^{(1)}{}_z\left(\frac{(C+1)z-(C-1)\,z'}{2}\right)a_\mu^{(1)}\left(z'\right)\right.\\
&\left.+\frac{1}{C+1}a_\mu^{(1)'}(z)\int_0^z dz' a_\gamma^{(1)}(z')\right]\\
&- \frac{1}{4\eta_g\nu_g^2}\left(k_g\frac{\omega^2}{\alpha_0^2} - 2\frac{\beta_0^2}{\alpha_0^2}k_g^3\right)\left[\frac{1}{2}\int_0^z dz' a_\gamma^{(1)}{}_z\left(\frac{(C+1)z-(C-1)\,z'}{2}\right)a_\mu^{(1)}\left(z'\right)\right.\\
&\left.-\frac{1}{C+1}a_\mu^{(1)'}(z)\int_0^z dz' a_\gamma^{(1)}(z')\right]\\
&+ \frac{k_g\left(k_g^2+\nu_g^2\right)}{8\nu_g^3}\left[\frac{1}{2}\int_0^z dz' a_\gamma^{(1)}{}_z\left(\frac{(C+1)z-(C-1)\,z'}{2}\right)a_\rho^{(1)}\left(z'\right)\right.\\
&\left.+\frac{1}{C+1}a_\rho^{(1)'}(z)\int_0^z dz' a_\gamma^{(1)}(z')\right]\\
&- \frac{k_g\left(k_g^2+\nu_g^2\right)}{8\eta_g\nu_g^2}\left[\frac{1}{2}\int_0^z dz' a_\gamma^{(1)}{}_z\left(\frac{(C+1)z-(C-1)\,z'}{2}\right)a_\rho^{(1)}\left(z'\right)\right.\\
&\left.-\frac{1}{C+1}a_\rho^{(1)'}(z)\int_0^z dz' a_\gamma^{(1)}(z')\right]
\end{aligned}
$$

$$
\begin{aligned}
&- \frac{1}{4\eta_g\nu_g^2}\left(\frac{\beta_0^2}{\alpha_0^2}Ck_g^3 + \nu_g^2 k_g - 2Ck_g^5\frac{\beta_0^2}{\omega^2} - 2k_g^3\nu_g^2\frac{\beta_0^2}{\omega^2}\right)\\
&\times\left[\frac{1}{2}\int_0^z dz' a_\rho^{(1)}{}_z\left(\frac{(C+1)z-(C-1)\,z'}{2}\right)a_\mu^{(1)}\left(z'\right) + \frac{1}{C+1}a_\mu^{(1)'}(z)\int_0^z dz' a_\rho^{(1)}(z')\right]\\
&- \frac{1}{4\eta_g\nu_g^2}\left(2\frac{\beta_0^2}{\alpha_0^2}Ck_g^3 - 2Ck_g^5\frac{\beta_0^2}{\omega^2} - 2k_g^3\nu_g^2\frac{\beta_0^2}{\omega^2}\right)\\
&\times\left[\frac{1}{2}\int_0^z dz' a_\mu^{(1)}{}_z\left(\frac{(C+1)z-(C-1)\,z'}{2}\right)a_\rho^{(1)}\left(z'\right) + \frac{1}{C+1}a_\rho^{(1)'}(z)\int_0^z dz' a_\mu^{(1)}(z')\right]\\
&+ \frac{1}{4\eta_g\nu_g^2}\left(\frac{\beta_0^2}{\alpha_0^2}C\nu_g^2 k_g + k_g^3 - 2k_g^5\frac{\beta_0^2}{\omega^2} - 2Ck_g^3\nu_g^2\frac{\beta_0^2}{\omega^2}\right)\\
&\times\left[\frac{1}{2}\int_0^z dz' a_\rho^{(1)}{}_z\left(\frac{(C+1)z-(C-1)\,z'}{2}\right)a_\mu^{(1)}\left(z'\right) - \frac{1}{C+1}a_\mu^{(1)'}(z)\int_0^z dz' a_\rho^{(1)}(z')\right]\\
&+ \frac{1}{4\eta_g\nu_g^2}\left(2\frac{\beta_0^2}{\alpha_0^2}k_g^3 - 2k_g^5\frac{\beta_0^2}{\omega^2} - 2Ck_g^3\nu_g^2\frac{\beta_0^2}{\omega^2}\right)\\
&\times\left[\frac{1}{2}\int_0^z dz' a_\mu^{(1)}{}_z\left(\frac{(C+1)z-(C-1)\,z'}{2}\right)a_\rho^{(1)}\left(z'\right) - \frac{1}{C+1}a_\rho^{(1)'}(z)\int_0^z dz' a_\mu^{(1)}(z')\right]\\
&- \frac{1}{4\eta_g^2\nu_g}\left(k_g^3 - 2k_g^5\frac{\beta_0^2}{\omega^2} + \frac{\beta_0^2}{\alpha_0^2}C^3\nu_g^2 k_g - 2C^3\nu_g^2 k_g^3\frac{\beta_0^2}{\omega^2}\right)\\
&\times\left[\frac{1}{2C}\int_0^z dz' a_\rho^{(1)}{}_z\left(\frac{(C+1)z+(C-1)\,z'}{2C}\right)a_\mu^{(1)}\left(z'\right) + \frac{1}{C+1}a_\mu^{(1)'}(z)\int_0^z dz' a_\rho^{(1)}(z')\right]\\
&- \frac{1}{4\eta_g^2\nu_g}\left(-2C^3\nu_g^2 k_g^3\frac{\beta_0^2}{\omega^2} - \frac{1}{2}k_g\frac{\omega^2}{\beta_0^2} + 2C^2\nu_g^2 k_g^3\frac{\beta_0^2}{\omega^2}\right)\\
&\times\left[\frac{1}{2C}\int_0^z dz' a_\mu^{(1)}{}_z\left(\frac{(C+1)z+(C-1)\,z'}{2C}\right)a_\rho^{(1)}\left(z'\right) + \frac{1}{C+1}a_\rho^{(1)'}(z)\int_0^z dz' a_\mu^{(1)}(z')\right]\\
&+ \frac{1}{4\eta_g\nu_g^2}\left(C\nu_g^2 k_g - 2C\nu_g^2 k_g^3\frac{\beta_0^2}{\omega^2} + \frac{\beta_0^2}{\alpha_0^2}k_g^3 - 2k_g^5\frac{\beta_0^2}{\omega^2}\right)\\
&\times\left[\frac{1}{2C}\int_0^z dz' a_\rho^{(1)}{}_z\left(\frac{(C+1)z+(C-1)\,z'}{2C}\right)a_\mu^{(1)}\left(z'\right) - \frac{1}{C+1}a_\mu^{(1)'}(z)\int_0^z dz' a_\rho^{(1)}(z')\right]\\
&+ \frac{1}{4\eta_g\nu_g^2}\left(2C^2\nu_g^2 k_g^3\frac{\beta_0^2}{\omega^2} - 2C\nu_g^2 k_g^3\frac{\beta_0^2}{\omega^2} - \frac{1}{2}k_g\frac{\omega^2}{\beta_0^2}\right)\\
&\times\left[\frac{1}{2C}\int_0^z dz' a_\mu^{(1)}{}_z\left(\frac{(C+1)z+(C-1)\,z'}{2C}\right)a_\rho^{(1)}\left(z'\right) - \frac{1}{C+1}a_\rho^{(1)'}(z)\int_0^z dz' a_\mu^{(1)}(z')\right],
\end{aligned}
$$

the solution for Eq. (50), i.e.,

$$\hat{G}_0^S\hat{V}_2^{SP}\hat{G}_0^P = -\hat{G}_0^S\hat{V}_1^{SP}\hat{G}_0^P\hat{V}_1^{PP}\hat{G}_0^P - \hat{G}_0^S\hat{V}_1^{SS}\hat{G}_0^S\hat{V}_1^{SP}\hat{G}_0^P,$$

is

$$
\begin{aligned}
&\frac{1}{4}\left(\frac{k_g}{\nu_g}+\frac{k_g}{\eta_g}\right)a_\rho^{(2)}(z) + \frac{\beta_0^2}{2\omega^2}k_g\left(\nu_g+\eta_g\right)\left(1-\frac{k_g^2}{\nu_g\eta_g}\right)a_\mu^{(2)}(z)\\
=&\Bigg\{-\frac{1}{2\eta_g\nu_g^2}\left[2(C-1)\nu_g^2 k_g^5\frac{\beta_0^4}{\omega^4} + \left(1-\frac{\beta_0^2}{\alpha_0^2}C\right)\nu_g^2 k_g^3\frac{\beta_0^2}{\omega^2}\right] - \frac{\beta_0^2}{\alpha_0^2}\frac{k_g^3}{\nu_g}\frac{\beta_0^2}{\omega^2} + \frac{k_g}{2\eta_g}\left(2k_g^2\frac{\beta_0^2}{\omega^2}-1\right)\\
&+\left(\frac{1}{2C}+\frac{1}{C+1}\right)\frac{1}{4\eta_g^2\nu_g}\left(6k_g^3 - 12k_g^5\frac{\beta_0^2}{\omega^2} - k_g\frac{\omega^2}{\beta_0^2} + 8k_g^7\frac{\beta_0^4}{\omega^4} + 8C^3\nu_g^2 k_g^5\frac{\beta_0^4}{\omega^4}\right.
\end{aligned}
$$

$$
\begin{aligned}
&-4\frac{\beta_0^2}{\alpha_0^2}C^3\nu_g^2k_g^3\frac{\beta_0^2}{\omega^2}\Bigg)\\
&-\left(\frac{1}{2C}-\frac{1}{C+1}\right)\frac{1}{4\eta_g\nu_g^2}\left(4\frac{\beta_0^2}{\alpha_0^2}k_g^3-8k_g^5\frac{\beta_0^2}{\omega^2}-k_g\frac{\omega^2}{\alpha_0^2}+2k_g^3-4C\nu_g^2k_g^3\frac{\beta_0^2}{\omega^2}+8C\nu_g^2k_g^5\frac{\beta_0^4}{\omega^4}\right.\\
&\left.-4\frac{\beta_0^2}{\alpha_0^2}k_g^5\frac{\beta_0^2}{\omega^2}+8k_g^7\frac{\beta_0^4}{\omega^4}\right)\Bigg\}a_\mu^{(1)}(z)a_\mu^{(1)}(z)\\
&+\left[\left(\frac{1}{2}+\frac{1}{C+1}\right)\frac{k_g}{8\eta_g\nu_g^2}\left(Ck_g^2+\nu_g^2\right)-\left(\frac{1}{2}-\frac{1}{C+1}\right)\frac{k_g}{8\eta_g\nu_g^2}\left(k_g^2+C\nu_g^2\right)\right.\\
&\left.+\left(\frac{1}{2C}+\frac{1}{C+1}\right)\frac{k_g}{8\eta_g^2\nu_g}\left(C^3\nu_g^2+k_g^2\right)-\left(\frac{1}{2C}-\frac{1}{C+1}\right)\frac{k_g}{8\eta_g\nu_g^2}\left(k_g^2+C\nu_g^2\right)\right]a_\rho^{(1)}(z)a_\rho^{(1)}(z)\\
&+\left[\left(\frac{1}{2}+\frac{1}{C+1}\right)\frac{\beta_0^2}{\alpha_0^2}\frac{1}{4\nu_g^3}k_g\left(k_g^2-\nu_g^2\right)+\left(\frac{1}{2}-\frac{1}{C+1}\right)\frac{1}{4\eta_g\nu_g^2}\left(k_g\frac{\omega^2}{\alpha_0^2}-2\frac{\beta_0^2}{\alpha_0^2}k_g^3\right)\right.\\
&\left.+\frac{\beta_0^2}{\alpha_0^2}\frac{k_g}{2\nu_g}\right]a_\mu^{(1)}(z)a_\gamma^{(1)}(z)\\
&-\left[\left(\frac{1}{2}+\frac{1}{C+1}\right)\frac{k_g\left(k_g^2+\nu_g^2\right)}{8\nu_g^3}-\left(\frac{1}{2}-\frac{1}{C+1}\right)\frac{k_g\left(k_g^2+\nu_g^2\right)}{8\eta_g\nu_g^2}\right]a_\rho^{(1)}(z)a_\gamma^{(1)}(z)\\
&-\left[\left(\frac{1}{2}+\frac{1}{C+1}\right)\frac{1}{4\eta_g\nu_g^2}\left(2\nu_g^2k_g^3\frac{\beta_0^2}{\omega^2}-\nu_g^2k_g+2Ck_g^5\frac{\beta_0^2}{\omega^2}-\frac{\beta_0^2}{\alpha_0^2}Ck_g^3\right)\right.\\
&\left.-\left(\frac{1}{2}-\frac{1}{C+1}\right)\frac{1}{4\eta_g\nu_g^2}\left(2C\nu_g^2k_g^3\frac{\beta_0^2}{\omega^2}-\frac{\beta_0^2}{\alpha_0^2}C\nu_g^2k_g+2k_g^5\frac{\beta_0^2}{\omega^2}-k_g^3\right)\right.\\
&\left.-\left(\frac{1}{2C}+\frac{1}{C+1}\right)\frac{1}{4\eta_g^2\nu_g}\left(3k_g^3+\frac{\beta_0^2}{\alpha_0^2}C^3\nu_g^2k_g-4C^3\nu_g^2k_g^3\frac{\beta_0^2}{\omega^2}-4k_g^5\frac{\beta_0^2}{\omega^2}-\frac{1}{2}k_g\frac{\omega^2}{\beta_0^2}\right)\right.\\
&\left.+\left(\frac{1}{2C}-\frac{1}{C+1}\right)\frac{1}{4\eta_g\nu_g^2}\left(C\nu_g^2k_g+2k_g^3+\frac{\beta_0^2}{\alpha_0^2}k_g^3-4k_g^5\frac{\beta_0^2}{\omega^2}-4C\nu_g^2k_g^3\frac{\beta_0^2}{\omega^2}-\frac{1}{2}k_g\frac{\omega^2}{\beta_0^2}\right)\right.\\
&\left.-(C-1)\frac{k_g^3}{2\eta_g}\frac{\beta_0^2}{\omega^2}\right]a_\rho^{(1)}(z)a_\mu^{(1)}(z)\\
&-\frac{1}{2\eta_g\nu_g^2}\left[2(C-1)\nu_g^2k_g^5\frac{\beta_0^4}{\omega^4}+\left(1-\frac{\beta_0^2}{\alpha_0^2}C\right)\nu_g^2k_g^3\frac{\beta_0^2}{\omega^2}\right]\\
&\times\int_0^z dz' {a_\mu^{(1)}}_z\left(\frac{(C+1)z-(C-1)\,z'}{2}\right)a_\mu^{(1)}\left(z'\right)\\
&+\frac{1}{4\eta_g^2\nu_g}\left(6k_g^3-12k_g^5\frac{\beta_0^2}{\omega^2}-k_g\frac{\omega^2}{\beta_0^2}+8k_g^7\frac{\beta_0^4}{\omega^4}+8C^3\nu_g^2k_g^5\frac{\beta_0^4}{\omega^4}-4\frac{\beta_0^2}{\alpha_0^2}C^3\nu_g^2k_g^3\frac{\beta_0^2}{\omega^2}\right)\\
&\times\left[\frac{1}{2C}\int_0^z dz' {a_\mu^{(1)}}_z\left(\frac{(C+1)z+(C-1)\,z'}{2C}\right)a_\mu^{(1)}\left(z'\right)+\frac{1}{C+1}a_\mu^{(1)'}(z)\int_0^z dz' a_\mu^{(1)}(z')\right]\\
&-\frac{1}{4\eta_g\nu_g^2}\left(4\frac{\beta_0^2}{\alpha_0^2}k_g^3-8k_g^5\frac{\beta_0^2}{\omega^2}-k_g\frac{\omega^2}{\alpha_0^2}+2k_g^3-4C\nu_g^2k_g^3\frac{\beta_0^2}{\omega^2}+8C\nu_g^2k_g^5\frac{\beta_0^4}{\omega^4}-4\frac{\beta_0^2}{\alpha_0^2}k_g^5\frac{\beta_0^2}{\omega^2}+8k_g^7\frac{\beta_0^4}{\omega^4}\right)\\
&\times\left[\frac{1}{2C}\int_0^z dz' {a_\mu^{(1)}}_z\left(\frac{(C+1)z+(C-1)\,z'}{2C}\right)a_\mu^{(1)}\left(z'\right)-\frac{1}{C+1}a_\mu^{(1)'}(z)\int_0^z dz' a_\mu^{(1)}(z')\right]\\
&+\frac{k_g\left(Ck_g^2+\nu_g^2\right)}{8\eta_g\nu_g^2}\left[\frac{1}{2}\int_0^z dz' {a_\rho^{(1)}}_z\left(\frac{(C+1)z-(C-1)\,z'}{2}\right)a_\rho^{(1)}\left(z'\right)\right.
\end{aligned}
$$

$$
\begin{aligned}
&+\frac{1}{C+1}a_\rho^{(1)'}(z)\int_0^z dz' a_\rho^{(1)}(z')\Bigg] \\
&-\frac{k_g\left(k_g^2+C\nu_g^2\right)}{8\eta_g\nu_g^2}\left[\frac{1}{2}\int_0^z dz' a_\rho^{(1)}{}_z\left(\frac{(C+1)z-(C-1)\,z'}{2}\right)a_\rho^{(1)}\left(z'\right)\right. \\
&\left.-\frac{1}{C+1}a_\rho^{(1)'}(z)\int_0^z dz' a_\rho^{(1)}(z')\right] \\
&+\frac{C^3k_g\nu_g^2+k_g^3}{8\eta_g^2\nu_g}\left[\frac{1}{2C}\int_0^z dz' a_\rho^{(1)}{}_z\left(\frac{(C+1)z+(C-1)\,z'}{2C}\right)a_\rho^{(1)}\left(z'\right)\right. \\
&\left.+\frac{1}{C+1}a_\rho^{(1)'}(z)\int_0^z dz' a_\rho^{(1)}(z')\right] \\
&-\frac{k_g\left(k_g^2+C\nu_g^2\right)}{8\eta_g\nu_g^2}\left[\frac{1}{2C}\int_0^z dz' a_\rho^{(1)}{}_z\left(\frac{(C+1)z+(C-1)\,z'}{2C}\right)a_\rho^{(1)}\left(z'\right)\right. \\
&\left.-\frac{1}{C+1}a_\rho^{(1)'}(z)\int_0^z dz' a_\rho^{(1)}(z')\right] \\
&+\frac{\beta_0^2}{\alpha_0^2}\frac{k_g\left(k_g^2-\nu_g^2\right)}{4\nu_g^3}\left[\frac{1}{2}\int_0^z dz' a_\gamma^{(1)}{}_z\left(\frac{(C+1)z-(C-1)\,z'}{2}\right)a_\mu^{(1)}\left(z'\right)\right. \\
&\left.+\frac{1}{C+1}a_\mu^{(1)'}(z)\int_0^z dz' a_\gamma^{(1)}(z')\right] \\
&+\frac{1}{4\eta_g\nu_g^2}\left(k_g\frac{\omega^2}{\alpha_0^2}-2\frac{\beta_0^2}{\alpha_0^2}k_g^3\right)\left[\frac{1}{2}\int_0^z dz' a_\gamma^{(1)}{}_z\left(\frac{(C+1)z-(C-1)\,z'}{2}\right)a_\mu^{(1)}\left(z'\right)\right. \\
&\left.-\frac{1}{C+1}a_\mu^{(1)'}(z)\int_0^z dz' a_\gamma^{(1)}(z')\right] \\
&-\frac{k_g\left(k_g^2+\nu_g^2\right)}{8\nu_g^3}\left[\frac{1}{2}\int_0^z dz' a_\gamma^{(1)}{}_z\left(\frac{(C+1)z-(C-1)\,z'}{2}\right)a_\rho^{(1)}\left(z'\right)\right. \\
&\left.+\frac{1}{C+1}a_\rho^{(1)'}(z)\int_0^z dz' a_\gamma^{(1)}(z')\right] \\
&+\frac{k_g\left(k_g^2+\nu_g^2\right)}{8\eta_g\nu_g^2}\left[\frac{1}{2}\int_0^z dz' a_\gamma^{(1)}{}_z\left(\frac{(C+1)z-(C-1)\,z'}{2}\right)a_\rho^{(1)}\left(z'\right)\right. \\
&\left.-\frac{1}{C+1}a_\rho^{(1)'}(z)\int_0^z dz' a_\gamma^{(1)}(z')\right] \\
&-\frac{1}{4\eta_g\nu_g^2}\left(2\nu_g^2k_g^3\frac{\beta_0^2}{\omega^2}-\nu_g^2k_g+2Ck_g^5\frac{\beta_0^2}{\omega^2}-\frac{\beta_0^2}{\alpha_0^2}Ck_g^3\right) \\
&\times\left[\frac{1}{2}\int_0^z dz' a_\rho^{(1)}{}_z\left(\frac{(C+1)z-(C-1)\,z'}{2}\right)a_\mu^{(1)}\left(z'\right)+\frac{1}{C+1}a_\mu^{(1)'}(z)\int_0^z dz' a_\rho^{(1)}(z')\right] \\
&+\frac{1}{4\eta_g\nu_g^2}\left(2C\nu_g^2k_g^3\frac{\beta_0^2}{\omega^2}-\frac{\beta_0^2}{\alpha_0^2}C\nu_g^2k_g+2k_g^5\frac{\beta_0^2}{\omega^2}-k_g^3\right) \\
&\times\left[\frac{1}{2}\int_0^z dz' a_\rho^{(1)}{}_z\left(\frac{(C+1)z-(C-1)\,z'}{2}\right)a_\mu^{(1)}\left(z'\right)-\frac{1}{C+1}a_\mu^{(1)'}(z)\int_0^z dz' a_\rho^{(1)}(z')\right] \\
&+(C-1)\frac{k_g^3}{2\eta_g}\frac{\beta_0^2}{\omega^2}\int_0^z dz' a_\mu^{(1)}{}_z\left(\frac{(C+1)z-(C-1)\,z'}{2}\right)a_\rho^{(1)}\left(z'\right)
\end{aligned}
$$

$$
\begin{aligned}
&- \frac{1}{4\eta_g^2\nu_g}\left(-2k_g^3 + 2C^3\nu_g^2 k_g^3\frac{\beta_0^2}{\omega^2} + 2k_g^5\frac{\beta_0^2}{\omega^2} + \frac{1}{2}k_g\frac{\omega^2}{\beta_0^2}\right)\\
&\times\left[\frac{1}{2C}\int_0^z dz' a_\mu^{(1)}{}_z\left(\frac{(C+1)z+(C-1)\,z'}{2C}\right)a_\rho^{(1)}\left(z'\right) + \frac{1}{C+1}a_\rho^{(1)'}(z)\int_0^z dz' a_\mu^{(1)}(z')\right]\\
&- \frac{1}{4\eta_g^2\nu_g}\left(-k_g^3 - \frac{\beta_0^2}{\alpha_0^2}C^3\nu_g^2 k_g + 2C^3\nu_g^2 k_g^3\frac{\beta_0^2}{\omega^2} + 2k_g^5\frac{\beta_0^2}{\omega^2}\right)\\
&\times\left[\frac{1}{2C}\int_0^z dz' a_\rho^{(1)}{}_z\left(\frac{(C+1)z+(C-1)\,z'}{2C}\right)a_\mu^{(1)}\left(z'\right) + \frac{1}{C+1}a_\mu^{(1)'}(z)\int_0^z dz' a_\rho^{(1)}(z')\right]\\
&- \frac{1}{4\eta_g\nu_g^2}\left(2k_g^3 - 2k_g^5\frac{\beta_0^2}{\omega^2} - 2C\nu_g^2 k_g^3\frac{\beta_0^2}{\omega^2} - \frac{1}{2}k_g\frac{\omega^2}{\beta_0^2}\right)\\
&\times\left[\frac{1}{2C}\int_0^z dz' a_\mu^{(1)}{}_z\left(\frac{(C+1)z+(C-1)\,z'}{2C}\right)a_\rho^{(1)}\left(z'\right) - \frac{1}{C+1}a_\rho^{(1)'}(z)\int_0^z dz' a_\mu^{(1)}(z')\right]\\
&- \frac{1}{4\eta_g\nu_g^2}\left(C\nu_g^2 k_g + \frac{\beta_0^2}{\alpha_0^2}k_g^3 - 2k_g^5\frac{\beta_0^2}{\omega^2} - 2C\nu_g^2 k_g^3\frac{\beta_0^2}{\omega^2}\right)\\
&\times\left[\frac{1}{2C}\int_0^z dz' a_\rho^{(1)}{}_z\left(\frac{(C+1)z+(C-1)\,z'}{2C}\right)a_\mu^{(1)}\left(z'\right) - \frac{1}{C+1}a_\mu^{(1)'}(z)\int_0^z dz' a_\rho^{(1)}(z')\right],
\end{aligned}
$$

and the solution for Eq. (51), i.e.,

$$\hat{G}_0^S\hat{V}_2^{SS}\hat{G}_0^S = -\hat{G}_0^S\hat{V}_1^{SP}\hat{G}_0^P\hat{V}_1^{PS}\hat{G}_0^S - \hat{G}_0^S\hat{V}_1^{SS}\hat{G}_0^S\hat{V}_1^{SS}\hat{G}_0^S,$$

is

$$
\begin{aligned}
&- \frac{1}{4}\left(1 - \frac{k_g^2}{\eta_g^2}\right)a_\rho^{(2)}(z) - \left[\frac{k_g^2+\eta_g^2}{4\eta_g^2} - \frac{2k_g^2}{k_g^2+\eta_g^2}\right]a_\mu^{(2)}(z)\\
=&-\left\{\frac{1}{8\eta_g^4}\left(8k_g^2\eta_g^2 - \frac{\omega^4}{\beta_0^4}\right) - \frac{1}{4\eta_g^2}\left(\frac{\omega^2}{\beta_0^2} - 4\frac{\beta_0^2}{\omega^2}\eta_g^2 k_g^2\right) - \frac{\beta_0^2}{\alpha_0^2}k_g^2\frac{\beta_0^2}{\omega^2}\right.\\
&\left.+\frac{1}{\eta_g^2(C+1)}\left[k_g^2\left(\frac{\beta_0^4}{\alpha_0^4}C^2 - 1\right) - 4k_g^4\frac{\beta_0^2}{\omega^2}\left(\frac{\beta_0^2}{\alpha_0^2}C^2 - 1\right) + 4k_g^6\frac{\beta_0^4}{\omega^4}(C^2-1)\right]\right\}a_\mu^{(1)}(z)a_\mu^{(1)}(z)\\
&- \left[\frac{1}{8\eta_g^4}\left(\eta_g^4 - k_g^4\right) + \frac{1}{4\eta_g^2}k_g^2(C-1)\right]a_\rho^{(1)}(z)a_\rho^{(1)}(z)\\
&+\left\{\frac{k_g^2}{\eta_g^2} - \frac{1}{\eta_g^2(C+1)}\left[k_g^2\left(\frac{\beta_0^2}{\alpha_0^2}C^2 - 1\right) - 2\frac{\beta_0^2}{\omega^2}k_g^4\left(C^2-1\right)\right]\right\}a_\mu^{(1)}(z)a_\rho^{(1)}(z)\\
&- \frac{1}{8\eta_g^4}\left(8k_g^2\eta_g^2 - \frac{\omega^4}{\beta_0^4}\right)a_\mu^{(1)'}(z)\int_0^z dz' a_\mu^{(1)}(z')\\
&- \frac{1}{8\eta_g^4}\left(\eta_g^4 - k_g^4\right)a_\rho^{(1)'}(z)\int_0^z dz' a_\rho^{(1)}(z')\\
&+\frac{k_g^2}{2\eta_g^2}\left[a_\mu^{(1)'}(z)\int_0^z dz' a_\rho^{(1)}(z') + a_\rho^{(1)'}(z)\int_0^z dz' a_\mu^{(1)}(z')\right]\\
&- \frac{1}{8\eta_g^2}\left(\eta_g^2 - 3k_g^2\right)\left[a_\mu^{(1)'}(z)\int_0^z dz' a_\rho^{(1)}(z') - a_\rho^{(1)'}(z)\int_0^z dz' a_\mu^{(1)}(z')\right]\\
&- \frac{1}{\eta_g^2(C+1)}\left[k_g^2\left(\frac{\beta_0^4}{\alpha_0^4}C^2 - 1\right) - 4k_g^4\frac{\beta_0^2}{\omega^2}\left(\frac{\beta_0^2}{\alpha_0^2}C^2 - 1\right) + 4k_g^6\frac{\beta_0^4}{\omega^4}(C^2-1)\right]
\end{aligned}
$$

$$
\begin{aligned}
&\times \int_0^z dz' a_\mu^{(1)}{}_z \left(\frac{2Cz-(C-1)\,z'}{(C+1)} \right) a_\mu^{(1)}\left(z'\right) \\
&- \frac{1}{4\eta_g^2} k_g^2 (C-1) \int_0^z dz' a_\rho^{(1)}{}_z \left(\frac{2Cz-(C-1)\,z'}{(C+1)} \right) a_\rho^{(1)}\left(z'\right) \\
&- \frac{1}{2\eta_g^2 (C+1)} \left[k_g^2 \left(\frac{\beta_0^2}{\alpha_0^2} C^2 - 1 \right) - 2 \frac{\beta_0^2}{\omega^2} k_g^4 \left(C^2-1\right) \right] \\
&\times \left[\int_0^z dz' a_\mu^{(1)}{}_z \left(\frac{2Cz-(C-1)\,z'}{(C+1)} \right) a_\rho^{(1)}\left(z'\right) + \int_0^z dz' a_\rho^{(1)}{}_z \left(\frac{2Cz-(C-1)\,z'}{(C+1)} \right) a_\mu^{(1)}\left(z'\right) \right] \\
&+ \frac{C k_g^2}{2(C+1)\eta_g^2} \left(\frac{\beta_0^2}{\alpha_0^2} - 1 \right) \\
&\times \left[\int_0^z dz' a_\mu^{(1)}{}_z \left(\frac{2Cz-(C-1)\,z'}{(C+1)} \right) a_\rho^{(1)}\left(z'\right) - \int_0^z dz' a_\rho^{(1)}{}_z \left(\frac{2Cz-(C-1)\,z'}{(C+1)} \right) a_\mu^{(1)}\left(z'\right) \right],
\end{aligned}
$$

where $\eta_g = C\nu_g, k_g^2 + \nu_g^2 = \omega^2/\alpha_0^2$ and $k_g^2 + \eta_g^2 = \omega^2/\beta_0^2$.

After we solve all (four) of the second order equations, future research is to perform numerical tests with all four components of data available.

5 Conclusion

In this paper, a framework and algorithm have been developed for more accurate target identification. The elastic non-linear inversion requires all four components of data. In this paper we analyzed an algorithm which inputs only $\hat{D}^{PP}$. Although $\hat{D}^{PP}$ can itself provide useful non-linear direct inversion results, the implication of this research is that further value would derive from actually measuring $\hat{D}^{PP}$, $\hat{D}^{PS}$, $\hat{D}^{SP}$ and $\hat{D}^{SS}$, as the method requires. For the case that all four components of data available, we also provided a consistent method to solve for all of the second terms.

Acknowledgements

The M-OSRP sponsors are thanked for supporting this research. We are grateful to Robert Keys and Douglas Foster for useful comments and suggestions. We have been partially funded by and are grateful for NSF-CMG award DMS-0327778 and DOE Basic Sciences award DE-FG02-05ER15697.

Appendix A

In this Appendix, we give the different coefficients before every linear quantity $(a_\gamma^{(1)}, a_\rho^{(1)}, a_\mu^{(1)})$ — different incidence angle θ. For P to P case, we have

$$
\begin{aligned}
k_g^{PP} &= \frac{\omega}{\alpha_0} \sin\theta^{PP}, \\
\nu_g^{PP} &= \frac{\omega}{\alpha_0} \cos\theta^{PP},
\end{aligned}
$$

For S to P case,

$$k_g^{PS} = \frac{\omega}{\beta_0}\sin\theta^{PS},$$
$$\nu_g^{PS} = \frac{\omega}{\alpha_0}\sqrt{1-\frac{\alpha_0^2}{\beta_0^2}\sin^2\theta^{PS}}$$
$$\eta_g^{PS} = \frac{\omega}{\beta_0}\cos\theta^{PS},$$

For P to S case,

$$k_g^{SP} = \frac{\omega}{\alpha_0}\sin\theta^{SP},$$
$$\nu_g^{SP} = \frac{\omega}{\alpha_0}\cos\theta^{SP}$$
$$\eta_g^{SP} = \frac{\omega}{\beta_0}\sqrt{1-\frac{\beta_0^2}{\alpha_0^2}\sin^2\theta^{SP}},$$

For S to S case,

$$k_g^{SS} = \frac{\omega}{\beta_0}\sin\theta^{SS},$$
$$\eta_g^{SS} = \frac{\omega}{\beta_0}\cos\theta^{SS},$$

Let the arguments of $a_\rho^{(1)}$ and $a_\mu^{(1)}$ in Eqs. (41), (42), (43) and (44) equal, we need

$$-2\nu_g^{PP} = -\nu_g^{PS} - \eta_g^{PS} = -\nu_g^{SP} - \eta_g^{SP} = -2\eta_g^{SS},$$

which leads to

$$2\frac{\omega}{\alpha_0}\cos\theta^{PP} = \frac{\omega}{\alpha_0}\sqrt{1-\frac{\alpha_0^2}{\beta_0^2}\sin^2\theta^{PS}} + \frac{\omega}{\beta_0}\cos\theta^{PS}$$
$$= \frac{\omega}{\alpha_0}\cos\theta^{SP} + \frac{\omega}{\beta_0}\sqrt{1-\frac{\beta_0^2}{\alpha_0^2}\sin^2\theta^{SP}} = 2\frac{\omega}{\beta_0}\cos\theta^{SS},$$

From the expression above, given θ^{PP}, we can find the corresponding θ^{PS}, θ^{SP} and θ^{SS}.

$$\theta^{PS} = \cos^{-1}\left[\frac{4b^2\cos^2\theta^{PP}+1-b^2}{4b\cos\theta^{PP}}\right],$$
$$\theta^{SP} = \cos^{-1}\left[\frac{4b^2\cos^2\theta^{PP}-1+b^2}{4b^2\cos\theta^{PP}}\right],$$
$$\theta^{SS} = \cos^{-1}\left(b\cos\theta^{PP}\right),$$

where $b = \frac{\beta_0}{\alpha_0}$.

References

Aki, K. and P. G. Richards. *Quantitative Seismology.* 2nd edition. University Science Books, 2002.

Araújo, F. V. *Linear and non-linear methods derived from scattering theory: backscattered tomography and internal multiple attenuation*. PhD thesis, Universidade Federal da Bahia, 1994.

Carvalho, P. M. *Free-surface multiple reflection elimination method based on nonlinear inversion of seismic data*. PhD thesis, Universidade Federal da Bahia, 1992.

Carvalho, P. M., A. B. Weglein, and R. H. Stolt. "Nonlinear inverse scattering for multiple suppression: Application to real data. part I." *62nd Ann. Internat. Mtg: Soc. of Expl. Geophys., Expanded Abstracts*. . Soc. Expl. Geophys., 1992. 1093–1095.

Clayton, R. W. and R. H. Stolt. "A Born-WKBJ inversion method for acoustic reflection data." *Geophysics* 46 (1981): 1559–1567.

Foster, D. J., R. G. Keys, and D. P. Schmitt. *Detecting subsurface hydrocarbons with elastic wavefields*. Springer-In Inverse Problems in Wave Progagation, Volume 90 of The IMA Volumes in Mathematics and its Applications, 1997.

Innanen, K. A. and A. B. Weglein. "Linear inversion for absorptive/dispersive medium parameters." *74th Annual Internat. Mtg., Soc. Expl. Geophys., Expanded Abstracts*. . Soc. Expl. Geophys., 2004. 1834–1837.

Innanen, K. A. and A. B. Weglein. "Towards non-linear construction of a Q-compensation operator directly from measured seismic reflection data." *75th Annual Internat. Mtg., Soc. Expl. Geophys., Expanded Abstracts*. . Soc. Expl. Geophys., 2005. 1693–1696.

Liu, F., A. B. Weglein K. A. Innanen, and B. G. Nita. "Extension of the non-linear depth imaging capability of the inverse scattering series to multidimensional media: strategies and numerical results." *9th Ann. Cong. SBGf, Expanded Abstracts*. . SBGf, 2005.

Liu, F., B. G. Nita, A. B. Weglein, and K. A. Innanen. "Inverse Scattering Series in the presence of lateral variations." *M-OSRP Annual Report* 3 (2004).

Liu, F. and A. B. Weglein. "Initial analysis of the inverse scattering series for a variable background." *M-OSRP Annual Report* 2 (2003): 210–225.

Matson, K. H. *An inverse-scattering series method for attenuating elastic multiples from multicomponent land and ocean bottom seismic data*. PhD thesis, University of British Columbia, 1997.

Ramírez, Adriana C. and Arthur B. Weglein. "An inverse scattering internal multiple elimination method: Beyond attenuation, a new algorithm and initial tests." *75th Annual Internat. Mtg., Soc. Expl. Geophys., Expanded Abstracts*. . Soc. Expl. Geophys., 2005. 2115–2118.

Shaw, S. A. and A. B. Weglein. "Imaging seismic reflection data at the correct depth without specifying an accurate velocity model: Initial examples of an inverse scattering subseries." *Frontiers of remote sensing information processing*. Ed. C. H. Chen. World Scientific Publishing Company, 2003. chapter 21, 469–484.

Shaw, S. A. and A. B. Weglein. "A leading order imaging series for prestack data acquired over a laterally invariant acoustic medium. Part II: Analysis for data missing low frequencies." *M-OSRP Annual Report* 3 (2004).

Shaw, S. A., A. B. Weglein, D. J. Foster, K. H. Matson, and R. G. Keys. "Convergence properties of a leading order depth imaging series." *73rd Annual Internat. Mtg., Soc. Expl. Geophys., Expanded Abstracts*. . Soc. Expl. Geophys., 2003. 937–940.

Shaw, S. A., A. B. Weglein, D. J. Foster, K. H. Matson, and R. G. Keys. "Isolation of a leading order depth imaging series and analysis of its convergence properties." *M-OSRP Annual Report* 2 (2003): 157–195.

Shaw, S. A., A. B. Weglein, D. J. Foster, K. H. Matson, and R. G. Keys. "Isolation of a leading order depth imaging series and analysis of its convergence properties." *Journal of Seismic Exploration* 2 (November 2004): 157–195.

Weglein, A. B., F. V. Araújo, P. M. Carvalho, R. H. Stolt, K. H. Matson, R. T. Coates, D. Corrigan, D. J. Foster, S. A. Shaw, and H. Zhang. "Inverse scattering series and seismic exploration." *Inverse Problems* 19 (2003): R27–R83.

Weglein, A. B., D. J. Foster, K. H. Matson, S. A. Shaw, P. M. Carvalho, and D. Corrigan. "Predicting the correct spatial location of reflectors without knowing or determining the precise medium and wave velocity: initial concept, algorithm and analytic and numerical example." *Journal of Seismic Exploration* 10 (2002): 367–382.

Weglein, A. B., F. A. Gasparotto, P. M. Carvalho, and R. H. Stolt. "An inverse-scattering series method for attenuating multiples in seismic reflection data." *Geophysics* 62 (1997): 1975–1989.

Weglein, A. B. and R. H. Stolt. 1992 "Approaches on linear and non-linear migration-inversion.". Personal Communication.

Weglein, A. B., P. B. Violette, and T. H. Keho. "Using multiparameter Born theory to obtain certain exact multiparameter inversion goals." *Geophysics* 51 (1986): 1069–1074.

Zhang, H. and A. B. Weglein. "The inverse scattering series for tasks associated with primaries: Depth imaging and direct non-linear inversion of 1D variable velocity and density acoustic media." *75th Annual Internat. Mtg., Soc. Expl. Geophys., Expanded Abstracts*. . Soc. Expl. Geophys., 2005. 1705–1708.

Comprehending and analyzing the leading order and higher order imaging closed forms derived from inverse scattering series

J. Zhang, F. Liu, K. A. Innanen, and A. B. Weglein

Abstract

All current leading-edge migration/imaging methods locate the depths of subsurface reflectors using the phase in the reflected data and the velocity above the reflector. The subseries for imaging without the velocity (Weglein et al., 2003), which is part of the whole inverse scattering series (ISS), has the capability of directly producing reflector images using only the data. The imaging subseries is a cascaded series in the sense that the coefficient of each term is again an infinite series (Shaw, 2005). Part of this cascaded series was captured and called leading-order imaging series (LOIS) (Shaw et al., 2003). Then, more imaging terms were identified and *added* to the LOIS. This more capable series is called higher order imaging series (HOIS) (Liu, 2006). It is worth mentioning that the HOIS has not captured all of the terms for imaging. Both LOIS and HOIS have closed forms. The closed form HOIS has an unusal implicit form that was developed by Liu (2006) using an intuitive leap and the conviction that only shallower events in the linear approximate image (α_1) should help any particular event to determine its location, through non-linear multiplicative communication. The same intuitive leap can be applied to the LOIS closed form. The closed forms without using Liu's intuitive leap seem unreasonable at present, since they need deeper medium information in order to locate shallower interfaces. However, the ISS only promise the final result will be correct, without guaranteeing any intermediate results are reasonable or correct. This is one of the lessons we learned from the application of ISS on free surface multiple removal. On free surface multiple removal, all of the free surface multiples will be eliminated after all of the multiple removing terms are added to the data. However, at any intermediate step, some free surface multiples may become even stronger than they were in the original data. More details on this issue will be discussed in the following.

1 Introduction

Migration/Imaging is the process of locating reflectors at depth using reflected seismic data. This process uses the arrival time of the signal and the wave velocity of the medium through which the signal traveled. Current migration algorithms obtain the latter from another procedure, velocity analysis. These migration algorithms are, on one hand, very stable. For example, with current data acquisition which often miss small and cross-line offsets measurements, and zero/low frequency information, these imaging algorithms manage to provide satisfactory results for most cases. On the other hand, for cases (e.g., sub-salt imaging) in which the velocity analysis has difficulties, the performance of velocity dependent migration procedures will be affected too. In these situations, one has two choices: either improving the performance of the velocity analysis, or pursuing a new imaging procedure which does not require the actual medium velocity. Efforts have been expended on both choices. This paper, among many others (Weglein et al., 2000; Shaw et al., 2002; Innanen and Weglein, 2003; Liu et al., 2005), is pursuing the latter choice.

The idea of performing imaging without the actual medium velocity is so contradictory to common sense that it is reasonable to ask: how could it be possible? We would like to answer this question by first pointing out that the velocity information that migration uses comes from nowhere but the

data. So essentially all information comes from the data (Figure 1a). We would argue that given this, the existence of such an algorithm that could *directly* produce the image of the subsurface, without a separate velocity analysis step (Figure 1b) is not counter-intuitive at all. The main difference is that, the imaging without the velocity algorithm derived from the ISS is capable of using the amplitude information of the data as well as the arrival time. The significance of this capability is explained below. Figure 2 illustrates the two primaries for a 1D normal incidence experiment. The arrival times of the two primaries are t_a and t_b respectively. Assuming the wave speed in the medium between the source and the first interface is c_0 (which is called the reference medium velocity), the water bottom is easy to locate: $z_a = t_a * c_0/2$. Imaging the second interface is also not difficult if the velocity of the medium between the two interfaces is known. However, note that the first signal contains more information than just the arrival time. Its amplitude directly relates to the property contrast across the first interface: $R = \frac{c_1 - c_0}{c_1 + c_0}$. So the velocity below the first interface can be obtained as long as the amplitude of the signal and the reference medium velocity are known. The question is whether or not such an algorithm can be found that can directly extract all of the necessary information from the data to perform imaging without finding the velocity through a separate step. The imaging without the velocity algorithm is such an algorithm.

The framework and logic about the ISS are discussed by Weglein et al. (2003). It mentioned that the whole ISS has very limited applicability due to convergence issues (Carvalho, 1992). So, certain terms are identified and grouped together to perform one task only (multiple removal, imaging, or inversion) and act like no other task exists at all. These subseries might have better convergence properties than the whole series. This is the idea of isolated task-specific subseries. In other words, it is the latter isolated task specific concept and math-physics interpretation that makes the inverse series practically useful.

The imaging capability within the inverse scattering series is a series in terms of powers of the distance between the pseodo depth and the actual depth, and the latter difference in depths, are in turn each be a power series in the data. If only the first term in the expansion of the difference between actual and pseudo depth in terms of the data is retained, the result is a leading order imaging series (Shaw et al., 2003) and has effectiveness when the overall difference between actual and reference properties is not large. If you retain more than the leading order terms in the data in the cascaded imaging series then this is called higher order imaging capture (Liu et al., 2006) and has a broader region of contrast accommodation. The capture called higher order imaging is not the full cascaded imaging series. These ideas were first put forward in Weglein et al. (2001) and Shaw et al. (2002). Both the leading order imaging series (LOIS) and the higher order imaging series (HOIS) have closed forms. The first step in performing imaging without the velocity is to obtain $\alpha_1(z)$ (Weglein et al., 2001; Shaw et al., 2002; Liu et al., 2005) which is very close to the Stolt migration result using reference medium velocity. Then we use the obtained LOIS and HOIS closed forms to improve the reflector locations in α_1. In this paper, through analysis of those closed forms and the work of Innanen (2005), their accuracy and meaning are discussed.

The leading-order closed-form (LOIS) imaging series is

$$\alpha^{LOIS}(z) = \alpha_1\Big(z - \frac{1}{2}\int_0^z \alpha_1(z')dz'\Big); \tag{1}$$

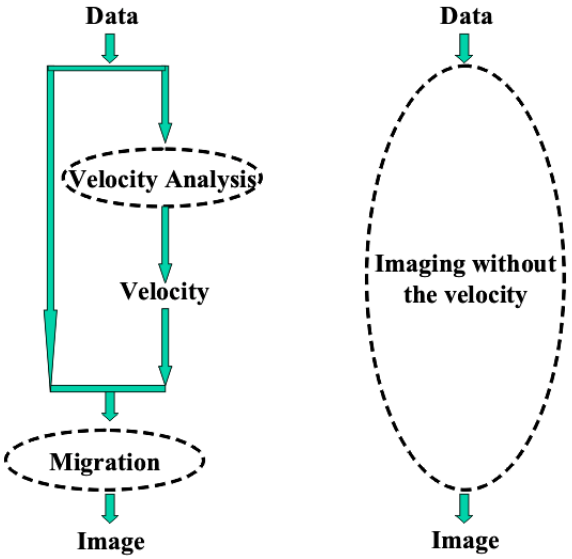

(a) Conventional

(b) Imaging without the velocity

Figure 1: Imaging strategies

and the high-order closed-form imaging series (HOIS) is

$$\alpha^{HOIS}\Big(z+\frac{1}{2}\int_0^z \frac{\alpha_1(z')}{1-\frac{1}{4}\alpha_1(z')}dz'\Big)=\alpha_1(z). \tag{2}$$

The functions $\alpha^{LOIS}(z)$ and $\alpha^{HOIS}(z)$ provide better reflector locations compared to α_1. One may notice that in Eq. 1, the argument of α^{LOIS} is very simple and that of α_1 is relatively complicated, while in Eq. 2, it is α^{HOIS} that has the relatively complicated argument. Why this transfer of complexity? What difference will it make? What is the performance/accuracy of these closed forms? We will try to answer these questions, without becoming too involved in the math or diagrams of the ISS.

2 Interpretation of the closed forms

There are several ways to interpret Eq. 1:

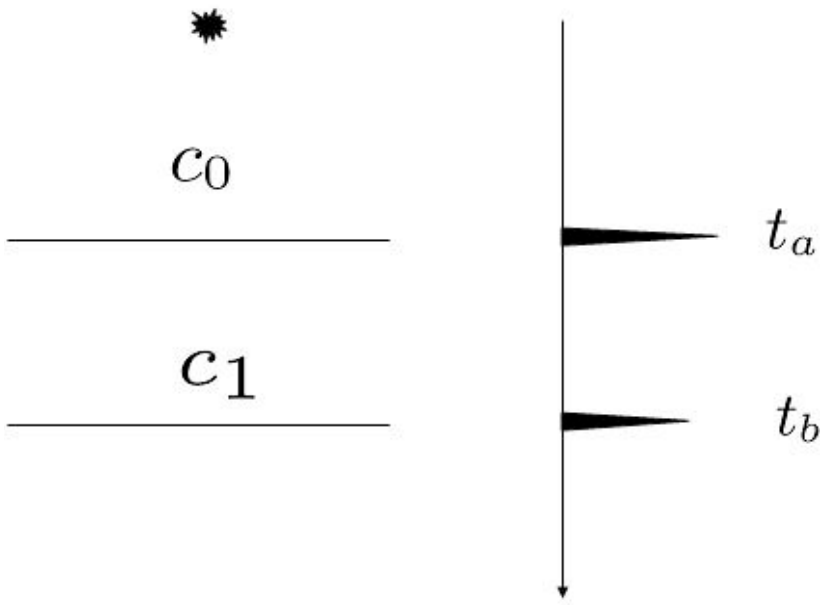

Figure 2: 1D normal incidence two primaries. Depth of the first and second interfaces are z_a and z_b respectively.

1. The value of α^{LOIS} at z equals the value of α_1 at $z - \frac{1}{2}\int_0^z \alpha_1(z')dz' = z'_b$; or,
2. The value of α^{LOIS} at $z = z'_b + \frac{1}{2}\int_0^z \alpha_1(z')dz'$ equals the value of α_1 at z'_b; or in reverse,
3. The value of α_1 at z'_b equals to the value of α^{LOIS} at $z = z'_b + \frac{1}{2}\int_0^z \alpha_1(z')dz'$.

Imagine that there is an interface at z'_b in α_1. Then based on the third interpretation, this interface will be moved to another depth z, and the distance to be moved is determined by: $\frac{1}{2}\int_0^z \alpha_1(z')dz'$, which is an integration to depth z, *not* z'_b. So, if z is bigger than z'_b, then α_1 values from greater depths contribute to the moving of this shallower interface. This conclusion is actually a little strange since the diagram analysis only permit shallower events helping the locations of deeper events. Even from physical instincts, it seems strange that the moving of shallower events care about deeper events. What is going on here?

Innanen (2005) proposed a coupled imaging-inversion algorithm. In an attempt to obtain the *imaging* only equation, a "natural" isolated form would seem to be

$$\alpha^{HOIS}(z) = \alpha_1\Big(z - \frac{1}{2}\int_0^z \frac{\alpha_1(z')}{1 - \frac{1}{4}\alpha_1(z')}dz'\Big), \tag{3}$$

which is very similar to Eq. 2 except where the complicated argument stays.

Eq. 3 was tested and found that the results were poor. Then from physical intuition, Liu intuitively moved the argument to the left hand side and obtained Eq. 2 which provided very good results (Liu, 2006). To understand this move, let's apply the same operation to Eq. 1:

$$\alpha^{SLOIS}\Big(z+\frac{1}{2}\int_0^z \alpha_1(z')dz'\Big)=\alpha_1(z), \tag{4}$$

where SLOIS denotes "Shifted LOIS". Let's analyze its meaning in a similar way:

1. The value of α^{SLOIS} at $z+\frac{1}{2}\int_0^z \alpha_1(z')dz'$ equals to the value of α_1 at z; or, reversely,
2. The value of α_1 at z equals to the value of α^{SLOIS} at $z+\frac{1}{2}\int_0^z \alpha_1(z')dz'$; so,
3. The value of α_1 at z_b' equals to the value of α^{SLOIS} at $z_b'+\frac{1}{2}\int_0^{z_b'} \alpha_1(z')dz'$.

Clearly, if it happens that there is an interface at z_b' in α_1 then it will be moved to depth z and the distance to move is determined by an integration to depth z_b'. No deeper events will contribute to the movement of shallower ones. Based on the idea that it is overburden information that is used to locate reflectors, it seems that Eq. 4 might be more reasonable than Eq. 1, just like Eq. 2 compared to Eq. 3.

3 Accuracy of the closed forms

Although neither of the two closed forms has the full imaging capability of the imaging subseries, in many cases they provide very promising results. For example, in Figures 3 and 4, for a relatively small contrast model, both the LOIS and HOIS result is very satisfactory (Liu, 2006). While in Figures 5-6, for a large contrast model, HOIS gives much better result compared to LOIS (Liu, 2006).

One might still want to know how well HOIS can locate the interface? In the following, through a simple analytic example, we would demonstrate analytically that the HOIS can correctly locate the first interface below water bottom.

In Figure 7, the depth of the water bottom is z_a and the interface below the water bottom is at z_b. The velocities are c_0 and c_1 for medium at $z<z_a$ and $z_a<z<z_b$ respectively. Using the reference medium velocity c_0, the interface z_a will be located correctly in α_1 since the reference medium is the correct velocity. But the interface at z_b will be located at $z_b'=z_a+\frac{c_0}{c_1}(z_b-z_a)$ which will be shallower than the correct depth. The objective of the imaging subseries is to shift the interface at z_b' to its correct location z_b. It would be interesting to evaluate the performance of the HOIS. According to Eq. 2, the interface at z_b' in α_1 will be shifted to a deeper depth (in this case) by the amount of

$$\delta z \;=\; \frac{1}{2}\int_0^{z_b'} \frac{\alpha_1(z'')}{1-\frac{1}{4}\alpha_1(z'')}dz''$$

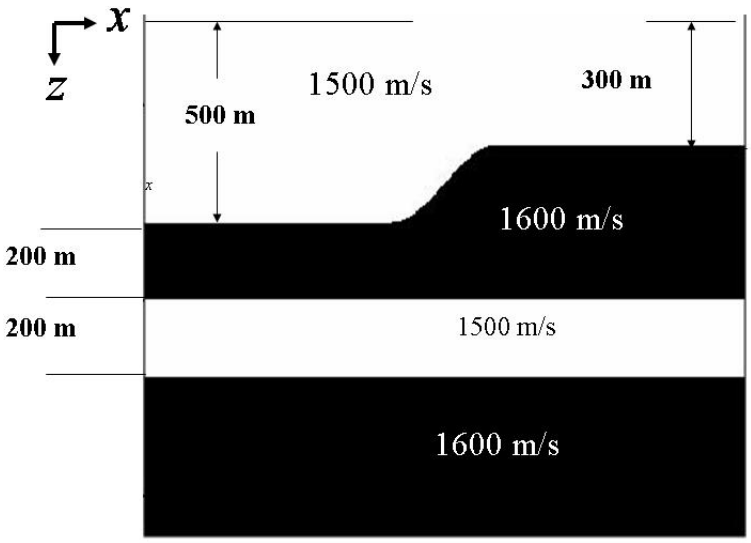

Figure 3: Small constrast model.

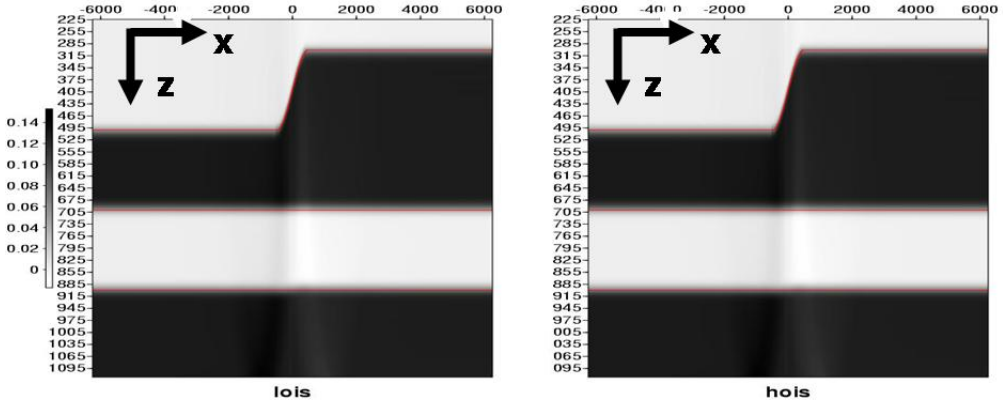

Figure 4: Satisfactory results.

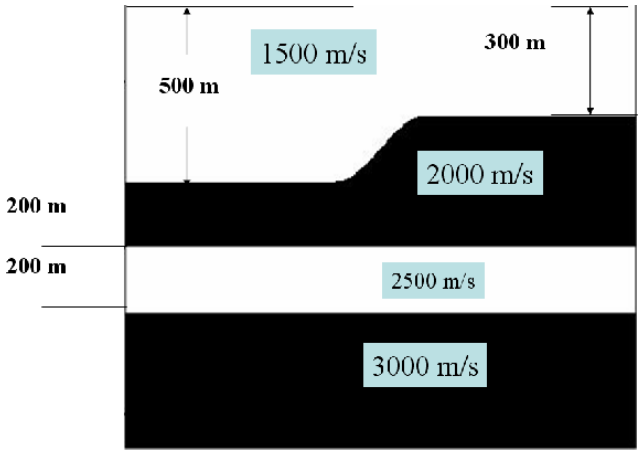

Figure 5: Large constrast model.

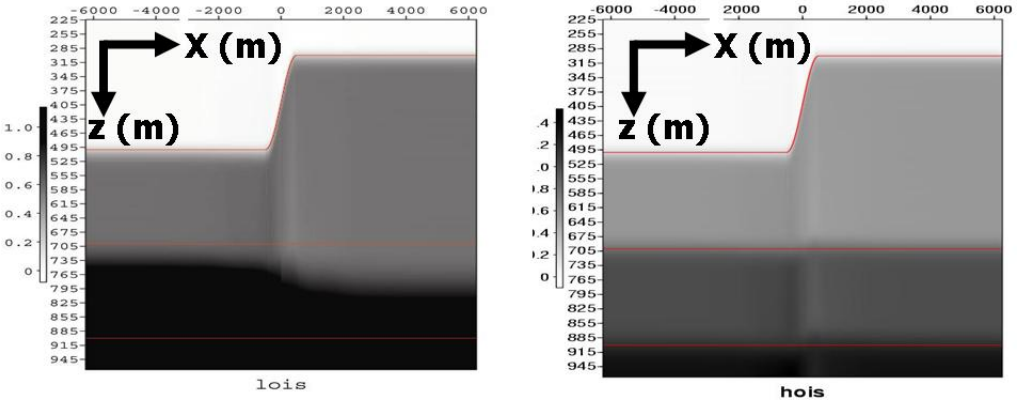

Figure 6: HOIS generates superior results.

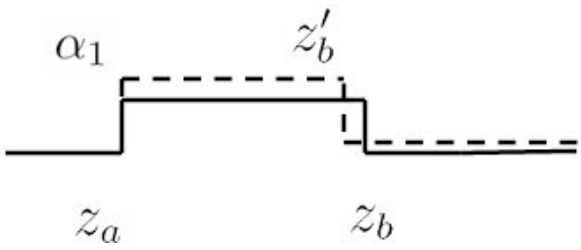

Figure 7: 1D normal incidence α and α_1.

$$\begin{aligned} &= (z_b' - z_a)\frac{2R}{1-R} \\ &= z_b - z_b', \end{aligned} \tag{5}$$

where $\alpha_1 = 4RH(z - z_a)$ and $R = \frac{c_1 - c_0}{c_1 + c_0}$ (Shaw et al., 2003). So, the correct amount of shifting has been performed by the HOIS for the first interface below the water bottom. Deeper interfaces in general will not be shifted accurately to the correct place by the HOIS.

4 Discussion

From the above analysis and previous numerical tests, there is no doubt that Eq.4 and Eq.2 provide similar or better results compared to Eq.1 and Eq.3. However, Eq.4 and Eq.2 are obtained using physical intuition at the end of derivation, while the straightforward application of the idea of isolated imaging subseries seems to produce Eq.1 and Eq.3. The intuitive leap is certainly beneficiary by providing better results. However, is it always necessary when the whole imaging subseries is pursued? Our current best understanding regarding this issue is that the ISS or the isolated imaging subseries promises that (in principle) the final imaging result will be correct, without guaranteeing that any part of the imaging subseries will be necessarily comprehensible to us in terms of the overall progress. Eq.1 and Eq.3 might not seem quite reasonable at the moment, but it is possible that it will eventually become comprehensible by adding more terms.

This is not the first time that terms within an isolated task specific subseries produce seemingly momentarily incomprehensible results. It happens when it is applied to remove free surface multiples. The free surface multiple removal (FSMR) algorithm derived from inverse scattering series removes the free surface multiples order by order. The second term when added to data will eliminate all of the first order free surface multiples, while at the same time, altering the amplitude of higher order multiples. And most importantly, it in general will boost the amplitude of higher order multiples, which seems strange and unreasonable, since the series is designed to eliminate multiples. But when further free surface removal terms are included, that original alteration (which sometimes has increased amplitude) of higher order multiples is necessary and deliberate to allow the next term in the FSMR series to remove them. Although this point has been explained previously (Carvalho,

1992; Weglein et al., 1997; Zhang and Weglein, 2005), in the following, we would like to illustrate it using simple diagrams without involving math.

In Figure 8a, the data contain primary and many different orders of free surface multiple. The first term in the ISS free surface multiple removal algorithm is the data set convolved with itself (Figure 8b). After adding Figure 8b to Figure 8a, we find that the first order free surface multiple has been eliminated (Figure 8c). However, instead of being removed or attenuated, the amplitude of the third order free surface multiple has been amplified. But if we keep on going, it will eventually be eliminated. For example, Figure 8d is the second term in the free surface multiple removal series. Adding it to Figure 8c produces Figure 8e, which eliminates the second order free surface multiple. The third order free surface multiple has at the same time been brought down to a smaller amplitude, ready to be removed by the third term. Note in the above demonstration, adaptive subtraction, which is impossible to avoid in real data, has not been mentioned. The burden of adaptive subtraction, however, can be lower if we use deghosted data and perform the convolution carefully by including factors such as obliquity factor, source wavelet and source and receiver depth.

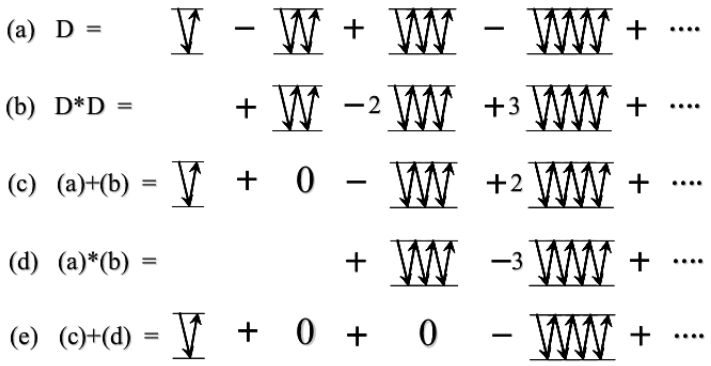

Figure 8: Demonstration of free surface multiple removal.

5 Conclusions

The difference and accuracy between different forms of imaging closed forms have been analyzed. None of the closed forms has captured the whole imaging subseries. This paper explains how

the implicit form of the HOIS closed form is comprehensible and reasonable. That HOIS closed form was deduced based on some intuitive sense of how capability beyond leading order imaging would appear in a closed form. Among points we are interested in communicating here are: (1) sometimes partial capture seems incomprehensible in isolation, but can become comprehensible when a broaden context, capture and goal is considered; and (2) real progress beyond current imaging capture will require staying close to the higher order imaging diagrams so it would be better to define what has been and what has not been accommodated within imaging algorithms.

6 Acknowledgements

We wish to thank Simon Shaw (ConocoPhillips) for his helpful discussions. The support of M-OSRP sponsors is greatly appreciated. This work has been partially funded by NSF-CMG award DMS-0327778 and DOE Basic Sciences award DE-FG02-05ER15697. Jingfeng Zhang appreciates support as the 2006-2007 ConocoPhillips fellow. Fang Liu appreciates support as the 2006-2007 GXT fellowship.

References

Carvalho, P. M. *Free-surface multiple reflection elimination method based on nonlinear inversion of seismic data*. PhD thesis, Universidade Federal da Bahia, 1992.

Innanen, K. A. "Reflector location using high-order inverse scattering series terms." *M-OSRP Annual Report* 4 (2005): 264–270.

Innanen, K. A. and A. B. Weglein. "Simultaneous Imaging and Inversion with the Inverse Scattering Series." *Proceedings of the Eighth International Congress of the SBGf and Fifth Latin American Geophysical Conference*. . SBGf, 2003.

Liu, F., A.B. Weglein, K.A. Innanen, and B.G Nita. "Extension of the non-linear depth imaging capability of the inverse scattering series to multidimensional media: strategies and numerical results." *SBGf (Sociedade Brasileira de Geofísica) Expanded Abstracts*. . SBGf, 2005.

Liu, Fang. *Multi-dimensional depth imaging without an adequate velocity model*. PhD thesis, University of Houston, 2006.

Liu, Fang, Arthur B. Weglein, Kristopher A. Innanen, and Bogdan G. Nita. "Multi-dimensional seismic imaging using the inverse scattering series." *76th Annual Internat. Mtg., Soc. Expl. Geophys., Expanded Abstracts*. . Soc. Expl. Geophys., 2006. 937–940.

Shaw, S. A. *An inverse scattering series algorithm for depth imaging of reflection data from a layered acoustic medium with an unknown velocity model*. PhD thesis, University of Houston, 2005.

Shaw, S. A., A. B. Weglein, D. J. Foster, K. H. Matson, and R. G. Keys. "Convergence properties of a leading order depth imaging series." *73rd Annual Internat. Mtg., Soc. Expl. Geophys., Expanded Abstracts*. . Soc. Expl. Geophys., 2003. 937–940.

Shaw, Simon A., A. B. Weglein, K. H. Matson, and D. J. Foster. "Cooperation of the leading order terms in an inverse-scattering subseries for imaging: 1-D analysis and evaluation.." *SEG Technical Program Expanded Abstracts* (2002): 2277–2280.

Weglein, A. B., F. V. Araújo, P. M. Carvalho, R. H. Stolt, K. H. Matson, R. T. Coates, D. Corrigan, D. J. Foster, S. A. Shaw, and H. Zhang. "Inverse Scattering Series and Seismic Exploration." *Inverse Problems* (2003): R27–R83.

Weglein, A. B., D. J. Foster, K. H. Matson, S. A. Shaw, P. M. Carvalho, and D. Corrigan. "An inverse-scattering sub-series for predicting the spatial location of reflectors without the precise reference medium and wave velocity." *71st Annual Internat. Mtg., Soc. Expl. Geophys., Expanded Abstracts*. . Soc. Expl. Geophys., 2001. 2108–2111.

Weglein, A. B., F. A. Gasparotto, P. M. Carvalho, and R. H. Stolt. "An Inverse-Scattering Series Method for Attenuating Multiples in Seismic Reflection Data." *Geophysics* 62 (November-December 1997): 1975–1989.

Weglein, A. B., K. H. Matson, D. J. Foster, P. M. Carvalho, D. Corrigan, and S. A. Shaw. "Imaging and inversion at depth without a velocity model: Theory, concepts and initial evaluation." *70th Annual Internat. Mtg., Soc. Expl. Geophys., Expanded Abstracts*. . Soc. Expl. Geophys., 2000. 1016–1019.

Zhang, J. and A. B. Weglein. "Extinction theorem deghosting method using towed streamer pressure data: Analysis of the receiver array effect on deghosting and subsequent free surface multiple removal." *75th Annual Internat. Mtg., Soc. Expl. Geophys., Expanded Abstracts*. . Soc. Expl. Geophys., 2005. 2095–2100.

Direct horizontal common image gathers without the velocity or "ironing"

F. Liu, A. B. Weglein, K. A. Innanen, B. G. Nita, and J. Zhang

Abstract

Traditional migration requires an accurate velocity to find an adequate image. There are circumstances where directly producing the velocity is difficult to realize and an indirect measurement of an adequate image is sought as a way to find the velocity. A necessary condition that a correctly located image would satisfy (with the correct velocity) is that images from different subsets of the data produce the image at the same depth. That is called a flat (i.e., horizontal) common-image gather. In AVO (Amplitude Variation with Offset) analysis, the amplitudes of reflected waves with different incident angles are studied to deduce lithology information beyond the structure map obtained by seismic imaging algorithms. The quantitative analysis of the amplitude, relies on common-image gathers being flat (or equivalently, at the same depth). But the waves with different incident angles will have different apparent velocities, resulting in different depths for the same image point at different angles, or non-flat common image gathers. In many scenarios, non-flat common-image gather are flattened by trim means at the cost of compromising zero-crossing and polarity-reversal information. This work presents an automatic solution based on the seismic imaging subseries of the inverse scattering series (ISS) that flattens the common image gather without knowing or determining the subsurface velocity, and without any harmful amplitude consequences.

This work illustrates that the higher-order imaging algorithm automatically produces as a simple and reasonable by product the horizontal common-image gather. Every image for different fixed angle θ-value produces its image at the same depth.

1 Introduction

Inverse scattering series (ISS) is a comprehensive theory for processing primaries and multiples without the traditional need for a subsurface velocity. Several task-specific subseries of ISS (Weglein et al., 2003) have been identified. These subseries correspond to classical objectives of seismic data processing: (1) eliminating free-surface multiple (Carvalho et al., 1991; Carvalho, 1992), (2) eliminating the internal multiples (Weglein et al., 1997; Araújo, 1994; Matson, 1997; Ramírez and Weglein, 2005), (3) imaging reflectors at depth (Weglein et al., 2000, 2002; Shaw et al., 2003; Innanen et al., 2004; Shaw, 2005; Liu, 2006), (4) determining the parameter changes across the reflectors (Zhang and Weglein, 2003, 2004; Zhang, 2006). This article is specific to task (3): the image of the same reflector in the same lateral coordinate, flattened and migrated to the same (actual) depth without knowing or determining the subsurface reflector or its overburden.

2 Description of the problem

For simplicity, consider an exploration problem in 2D where z_s (the elevation of the source) and z_g (the elevation of the receiver) are fixed. In this case, the seismic data is considered a function of three variables: x_s (the horizontal coordinate of the source), x_g (the horizaontal coordinate of the receivers), and t (time).

Physical properties at points in the subsurface, including reflector location in space, are not in any way dependent on the surface reflection data, or any subset of the data, used to determine or estimate those properties. That criteria is used in current leading-edge imaging as a necessary condition that an imaging algorithm with a correct velocity would satisfy. For example, images from different offset components of the data ought to locate at the same point in space if the velocity is correct. That concept is simple but in practice often not easy to realize. Methods to force or "iron" the common-image gather data flat and horizontal can have very serious and harmful consequences on subsequent analysis with lost polarity reversals and difficulty identifying class I and class II AVO anomalies.

In this paper we demonstrate that the higher-order velocity-independent imaging subseries automatically produces the flat common-image gather, as you would expect from an imaging algorithm that produces the image at the correct depth. Not only is there no velocity, but the flatness is achieved without damaging the offset dependent amplitude information in the imaged data.

This phenomenon can be illustrated by the two experiments shown in Figure 1.

Although Experiment 1 and Experiment 2 correspond to the same earth, their incident wavefields are different, and consequently the input data and seismic imaging results will be different, as illustrated in Figure 2.

The phenomena described above will compromise the AVO analysis, where the reflection event from the same reflection point should be flat. Flattened events are very desirable for quantitative estimation of the reflection strength. This phenomena had already been studied in Shaw (2005) for earth even without lateral variation and dealt with by using the leading order imaging subseries.

3 Theory

For a constant-density acoustic model, the mathematical description of the 2D wave-propagation is,

$$\left(\frac{\partial^2}{\partial x^2}+\frac{\partial^2}{\partial z^2}+\frac{\omega^2}{c^2(x,z)}\right)G(x,z,x_s,z_s,\omega)=\delta(x-x_s)\delta(z-z_s), \tag{1}$$

where ω is the temporary frequency (the Fourier conjugate of time t), $G(x,z,x_s,z_s,\omega)$ is the wavefield, the function $c(x,z)$ is the velocity field.

Equation (1) can be systematically solved by the inverse scattering series (Weglein et al., 2003) with the help of a wave parapagation in a much simpler reference velocity c_0,

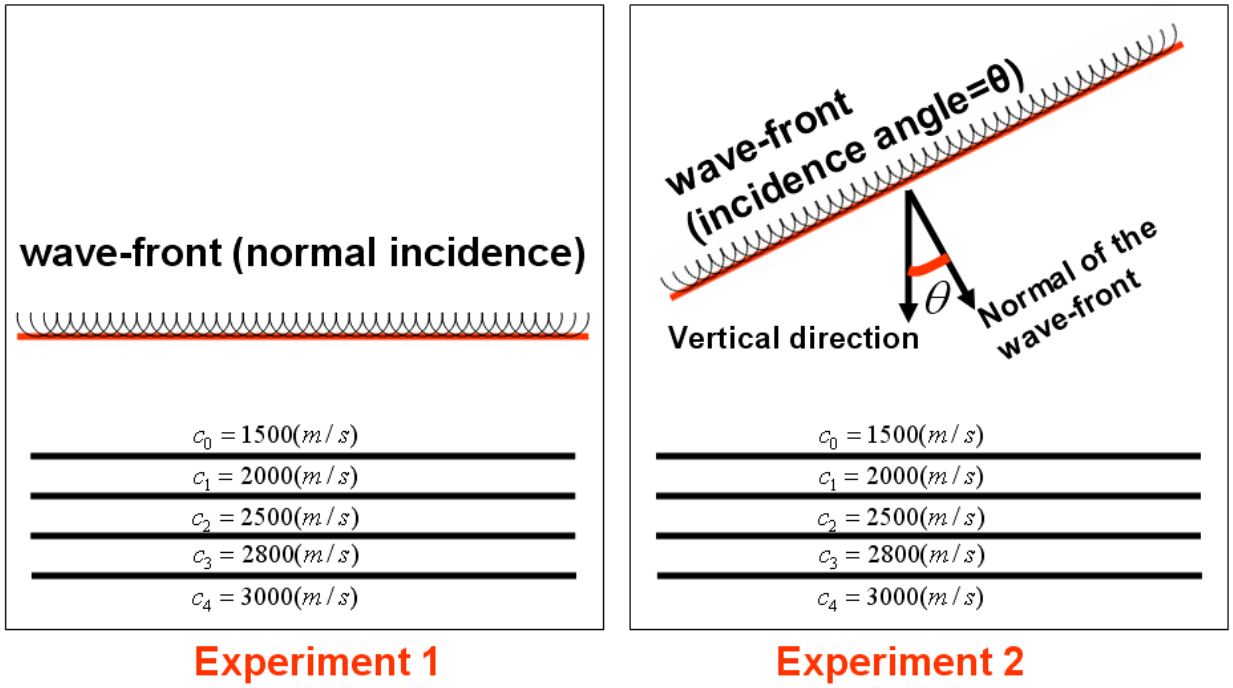

Figure 1: *In Experiment 1 (left panel), a normal incident plane wave is used to study an earth without lateral variation. In Experiment 2 (right panel), a plane wave with non-zero incident angle θ is used to study the same earth as in Experiment 1.*

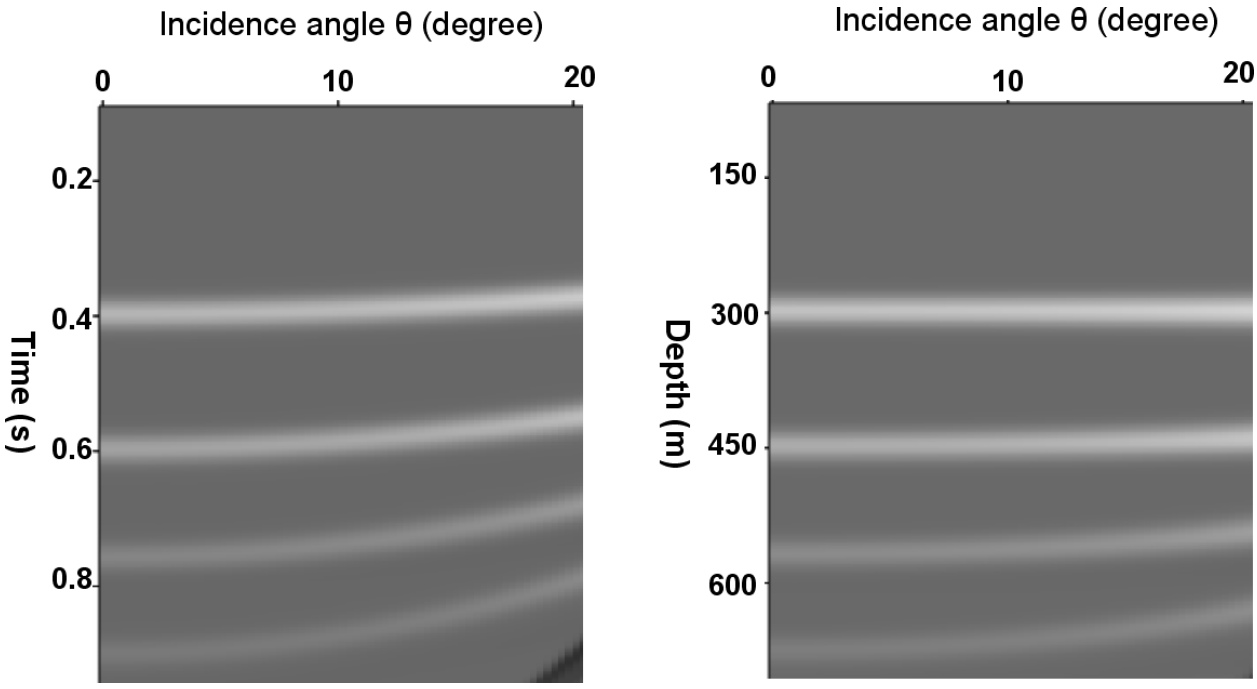

Figure 2: The left panel is the input data with different angles. The right panel is the corresponding common image gather (FK migration with homogeneous water velocity $c_0 = 1500m/s$) for different incident angles. It is obvious that no event in the input data is flat. In the common image gather, the first reflector (water bottom) is flattened, but the reflectors below are still curved.

$$\left(\frac{\partial^2}{\partial x^2}+\frac{\partial^2}{\partial z^2}+\frac{\omega^2}{c_0^2}\right)G_0(x,z,x_s,z_s\omega)=\delta(x-x_s)\delta(z-z_s), \tag{2}$$

where $G_0(x,z,x_s,z_s\omega)$ is the reference wave-field.

In the inverse series, equation (1) is computed in an order-by-order fashion via the inverse scattering series (equation (11)$\sim$(13) of Weglein et al. (2003)) as,

$$G_0k^2\alpha_1G_0=D=G-G_0, \tag{3}$$

$$G_0k^2\alpha_2G_0=-G_0k^2\alpha_1G_0k^2\alpha_1G_0, \tag{4}$$

$$\begin{aligned}G_0k^2\alpha_3G_0=&-G_0k^2\alpha_1G_0k^2\alpha_2G_0-G_0k^2\alpha_2G_0k^2\alpha_1G_0\\&-G_0k^2\alpha_1G_0k^2\alpha_1G_0k^2\alpha_1G_0,\end{aligned} \tag{5}$$

where $k=\omega/c_0$; D in equation (3) is the input data for the inverse scattering series and is the difference between the actual wavefield G and the reference wavefield G_0; α_1, α_2, $\cdots$ are iteratively computed and can be used to construct $\alpha=\alpha_1+\alpha_2+\alpha_3+\cdots$, which is related to the subsurface geology via $\alpha=1-c_0^2/c^2(x,z)$. Equation (3) can be solved via Fourier transform. Following the notation in Clayton and Stolt (1981), we use k_z, k_g, k_s, k_m and k_h to denote the Fourier conjugate of z, x_g, x_s, $x_m=0.5(x_g+x_s)$ and $x_h=x_g-x_s$ respectively. In the examples in this article, the reference velocity (the velocity actually used in migration) c_0 is chosen as whole-space constant water velocity. The detailed derivation of the equations in this article can be found in Liu (2006) and the final solution is summarized below.

4 The solution of the first term α_1

The data is chosen according to the following relation,

$$k_h=k_g+k_s=2\tfrac{\omega}{c_0}\sin(\theta)\qquad\qquad k_g-k_s=k_m\ . \tag{6}$$

where the constant θ is the incident angle of synthesized plane wave by Radon transform defined in the CMP (common-mid point) gather (see equation (9)). With equation (6) as constraint, the temporary frequency ω can be expressed as a function of k_m and k_z,

$$\omega=\frac{c_0k_z}{2}\sqrt{\frac{k_z^2+k_m^2}{k_z^2\cos^2(\theta)-k_m^2\sin^2(\theta)}}. \tag{7}$$

With ω defined in equation (7), our generalized migration formulism can be expressed as,

$$\widetilde{\widetilde{\alpha}}_1(k_m, k_z) = -\frac{4q_g q_s}{\omega^2/c_0^2} \int_{-\infty}^{\infty} dx_m e^{-ik_m x_m} \int_{-\infty}^{\infty} d\tau e^{i\omega\tau} D^{\tau p}(x_m, \tau). \tag{8}$$

where the double tidle signs in the equation above are used to denote the fact that the expression had been Fourier transformed twice from its original form in the spatial domain (x, z) to frequency-wave number domain (k_m, k_z), and $D^{\tau p}$ is computed via Radon transform,

$$D^{\tau p}(x_m, \tau) = \int_{-\infty}^{\infty} dx_h D\left(x_m + \frac{x_h}{2}, x_m - \frac{x_h}{2}, \tau + x_h \frac{\sin(\theta)}{c_0}\right). \tag{9}$$

Equation (6) of Liu et al. (2006) can be considered as a special case of equation (8) where the angle θ is chosen as zero.

5 Higher order imaging subseries

The higher-order imaging subseries (HOIS) in equation (11) of Liu et al. (2006) is generalized for non-zero θ as,

$$\alpha_{HOIS}\left(x, z + \frac{1}{2}\int_0^z \frac{\alpha_1(x, z')dz'}{\cos^2\theta - 0.25\alpha_1(x, z')}\right) = \alpha_1(x, z) \tag{10}$$

Interested readers may refer to Liu (2006) for detailed derivation and discussion for equation (10).

6 Numerical examples

The synthetic data set (see examples in Figure 4) used in this article was generated upon a salt model shown in Figure 3.

The linear images (α_1) of the inverse scattering series with different angles are calculated via equation (8) and the imaging results for two typical angles are shown in Figure 5 and Figure 6.

In order to consistently use the migration result in Figure 5 and Figure 6 in AVO analysis, it is very desirable that they share the same depth. In order to study the performance of our algorithm in different geological conditions, we picked four locations (illustrated by the vertical green lines in Figure 5). It is clear that, in α_1 with water speed, only the images of the water-bottom share

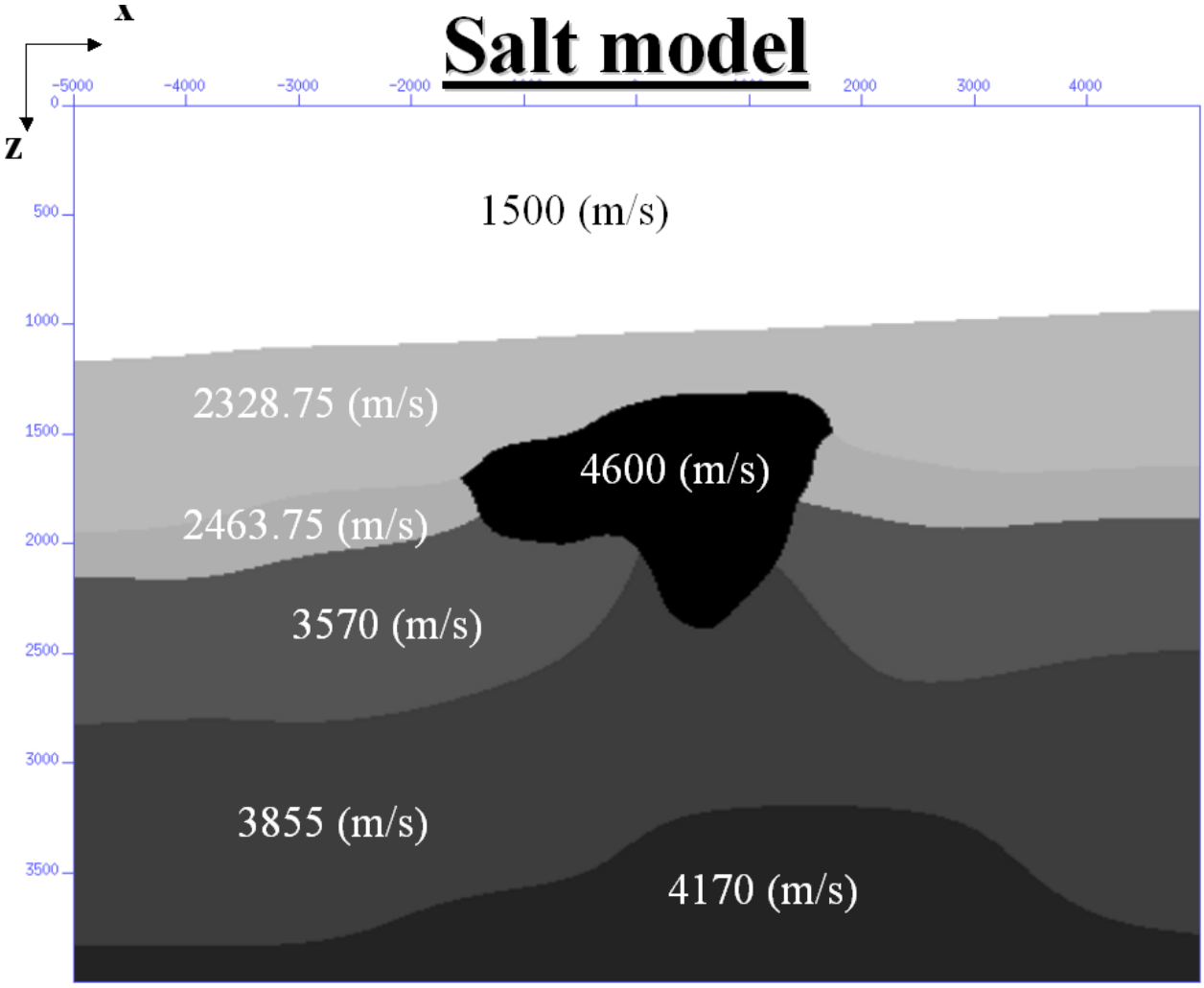

Figure 3: *A salt model designed by Peter Traynin from ExxonMobil.*

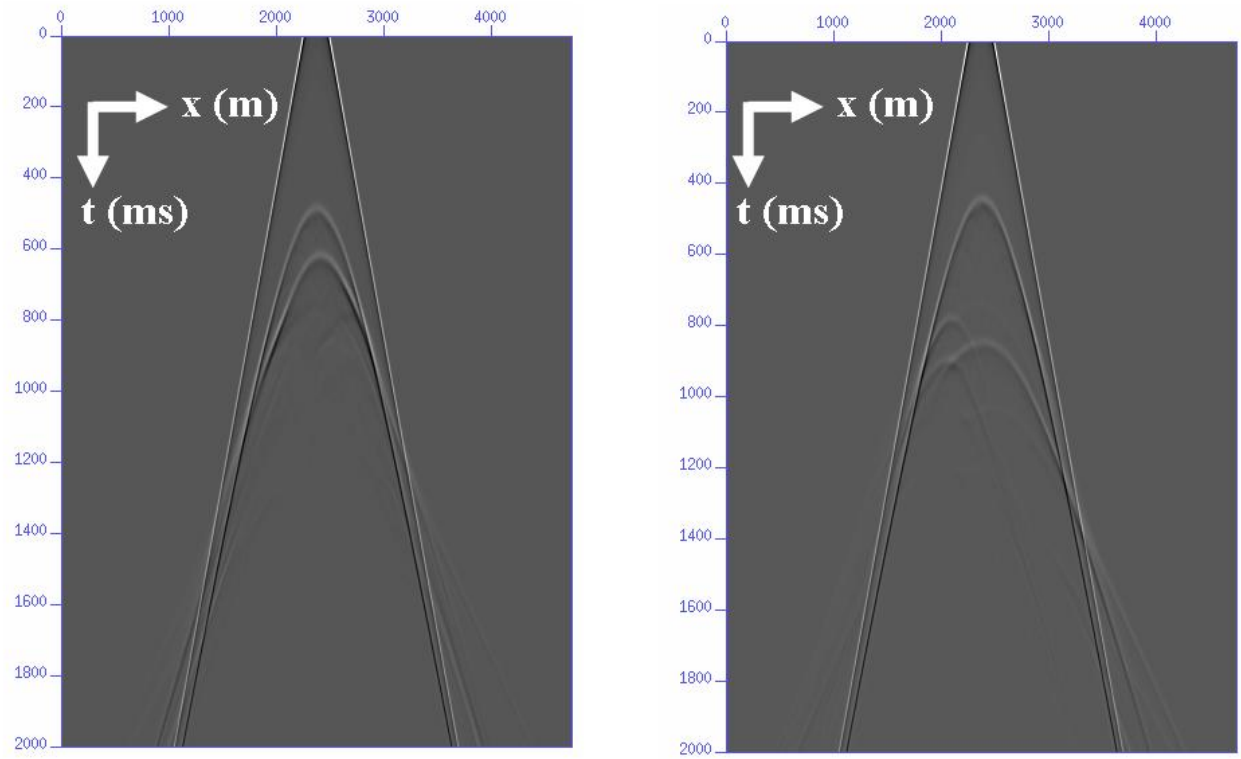

Figure 4: *Two typical shot gathers extracted from the data set generated from the salt model in Figure 3.*

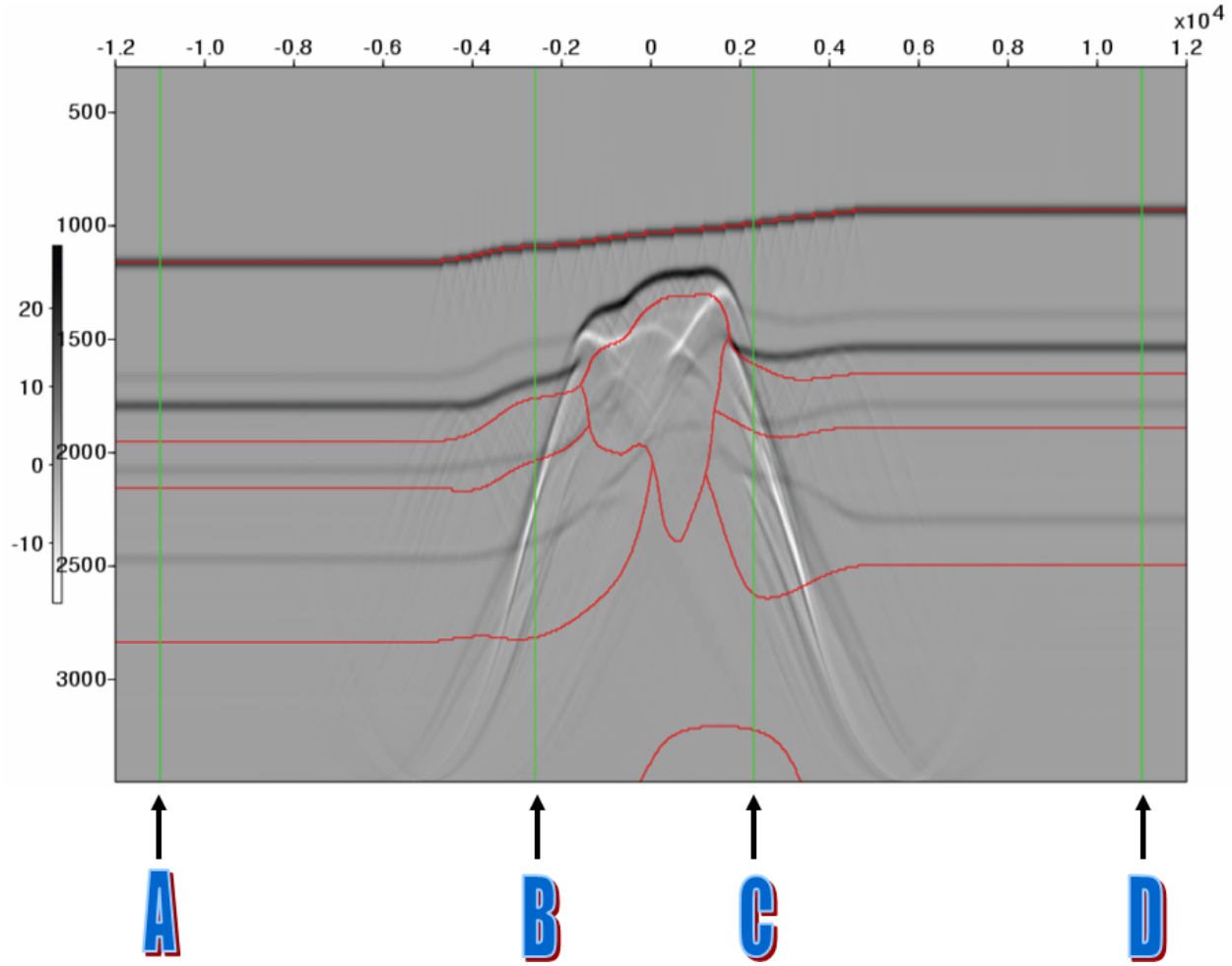

Figure 5: *The linear image α_1 (see equation (8)) with $\theta = 0°$. In this figure and Figure (6, 7, 8, 13), partial derivative over z operation $\partial/\partial z$ is taken before the display, and the red lines are bench-marks indicating the actual location of various reflectors. The vertical green lines indicate four location in the x-coordinate where the common-image gather is extracted and studied in detail. Those four loctions are denoted as A, B, C, and D, respectively, as indicated by the symbols below each location.*

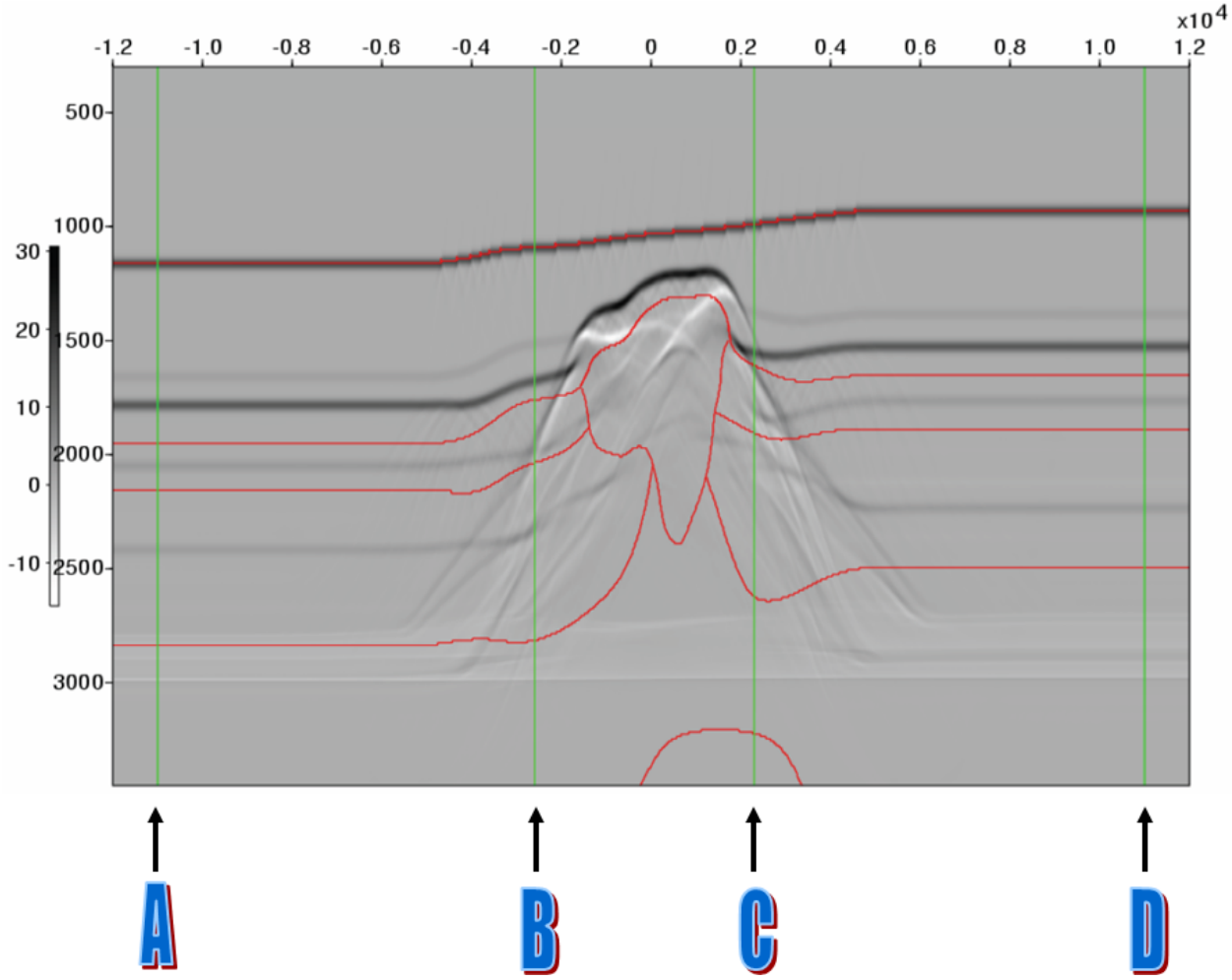

Figure 6: *The linear image α_1 (see equation (8)) with $\theta = 9°$. Due to the truncation artifacts (below 2500m) caused by unavailability of the data, $\theta = 9°$ is the maximal angle we studied in this article.*

the same depth, as indicated by the flat water-bottom in the common-image gather in Figure 9(a), 10(a), 11(a), 12(a). The images of the reflectors below the water-bottom are not flat, as indicated by the bumpy refletors in Figure 9(a), 10(a), 11(a), 12(a). Since the angles we studied in this example are very small (between 0° and 9°), the curvature of the non-flat events is not easily visible. For display purpose, we duplicate each imaging result for an angle 100 times. We then introduce 100 copies of imaging result for another angle θ, etc, $\cdots$. Since the imaging result for a specific angle is duplicated 100 times, this 100 identical traces will produce a smooth-looking background. In this manner, even the small changes between the imaging results of adjacent angles can be easily seen against the smooth background produced by trace duplication.

After the application of the higher-order imaging subseries, all the reflection events become horizontal, see Figure 9(c), 10(c), 11(c), 12(c). There is clearly lots of useful information in the common image gathers, either in α_1, or in the higher-order imaging subseries: the reflection events are much more coherent than the un-collapsed diffraction energy; the diffraction energy looks more diffusive than in the original (x, z)-domain; the difference between the diffraction events and reflection events become more obvious.

Since after applying the higher-order imaging subseries, all the reflection events are imaged to the same location, where the diffraction events are further dispersed into different locations, as indicated by Figure 9, 10, 11, 12, it is reasonable to sum all the higher-order images together to have an improved image with better signal/noise ratio, as displayed in Figure 13.

7 Conclusions

In this paper, the efficacy of the higher order imaging subseries is further demonstrated by automatically and accurately producing common-image gathers, without the velocity, and with amplitude intact and ready for subsequent AVO analysis.

8 Acknowledgments

The authors would like to thank GX Technology for granting Fang 2006-2007 GXT fellowship, Peter Traynin from ExxonMobil for providing the salt model. We thank Simon Shaw and all M-OSRP members and sponsors. This work has been partially funded by NSF-CMG award DMS-0327778 and DOE Basic Science award DE-FG02-05ER15697.

References

Araújo, F. V. *Linear and non-linear methods derived from scattering theory: backscattered tomography and internal multiple attenuation.* PhD thesis, Universidade Federal da Bahia, 1994.

Carvalho, P. M. *Free-surface multiple reflection elimination method based on nonlinear inversion of seismic data.* PhD thesis, Universidade Federal da Bahia, 1992.

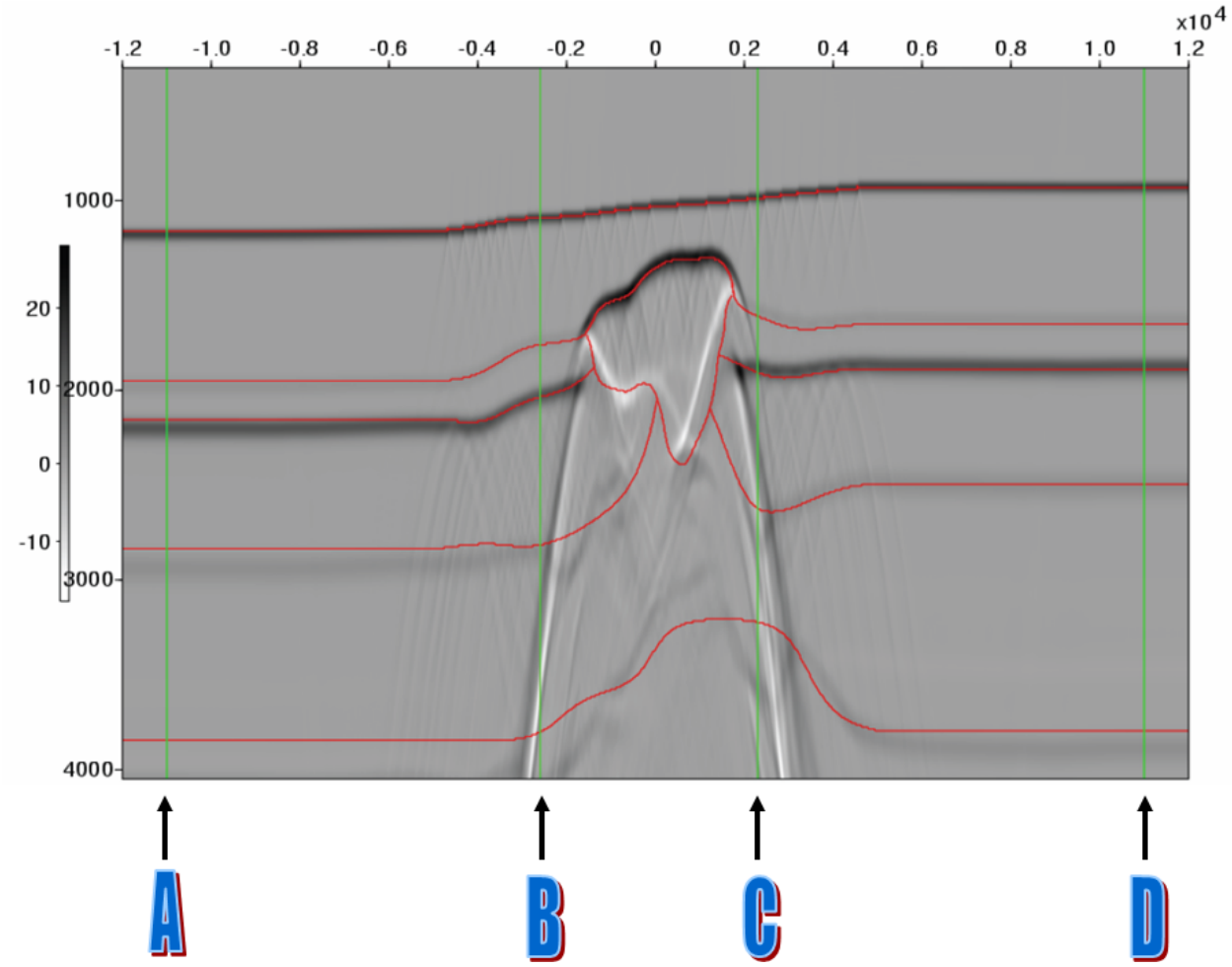

Figure 7: *The higher-order imaging subseries (see equation (10)) with* $\theta = 0°$.

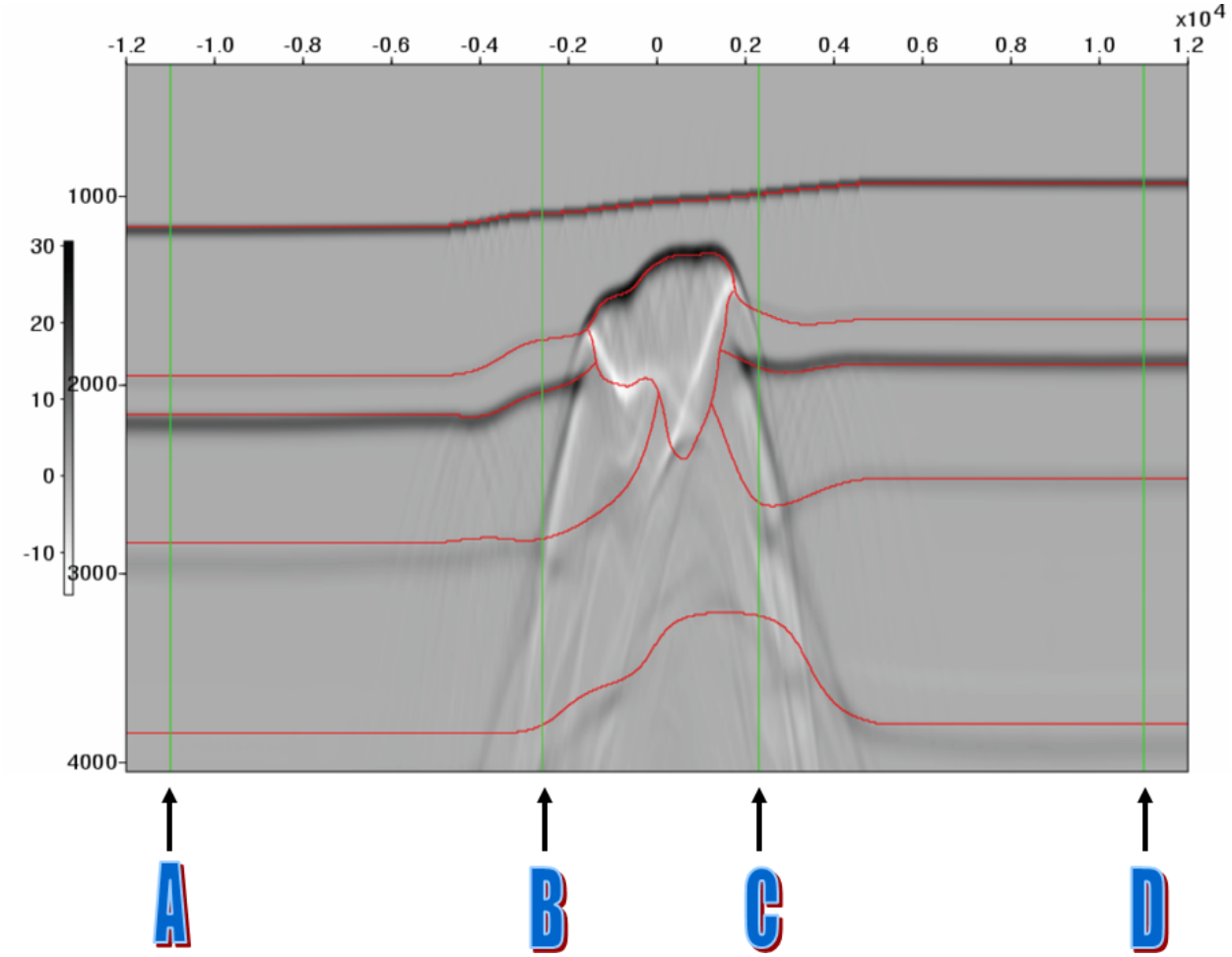

Figure 8: *The higher-order imaging subseries (see equation (10)) with* $\theta = 9°$.

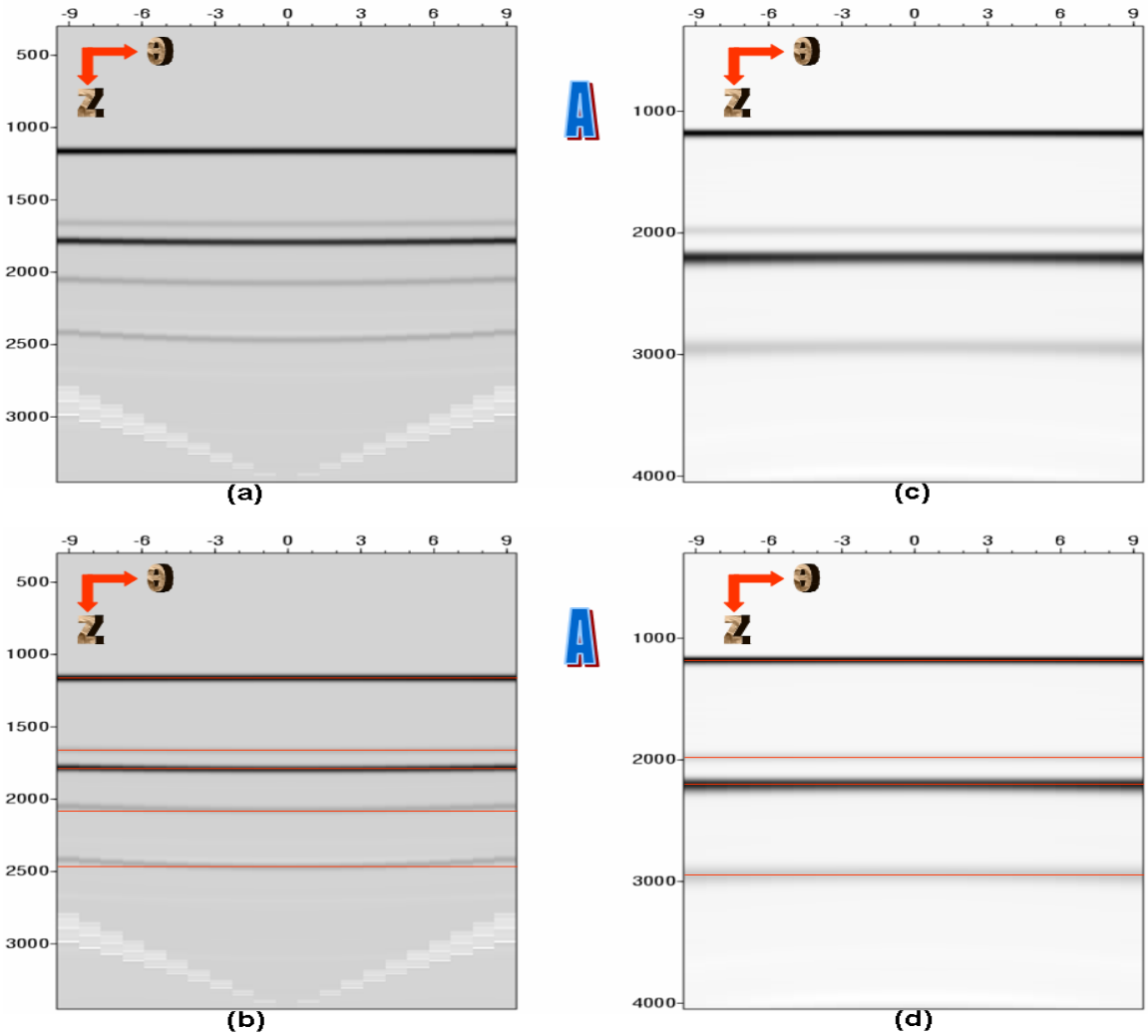

Figure 9: The common-image gather taken from location A in Figure 5, where $x = -11,000m$. There are only reflection events visible in this region since the lateral variation is very small. (a) is the common image gather taken from the linear image α_1, (b) is same as (a) except for the fact that horizontal red lines are drawn to bench-mark the flatness of the common-image gather. It is noticeable that the fourth reflector (around the fourth red-lines in (b)) is not flat, and it is obvious that the fifth (around the fifth red-lines in (b)) is not flat. (c) is the common image gather taken from the higher-order image series, (d) is same as (c) except for the fact that horizontal red lines are drawn to bench-mark the flatness of the common-image gather. It is obvious that all reflectors become flat.

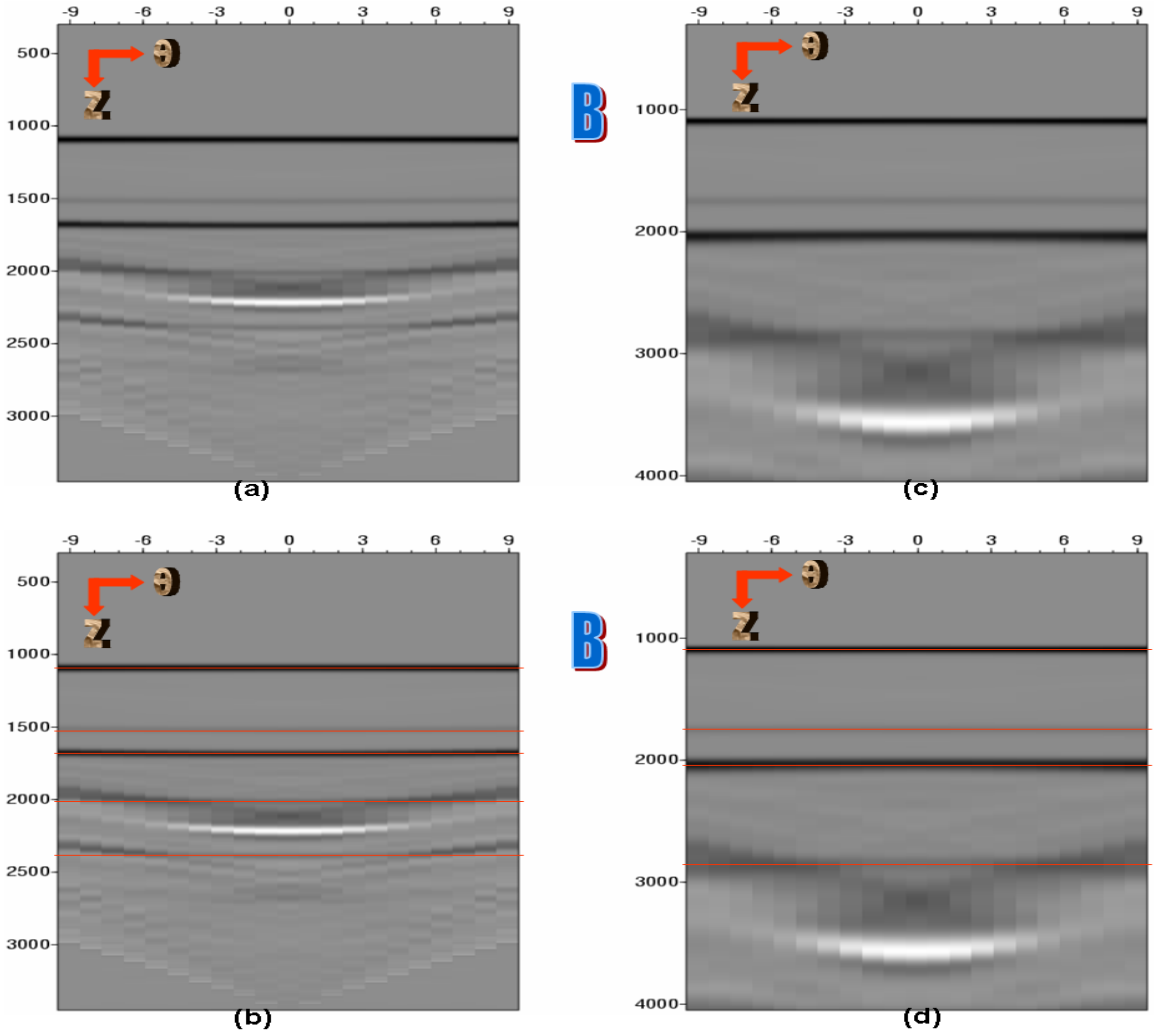

Figure 10: The common-image gather taken from location B in Figure 5, where $x = -2,600m$. There are reflection and diffraction events visible in this region since the lateral variation is big. (a) is the common image gather taken from the linear image α_1, (b) is same as (a) except for the fact that horizontal red lines are drawn to bench-mark the flatness of the common-image gather. Please notice that although the fourth and fifth reflectors (around the fourth and fifth red horizontal lines in (c)) are noticeably curved, they are much flatter and more coherent than the diffraction events. (c) is the common image gather taken from the higher-order image series, (d) is same as (c) except for the fact that horizontal red lines are drawn to bench-mark the flatness of the common-image gather. It is obvious that all reflectors become flat, although the fourth reflector is noisy due to un-clasped diffractions.

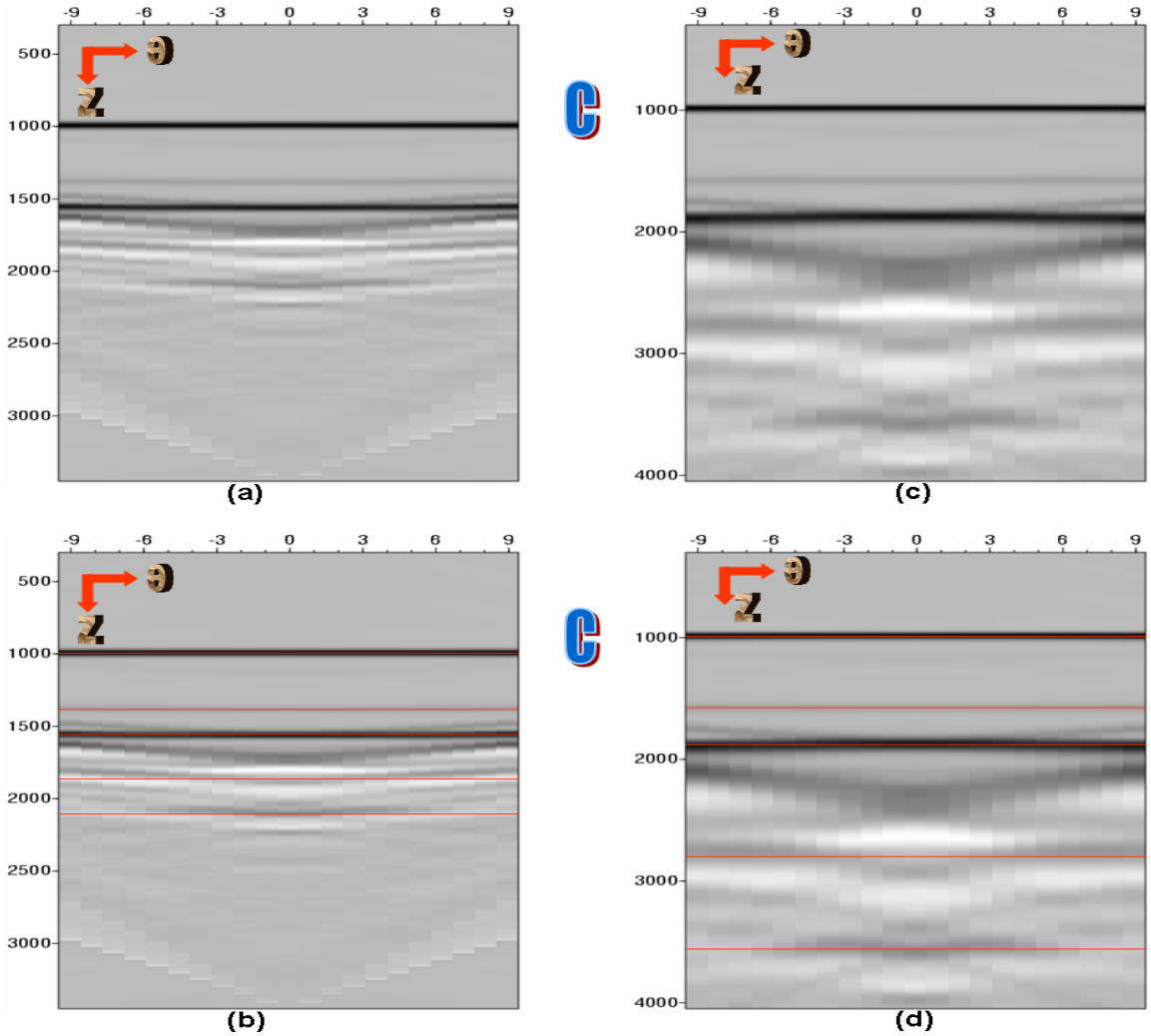

Figure 11: The common-image gather taken from location C in Figure 5, where $x = 2,300m$. There are reflection and diffraction events visible in this region since the lateral variation is big. (a) is the common image gather taken from the linear image α_1, (b) is same as (a) except for the fact that horizontal red lines are drawn to bench-mark the flatness of the common-image gather. Please notice that although the fourth and fifth reflectors (around the fourth and fifth red horizontal lines in (c)) are noticeably curved, they are much flatter and more coherent than the diffraction events. (c) is the common image gather taken from the higher-order image series, (d) is same as (c) except for the fact that horizontal red lines are drawn to bench-mark the flatness of the common-image gather. It is obvious that all reflectors become much flatter, although the fourth and fifth reflectors are noisy due to un-clasped diffractions.

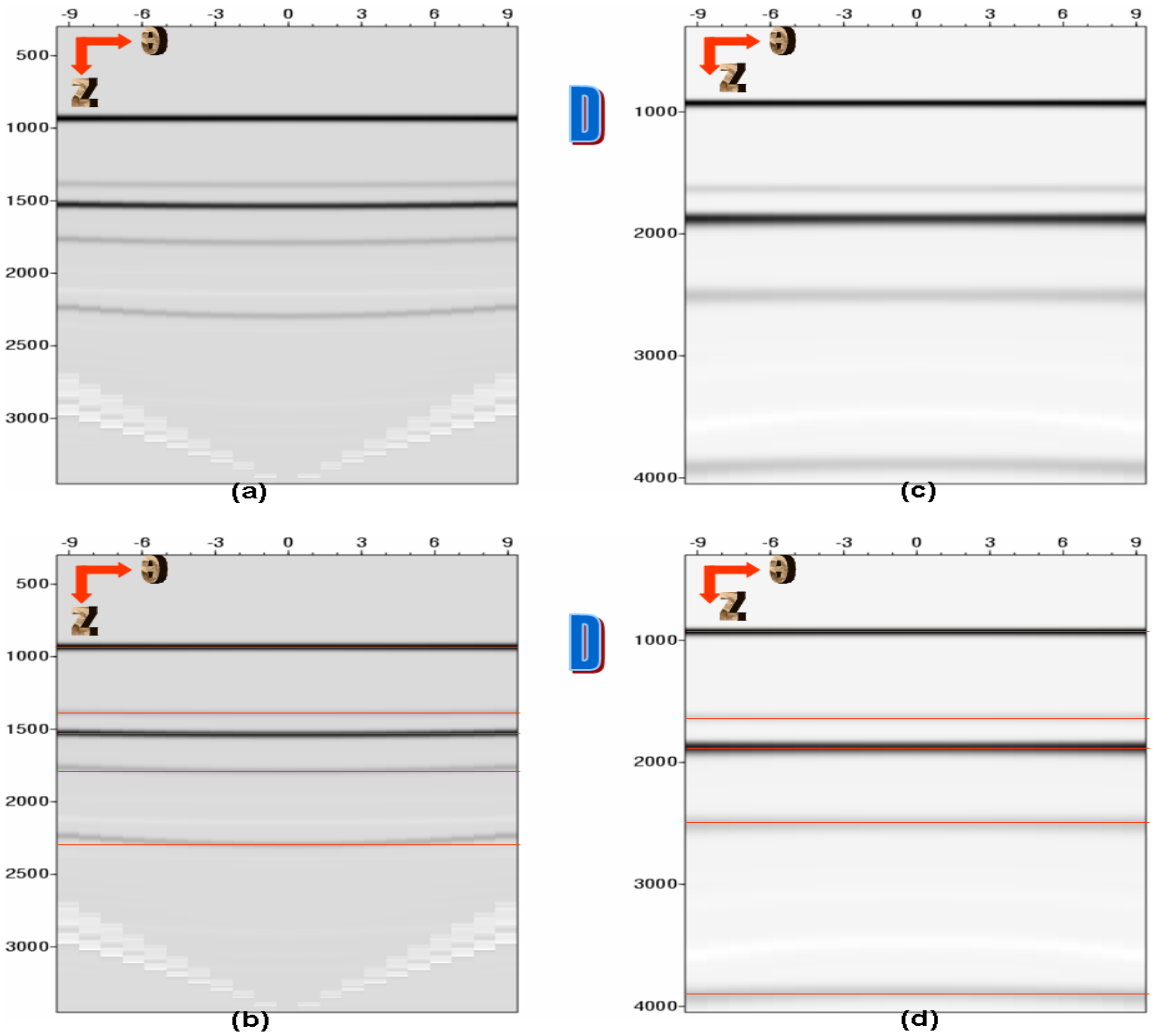

Figure 12: The common-image gather taken from location D in Figure 5, where $x = 11,000m$. There are only reflection events visible in this region since the lateral variation is very small. (a) is the common image gather taken from the linear image α_1, (b) is same as (a) except for the fact that horizontal red lines are drawn to bench-mark the flatness of the common-image gather. It is noticeable that the fourth reflector (around the fourth red-lines in (b)) is not flat, and it is obvious that the fifth (around the fifth red-lines in (b)) is not flat. (c) is the common image gather taken from the higher-order image series, (d) is same as (c) except for the fact that horizontal red lines are drawn to bench-mark the flatness of the common-image gather. It is obvious that all reflectors become flat.

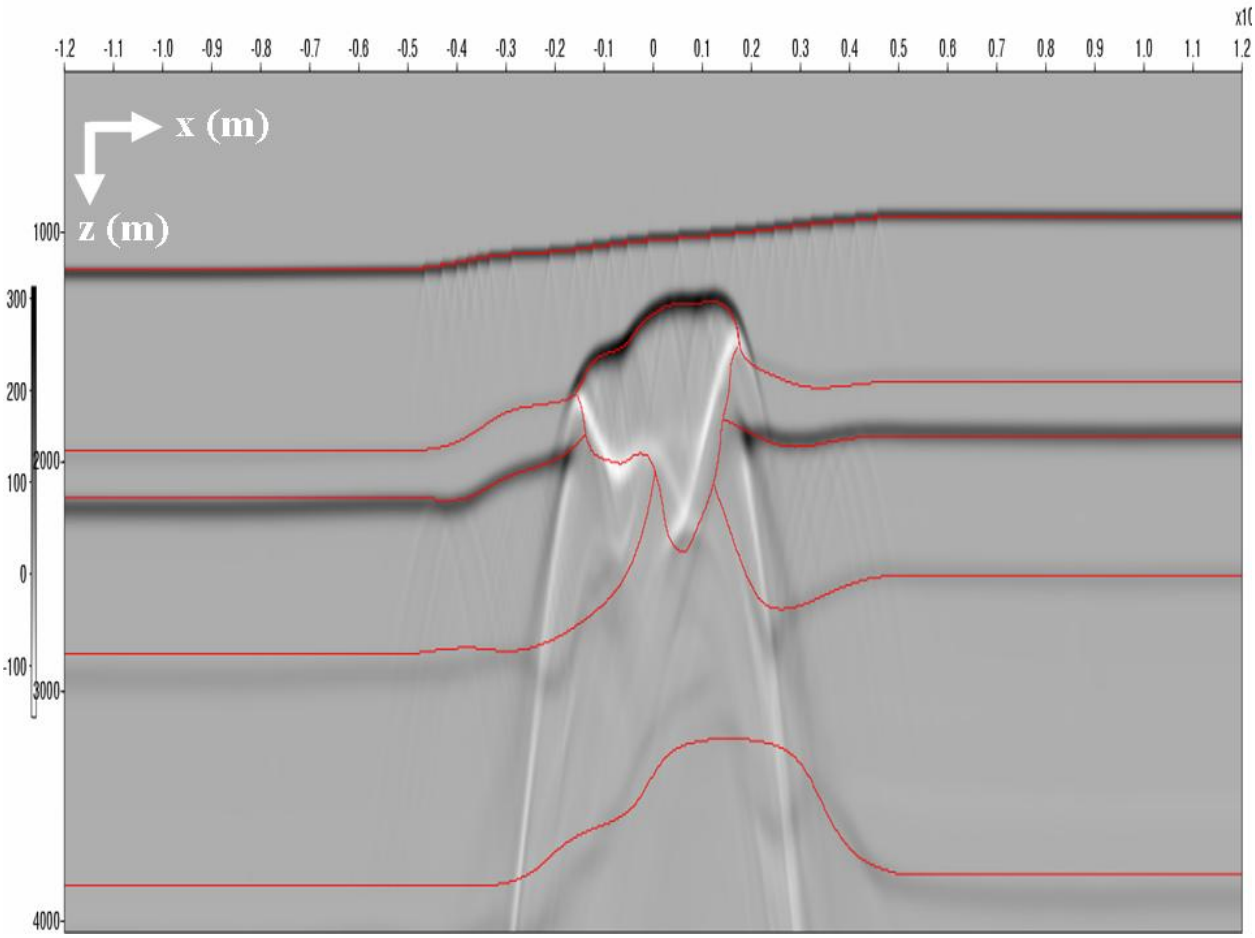

Figure 13: *The sum of all the higher-order images. Since the reflection events are migrated to the same depth by the higher-order imaging subseries, they sum to each other constructively. But the residual diffractions are not migrated to the same depth, and hence they sum to each other destructively and become much weaker compared to the imaging result for any single fixed angle θ.*

Carvalho, P. M., A. B. Weglein, and R. H. Stolt. "Examples of a nonlinear inversion method based on the T-matrix of scattering theory: Application to multiple suppression." *61st Ann. Internat. Mtg: Soc. of Expl. Geophys., Expanded Abstracts*. . Soc. Expl. Geophys., 1991. 1319–1322.

Clayton, R. W. and R. H. Stolt. "A Born-WKBJ inversion method for acoustic reflection data." *Geophysics* 46 (1981): 1559–1567.

Innanen, K. A., A. B. Weglein, and T. J. Ulrych. "Basic numerics in the non-linear inversion of primaries: simultaneous imaging and inversion II." *M-OSRP Annual Report* 3 (2004).

Liu, Fang. *Multi-dimensional depth imaging without an adequate velocity model*. PhD thesis, University of Houston, 2006.

Liu, Fang, Arthur B. Weglein, Kristopher A. Innanen, and Bogdan G. Nita. "Multi-dimensional seismic imaging using the inverse scattering series." *76th Annual Internat. Mtg., Soc. Expl. Geophys., Expanded Abstracts*. . Soc. Expl. Geophys., 2006. 937–940.

Matson, K. H. *An inverse-scattering series method for attenuating elastic multiples from multi-component land and ocean bottom seismic data*. PhD thesis, University of British Columbia, 1997.

Ramírez, A. C. and A.B. Weglein. "An inverse scattering internal multiple elimination method: Beyond attenuation, a new algorithm and initial tests." *SEG Expanded Abstracts.* (2005): 2115–2118.

Shaw, S. A., A. B. Weglein, D. J. Foster, K. H. Matson, and R. G. Keys. "Convergence properties of a leading order depth imaging series." *73rd Annual Internat. Mtg., Soc. Expl. Geophys., Expanded Abstracts*. . Soc. Expl. Geophys., 2003. 937–940.

Shaw, Simon. A. *An inverse scattering series algorithm for depth imaging of reflection data from a layered acoustic medium with an unknown velocity model*. PhD thesis, University of Houston, 2005.

Weglein, A. B., F. V. Araújo, P. M. Carvalho, R. H. Stolt, K. H. Matson, R. T. Coates, D. Corrigan, D. J. Foster, S. A. Shaw, and H. Zhang. "Inverse scattering series and seismic exploration." *Inverse Problems* 19 (2003): R27–R83.

Weglein, A. B., D. J. Foster, K. H. Matson, S. A. Shaw, P. M. Carvalho, and D. Corrigan. "Predicting the correct spatial location of reflectors without knowing or determining the precise medium and wave velocity: initial concept, algorithm and analytic and numerical example." *Journal of Seismic Exploration* 10 (2002): 367–382.

Weglein, A. B., F. A. Gasparotto, P. M. Carvalho, and R. H. Stolt. "An inverse-scattering series method for attenuating multiples in seismic reflection data." *Geophysics* 62 (1997): 1975–1989.

Weglein, A. B., K. H. Matson, D. J. Foster, P. M. Carvalho, D. Corrigan, and S. A. Shaw. "Imaging and inversion at depth without a velocity model: theory, concepts and initial evaluation." *70th Annual Internat. Mtg., Soc. Expl. Geophys., Expanded Abstracts*. . Soc. Expl. Geophys., 2000. 1016–1019.

Zhang, H. and A. B. Weglein. "Target identification using the inverse scattering series: inversion of large-contrast, variable velocity and density acoustic media." *M-OSRP Annual Report* 2 (2003).

Zhang, H. and A. B. Weglein. "Target identification using the inverse scattering series: data requirements for the direct inversion of large-contrast, inhomogeneous elastic media." *M-OSRP Annual Report* 3 (2004).

Zhang, Haiyan. *Direct non-linear acoustic and elastic inversion: towards fundamentally new comprehensive and realistic target identification.* PhD thesis, University of Houston, 2006.

The first term of the inverse scattering series: practical strategies and issues

F. Liu, A. B. Weglein, B. G. Nita, K. A. Innanen, J. Zhang

Abstract

The first step of the inverse scattering series is the calculation of α_1. The parameter α_1 can be seen as the perturbation in the Born approximation. The first-order approximation to the velocity perturbation, α_1, as well as similar first-order perturbation forms are extensively used in the following procedures: internal multiple removal algorithms (in the form of a model-type independent first-order perturbation form b_1), the leading-order imaging subseries, the simultaneous imaging and inversion subseries, and the higher-order imaging subseries. The best-effort calculation of α_1 is very critical for the subsequent implementations. This article summarizes our best efforts to achieve an α_1 with imperfect data acquisition. The discussion is based on 2D, but can be extended to 3D with very little modification.

1 Introduction

In the inverse scattering series (Weglein et al., 2003), the first term is the migration inversion (Clayton and Stolt, 1981) result based on the inaccurate velocity field c_0. The basic idea of the inverse scattering series is to construct the second term, the third term, etc., using this as input. Compared with the true earth, this starting point is generally dramatically different, due to the inaccurate reference velocity (or migration velocity) used in migration. This implies that, we have a long way to go to reach our inverse objectives. The purpose of this article is to describe the practical construction of the linear term.

There are several lessons from our experience: (1) implementation steps must honor the physics in the inverse scattering series; (2) argument based on ray theory should be used carefully. In this paper, we are going to describe the implementation of α_1 used to achieve the 2D velocity-independent acoustic imaging results shown in Liu (2006). The reason why we need an accurate and reliable calculation of α_1 from measured data is that α_1 is the input to further processing in the inverse scattering series. And α_1 as an input for processing data non-linearly requires amplitude and phase information to be treated appropriately.

2 Theory

For a constant-density acoustic model, the mathematical description of the wave-propagation problem is,

$$\left(\frac{\partial^2}{\partial x^2}+\frac{\partial^2}{\partial z^2}+\frac{\omega^2}{c^2(x,z)}\right)P(x,z,x_s,z_s,\omega)=\delta(x-x_s)\delta(z-z_s)A(\omega), \tag{1}$$

where ω is the temporal frequency (the Fourier conjugate of time t), $P(x, z, x_s, z_s, \omega)$ is the wave-field, $A(\omega)$ is the **source signature** (or **wavelet**) in the frequency domain, and the function $c(x, z)$ is the velocity field governing the wave propagation in the subsurface. If the wavelet is known and its effect had been compensated for, we can use $A(\omega) = 1$, and the corresponding wave-field is called the **Green's function** (or **impulse response**) in the medium $c(x, z)$,

$$\left(\frac{\partial^2}{\partial x^2} + \frac{\partial^2}{\partial z^2} + \frac{\omega^2}{c^2(x,z)}\right) G(x, z, x_s, z_s, \omega) = \delta(x - x_s)\delta(z - z_s). \tag{2}$$

The inverse scattering series (ISS) is a procedure to construct the medium property distribution $c(x, z)$ using an arbitrary reference velocity c_0 and its corresponding Green's function G_0,

$$\left(\frac{\partial^2}{\partial x^2} + \frac{\partial^2}{\partial z^2} + \frac{\omega^2}{c_0^2(x,z)}\right) G_0(x, z, x_s, z_s, \omega) = \delta(x - x_s)\delta(z - z_s). \tag{3}$$

Although in the ISS, the reference medium can be arbitrary, it is chosen to be homogeneous in the current imaging subseries. Hence $c_0(x, z) = c_0$. The major reason to choose the constant reference velocity is the availability of the analytic solution for its Green's function and exact analytic inverse for the corresponding integral equation.

The input data D (available only on the measurement surface) for the inverse scattering series is the difference between the Green's function in the actual and reference medium:

$$D(x_g, z_g, x_s, z_s, \omega) = G(x_g, z_g, x_s, z_s, \omega) - G_0(x_g, z_g, x_s, z_s, \omega) \tag{4}$$

The data in the inverse scattering series can also be considered as the recorded wave-field G with the direct arrival G_0 removed.

With the data defined in equation (4), the first term of the inverse series can be computed as,

$$D(x_g, z_g, x_s, z_s, \omega) = \int_{-\infty}^{\infty} dz' \int_{-\infty}^{\infty} dx' G_0(x_g, z_g, x', z', \omega) V_1(x', z') G_0(x', z', x_s, z_s, \omega), \tag{5}$$

where

$$V_1(x, z) = \frac{\omega^2}{c_0^2} \alpha_1(x, z), \tag{6}$$

and $\alpha_1(x, z)$ is the 1^{st}-order component of the wavespeed perturbation $\alpha(x, z) = \sum_{n=1}^{\infty} \alpha_n(x, z)$, whose reconstruction is the aim of the inverse scattering series.

In equation (3), if the reference velocity c_0 is constant, we have the Green's function in the reference medium (Morse and Feshbach, 1953, Equation (7.2.18)),

$$G_0(x_g, z_g, x_s, z_s, \omega) = \frac{1}{2\pi} \int_{-\infty}^{\infty} dk_g \frac{e^{ik_g(x_g - x_s)} e^{iq_g|z_g - z_s|}}{2iq_g}, \tag{7}$$

where k_g is the Fourier conjugate to x_g, $q_g = \text{sgn}(\omega)\sqrt{(\omega/c_0)^2 - k_g^2}$. The quantities (x_g, z_g) and (x_s, z_s) denote the spatial coordinates of the receivers and sources, respectively. Throughout this article, the function sgn is defined as the sign of its argument:

$$\text{sgn}(x) = \begin{cases} 1 & (x > 0) \\ 0 & (x = 0) \\ -1 & (x < 0) \end{cases} \tag{8}$$

For convenience, let me summarize all the variables and their corresponding Fourier conjugates in the table below:

Physical meaning	Variable name	Fourier conjugate
x-coordinate of the receiver	x_g	k_g
x-coordinate of the source	x_s	k_s
Time	t	ω
x-coordinate of the mid-point	$x_m = 0.5(x_g + x_s)$	$k_m = k_g - k_s$
Offset	$x_h = x_g - x_s$	$k_h = k_g + k_s$

With the Green's function defined in equation (7), equation (5) can be elegantly solved by applying two nested Fourier transforms [1]: $\int_{-\infty}^{\infty} dx_g \int_{-\infty}^{\infty} dx_s e^{ik_s x_s - ik_g x_g}$, over the lateral source and receiver coordinates to obtain α_1. After the Fourier transform above, the nested integral on the right-hand-side of equation (5) is reduced to a simple product:

$$\widetilde{\widetilde{D}}\,(k_g, k_s, \omega) = -\frac{\omega^2}{4q_g q_s c_0^2} \widetilde{\widetilde{\alpha}}_1(k_g - k_s, q_g + q_s), \tag{9}$$

where $\widetilde{\widetilde{\alpha}}_1$ is the double Fourier transform of $\alpha_1(x, z)$:

$$\widetilde{\widetilde{\alpha}}_1(k_m, k_z) = \int_{-\infty}^{\infty} dx e^{-ik_m x} \int_{-\infty}^{\infty} dz e^{ik_z z} \alpha_1(x, z),$$

and $q_g = \text{sgn}(\omega)\sqrt{(\omega/c_0)^2 - k_g^2}$, $q_s = \text{sgn}(\omega)\sqrt{(\omega/c_0)^2 - k_s^2}$. $\widetilde{\widetilde{D}}$ is the triple Fourier transform of the data $D(x_g, x_s, t)$:

$$\widetilde{\widetilde{D}}\,(k_g, k_s, \omega) = \int_{-\infty}^{\infty} dx_g e^{ik_g x_g} \int_{-\infty}^{\infty} dx_s e^{-ik_s x_s} \int_{-\infty}^{\infty} dt e^{i\omega t} D(x_g, x_s, t).$$

[1] Note that the "sign convention" of the Fourier transform is different for the source and geophone coordinates. See Clayton and Stolt (1981) for detail of this choice of Fourier transform.

In this article, We put the tilde sign $\sim$ on top of a function to express its Fourier transform. Equation (9) can be rearranged as:

$$\widetilde{\widetilde{\alpha}}_1(k_g - k_s, q_g + q_s) = -4\frac{q_g q_s}{\omega^2/c_0^2}\widetilde{\widetilde{D}}\left(k_g, k_s, \omega\right), \tag{10}$$

By a simple transformation of coordinates, the data can be transformed to the mid-point x_m and offset x_h coordinate,

$$x_m = \frac{x_g + x_s}{2} \qquad , \qquad x_h = x_g - x_s. \tag{11}$$

Equation (10) can be written in an equivalent form,

$$\widetilde{\widetilde{\alpha}}_1(k_m, k_z) = -4\frac{q_g q_s}{\omega^2/c_0^2}\widetilde{\widetilde{D}}\left(k_m, k_h, k_z\right). \tag{12}$$

It is clear that there is one extra degree of freedom in the data than in α_1, and the reduction of the extra freedom is not unique. The reduction methods in this article are based on the ability to reduce to the redundant freedom to what had been achieved by Zhang and Weglein (2004); Shaw and Weglein (2004a); Liu et al. (2005).

In Liu et al. (2005), the extra degree of freedom is fixed by choosing the offset conjugate k_h to be zero.

The extra freedom in the data has been studied by Zhang and Weglein (2004), by fixing the ratio between ω and $q_g = q_s$,

$$\begin{aligned} &q_g = q_s = \frac{\omega}{c_0}\cos(\theta), \qquad \text{where :} \qquad \theta = \text{constant}, \\ &k_g = k_s. \end{aligned} \tag{13}$$

Similar treatment can be found from the first equation in page-161 of Shaw and Weglein (2004a). Our objective is to generalize the work mentioned above to allow **both** lateral variations in the medium **and** extra freedom in the data. This extra freedom is critical for research beyond seismic imaging, i.e., amplitude analysis for parameter inversion.

To generalize equation (13), we define a fixed angle θ without restricting $k_h = k_g - k_s = 0$:

$$k_g + k_s = 2\frac{\omega}{c_0}\sin\left(\theta\right). \tag{14}$$

The result used by Liu et al. (2005) can be considered as the special case of $\theta = 0$. With this data choice, the relationship in Liu et al. (2005) can be generalized as:

$$k_h = k_g + k_s = 2\frac{\omega}{c_0}\sin(\theta) \qquad\qquad k_g - k_s = k_m \ . \tag{15}$$

One important reason to choose angle θ as our parameterization is that parameter inversion is normally done as a function of angle. Please notice that the angle is defined in the offset domain, the coordinate orthogonal to the mid-point coordinate. A comprehensive description of the variables in this articles is provided in table (2).

For an arbitrary angle θ, we will solve equation (10) under the constraint of equation (15). Consequently, for each k_m and ω, the corresponding vertical wave-number k_z can be calculated by:

$$\begin{aligned} k_z = q_g + q_s = \operatorname{sgn}(\omega)\sqrt{\left(\frac{\omega}{c_0}\right)^2 - \left(\frac{\omega}{c_0}\sin(\theta) + \frac{k_m}{2}\right)^2} \\ + \operatorname{sgn}(\omega)\sqrt{\left(\frac{\omega}{c_0}\right)^2 - \left(\frac{\omega}{c_0}\sin(\theta) - \frac{k_m}{2}\right)^2}. \end{aligned}$$

For fixed k_m and θ, let us consider the equation above as a function of ω:

$$k_z = \kappa(\omega). \tag{16}$$

For the same fixed k_m and θ, the relation above can be inverted to express ω as a function of k_z:

$$\omega = \kappa^{-1}(k_z) = \frac{c_0 k_z}{2}\sqrt{\frac{k_z^2 + k_m^2}{k_z^2\cos^2(\theta) - k_m^2\sin^2(\theta)}}. \tag{17}$$

With ω being defined in equation (17), our generalized formalism can be expressed as:

$$\begin{aligned} \widetilde{\widetilde{\alpha}}_1(k_m, k_z) &= -\frac{4q_g q_s}{\omega^2/c_0^2}\widetilde{\widetilde{D}}\left(\frac{\omega\sin(\theta)}{c_0} + \frac{k_m}{2}, \frac{\omega\sin(\theta)}{c_0} - \frac{k_m}{2}, \omega\right) \\ &= -\frac{4q_g q_s}{\omega^2/c_0^2}\int_{-\infty}^{\infty} dx_g e^{-ik_g x_g}\int_{-\infty}^{\infty} dx_s e^{ik_s x_s}\int_{-\infty}^{\infty} dt e^{i\omega t} D(x_g, x_s, t). \end{aligned} \tag{18}$$

Let us change the integration variable from (x_g,x_s) to ($x_m = 0.5(x_g + x_s)$, $x_h = x_g - x_s$):

$$
\begin{aligned}
&-\frac{4q_gq_s}{\omega^2/c_0^2}\int\limits_{-\infty}^{\infty}dx_m\int\limits_{-\infty}^{\infty}dx_he^{-ik_g[x_m+0.5x_h]}e^{ik_s[x_m-0.5x_h]}\int\limits_{-\infty}^{\infty}dte^{i\omega t}D\left(x_m+0.5x_h,x_m-0.5x_h,t\right)\\
&=-\frac{4q_gq_s}{\omega^2/c_0^2}\int\limits_{-\infty}^{\infty}dx_me^{-i(k_g-k_s)x_m}\int\limits_{-\infty}^{\infty}dx_he^{-i(k_g+k_s)x_h/2}\int\limits_{-\infty}^{\infty}dte^{i\omega t}D\left(x_m+0.5x_h,x_m-0.5x_h,t\right)\\
&=-\frac{4q_gq_s}{\omega^2/c_0^2}\int\limits_{-\infty}^{\infty}dx_me^{-ik_mx_m}\int\limits_{-\infty}^{\infty}dx_he^{-i\frac{\omega\sin(\theta)}{c_0}x_h}\int\limits_{-\infty}^{\infty}dte^{i\omega t}D\left(x_m+0.5x_h,x_m-0.5x_h,t\right)\\
&=-\frac{4q_gq_s}{\omega^2/c_0^2}\int\limits_{-\infty}^{\infty}dx_me^{-ik_mx_m}\int\limits_{-\infty}^{\infty}dt\int\limits_{-\infty}^{\infty}dx_he^{i\omega\left[t-\frac{\sin(\theta)x_h}{c_0}\right]}D\left(x_m+0.5x_h,x_m-0.5x_h,t\right)
\end{aligned}
$$

With another change of the integration variable from t to $(\tau = t - \frac{\sin(\theta)x_h}{c_0})$, the expression above can be written as:

$$
\begin{aligned}
&-\frac{4q_gq_s}{\omega^2/c_0^2}\int\limits_{-\infty}^{\infty}dx_me^{-ik_mx_m}\int\limits_{-\infty}^{\infty}e^{i\omega\tau}d\tau\int\limits_{-\infty}^{\infty}dx_hD\left(x_m+0.5x_h,x_m-0.5x_h,\tau+\frac{\sin(\theta)x_h}{c_0}\right)\\
&=-\frac{4q_gq_s}{\omega^2/c_0^2}\int\limits_{-\infty}^{\infty}dx_me^{-ik_mx_m}\int\limits_{-\infty}^{\infty}d\tau e^{i\omega\tau}D^{\tau p}\left(x_m,\tau\right)
\end{aligned}
$$

where $D^{\tau p}$ is simply the linear Radon transform of all traces within a **CMP** gather [2]:

$$
D^{\tau p}\left(x_m,\tau\right)=\int\limits_{-\infty}^{\infty}dx_hD\left(x_m+\frac{x_h}{2},x_m-\frac{x_h}{2},\tau+x_h\frac{\sin\left(\theta\right)}{c_0}\right). \tag{19}
$$

The equation above is defined for the expression of α_1 :

$$
\widetilde{\widetilde{\alpha}}_1\left(k_m,k_z\right)=-\frac{4q_gq_s}{\omega^2/c_0^2}\int\limits_{-\infty}^{\infty}dx_me^{-ik_mx_m}\int\limits_{-\infty}^{\infty}d\tau e^{i\omega\tau}D^{\tau p}\left(x_m,\tau\right). \tag{20}
$$

Equation (20) can be Fourier transformed from k_z to z by the Fourier operator $(1/2\pi)\int\limits_{-\infty}^{\infty}dk_ze^{-ik_zz}$. But for our purposes, when an angle $\theta \neq 0$ is used, there is a lower limit for the k_z value, namely

[2] CMP means "common mid-point". A **CMP**-gather is the set of seismic data sharing the same mid-point x_m.

$\min(|k_z|)$, defined in eqiation (23). Therefore, our Fourier transform back into space is actually band-limited:

$$\widetilde{\alpha}_1(k_m, z) = \int_{-\infty}^{\infty} dx_m e^{-ik_m x_m} \int_{-\infty}^{\infty} d\tau D^{\tau p} \frac{1}{2\pi} \int_{|k_z|>\min(|k_z|)} dk_z \frac{-4q_g q_s}{\omega^2/c_0^2} e^{i\omega\tau} e^{-ik_z z}. \tag{21}$$

Please notice that in the equation above, the rightmost integral is independent of the data, we only need to calculate it once, and used for later FK-migration tasks,

$$f(k_m, \tau, z) = \frac{1}{2\pi} \int_{|k_z|>\min(|k_z|)} dk_z \frac{-4q_g q_s}{\omega^2/c_0^2} e^{i(\omega\tau - k_z z)}. \tag{22}$$

For the calculation of the factor $f(k_m, \tau, z)$ in equation (22), we kept the uniform sampling in k_z to allow the Fast Fourier Transform, and the frequency ω in the integral is computed via equation (17).

The advantage of pre-calculating $f(k_m, \tau, z)$ in equation (22) first, and used for later migration task is the saving in computation.

The advantages of expressing data in equation (19) are: (1) an easier cut of the direct-arrivals, and (2), very straightforward control over the amplitude and waveform [3].

There are also pre-processing procedures that can be more easily and quickly done in the $\tau - p$ domain (the data after slant stacking) than in the original domain; the computation cost can be greatly reduced since the freedom of the data is reduced.

Missing spectrum

In equation (20), the frequency ω is calculated as in equation (17). Only in the special case of $\theta = 0$, can we sweep the data in the (k_g, k_s, ω) domain to achieve a complete spectrum of α_1 for $-\infty \le k_m \le +\infty$, and $-\infty \le k_z \le +\infty$. Otherwise, for $k_m \neq 0$, there is always a missing band in the spectrum. The efforts below are meant to maximally gather the frequency contents available in the spectrum of α_1.

If we require that both q_g and q_s are real, we have:

$$\left|\frac{\omega}{c_0}\right| \ge \left|\frac{\omega \sin(\theta)}{c_0} \pm \frac{k_m}{2}\right|$$

[3] The sources in seismic exploration are localized in space, which produce reflection data with varying waveform for different offsets even for the simplest horizontal reflectors. But after applying the linear Radon transform, which can be easily implemented, we have a physical problem with plane-wave incidence. For a horizontal reflector, the reflection responses to an incident plan-wave share the same waveform for different incident angles.

Let us consider an easy case where $\omega \geq 0$. We require:

$$\begin{pmatrix} \frac{\omega}{c_0} \geq \pm\left(\frac{\omega\sin(\theta)}{c_0} + \frac{k_m}{2}\right) & \Longrightarrow & \omega \geq \frac{\pm 0.5 k_m c_0}{1 \mp \sin(\theta)} \\ \frac{\omega}{c_0} \geq \pm\left(\frac{\omega\sin(\theta)}{c_0} - \frac{k_m}{2}\right) & \Longrightarrow & \omega \geq \frac{\mp 0.5 k_m c_0}{1 \mp \sin(\theta)} \end{pmatrix}$$
$$\Longrightarrow \omega \geq \frac{|0.5 k_m| c_0}{1 - |\sin(\theta)|} = \max\left(\frac{\mp 0.5 k_m c_0}{1 \mp \sin(\theta)}, \frac{\pm 0.5 k_m c_0}{1 \mp \sin(\theta)}\right)$$

Likewise, for $\omega < 0$, we have:

$$\begin{pmatrix} -\frac{\omega}{c_0} \geq \pm\left(\frac{\omega\sin(\theta)}{c_0} + \frac{k_m}{2}\right) & \Longrightarrow & \omega \leq \frac{\pm 0.5 k_m c_0}{-1 \mp \sin(\theta)} \\ -\frac{\omega}{c_0} \geq \pm\left(\frac{\omega\sin(\theta)}{c_0} - \frac{k_m}{2}\right) & \Longrightarrow & \omega \leq \frac{\mp 0.5 k_m c_0}{-1 \mp \sin(\theta)} \end{pmatrix}$$
$$\Longrightarrow \omega \leq \frac{-|0.5 k_m| c_0}{1 - |\sin(\theta)|} = \min\left(\frac{\mp 0.5 k_m c_0}{-1 \mp \sin(\theta)}, \frac{\pm 0.5 k_m c_0}{-1 \mp \sin(\theta)}\right)$$

Combining the two relations above, we have:

$$|\omega| \geq \frac{1}{2} \frac{|k_m| c_0}{1 - |\sin(\theta)|}$$

Let us denote the lower limit above as: $\omega_{\min}$, the relation above can be expressed as,

$$\omega_{\min} = \frac{1}{2} \frac{|k_m| c_0}{1 - |\sin(\theta)|}$$

I then consider when the lower-limit $\omega_{\min}$ is reached, what would be all the possible values for the corresponding k_z:

$$\left(\frac{\omega\sin(\theta)}{c_0} \pm \frac{k_m}{2}\right)^2 = \left(\frac{0.5\,|k_m|\,c_0}{1 - |\sin(\theta)|}\frac{\sin(\theta)}{c_0} \pm \frac{k_m}{2}\right)^2 = \frac{k_m^2}{4}\left(\frac{\sin(\theta)}{1 - |\sin(\theta)|} \pm 1\right)^2$$
$$= \frac{k_m^2}{4}\left(\frac{\sin(\theta) \mp |\sin(\theta)| \pm 1}{1 - |\sin(\theta)|}\right)^2$$
$$= \begin{pmatrix} \frac{k_m^2}{4}\left(\frac{1}{1-|\sin(\theta)|}\right)^2 = \frac{\omega_{\min}^2}{c_0^2} \\ \texttt{or} \\ \frac{k_m^2}{4}\left(\frac{1-2|\sin(\theta)|}{1-|\sin(\theta)|}\right)^2 = \frac{\omega_{\min}^2}{c_0^2}\left(1 - 2\,|\sin(\theta)|\right)^2 \end{pmatrix}.$$

Consequently, in this case, the k_z value will be,

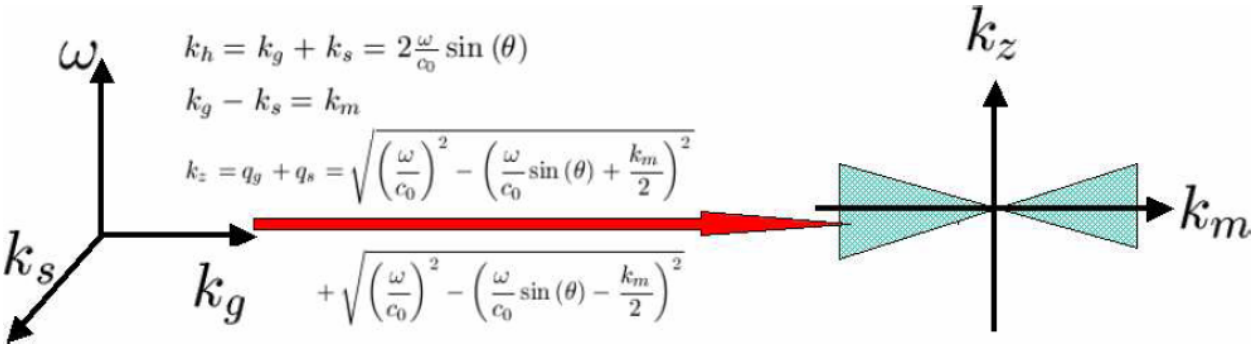

Figure 1: In the (k_m, k_z)-plane, the spectrum is missing for the two shaded triangular regions.

$$k_z = q_g + q_s = \sqrt{\frac{\omega^2}{c_0^2} - \left(\frac{\omega\sin(\theta)}{c_0} + \frac{k_m}{2}\right)^2} + \sqrt{\frac{\omega^2}{c_0^2} - \left(\frac{\omega\sin(\theta)}{c_0} - \frac{k_m}{2}\right)^2}$$
$$= \frac{\omega_{\min}}{c_0}\sqrt{1 - \{1 - 2|\sin(\theta)|\}^2} = 2\frac{\omega_{\min}}{c_0}\sqrt{|\sin(\theta)| - |\sin^2(\theta)|} = |k_m|\sqrt{\frac{|\sin(\theta)|}{1 - |\sin(\theta)|}}.$$

Consequently, we have the low limit for k_z,

$$\min(|k_z|) = |k_m|\sqrt{\frac{|\sin(\theta)|}{1 - |\sin(\theta)|}}. \tag{23}$$

From equation (23), it is clear that the lower-limit for k_z is proportional to k_m. The missing part of the spectrum is displayed in the shaded region of Fig. 1.

The slope of the boundary of the shaded regions in the figure above is $\sqrt{\frac{|\sin(\theta)|}{1-|\sin(\theta)|}}$, it will be empty if $\theta = 0$. This means that for the special case of $\theta = 0$, the shaded region vanishes and the spectrum is complete.

During the process of Fourier transform the spectrum is put back into space, i.e., the right-most integral in equation (21), we must keep in mind the missing spectrum in Fig. (1).

3 What is the "ideal" and adequate data acquisition?

In the α_1 calculation, we have to Fourier transform the input data in equation (4) into wave-number domain,

$$\widetilde{\widetilde{D}}(k_g, k_s, t) = \int_{-\infty}^{\infty} dx_g \int_{-\infty}^{\infty} dx_s e^{i(k_g x_g - k_s x_s)} D(x_g, x_s, t) \tag{24}$$

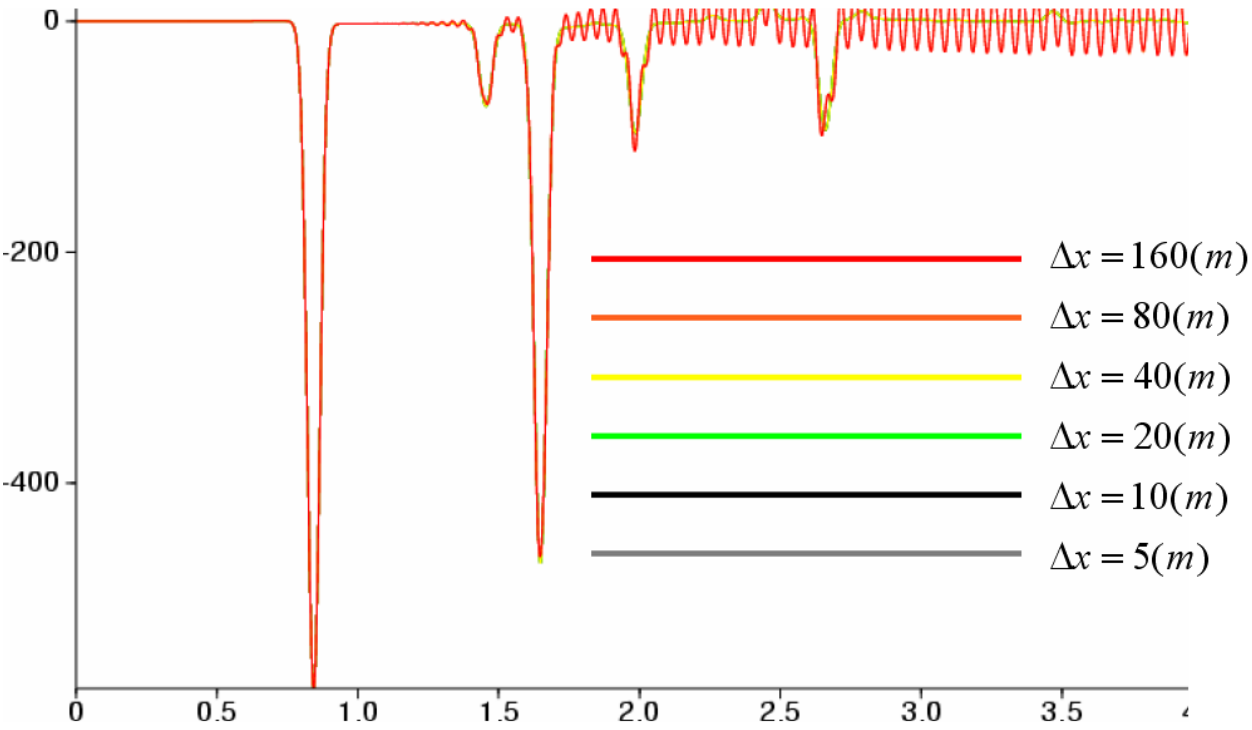

Figure 2: $\tau - p$ transform with different Δx. The gray ($\Delta x = 5$) and black ($\Delta x = 10$) curves are not visible since they are covered by green ($\Delta x = 20$) curve. For large time, little difference between green ($\Delta x = 20$) and yellow ($\Delta x = 40$) is visible. After Δx increases to $80m$ (orange) or $160m$ (red), the negative effects of sparse sampling in the x-direction is clearly visible for large time (from $1.5s$ an on). For small time, i.e., $t < 1.2s$, only the red curve ($\Delta x = 160$) is visible because all the other curves share the same value, and hence were covered by the last drawn red curve.

Any single value in the wave-number spectrum (for example, a single $\widetilde{\widetilde{D}}(k_g, k_s, t)$) requires the wave field at every source and receiver location $-\infty \leq x_g, x_s \leq \infty$. This implies two sampling issues: (1) infinitely small sampling intervals; and (2) infinitely large aperture from $-\infty$ to ∞; practical seismic acquisition clearly does not permit this.

Let's discuss those two issues separately. The first issue does not tend to cause problems, since the wave fields are used in integrals, a reasonably fine sampling rate gives a very good result. In Fig. (2), we show the effects of different Δx (sampling rate in the horizontal direction) in the $\tau - p$ transform in equation (19) (a step most sensitive to Δx). It is obvious that a sampling interval of $20m$ gives an almost exactly same result as the one given by a sampling rate of $5m$. We further obtain good results with $\Delta x = 40m$, a sampling rate already provided by current seismic acquisition.

The wave-field used in equation (24) is the wave-field at a receiver point due to a localized source. Source and receiver array will tend to affect the accuracy of the integral. We have not yet tested the imaging subseries with regard to this issue.

The second issue states that, theoretically, we need the data from $-\infty < x < \infty$ to properly do

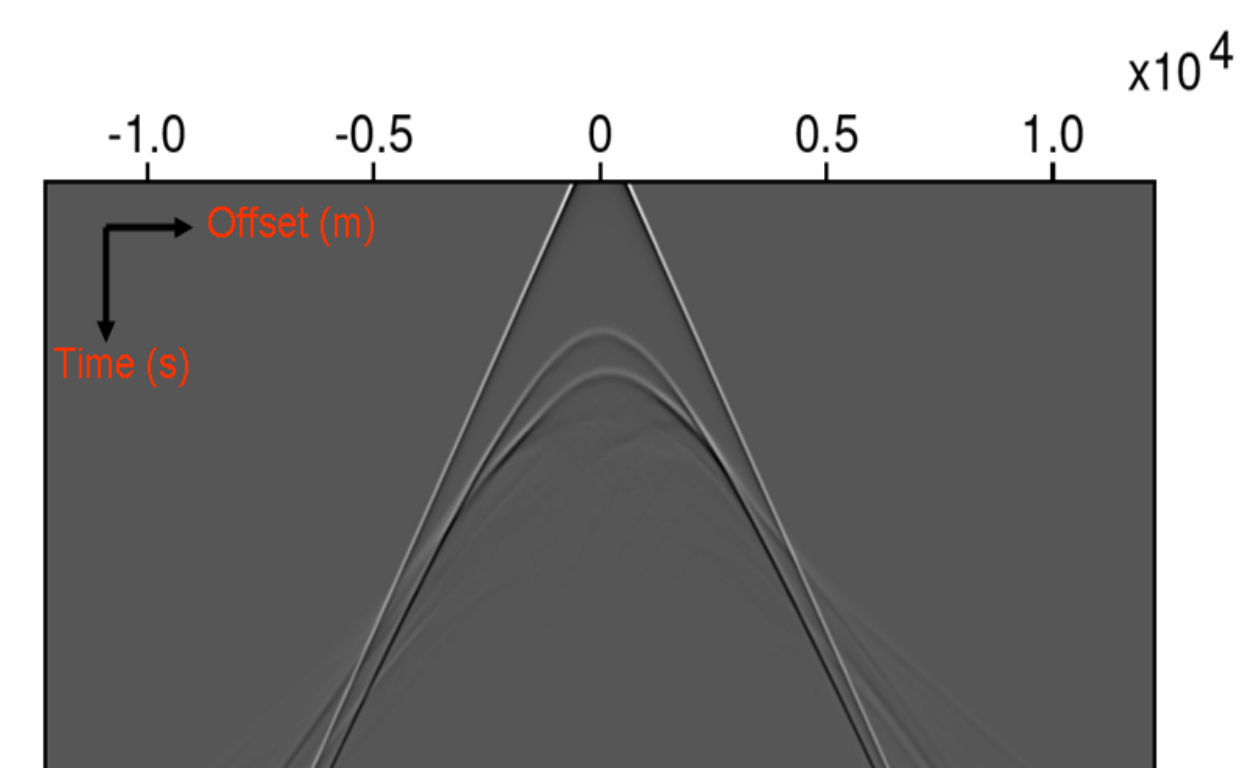

Figure 3: A sample shot gather. The recording length of this shot gather is $T_M = 4.2(s)$, and for this duration, the wave energy had not reached the phones at the left and right edge. For this recording duration, we will receive no additional wave energy from the source if we increase the horizontal aperture.

the Fourier transform, a very daunting requirement for the current seismic acquisition. But in the actual implementation, if the maximal recording time is T_M, then due to the finite speed of the wave propagation, wave energy can only have traveled a finite distance away from the source, and hence we only need a finite aperture in the lateral direction. This can be illustrated by the example in Fig. (3). In the example in Fig. (3), the maximal offset is $12,250m$, which is much larger than the one in standard practice. Further research is needed to study the effects of missing data in the small and large offsets. We have not yet tested our algorithms against this issue. However, Stolt and Benson (1987); Stolt (2002); Ramírez et al. (2007) have provided many methods for data reconstruction and extrapolation that can be used to extend the recorded data offset to the desired one.

4 Pre-processing

Inverse scattering imaging subseries assumes that the following tasks have already been achieved: wavelet estimation, data reconstruction and regularization, de-ghosting, free-surface multiple removal, internal multiple removal, etc.

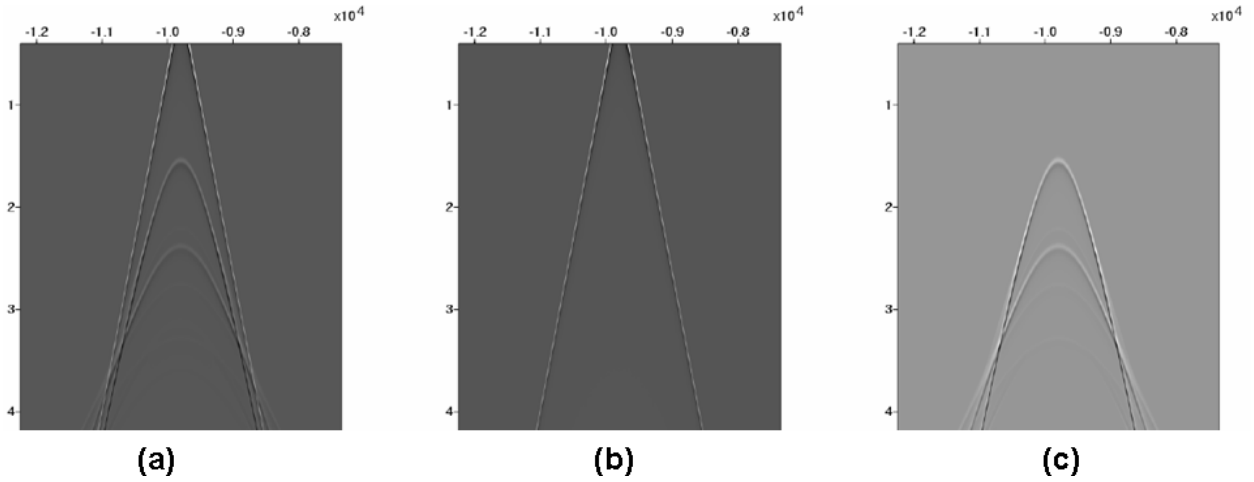

Figure 4: A shot gather from finite difference modleing in shown in (a), the direct arrival (see (b)) is generated using a whole space homogeneous water speed. The direct arrival is removed by subtracting (b) from (a), and pure reflection data is shown in (c). This is the only pre-processing actually happened here.

4.1 Wavelet estimation, de-ghosting, free-surface multiple removal

In practice, normally both the source and the receiver are located very close to the air-water interface, termed the free-surface. The presence of the free-surface will generate ghosts and free-surface multiples. The effects of free-surface can be removed using de-ghosting (Weglein et al., 2000, 2002; Zhang and Weglein, 2005, 2006) and free-surface multiple removal (Carvalho et al., 1991; Weglein et al., 1992; Carvalho and Weglein, 1994). After de-ghosting and free-surface multiple removal, the marine seismic experiment can be considered as if the free-surface does not exist. In the finite-difference modeling, we avoid the free-surface issue by putting a free-surface very far away from the sources and receivers such that the presence of the free-surface is not visible in the input data (see Fig. 4(a)). We generate the direct wave using whole-space homogeneous water velocity (see Fig. 4(b)), then subtract the direct wave from the original data to produce pure reflection data in Fig. 4(c).

Although we assume internal multiples have been removed from the input data, in finite-difference modeling procedure, there is no way of excluding internal multiples. However, since the major task of this research is seismic imaging, and since their amplitudes are very small here, we have not removed them from the data.

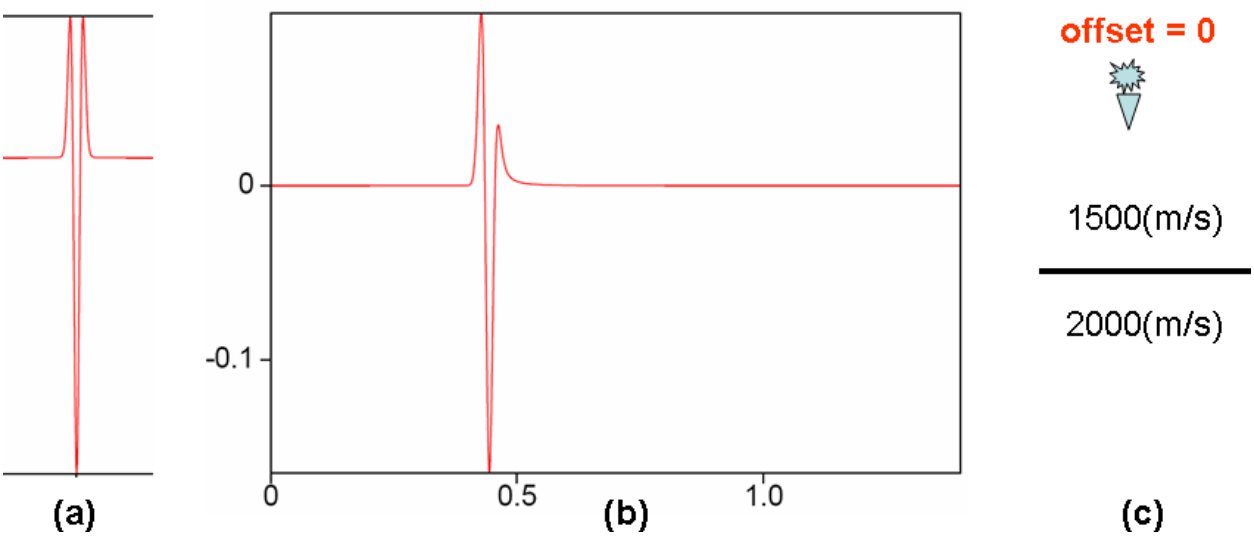

Figure 5: The temporal variation of the Ricker wavelet is shown in (a), please notice its symmetrical side lobes. Even for the simplest geology and acquisition geometry shown in (c), the asymmetrical recorded reflection packet, shown in (b), is noticeably different from the symmetrical-looking wavelet.

5 Wavelet estimtion and reconstruction

5.1 What is "wavelet"?

In this article, by "wavelet" we mean the source term on the right-hand-side of the wave equation (for example, $\widetilde{A}(\omega)$ in equation (1)), not the discrete wave packet recorded by the phones [4]. Fig (5) illustrate the difference. Fig 5-(a) is the temporal variation of the wavelet; Fig 5-(b) is the reflection wave packet recorded at zero offset; the configuration of the experiment is shown in Fig 5-(c). It is obvious that the symmetrical shape of the Ricker wavelet is not kept by the reflection data, event in the simplest geology without lateral variation.

Interested readers may refer to Weglein and Secrest (1990); Guo (2004) for a comprehensive description of wavelet estimations.

5.2 Wavelet reconstruction

Ideally speaking, in order to have a Green's function, the $A(\omega)$ term in the right-hand side of equation (1) should be a constant. In the time domain, a constant $A(\omega)$ implies an ideal spike,

[4]This is different from the definition of the wavelet popular in exploration seismology. According to the SEG website, the definition of wavelet, for example, "embedded wavelet", "basic wavelet", or "equivalent wavelet" is the time-domain reflection shape from a single positive reflector at normal incidence.

$$A(\omega) = 1 \qquad \Leftrightarrow \qquad \frac{1}{2\pi}\int_{-\infty}^{\infty} d\omega A(\omega) e^{-i\omega t} = \delta(t),$$

where $\delta(t)$ is the Dirac δ-function. Ideal δ-function changes infinitely rapidly at $t = 0$; it can neither be generated by any mechanical or electronical means, nor can it propagate through the subsurface medium. Dirac δ-function and Green's functions are popularly used in method derivations bacause they best express the principle of superposition and are best for mathematical manipulations. Luckily, the inverse scattering imaging algorithms of Shaw et al. (2003); Shaw and Weglein (2003); Shaw et al. (2004); Shaw and Weglein (2004b); Shaw (2005); Liu (2006) do not require the idealistic spike wavelet to work effectively, but a band-limited δ-function, just as the free-surface multiple and internal multiple removal algorithms (Carvalho, 1992; Araújo, 1994; Weglein et al., 1997; Matson, 1997). For example, Shaw (2005) used a wavelet which is a box function in the frequency domain; in Liu (2006), the wavelet is recovered to a smooth Gaussian function. In both cases, the missing high frequency do not cause any problem for the series. Actually, the lower the frequency, the faster the convergance rate, as observed by Shaw et al. (2004).

In practice, high frequencies are missing due to attenuation, low frequencies are also missing due to the finite energy of the source, spectrum limit of the phones, etc. Shaw (2005) obtained good results with wavelet missing low frequency information. In this section, we demonstrate how to recover the low frequency information using simple techniques of integration.

Our first example of band-limited wavelet is the wavelet which is the first derivative of Gaussian. Equation (25) shows the temporal variation $A(t)$ and frequency spectrum $\widetilde{A}(\omega)$ of a typical Gaussian derivative wavelet. The low frequency energy gradually vanishes when frequency approaches zero. Although zero frequency is missing, this wavelet can be easily reconstructed back to a Gaussian wavelet by a straight-forward temporal integral in equation (26).

$$A(t) = -\frac{a}{4}\sqrt{\frac{a}{\pi}} t e^{-at^2/4} \qquad \Leftrightarrow \qquad \widetilde{A}(\omega) = -i\omega e^{-\omega^2/a} \tag{25}$$

$$\int_{-\infty}^{t} d\tau A(\tau) = \int_{-\infty}^{t} d\tau - \frac{a}{4}\sqrt{\frac{a}{\pi}} \tau e^{-a\tau^2/4} = \sqrt{\frac{a}{4\pi}} e^{-at^2/4} \tag{26}$$

The procedure in equation (26) works fine for the Gaussian-derivative wavelet, but it is not generally sufficient for any wavelet. For example, the most popular wavelet in the exploration seismology is the second derivative of Gaussian, or the Ricker wavelet, whose temporal variation and frequency spectrum are shown in equation (27).

$$A(t) = -\frac{a}{4}\sqrt{\frac{a}{\pi}} \left(1 - 0.5at^2\right) e^{-at^2/4} \qquad \Leftrightarrow \qquad \widetilde{A}(\omega) = -\omega^2 e^{-\omega^2/a} \tag{27}$$

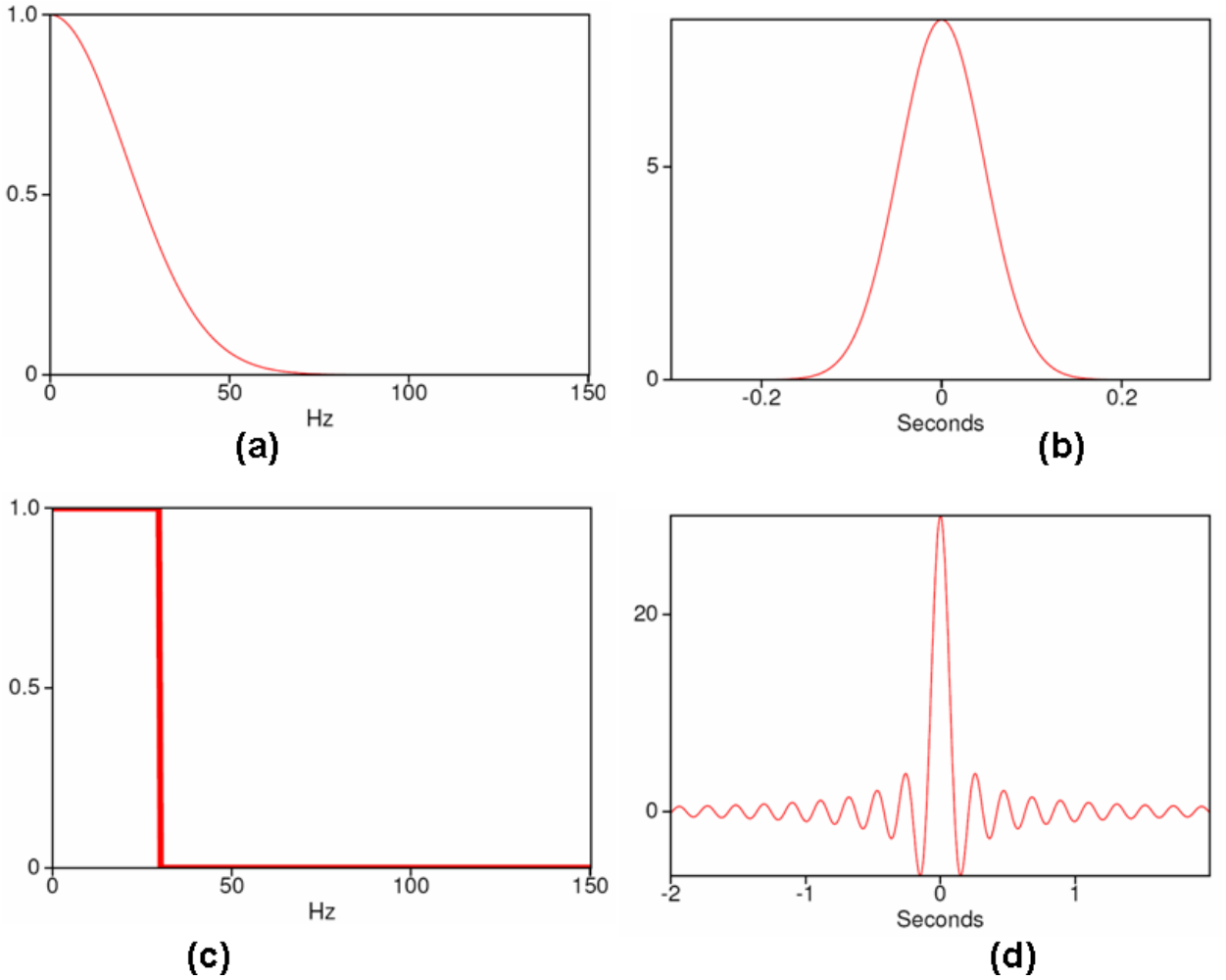

Figure 6: Examples of band-limited wavelets successfully used in the imaging subseries. Liu (2006) reconstruct the wavelet in the seismic data to Gaussian (see (a) and (b) for its frequency spectrum and temporal variation). Shaw et al. (2004) use Sinc wavelet, whose frequency spectrum and temporal variation is shown (c) and (d), respectively. In both wavelet, the high frequencies are missing, but both wavelets had been demonstrated to be sufficient for the purpose of the imaging subseries.

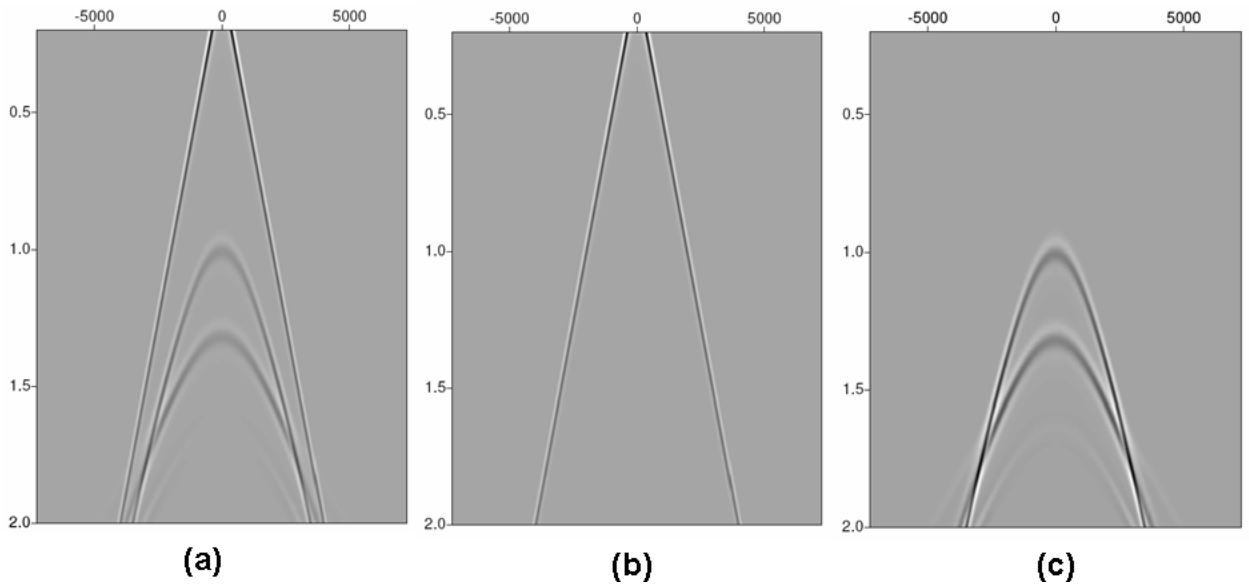

Figure 7: The input data for the experiment to recover Ricker wavelet to Gaussian. The data in (a) is generated using finite-difference modeling with a Ricker wavelet in equation (27). The direct wave in (b) was generated using whole-space water speed and was subtracted from (a) to obtain the input data in (c).

If we integrate it over time once, we only reach the first derivative of Gaussian, still not sufficient for the imaging subseries. But if we integrate it twice, as indicated in equation (28), we can reconstruct Gaussian,

$$\int_{-\infty}^{t} du \int_{-\infty}^{u} dv \frac{-a}{4}\sqrt{\frac{a}{\pi}}\left(1-0.5av^2\right)e^{-av^2/4} = \int_{-\infty}^{t} du(t-u)\left(\frac{a}{4}\sqrt{\frac{a}{\pi}}\left(0.5au^2-1\right)e^{-au^2/4}\right) \qquad (28)$$

Let's look at one numerical example to study the transformation of the Ricker wavelet. The finite difference input data in Fig. (7) was generated using a Ricker wavelet in equation (27). Then a Radon transform (see equation (19) was performed, the zero-angle Radon transform result was shown in Fig. (8). It is clear that although each reflector in the trace had been well recovered to the first dervative of Gaussian (the integral of the Ricker wavelet). We then apply the reconstruct method in equation (28) to reach the satisfactory recovery in Fig. (9).

So far, the treatment for band-limited wavelet to make it ready for the imaging subseries are very encouraging, although we demonstrated the solution in a case by case sense, and we do not have a general solution for this topic.

In this article, we focused on recovering the wavelet in the data to Gaussian since studying missing low frequency is not the main topic of this research. For more detailed study, interested reader may refer to Shaw and Weglein (2004b).

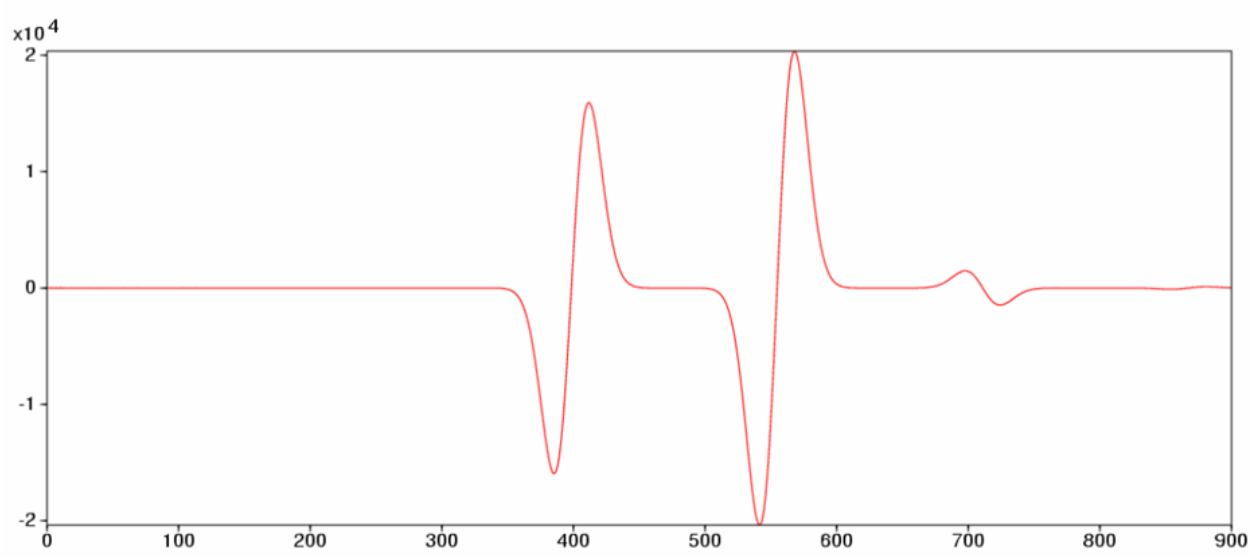

Figure 8: The zero-angle Radon transform of the data in Fig. 7(c).

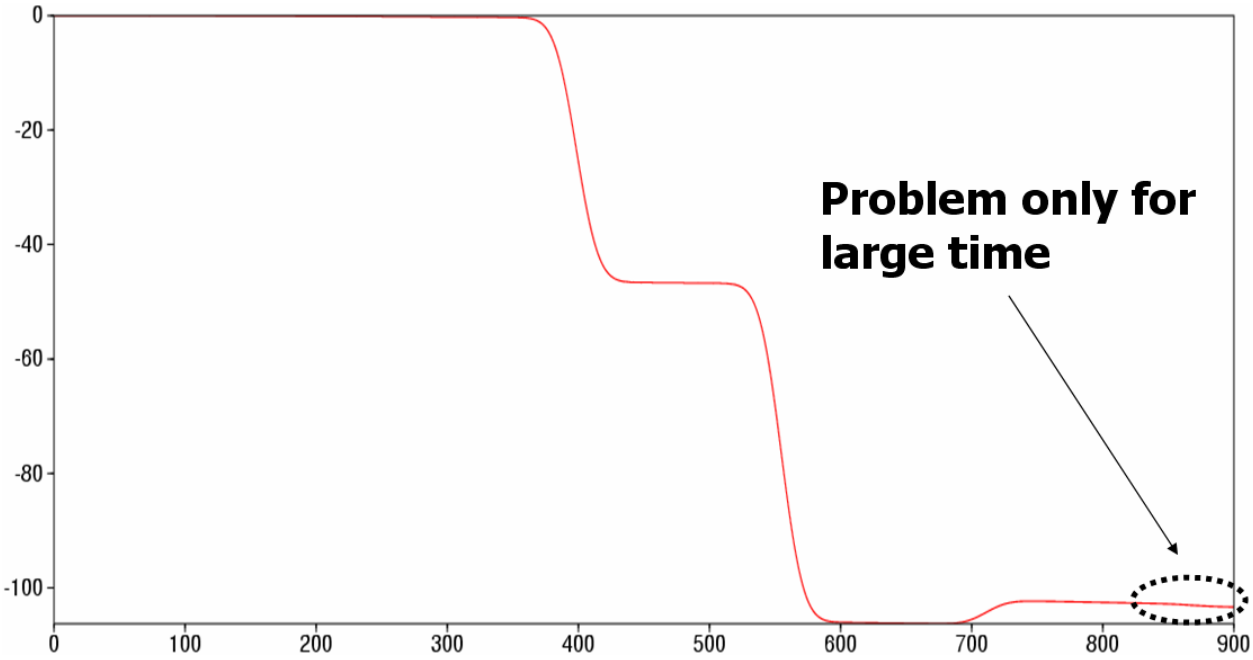

Figure 9: The recovery of a Ricker wavelet to Gaussian. The input data are generated from a layered medium using finite-difference modeling. The recovery is done by integrating over time twice. The α_1 trace again had the box looking of an impedance display. Ricker wavelet contains far less low-frequency information than the first derivative of Gaussian, but its recovery is achieved using a little treatment.

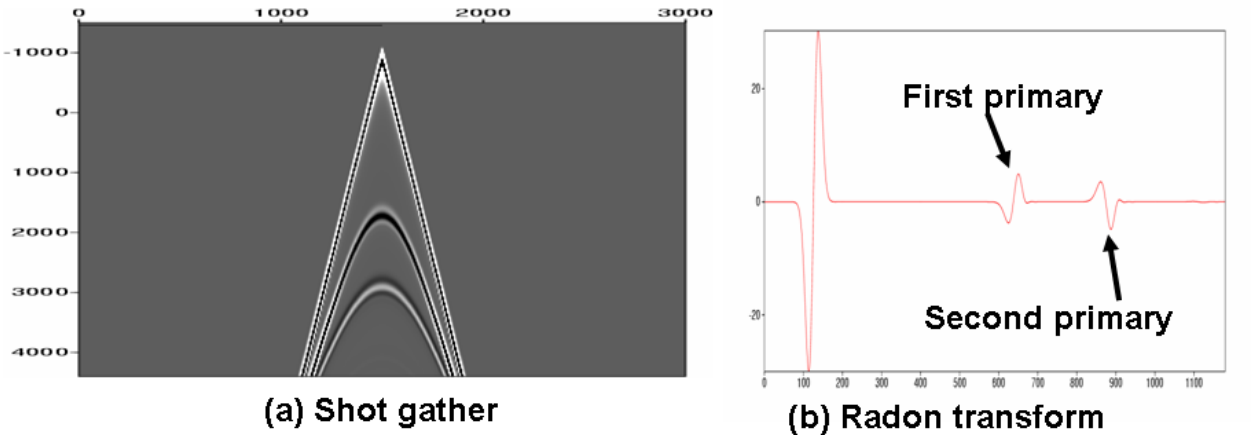

Figure 10: (a): A shot gather generated by a 3^{rd}-party finite difference software. (b): Zero-angle Radon transform result.

Due to that fact that the accurate implementation of the wavelet is not critical for the purposes of developing current seismic imaging algorithms, the most critical information for them is the travel-time. Consequently, the accurate implementation of the wavelet is not the most important objective for many numerical modeling procedures. Let's illustrate this issue with one very simple example. A 3^{rd} party finite difference modeling software was used to generate a shot gather upon a layered medium. The software was given the maximal freedom to choose the peak frequency and the sampling rate in time, we only specify the geological model and the sampling rate in space. Although the 3^{rd}-party program applies transparent boundary conditions to minimize the boundary artifacts, we made the model so big (width=15000m, height=5000m) that the receivers will not receive the unwanted boundary-artifacts from the top, bottom, left and right edges.

From its documentation, we know the 3^{rd} modeling code uses the Ricker wavelet. The data was shown in the left of Fig. (10), it's clear that the linear travel time of the direct wave, and the hyperbolic look of the reflection data, are all very reasonable. But if we sum all the traces together (zero-angle Radon transform), we obtain the resulting trace shown on the right of Fig. (10). Let's look at the wave-form of the first and second primary. Due to the fact that the integral of Ricker is the first derivative of Gaussian, the positive lobe and negative lobe should be of the same size. But in this case, the differences in the sizes of the positive and negative lobes are 32.8 and 35.6 percent, respectively.

6 Migrate the DC-component separately

Let's consider a model without lateral variation. For this model, the result from equation (19) has no lateral variation, i.e., is not a function of x_m. It's Fourier transform in equation (20) will be a δ-function in space because the Fourier transform of a constant is a δ-function. Spiky spectrum like this is often straight-forwardly approximated by an array of floating points. We found that a much better process is to remove the DC component from the data. Then we have a data without

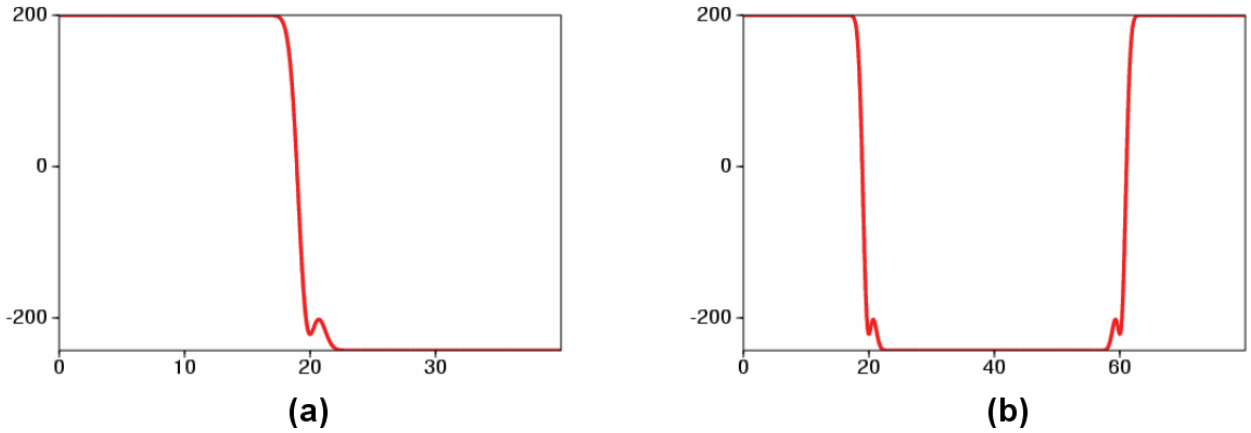

Figure 11: The idea of duplicate a function to make it even with respect to the middle. In this case, an uneven function in (a) is duplicated on the right by its mirror image to construct an even function in (b).

DC-component. The nice property of the data without DC-component is that, its spectrum is no longer spiky, and we don't have the problem of approximate the spiky spectrum.

The spiky spectrum is actually essential for a earth model which extends to infinity. For example, if we have a function that has values in $-X < x < X$, the sampling rate for the earth model spectrum, which is proportional to the reciprocal of X, approaches zero if X approaches infinity. If we localize the non-vanishing range of the data, its spectrum will no longer be spiky and we can well approximate it by an affordable sampling rate. Our idea is to subtract a DC component from the data. And we hope after subtracting the DC component, the data will be localized.

The problem for this idea is that, the left and right edges of the data are generally different, this implies that we have different DC component to the left than to the right. For this kind of data, no matter how we choose the DC component, the data cannot vanish on both edges. The approach we used is to produce a mirror image of the data on the other side of the edge. And by doing so, we have a data which is even with respect to the center. The idea of duplication is summarized in Fig. (11). In all the models we had tested, the lateral variation on both edges are very small and the duplication will not introduce much artifacts. If we choose the single trace at the left edge, we have a data which vanishes to the left and right edge, and hence becomes localized in the x-direction. Another nice property of this approach is that, since after the removal of the DC-component, the data near the edges vanish, there is no boundary artifacts at the edges.

For the salt model we had tested, the $\tau - p$ transform result is shown in Fig. (12). It was duplicated on the right edge to have the symmetrical data in Fig. (13). The data in Fig. (13) was migrated using equation (21) to have the FK migration result in Fig. (14).

The DC-component has no lateral variation, and can be migrated by a simple rescale, very little extra work is introduced.

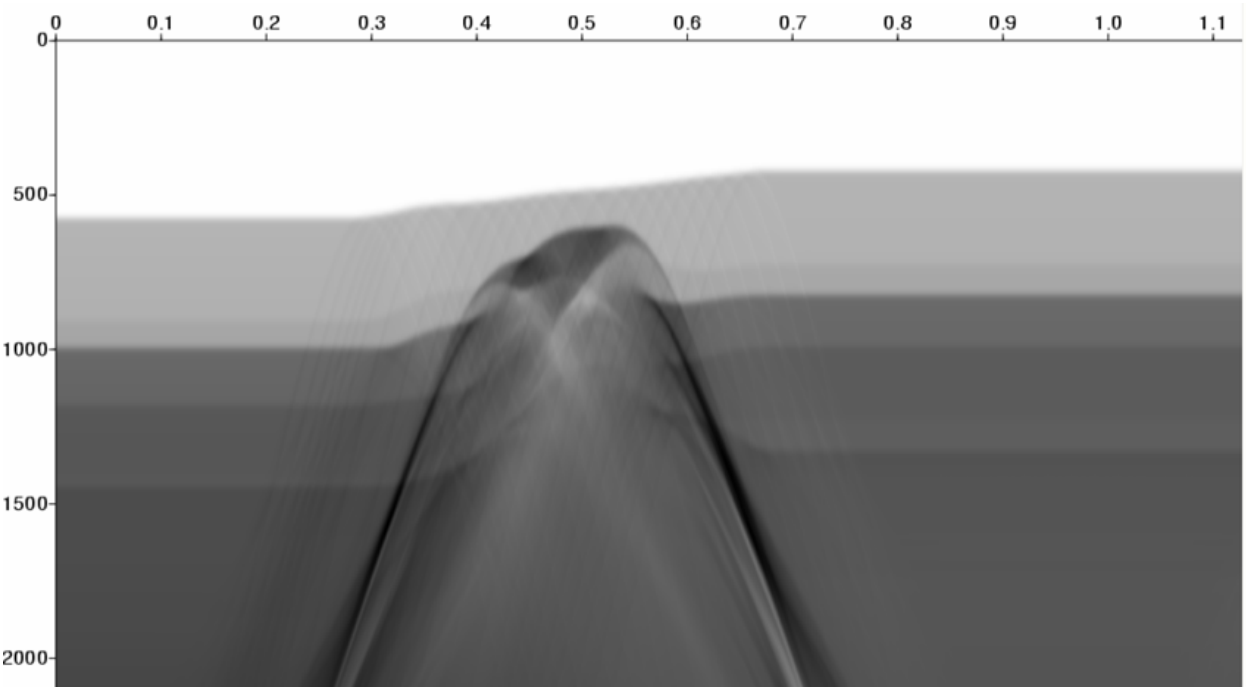

Figure 12: The data after $\tau - p$ transform for the salt model.

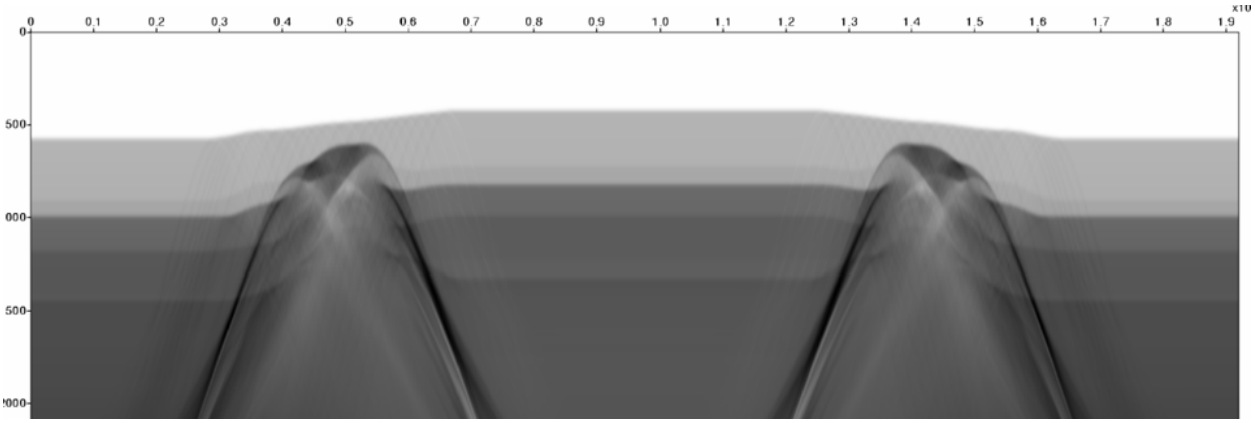

Figure 13: The data in Fig. (12) was duplicated to the right to make left and right edges identical.

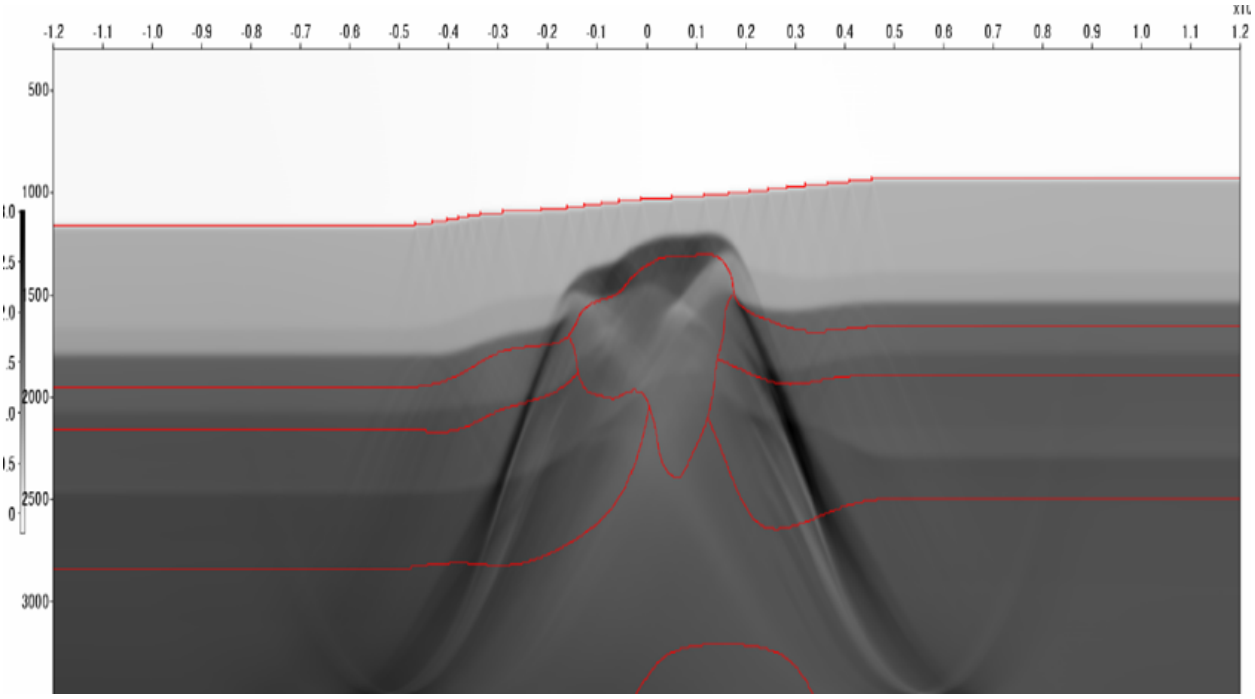

Figure 14: The FK migration result using the data in Fig. (13). The right half is removed since it is just the mirror image of the left half.

7 Caution against using post-stack data

Pre-stack data has more degrees of freedom than the target subsurface geology. However, post-stack data has the same degrees of freedom as the the target subsurface geology. In practice, post-stack sections were migrated to achieve the depth image. We highly recommend the original pre-stack data against post-stack intermediate results.

8 Conclusions

We explained our implementation for α_1 in terms of synthetic acoustic data. The computation of α_1 is very important for the inverse scattering series because it is the input for nonlinear processing that requires amplitude and phase information to be preserved in α_1. In the process of preparing α_1, we found that it is very important to try our best to live up to the physics in the inverse scatttering equations, especially the physics in the understanding of wavelet, sampling, aperture, and better approximation of the spiky spectrum of the earth. Techniques such as duplicating the data on the edge, migrating the DC component separately, pre-calculating the migration operator are proven to be helpful for us on the way towards the best effort α_1.

9 Acknowledgments

The authors would like to thank GX Technology for granting Fang 2006-2007 GXT fellowship, Peter Traynin from ExxonMobil for providing the salt model. We thank Simon Shaw and all M-OSRP members and sponsors. This work has been partially funded by NSFCMG award DMS-0327778 and DOE Basic Energy Sciences award DE-FG02- 05ER15697.

References

Araújo, F. V. *Linear and non-linear methods derived from scattering theory: backscattered tomography and internal multiple attenuation*. PhD thesis, Universidade Federal da Bahia, 1994.

Carvalho, P. M. *Free-surface multiple reflection elimination method based on nonlinear inversion of seismic data*. PhD thesis, Universidade Federal da Bahia, 1992.

Carvalho, P. M. and A. B. Weglein. "Wavelet estimation for surface multiple attenuation using a simulated annealing algorithm." *64th Ann. Internat. Mtg: Soc. of Expl. Geophys., Expanded Abstracts*. . Soc. Expl. Geophys., 1994. 1481–1484.

Carvalho, P. M., A. B. Weglein, and R. H. Stolt. "Examples of a nonlinear inversion method based on the T-matrix of scattering theory: Application to multiple suppression." *61st Ann. Internat. Mtg: Soc. of Expl. Geophys., Expanded Abstracts*. . Soc. Expl. Geophys., 1991. 1319–1322.

Clayton, R. W. and R. H. Stolt. "A Born-WKBJ inversion method for acoustic reflection data." *Geophysics* 46 (1981): 1559–1567.

Guo, Z. *Single streamer wavelet estimation: Extending Extinction Theorem concepts towards a practical solution*. PhD thesis, University of Houston, 2004.

Liu, F., A. B. Weglein, B. G. Nita, and K. A. Innanen. "Inverse scattering series for vertically and laterally varying media: application to velocity independent depth imaging." *M-OSRP Annual Report* 4 (2005).

Liu, Fang. *Multi-dimensional depth imaging without an adequate velocity model*. PhD thesis, University of Houston, 2006.

Matson, K. H. *An inverse-scattering series method for attenuating elastic multiples from multi-component land and ocean bottom seismic data*. PhD thesis, University of British Columbia, 1997.

Morse, P. M. and H. Feshbach. *Methods of theoretical physics*. McGraw-Hill Book Co., 1953.

Ramírez, A. C., K. Hokstad, and E. Otnes. "Data driven regularization/extrapolation using interferometry with the direct wave." *EAGE 69th Conference & Exhibition London, UK* (2007).

Shaw, S. A. and A. B. Weglein. "Imaging seismic reflection data at the correct depth without specifying an accurate velocity model: Initial examples of an inverse scattering subseries." *Frontiers of remote sensing information processing*. Ed. C. H. Chen. World Scientific Publishing Company, 2003. chapter 21, 469–484.

Shaw, S. A. and A. B. Weglein. "A leading order imaging series for prestack data acquired over a laterally invariant acoustic medium. Part I: Derivation and preliminary analysis." *M-OSRP Annual Report* 3 (2004).

Shaw, S. A. and A. B. Weglein. "A leading order imaging series for prestack data acquired over a laterally invariant acoustic medium. Part II: Analysis for data missing low frequencies." *M-OSRP Annual Report* 3 (2004).

Shaw, S. A., A. B. Weglein, D. J. Foster, K. H. Matson, and R. G. Keys. "Isolation of a leading order depth imaging series and analysis of its convergence properties." *M-OSRP Annual Report* 2 (2003): 157–195.

Shaw, S. A., A. B. Weglein, D. J. Foster, K. H. Matson, and R. G. Keys. "Isolation of a leading order depth imaging series and analysis of its convergence properties." *Journal of Seismic Exploration* 2 (November 2004): 157–195.

Shaw, Simon. A. *An inverse scattering series algorithm for depth imaging of reflection data from a layered acoustic medium with an unknown velocity model*. PhD thesis, University of Houston, 2005.

Stolt, R[] H[]. "Seismic data mapping and reconstruction." *Geophysics* 67 (2002): 890–908.

Stolt, R. H. and Benson. *Seismic Migration*. Society of Exploration Geophysicists, 1987.

Weglein, A. B., F. V. Araújo, P. M. Carvalho, R. H. Stolt, K. H. Matson, R. T. Coates, D. Corrigan, D. J. Foster, S. A. Shaw, and H. Zhang. "Inverse scattering series and seismic exploration." *Inverse Problems* 19 (2003): R27–R83.

Weglein, A. B., P. M. Carvalho, and R. H. Stolt. "Nonlinear inverse scattering for multiple suppression: Application to real data. part I." *62nd Ann. Internat. Mtg: Soc. of Expl. Geophys., Expanded Abstracts*. . Soc. Expl. Geophys., 1992. 1093–1095.

Weglein, A. B., F. A. Gasparotto, P. M. Carvalho, and R. H. Stolt. "An inverse-scattering series method for attenuating multiples in seismic reflection data." *Geophysics* 62 (1997): 1975–1989.

Weglein, A. B. and B. G. Secrest. "Wavelet estimation for a multidimensional acoustic or elastic earth." *Geophysics* 55 (1990): 902–913.

Weglein, A. B., S. A. Shaw, K. H. Matson, J. L. Sheiman, R. H. Stolt, T. H. Tan, A. Osen, G. Correa, K. A. Innanen, Z. Guo, and J. Zhang. "New approaches to deghosting towed-streamer and ocean-bottom pressure measurements." *72nd Annual Internat. Mtg., Soc. Expl. Geophys., Expanded Abstracts*. . Soc. Expl. Geophys., 2002. 1016–1019.

Weglein, A. B., T. H. Tan, K. H. Matson, S. A. Shaw, and D. J. Foster. "Prediction of the wavefield anywhere above an ordinary towed streamer: Applications to source wavelet estimation, demultiple, and imaging." *70th Annual Internat. Mtg., Soc. Expl. Geophys., Expanded Abstracts.* . Soc. Expl. Geophys., 2000. 2413–2415.

Zhang, H. and A. B. Weglein. "Target identification using the inverse scattering series: data requirements for the direct inversion of large-contrast, inhomogeneous elastic media." *M-OSRP Annual Report* 3 (2004).

Zhang, J. and A. B. Weglein. "Extinction Theorem deghosting method using towed streamer pressure data: Analysis of the receiver array effect on deghosting and subsequent free surface multiple removal." *M-OSRP Annual Report* 4 (2005).

Zhang, J. and A. B. Weglein. "Application of extinction theorem deghosting method on ocean bottom data." *76th Annual Internat. Mtg., Soc. Expl. Geophys., Expanded Abstracts.* . Soc. Expl. Geophys., 2006. 2694–2678.

Note on velocity independent contributions in the inverse scattering series for processing primaries

A. C. Ramírez, B. G. Nita, A. B. Weglein and E. Otnes

Abstract

Direct-inversion denotes an algorithm that inputs data and outputs medium properties without any modeling. More than 20 years ago, based on the inverse scattering series, Weglein et al. (1981, 1997) imagined direct inversion as a progression of specific and independent operations acting on the data: (1) removal of free-surface multiples; (2) removal of internal multiples; (3) imaging of primaries at their correct depth location; and finally (4) AVO inversion for earth properties. Since the overall direct inversion method in the inverse scattering series operates without any a priori subsurface information, then each one of the four tasks must achieve its goal without any subsurface information as well. The direct inversion series and task specific approach must allow the separation of an imaging subseries from the full series. We present and propose a formalism to find the velocity independent contributions (up to second order in the data) in the inverse scattering series for processing primaries. These contributions are found in terms of a general perturbation, such as the one that was used to find a model type independent internal multiple algorithm. With this perturbation, a separation into two terms of the second order term in the series is performed. The first term does not require knowledge of the earth model type or any subsurface information. The second term in this formalism requires the specification of a model type in order to be computed. When a model type is given, such an acoustic or elastic type, the second part of this term is readily computable. We want to find a general formulation for imaging terms within the inverse series that does not require this specification. Hence, we identify and select only the parts that do not require a model type, and use diagrams to select the terms that we expect will be involved only in the imaging task. We present our initial efforts to this approach.

Introduction

One of the most important objectives of seismic imaging is to place reflectors in their correct spatial location. Seismic imaging beneath complex media (e.g. image beneath salt in locations like deep water GOM) is one of the most challenging problems faced in seismic exploration. The reason is that the success of current methods for imaging seismic data depends on the degree to which we can estimate earth properties above the target, in particular changes in velocity. Even in cases where an accurate velocity model exists or can be obtained, combinations of lateral varying velocity and a range of reflector dip can make current imaging methods fail. A highly accurate estimate of velocity or earth-properties is difficult to achieve in practice and, even when it is achievable, the current imaging technology has shortcomings. This provides a strong motivation for new thinking and for studying new algorithms where fewer assumptions would provide more effectiveness under complex circumstances.

Previously, a subseries of the inverse series in an acoustic medium had been isolated –for a 1D normal incidence experiment (Shaw et al., 2002; Shaw and Weglein, 2003; Innanen, 2003), for 1D prestack data (Shaw, 2005) and for 2D data (Liu et al., 2005, 2006)- that moves reflectors towards their correct spatial location using an inadequate constant reference velocity. We are using the inverse scattering series, a multidimensional direct inversion procedure, to derive a formalism that, if successful, would accurately depth image seismic data directly in terms of data itself and a background medium without any subsurface information. Unlike the present state of the art procedures, this formalism does not make any a priori assumptions on the type and properties of the medium investigated. In practice, these assumptions are often erroneous and can lead to algorithm failures.

In this work, we present our initial efforts to locate and isolate velocity independent imaging terms from the inverse scattering series using a generalized perturbation operator. Our efforts launched from the knowledge and lessons provided by the internal multiple algorithm (Araújo, 1994; Araújo et al., 1994; Weglein et al., 2003) in which a model type independent theory was derived as a subseries of the inverse scattering series using this generalized form of the perturbation operator. These subseries have been effectively used to attenuate multiples in towed streamer, multi-component ocean bottom, and on-shore synthetic and field datasets (Coates and Weglein, 1996; Matson et al., 1999) without the requirement of a priori information concerning the subsurface. At the same time, the present work aims to the future generalization of the ideas presented by Weglein et al. (2000) in which the concept of total wavefield at depth with a direct algorithm that only depends on measured data and a background medium was first proposed. This concept combined with an imaging condition attempts to locate the total wavefield at its correct space location (the idea was further developed by Weglein et al. (2006)). Their formulation uses an acoustic model type for the perturbation operator, and uses the complete perturbation at every order of approximation instead of selecting only the velocity independent imaging terms. Our goals are a step beyond Weglein et al. (2006)) novel idea. We are proposing to use only the imaging terms in the wavefield at depth series described in Nita et al. (2007). We expect the output to be an image of the data at the correct spatial location, but, with incorrect amplitude information. Our stretch goal is similar to the one for the internal multiple algorithm in which the selected terms use what is possible to achieve within the inverse scattering subseries for multiples without discussing a model type. An accurate image of the wavefield at depth that only uses imaging terms from the inverse series, could be reached with the theory developed in this report combined with a model type independent version of the work presented by Nita et al. (2007).

Derivation for the velocity independent imaging terms with a generalized perturbation operator

Note: The material presented in this section is well known. It follows the definitions and concepts introduced by Weglein et al. (1981, 1997), and further developed in Weglein et al. (2000, 2003).

In principle, the inverse scattering series allows for all seismic processing goals to be achieved directly and explicitly in terms of only measured data and a reference background. It never attempts to

change the imprecise input (background medium properties) towards precise input (actual medium properties); it predicts precise output in terms of imprecise input.

The inverse scattering multiple removal technology, demonstrated efficacy and an advantage over model-dependent methods by providing added value under complex and ill-defined geologic subsurface conditions. The same complex conditions are, nowadays, the main obstacle to effective data imaging, since an accurate description of the earth properties (velocity in particular) is not achievable. Our conjecture is that identifying velocity independent imaging terms with a generalized perturbation by following the lessons learned in the internal multiple removal work will lead to a similar level of effectiveness for imaging primaries. The formalism we propose aims to image primaries at their correct spatial location with no requirement or estimate of any subsurface's property.

We start by recognizing that potential exists and resides within the inverse scattering series,

$$
\begin{aligned}
(G_0V_1G_0)_{ms} &= D && (1)\\
(G_0V_2G_0)_{ms} &= -(G_0V_1G_0V_1G_0)_{ms} && (2)\\
(G_0V_3G_0)_{ms} &= -(G_0V_1G_0V_1G_0V_1G_0 + G_0V_1G_0V_2 - G_0V_2G_0V_1)_{ms} && (3)\\
&\vdots
\end{aligned}
$$

where the subscript ms refers to evaluation at the measurement surface, G_0 is the reference Green's function, $\sum_i^\infty V_i$ is the i^{th} approximation of the perturbation V, i denotes the order in the data and we define the perturbation operator V as the difference between the differential wave operators: $V = L_0 - L$. The differential operators L_0 and L define the wave propagation in reference and actual medium, respectively. In the following we are not going to give a specific form to V in terms of a model type. Instead, we are going to give it spatial and frequency degrees of freedom. In principle, enough to include different earth model types.

We are going to start off by assuming that the actual medium varies only in depth (later, we are going to generalize the result to a multi-D earth). This will help to simplify the analysis and location of the velocity independent imaging terms. Within this formulation we are going to split the inverse scattering terms into a part achievable only through a model type specification and a part that does not require that knowledge. We then select the part that is independent of a model type and further separate it into imaging and inversion terms by looking at their diagram and using analogies from diagrams and results in the forward series (Matson, 1996; Nita et al., 2004; Innanen and Weglein, 2003; Ramírez and Otnes, 2006). The reasoning behind this idea comes from the internal multiple experience (Weglein, 1995; Weglein et al., 1997, 2003), where the third term in the inverse series was examined and split into a model type dependent and independent part. The part that did not require knowledge of the earth properties, was put into a "W" Feynman diagram (Feynman, 1949; Weglein et al., 2003) as a result of the conjecture that, "if you achieved this, then you would have reached an algorithm that attenuates multiples without requiring any subsurface information". This conjecture for the internal multiples algorithm has been demonstrated to be successful when applied to synthetic and real data examples under complex geology (Coates and Weglein, 1996; Matson et al., 1999). We start with the same conjecture, "if we can look at the inverse series and locate the terms that process primaries without requiring a model type, and, separate these terms

to identify the parts corresponding to diagrams that act on location issues only, then we would have reached our goal of locating model type independent imaging terms". These terms are then going to be used as input for the wavefield at depth algorithm, and we expect to obtain an algorithm with properties similar to the ones of the internal multiple algorithm.

In the following sections, we calculate the first and second orders of the velocity independent imaging terms within the inverse scattering series using a generalized perturbation operator, all in terms of the data and the reference medium only.

Calculation of the effective data

Using a homogeneous reference Green's function,

$$G_0(z|z';\omega) = \frac{e^{ik|z-z'|}}{2ik},$$

into the first equation in the inverse scattering series,$D = G_0 V_1 G_0$, we obtain

$$\begin{aligned} D(z_g|z_s;\omega) &= \int_{-\infty}^{\infty} dz' \int_{-\infty}^{\infty} dz'' \; \frac{e^{ik(z'-z_g)}}{2ik} V_1(z'|z'';\omega) \frac{e^{ik(z''-z_s)}}{2ik}, \\ D(z_g|z_s;\omega) &= \int_{-\infty}^{\infty} dz' \int_{-\infty}^{\infty} dz'' \; \frac{e^{ik(z'-z_g)}}{2ik} V_1(z'|z'';\omega) \frac{e^{ik(z''-z_s)}}{2ik}, \\ D(z_g|z_s;\omega) &= \frac{1}{2ik} e^{-ik(z_s+z_g)} V_1(k|k;\omega) \frac{1}{2ik}, \end{aligned} \tag{4}$$

It is observed that the first order of the perturbation has 2 degrees of freedom, 1 degree for space freedom (in a 1D experiment there is only one depth variable, hence $z' = z''$) and 1 degree for frequency/time freedom. The data, for a 1D normal incident field only has one degree of freedom since the depth variables z_g and z_s are constant locations for receiver and source, respectively. The fact that the data has less degrees of freedom than the perturbation creates a problem. The perturbation wants all possible combinations of the k and ω, and the only way to fulfill this requirement is by measuring the data everywhere. We can find a solution for this problem by constraining k to be equal to ω/c_0. This provides a form to calculate the on-shell projection of the perturbation, which is the part of the perturbation achievable only from the measured data at z_g.

$$D(z_g|z_s;\omega) = \frac{1}{2ik} e^{-ik(z_s+z_g)} V_1(2k) \frac{1}{2ik} \tag{5}$$

The last step is possible since k depends on ω according to the relation $k = \omega/c_0$.

Introducing the definition for the effective data $\frac{b_1(z_g|z_s;k_z)}{2ik} = D(z_g|z_s;\omega/c_0) = D(z_g|z_s;k_z)$ into equation 5 (Araújo et al., 1994), yields

$$b_1(z_g|z_s;k_z) = \frac{1}{2ik} e^{-ik(z_s+z_g)} V_1(2k) \tag{6}$$

where $k_z = 2k$ is defined as the vertical wavenumber. This is the general form of the effective data. However, for the sake of simplicity, in the following calculations we will assume that $z_s = z_g = 0$ and write $b_1(z_g = 0|z_s = 0;k_z) = b_1(k_z)$.

Calculation of the second order term

The second equation in the inverse scattering series, $G_0V_2G_0 = -G_0V_1G_0V_1G_0$, gives

$$\frac{1}{2ik}V_2(2k)\frac{1}{2ik} = \int_{-\infty}^{\infty} dz \int_{-\infty}^{\infty} dz' \frac{e^{ikz}}{2ik} V_1(z|z';\omega) \int_{-\infty}^{\infty} dz'' \int_{-\infty}^{\infty} dz''' \frac{e^{ik|z'-z''|}}{2ik} V_1(z''|z''';\omega)\frac{e^{ikz'''}}{2ik}. \tag{7}$$

We separate the contributions of the absolute value in the second integral into the part that acts when $z > z'$ and when $z' > z$ by using Heaviside step functions $H(z-z')$ and $H(z'-z)$,respectively,

$$\begin{aligned} V_2(2k) &= \int_{-\infty}^{\infty} dz \int_{-\infty}^{\infty} dz' e^{ikz} V_1(z|z';\omega) \int_{-\infty}^{\infty} dz'' \int_{-\infty}^{\infty} dz''' \frac{e^{ik(z'-z'')}}{2ik} H(z'-z'')V_1(z''|z''';\omega)e^{ikz'''}, \\ &= \int_{-\infty}^{\infty} dz \int_{-\infty}^{\infty} dz' e^{ikz} V_1(z|z';\omega) \int_{-\infty}^{\infty} dz'' \int_{-\infty}^{\infty} dz''' \frac{e^{ik(z''-z')}}{2ik} H(z''-z')V_1(z''|z''';\omega)e^{ikz'''}. \end{aligned} \tag{8}$$

which becomes

$$V_2(2k) = 2\int_{-\infty}^{\infty} dz \int_{-\infty}^{\infty} dz' e^{ikz} V_1(z|z';\omega) \int_{-\infty}^{\infty} dz'' \int_{-\infty}^{\infty} dz''' \frac{e^{ik(z''-z')}}{2ik} H(z''-z')V_1(z''|z''';\omega)e^{ikz'''}. \tag{9}$$

Introducing the Heaviside integral representation,

$$H(z''-z') = \lim_{\epsilon\to 0}\frac{1}{2\pi}\int_{-\infty}^{\infty}\frac{1}{i(p-i\epsilon)}e^{-ip(z''-z')}dp, \tag{10}$$

into equation 9, we obtain

$$\begin{aligned} V_2(2k) = 2 &\lim_{\epsilon\to 0}\frac{1}{2\pi}\int_{-\infty}^{\infty} dz \int_{-\infty}^{\infty} dz' e^{ikz} V_1(z|z';\omega) \int_{-\infty}^{\infty} dz'' \int_{-\infty}^{\infty} dz''' \frac{e^{ik(z''-z')}}{2ik} \\ &\int_{-\infty}^{\infty} dp \frac{e^{-ip(z''-z')}}{i(p-i\epsilon)} V_1(z''|z''';\omega)e^{ikz'''}, \\ = 2 &\lim_{\epsilon\to 0}\frac{1}{2\pi}\frac{1}{2ik}\int_{-\infty}^{\infty} dp \frac{1}{i(p-i\epsilon)} \int_{-\infty}^{\infty} dz e^{ikz} \int_{-\infty}^{\infty} dz' V_1(z|z';\omega)e^{i(-k+p)z'} \int_{-\infty}^{\infty} dz'' e^{i(k-p)z''} \\ &\int_{-\infty}^{\infty} dz''' V_1(z''|z''';\omega)e^{ikz'''}. \end{aligned}$$

recognizing that the last two integrals are simple Fourier transforms, we get

$$V_2(2k) = 2\lim_{\epsilon\to 0}\frac{1}{2\pi}\int_{-\infty}^{\infty} dp \frac{1}{2ik}\frac{V_1(k|-k+p;\omega)V_1(k-p|k;\omega)}{i(p-i\epsilon)}.$$

This integral can be solved through a contour integral, which will be separated into a principal value (P.V.) and the contribution around the pole $p = i\epsilon$.

$$V_2(2k) = \lim_{\epsilon \to 0} \frac{2}{2i\pi} \int_{-\infty}^{\infty} dp \; i\pi \; \delta(p - i\epsilon) \frac{V_1(k| - k + p; \omega) V_1(k - p|k; \omega)}{2ik} + P.V. \left(\frac{1}{i(p - i\epsilon)} \right). \quad (11)$$

The portion of V_2 which depends on the principal value part of the integral is not computable in terms of the data without specifying a model type. We will exclude that part from the computation. Then, we select the contribution from integrating around the pole and take the limit as $\epsilon \to 0$ to obtain

$$\begin{aligned} V_2(2k) &= \frac{1}{2ik} V_1(k| - k; \omega) V_1(k|k; \omega), \\ &= \frac{1}{2ik} V_1(0) V_1(2k). \end{aligned} \quad (12)$$

where only the on-shell projection of the perturbation was used. In terms of effective data, the previous result reads

$$b_2(k_z) = b_1(0) b_1(k_z). \quad (13)$$

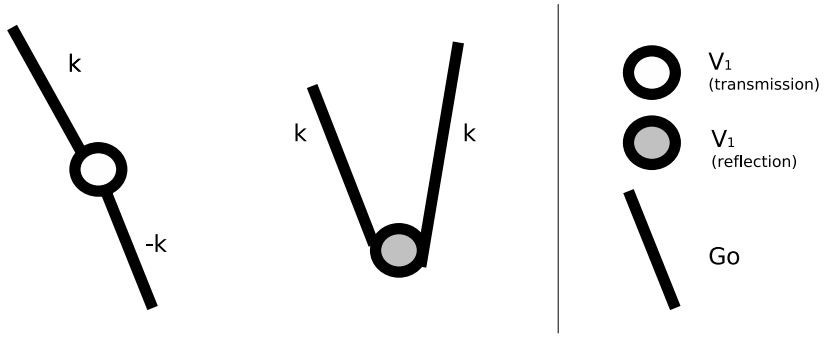

Figure 1: Transmission and reflection diagram for the second order model type independent terms in the inverse scattering series.

The original interpretation of the result in equations 12 and 13 was that transmission data was needed since $b_1(0)$ and $V_1(k| - k; \omega)$ represent a vector that gets transmitted (the transmition diagram for $V_1(k| - k; \omega)$ and the reflection diagram for $V_1(k| - k; \omega)$ are shown in Figure 1). However, by performing a Fourier transform and setting $k = 0$, we can write equation 13 in terms of reflection data only,

$$b_2(k_z) = b_1(0) b_1(k_z) = \left(\int_{-\infty}^{\infty} dz \; b_1(z) \right) \left(\int_{-\infty}^{\infty} dz' \; b_1(z') e^{ik_z z'} \right). \quad (14)$$

where z represents the pseudodepth $z = c_0 t/2$ at constant velocity c_0, and its the conjugate variable of k_z.

Figure 2: A diagram for the term b_{22}. The information from the primary above is given to the deeper primary.

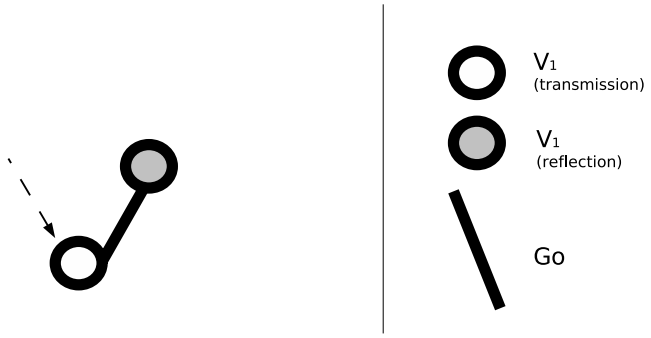

Figure 3: A diagram for the term b_{23}. The deeper primary gives amplitude information to the shallower primary.

Separation of b_2 into task independent terms

The identification of the imaging term comes from two sources: 1) an analogy with the diagrams in the forward series that produce the correct travel time in the predicted wavefield and, 2) from the imaging only diagrams identified within the imaging subseries for 1-parameter acoustic media. Following the derivation of the internal multiple algorithm, the result in equation 14 can be separated into different task specific contributions depending on the relative positions of the pseudodepths z and z'. Thus,

$$\begin{aligned} b_2(k_z) = &\int_{-\infty}^{\infty} dz_1\ b_1(z_1) \int_{-\infty}^{\infty} dz_2\ b_1(z_2) e^{ik_z z_2}\ \delta(z_2 - z_1) \\ &+ \int_{-\infty}^{\infty} dz_1\ b_1(z_1) \int_{-z_1+\epsilon}^{\infty} dz_2\ b_1(z_2) e^{ik_z z_2} \\ &+ \int_{-\infty}^{\infty} dz_1\ b_1(z_1) \int_{-\infty}^{z_1-\epsilon} dz_2\ b_1(z_2) e^{ik_z z_2} \\ b_2(k_z) = &\int_{-\infty}^{\infty} dz_1 b_1^2(z_1) e^{ik_z z_1} + \int_{-\infty}^{\infty} dz_1\ b_1(z_1) \int_{-z_1+\epsilon}^{\infty} dz_2\ b_1(z_2) e^{ik_z z_2} \end{aligned}$$

$$+\int_{-\infty}^{\infty} dz_1\ b_1(z_1)\int_{-\infty}^{z_1-\epsilon} dz_2\ b_1(z_2)e^{ik_z z_2} \tag{15}$$

$$=b_{21}+b_{22}+b_{23}. \tag{16}$$

By analogy with the internal multiple elimination series diagrams (Weglein et al., 1997; Ramírez and Weglein, 2005) and the imaging series (Shaw et al., 2002), the first term (b_{21}) contains a self interaction and is expected to be an amplitude corrector. A second analogy with the separate diagrams in the imaging series (Shaw and Weglein, 2003) and the transmission-like diagrams in the forward series (Ramírez and Otnes, 2006) leads to an interpretation of b_{22} as the candidate for the velocity independent imaging term. These statements can be supported by the following analytic example:

1D Analytic example

Imagine a 1D experiment with two reflectors and a plane wave source. The primary-only data for this experiment is

$$D(t) = R_1\delta(t-t_1) + R_2'\delta(t-t_2), \tag{17}$$

$$D(k_z) = b_1(k_z) = R_1 e^{ik_z z_1} + R_2' e^{ik_z z_2}, \tag{18}$$

hence,

$$b_1(z) = R_1\delta(z-z_1) + R_2'\delta(z-z_2). \tag{19}$$

With these data, we find the following second order terms:

The first term,

$$b_{21}(k_z) = R_1^2 e^{ik_z z_1} + R_2'^2 e^{ik_z z_2}, \tag{20}$$

is clearly an amplitude term since it does not change the depth/time/phase of the data.

The second term,

$$b_{22}(k_z) = \int_{-\infty}^{\infty} dz \left(R_1\delta(z-z_1) + R_2'\delta(z-z_2)\right) \left(R_1 e^{ik_z z_1}H(z_1-z) + R_2' e^{ik_z z_2}H(z_2-z)\right) \tag{21}$$

$$= R_1^2 e^{ik_z z_1}H(z_1-z_1) + R_1R_2' e^{ik_z z_2}H(z_2-z_1) + R_1R_2' e^{ik_z z_1}H(z_1-z_2) + R_2'^2 e^{ik_z z_2}H(z_2-z_1) \tag{22}$$

$$= R_1R_2' e^{ik_z z_2}H(z_2-z_1), \tag{23}$$

allows nonlinear communication between the primaries, and the extra contribution is given to the deeper primary (see Figure 2).

The third term,

$$b_{23}(k_z) = \int_{-\infty}^{\infty} dz \left(R_1\delta(z-z_1) + R_2'\delta(z-z_2)\right) \left(R_1 e^{ik_z z_1} H(z-z_1) + R_2' e^{ik_z z_2} H(z-z_2)\right) \quad (24)$$

$$= R_1^2 e^{ik_z z_1} H(z_1-z_1) + R_1 R_2' e^{ik_z z_2} H(z_1-z_2) + R_1 R_2' e^{ik_z z_1} H(z_2-z_1) + R_2'^2 e^{ik_z z_2} H(z_1-z_2) \quad (25)$$

$$= R_1 R_2' e^{ik_z z_1} H(z_2-z_1), \quad (26)$$

allows the deeper reflector to contribute to the one above it. It is not imaging and not an amplitude term since. Further research is required to understand the purpose of this term (see Figure 3).

Extension to multi-D

Calculation of the effective data

Starting with equation 1

$$D(\boldsymbol{x_g}, z_g|\boldsymbol{x_s}, z_s;\omega) = \int_{-\infty}^{\infty} d\boldsymbol{x} \int_{-\infty}^{\infty} d\boldsymbol{x}' \int_{-\infty}^{\infty} dz \int_{-\infty}^{\infty} dz' G_0(\boldsymbol{x_g} z_g|\boldsymbol{x}, z;\omega) V_1(\boldsymbol{x}, z|\boldsymbol{x}', z';\omega) G_0(\boldsymbol{x}', z'|\boldsymbol{x_s}, z_s;\omega) \quad (27)$$

where $\boldsymbol{x_g}$, z_g, $\boldsymbol{x_s}$ and z_s are the spatial coordinates corresponding to source and receiver locations used to record the data D.

The Green's function propagating in a homogeneous medium is given by

$$G_0(\boldsymbol{x_g}, z_g|\boldsymbol{x}, z, \omega) = -\frac{1}{2\pi} \int_{-\infty}^{\infty} dk_g e^{ik_g(x_g - x)} \frac{e^{iq_g|z-z_g|}}{2iq_g}, \quad (28)$$

where k_g is the horizontal wavenumber and q_g is the vertical wavenumber defined as $k_z = \sqrt{k^2 - k_x^2}$ and $k = \omega/c_0$. The corresponding Green's function for the source side wavenumbers k_s and q_s is given by

$$G_0(\boldsymbol{x}, z|\boldsymbol{x_s}, z_s, \omega) = -\frac{1}{2\pi} \int_{-\infty}^{\infty} dk_s e^{ik_s(x - x_s)} \frac{e^{iq_s|z-z_s|}}{2iq_s}. \quad (29)$$

Using the Green's functions in equations 28 and 29 in equation 27, we find,

$$D(\boldsymbol{x_g}, z_g|\boldsymbol{x_s}, z_s;\omega) = \left(\frac{1}{2\pi}\right)^2 \int_{-\infty}^{\infty} d\boldsymbol{x} \int_{-\infty}^{\infty} d\boldsymbol{x}' \int_{-\infty}^{\infty} dz \int_{-\infty}^{\infty} dz' \int_{-\infty}^{\infty} dk_g \; e^{ik_g(x_g - x)} \frac{e^{iq_g|z-z_g|}}{2iq_g} V_1(\boldsymbol{x}, z|\boldsymbol{x}', z';\omega) \times \int_{-\infty}^{\infty} dk_s e^{ik_s(x' - x_s)} \frac{e^{iq_s|z'-z_s|}}{2iq_s}, \quad (30)$$

and, performing a Fourier transform over the horizontal coordinates x_s and x_g,

$$D(\boldsymbol{k_g}, z_g|\boldsymbol{k_s}, z_s; \omega) = \left(\frac{1}{2\pi}\right)^2 \int_{-\infty}^{\infty} dx_g e^{-ik_g^{'}x_g} \int_{-\infty}^{\infty} dx_g e^{ik_s^{'}x_s} \int_{-\infty}^{\infty} d\boldsymbol{x} \int_{-\infty}^{\infty} d\boldsymbol{x}^{'} \int_{-\infty}^{\infty} dz \int_{-\infty}^{\infty} dz^{'} \int_{-\infty}^{\infty} dk_g e^{ik_g(x_g - x)} \frac{e^{iq_g|z-z_g|}}{2iq_g} V_1(\boldsymbol{x}, z|\boldsymbol{x}^{'}, z^{'}; \omega) \int_{-\infty}^{\infty} dk_s e^{ik_s(x^{'} - x_s)} \frac{e^{iq_s|z^{'}-z_s|}}{2iq_s}. \tag{31}$$

The integrals over source and receiver coordinates give a contribution of $2\pi\delta(k_g^{'} - k_g)$ and $2\pi\delta(k_s^{'} - k_s)$, respectively, which allow us to easily solve the integrals over k_g and k_s, to obtain

$$D(\boldsymbol{k_g}, z_g|\boldsymbol{k_s}, z_s; \omega) = \int_{-\infty}^{\infty} d\boldsymbol{x} \int_{-\infty}^{\infty} d\boldsymbol{x}^{'} \int_{-\infty}^{\infty} dz \int_{-\infty}^{\infty} dz^{'} e^{-ik_g x} \frac{e^{iq_g|z-z_g|}}{2iq_g} V_1(\boldsymbol{x}, z|\boldsymbol{x}^{'}, z^{'}; \omega) e^{ik_s x} \frac{e^{iq_s|z-z_s|}}{2iq_s}. \tag{32}$$

In a surface seismic experiment $z_g > z$ and $z_s > z$, since the perturbation operator $V(\boldsymbol{x}, z)$ has its support only below the measurement surface. At the measurement surface and above, the reference medium is assumed and selected to correspond to the actual medium. Hence, there is no need for the absolute values in equation 32, and the solution of the integrals gives

$$D(\boldsymbol{k_g}, z_g|\boldsymbol{k_s}, z_s; \omega) = \frac{e^{-iq_g z_g} e^{-iq_s z_s}}{-4q_g q_s} V_1(k_g, q_g|k_s, q_s; \omega). \tag{33}$$

The effective data $b_1(k_g, k_s, q_g + q_s)$ is defined as a source obliquity factor times the measured values of the scattered field, $D(k_g, k_s, \omega)$,

$$b_1(k_g, z_g|k_s, z_s; q_g + q_s) = -2iq_s D(k_g, z_g|k_s, z_s; \omega) = \frac{e^{-iq_g z_g} e^{-iq_s z_s}}{-2iq_g} V_1(k_g, q_g|k_s, q_s; \omega), \tag{34}$$

where the vectors $\boldsymbol{k_g} = (k_g, -q_g)$ and $\boldsymbol{k_s} = (k_s, -q_s)$ are constrained by $|\boldsymbol{k_g}| = |\boldsymbol{k_s}| = \omega/c_0$ and the third variable dependence in the effective data is denoted by k_z. Once more, we are only computing the part of the perturbation operator achievable with measurements at the surface, which is the on-shell part of the operator. To find the general form of the operator, $V_1(k_g, q_g|k_s, q_s; \omega)$, explicitly in terms of data would require measurement of the data everywhere. Since we only have data at the measurement surface, only a projection of this operator is achievable. Hence, we need to relate the vertical wavenumbers with ω and the horizontal wavenumbers. The formalism that provides the possibility to achieve an on-shell projection of the perturbation operator in terms of surface data was provided by Razavy (1975) and reviewed by Weglein et al. (2003).

The variable k_z is defined as

$$k_z = -(q_g + q_s) \tag{35}$$

and it is the Fourier conjugate of the pseudodepth variable z. In equation 35

$$q_g = sgn\ \omega\sqrt{\frac{\omega^2}{c_0^2} - k_g^2}, \tag{36}$$

and

$$q_s = sgn\ \omega\sqrt{\frac{\omega^2}{c_0^2} - k_s^2}. \tag{37}$$

Calculation of the second order term

We now start with the second equation in the inverse series, equation 2,

$$\begin{aligned}\int_{-\infty}^{\infty} d\boldsymbol{x} \int_{-\infty}^{\infty} d\boldsymbol{x}^{'} \int_{-\infty}^{\infty} dz \int_{-\infty}^{\infty} dz^{'}\ G_0(\boldsymbol{x_g} z_g|\boldsymbol{x}, z, \omega) V_2(\boldsymbol{x}, z|\boldsymbol{x}^{'}, z^{'}; \omega) G_0(\boldsymbol{x}^{'}, z^{'}|\boldsymbol{x_s}, z_s, \omega) = \\ - \int_{-\infty}^{\infty} d\boldsymbol{x} \int_{-\infty}^{\infty} d\boldsymbol{x}^{'} \int_{-\infty}^{\infty} dz \int_{-\infty}^{\infty} dz^{'} G_0(\boldsymbol{x_g} z_g|\boldsymbol{x}, z, \omega) V_1(\boldsymbol{x}, z|\boldsymbol{x}^{'}, z^{'}; \omega) \int_{-\infty}^{\infty} d\boldsymbol{x}^{''} \int_{-\infty}^{\infty} d\boldsymbol{x}^{''} \\ \times \int_{-\infty}^{\infty} dz^{'''} \int_{-\infty}^{\infty} dz^{'''} G_0(\boldsymbol{x}^{'}, z^{'}|\boldsymbol{x}^{''}, z^{''}, \omega) V_1(\boldsymbol{x}^{''}, z^{''}|\boldsymbol{x}^{'''}, z^{'''}; \omega) G_0(\boldsymbol{x}^{'''}, z^{'''}|\boldsymbol{x_s}, z_s, \omega)\end{aligned} \tag{38}$$

To solve this equation, we start by introducing the reference Green's functions, equations 28 and 29, and performing a Fourier transform over the horizontal coordinates $\boldsymbol{x_s}$ and $\boldsymbol{x_g}$.

The left hand side is solved in the same way as the equation for V_1 is solved in the previous section.

$$l.h.s.(k_g, q_g|k_s, q_s; \omega) = \frac{e^{-iq_g z_g} e^{-iq_s z_s}}{-4q_g q_s} V_2(k_g, q_g|k_s, q_s; \omega). \tag{39}$$

In terms of the second order effective data b_2,

$$b_2(k_g, q_g|k_s, q_s; \omega) = \frac{e^{-iq_g z_g} e^{-iq_s z_s}}{-2iq_g} V_2(k_g, q_g|k_s, q_s; \omega). \tag{40}$$

For the right hand side, we recognize that for a surface seismic experiment $z > z_s$ and $z > z_g$, then,

$$\begin{aligned}r.h.s.(k_g, q_g|k_s, q_s; \omega) = \left(\frac{1}{2\pi}\right)^2 \int_{-\infty}^{\infty} dx_g e^{-ik_g^{'}\boldsymbol{x_g}} \int_{-\infty}^{\infty} dx_s e^{ik_s^{'}\boldsymbol{x_s}} \\ \int_{-\infty}^{\infty} d\boldsymbol{x} \int_{-\infty}^{\infty} d\boldsymbol{x}^{'} \int_{-\infty}^{\infty} dz \int_{-\infty}^{\infty} dz^{'} \int_{-\infty}^{\infty} dk_g e^{ik_g(x_g - x)} \frac{e^{iq_g(z - z_g)}}{2iq_g} V_1(\boldsymbol{x}, z|\boldsymbol{x}^{'}, z^{'}; \omega) \\ \int_{-\infty}^{\infty} d\boldsymbol{x}^{''} \int_{-\infty}^{\infty} d\boldsymbol{x}^{'''} \int_{-\infty}^{\infty} dz^{''} \int_{-\infty}^{\infty} dz^{'''} \int_{-\infty}^{\infty} dk_\lambda e^{ik_\lambda(x^{'} - x^{''})} \frac{e^{iq_\lambda|z^{'} - z^{''}|}}{-2iq_\lambda}\end{aligned}$$

$$\times V_1(\boldsymbol{x}^{''}, z^{''}|\boldsymbol{x}^{'''}, z^{'''}; \omega) \int_{-\infty}^{\infty} dk_s e^{ik_s(x^{'''}-x_s)} \frac{e^{iq_s(z^{'''}-z_s)}}{2iq_s}. \quad (41)$$

The integrals over horizontal variables $\boldsymbol{x_g}$ and $\boldsymbol{x_s}$ give a factor of $2\pi\delta(k_g - k_\lambda)$ and $2\pi\delta(k_s - k_\lambda)$, respectively. Next, we solve the integrals over horizontal wavenumbers k_g and k_s and rearrange the order of integration, to obtain

$$\begin{aligned} r.h.s.(k_g, q_g|k_s, q_s; \omega) = & \int_{-\infty}^{\infty} dk_\lambda \int_{-\infty}^{\infty} dz \int_{-\infty}^{\infty} dz^{'} \frac{e^{iq_g(z-z_g)}}{2iq_g} \int_{-\infty}^{\infty} d\boldsymbol{x} \int_{-\infty}^{\infty} d\boldsymbol{x}^{'} e^{-ik_g x} V_1(\boldsymbol{x}, z|\boldsymbol{x}^{'}, z^{'}; \omega) e^{ik_\lambda x^{'}} \\ & \int_{-\infty}^{\infty} dz^{''} \int_{-\infty}^{\infty} dz^{'''} \frac{e^{iq_\lambda|z'-z''|}}{-2iq_\lambda} \int_{-\infty}^{\infty} d\boldsymbol{x}^{''} \int_{-\infty}^{\infty} d\boldsymbol{x}^{'''} \frac{e^{iq_s(z'''-z_s)}}{2iq_s} \\ & \times \quad e^{-ik_\lambda x^{''}} V_1(\boldsymbol{x}^{''}, z^{''}|\boldsymbol{x}^{'''}, z^{'''}; \omega) e^{ik_s x^{'''}}, \end{aligned} \quad (42)$$

which becomes

$$\begin{aligned} r.h.s.(k_g, q_g|k_s, q_s; \omega) = & \int_{-\infty}^{\infty} dk_\lambda \int_{-\infty}^{\infty} dz \int_{-\infty}^{\infty} dz^{'} \frac{e^{iq_g(z-z_g)}}{2iq_g} V_1(k_g, z|k_\lambda, z^{'}; \omega) \\ & \int_{-\infty}^{\infty} dz^{''} \int_{-\infty}^{\infty} dz^{'''} \frac{e^{iq_\lambda|z'-z''|}}{-2iq_\lambda} V_1(k_\lambda, z^{''}|k_s, z^{'''}; \omega) \frac{e^{iq_s(z'''-z_s)}}{2iq_s}, \end{aligned} \quad (43)$$

We introduce the Heaviside step functions $H(z - z')$ and $H(z' - z)$ to separate the contributions of the absolute value in the second exponential for $z > z'$ and $z' > z$, respectively, and write

$$\begin{aligned} r.h.s.(k_g, q_g|k_s, q_s; \omega) = \lim_{\epsilon \to 0} & \frac{1}{2\pi} \int_{-\infty}^{\infty} dk_\lambda \int_{-\infty}^{\infty} dz \int_{-\infty}^{\infty} dz^{'} \frac{e^{iq_g(z-z_g)}}{2iq_g} V_1(k_g, z|k_\lambda, z^{'}; \omega) \int_{-\infty}^{\infty} dz^{''} \int_{-\infty}^{\infty} dz^{'''} \\ & \times \quad \frac{1}{-2iq_\lambda} \left(e^{iq_\lambda(z'-z'')} \int_{-\infty}^{\infty} dp \frac{e^{-ip(z'-z'')}}{i(p-i\epsilon)} + e^{iq_\lambda(z''-z')} \int_{-\infty}^{\infty} dp \frac{e^{-ip(z''-z')}}{i(p-i\epsilon)} \right) \\ & \times \quad V_1(k_\lambda, z^{''}|k_s, z^{'''}; \omega) \frac{e^{iq_s(z'''-z_s)}}{2iq_s} \end{aligned} \quad (44)$$

where the Heaviside integral representation (equation 10) was used. Rearranging the order of integration and solving the integrals over z' and z, we find

$$\begin{aligned} r.h.s.(k_g, q_g|k_s, q_s; \omega) = \lim_{\epsilon \to 0} & \frac{1}{2\pi} \int_{-\infty}^{\infty} dk_\lambda \frac{e^{-iq_s z_s} e^{-iq_g z_g}}{-(2iq_\lambda)(2iq_g)(2iq_s)} \int_{-\infty}^{\infty} dp \frac{1}{i(p-i\epsilon)} \\ & \times [\ V_1(k_g, q_g|k_\lambda, q_\lambda - p; \omega)\ V_1(k_\lambda, -q_\lambda + p|k_s, q_s; \omega) \\ & + \ V_1(k_g, q_g|k_\lambda, -q_\lambda + p; \omega)\ V_1(k_\lambda, q_\lambda - p|k_s, q_s; \omega)\ ]. \end{aligned} \quad (45)$$

We solve the integral over p through a contour integral, which separates it into a principal value and a contribution around the pole at $p = i\epsilon$ (see the solution for equation 11). The principal value part of this integral can only be solved by specifying a model type. This part is ignored in this formalism.

The contribution from the pole is the only part achievable without the need for a model type. We are interested in locating an imaging term that does not require knowledge of the earth subsurface

properties. Therefore, we exclude the principal value and obtain an expression for the second order inverse scattering equation that only depends on data and propagation in the background medium,

$$\frac{e^{-iq_g z_g}e^{-iq_s z_s}}{-4q_g q_s}V_2(k_g,q_g|k_s,q_s;\omega) = \frac{1}{2}\int_{-\infty}^{\infty}dk_\lambda \frac{e^{-iq_s z_s}e^{-iq_g z_g}}{-(2iq_\lambda)(2iq_g)(2iq_s)} \times [\ V_1(k_g,q_g|k_\lambda,q_\lambda;\omega)\ V_1(k_\lambda,-q_\lambda|k_s,q_s;\omega) + V_1(k_g,q_g|k_\lambda,-q_\lambda;\omega)\ V_1(k_\lambda,q_\lambda|k_s,q_s;\omega)\ ]. \quad (46)$$

This result is related to the effective data. Using the definition in equation 34, such that,

$$V_1(k_1,q_1|k_2,q_2;\omega) = \frac{-2iq_1}{e^{-iq_1 z_g}e^{-iq_2 z_s}}b_1(k_1,z_g|k_2,z_s;q_1+q_2), \quad (47)$$

Hence,

$$\frac{e^{-iq_g z_g}e^{-iq_s z_s}}{-4q_g q_s}V_2(k_g-k_s,-q_g-q_s) = \frac{1}{2}\int_{-\infty}^{\infty}dk_\lambda \frac{e^{-iq_s z_s}e^{-iq_g z_g}}{(-2iq_\lambda)(-2iq_g)(-2iq_s)} \times [\frac{-2iq_g}{e^{-iq_g z_g}e^{iq_\lambda z_s}}b_1(k_g,z_g|k_\lambda,z_s,q_g-q_\lambda)\ \frac{-2iq_\lambda}{e^{-iq_\lambda z_g}e^{-iq_s z_s}}b_1(k_\lambda,z_g|k_s,z_s;q_\lambda+q_s) + \frac{-2iq_g}{e^{-iq_g z_g}e^{-iq_\lambda z_s}}b_1(k_g,z_g|k_\lambda,z_s,q_g+q_\lambda)\ \frac{-2iq_\lambda}{e^{iq_\lambda z_g}e^{-iq_s z_s}}b_1(k_\lambda,z_g|k_s,z_s;-q_\lambda+q_s)]. \quad (48)$$

Factoring the common terms and using equation 40, leads to

$$b_2(k_g,z_g|k_s,z_s,q_g+q_s) = \frac{1}{2}\int_{-\infty}^{\infty}dk_\lambda \times [e^{iq_\lambda(z_s-z_g)}b_1(k_g,z_g|k_\lambda,z_s,q_g-q_\lambda)\ b_1(k_\lambda,z_g|k_s,z_s;q_\lambda+q_s) + e^{iq_\lambda(z_g-z_s)}b_1(k_g,z_g|k_\lambda,z_s,q_g+q_\lambda)\ b_1(k_\lambda,z_g|k_s,z_s;-q_\lambda+q_s)]. \quad (49)$$

In clear analogy with the 1D case, we take a closer look at the third variable dependence of b_1. The subtraction of vertical wavenumbers resembles transmission effects while the addition is related to reflection. The imaging part of equation 49, will then be the combination of transmission-like data imaged at a shallower pseudodepth than the reflection-like data. Note that both parts of the data (reflection-like and transmission-like parts) are going to be written in terms of surface reflection data. However, to find the task specific term that only cares about locating the reflectors at their correct depth, we need to remember the history of that part of the data in the wavenumber domain.

Hence, to find the velocity independent imaging second order term, we write the previous result using a simple constant velocity Stolt migration for the effective data,

$$b_2(k_g,z_g|k_s,z_s,q_g+q_s) = \frac{1}{2}\int_{-\infty}^{\infty}dk_\lambda \times [e^{iq_\lambda(z_s-z_g)}\int_{-\infty}^{\infty}dz_1 \underline{e^{-i(q_g-q_\lambda)z_1}b_1(k_g,z_g|k_\lambda,z_s,z_1)}\ \int_{-\infty}^{\infty}dz_2 e^{-i(q_\lambda+q_s)z_2}b_1(k_\lambda,z_g|k_s,z_s;z_2)$$

$$+\ e^{iq_\lambda(z_g-z_s)}\int_{-\infty}^{\infty}dz_1e^{-i(q_g+q_\lambda)z_1}b_1(k_g,z_g|k_\lambda,z_s,z_1)\ \int_{-\infty}^{\infty}dz_2\underline{e^{-i(-q_\lambda+q_s)z_2}b_1(k_\lambda,z_g|k_s,z_s;z_2)}],$$

where the underlined terms are the ones coming from transmission-like diagrams.

Finally, we split this result into its task specific components, $b_2 = b_{21} + b_{22} + b_{23}$, where

$$\begin{aligned}b_{21}(k_g,z_g|k_s,z_s,q_g+q_s) =&\ \frac{1}{2}\int_{-\infty}^{\infty}dk_\lambda\int_{-\infty}^{\infty}dz_1\int_{-\infty}^{\infty}dz_2e^{-iq_gz_1}e^{-iq_sz_2}\left(e^{iq_\lambda(z_s-z_g)}e^{iq_\lambda(z_1-z_2)}+e^{iq_\lambda(z_g-z_s)}e^{iq_\lambda(z_2-z_1)}\right)\\ &\times\ b_1(k_g,z_g|k_\lambda,z_s,z_1)\ b_1(k_\lambda,z_g|k_s,z_s;z_2)\delta(z_1-z_2),\\ =&\ \frac{1}{2}\int_{-\infty}^{\infty}dk_\lambda\int_{-\infty}^{\infty}dz_1e^{-i(q_g+q_s)z_1}\left(e^{iq_\lambda(z_s-z_g)}+e^{iq_\lambda(z_g-z_s)}\right)\\ &\times\ b_1(k_g,z_g|k_\lambda,z_s,z_1)\ b_1(k_\lambda,z_g|k_s,z_s;z_1)\end{aligned}$$

is the self interacting term, an amplitude corrector (yet to be tested) according to the lessons provided by the analysis of the imaging subseries of inverse series (Shaw et al., 2002; Weglein et al., 2003; Liu et al., 2006), the inverse scattering internal multiple leading and higher order terms (Weglein et al., 1997; Ramírez and Weglein, 2005), as well as the diagrams from the forward series (Innanen and Weglein, 2003; Nita et al., 2004; Ramírez and Otnes, 2006).

The remaining part can be further separated into

$$\begin{aligned}b_{22}(k_g,z_g|k_s,z_s,q_g+q_s) =&\ \frac{1}{2}\int_{-\infty}^{\infty}dk_\lambda\\ &\times\ [e^{iq_\lambda(z_s-z_g)}\int_{-\infty}^{\infty}dz_1\underline{e^{-i(q_g-q_\lambda)z_1}b_1(k_g,z_g|k_\lambda,z_s,z_1)}\ \int_{z_1+\epsilon}^{\infty}dz_2e^{-i(q_\lambda+q_s)z_2}b_1(k_\lambda,z_g|k_s,z_s;z_2)\\ &+\ e^{iq_\lambda(z_g-z_s)}\int_{-\infty}^{\infty}dz_1e^{-i(q_g+q_\lambda)z_1}b_1(k_g,z_g|k_\lambda,z_s,z_1)\ \int_{z_1+\epsilon}^{\infty}dz_2\underline{e^{-i(-q_\lambda+q_s)z_2}b_1(k_\lambda,z_g|k_s,z_s;z_2)}],\end{aligned}$$

and,

$$\begin{aligned}b_{23}(k_g,z_g|k_s,z_s,q_g+q_s) =&\ \frac{1}{2}\int_{-\infty}^{\infty}dk_\lambda\\ &\times\ [e^{iq_\lambda(z_s-z_g)}\int_{-\infty}^{\infty}dz_1\underline{e^{-i(q_g-q_\lambda)z_1}b_1(k_g,z_g|k_\lambda,z_s,z_1)}\ \int_{-\infty}^{z_1-\epsilon}dz_2e^{-i(q_\lambda+q_s)z_2}b_1(k_\lambda,z_g|k_s,z_s;z_2)\\ &+\ e^{iq_\lambda(z_g-z_s)}\int_{-\infty}^{\infty}dz_1e^{-i(q_g+q_\lambda)z_1}b_1(k_g,z_g|k_\lambda,z_s,z_1)\ \int_{-\infty}^{z_1-\epsilon}dz_2\underline{e^{-i(-q_\lambda+q_s)z_2}b_1(k_\lambda,z_g|k_s,z_s;z_2)}].\end{aligned}$$

Following the analysis made in the 1D numerical example in this report, intuition yields that an imaging-only part of b_{22} and b_{23} would be the part that contains reflection-like data at a shallower pseudodepth. This is in agreement to the analysis and experience gained from the higher order imaging work by Liu et al. (2006), in which only the shallower events give nonlinear contributions towards correcting the depth of the deeper once. Hence,

$$b_2^{VIi}(k_g,z_g|k_s,z_s,q_g+q_s) =\ \frac{1}{2}\int_{-\infty}^{\infty}dk_\lambda$$

$$\times \; [e^{iq_\lambda(z_s-z_g)} \int_{-\infty}^{\infty} dz_1 \underline{e^{-i(q_g-q_\lambda)z_1} b_1(k_g, z_g|k_\lambda, z_s, z_1)} \int_{z_1+\epsilon}^{\infty} dz_2 e^{-i(q_\lambda+q_s)z_2} b_1(k_\lambda, z_g|k_s, z_s; z_2)$$
$$+ \; e^{iq_\lambda(z_g-z_s)} \int_{-\infty}^{\infty} dz_1 e^{-i(q_g+q_\lambda)z_1} b_1(k_g, z_g|k_\lambda, z_s, z_1) \int_{-\infty}^{z_1-\epsilon} dz_2 \underline{e^{-i(-q_\lambda+q_s)z_2} b_1(k_\lambda, z_g|k_s, z_s; z_2)}].$$

would be the velocity independent imaging (VIi) term (second order in the measured data). This term needs to be introduced into the wavefield at depth for the imaging formalism by Nita et al. (2007).

Conclusions

Current imaging technology makes assumptions about the nature of the earth that are often violated in practice, leading to algorithm failures. There are two ways in which we can address the violation of an assumption: attempt to better satisfy the assumption, or derive a different method that does not make that assumption. Shaw et al. (2002); Shaw and Weglein (2003) as well as Shaw (2005) presented 1D pre-stack and post-stack theory and synthetic examples of the 1-parameter leading order acoustic inverse scattering imaging algorithm and, the theory was extended to its 2D version and further developed by Liu et al. (2005, 2006) and tested on 2D acoustic finite difference data, giving encouraging results.

We showed the steps involved in the calculation of the second term in the inverse series employing only the part of a general perturbation operator which does not depend on a medium's model type. This part of the second term was further separated into terms containing self interactions and terms containing transmission-like diagrams. A part of the second term was identified as a candidate for a velocity independent imaging term, second order in the data. Our efforts aim to provide to the processing of primaries, the same capability that was earlier brought to the removal of multiples. Multiple removal can occur today without subsurface information, whereas, primaries remain captured by the need to provide subsurface information for the goals of depth imaging and inversion. The purpose is to put them on an equal footing. To this end, Nita et al. (2007) generalize the method described by Weglein et al. (2000) for extending the inverse-scattering series to predict the total wavefield at depth without knowing the propagation medium. The theory is being extended by identifying and using only velocity independent imaging terms in terms of a generalized perturbation operator. Our goal is to be able to locate reflectors at their correct location in space, in a model type independent fashion, analogous to what was earlier achieved for removing multiples with the inverse series formalism. However, the amplitudes of the reflectors are not going to be actual reflection coefficients, since only imaging terms would be used.

Acknowledgments

The support of M-OSRP sponsors and personnel is gratefully acknowledged. This research was partially supported by the NSF-CMG award DMS-0327778 DOE Basic Energy Sciences award DE-FG02-05ER15697.

References

Araújo, F. V. *Linear and non-linear methods derived from scattering theory: backscattering tomography and internal-multiple attenuation.* PhD thesis, Universidade Federal da Bahia, Brazil, 1994. in Portuguese.

Araújo, F. V., A. B. Weglein, P. M. Carvalho, , and R. H Stolt. "Inverse scattering series for multiple attenuation: An example with surface and internal multiples.." *SEG Expanded Abstracts, 1039-1041* (1994).

Coates, R. T. and A. B. Weglein. "Internal multiple attenuation using inverse scattering: results from prestack 1D and 2D acoustic and elastic synthetics.." *SEG Expanded Abstracts* (1996).

Feynman, R. P. "Space-Time Approach to Quantum Electrodynamics.." *Phys. Rev. 76* (1949): 769–789.

Innanen, K. A. *Methods for the treatment of acoustic and absorptive/dispersive wavefield measurements.* PhD thesis, University of British Columbia, 2003.

Innanen, K. A. and A. B. Weglein. "Construction of absorptive/dispersive wave fields with the forward scattering series." *Journal of Seismic Exploration* 12 (2003): 259–282.

Liu, F., A.B. Weglein, K.A. Innanen, and B. G. Nita. "Extension of the non-linear depth imaging capability of the inverse scattering series to multidimensional media: strategies and numerical results." 2005.

Liu, F., A.B. Weglein, K.A. Innanen, and B. G. Nita. "Multi-dimensional seismic imaging using the inverse scattering series." *SEG Technical Program Expanded Abstracts* (2006).

Matson, K. "The relationship between scattering theory and the primaries and multiples of reflection seismic data." *Journal of Seismic Exploration* 5 (1996).

Matson, K., D. Corrigan, A. Weglein, Chi-Yuh Young, and P. Carvalho. "Inverse scattering internal multiple attenuation: results from complex synthetic and field data examples.." *SEG 1999 Expanded Abstracts.* 1999.

Nita, B. G., K. H. Matson, and A. B. Weglein. "Forward Scattering Series and Seismic Events: Far Field Approximations, Critical and Postcritical Events." *Society for Industrial and Applied Mathematics* 64 (2004): 21672185.

Nita, B. G., A. C. Ramírez, A. B. Weglein, and E. Otnes. "Model type independent imaging." *Technical Report, M-OSRP annual meeting* (2007).

Ramírez, A. C. and E. Otnes. "Forward scattering series for 2-parameter acoustic media: analysis and implications to the inverse scattering task-specific subseries." *Submitted to Commun. Comput. Phys.* (2006).

Ramírez, A. C. and A.B. Weglein. "An inverse scattering internal multiple elimination method: Beyond attenuation, a new algorithm and initial tests." *SEG Expanded Abstracts.* (2005): 2115–2118.

Razavy, M. "Determination of the wave velocity in an inhomogenous medium from the reflection coefficient." *J. Acoust. Soc. Am.* 58 (November 1975): 956–963.

Shaw, S. A. *An inverse scattering series algorithm for depth imaging of reection data from a layered acoustic medium with an unknown velocity model.* PhD thesis, University of Houston, Houston, TX, USA., 2005.

Shaw, S. A. and A. B. Weglein. "Imaging seismic reflection data at the correct depth without specifying an accurate velocity model: initial numerical examples of an inverse scattering subseries." *in Frontiers of remote sensing information processing, C.H. Chen (ed.), World Scientic Publishing Co* (2003).

Shaw, Simon A., A. B. Weglein, K. H. Matson, and D. J. Foster. "Cooperation of the leading order terms in an inverse-scattering subseries for imaging: 1-D analysis and evaluation.." *SEG Technical Program Expanded Abstracts* (2002).

Weglein, A. B. "Multiple attenuation: Recend advances and the road ahead." *SEG Technical Program Expanded Abstracts* (1995).

Weglein, A. B., F. V. Araujo, P. M. Carvalho, R. H. Stolt, K. H. Matson, R. T. Coates, D. Corrigan, D. J. Foster, S. A. Shaw, and H. Zhang. "Topical Review: Inverse scattering series and seismic exploration." *Inverse Problems* 19 (2003): 27–83.

Weglein, A. B., F. V. Araujo Gasparotto, P. M. Carvalho, and R. H. Stolt. "An inverse-scattering series method for attenuating multiples in seismic reflection data.." *Geophysics* 62 (1997): 1975–1989.

Weglein, A. B., W. E. Boyse, and J. E. Anderson. "Obtaining three-dimensional velocity information directly from reflection seismic data: an inverse scattering formalism." *Geophysics* 46 (1981): 1116–1120.

Weglein, A. B., B. G. Nitam, K. A. Innanen, E. Otnes, S. A. Shaw, F. Liu, H. Zhang, A. C. Ramírez, J. Zhang, G. L. Pavlis, and C. Fan. "Using the inverse scattering series to predict the wavefield at depth and the transmitted wavefield without an assumption about the phase of the measured reflection data or back propagation in the overburden." *Geophysicsn* 71 (2006): SI125–SI137.

Weglein, A. B., T. H. Tan, S. A. Shaw, K. H. Matson, and D. J. Foster. "Prediction of the wavefield anywhere above an ordinary towed streamer: application to source waveform estimation, demultiple, deghosting, data reconstruction and imaging." *SEG Expanded Abstracts* (2000).

Calculation and imaging of the non-linear 2D wavefield at depth in terms of the data and without any assumptions about the medium

B. G. Nita, A. C. Ramirez, A. B. Weglein, E. Otnes

Abstract

We show the steps involved in the calculation and imaging of the second order wavefield at depth using the inverse scattering series. In the calculations we employ only the part of the perturbation operator which does not depend on a medium's model type. The calculations and result only require the recorded data and the Green's function of the homogeneous background without any a priori assumptions on the medium that's being investigated.

1 Introduction

Inverse scattering series provides the opportunity to determine a multidimensional unknown medium directly from the measured data without making any intermediate determinations of, or assumptions on, the medium under investigation. The inversion process can be thought of as a sequence of independent tasks (1) free surface multiple removal (2) internal multiple removal (3) imaging the reflectors at depth and (4) identifying the medium properties changing across the reflectors. Each task can be associated with a subseries of the full inverse scattering series which only provides the respective capability without affecting the other tasks. For a description of the logic and the history of the subseries method see Weglein et al. (2003).

For the first two tasks, free surface and internal multiple elimination, model type independent subseries and algorithms have been found and applied extensively in the oil industry (see e.g. Weglein et al. (1997) and Weglein et al. (2003) and references therein). For the third task of imaging the reflectors at depth, algorithms have been found and tested for 1D and multi-D acoustic media (Shaw, 2001; Weglein et al., 2001; Shaw, 2002; Shaw and Weglein, 2003; Shaw et al., 2003; Shaw, 2003; Weglein et al., 2003; Shaw et al., 2004; Shaw, 2005; Liu et al., 2005, 2006, 2007).

This research investigates a possible model type independent methodology to calculate and image the wavefield at depth from the inverse scattering series using only recorded data. Roughly speaking, the method uses the calculated and task specific separated perturbation operator V, in the forward scattering series, to calculate different orders of the scattered field at any depth. The subsequent imaging of this wavefield at depth is performed similarly to the imaging step in $f-k$ depth migration algorithms. For an acoustic medium, the method was first described in Weglein et al. (2000) where the first order wavefield at depth was calculated. In this paper we investigate the possibility of performing these calculations in a model type independent environment for the first and the second orders wavefield at depth.

One important conclusions that comes out of this calculations is that, when the actual medium is unknown, calculating the wavefield at depth for one frequency requires all frequencies in the

wavefield on the measurement surface (data). This is fundamentally different from migration algorithms, which assume the medium is known, and which can extrapolate, at depth, each frequency individually (by performing a phase-shift for example). This was originally noted in Weglein et al. (2000) for the first order of the acoustic wavefield at depth calculated using the inverse scattering series. Here we discover the same characteristic for the wavefield at depth without a specified model type for both first and second order.

The paper starts with the necessary background, definitions and description of the method, in Section 2, and then proceeds with the calculation of the first and second orders of the wavefield at depth in Sections 3 and 4 respectively. Section 5 shows how this part of the field can be imaged. We end the paper with conclusions and discussion of future research directions. Throughout the paper we use the following conventions for Fourier transforming over the space and time coordinates. For the Fourier transform over the horizontal variable x, we are going to use the different sign convention for the transformation over the source and receiver coordinates. Accordingly, the forward Fourier transform of a real function f over the horizontal source coordinate x_s is going to be

$$f(k_{xs}) = \int_{-\infty}^{\infty} f(x_s) e^{ik_{xs}x_s} dx_s, \tag{1}$$

where k_{xs} is the associated horizontal wavenumber. The forward Fourier transform of f over the horizontal receiver coordinate x_g is going to be

$$f(k_{xg}) = \int_{-\infty}^{\infty} f(x_g) e^{-ik_{xg}x_g} dx_g, \tag{2}$$

where k_{xg} is, same as before, the associated horizontal wavenumber. The corresponding inverse Fourier transforms are

$$f(x_s) = \frac{1}{2\pi} \int_{-\infty}^{\infty} f(k_{xs}) e^{-ik_{xs}x_s} dk_{xs} \tag{3}$$

and

$$f(x_g) = \frac{1}{2\pi} \int_{-\infty}^{\infty} f(k_{xg}) e^{ik_{xg}x_g} dk_{xg} \tag{4}$$

respectively. There will be no such distinction for the vertical coordinates/wavenumbers. The Fourier transform of, say, $f(z)$ will be

$$f(q) = \int_{-\infty}^{\infty} f(z) e^{iqz} dz \tag{5}$$

and the inverse Fourier transform of $f(q)$ will be

$$f(z) = \frac{1}{2\pi} \int_{-\infty}^{\infty} f(q) e^{-iqz} dq \tag{6}$$

The forward Fourier transform over the time coordinate t is

$$f(\omega) = \int_{-\infty}^{\infty} f(t) e^{i\omega t} dt, \tag{7}$$

where ω is the temporal frequency. Its corresponding inverse Fourier transform will be given by

$$f(t) = \frac{1}{2\pi} \int_{-\infty}^{\infty} f(\omega) e^{-i\omega t} d\omega. \tag{8}$$

2 Background

In operator form, the differential equations describing wave propagation in an actual and a reference medium can be written as

$$\mathbf{LG} = -\mathbf{I} \tag{9}$$

and

$$\mathbf{L_0G_0} = -\mathbf{I}, \tag{10}$$

where $\mathbf{L}$, $\mathbf{L_0}$ and $\mathbf{G}$, $\mathbf{G_0}$ are the actual and reference differential and Green's operators, respectively, for a single temporal frequency and $\mathbf{I}$ is the identity operator. The above equations (9) and (10) assume that the source and receiver signatures have been deconvolved. The perturbation, $\mathbf{V}$, and the scattered field operator, ψ_s, are defined as

$$\mathbf{V} = \mathbf{L} - \mathbf{L_0}, \tag{11}$$

$$\psi_\mathbf{s} = \mathbf{G} - \mathbf{G_0}. \tag{12}$$

The fundamental equation of scattering theory, the Lippmann–Schwinger equation, relates ψ_s, $\mathbf{G_0}$, $\mathbf{V}$, and $\mathbf{G}$ (see, e.g., Taylor (1972)):

$$\psi_s = \mathbf{G} - \mathbf{G_0} = \mathbf{G_0VG}. \tag{13}$$

The Lippmann-Schwinger equation (13) is valid everywhere, inside or outside the support of $\mathbf{V}$. Expressions for $\mathbf{L}$, $\mathbf{L_0}$ and $\mathbf{V}$, in the case of a pressure wavefield propagating in inhomogeneous acoustic and elastic media, have been given in Clayton and Stolt (1981) and Stolt and Weglein (1985). Equation (13) can be expanded in an infinite series by substituting $\mathbf{G} = \mathbf{G_0} - \mathbf{G_0VG}$ into the right-hand side repeatedly to obtain

$$\begin{aligned} \psi_s &= \mathbf{G_0VG_0} + \mathbf{G_0VG_0VG} \\ \psi_s &= \mathbf{G_0VG_0} + \mathbf{G_0VG_0VG_0} + \mathbf{G_0VG_0VG_0VG} \\ &\vdots \end{aligned} \tag{14}$$

and so on. By repeating this process an infinite number of times we imagine that we can drop the last term containing the Green's function of the actual medium, $\mathbf{G}$, in favor of an infinite series, and write the scattered field as

$$\psi_s \equiv \mathbf{G} - \mathbf{G_0} = \mathbf{G_0VG_0} + \mathbf{G_0VG_0VG_0} + \cdots \quad . \tag{15}$$

When convergent (see e.g. Matson (1996) and Nita et al. (2004)), this series, the forward scattering series, constructs the scattered field operator ψ_s, everywhere inside or outside the medium, as a sum of terms representing propagations in the reference medium ($\mathbf{G_0}$) and interactions with the inhomogeneity represented by the perturbation operator $\mathbf{V}$. For example, one could use this expression to calculate the reflected or transmitted response of the medium everywhere. The data recorded in a seismic experiment is usually considered to be the scattered field on the measurement surface

$$(\psi_s)_{MS} = \mathbf{D} \tag{16}$$

Next we consider the expansion of the perturbation V and the scattered field ψ_s as a series in orders of the data $\mathbf{D}$ and write

$$\mathbf{V} = \mathbf{V_1} + \mathbf{V_2} + \mathbf{V_3} + \dots \tag{17}$$

and

$$\psi_s = \psi_s^1 + \psi_s^2 + \psi_s^3 + \dots \tag{18}$$

respectively, where V_i and ψ_s^i are terms of order i in the data $\mathbf{D}$. Notice, for example, that, on the measurement surface, we have

$$\begin{aligned} (\psi_s^1)_{MS} &= \mathbf{D} \\ (\psi_s^i)_{MS} &= 0, \ i \geq 2. \end{aligned} \tag{19}$$

Plugging the series in (17) and (18) into the forward scattering series (15) we find

$$\begin{aligned} \psi_s^1 + \psi_s^2 + \psi_s^3 + \dots = {} & \mathbf{G_0 V_1 G_0} + \mathbf{G_0 V_2 G_0} + \mathbf{G_0 V_3 G_0} \dots \\ & + \mathbf{G_0 V_1 G_0 V_1 G_0} + \mathbf{G_0 V_1 G_0 V_2 G_0} + \mathbf{G_0 V_2 G_0 V_1 G_0} + \dots \\ & + \mathbf{G_0 V_1 G_0 V_1 G_0 V_1 G_0} + \dots \\ & + \dots \ . \end{aligned} \tag{20}$$

Equating like orders in the data in the equation above we find

$$\psi_s^1 = \mathbf{G_0 V_1 G_0} \tag{21}$$

$$\psi_s^2 = \mathbf{G_0 V_2 G_0} + \mathbf{G_0 V_1 G_0 V_1 G_0} \tag{22}$$

$$\psi_s^3 = \mathbf{G_0 V_3 G_0} + \mathbf{G_0 V_2 G_0 V_1 G_0} + \mathbf{G_0 V_1 G_0 V_2 G_0} + \mathbf{G_0 V_1 G_0 V_1 G_0 V_1 G_0} \tag{23}$$

$$\vdots \ .$$

On the measurements surface, and because of (19), equations (21)-(23) provide an algorithm for computing V_i, $i \geq 1$

$$D = (\mathbf{G_0 V_1 G_0})_{ms} \tag{24}$$

$$0 = (\mathbf{G_0 V_2 G_0} + \mathbf{G_0 V_1 G_0 V_1 G_0})_{ms} \tag{25}$$

$$0 = (\mathbf{G_0 V_3 G_0} + \mathbf{G_0 V_2 G_0 V_1 G_0} + \mathbf{G_0 V_1 G_0 V_2 G_0} + \mathbf{G_0 V_1 G_0 V_1 G_0 V_1 G_0})_{ms} \tag{26}$$

$$\vdots \ .$$

One can then calculate $\mathbf{V}$ as a series $\mathbf{V} = \mathbf{V_1} + \mathbf{V_2} + \mathbf{V_3} + ...$ This approach and task specific subseries associated with the series for $\mathbf{V}$ were studied (see e.g. Weglein et al. (2003) and references therein) and continue to be studied. Most importantly, the subseries method provided model type independent algorithms for free surface and internal multiple elimination. Subseries for moving reflectors at the correct depth have been found for the acoustic case (Shaw (2005), Liu et al. (2006)) and research efforts are under way to generalize the subseries to a model type independent algorithm (Ramírez et al. (2007)).

However equations (21)-(23) also provide a different method for computing the wavefield at depth in two steps (see also Weglein et al. (2000) and Weglein et al. (2006)). In the first step we restrict

these equations to the measurement surface to obtain (24)-(26). From these equations we can calculate $\mathbf{V_i}$, $i \geq 1$. In a second step we use the fully unrestricted equations (21)-(23), now with known $\mathbf{V_i}$'s, to calculate ψ_s^i, $i \geq 1$, at any depth. The connection between the two steps is realized through the perturbation operator $\mathbf{V}$, a quantity which only depends on the actual medium (for a fixed reference medium) and does not change from one equation to another. We emphasize that this calculation of the wavefield at depth is performed starting with the data and a reference medium and does not require any features of the actual medium. There are several important features of this calculation that will be evident in the following section. First, in the calculation of $\mathbf{V_i}$, only the model type independent part (as described in Weglein et al. (2003), Ramírez et al. (2007)) is retained and the part that depends on the medium properties is ignored. Second, since what we are trying to achieve is the extrapolation of the wavefield at depth without any change in amplitude, we only use the terms in the series that correct for the reflectors mislocation, as found in Shaw (2005).

In the following sections we calculate the first and second orders of the wavefield at depth in terms of the data and the reference medium only.

3 The calculation of the first order wavefield at depth ψ_s^1

We start with equation (21)

$$\psi_s^1 = \mathbf{G}_0\mathbf{V_1}\mathbf{G}_0 \tag{27}$$

or, in a coordinate system,

$$\psi_s^1(x_1, z_1, x_2, z_2; \omega_1) = \int dx'dx''dz'dz''G_0(x_1, z_1, x', z'; \omega_1)V_1(x', z', x'', z'', \omega_1)G_0(x'', z'', x_2, z_2; \omega_1) \tag{28}$$

where (see Appendix 6)

$$G_0(x_1, z_1, x', z', \omega_1) = \left(\frac{1}{2\pi}\right)^2 \int_{-\infty}^{\infty} dk_g \int_{-\infty}^{\infty} dq_1 \frac{e^{ik_g(x_1-x')}e^{iq_1(z'-z_1)}}{k_g^2 + q_1^2 - \frac{\omega_1^2}{c_0^2} - i\epsilon} \tag{29}$$

and

$$G_0(x'', z'', x_2, z_2, \omega_1) = \left(\frac{1}{2\pi}\right)^2 \int_{-\infty}^{\infty} dk_s \int_{-\infty}^{\infty} dq_2 \frac{e^{ik_s(x''-x_2)}e^{iq_2(z''-z_2)}}{k_s^2 + q_2^2 - \frac{\omega_1^2}{c_0^2} - i\epsilon} \tag{30}$$

and where x_1, z_1, x_2 and z_2 are arbitrary coordinates. Notice that in the equations for the Green's functions given above we have associated the space variables x_1, z_1, x_2 and z_2 with the wavenumbers k_g, q_1, k_s, q_2 satisfying the dispersion relations

$$k_g^2 + q_1^2 = \frac{\omega_1^2}{c_0^2}, \quad k_s^2 + q_2^2 = \frac{\omega_1^2}{c_0^2}. \tag{31}$$

Fourier transforming equation (28) over all space variables (i.e. applying on both sides the integral operators $\int_{-\infty}^{\infty} dx_1 e^{-ik'_g x_1}$, $\int_{-\infty}^{\infty} dx_2 e^{ik'_s x_2}$, $\int_{-\infty}^{\infty} dz_1 e^{iq'_1 z_1}$ and $\int_{-\infty}^{\infty} dz_2 e^{iq'_2 z_2}$) we find

$$\begin{aligned}\psi_s^1(k'_g,q'_1,k'_s,q'_2;\omega_1) = \left(\frac{1}{2\pi}\right)^4 \int dx'dx''dz'dz'' \int_{-\infty}^{\infty} dk_g \int_{-\infty}^{\infty} dx_1 e^{ix_1(k_g-k'_g)} \int_{-\infty}^{\infty} dk_s \int_{-\infty}^{\infty} dx_1 e^{-ix_2(k_s-k'_s)} \\ \times \int_{-\infty}^{\infty} dq_1 \int_{-\infty}^{\infty} dz_1 e^{iz_1(q'_1-q_1)} \int_{-\infty}^{\infty} dq_2 \int_{-\infty}^{\infty} dz_2 e^{iz_2(q'_2-q_2)} \\ \times \frac{e^{-ix'k_g} e^{ix''k_s}}{k_g^2+q_1^2-\frac{\omega_1^2}{c_0^2}-i\epsilon} V_1(x',z',x'',z'',\omega_1) \frac{e^{iz'q_1} e^{iz''q_2}}{k_s^2+q_2^2-\frac{\omega_1^2}{c_0^2}-i\epsilon}\end{aligned} \tag{32}$$

which becomes

$$\begin{aligned}\psi_s^1(k'_g,q'_1,k'_s,q'_2;\omega_1) = \left(\frac{1}{2\pi}\right)^4 \int dx'dx''dz'dz'' \int_{-\infty}^{\infty} dk_g \delta(k_g-k'_g) \int_{-\infty}^{\infty} dk_s \delta(k_s-k'_s) \\ \times \int_{-\infty}^{\infty} dq_1 \delta(q'_1-q_1) \int_{-\infty}^{\infty} dq_2 \delta(q'_2-q_2) \\ \times \frac{e^{-ix'k_g} e^{ix''k_s}}{k_g^2+q_1^2-\frac{\omega_1^2}{c_0^2}-i\epsilon} V_1(x',z',x'',z'',\omega_1) \frac{e^{iz'q_1} e^{iz''q_2}}{k_s^2+q_2^2-\frac{\omega_1^2}{c_0^2}-i\epsilon}\end{aligned} \tag{33}$$

or, after simplifying the delta functions and eliminating the primed notation from the wavenumbers,

$$\psi_s^1(k_g,q_1,k_s,q_2;\omega_1) = \int dx'dx''dz'dz'' \frac{e^{-ix'k_g} e^{ix''k_s}}{k_g^2+q_1^2-\frac{\omega_1^2}{c_0^2}-i\epsilon} V_1(x',z',x'',z'',\omega_1) \frac{e^{iz'q_1} e^{iz''q_2}}{k_s^2+q_2^2-\frac{\omega_1^2}{c_0^2}-i\epsilon}. \tag{34}$$

The last four integrals can also be regarded as Fourier transforms over x', x'', z' and z'' so that the last expression can be written as

$$\psi_s^1(k_g,q_1,k_s,q_2;\omega_1) = \frac{1}{k_g^2+q_1^2-\frac{\omega_1^2}{c_0^2}-i\epsilon} V_1(k_g,-q_1,k_s,-q_2,\omega_1) \frac{1}{k_s^2+q_2^2-\frac{\omega_1^2}{c_0^2}-i\epsilon}. \tag{35}$$

From Appendix 6 equation (146) we have that

$$V_1(k_g,-q_g,-k_s,-q_s,\omega) = -4q_g q_s e^{iq_g z_g} e^{iq_s z_s} D(k_g,k_s,\omega) \tag{36}$$

where we emphasize that while the horizontal wavenumbers are the same in the two equations, the vertical wavenumbers are different and are related to the horizontal ones through different frequencies ω and ω_1. To avoid confusions (see also Appendix 6) we rewrite the last equation as

$$V_1(k_g,-q_g,-k_s,-q_s,\omega) = -4q_g q_s e^{iq_g z_g} e^{iq_s z_s} D(k_g,k_s,q_g+q_s). \tag{37}$$

It is important to notice that the V_1 on the left is the 3-dimensional projection of the fully 5-dimensional V_1 operator (so chosen by ignoring the P.V. part of the Green's function, see Appendix 6). The independent variables on the left are k_g, k_s and $q_g + q_s$. With this in mind we write

$$V_1(k_g, -q_1, -k_s, -q_2, \omega_1) = \frac{1}{2\pi} \int_{-\infty}^{\infty} d(-q_g - q_s)\delta(q_g + q_s - q_1 - q_2) V_1(k_g, -q_g, -k_s, -q_s, \omega) \quad (38)$$

or

$$V_1(k_g, -q_1, -k_s, -q_2, \omega_1) = -\frac{1}{2\pi} \int_{-\infty}^{\infty} d(-q_g - q_s)\delta(q_g + q_s - q_1 - q_2) q_g q_s e^{iq_g z_g} e^{iq_s z_s} D(k_g, k_s, \omega). \quad (39)$$

Equation (39) leads to a relationship between the sums of the vertical wavenumbers,

$$q_g + q_s = q_1 + q_2, \quad (40)$$

which, in turn, allows us to calculate ω_1 in terms of ω as (see Appendix 6 equation (152)) as

$$\frac{\omega_1^2}{c_0^2} = \frac{\left[(q_g + q_s)^2 + k_g^2 + k_s^2\right]^2 - 4k_g^2 k_s^2}{4(q_g + q_s)^2}. \quad (41)$$

With this particular ω_1, equation (39) for V_1 becomes

$$V_1(k_g, -q_1, k_s, -q_2, \omega_1) = -4q_g q_s e^{iq_g z_g} e^{iq_s z_s} D(k_g, k_s, \omega) \quad (42)$$

so the final expression for ψ_s^1

$$\psi_s^1(k_g, q_1, k_s, q_2; \omega_1) = \frac{-4q_g q_s e^{iq_g z_g} e^{iq_s z_s} D(k_g, k_s, \omega)}{\left(k_g^2 + q_1^2 - \frac{\omega_1^2}{c_0^2} - i\epsilon\right)\left(k_s^2 + q_2^2 - \frac{\omega_1^2}{c_0^2} - i\epsilon\right)} \quad (43)$$

in which the variables are related by the dispersion relationships

$$k_g^2 + q_1^2 = \frac{\omega_1^2}{c_0^2}, \quad k_s^2 + q_2^2 = \frac{\omega_1^2}{c_0^2} \quad (44)$$

$$k_g^2 + q_g^2 = \frac{\omega^2}{c_0^2}, \quad k_s^2 + q_s^2 = \frac{\omega^2}{c_0^2} \quad (45)$$

and

$$\frac{\omega_1^2}{c_0^2} = \frac{\left[(q_g + q_s)^2 + k_g^2 + k_s^2\right]^2 - 4k_g^2 k_s^2}{4(q_g + q_s)^2}. \quad (46)$$

For the acoustic case, equation (43) was obtained in Weglein et al. (2000) and it was discussed in Weglein et al. (2006). In the next section we calculate the second order wavefield at depth, ψ_s^2.

4 The calculation of the second order wavefield at depth ψ_s^2

We start with equation (22)

$$\psi_s^2 = \mathbf{G_0 V_2 G_0} + \mathbf{G_0 V_1 G_0 V_1 G_0}. \tag{47}$$

For convenience, we will denote

$$\psi_s^{21} = \mathbf{G_0 V_1 G_0 V_1 G_0} \tag{48}$$

$$\psi_s^{22} = \mathbf{G_0 V_2 G_0}. \tag{49}$$

4.1 The calculation of ψ_s^{21}

We start with

$$\psi_s^{21} = \mathbf{G_0 V_1 G_0 V_1 G_0} \tag{50}$$

or, with coordinates,

$$\psi_s^{21}(x_1, z_1, x_2, z_2; \omega_1) = \int dx' dx'' dz' dz'' G_0(x_1, z_1, x', z'; \omega_1) V_1(x', z', x'', z'', \omega_1)$$
$$\times \int dx''' dx^{iv} dz''' dz^{iv} G_0(x'', z'', x''', z'''; \omega_1) V_1(x''', z''', x^{iv}, z^{iv}, \omega_1) G_0(x^{iv}, z^{iv}, x_s, z_s; \omega_1) \tag{51}$$

where x_1, z_1, x_2 and z_2 are arbitrary coordinates and, as before, the Green's functions have the expressions (see Appendix 6)

$$G_0(x_1, z_1, x', z', \omega_1) = \left(\frac{1}{2\pi}\right)^2 \int_{-\infty}^{\infty} dk_g \int_{-\infty}^{\infty} dq_1 \frac{e^{ik_g(x_1 - x')} e^{iq_1(z' - z_1)}}{k_g^2 + q_1^2 - \frac{\omega_1^2}{c_0^2} - i\epsilon}, \tag{52}$$

$$G_0(x^{iv}, z^{iv}, x_2, z_2, \omega_1) = \left(\frac{1}{2\pi}\right)^2 \int_{-\infty}^{\infty} dk_s \int_{-\infty}^{\infty} dq_2 \frac{e^{ik_s(x^{iv} - x_2)} e^{iq_2(z^{iv} - z_2)}}{k_s^2 + q_2^2 - \frac{\omega_1^2}{c_0^2} - i\epsilon}. \tag{53}$$

and

$$G_0(x'', z'', x''', z''', \omega_1) = \frac{1}{2\pi} \int_{-\infty}^{\infty} dk_{\lambda_1} \frac{e^{ik_{\lambda_1}(x'' - x''')} e^{iq_{\lambda_1}|z'' - z'''|}}{2iq_{\lambda_1}}. \tag{54}$$

where $q_{\lambda_1} = \sqrt{\frac{\omega_1^2}{c_0^2} - k_{\lambda_1}^2}$. In the expressions of the Green's functions above we have associated the spatial variables x_1, z_1, x_2 and z_2 with the wavenumbers k_g, q_1, k_s and q_2 respectively. The wavenumbers satisfy the dispersion relations

$$k_g^2 + q_1^2 = \frac{\omega_1^2}{c_0^2}, \quad k_s^2 + q_2^2 = \frac{\omega_1^2}{c_0^2}, \quad k_{\lambda_1}^2 + q_{\lambda_1}^2 = \frac{\omega_1^2}{c_0^2}. \tag{55}$$

Fourier transforming equation (51) over all spatial arguments of ψ_s^{21} (i.e. applying on both sides the integral operators $\int_{-\infty}^{\infty} dx_1 e^{-ik'_g x_1}$, $\int_{-\infty}^{\infty} dx_2 e^{ik'_s x_2}$, $\int_{-\infty}^{\infty} dz_1 e^{iq'_1 z_1}$ and $\int_{-\infty}^{\infty} dz_2 e^{iq'_2 z_2}$) we find

$$\psi_s^{21}(k'_g,q'_1,k'_s,q'_2;\omega_1) = \left(\frac{1}{2\pi}\right)^5 \int dk_{\lambda_1} \frac{1}{2iq_{\lambda_1}} \int dx'dx''dz'dz''dx'''dx^{iv}dz'''dz^{iv}$$
$$\int dk_g \int dx_1 e^{ix_1(k_g-k'_g)} \int dk_s \int dx_1 e^{-ix_2(k_s-k'_s)} \int dq_1 \int dz_1 e^{iz_1(q'_1-q_1)} \int dq_2 \int dz_2 e^{iz_2(q'_2-q_2)}$$
$$\times \frac{e^{-ix'k_g}e^{ix''k_{\lambda_1}}}{k_g^2+q_1^2-\frac{\omega_1^2}{c_0^2}-i\epsilon} V_1(x',z',x'',z'',\omega_1) \frac{e^{-ix'''k_{\lambda_1}}e^{ix^{iv}k_s}}{k_s^2+q_2^2-\frac{\omega_1^2}{c_0^2}-i\epsilon} V_1(x''',z''',x^{iv},z^{iv},\omega_1) e^{iz'q_1} e^{iq_{\lambda_1}|z''-z'''|} e^{iz^{iv}q_2} \tag{56}$$

which becomes

$$\psi_s^{21}(k'_g,q'_1,k'_s,q'_2;\omega_1) = \left(\frac{1}{2\pi}\right)^5 \int dk_{\lambda_1} \frac{1}{2iq_{\lambda_1}} \int dx'dx''dz'dz''dx'''dx^{iv}dz'''dz^{iv} \int dk_g \delta(k_g-k'_g)$$
$$\times \int dk_s \delta(k_s-k'_s) \int dq_1 \delta(q'_1-q_1) \int dq_2 \delta(q'_2-q_2) V_1(x',z',x'',z'',\omega_1)$$
$$\times \frac{e^{-ix'k_g}e^{ix''k_{\lambda_1}}}{k_g^2+q_1^2-\frac{\omega_1^2}{c_0^2}-i\epsilon} \frac{e^{-ix'''k_{\lambda_1}}e^{ix^{iv}k_s}}{k_s^2+q_2^2-\frac{\omega_1^2}{c_0^2}-i\epsilon} V_1(x''',z''',x^{iv},z^{iv},\omega_1) e^{iz'q_1} e^{iq_{\lambda_1}|z''-z'''|} e^{iz^{iv}q_2} \tag{57}$$

or, after simplifying the delta functions and eliminating the primed notation on the wavenumbers,

$$\psi_s^{21}(k_g,q_1,k_s,q_2;\omega_1) = \frac{1}{2\pi} \int_{-\infty}^{\infty} dk_{\lambda_1} \frac{1}{2iq_{\lambda_1}} \int dx'dx''dz'dz''dx'''dx^{iv}dz'''dz^{iv} e^{iz'q_1} e^{iq_{\lambda_1}|z''-z'''|} e^{iz^{iv}q_2}$$
$$\times \frac{e^{-ix'k_g}e^{ix''k_{\lambda_1}}}{k_g^2+q_1^2-\frac{\omega_1^2}{c_0^2}-i\epsilon} \frac{e^{-ix'''k_{\lambda_1}}e^{ix^{iv}k_s}}{k_s^2+q_2^2-\frac{\omega_1^2}{c_0^2}-i\epsilon} V_1(x',z',x'',z'',\omega_1) V_1(x''',z''',x^{iv},z^{iv},\omega_1). \tag{58}$$

The integrals over x', x'', x''', x^{iv}, z' and z^{iv} are Fourier transform so we can further simplify into

$$\psi_s^{21}(k_g,q_1,k_s,q_2;\omega_1) = \frac{1}{4\pi i} \frac{1}{k_g^2+q_1^2-\frac{\omega_1^2}{c_0^2}-i\epsilon} \frac{1}{k_s^2+q_2^2-\frac{\omega_1^2}{c_0^2}-i\epsilon} \int dk_{\lambda_1} \frac{1}{q_{\lambda_1}} \int dz''$$
$$\times V_1(k_g,-q_1,-k_{\lambda_1},z'',\omega_1) \int dz''' e^{iq_{\lambda_1}|z''-z'''|} V_1(k_{\lambda_1},z''',-k_s,-q_2,\omega_1). \tag{59}$$

Next we use the Heaviside step function H to express the absolute values and write

$$e^{iq_{\lambda_1}|z''-z'|} = e^{iq_{\lambda_1}(z'-z'')} H(z'-z'') + e^{iq_{\lambda_1}(z''-z')} H(z''-z'). \tag{60}$$

Moreover we use the integral representation of H (reference)

$$H(z) = \lim_{\epsilon\to 0} \frac{1}{2\pi} \int_{-\infty}^{\infty} dp \frac{1}{i(p-i\epsilon)} e^{-ipz}. \tag{61}$$

With this, the expression of ψ_s^{21} becomes

$$\psi_s^{21}(k_g,q_1,k_s,q_2;\omega_1) = \frac{1}{4\pi i}\frac{1}{k_g^2+q_1^2-\frac{\omega_1^2}{c_0^2}-i\epsilon}\frac{1}{k_s^2+q_2^2-\frac{\omega_1^2}{c_0^2}-i\epsilon}\int dk_{\lambda_1}\frac{1}{q_{\lambda_1}}\int dz'' V_1(k_g,-q_1,-k_{\lambda_1},z'',\omega_1)$$
$$\times\left[\int dz''' e^{iq_{\lambda_1}(z''-z''')}\lim_{\epsilon\to 0}\frac{1}{2\pi}\int_{-\infty}^{\infty} dp\frac{1}{i(p-i\epsilon)}e^{-ip(z''-z''')}V_1(k_{\lambda_1},z''',-k_s,-q_2,\omega_1)\right.$$
$$\left.+\int dz''' e^{iq_{\lambda_1}(z'''-z'')}\lim_{\epsilon\to 0}\frac{1}{2\pi}\int_{-\infty}^{\infty} dp\frac{1}{i(p-i\epsilon)}e^{-ip(z'''-z'')}V_1(k_{\lambda_1},z''',-k_s,-q_2,\omega_1)\right] \tag{62}$$

Rearranging the order of integration and solving the Fourier transforms over dz'' and dz''' we find

$$\psi_s^{21}(k_g,q_1,k_s,q_2;\omega_1) = \frac{1}{8\pi^2 i}\frac{1}{k_g^2+q_1^2-\frac{\omega_1^2}{c_0^2}-i\epsilon}\frac{1}{k_s^2+q_2^2-\frac{\omega_1^2}{c_0^2}-i\epsilon}\int_{-\infty}^{\infty} dk_{\lambda_1}\frac{1}{q_{\lambda_1}}$$
$$\times\left[\lim_{\epsilon\to 0}\int_{-\infty}^{\infty} dp\frac{V_1(k_g,-q_1,-k_{\lambda_1},-q_{\lambda_1}+p,\omega_1)V_1(k_{\lambda_1},q_{\lambda_1}-p,-k_s,-q_2,\omega_1)}{i(p-i\epsilon)}\right.$$
$$\left.+\lim_{\epsilon\to 0}\int_{-\infty}^{\infty} dp\frac{V_1(k_g,-q_1,-k_{\lambda_1},q_{\lambda_1}-p,\omega_1)V_1(k_{\lambda_1},-q_{\lambda_1}+p,-k_s,-q_2,\omega_1)}{i(p-i\epsilon)}\right] \tag{63}$$

The two dp integrals can be separated into a principal value and a contribution from contour integrals around the pole $p=i\epsilon$. The portion of V_2 which depends on the principal value part of that integral, is not computable in terms of the data without specifying a model type. In conclusion we will exclude that part from the computation. The contribution from integrating around the contour integrals around the pole leads to

$$\psi_s^{21}(k_g,q_1,k_s,q_2;\omega_1) = \frac{1}{8\pi^2 i}\frac{1}{k_g^2+q_1^2-\frac{\omega_1^2}{c_0^2}-i\epsilon}\frac{1}{k_s^2+q_2^2-\frac{\omega_1^2}{c_0^2}-i\epsilon}\int_{-\infty}^{\infty} dk_{\lambda_1}\frac{1}{q_{\lambda_1}}$$
$$\times\left[\lim_{\epsilon\to 0}\int_{-\infty}^{\infty} dp\; i\pi\delta(p-i\epsilon)V_1(k_g,-q_1,-k_{\lambda_1},-q_{\lambda_1}+p,\omega_1)V_1(k_{\lambda_1},q_{\lambda_1}-p,-k_s,-q_2,\omega_1)\right.$$
$$\left.+\lim_{\epsilon\to 0}\int_{-\infty}^{\infty} dp\; i\pi\delta(p-i\epsilon)V_1(k_g,-q_1,-k_{\lambda_1},q_{\lambda_1}-p,\omega_1)V_1(k_{\lambda_1},-q_{\lambda_1}+p,-k_s,-q_2,\omega_1)\right] \tag{64}$$

or

$$\psi_s^{21}(k_g,q_1,k_s,q_2;\omega_1) = \frac{1}{8\pi}\frac{1}{k_g^2+q_1^2-\frac{\omega_1^2}{c_0^2}-i\epsilon}\frac{1}{k_s^2+q_2^2-\frac{\omega_1^2}{c_0^2}-i\epsilon}\int_{-\infty}^{\infty} dk_{\lambda_1}\frac{1}{q_{\lambda_1}}$$

$$\times [V_1(k_g, -q_1, -k_{\lambda_1}, -q_{\lambda_1}, \omega_1)V_1(k_{\lambda_1}, q_{\lambda_1}, -k_s, -q_2, \omega_1)$$
$$+V_1(k_g, -q_1, -k_{\lambda_1}, q_{\lambda_1}, \omega_1)V_1(k_{\lambda_1}, -q_{\lambda_1}, -k_s, -q_2, \omega_1)]\,. \tag{65}$$

Next we relate V_1 in vertical numbers q_1, q_2 and V_1 in vertical numbers q_g, q_s. As noted before, this leads to two sets of relationships between the sums of the vertical wavenumbers,

$$q_g + q_\lambda = q_1 + q_{\lambda_1} \tag{66}$$
$$q_\lambda - q_s = q_{\lambda_1} - q_2 \tag{67}$$

and

$$q_g - q_\lambda = q_1 - q_{\lambda_1} \tag{68}$$
$$q_\lambda + q_s = q_{\lambda_1} + q_2. \tag{69}$$

where

$$q_{\lambda_1} = \sqrt{\frac{\omega_1^2}{c_0^2} - k_\lambda^2}, \quad q_\lambda = \sqrt{\frac{\omega^2}{c_0^2} - k_\lambda^2}. \tag{70}$$

Each of the two sets of equations for the vertical wavenumbers has to be satisfied simultaneously. Notice that these equations provide a unique and consistent formula for ω_1, in terms of ω, which can be discovered by, for example, subtracting equations (66) and (67) and adding equations (68) and (69). The relationship is (see also equation (40))

$$q_g + q_s = q_1 + q_2, \tag{71}$$

which leads to (see Appendix 6 equation (152) and also Section 3)

$$\frac{\omega_1^2}{c_0^2} = \frac{\left[(q_g + q_s)^2 + k_g^2 + k_s^2\right]^2 - 4k_g^2 k_s^2}{4(q_g + q_s)^2}. \tag{72}$$

With this particular ω_1, equation (65) for ψ_s^{21} becomes

$$\psi_s^{21}(k_g, q_1, k_s, q_2; \omega_1) = \frac{1}{8\pi} \frac{1}{k_g^2 + q_1^2 - \frac{\omega_1^2}{c_0^2} - i\epsilon} \frac{1}{k_s^2 + q_2^2 - \frac{\omega_1^2}{c_0^2} - i\epsilon} \int dk_\lambda \frac{1}{q_{\lambda_1}}$$
$$\times [V_1(k_g, -q_g, -k_\lambda, -q_\lambda, \omega)V_1(k_\lambda, q_\lambda, -k_s, -q_s, \omega) + V_1(k_g, -q_g, -k_\lambda, q_\lambda, \omega)V_1(k_\lambda, -q_\lambda, -k_s, -q_2, \omega)]\,. \tag{73}$$

Next we plug in the expressions for V_1's in terms of the measured data. From equations (172), (173), (174) and (175) in Appendix 6 we have

$$V_1(k_g, -q_g, -k_\lambda, -q_\lambda, \omega) = -4q_g q_\lambda e^{iq_g z_g} e^{iq_\lambda z_s} D(k_g, k_\lambda, q_g + q_\lambda), \tag{74}$$

$$V_1(k_\lambda, q_\lambda, -k_s, -q_s, \omega) = 4q_\lambda q_s e^{-iq_\lambda z_g} e^{iq_s z_s} D(k_\lambda, k_s, -q_\lambda + q_s) \tag{75}$$

$$V_1(k_g, -q_g, -k_\lambda, q_\lambda, \omega) = 4q_g q_\lambda e^{iq_g z_g} e^{-iq_\lambda z_s} D(k_g, k_\lambda, q_g - q_\lambda) \tag{76}$$

and

$$V_1(k_\lambda, -q_\lambda, -k_s, -q_2, \omega) = -4q_\lambda q_s e^{iq_\lambda z_g} e^{iq_s z_s} D(k_\lambda, k_s, q_\lambda + q_s) \tag{77}$$

and so equation (73) becomes

$$\begin{aligned}\psi_s^{21}(k_g, q_1, k_s, q_2; \omega_1) = &-\frac{2q_g q_s}{\pi} \frac{e^{iq_g z_g}}{k_g^2 + q_1^2 - \frac{\omega_1^2}{c_0^2} - i\epsilon} \frac{e^{iq_s z_s}}{k_s^2 + q_2^2 - \frac{\omega_1^2}{c_0^2} - i\epsilon} \\ &\times \int_{-\infty}^{\infty} dk_\lambda \frac{q_\lambda^2}{q_{\lambda_1}} \Big[e^{iq_\lambda(z_s - z_g)} D(k_g, k_\lambda, q_g + q_\lambda) D(k_\lambda, k_s, -q_\lambda + q_s) \\ &+ e^{iq_\lambda(z_g - z_s)} D(k_g, k_\lambda, q_g - q_\lambda) D(k_\lambda, k_s, q_\lambda + q_s) \Big]. \end{aligned} \tag{78}$$

Similar to what is described in Appendix 6 we are going to separate the expression of ψ_s^{21} into an imaging part and an inversion part and use the former and discard the latter for our calculation of the second order wavefield at depth. To separate, we write the data terms as Fourier integrals over vertical wavenumbers as

$$D(k_g, k_\lambda, q_g + q_\lambda) = \int_{-\infty}^{\infty} dz_1 e^{iz_1(q_g + q_\lambda)} D(k_g, k_\lambda, z_1), \tag{79}$$

$$D(k_\lambda, k_s, -q_\lambda + q_s) = \int_{-\infty}^{\infty} dz_2 e^{iz_2(-q_\lambda + q_s)} D(k_\lambda, k_s, z_2) \tag{80}$$

$$D(k_g, k_\lambda, q_g - q_\lambda) = \int_{-\infty}^{\infty} dz_3 e^{iz_3(q_g - q_\lambda)} D(k_g, k_\lambda, z_3) \tag{81}$$

$$D(k_\lambda, k_s, q_\lambda + q_s) = \int_{-\infty}^{\infty} dz_4 e^{iz_4(q_\lambda + q_s)} D(k_\lambda, k_s, z_4), \tag{82}$$

and rewrite equation (78) as

$$\begin{aligned}\psi_s^{21}(k_g, q_1, k_s, q_2; \omega_1) = &-\frac{2q_g q_s}{\pi} \frac{e^{iq_g z_g}}{k_g^2 + q_1^2 - \frac{\omega_1^2}{c_0^2} - i\epsilon} \frac{e^{iq_s z_s}}{k_s^2 + q_2^2 - \frac{\omega_1^2}{c_0^2} - i\epsilon} \int_{-\infty}^{\infty} dk_\lambda \frac{q_\lambda^2}{q_{\lambda_1}} \\ &\Bigg[e^{iq_\lambda(z_s - z_g)} \int_{-\infty}^{\infty} dz_1 e^{iz_1(q_g + q_\lambda)} D(k_g, k_\lambda, z_1) \int_{-\infty}^{\infty} dz_2 e^{iz_2(-q_\lambda + q_s)} D(k_\lambda, k_s, z_2) \\ &+ e^{iq_\lambda(z_g - z_s)} \int_{-\infty}^{\infty} dz_3 e^{iz_3(q_g - q_\lambda)} D(k_g, k_\lambda, z_3) \int_{-\infty}^{\infty} dz_4 e^{iz_4(q_\lambda + q_s)} D(k_\lambda, k_s, z_4) \Bigg]. \end{aligned} \tag{83}$$

Depending on the relative position of the two pseudo-depths z_1, z_2, z_3 and z_4 we can further separate the last expression into

$$\psi_s^{21}(k_g,q_1,k_s,q_2;\omega_1) = -\frac{2q_gq_s}{\pi}\frac{e^{iq_gz_g}}{k_g^2+q_1^2-\frac{\omega_1^2}{c_0^2}-i\epsilon}\frac{e^{iq_sz_s}}{k_s^2+q_2^2-\frac{\omega_1^2}{c_0^2}-i\epsilon}\int_{-\infty}^{\infty}dk_\lambda\frac{q_\lambda^2}{q_{\lambda_1}}e^{iq_\lambda(z_s-z_g)}$$
$$\left[\int_{-\infty}^{\infty}dz_1e^{iz_1(q_g+q_\lambda)}D(k_g,k_\lambda,z_1)\int_{-\infty}^{\infty}dz_2e^{iz_2(-q_\lambda+q_s)}D(k_\lambda,k_s,z_2)\delta(z_2-z_1)\right.$$
$$+\int_{-\infty}^{\infty}dz_1e^{iz_1(q_g+q_\lambda)}D(k_g,k_\lambda,z_1)\int_{z_1+\epsilon}^{\infty}dz_2e^{iz_2(-q_\lambda+q_s)}D(k_\lambda,k_s,z_2)$$
$$\left.+\int_{-\infty}^{\infty}dz_1e^{iz_1(q_g+q_\lambda)}D(k_g,k_\lambda,z_1)\int_{-\infty}^{z_1-\epsilon}dz_2e^{iz_2(-q_\lambda+q_s)}D(k_\lambda,k_s,z_2)\right]$$
$$-\frac{2q_gq_s}{\pi}\frac{e^{iq_gz_g}}{k_g^2+q_1^2-\frac{\omega_1^2}{c_0^2}-i\epsilon}\frac{e^{iq_sz_s}}{k_s^2+q_2^2-\frac{\omega_1^2}{c_0^2}-i\epsilon}\int_{-\infty}^{\infty}dk_\lambda\frac{q_\lambda^2}{q_{\lambda_1}}e^{iq_\lambda(z_g-z_s)}$$
$$\left[\int_{-\infty}^{\infty}dz_3e^{iz_3(q_g-q_\lambda)}D(k_g,k_\lambda,z_3)\int_{-\infty}^{\infty}dz_4e^{iz_4(q_\lambda+q_s)}D(k_\lambda,k_s,z_4)\delta(z_3-z_4)\right.$$
$$+\int_{-\infty}^{\infty}dz_3e^{iz_3(q_g-q_\lambda)}D(k_g,k_\lambda,z_3)\int_{z_3+\epsilon}^{\infty}dz_4e^{iz_4(q_\lambda+q_s)}D(k_\lambda,k_s,z_4)$$
$$\left.+\int_{-\infty}^{\infty}dz_3e^{iz_3(q_g-q_\lambda)}D(k_g,k_\lambda,z_3)\int_{-\infty}^{z_3-\epsilon}dz_4e^{iz_4(q_\lambda+q_s)}D(k_\lambda,k_s,z_4)\right] \tag{84}$$

or, after solving the integral containing the delta function,

$$\psi_s^{21}(k_g,q_1,k_s,q_2;\omega_1) = -\frac{2q_gq_s}{\pi}\frac{e^{iq_gz_g}}{k_g^2+q_1^2-\frac{\omega_1^2}{c_0^2}-i\epsilon}\frac{e^{iq_sz_s}}{k_s^2+q_2^2-\frac{\omega_1^2}{c_0^2}-i\epsilon}\int_{-\infty}^{\infty}dk_\lambda\frac{q_\lambda^2}{q_{\lambda_1}}e^{iq_\lambda(z_s-z_g)}$$
$$\left[2\pi\int_{-\infty}^{\infty}dz_1e^{iz_1(q_g+q_s)}D(k_g,k_\lambda,z_1)D(k_\lambda,k_s,z_1)\right.$$
$$+\int_{-\infty}^{\infty}dz_1e^{iz_1(q_g+q_\lambda)}D(k_g,k_\lambda,z_1)\int_{z_1+\epsilon}^{\infty}dz_2e^{iz_2(-q_\lambda+q_s)}D(k_\lambda,k_s,z_2)$$
$$\left.+\int_{-\infty}^{\infty}dz_1e^{iz_1(q_g+q_\lambda)}D(k_g,k_\lambda,z_1)\int_{-\infty}^{z_1-\epsilon}dz_2e^{iz_2(-q_\lambda+q_s)}D(k_\lambda,k_s,z_2)\right]$$

$$
\begin{aligned}
&-\frac{2q_g q_s}{\pi}\frac{e^{iq_g z_g}}{k_g^2+q_1^2-\frac{\omega_1^2}{c_0^2}-i\epsilon}\frac{e^{iq_s z_s}}{k_s^2+q_2^2-\frac{\omega_1^2}{c_0^2}-i\epsilon}\int\limits_{-\infty}^{\infty}dk_\lambda\frac{q_\lambda^2}{q_{\lambda_1}}e^{iq_\lambda(z_g-z_s)}\\
&\Bigg[2\pi\int\limits_{-\infty}^{\infty}dz_3e^{iz_3(q_g+q_s)}D(k_g,k_\lambda,z_3)D(k_\lambda,k_s,z_3)\\
&+\int\limits_{-\infty}^{\infty}dz_3e^{iz_3(q_g-q_\lambda)}D(k_g,k_\lambda,z_3)\int\limits_{z_3+\epsilon}^{\infty}dz_4e^{iz_4(q_\lambda+q_s)}D(k_\lambda,k_s,z_4)\\
&+\int\limits_{-\infty}^{\infty}dz_3e^{iz_3(q_g-q_\lambda)}D(k_g,k_\lambda,z_3)\int\limits_{-\infty}^{z_3-\epsilon}dz_4e^{iz_4(q_\lambda+q_s)}D(k_\lambda,k_s,z_4)\Bigg].
\end{aligned}
\tag{85}
$$

As also noted in Appendix 6, the first term in each square bracket in equation (85) is similar to an amplitude corrector and it will be ignored in the following calculations. The second term in the first square bracket and the third in the second square bracket are similar to depth correctors (see e.g. Shaw (2005), Liu et al. (2006) Ramirez and Otnes (2007)). For the purpose of this paper we will only keep these (imaging) terms and arrive to our final expression

$$
\begin{aligned}
\psi_s^{21_{IM}}(k_g,q_1,k_s,q_2;\omega_1) &= -\frac{2q_g q_s}{\pi}\frac{e^{iq_g z_g}}{k_g^2+q_1^2-\frac{\omega_1^2}{c_0^2}-i\epsilon}\frac{e^{iq_s z_s}}{k_s^2+q_2^2-\frac{\omega_1^2}{c_0^2}-i\epsilon}\int\limits_{-\infty}^{\infty}dk_\lambda\frac{q_\lambda^2}{q_{\lambda_1}}\\
&\Bigg[e^{iq_\lambda(z_s-z_g)}\int\limits_{-\infty}^{\infty}dz_1e^{iz_1(q_g+q_\lambda)}D(k_g,k_\lambda,z_1)\int\limits_{z_1+\epsilon}^{\infty}dz_2e^{iz_2(-q_\lambda+q_s)}D(k_\lambda,k_s,z_2)\\
&+e^{iq_\lambda(z_g-z_s)}\int\limits_{-\infty}^{\infty}dz_3e^{iz_3(q_g-q_\lambda)}D(k_g,k_\lambda,z_3)\int\limits_{-\infty}^{z_3-\epsilon}dz_4e^{iz_4(q_\lambda+q_s)}D(k_\lambda,k_s,z_4)\Bigg],
\end{aligned}
\tag{86}
$$

in which the variables are related by the dispersion relationships

$$
k_g^2+q_1^2=\frac{\omega_1^2}{c_0^2}\quad k_s^2+q_2^2=\frac{\omega_1^2}{c_0^2} \tag{87}
$$

$$
k_g^2+q_g^2=\frac{\omega^2}{c_0^2}\quad k_s^2+q_s^2=\frac{\omega^2}{c_0^2} \tag{88}
$$

and

$$
\frac{\omega_1^2}{c_0^2}=\frac{\left[(q_g+q_s)^2+k_g^2+k_s^2\right]^2-4k_g^2k_s^2}{4(q_g+q_s)^2}. \tag{89}
$$

4.2 The calculation of ψ_s^{22}

For ψ_s^{22} the calculations are similar to the ones in Section 3 and we can find

$$\psi_s^{22}(k_g,q_1,k_s,q_2;\omega_1)=\frac{1}{k_g^2+q_1^2-\frac{\omega_1^2}{c_0^2}-i\epsilon}V_2(k_g,-q_1,-k_s,-q_2,\omega_1)\frac{1}{k_s^2+q_2^2-\frac{\omega_1^2}{c_0^2}-i\epsilon}. \tag{90}$$

It is again important to notice that the V_2 on the right is the 3-dimensional projection of the fully 5-dimensional V_2 operator. The independent variables on the right are k_g, k_s and q_1+q_2. With this in mind we write (see also Appendix 6)

$$V_2(k_g,-q_1,-k_s,-q_2,\omega_1)=\frac{1}{2\pi}\int_{-\infty}^{\infty}d(-q_g-q_s)\delta(q_g+q_s-q_1-q_2)V_2(k_g,-q_g,-k_s,-q_s,\omega). \tag{91}$$

This last equation leads to the same relationship between the sums of the vertical wavenumbers,

$$q_g+q_s=q_1+q_2, \tag{92}$$

which, in turn, allows us to calculate ω_1 in terms of ω as (see Appendix 6 equation (152))

$$\frac{\omega_1^2}{c_0^2}=\frac{\left[(q_g+q_s)^2+k_g^2+k_s^2\right]^2-4k_g^2k_s^2}{4(q_g+q_s)^2}. \tag{93}$$

Note that this value of ω_1 is consistent with the previous values obtained in the calculation of V_1 and ψ_s^1. With this particular ω_1, the equation for V_2 becomes

$$V_2(k_g,-q_1,-k_s,-q_2,\omega_1)=V_2(k_g,-q_g,-k_s,-q_s,\omega). \tag{94}$$

In this expression, consistent with our previous remarks, we will only use the imaging part of V_2 as calculated in equation (185) in Appendix 6

$$V_2^{IM}(k_g,-q_1,-k_s,-q_2,\omega_1)=V_2^{IM}(k_g,-q_g,-k_s,-q_s,\omega)=\frac{2q_gq_se^{i(q_gz_g+q_sz_s)}}{\pi}\int_{-\infty}^{\infty}dk_\lambda q_\lambda$$
$$\times\left[e^{iq_\lambda(z_s-z_g)}\int_{-\infty}^{\infty}dz_1e^{iz_1(q_g+q_\lambda)}D(k_g,k_\lambda,z_1)\int_{z_1+\epsilon}^{\infty}dz_2e^{iz_2(-q_\lambda+q_s)}D(k_\lambda,k_s,z_2)\right.$$
$$\left.+e^{iq_\lambda(z_g-z_s)}\int_{-\infty}^{\infty}dz_3e^{iz_3(q_g-q_\lambda)}D(k_g,k_\lambda,z_3)\int_{-\infty}^{z_3-\epsilon}dz_4e^{iz_4(q_\lambda+q_s)}D(k_\lambda,k_s,z_4)\right]. \tag{95}$$

The final expression for $\psi_s^{22_{IM}}$ is then

$$\psi_s^{22_{IM}}(k_g,q_1,k_s,q_2;\omega_1)=\frac{2}{\pi}\frac{q_gq_s}{k_g^2+q_1^2-\frac{\omega_1^2}{c_0^2}-i\epsilon}\frac{e^{i(q_gz_g+q_sz_s)}}{k_s^2+q_2^2-\frac{\omega_1^2}{c_0^2}-i\epsilon}\int_{-\infty}^{\infty}dk_\lambda q_\lambda$$

$$\times \left[e^{iq_\lambda(z_s-z_g)} \int_{-\infty}^{\infty} dz_1 e^{iz_1(q_g+q_\lambda)} D(k_g,k_\lambda,z_1) \int_{z_1+\epsilon}^{\infty} dz_2 e^{iz_2(-q_\lambda+q_s)} D(k_\lambda,k_s,z_2) \right.$$
$$\left. + e^{iq_\lambda(z_g-z_s)} \int_{-\infty}^{\infty} dz_3 e^{iz_3(q_g-q_\lambda)} D(k_g,k_\lambda,z_3) \int_{-\infty}^{z_3-\epsilon} dz_4 e^{iz_4(q_\lambda+q_s)} D(k_\lambda,k_s,z_4) \right]. \quad (96)$$

in which the variables are related by the dispersion relationships

$$k_g^2+q_1^2=\frac{\omega_1^2}{c_0^2}, \quad k_s^2+q_2^2=\frac{\omega_1^2}{c_0^2}, \quad (97)$$

$$k_g^2+q_g^2=\frac{\omega^2}{c_0^2}, \quad k_s^2+q_s^2=\frac{\omega^2}{c_0^2}, \quad k_\lambda^2+q_\lambda^2=\frac{\omega^2}{c_0^2} \quad (98)$$

and

$$\frac{\omega_1^2}{c_0^2}=\frac{\left[(q_g+q_s)^2+k_g^2+k_s^2\right]^2-4k_g^2k_s^2}{4(q_g+q_s)^2}. \quad (99)$$

4.3 Solution for ψ_s^{2IM}

Combining equations (86) and (96) we find

$$\psi_s^{2IM}(k_g,q_1,k_s,q_2;\omega_1)=\frac{2q_gq_s}{\pi}\frac{e^{iq_gz_g}}{k_g^2+q_1^2-\frac{\omega_1^2}{c_0^2}-i\epsilon}\frac{e^{iq_sz_s}}{k_s^2+q_2^2-\frac{\omega_1^2}{c_0^2}-i\epsilon}\int_{-\infty}^{\infty} dk_\lambda \frac{q_\lambda}{q_{\lambda_1}}(q_{\lambda_1}-q_\lambda)$$
$$\times \left[e^{iq_\lambda(z_s-z_g)} \int_{-\infty}^{\infty} dz_1 e^{iz_1(q_g+q_\lambda)} D(k_g,k_\lambda,z_1) \int_{z_1+\epsilon}^{\infty} dz_2 e^{iz_2(-q_\lambda+q_s)} D(k_\lambda,k_s,z_2) \right.$$
$$\left. + e^{iq_\lambda(z_g-z_s)} \int_{-\infty}^{\infty} dz_3 e^{iz_3(q_g-q_\lambda)} D(k_g,k_\lambda,z_3) \int_{-\infty}^{z_3-\epsilon} dz_4 e^{iz_4(q_\lambda+q_s)} D(k_\lambda,k_s,z_4) \right] \quad (100)$$

in which, again, the variables are related by the dispersion relationships

$$k_g^2+q_1^2=\frac{\omega_1^2}{c_0^2}, \quad k_s^2+q_2^2=\frac{\omega_1^2}{c_0^2}, \quad k_\lambda^2+q_{\lambda_1}^2=\frac{\omega_1^2}{c_0^2} \quad (101)$$

$$k_g^2+q_g^2=\frac{\omega^2}{c_0^2}, \quad k_s^2+q_s^2=\frac{\omega^2}{c_0^2}, \quad k_\lambda^2+q_\lambda^2=\frac{\omega^2}{c_0^2} \quad (102)$$

and

$$\frac{\omega_1^2}{c_0^2}=\frac{\left[(q_g+q_s)^2+k_g^2+k_s^2\right]^2-4k_g^2k_s^2}{4(q_g+q_s)^2}. \quad (103)$$

5 Imaging the wavefield at depth

Equation (18) provides a formula for the scattered wavefield everywhere inside or outside the actual medium

$$\psi_s = \psi_s^1 + \psi_s^2 + \psi_s^3 + \dots. \tag{104}$$

Plugging in the expressions we found for the first and second orders, ψ_s^1 and ψ_s^2, in equations (43) and (100) respectively, we find

$$\begin{aligned}
\psi_s^{2nd}(k_g, q_1, k_s, q_2; \omega_1) = & \frac{-4q_g q_s e^{iq_g z_g} e^{iq_s z_s}}{\left(k_g^2 + q_1^2 - \frac{\omega_1^2}{c_0^2} - i\epsilon\right)\left(k_s^2 + q_2^2 - \frac{\omega_1^2}{c_0^2} - i\epsilon\right)} \\
& \Bigg\{ D(k_g, z_g, k_s, z_s, \omega) + \frac{1}{2\pi} \int_{-\infty}^{\infty} dk_\lambda \frac{q_\lambda}{q_{\lambda_1}} (q_\lambda - q_{\lambda_1}) \\
& \times \Bigg[e^{iq_\lambda(z_s - z_g)} \int_{-\infty}^{\infty} dz_1 e^{iz_1(q_g + q_\lambda)} D(k_g, k_\lambda, z_1) \int_{z_1+\epsilon}^{\infty} dz_2 e^{iz_2(-q_\lambda + q_s)} D(k_\lambda, k_s, z_2) \\
& + e^{iq_\lambda(z_g - z_s)} \int_{-\infty}^{\infty} dz_3 e^{iz_3(q_g - q_\lambda)} D(k_g, k_\lambda, z_3) \int_{-\infty}^{z_3-\epsilon} dz_4 e^{iz_4(q_\lambda + q_s)} D(k_\lambda, k_s, z_4) \Bigg] \Bigg\}.
\end{aligned} \tag{105}$$

To image this wavefield we first transform it into the depth domain by inverse Fourier transforming over the vertical wavenumbers to obtain

$$\psi_s^{2nd}(k_g, k_s, z; \omega_1) = \int_{-\infty}^{\infty} dk_z \; e^{ik_z z} \psi_s^{2nd}(k_g, q_1, k_s, q_2; \omega_1) \tag{106}$$

where $k_z = q_1 + q_2$. Then we integrate over all temporal frequencies, which amounts in applying the imaging condition, to obtain

$$I(k_g, k_s, z) = \int_{-\infty}^{\infty} d\omega_1 \psi_s^{2nd}(k_g, k_s, z; \omega_1), \tag{107}$$

and finally we transform over the horizontal wavenumbers to obtain the image in the space domain

$$I(x, z) = \frac{1}{2\pi} \int_{-\infty}^{\infty} d(k_g - k_s) e^{-i(k_g - k_s)x} I(k_g, k_s, z). \tag{108}$$

6 Conclusions

In this report we describe an approach to calculating and imaging the wavefield at depth using the inverse scattering series. The method does not make any assumptions on the medium under

investigations and only inputs the recorded data on the measurement surface and a background acoustic Green's function. Roughly speaking, the method uses the calculated and task specific separated perturbation operator $\mathbf{V}$, in the forward scattering series, to calculate different orders of the scattered field at any depth. For an acoustic medium, the method was presented in Weglein et al. (2000) where the first order wavefield was calculated. Here we proceed without specifying an actual model type. The main results of this paper are the calculated first and second orders wavefield at depth, equations (43) and (100) respectively.

It is important to notice that the calculation of the second order wavefield at depth uses the formula (see equation (22))

$$\psi_s^2 = \mathbf{G_0 V_2 G_0} + \mathbf{G_0 V_1 G_0 V_1 G_0} \tag{109}$$

and hence $\mathbf{V_1}$ and $\mathbf{V_2}$ are required for the calculation (see theri calculated expressions in the Appendices). There are two important related choices that we made in this calculation and that are worth mentioning. First, instead of putting through the equation the full expression of $\mathbf{V_2}$, we separated it and determined just the piece which corrects for the wrong depth and used that part only. Second, consistently with the first choice, instead of using the full second term on the right side of the above equation for ψ_s^2 we, again, separated the term, determined the part which corrects for the wrong depth and used that part only. The motivation behind these choices is simple: the full expression of $\mathbf{V}$ will construct the full wavefield at depth, including primaries and multiples (as shown for example in Matson (1996)). Since what we are trying to construct is the image at depth of data containing primaries only, it was reasonable to assume that this will be achieved by the part in V which only corrects for depth. Further analytical and numerical examples will verify this hypothesis.

We emphasize one important conclusion that comes out of the two expressions of the first and second orders wavefield at depth. When using inverse scattering methods, the actual medium is assumed to be unknown and no a priori assumptions are made about its properties. As a consequence, calculating the wavefield at depth for one frequency requires all frequencies in the data. This is fundamentally different from well known migration algorithms, which assume the velocity profile of the medium can be a priori found, and which, hence, can extrapolate, at depth, each frequency individually (by performing a phase-shift in the wavenumber-frequency domain for example). This was originally noted in Weglein et al. (2000) for the first order of the acoustic wavefield at depth calculated using the inverse scattering series. Here we discovered the same characteristic for the wavefield at depth without a specified model type for both first and second order.

Acknowledgments

Bogdan G. Nita, Arthur B. Weglein and Adriana C. Ramirez were supported by the NSF-CMG award DMS-0327778 and the DOE Basic Energy Sciences award DE-FG02-05ER15697. The support of the M-OSRP sponsors is also gratefully acknowledged.

References

Aki, K. and P. G. Richards. *Quantitative Seismology.* 2nd edition. University Science Books, 2002.

Clayton, R. W. and R. H. Stolt. "A Born-WKBJ inversion method for acoustic reflection data." *Geophysics* 46 (1981): 1559–1567.

Liu, F., A. B. Weglein, K. A. Innanen, and B. G. Nita. "Multi-dimensional seismic imaging using the inverse scattering series." *Proceedings of the 76th Annual Meeting of the Society of Exploration Geophysicists, New Orleans, LA.* . Soc. Expl. Geophys., 2006.

Liu, F., A. B. Weglein, K. A. Innanen, B. G. Nita, and J. Zhang. "A comprehensive strategy for removing multiples and depth imaging primaries without subsurface information: Direct horizontal common image gathers without the velocity or "ironing"." *Proceedings of the 77th Annual Meeting of the Society of Exploration Geophysicists, San Antonio, TX.* . Soc. Expl. Geophys., 2007.

Liu, F., A.B. Weglein, K.A. Innanen, and B.G Nita. "Extension of the non-linear depth imaging capability of the inverse scattering series to multidimensional media: strategies and numerical results." 2005.

Matson, K. H. "The relationship between scattering theory and the primaries and multiples of reflection seismic data." *Journal of Seismic Exploration* 5 (1996): 63–78.

Nita, B. G., K. H. Matson, and A. B. Weglein. "Forward scattering series and seismic events: Far field approximations, critical and postcritical events." *SIAM Journal of Applied Mathematics* 64 (2004): 2167–2185.

Ramírez, A. C., B. G. Nita, A. B. Weglein, and E. Otnes. "Model type independent contributions in the inverse scattering series for processing primaries." *MOSRP06 Annual Report (this volume)* (2007).

Ramirez, A. C. and E. Otnes. "Forward scattering series for 2-parameter acoustic media: analysis and implications to the inverse scattering task-specific subseries." *Submitted to Commun. Comput. Phys.* (2007).

Shaw, S. A. "An inverse scattering sub-series for predicting the correct spatial location of reflectors: Initial analysis, testing and evaluation." *7th Internat. Conf. of the SBGf, Expanded Abstracts.* . 2001.

Shaw, S. A. "Cooperation of the leading order terms in an inverse scattering subseries for imaging: 1-D analysis and evaluation." *Proceedings of the 72nd Annual Meeting of the Society of Exploration Geophysicists, Salt Lake City, UT, USA.*. . Soc. Expl. Geophys., 2002.

Shaw, S. A. "Analytical and numerical examples of leading order imaging series." *8th Internat. Conf. of the SBGf, Expanded Abstracts.* . 2003.

Shaw, S. A. *An inverse scattering series algorithm for depth imaging of reflection data from a layered acoustic medium with an unknown velocity model*. PhD thesis, University of Houston, 2005.

Shaw, S. A. and A. B. Weglein. "Imaging seismic reflection data at the correct depth without specifying an accurate velocity model: Initial examples of an inverse scattering subseries." *Frontiers of remote sensing information processing*. Ed. C. H. Chen. World Scientific Publishing Company, 2003. chapter 21, 469–484.

Shaw, S. A., A. B. Weglein, D. J. Foster, K. H. Matson, and R. G. Keys. "Convergence properties of a leading order depth imaging series." *73rd Annual Internat. Mtg., Soc. Expl. Geophys., Expanded Abstracts*. . Soc. Expl. Geophys., 2003. 937–940.

Shaw, S. A., A. B. Weglein, D. J. Foster, K. H. Matson, and R. G. Keys. "Isolation of a leading order depth imaging series and analysis of its convergence properties." *Journal of Seismic Exploration* 2 (November 2004): 157–195.

Stolt, R. H. and A. B. Weglein. "Migration and inversion of seismic data." *Geophysics* 50 (1985): 2458–2472.

Taylor, J. R. *Scattering theory: the quantum theory of nonrelativistic collisions*. John Wiley & Sons, Inc., 1972.

Weglein, A. B., D. J. Foster, K. H. Matson, S. A. Shaw, P. M. Carvalho, and D. Corrigan. "An inverse-scattering sub-series for predicting the spatial location of reflectors without the precise reference medium and wave velocity." *71st Annual Internat. Mtg., Soc. Expl. Geophys., Expanded Abstracts*. . Soc. Expl. Geophys., 2001. 2108–2111.

Weglein, A. B., K. H. Matson, D. J. Foster, P. M. Carvalho, D. Corrigan, and S. A. Shaw. "Imaging and inversion at depth without a velocity model: theory, concepts and initial evaluation." *70th Annual Internat. Mtg., Soc. Expl. Geophys., Expanded Abstracts*. . Soc. Expl. Geophys., 2000. 1016–1019.

Weglein, A. B., B. G. Nita, K. A. Innanen, E. Otnes, S. A. Shaw, F. Liu, H. Zhang, A. C. Ramirez, J. Zhang, G. L. Pavlis, and C. Fan. "Using the inverse scattering series to predict the wavefield at depth and the transmitted wavefield without an assumption about the phase of the measured data or back propagation in the overburden." *Geophysics* 71 (2006): SI125–SI137.

Weglein, Arthur B., Fernanda V. Araújo, Paulo M. Carvalho, Robert H. Stolt, Kenneth H. Matson, Richard T. Coats, Dennis Corrigan, Douglas J. Foster, Simon A. Shaw, and Haiyan Zhang. "Inverse Scattering Series and Seismic Exploration." *Inverse Problems* (2003): R27–R83.

Weglein, Arthur B., Fernanda Araújo Gasparotto, Paulo M. Carvalho, and Robert H. Stolt. "An Inverse-Scattering Series Method for Attenuating Multiples in Seismic Reflection Data." *Geophysics* 62 (November-December 1997): 1975–1989.

Appendices

A. Green's function in an infinite homogeneous space

Consider the homogeneous acoustic wave equation (see also equation (10))

$$\nabla^2\phi(\mathbf{x},t) - \frac{1}{c_0^2}\frac{\partial^2\phi(\mathbf{x},t)}{\partial t^2} = -\delta(\mathbf{x})\delta(t) \tag{110}$$

where $\mathbf{x} = (x_g - x_s, z_g - z_s)$ is the vector connecting the source of the wave to the point where the wave is measured (the receiver) and where we assume that the source goes off at time $t = 0$. In the frequency domain, the solution to equation (110) in an infinite homogeneous space is (see e.g. Aki and Richards (2002))

$$\phi(\mathbf{x},\omega) = \frac{1}{R}e^{i\omega\left(\frac{R}{c_0}\right)} \tag{111}$$

where $R = |\mathbf{x}| = \sqrt{(x_g - x_s)^2 + (z_g - z_s)^2}$. This is the Green's function of the acoustic wave equation in an infinite homogeneous space and it is usually denoted by

$$G_0(x_g, z_g, x_s, z_s, \omega) = \frac{1}{R}e^{i\omega\left(\frac{R}{c_0}\right)} \tag{112}$$

In the following we will use ϕ and G_0 interchangeably.

In terms of its Fourier transform over all space coordinates, we can also write ϕ as

$$\phi(\mathbf{x},t) = \frac{1}{(2\pi)^2}\int_{-\infty}^{\infty}dk_x\int_{-\infty}^{\infty}dq\phi(\mathbf{k},t)e^{i\mathbf{k}\cdot\mathbf{x}} \tag{113}$$

where $\mathbf{k} = (k, q)$ is the wavenumber vector, with horizontal and vertical components, associated with $\mathbf{x}$. Notice that we also have

$$\nabla^2\phi(\mathbf{x},t) = \frac{1}{(2\pi)^2}\int_{-\infty}^{\infty}dk_x\int_{-\infty}^{\infty}dq\phi(\mathbf{k},t)(-k_x^2 - q^2)e^{i\mathbf{k}\cdot\mathbf{x}}, \tag{114}$$

$$-\frac{1}{c_0^2}\frac{\partial^2\phi(\mathbf{x},t)}{\partial t^2} = \frac{1}{(2\pi)^2}\int_{-\infty}^{\infty}dk_x\int_{-\infty}^{\infty}dq\phi(\mathbf{k},t)\frac{\omega^2}{c_0^2}e^{i\mathbf{k}\cdot\mathbf{x}} \tag{115}$$

and

$$-\delta(\mathbf{x}) = -\frac{1}{(2\pi)^2}\int_{-\infty}^{\infty}dk_x\int_{-\infty}^{\infty}dqe^{i\mathbf{k}\cdot\mathbf{x}}. \tag{116}$$

Putting these last three expressions back into equation (110) and transforming to frequency domain we find

$$\frac{1}{(2\pi)^2}\int_{-\infty}^{\infty}dk_x\int_{-\infty}^{\infty}dq\phi(\mathbf{k},\omega)\left(\frac{\omega^2}{c^2} - k^2 - q^2\right)e^{i\mathbf{k}\cdot\mathbf{x}} = -\frac{1}{(2\pi)^2}\int_{-\infty}^{\infty}dk_x\int_{-\infty}^{\infty}dqe^{i\mathbf{k}\cdot\mathbf{x}}. \tag{117}$$

By equating the integrands we find

$$G_0(k,q,\omega) = \phi(k,q,\omega) = \frac{1}{k^2+q^2-\frac{\omega^2}{c_0^2}}. \tag{118}$$

Then from (112) and the double inverse Fourier transform of (118)

$$G_0(x_g,z_g,x_s,z_s,\omega) = \frac{1}{R}e^{i\omega\left(\frac{R}{c_0}\right)} = \frac{1}{(2\pi)^2}\int_{-\infty}^{\infty}dk_x\int_{-\infty}^{\infty}dq\frac{e^{i\mathbf{k}\cdot\mathbf{x}}}{k^2+q^2-\frac{\omega^2}{c_0^2}}. \tag{119}$$

The first expression is a cylindrical wave propagating from the source to the receiver with speed c_0. The right side represents a superposition of planewaves over the entire range of wavenumbers k and q. These planewaves have the arbitrary velocity $\frac{\omega}{|\mathbf{k}|}$ which varies from 0 to ∞. In order to write the expression on the right as a superposition of planewaves traveling at the same speed c_0, we have to perform one of the integrations with respect to one of the two wavenumbers. We will do this over the vertical wavenumber q, then comment on this calculation to obtain equivalent forms for the Green's function.

The Weyl Integral form of the Green's function

To integrate the right side of equation (119) with respect to q we apply residue theorem. We complexify q and notice that the poles of the integrand are at

$$q = \pm\sqrt{\frac{\omega^2}{c_0^2}-k^2} \tag{120}$$

with some of them lying on the real q axis, i.e. along the integration path. To make the integrand analytic along the real q axis, a small attenuation is introduced through an imaginary part in the velocity c_0 (see Aki and Richards (2002)) so that the new velocity c_0^{new} is

$$\frac{1}{c_0^{new}} = \frac{1}{c_0} + i\varepsilon \tag{121}$$

with ε being a small parameter such that $\varepsilon > 0$ for $\omega > 0$. This attenuation effects in a shift of the poles away from the real q axis and into the first and the third quadrant in the complex q plane. We define the poles in the first quadrant as

$$q = +\sqrt{\frac{\omega^2}{c_0^2}-k^2} \tag{122}$$

and the poles in the third quadrant as

$$q = -\sqrt{\frac{\omega^2}{c_0^2}-k^2}. \tag{123}$$

Notice that in the first quadrant both the imaginary and the real part of q are positive, while in the third quadrant both the imaginary and the real part of q are negative. We now apply Cauchy's theorem to calculate the integral.

For positive $z_g - z_s$ a factor of $e^{iq(z_g - z_s)}$ will cancel the integrand if taken around a sufficiently large semicircle in the upper half complex q-plane. This implies that adding this semicircle to the integration path will not change the value of the integral and hence it can be used to close the integration path. Cauchy's theorem implies

$$\phi = P.V. + i\pi\delta\left(q - \sqrt{\frac{\omega^2}{c_0^2} - k^2}\right) = P.V. + \frac{e^{-i\omega t}}{2\pi}\int_{-\infty}^{\infty} dk_x \frac{e^{i[k(x_g - x_s) + iq(z_g - z_s)]}}{2iq}, \tag{124}$$

where k and q now satisfy the dispersion relation

$$k^2 + q^2 = \frac{\omega^2}{c_0^2}. \tag{125}$$

For negative $z_g - z_s$ the same factor $e^{iq(z_g - z_s)}$ will cancel the integrand if taken around a sufficiently large semicircle in the lower half complex q-plane. We add the semicircle to close the integration path and obtain, from Cauchy's theorem,

$$\phi = P.V + i\pi\delta\left(q + \sqrt{\frac{\omega^2}{c_0^2} - k^2}\right) = P.V. + \frac{e^{-i\omega t}}{2\pi}\int_{-\infty}^{\infty} dk_x \frac{e^{i[k(x_g - x_s) + iq(z_s - z_g)]}}{2iq}. \tag{126}$$

where, again, k and q satisfy the dispersion relation

$$k^2 + q^2 = \frac{\omega^2}{c_0^2}. \tag{127}$$

The results in equations (124) and (126) can be summarized in the Weyl integral

$$G(x_g, z_g, x_s, z_s; \omega) = P.V. + \frac{1}{2\pi}\int_{-\infty}^{\infty} dk_x \frac{e^{i[k(x_g - x_s) + iq|z_g - z_s|]}}{2iq} \tag{128}$$

where

$$q = \sqrt{\frac{\omega^2}{c_0^2} - k^2} \tag{129}$$

and the sign of q is chosen such that the $Im\ q > 0$.

In the history of the development of a model type independent internal multiple algorithm it was determined that the portion of V_2 which depends on the principal value part of the contribution from G_0 is not computable from surface data without assuming a model type. For this reason we will also ignore the principal value part of the Green's function and investigate the usefulness of a wavefield at depth formula derived by considering the model type independent part of V_2 only. The Green's function that we are going to use hence is

$$G(x_g, z_g, x_s, z_s; \omega) = \frac{1}{2\pi}\int_{-\infty}^{\infty} dk_x \frac{e^{i[k(x_g - x_s) + iq|z_g - z_s|]}}{2iq}. \tag{130}$$

An alternative formula for the Green's function

It is also useful to have an alternative expression for the Green's function, e.g. in the wavenumber / frequency domain. Recall from equation (118) that such a form is close to

$$G_0(k,q,\omega) = \frac{1}{k^2 + q^2 - \frac{\omega^2}{c_0^2}}. \tag{131}$$

However, because of the dispersion relations, which we now have to impose, and the poles located on the real q axis we have to rewrite it as

$$G_0(k,q,\omega) = \frac{1}{k^2 + q^2 - \frac{\omega^2}{c_0^2} - i\epsilon} \tag{132}$$

where the selection of $\pm\epsilon$ leads to a causal/anticausal Green's function (here chosen as causal) and where, as before,

$$q = \sqrt{\frac{\omega^2}{c_0^2} - k^2} \tag{133}$$

and the sign of q is chosen such that the $Im\ q > 0$. If we wanted to work with this form in the space domain we would have to double inverse Fourier transform over the horizontal and vertical wavenumbers and obtain

$$G(x_g, z_g, x_s, z_s; \omega) = \left(\frac{1}{2\pi}\right)^2 \int_{-\infty}^{\infty} dk \int_{-\infty}^{\infty} dq \frac{e^{-ik(x_g - x_s)} e^{-iq(z_g - z_s)}}{k^2 + q^2 - \frac{\omega^2}{c_0^2} - i\epsilon}. \tag{134}$$

It is worth mentioning, even though this does not appear explicitly, that this Green's function represents only the part equivalent to the $i\pi\delta$ contribution described by formula (130) and with the principal value discarded.

B. The calculation of V_1

Start with equation (24)

$$D = (\mathbf{G_0 V_1 G_0})_{ms} \tag{135}$$

where D is the data, G_0 is the Greens function of the reference medium and $V_1(x', z', x'', z'', \omega)$ is the first order component of the perturbation V. In coordinates, this equation can be written as

$$D(x_g, x_s, \omega) = \int dx' dx'' dz' dz'' G_0(x_g, z_g, x', z', \omega) V_1(x', z', x'', z'', \omega) G_0(x'', z'', x_s, z_s, \omega) \tag{136}$$

where x_g, z_g, x_s and z_s are the spatial coordinates of the source of the wave and the receiver used to record the data and where we have omitted the vertical coordinates arguments in the data since

they are fixed given numbers (not actual variables). In this equation we will use the following expressions for the Green's functions

$$G_0(x_g, z_g, x', z', \omega) = \frac{1}{2\pi} \int_{-\infty}^{\infty} dk_g \frac{e^{ik_g(x_g - x')} e^{iq_g|z' - z_g|}}{2iq_g} \tag{137}$$

and

$$G_0(x'', z'', x_s, z_s, \omega) = \frac{1}{2\pi} \int_{-\infty}^{\infty} dk_s \frac{e^{ik_s(x'' - x_s)} e^{iq_s|z'' - z_s|}}{2iq_s} \tag{138}$$

where k_g, q_g, k_s and q_s are the wavenumbers associated with x_g, z_g, x_s and z_s respectively and which satisfy the dispersion relations

$$k_g^2 + q_g^2 = \frac{\omega^2}{c_0^2}, \quad k_s^2 + q_s^2 = \frac{\omega^2}{c_0^2}. \tag{139}$$

Plugging these expressions of the Green's functions into equation (136) we find

$$D(x_g, x_s, \omega) = \int dx' dx'' dz' dz'' \frac{1}{2\pi} \int_{-\infty}^{\infty} dk_g \frac{e^{ik_g(x_g - x')} e^{iq_g|z' - z_g|}}{2iq_g} V_1(x', z', x'', z'', \omega) \frac{1}{2\pi} \int_{-\infty}^{\infty} dk_s \frac{e^{ik_s(x'' - x_s)} e^{iq_s|z'' - z_s|}}{2iq_s}. \tag{140}$$

Next we apply Fourier transforms on x_g and x_s, i.e. we apply, on both sides, the integral operators $\int_{-\infty}^{\infty} dx_g e^{-ik_g' x_g}$ and $\int_{-\infty}^{\infty} dx_s e^{ik_s' x_s}$ and obtain

$$\begin{aligned} D(k_g', k_s', \omega) = \frac{1}{2\pi} \int_{-\infty}^{\infty} dk_g \int_{-\infty}^{\infty} dx_g e^{-ix_g(k_g' - k_g)} \frac{1}{2\pi} \int_{-\infty}^{\infty} dk_s \int_{-\infty}^{\infty} dx_s e^{ix_s(k_s' - k_s)} \\ \times \int dx' dx'' dz' dz'' \frac{e^{-ik_g x'} e^{iq_g|z' - z_g|}}{2iq_g} V_1(x', z', x'', z'', \omega) \frac{e^{ik_s x''} e^{iq_s|z'' - z_s|}}{2iq_s} \end{aligned} \tag{141}$$

or

$$\begin{aligned} D(k_g', k_s', \omega) = \frac{1}{2\pi} \int_{-\infty}^{\infty} dk_g \delta(k_g' - k_g) \frac{1}{2\pi} \int_{-\infty}^{\infty} dk_s \delta(k_s' - k_s) \\ \times \int dx' dx'' dz' dz'' \frac{e^{-ik_g x'} e^{iq_g|z' - z_g|}}{2iq_g} V_1(x', z', x'', z'', \omega) \frac{e^{ik_s x''} e^{iq_s|z'' - z_s|}}{2iq_s} \end{aligned} \tag{142}$$

After solving the first two integrals and changing the notation for the wavenumbers from prime to non primed quantities (for simplicity) we obtain

$$D(k_g, k_s, \omega) = \int dx' dx'' dz' dz'' \frac{e^{-ik_g x'} e^{iq_g|z' - z_g|}}{2iq_g} V_1(x', z', x'', z'', \omega) \frac{e^{ik_s x''} e^{iq_s|z'' - z_s|}}{2iq_s} \tag{143}$$

and, after factoring and additional assumption that $z' > z_g$ and $z' > z_s$ (which is reasonable since the depth of the scatterer is always larger than the depth of the sources and receivers in a surface seismic experiment and when the positive z-axis points downward), we find

$$D(k_g, k_s, \omega) = \frac{e^{-iq_g z_g} e^{-iq_s z_s}}{-4q_g q_s} \int dx' dx'' dz' dz'' e^{iz' q_g} e^{iq_s z''} e^{-ix' k_g} e^{ik_s x''} V_1(x', z', x'', z'', \omega), \tag{144}$$

and finally

$$D(k_g, k_s, \omega) = \frac{e^{-iq_g z_g} e^{-iq_s z_s}}{-4q_g q_s} V_1(k_g, -q_g, -k_s, -q_s, \omega). \tag{145}$$

From here we can calculate V_1 in the wavenumbers domain to be

$$V_1(k_g, -q_g, -k_s, -q_s, \omega) = -4q_g q_s e^{iq_g z_g} e^{iq_s z_s} D(k_g, k_s, \omega). \tag{146}$$

C. Relation between ω_1 and ω

Here we show how we can calculate ω_1 in terms of ω such that equation (40)

$$q_g + q_s = q_1 + q_2, \tag{147}$$

is satisfied. Squaring both sides of

$$q_g + q_s = \sqrt{\frac{\omega_1^2}{c_0^2} - k_g^2} + \sqrt{\frac{\omega_1^2}{c_0^2} - k_s^2} \tag{148}$$

we find, after rearranging terms,

$$(q_g + q_s)^2 + k_g^2 + k_s^2 - 2\frac{\omega_1^2}{c_0^2} = 2\sqrt{\left(\frac{\omega_1^2}{c_0^2} - k_g^2\right)\left(\frac{\omega_1^2}{c_0^2} - k_s^2\right)}. \tag{149}$$

After squaring one more time we find

$$\left[(q_g + q_s)^2 + k_g^2 + k_s^2 - 2\frac{\omega_1^2}{c_0^2}\right]^2 = 4\left(\frac{\omega_1^2}{c_0^2} - k_g^2\right)\left(\frac{\omega_1^2}{c_0^2} - k_s^2\right) \tag{150}$$

or, after some cancellations,

$$\left[(q_g + q_s)^2 + k_g^2 + k_s^2\right]^2 - 4\frac{\omega_1^2}{c_0^2}(q_g + q_s)^2 = 4k_g^2 k_s^2. \tag{151}$$

From here we obtain

$$\frac{\omega_1^2}{c_0^2} = \frac{\left[(q_g + q_s)^2 + k_g^2 + k_s^2\right]^2 - 4k_g^2 k_s^2}{4(q_g + q_s)^2} \tag{152}$$

which is the desired formula.

D. The calculation and separation of V_2

Start with equation (25)

$$0 = (\mathbf{G_0 V_2 G_0} + \mathbf{G_0 V_1 G_0 V_1 G_0})_{ms} \tag{153}$$

or

$$(-\mathbf{G_0 V_1 G_0 V_1 G_0})_{ms} = (\mathbf{G_0 V_2 G_0})_{ms}. \tag{154}$$

For the right hand-side of equation (154) we find similarly to the calculation of V_1 (see equation (145))

$$RHS = G_0 V_2 G_0 = \frac{e^{-i(q_g z_g + q_s z_s)}}{-4 q_g q_s} V_2(k_g, -q_g, -k_s, -q_s, \omega), \tag{155}$$

where, as before, k_g, q_g, k_s and q_s are the wavenumbers associated with x_g, z_g, x_s and z_s (source and receiver coordinates) respectively and which satisfy the dispersion relations

$$k_g^2 + q_g^2 = \frac{\omega^2}{c_0^2}, \quad k_s^2 + q_s^2 = \frac{\omega^2}{c_0^2}. \tag{156}$$

The left hand-side of equation (154) is

$$\begin{aligned} LHS = -(\mathbf{G_0 V_1 G_0 V_1 G_0}) = -\int dx' dx'' dz' dz'' G_0(x_g, z_g, x', z', \omega) V_1(x', x'', z', dz'', \omega) \\ \times \int dx''' dx^{iv} dz''' dz^{iv} G_0(x'', z'', x''', z''', \omega) V_1(x''', x^{iv}, z''', dz^{iv}, \omega) G_0(x^{iv}, z^{iv}, x_s, z_s, \omega) \end{aligned} \tag{157}$$

where the Green's functions are (see Appendix 6)

$$G_0(x_g, z_g, x', z', \omega) = \frac{1}{2\pi} \int_{-\infty}^{\infty} dk_g \frac{e^{ik_g(x_g - x')} e^{iq_g|z' - z_g|}}{2iq_g}, \tag{158}$$

$$G_0(x'', z'', x''', z''', \omega) = \frac{1}{2\pi} \int_{-\infty}^{\infty} dk_\lambda \frac{e^{ik_\lambda(x'' - x''')} e^{iq_\lambda|z''' - z''|}}{2iq_\lambda} \tag{159}$$

and

$$G_0(x^{iv}, z^{iv}, x_s, z_s, \omega) = \frac{1}{2\pi} \int_{-\infty}^{\infty} dk_s \frac{e^{ik_s(x^{iv} - x_s)} e^{iq_s|z^{iv} - z_s|}}{2iq_s}. \tag{160}$$

Plugging these expressions into equation (157) and then Fourier transforming it over x_g and x_s (i.e. applying on both sides the integral operators $\int_{-\infty}^{\infty} dx_g e^{-ik_g x_g}$ and $\int_{-\infty}^{\infty} dx_s e^{ik_s x_s}$) we find

$$LHS = \frac{e^{-i(q_g z_g + q_s z_s)}}{16\pi i q_g q_s} \int dk_\lambda \frac{1}{q_\lambda} \int dz'' dz''' e^{iq_\lambda|z'' - z'''|} V_1(k_g, -q_g, -k_\lambda, z'', \omega) V_1(k_\lambda, z''', -k_s, -q_s, \omega). \tag{161}$$

Next we use the Heaviside step function H to express the absolute values and write

$$e^{iq_\lambda|z''-z'''|} = e^{iq_\lambda(z''-z''')}H(z''-z''') + e^{iq_\lambda(z'''-z'')}H(z'''-z''). \tag{162}$$

Moreover we use the integral representation of H (reference)

$$H(z) = \lim_{\epsilon\to 0}\frac{1}{2\pi}\int_{-\infty}^{\infty} dp \frac{1}{i(p-i\epsilon)}e^{-ipz}. \tag{163}$$

With these considerations, the LHS term becomes

$$LHS = \frac{1}{2\pi}\frac{e^{-iq_g z_g}e^{-iq_s z_s}}{8iq_g q_s}\int dk_\lambda \frac{1}{q_\lambda}\int dz''dz''' V_1(k_g,-q_g,-k_\lambda,z'',\omega)V_1(k_\lambda,z''',-k_s,-q_s,\omega)$$
$$\times\left(e^{iq_\lambda(z''-z''')}\lim_{\epsilon\to 0}\frac{1}{2\pi}\int_{-\infty}^{\infty} dp\frac{1}{i(p-i\epsilon)}e^{-ip(z''-z''')} + e^{iq_\lambda(z'''-z'')}\lim_{\epsilon\to 0}\frac{1}{2\pi}\int_{-\infty}^{\infty} dp\frac{1}{i(p-i\epsilon)}e^{-ip(z'''-z'')}\right) \tag{164}$$

or

$$\begin{aligned} LHS = \left(\frac{1}{2\pi}\right)^2 \frac{e^{-iq_g z_g}e^{-iq_s z_s}}{8iq_g q_s}\Bigg[&\int dk_\lambda \frac{1}{q_\lambda}\lim_{\epsilon\to 0}\int dp\frac{1}{i(p-i\epsilon)}\int dz''dz''' \\ &\times e^{iq_\lambda(z''-z''')}e^{-ip(z''-z''')}V_1(k_g,-q_g,-k_\lambda,z'',\omega)V_1(k_\lambda,z''',-k_s,-q_s,\omega) \\ &+\int dk_\lambda \frac{1}{q_\lambda}\lim_{\epsilon\to 0}\int dp\frac{1}{i(p-i\epsilon)}\int dz''dz''' \\ &\times e^{iq_\lambda(z'''-z'')}e^{-ip(z'''-z'')}V_1(k_g,-q_g,-k_\lambda,z'',\omega)V_1(k_\lambda,z''',-k_s,-q_s,\omega)\Bigg]. \end{aligned} \tag{165}$$

Next we treat the dz' and dz'' integrals as Fourier transforms and obtain

$$\begin{aligned} LHS = \left(\frac{1}{2\pi}\right)^2 &\frac{e^{-iq_g z_g}e^{-iq_s z_s}}{8iq_g q_s} \\ &\times\Bigg[\int_{-\infty}^{\infty} dk_\lambda \frac{1}{q_\lambda}\lim_{\epsilon\to 0}\int_{-\infty}^{\infty} dp\frac{V_1(k_g,-q_g,-k_\lambda,-q_\lambda+p,\omega)V_1(k_\lambda,q_\lambda-p,-k_s,-q_s,\omega)}{i(p-i\epsilon)} \\ &+\int_{-\infty}^{\infty} dk_\lambda \frac{1}{q_\lambda}\lim_{\epsilon\to 0}\int_{-\infty}^{\infty} dp\frac{V_1(k_g,-q_g,-k_\lambda,q_\lambda-p,\omega)V_1(k_\lambda,-q_\lambda+p,-k_s,-q_s,\omega)}{i(p-i\epsilon)}\Bigg] \end{aligned} \tag{166}$$

The two dp integrals can be separated into a principal value and a contribution from contour integrals around the pole $p = i\epsilon$. The portion of V_2 which depends on the principal value part of that integral, is not computable in terms of the data without specifying a model type. In conclusion we will exclude that part from the computation. The contribution from integrating around the contour integrals around the pole leads to

$$LHS = \left(\frac{1}{2\pi}\right)^2 \frac{e^{-iq_g z_g}e^{-iq_s z_s}}{8iq_g q_s}$$

$$\times \left[\int dk_\lambda \frac{1}{q_\lambda} \lim_{\epsilon \to 0} \int dp \; i\pi\delta(p - i\epsilon) V_1(k_g, -q_g, -k_\lambda, -q_\lambda + p, \omega) V_1(k_\lambda, q_\lambda - p, -k_s, -q_s, \omega) \right.$$
$$\left. + \int dk_\lambda \frac{1}{q_\lambda} \lim_{\epsilon \to 0} \int dp \; i\pi\delta(p - i\epsilon) V_1(k_g, -q_g, -k_\lambda, q_\lambda - p, \omega) V_1(k_\lambda, -q_\lambda + p, -k_s, -q_s, \omega) \right] \quad (167)$$

or

$$LHS = \frac{1}{4\pi} \frac{e^{-iq_g z_g} e^{-iq_s z_s}}{8 q_g q_s} \int dk_\lambda \frac{1}{q_\lambda} \left[V_1(k_g, -q_g, -k_\lambda, -q_\lambda, \omega) V_1(k_\lambda, q_\lambda, -k_s, -q_s, \omega) \right.$$
$$\left. + V_1(k_g, -q_g, -k_\lambda, q_\lambda, \omega) V_1(k_\lambda, -q_\lambda, -k_s, -q_s, \omega) \right]. \quad (168)$$

Next, we relate V_1 to the data. From equation (146) obtained in Appendix 6 we have

$$V_1(k_g, -q_g, -k_s, -q_s, \omega) = -4 q_g q_s e^{iq_g z_g} e^{iq_s z_s} D(k_g, k_s, \omega). \quad (169)$$

To avoid confusion we will relate the temporal frequency ω with the sum of the vertical wavenumbers and write

$$V_1(k_g, -q_g, -k_s, -q_s, \omega) = -4 q_g q_s e^{iq_g z_g} e^{iq_s z_s} D(k_g, k_s, q_g + q_s). \quad (170)$$

To calculate the first V_1 in the equation (168) we write

$$V_1(k_g, -q_g, x, z, \omega) = \frac{1}{2\pi} \int d(-k_s) e^{-i(-k_s)x} \frac{1}{2\pi} \int d(-q_s) e^{i(-q_s)z} V_1(k_g, -q_g, -k_s, -q_s, \omega), \quad (171)$$

and then

$$V_1(k_g, -q_g, -k_\lambda, -q_\lambda, \omega) = \int dx e^{i(-k_\lambda)x} \int dz e^{-i(-q_\lambda)z} V_1(k_g, -q_g, x, z, \omega)$$
$$= \int dx e^{i(-k_\lambda)x} \int dz e^{-i(-q_\lambda)z} \frac{1}{2\pi} \int d(-k_s) e^{-i(-k_s)x} \frac{1}{2\pi} \int d(-q_s) e^{i(-q_s)z} V_1(k_g, -q_g, -k_s, -q_s, \omega)$$
$$= \frac{1}{2\pi} \int d(-k_s) \delta(k_s - k_\lambda) \frac{1}{2\pi} \int d(-q_s) \delta(q_s - q_\lambda) \left[-4 q_g q_s e^{iq_g z_g} e^{iq_s z_s} D(k_g, k_s, q_g + q_s) \right]$$
$$= -4 q_g q_\lambda e^{iq_g z_g} e^{iq_\lambda z_s} D(k_g, k_\lambda, q_g + q_\lambda). \quad (172)$$

Similarly we find

$$V_1(k_\lambda, q_\lambda, -k_s, -q_s, \omega) = 4 q_\lambda q_s e^{-iq_\lambda z_g} e^{iq_s z_s} D(k_\lambda, k_s, -q_\lambda + q_s), \quad (173)$$

$$V_1(k_g, -q_g, -k_\lambda, q_\lambda, \omega) = 4 q_g q_\lambda e^{iq_g z_g} e^{-iq_\lambda z_s} D(k_g, k_\lambda, q_g - q_\lambda) \quad (174)$$

and

$$V_1(k_\lambda, -q_\lambda, -k_s, -q_s, \omega) = -4 q_\lambda q_s e^{iq_\lambda z_g} e^{iq_s z_s} D(k_\lambda, k_s, q_\lambda + q_s). \quad (175)$$

With these expressions, equation (168) becomes

$$LHS = -\frac{1}{2\pi} \int dk_\lambda q_\lambda \left[e^{iq_\lambda (z_s - z_g)} D(k_g, k_\lambda, q_g + q_\lambda) D(k_\lambda, k_s, -q_\lambda + q_s) \right.$$
$$\left. + e^{iq_\lambda (z_g - z_s)} D(k_g, k_\lambda, q_g - q_\lambda) D(k_\lambda, k_s, q_\lambda + q_s) \right]. \quad (176)$$

To separate this expression into imaging-only and inversion-only parts we write all data terms as Fourier integrals over vertical wavenumbers as

$$D(k_g, k_\lambda, q_g + q_\lambda) = \int dz_1 e^{iz_1(q_g+q_\lambda)} D(k_g, k_\lambda, z_1), \tag{177}$$

$$D(k_\lambda, k_s, -q_\lambda + q_s) = \int dz_2 e^{iz_2(-q_\lambda+q_s)} D(k_\lambda, k_s, z_2) \tag{178}$$

$$D(k_g, k_\lambda, q_g - q_\lambda) = \int dz_3 e^{iz_3(q_g-q_\lambda)} D(k_g, k_\lambda, z_3) \tag{179}$$

$$D(k_\lambda, k_s, q_\lambda + q_s) = \int dz_4 e^{iz_4(q_\lambda+q_s)} D(k_\lambda, k_s, z_4), \tag{180}$$

then we rewrite equation (176) as

$$\begin{aligned} LHS = -\frac{1}{2\pi} \int dk_\lambda q_\lambda \Bigg[& e^{iq_\lambda(z_s-z_g)} \int dz_1 e^{iz_1(q_g+q_\lambda)} D(k_g, k_\lambda, z_1) \int dz_2 e^{iz_2(-q_\lambda+q_s)} D(k_\lambda, k_s, z_2) \\ & + e^{iq_\lambda(z_g-z_s)} \int dz_3 e^{iz_3(q_g-q_\lambda)} D(k_g, k_\lambda, z_3) \int dz_4 e^{iz_4(q_\lambda+q_s)} D(k_\lambda, k_s, z_4) \Bigg]. \end{aligned} \tag{181}$$

Depending on the relative position of the two pseudo-depths z_1, z_2, z_3 and z_4 we can further separate the last expression into

$$\begin{aligned} LHS = & -\frac{1}{2\pi} \int dk_\lambda q_\lambda e^{iq_\lambda(z_s-z_g)} \\ & \Bigg[\int_{-\infty}^{\infty} dz_1 e^{iz_1(q_g+q_\lambda)} D(k_g, k_\lambda, z_1) \int_{-\infty}^{\infty} dz_2 e^{iz_2(-q_\lambda+q_s)} D(k_\lambda, k_s, z_2) \delta(z_2 - z_1) \\ & + \int_{-\infty}^{\infty} dz_1 e^{iz_1(q_g+q_\lambda)} D(k_g, k_\lambda, z_1) \int_{z_1+\epsilon}^{\infty} dz_2 e^{iz_2(-q_\lambda+q_s)} D(k_\lambda, k_s, z_2) \\ & + \int_{-\infty}^{\infty} dz_1 e^{iz_1(q_g+q_\lambda)} D(k_g, k_\lambda, z_1) \int_{-\infty}^{z_1-\epsilon} dz_2 e^{iz_2(-q_\lambda+q_s)} D(k_\lambda, k_s, z_2) \Bigg] \\ & - \frac{1}{4\pi} \int_{-\infty}^{\infty} dk_\lambda q_\lambda e^{iq_\lambda(z_g-z_s)} \\ & \Bigg[\int_{-\infty}^{\infty} dz_3 e^{iz_3(q_g-q_\lambda)} D(k_g, k_\lambda, z_3) \int_{-\infty}^{\infty} dz_4 e^{iz_4(q_\lambda+q_s)} D(k_\lambda, k_s, z_4) \delta(z_3 - z_4) \\ & + \int_{-\infty}^{\infty} dz_3 e^{iz_3(q_g-q_\lambda)} D(k_g, k_\lambda, z_3) \int_{z_3+\epsilon}^{\infty} dz_4 e^{iz_4(q_\lambda+q_s)} D(k_\lambda, k_s, z_4) \end{aligned}$$

$$+\int_{-\infty}^{\infty} dz_3 e^{iz_3(q_g-q_\lambda)} D(k_g,k_\lambda,z_3) \int_{-\infty}^{z_3-\epsilon} dz_4 e^{iz_4(q_\lambda+q_s)} D(k_\lambda,k_s,z_4)\Bigg] \tag{182}$$

or, after solving the integrals containing the delta function,

$$\begin{aligned} LHS = &-\frac{1}{2\pi}\int_{-\infty}^{\infty} dk_\lambda q_\lambda e^{iq_\lambda(z_s-z_g)} \Bigg[2\pi \int_{-\infty}^{\infty} dz_1 e^{iz_1(q_g+q_s)} D(k_g,k_\lambda,z_1) D(k_\lambda,k_s,z_1) \\ &+\int_{-\infty}^{\infty} dz_1 e^{iz_1(q_g+q_\lambda)} D(k_g,k_\lambda,z_1) \int_{z_1+\epsilon}^{\infty} dz_2 e^{iz_2(-q_\lambda+q_s)} D(k_\lambda,k_s,z_2) \\ &+\int_{-\infty}^{\infty} dz_1 e^{iz_1(q_g+q_\lambda)} D(k_g,k_\lambda,z_1) \int_{-\infty}^{z_1-\epsilon} dz_2 e^{iz_2(-q_\lambda+q_s)} D(k_\lambda,k_s,z_2)\Bigg] \\ &-\frac{1}{4\pi}\int_{-\infty}^{\infty} dk_\lambda q_\lambda e^{iq_\lambda(z_g-z_s)} \Bigg[2\pi \int_{-\infty}^{\infty} dz_3 e^{iz_3(q_g+q_s)} D(k_g,k_\lambda,z_3) D(k_\lambda,k_s,z_3) \\ &+\int_{-\infty}^{\infty} dz_3 e^{iz_3(q_g-q_\lambda)} D(k_g,k_\lambda,z_3) \int_{z_3+\epsilon}^{\infty} dz_4 e^{iz_4(q_\lambda+q_s)} D(k_\lambda,k_s,z_4) \\ &+\int_{-\infty}^{\infty} dz_3 e^{iz_3(q_g-q_\lambda)} D(k_g,k_\lambda,z_3) \int_{-\infty}^{z_3-\epsilon} dz_4 e^{iz_4(q_\lambda+q_s)} D(k_\lambda,k_s,z_4)\Bigg]. \end{aligned} \tag{183}$$

The first term in each square bracket in equation (183) is similar to an amplitude corrector (see e.g. Shaw (2005)) and it will be ignored for the purpose of this paper. The second term in the first square bracket and the third in the second square bracket are similar to depth correctors (see e.g. Shaw (2005), Liu et al. (2006) Ramirez and Otnes (2007)). For the purpose of this paper we will only keep these (imaging) terms and arrive to our final expression

$$\begin{aligned} LHS = &-\frac{1}{2\pi}\int dk_\lambda q_\lambda \Bigg[e^{iq_\lambda(z_s-z_g)} \int_{-\infty}^{\infty} dz_1 e^{iz_1(q_g+q_\lambda)} D(k_g,k_\lambda,z_1) \int_{z_1+\epsilon}^{\infty} dz_2 e^{iz_2(-q_\lambda+q_s)} D(k_\lambda,k_s,z_2) \\ &+e^{iq_\lambda(z_g-z_s)} \int_{-\infty}^{\infty} dz_3 e^{iz_3(q_g-q_\lambda)} D(k_g,k_\lambda,z_3) \int_{-\infty}^{z_3-\epsilon} dz_4 e^{iz_4(q_\lambda+q_s)} D(k_\lambda,k_s,z_4)\Bigg]. \end{aligned} \tag{184}$$

Combining equations (155) and (184) we find the imaging part of V_2 to be

$$V_2^{IM}(k_g,-q_g,-k_s,-q_s,\omega) = \frac{2q_g q_s e^{i(q_g z_g+q_s z_s)}}{\pi} \int_{-\infty}^{\infty} dk_\lambda q_\lambda$$

$$\times \left[e^{iq_\lambda(z_s-z_g)} \int_{-\infty}^{\infty} dz_1 e^{iz_1(q_g+q_\lambda)} D(k_g,k_\lambda,z_1) \int_{z_1+\epsilon}^{\infty} dz_2 e^{iz_2(-q_\lambda+q_s)} D(k_\lambda,k_s,z_2) \right.$$

$$\left. + e^{iq_\lambda(z_g-z_s)} \int_{-\infty}^{\infty} dz_3 e^{iz_3(q_g-q_\lambda)} D(k_g,k_\lambda,z_3) \int_{-\infty}^{z_3-\epsilon} dz_4 e^{iz_4(q_\lambda+q_s)} D(k_\lambda,k_s,z_4) \right] . \quad (185)$$

Progressing 1D elastic media imaging using inverse scattering series: analytical PP-data preparation and constant velocity migration

S. Jiang, F. Liu, J. Zhang, and A. B. Weglein

Abstract

In this report, considering a 1D two-interface elastic media with three parameters, we present an analytic expression for PP-data and the migration result by constant velocity of reference media, which is a preliminary step for the eventual evaluation of 1D elastic media imaging independent of velocity by utilizing the inverse scattering series. The reflection and transmission coefficients of the PP-data are calculated using Zoeppritz' equations and only considering reflected primaries of compressional waves. We present the PP-data in the frequency domain, Fourier transform it to the time domain, and migrate it to the pseudo-depth domain with a constant velocity of the reference media. In all of the three domains, the reflection and transmission coefficients all depend on the angles of the incident wave. The numerical evaluation of the migrated PP-data in the pseudo-depth domain shows that the pseudo-depth of the second reflector in the PP-data changes with variation of the incident angle. The transformation of the data by a constant velocity migration to the pseudo-depth domain is in anticipation of the process performed on the measured data in the 1^{st} equation of the inverse scattering series. The analytic expressions of PP-data reported in this paper provide a valuable perspective and basis for further development of both velocity-independent imaging and non-linear AVO for 1D elastic multi-parameter media, and further value for synthetic generation of the other three data components: PS-data, SP-data and SS-data.

1 Introduction

In seismic exploration, the objective is to determine subsurface earth properties from the recorded wavefield generated from a man-made source of energy on or near the surface of the earth, that goes through and is reflected back from the subsurface. The quality of the recorded data, i.e. the wave field, plays a very important role in the location and delineation of subsurface targets, and in estimating the type and extent of rock and fluid properties for their hydrocarbon potential. But current depth imaging algorithms, one of the standard steps in seismic exploration, have limited ability in capturing the exact depth of subsurface structure of the earth in geologically complex areas where exact or well approximated velocity models are hard to access.

The inverse scattering theory and hence the inverse scattering series is a comprehensive theory and a multi-dimensional direct inversion procedure to directly achieve seismic processing objectives step by step *without a priori knowledge* of the subsurface of the earth (Weglein et al., 2000, 2003). As a result, it has the potential of avoiding the demand of an adequate velocity model to achieve the objectives of seismic exploration. The inverse scattering series is used as a framework from which to seek and identify uncoupled task-specific subseries.These are classified as: (1) free-surface related multiple removal subseries; (2) internal multiple removal subseries; (3) depth-imaging subseries;

and (4) property inversion subseries. The achievement of each task is expressed as a nonlinear series in terms of only the *output data* of the previous task and a chosen *reference Green's function*.

As one of important tasks in the inverse scattering series, the depth imaging subseries has been developing and progressing toward a more practical and comprehensive state. As a starting point, a 1D laterally invariant acoustic medium was considered (Shaw et al., 2002; Shaw and Weglein, 2003; Shaw et al., 2003, 2004; Shaw, 2005). In these papers, a leading order imaging subseries (*LOIS*) is separated from the whole series and written as a closed form. The application of *LOIS* and its closed form on the 1.5D acoustic medium achieves an accurate depth delineation of the subsurface reflectors with no absolutely a priori knowledge of the subsurface velocity. The test shows the powerful capability of the inverse scattering series. How about 2D medium with lateral variation,too? Liu et al. (2004, 2005) derived the higher order imaging subseries (*HOIS*) and its closed form for a 2D acoustic medium with both lateral and vertical variation. The implementation of the *HOIS* and its closed form on 2D acoustic media (Liu, 2006) shows very encouraging results, especially the success of accurate depth imaging of a 2D salt model as a typical example of complex geological area with big velocity contrast. And the extension of 2D acoustic imaging closed form to a 3D acoustic medium is direct. Innanen and Weglein (2003), Innanen (2005) captured a simultaneous imaging and inversion subseries (*SII*) at leading order and higher order for 1.5D acoustic case and obtained a closed form of this coupled tasks. All of this pioneering work encourages us to push the imaging theory a further step and stimulate us in the future research to seek a better whole closed form of the acoustic media which can cast a wider net for more terms in the series and extend these closed forms to more complicated media. In particular, we here consider 1D or even multi-D elastic medium with multi-parameters.

In this report, we take a step towards exploring a depth-imaging subseries for an elastic medium. The research plan is: First, to generate synthetic data for a 1D multi-layer elastic medium with multi-parameters. Second, to determine the physical meaning of the imaging-only integrals (Zhang and Weglein, 2005, 2006) by using the synthetic data, and further seek an extension of the imaging closed form to elastic media.

This paper consists of the following sections: *Section 2* is a short introduction to the inverse scattering series. *Section 3* will present the analytic expression of PP-data in three different domains for a 1D three-layer elastic medium with three parameters, and the formulae to calculate reflected and transmitted coefficients will also be listed. To get a clearer understanding of the PP-data in pseudo-depth domain by a constant veloctiy migration, *Section 4* shows the results of numerical evaluation for several chosen models. A research plan and imaging strategy for 1D multi-parameter elastic media will be discussed in the last section.

2 Inverse scattering theory and series

Scattering theory is a form of perturbation analysis. Generally speaking, it describes how a perturbation in the properties of a medium relates a perturbation to a wavefield that experiences that perturbed medium. Consider the two differential equations governing wave propagation in these

media (Weglein et al., 2003):

$$LG = \delta(\mathbf{r} - \mathbf{r_s}), \tag{1}$$

$$L_0 G_0 = \delta(\mathbf{r} - \mathbf{r_s}). \tag{2}$$

where L, L_0 and G, G_0 are the actual and reference differential operators and Green functions, respectively, for a single temporal frequency, ω, and $\delta(\mathbf{r} - \mathbf{r_s})$ is the Dirac delta function.$\mathbf{r}$ and $\mathbf{r_s}$ are the field point and source location, respectively.
We define the perturbation operator $V = L_0 - L$, and scattered field operator $\Psi_s = G - G_0$ (Weglein et al., 2002). The Lippmann-Schwinger equation is the fundamental equation of scattering theory which is an operator identity that relates Ψ_s, G_0, V and G (Taylor, 1972):

$$\Psi_s = G - G_0 = G_0 V G. \tag{3}$$

The so-called Born series can be obtained by iterating this equation back into itself,

$$\Psi_s = G_0 V G_0 + G_0 V G_0 V G_0 + \cdots = (\Psi_s)_1 + (\Psi_s)_2 + \cdots, \tag{4}$$

where $(\Psi_s)_n$ is the portion of Ψ_s that is the n^{th} order in V. The measured value of Ψ_s is the data, D, where $D = (\Psi_s)_{ms} = (\Psi_s)_{\text{on the measurement surface}}$.

Expanding V as a series in orders of D (Weglein et al., 1997),

$$V = V_1 + V_2 + V_3 + \cdots, \tag{5}$$

then substituting equation (5) into equation (4) and evaluating equation (4) on the measurement surface yields,

$$D = [G_0(V_1 + V_2 + \cdots)G_0]_{ms} + [G_0(V_1 + V_2 + \cdots)G_0(V_1 + V_2 + \cdots)G_0]_{ms} + \cdots \tag{6}$$

Setting terms of equal order in the data equal, leads to the equations that determine V_1, V_2, ... directly from D and G_0.

$$D = [G_0 V_1 G_0]_{ms}, \tag{7}$$

$$0 = [G_0 V_2 G_0]_{ms} + [G_0 V_1 G_0 V_1 G_0]_{ms}, \tag{8}$$

$$0 = [G_0 V_3 G_0]_{ms} + [G_0 V_1 G_0 V_2 G_0]_{ms} + [G_0 V_2 G_0 V_1 G_0]_{ms} + [G_0 V_1 G_0 V_1 G_0 V_1 G_0]_{ms}, \tag{9}$$

$$\vdots$$

3 Data preparation for 1D elastic media with two interfaces

In this section, we will consider a 1D elastic medium model with three parameters (i.e. bulk modulus, shear modulus and density) for the three layer case. First, we will show the model we have used to generate the data we need; second, a calculation of reflection and transmission coefficients will be presented by employing Zoeppritz' equation; finally, we will give three different analytic expressions in three domains: the frequency domain, the time domain, and the pseudo-depth domain.

3.1 The 1D two-interface elastic media model

In a 1D two-interface elastic medium model with three parameters, we consider an incident compressional wave with incident angle θ_0, the angle between the incident wave and the normal to the planar elastic layer. The response of this incident compressional wave will consist of a converted shear wave (or S-wave) and a compressional wave (or P-wave). We will consider only primaries of compressional waves (see Figure 1).

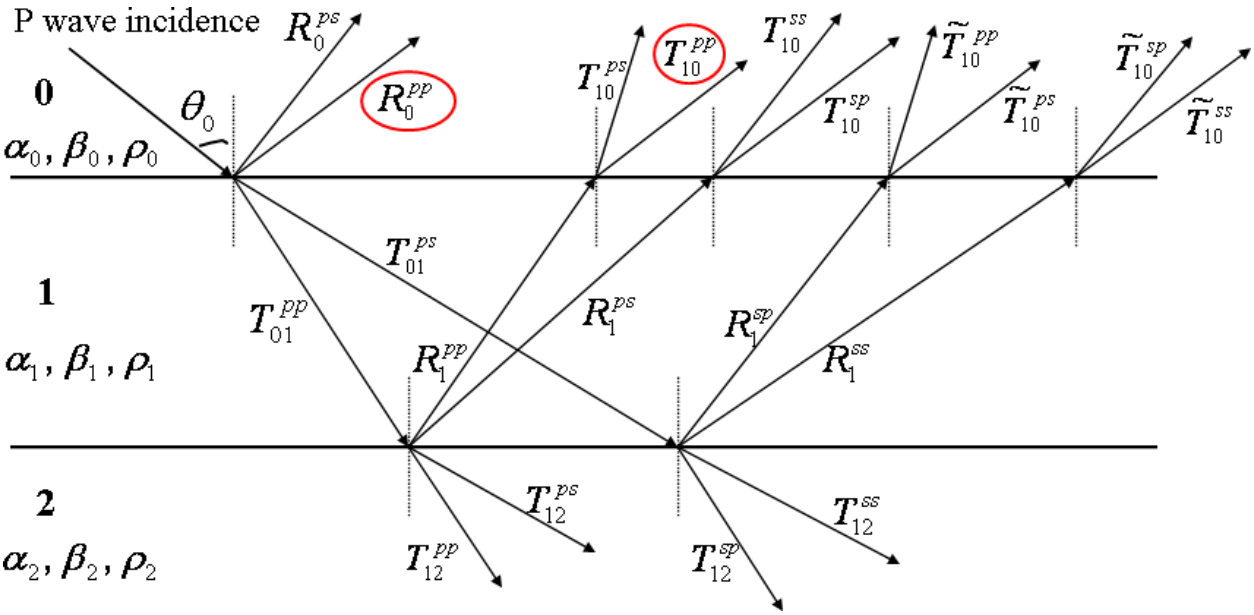

Figure 1: *Response of incident compressional wave on a 1D two-interface elastic media with three parameters. α_i, β_i and ρ_i $(i = 0, 1, 2)$ are the compressional wave velocity, shear wave velocity and density of the three layers, respectively. R_i^{pp}, R_i^{ss}, R_i^{ps} and R_i^{sp} denote the reflection coefficients of P-wave to P-wave, S-wave to S-wave, S-wave converted from P-wave and P-wave converted from S-wave, respectively, on the i^{th} interface; and similarly for T_{ij}^{pp}, T_{ij}^{ss}, T_{ij}^{ps} and T_{ij}^{sp} denoting the transmission coefficients from the i^{th} layer to the j^{th} layer in the media.*

3.2 Calculation of reflection and transmission coefficients

The calculation of the reflection and transmission coefficients in the above model can be found in many references, textbooks and papers, e.g., Ewing et al. (1957) which uses Knott's equations, and Achenbach (1973), Aki and Richards (2002), Foster et al. (1997), all of which use Zoeppritz' equations. Sheriff and Geldart (1994) use both methods. Here we will use the results listed in *Chapter* 5 of Aki and Richards (2002).

Let i_1 and j_1 denote the incident angle of the downgoing P-wave and downgoing S-wave, respectively; i_2 and j_2 denote the incident angle of the upgoing P-wave and upgoing S-wave, as shown as the four cases in Figure 2.

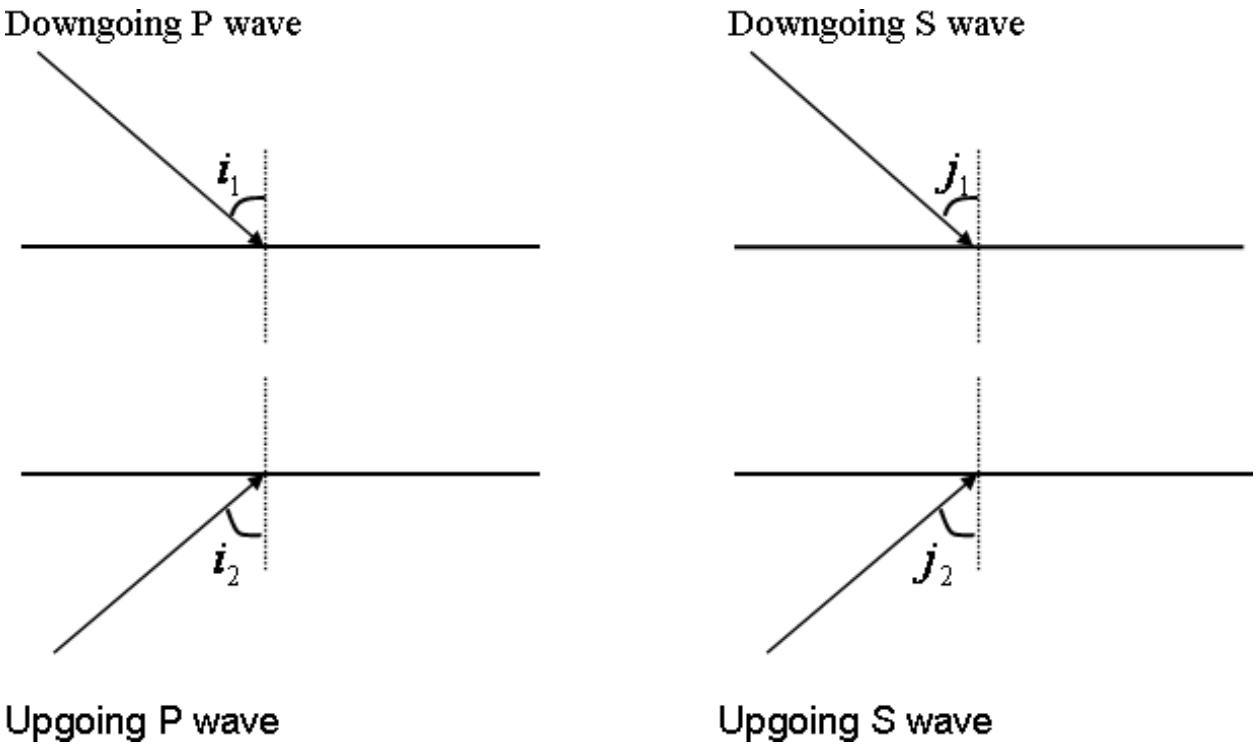

Figure 2: *The four possible cases with different incident angles in the layers*

In the next section, we will only consider the PP-data, which will require the following four kinds of reflection and transmission coefficients:

$$\begin{aligned} R_0^{pp} &= (\grave{P}\acute{P})_0 \\ &= \frac{1}{D}\left[\left(b\frac{\cos i_1}{\alpha_0} - c\frac{\cos i_2}{\alpha_1}\right)F - \left(a + d\frac{\cos i_1}{\alpha_0}\frac{\cos j_2}{\beta_1}\right)Hp^2\right], \qquad (10) \\ R_1^{pp} &= (\grave{P}\acute{P})_1 \\ &= \frac{1}{D}\left[\left(b\frac{\cos i_1}{\alpha_1} - c\frac{\cos i_2}{\alpha_2}\right)F - \left(a + d\frac{\cos i_1}{\alpha_1}\frac{\cos j_2}{\beta_2}\right)Hp^2\right], \qquad (11) \\ T_{01}^{pp} &= (\grave{P}\grave{P})_0 \\ &= 2\rho_0\frac{\cos i_1}{\alpha_0}F\alpha_0/(\alpha_1 D), \qquad (12) \\ T_{10}^{pp} &= (\acute{P}\acute{P})_1 \\ &= 2\rho_1\frac{\cos i_2}{\alpha_1}F\alpha_1/(\alpha_0 D), \qquad (13) \end{aligned}$$

where p is the horizontal component of slowness of each wave, and where

$$a = \rho_2(1-2\beta_2^2p^2) - \rho_1(1-2\beta_1^2p^2), \qquad b = \rho_2(1-2\beta_2^2p^2) + 2\rho_1\beta_1^2p^2; \qquad (14)$$

$$c = \rho_1(1-2\beta_1^2p^2) + 2\rho_2\beta_2^2p^2, \qquad d = 2(\rho_2\beta_2^2 - \rho_1\beta_1^2); \qquad (15)$$

$$E = b\frac{\cos i_1}{\alpha_1} + c\frac{\cos i_2}{\alpha_2}, \qquad F = b\frac{\cos j_1}{\beta_1} + c\frac{\cos j_2}{\beta_2}; \tag{16}$$

$$G = a - d\frac{\cos i_1}{\alpha_1}\frac{\cos j_2}{\beta_2}, \qquad H = a - d\frac{\cos i_2}{\alpha_2}\frac{\cos j_1}{\beta_1}; \tag{17}$$

$$D = EF + GHp^2. \tag{18}$$

One point which should be kept in mind is that the real values of the above parameters should be calculated by substituting the corresponding medium parameters in the layers into those formula.

The incident, reflected and transmitted angles of the p-wave and s-wave in two different layers must comply with Snell's law. For the 1^{st} interface, it is

$$\frac{\sin\theta_0}{\alpha_0} = \frac{\sin i_1}{\alpha_0} = \frac{\sin i_2}{\alpha_1} = \frac{\sin j_1}{\beta_0} = \frac{\sin j_2}{\beta_1} = p, \tag{19}$$

and hence,

$$\cos i_1 = \sqrt{1-\sin^2 i_1} = \sqrt{1-\alpha_0^2 p^2} \equiv x_0, \tag{20}$$

$$\cos i_2 = \sqrt{1-\sin^2 i_2} = \sqrt{1-\alpha_1^2 p^2} \equiv x_1, \tag{21}$$

$$\cos j_1 = \sqrt{1-\sin^2 j_1} = \sqrt{1-\beta_0^2 p^2} \equiv y_0, \tag{22}$$

$$\cos j_2 = \sqrt{1-\sin^2 j_2} = \sqrt{1-\beta_1^2 p^2} \equiv y_1. \tag{23}$$

However, for the 2^{nd} interface, the formula changes to

$$\frac{\sin\theta_0}{\alpha_0} = \frac{\sin i_1}{\alpha_1} = \frac{\sin i_2}{\alpha_2} = \frac{\sin j_1}{\beta_1} = \frac{\sin j_2}{\beta_2} = p, \tag{24}$$

and hence,

$$\cos i_1 = \sqrt{1-\sin^2 i_1} = \sqrt{1-\alpha_1^2 p^2} \equiv x_1, \tag{25}$$

$$\cos i_2 = \sqrt{1-\sin^2 i_2} = \sqrt{1-\alpha_2^2 p^2} \equiv x_2, \tag{26}$$

$$\cos j_1 = \sqrt{1-\sin^2 j_1} = \sqrt{1-\beta_1^2 p^2} \equiv y_1, \tag{27}$$

$$\cos j_2 = \sqrt{1-\sin^2 j_2} = \sqrt{1-\beta_2^2 p^2} \equiv y_2. \tag{28}$$

3.3 Data in different domains

In this section the analytic expressions of PP-data in three different domains will be shown. The mathematical derivation is found in the Appendix of this report.

3.3.1 In the frequency ω domain

Considering primaries only, the data in the frequency domain is

$$\begin{aligned}\widetilde{D}^{pp}(\omega,\theta_0) &= R_0^{pp}(\theta_0)\frac{e^{2i\nu_g a}}{4\pi i\nu_g} + T_{01}^{pp}(\theta_0)R_1^{pp}(\theta_0)T_{10}^{pp}(\theta_0)\frac{e^{2i\nu_g a+2iq_g(b-a)}}{4\pi i\nu_g} \\ &= R_0^{pp}(\theta_0)\frac{e^{2i\nu_g a}}{4\pi i\nu_g} + R_1^{'pp}(\theta_0)\frac{e^{2i\nu_g a+2iq_g(b-a)}}{4\pi i\nu_g}, \end{aligned} \tag{29}$$

where a, b are the real depths of the 1^{st} and 2^{nd} interfaces of the model,and $R_1^{'pp} \equiv T_{01}^{pp}R_1^{pp}T_{10}^{pp}$. The quantities ν_g and q_g are the vertical compressional wave number in the 1^{st} and 2^{nd} layer, respectively, and defined as

$$\nu_g = k_0\cos i_1 = k_0\cos\theta_0 = \frac{\omega}{\alpha_0}x_0, \tag{30}$$

$$q_g = k_1\cos i_2 = k_1\sqrt{1-\alpha_1^2p^2} = \frac{\omega}{\alpha_1}x_1. \tag{31}$$

The reflection and transmission coefficients are obtained through equation (10) $--$ (13). Notice this analytic PP-data is a function of incident angle θ_0.

3.3.2 In the time t domain

The same data in equation (29) expressed in the time domain will be

$$\begin{aligned}D^{pp}(t,\theta_0) = &- \frac{\alpha_0}{2\cos\theta_0}R_0^{pp}(\theta_0)H\left(t - x_0\frac{2a}{\alpha_0}\right) \\ &- \frac{\alpha_0}{2\cos\theta_0}R_1^{'pp}(\theta_0)H\left(t - x_0\frac{2a}{\alpha_0} - x_1\frac{2(b-a)}{\alpha_1}\right), \end{aligned} \tag{32}$$

where x_0, x_1 defined in equation (20) are functions of incident angle θ_0, which means the arrival time for the two primaries corresponding to the two interfaces will change with the different incident angles.

3.3.3 In the pseudo-depth z domain

When we migrate the data expressed by equation (29) with the constant velocity of the reference velocity, it is transformed into the pseudo-depth z domain and takes the following form:

$$D^{pp}(z,\theta_0) = -R_0^{pp}(\theta_0)H(z-a) - R_1^{'pp}(\theta_0)H\left(z-b'(\theta_0)\right), \tag{33}$$

where b' is the pseudo-depth of the 2^{nd} interface of the 1D elastic model, and takes the following form,

$$b'(\theta_0) = a + (b-a)\frac{\alpha_0\sqrt{1-\alpha_1^2p^2}}{\alpha_1\sqrt{1-\alpha_0^2p^2}} = a + (b-a)\frac{\alpha_0x_1}{\alpha_1x_0}, \tag{34}$$

$$x_0 \equiv \cos i_1 = \sqrt{1 - \sin^2 i_1} = \sqrt{1 - \alpha_0^2 p^2}, \tag{35}$$

$$x_1 \equiv \cos i_2 = \sqrt{1 - \sin^2 i_2} = \sqrt{1 - \alpha_1^2 p^2}. \tag{36}$$

Inspection of equation (33) reveals that in the pseudo-depth domain, the 1^{st} interface is exactly located at a, and this depth does not change with the incident angle θ_0. This is understood by taking a look at the mathematical derivation of the data from frequency domain to the pseudo-depth domain: we are migrating the data with the reference velocity, the velocity of the 1^{st} layer! So, the 1^{st} interface is exactly located in the data.

However, the location of the 2^{nd} interface in the data is not well located, because b' is a pseudo-depth and is a function of the incident angle θ_0. As mentioned, we are migrating the data with a wrong velocity, the velocity of the 1^{st} layer, as the velocity of the 2^{nd} layer.

4 Constant velocity migration of PP-data in pseudo-depth z domain: numerical results

To obtain some "taste" of what the constant velocity migration on PP-data looks like in the pseudo-depth domain, we will numerically evaluate equation (33) for the following five models (for all of the five models, the real depths are: $a = 160m$, $b = 365m$):

Model 1:
$\rho_0 = 2.27g/cm^3, \rho_1 = 2.32g/cm^3, \rho_2 = 2.50g/cm^3; \alpha_0 = 3251m/s, \alpha_1 = 3507m/s, \alpha_2 = 3380m/s; \beta_0 = 2138m/s, \beta_1 = 2116m/s, \beta_2 = 2200m/s.$

Model 2:
$\rho_0 = 2.27g/cm^3, \rho_1 = 2.80g/cm^3, \rho_2 = 2.50g/cm^3; \alpha_0 = 3251m/s, \alpha_1 = 2467m/s, \alpha_2 = 3780m/s; \beta_0 = 2138m/s, \beta_1 = 2516m/s, \beta_2 = 2000m/s.$

Model 3:
$\rho_0 = 2.27g/cm^3, \rho_1 = 1.60g/cm^3, \rho_2 = 2.50g/cm^3; \alpha_0 = 3251m/s, \alpha_1 = 2467m/s, \alpha_2 = 3780m/s; \beta_0 = 2138m/s, \beta_1 = 2516m/s, \beta_2 = 2000m/s.$

Model 4:
$\rho_0 = 2.27g/cm^3, \rho_1 = 1.80g/cm^3, \rho_2 = 2.00g/cm^3; \alpha_0 = 3251m/s, \alpha_1 = 2807m/s, \alpha_2 = 3580m/s; \beta_0 = 2138m/s, \beta_1 = 2516m/s, \beta_2 = 2000m/s.$

Model 5:
$\rho_0 = 2.27g/cm^3, \rho_1 = 1.80g/cm^3, \rho_2 = 2.00g/cm^3; \alpha_0 = 3251m/s, \alpha_1 = 2807m/s, \alpha_2 = 3580m/s; \beta_0 = 2738m/s, \beta_1 = 2200m/s, \beta_2 = 1800m/s.$

The reflection and transmission coefficients are calculated from equation (10)−−(13). The numerical results and comparison among them are shown in Figure 3, Figure 4 and Figure 5, respectively.

We have purposefully chosen our models. For example, we choose *Model 2* with bigger velocity contrast than *Model 1* and the resulting numerical results show a larger "gap" between the pseudo-depth and the real depth of the 2^{nd} interface for *Model 2* than *Model 1*; the difference between

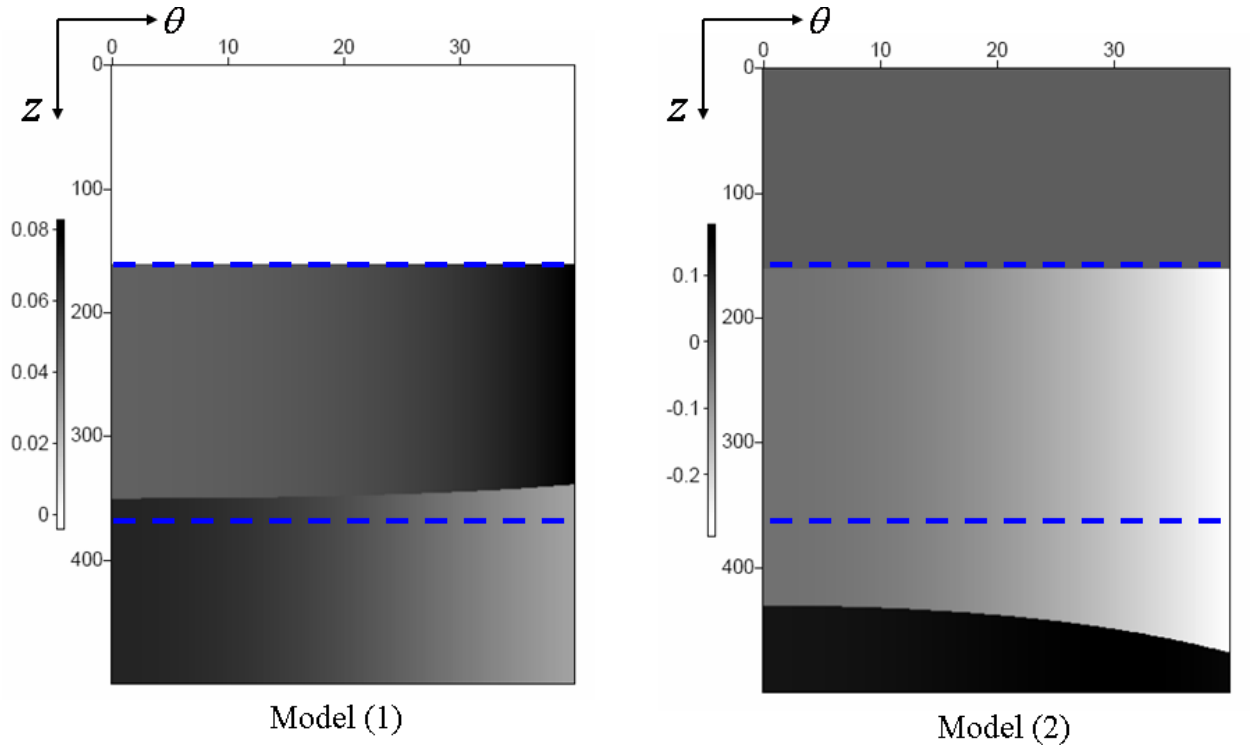

Figure 3: *Numerical evaluation and comparison of PP-data for Model* 1 *and Model* 2 *in pseudo-depth domain. In the figures, the two blue dash lines are the real depth of the* 1^{st} *and* 2^{nd} *interfaces, respectively.*

Model 3 and *Model 2* is the density change of the 2^{nd} layer and numerical comparison between the two models shows that density change will not effect the location of the pseudo-depth of the 2^{nd} interface; and the comparison between *Model 4* and *Model 5* shows that the change of shear wave velocity only will also not change the location of the pseudo-depth of the 2^{nd} interface in the PP-data. But notice that any change of these parameters in these models will alter the value of reflection and transmission coefficients.

5 1D elastic media imaging with PP-data only: Plan

The inverse scattering series is a direct, non-linear inverse procedure for the reconstruction of an unknown spatial distribution of multidimensional medium parameters in terms of only measurements of a reflected wave field (Liu et al., 2005). In the case of 1D variable velocity and density acoustic media (Zhang and Weglein, 2005), the 2^{nd} equation of the inverse scattering series is presented such that inversion-only terms and imaging-only terms are separated. The imaging-only term includes only integrals of the difference between the two medium parameters α_1 and β_1, rather than the α_1 in the integral of the imaging term in 1D acoustic case (Weglein et al., 2002; Shaw et al., 2004), where a leading order imaging subseries was present as a depth shift of the integral of α_1. The research on the 1D elastic media with three variable parameters (Zhang and Weglein, 2006) shows that

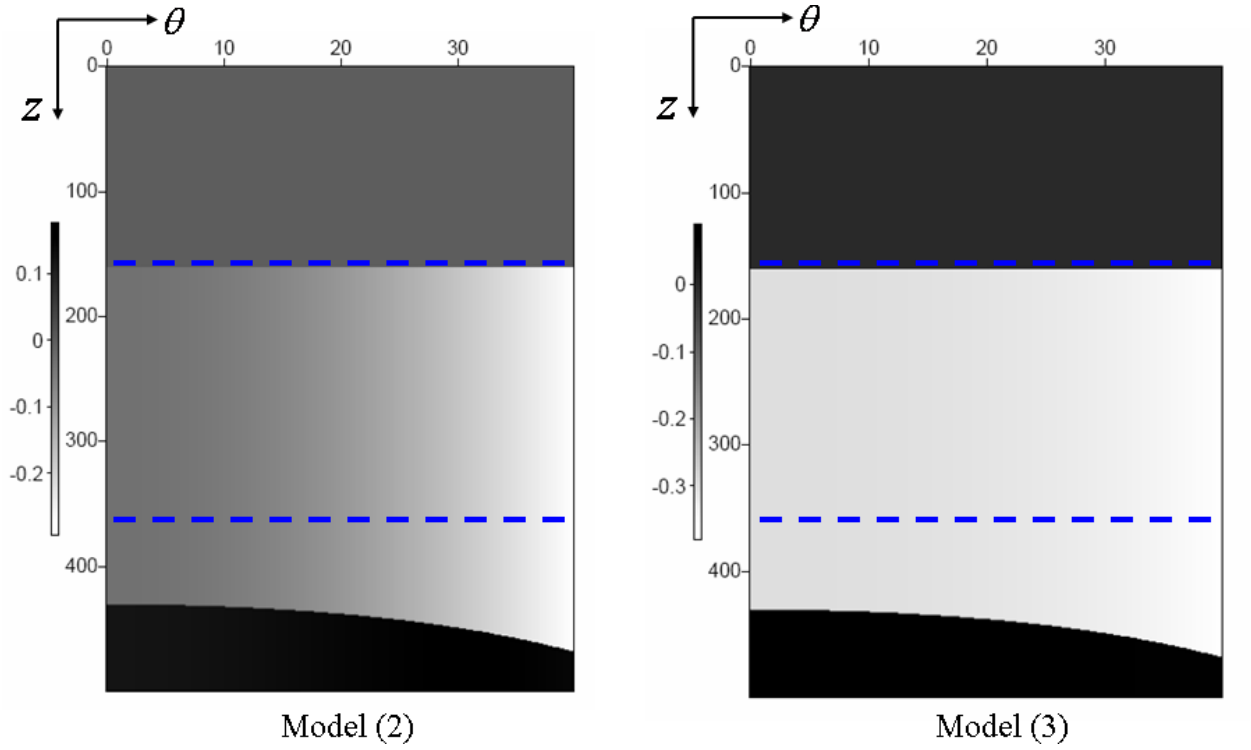

Figure 4: *Numerical evaluation and comparison of PP-data for Model* 2 *and Model* 3 *in pseudo-depth domain. In the figures, the two blue dash lines are the real depth of the* 1^{st} *and* 2^{nd} *interfaces, respectively.*

with PP-data only the imaging terms include integrals of the difference between $a_\gamma^{(1)}$ and $a_\rho^{(1)}$, two parameters of the three. All of these comparison indicate an extension of the leading order imaging subseries in the 1D one parameter acoustic media to the other two cases by only substituting α_1 inside the depth shift integral with the difference term (Weglein, 2006 Annual Report). Hence, the medium parameters at 1^{st} order must be obtained before starting the extension of the imaging formula. In this section, we will discuss the case of 1D elastic media with three variable parameters (Zhang and Weglein, 2006), to work toward an analytical expression of the three parameters from the 1^{st} ISS equation.

By using equation (7) and doing a Fourier transform on both sides of the equation, we get(Zhang and Weglein, 2006),

$$\widetilde{D}^{pp}(\omega,\theta) = -\frac{1}{4}(1-\tan^2\theta)\widetilde{a_\rho^{(1)}}(2\nu_g) - \frac{1}{4}(1+\tan^2\theta)\widetilde{a_\gamma^{(1)}}(2\nu_g) + \frac{2\beta_0^2\sin^2\theta}{\alpha_0^2}\widetilde{a_\mu^{(1)}}(2\nu_g). \tag{37}$$

After doing an inverse Fourier transform over $2\nu_g$, we write the above equation as,

$$-4D^{pp}(z,\theta) = A(\theta)a_\rho^{(1)}(z) + B(\theta)a_\gamma^{(1)}(z) + C(\theta)a_\mu^{(1)}(z), \tag{38}$$

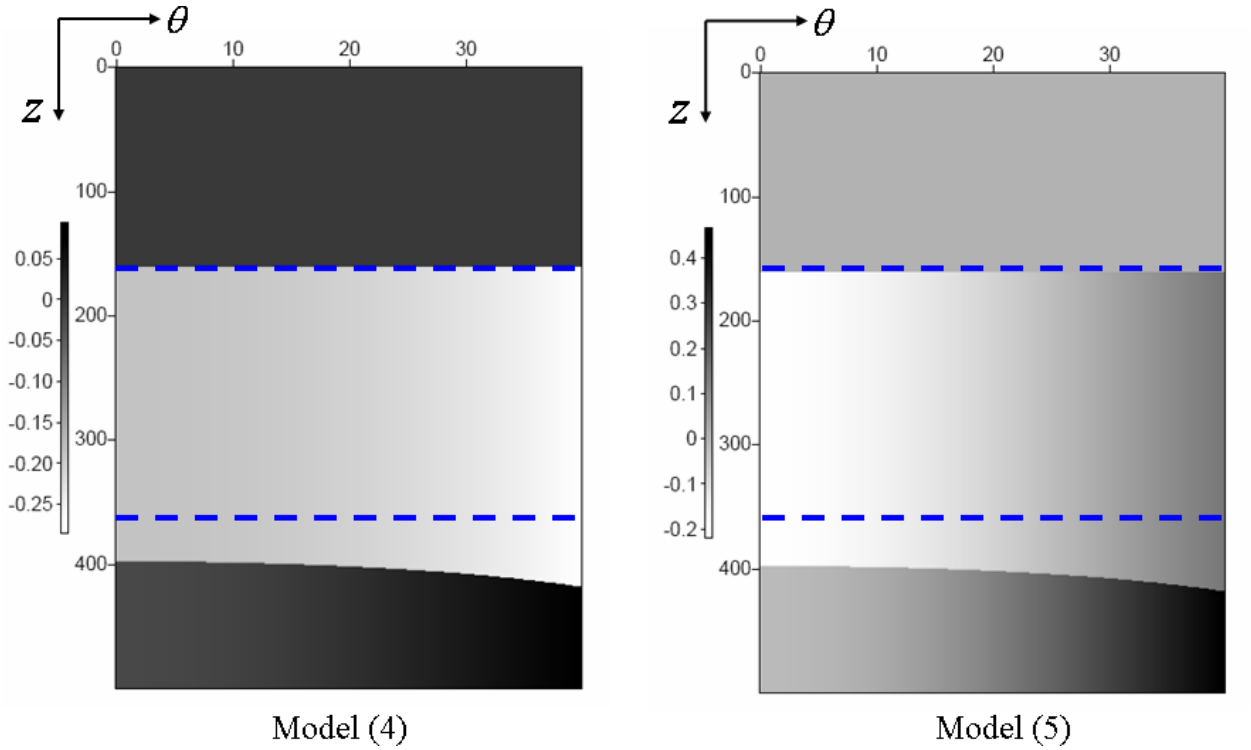

Figure 5: *Numerical evaluation and comparison of PP-data for Model 4 and Model 5 in pseudo-depth domain. In the figures, the two blue dash lines are the real depth of the 1^{st} and 2^{nd} interfaces, respectively.*

where $D^{pp}(z,\theta)$ is the PP-data in pseudo-depth z domain and,

$$A(\theta) = 1 - \tan^2\theta, \quad B(\theta) = 1 + \tan^2\theta, \quad C(\theta) = -8\frac{\beta_0^2 \sin^2\theta}{\alpha_0^2}. \tag{39}$$

$$a_\rho \equiv \frac{\rho}{\rho_0} - 1, \qquad a_\gamma \equiv \frac{\gamma}{\gamma_0} - 1, \qquad a_\mu \equiv \frac{\mu}{\mu_0} - 1. \tag{40}$$

The quantity ρ denotes density, $\gamma = \rho\alpha^2$ denotes bulk modulus, and $\mu = \rho\beta^2$ denotes shear modulus.

Next we solve equation (38) by using three different incident angles θ. The three different equations written in matrix form are

$$\begin{pmatrix} A(\theta_1) & B(\theta_1) & C(\theta_1) \\ A(\theta_2) & B(\theta_2) & C(\theta_2) \\ A(\theta_3) & B(\theta_3) & C(\theta_3) \end{pmatrix} \begin{pmatrix} a_\rho^{(1)}(z) \\ a_\gamma^{(1)}(z) \\ a_\mu^{(1)}(z) \end{pmatrix} = -4 \begin{pmatrix} D^{pp}(z,\theta_1) \\ D^{pp}(z,\theta_2) \\ D^{pp}(z,\theta_3) \end{pmatrix}, \tag{41}$$

or, simply,

$$\mathbf{MP} = \mathbf{D}, \tag{42}$$

where $\mathbf{M}$, $\mathbf{P}$ and $\mathbf{D}$ are the corresponding matrices in equation (41). To solve the matrix equation (42) to get the parameters, we just need to get the inverse matrix of $\mathbf{M}$, i.e., $\mathbf{P} = \mathbf{M}^{-1}\mathbf{D}$.

After using the PP-data in pseudo-depth domain and substituting it into the above matrix equation, we can provide analytical expressions of the parameters to first order. Therefore, we can take the difference between them, and provide the required input to the extended imaging formula. But the analytical result in this research reveals some new issues: more than two pseudo-depths pop up in the three-layer model. This issue comes from the pseudo-depth dependence of incident angle in the data when we try to solve the matrix equation (41) by employing three different incident angles. Currently research into this issue is still in progress.

6 Conclusion

In this report, as a starting point to seek an imaging algorithm in 1D elastic media, an analytical expression of D^{pp} for a 1D three-layer elastic medium is presented in the frequency domain, the time domain and in the pseudo-depth domain, respectively. The D^{pp} migrated with the constant velocity of the reference media in the pseudo-depth domain will be utilized in the imaging algorithm for 1D elastic media in future research. The procedure to obtain the PP-data in this paper will also supply further value as a framework for the preparation of the other three components of data in elastic media, i.e., D^{ps}, D^{sp} and D^{ss}, and therefore be helpful for the accessability of a full non-linear inversion algorithm.

7 Acknowledgements

We are grateful to all M-OSRP sponsors for long-term encouragement and support in this research. All members in M-OSRP are thanked for the help of finishing this paper and valuable discussions in this research program. This work has been partially funded by NSF-CMG award DMS-0327778 and DOE Basic Energy Science award DE-FG02-05ER15697.

References

Achenbach, J. D. *Wave propagation in elastic solids*. 1st ed. edition. Amsterdam: North-Holland; New York: American Elsevier, 1973.

Aki, K. and P. G. Richards. *Quantitative Seismology*. 2nd edition. University Science Books, 2002.

Ewing, W. M., W. S. Jardetzky, and F. Press. *Elastic waves in layered media*. McGraw-Hill Book Co., 1957.

Foster, D. J., R. G. Keys, and D. P. Schmitt. "Detecting subsurface hydrocarbons with elastic wavefields." *Inverse Problems in Wave Propagation* Volume 90 of the IMA Volumes in Mathematics and its Application (1997): 195–217.

Innanen, K. A. "Two non-linear forward and inverse approximations for wave fields in the presence of sustained medium perturbations." *Proceedings of the 75th Annual Meeting of the Society of Exploration Geophysicists, Houston, TX.* . Soc. Expl. Geophys., 2005.

Innanen, K. A. and A. B. Weglein. "Simultaneous Imaging and Inversion with the Inverse Scattering Series." *Proceedings of the Eighth International Congress of the SBGf and Fifth Latin American Geophysical Conference*. . SBGf, 2003.

Liu, F., B. G. Nita, A. B. Weglein, and K. A. Innanen. "Inverse Scattering Series in the presence of lateral variations." *M-OSRP Annual Report* 3 (2004).

Liu, F., A.B. Weglein, K.A. Innanen, and B.G Nita. "Extension of the non-linear depth imaging capability of the inverse scattering series to multidimensional media: strategies and numerical results." 2005.

Liu, Fang. *Multi-Dimensional Depth Imaing without an Adequate Velocity model*. PhD thesis, University of Houston, 2006.

Shaw, S. A. *An inverse scattering series algorithm for depth imaging of reflection data from a layered acoustic medium with an unknown velocity model*. PhD thesis, University of Houston, 2005.

Shaw, S. A. and A. B. Weglein. "Imaging seismic reflection data at the correct depth without specifying an accurate velocity model: Initial examples of an inverse scattering subseries." *Frontiers of remote sensing information processing*. Ed. C. H. Chen. World Scientific Publishing Company, 2003. chapter 21, 469–484.

Shaw, S. A., A. B. Weglein, D. J. Foster, K. H. Matson, and R. G. Keys. "Convergence properties of a leading order depth imaging series." *73rd Annual Internat. Mtg., Soc. Expl. Geophys., Expanded Abstracts*. . Soc. Expl. Geophys., 2003. 937–940.

Shaw, S. A., A. B. Weglein, D. J. Foster, K. H. Matson, and R. G. Keys. "Isolation of a leading order depth imaging series and analysis of its convergence properties." *Journal of Seismic Exploration* 2 (November 2004): 157–195.

Shaw, Simon A., A. B. Weglein, K. H. Matson, and D. J. Foster. "Cooperation of the leading order terms in an inverse-scattering subseries for imaging: 1-D analysis and evaluation.." *SEG Technical Program Expanded Abstracts* (2002): 2277–2280.

Sheriff, R. E. and L. P. Geldart. *Exploration Seismology*. Ed. Klaus Helbig and Sven Treitel. Volume 2nd ed. . Cambridge; New York: Cambridge University Press, 1994.

Taylor, J. R. *Scattering theory: the quantum theory of nonrelativistic collisions*. John Wiley & Sons, Inc., 1972.

Weglein, A. B., F. V. Araújo, P. M. Carvalho, R. H. Stolt, K. H. Matson, R. T. Coates, D. Corrigan, D. J. Foster, S. A. Shaw, and H. Zhang. "Inverse Scattering Series and Seismic Exploration." *Inverse Problems* (2003): R27–R83.

Weglein, A. B., D. J. Foster, K. H. Matson, S. A. Shaw, P. M. Carvalho, and D. Corrigan. "Predicting the correct spatial location of reflectors without knowing or determining the precise medium and wave velocity: initial concept, algorithm and analytic and numerical example." *Journal of Seismic Exploration* 10 (2002): 367–382.

Weglein, A. B., F. A. Gasparotto, P. M. Carvalho, and R. H. Stolt. "An Inverse-Scattering Series Method for Attenuating Multiples in Seismic Reflection Data." *Geophysics* 62 (November-December 1997): 1975–1989.

Weglein, A. B., K. H. Matson, D. J. Foster, P. M. Carvalho, D. Corrigan, and S. A. Shaw. "Imaging and inversion at depth without a velocity model: Theory, concepts and initial evaluation." *70th Annual Internat. Mtg., Soc. Expl. Geophys., Expanded Abstracts.* . Soc. Expl. Geophys., 2000. 1016–1019.

Zhang, H. and A.B. Weglein. "The inverse scattering series for tasks associated with primaries: depth imaging and direct non-linear inversion of 1D variable velocity and density acoustic media." *SEG Technical Program Expanded Abstracts.* 2005, 1705–1708.

Zhang, H. and A.B. Weglein. "Direct non-linear inversion of multi-parameter 1D elastic media using the inverse scattering series." *M-OSRP 2005 Annual Meeting.* 2006, 284–311.

Appendix

Derivation of PP-data in time domain and pseudo-depth domain

First, let's see how to get the PP-data from frequency domain to time domain. Let's perform a Fourier transform over ω for equation (29),

$$\begin{aligned}
D^{pp}(t,\theta_0) &= \int_{-\infty}^{\infty} e^{-i\omega t}\widetilde{D}^{pp}(\omega,\theta_0)d\omega \\
&= \frac{1}{2\pi}R_0^{pp}\int_{-\infty}^{\infty} e^{-i\omega t}\frac{e^{2i\nu_g a}}{2i\nu_g}d\omega + \frac{1}{2\pi}R_1^{'pp}\int_{-\infty}^{\infty} e^{-i\omega t}\frac{e^{2i\nu_g a+2iq_g(b-a)}}{2i\nu_g}d\omega \\
&= \frac{1}{2\pi}R_0^{pp}\int_{-\infty}^{\infty} e^{-i\omega t}\frac{\alpha_0 e^{i\omega\frac{2a}{\alpha_0}\cos\theta_0}}{2i\omega\cos\theta_0}d\omega + \frac{1}{2\pi}R_1^{'pp}\int_{-\infty}^{\infty} e^{-i\omega t}\frac{\alpha_0 e^{i\omega(\frac{2a}{\alpha_0}\cos\theta_0+\frac{2(b-a)}{\alpha_1}\cos\imath_2)}}{2i\omega\cos\theta_0}d\omega \\
&= -\frac{1}{2\pi}R_0^{pp}\int_{-\infty}^{\infty}d\omega\int_{-\infty}^{t}dt'\frac{\alpha_0}{2\cos\theta_0}e^{-i\omega(t'-\frac{2a}{\alpha_0}\cos\theta_0)} \\
&\quad -\frac{1}{2\pi}R_1^{'pp}\int_{-\infty}^{\infty}d\omega\int_{-\infty}^{t}dt'\frac{\alpha_0}{2\cos\theta_0}e^{-i\omega(t'-\frac{2a}{\alpha_0}\cos\theta_0-\frac{2(b-a)}{\alpha_1}\cos i_2)} \qquad (43)
\end{aligned}$$

Exchanging the integral order of $d\omega$ and dt',we get

$$\begin{aligned}
D^{pp}(t,\theta_0) &= -R_0^{pp}\int_{-\infty}^{t}dt'\frac{\alpha_0}{2\cos\theta_0}\delta(t'-\frac{2a}{\alpha_0}\cos\theta_0) \\
&\quad -R_1^{'pp}\int_{-\infty}^{t}dt'\frac{\alpha_0}{2\cos\theta_0}\delta\left(t'-\frac{2a}{\alpha_0}\cos\theta_0-\frac{2(b-a)}{\alpha_1}\cos i_2\right) \\
&= -\frac{\alpha_0}{2x_0}R_0^{pp}(\theta_0)H\left(t-x_0\frac{2a}{\alpha_0}\right)-\frac{\alpha_0}{2x_0}R_1^{'pp}(\theta_0)H\left(t-x_0\frac{2a}{\alpha_0}-x_1\frac{2(b-a)}{\alpha_1}\right) \qquad (44)
\end{aligned}$$

where x_0 and x_1 are defined in equation (20).

Now let's see how to get the PP-data from frequency domain to pseudo-depth domain. Let's perform an inverse Fourier transform over $2\nu_g$ for equation (29),

$$\begin{aligned}
D^{pp}(z,\theta_0) &= \int_{-\infty}^{\infty} e^{-2i\nu_g z}\widetilde{D}^{pp}(\omega,\theta_0)d(2\nu_g) \\
&= \frac{1}{2\pi}R_0^{pp}\int_{-\infty}^{\infty}\frac{e^{-2i\nu_g z}e^{2i\nu_g a}}{2i\nu_g}d(2\nu_g) + \frac{1}{2\pi}R_1^{'pp}\int_{-\infty}^{\infty}\frac{e^{-2i\nu_g z}e^{2i\nu_g a+2iq_g(b-a)}}{2i\nu_g}d(2\nu_g) \\
&= -\frac{1}{2\pi}R_0^{pp}\int_{-\infty}^{\infty}d(2\nu_g)\int_{-\infty}^{z}dz'e^{-2i\nu_g(z'-a)} \\
&\quad +\frac{1}{2\pi}R_1^{'pp}\int_{-\infty}^{\infty}d(2\nu_g)\frac{1}{2i\nu_g}e^{2i\nu_g a+2i\nu_g\frac{\alpha_0 x_1}{\alpha_1 x_0}(b-a)}e^{-2i\nu_g z} \\
&= -\frac{1}{2\pi}R_0^{pp}\int_{-\infty}^{z}dz'\int_{-\infty}^{\infty}d(2\nu_g)e^{-2i\nu_g(z'-a)} \\
&\quad -\frac{1}{2\pi}R_1^{'pp}\int_{-\infty}^{z}dz'\int_{-\infty}^{\infty}d(2\nu_g)e^{2i\nu_g a+2i\nu_g\frac{\alpha_0 x_1}{\alpha_1 x_0}(b-a)}e^{-2i\nu_g z}
\end{aligned}$$

$$
\begin{aligned}
&= -R_0^{pp}\int_{-\infty}^{z} dz'\delta(z'-a) - R_1^{'pp}\int_{-\infty}^{z} dz'\int_{-\infty}^{\infty} d(2\nu_g)e^{-2i\nu_g(z'-b')} \\
&= -R_0^{pp}(\theta_0)H(z-a) - R_1^{'pp}(\theta_0)\int_{-\infty}^{z} dz'\delta(z'-b') \\
&= -R_0^{pp}(\theta_0)H(z-a) - R_1^{'pp}(\theta_0)H(z-b') \qquad (45)
\end{aligned}
$$

In the above derivation, we used the following relation between q_g and ν_g:

$$
\begin{aligned}
q_g &= \frac{\omega}{\alpha_1}\cos i_2 = \frac{\omega}{\alpha_1}x_1 \\
&= \frac{\omega}{\alpha_0}x_0\frac{\alpha_0 x_1}{\alpha_1 x_0} = \nu_g\frac{\alpha_0 x_1}{\alpha_1 x_0} \qquad (46)
\end{aligned}
$$

where x_0 and x_1 are defined in equation (20).

On the construction of a multidimensional absorptive-dispersive medium model via direct linear inversion

K. A. Innanen, J. E. Lira and A. B. Weglein

Abstract

We describe the extension of previous scattering inverse methods for absorptive-dispersive media to include arbitrary multi-dimensional distributions of P-wave velocity and Q, which may be determined to first order from reflected seismic primary data with an inverse scattering formulation. This is relevant in two ways: as a standalone theory for Q estimation that amongst other things tells us about the sufficiency of reflection data to distinguish between variations in wavespeed vs. an attenuation parameter; and as the starting point for multi-parameter, multi-dimensional extensions to the inverse scattering series non-linear Q compensation methods currently under study.

1 Introduction

The ability of direct linear inverse scattering methods to determine spatial distributions of absorptive-dispersive (hereafter A-D) medium parameters from reflected seismic primaries is considered. The availability in principle of a well-posed direct linear inverse problem of this kind is itself of interest, because it tells us about the sufficiency of reflection data to distinguish between variations in wavespeed vs. an attenuation parameter, or quality factor (Q). Practical reasons for posing and studying this problem, meanwhile, are twofold. Consider as a first instance, that the reference medium and the actual medium (i.e., the two media used within a scattering formalism) are close to one another down to an interface of interest. The corresponding linear inversion provides a fully wave-theoretic (although approximate) formalism for the estimation of the Q contrast at that interface.

But, in addition to providing Q information, linear inverse theory for A-D media is directly relevant to the construction of *non-linear* processing operators designed to act on seismic reflection data with non-negligible Q. The inverse scattering series has served as a framework from which to derive a set of direct processing algorithms for reflection seismic data (Weglein et al., 2003). The series as a whole, and all derivative algorithms, operate only in terms of the measured data and a highly simplified reference Green's operator, trading the requirement for prior knowledge of medium variability for (1) highly non-linear algorithms and (2) an exacting requirement on data coverage and fidelity. Algorithms for primary processing, e.g., for reflector location (Weglein et al., 2001; Shaw et al., 2004; Shaw, 2005; Innanen, 2005; Liu et al., 2005, 2006), and for non-linear inversion (Zhang and Weglein, 2006a,b), seek to directly locate reflectors and directly determine their amplitudes by operating *on* the linear inversion result *with* the linear inversion result. Hence the linear inversion output is at the heart of any given non-linear processing regimen, and therefor remains of importance regardless of its proximity to the actual medium. Non-linear processing algorithms,

based on the inverse scattering series, which would perform "Q-related" tasks (i.e., Q estimation and compensation) have been considered theoretically, and indeed successful construction of such operators has been shown numerically for a restricted set of 1D models (Innanen and Weglein, 2003, 2005). To begin extending such prototype algorithms to accommodate less restricted models (applicable, for instance, to multi-dimensional, multi-parameter media) requires that the theory for linear inversion be developed to at least that extended level of realism, which is not the current state of affairs. Previous research has been within a depth-varying setting (Innanen, 2003; Innanen and Weglein, 2004). The current paper provides that development and extension.

1.1 Linear inversion of reflected primaries

Linear inversion of reflected seismic primaries with inverse scattering methods (Cohen and Bleistein, 1977; Bleistein, 1979) can be considered as the formal underpinning for much of modern seismic imaging and inverse theory. For instance, as cast for multiple parameters (Raz, 1981; Clayton and Stolt, 1981) it forms a theoretical basis for linear AVO and migration-inversion (Stolt and Weglein, 1985; Weglein and Stolt, 1999), whereas formulated as a generalized Radon transform (Beylkin, 1985; Bleistein, 1987) it becomes a Kirchhoff-like migration operator that maintains the integrity of the reflection coefficient (in the geometrical-optical limit). Furthermore, as we discuss below, the non-linear inverse scattering series, and algorithms based upon it, use output of the linear inverse as their main input (Weglein et al., 2003). Our parochial interest in (*i*) determining the sufficiency of reflection data to distinguish between variations in *P-wave velocity* (referred to as wavespeed in this paper) and Q, (*ii*) producing a multi-dimensional wave-theoretic inverse algorithm, and (*iii*) using a homogeneous reference medium, lead us to follow Clayton and Stolt (1981) most closely.

1.2 Q estimation

The determination of an appropriately parametrized A-D medium from reflection data involves a component that can be considered a form of Q-estimation. There exist a large number of Q-estimation tools and techniques, including rise-time and spectral ratio methods (Tonn, 1991), methods based on the behavior of attenuated events across scale (Kjartansson, 1979b; Innanen, 2003), modelling and inversion of data amplitude spectra, and their peaks or centroids (Zhang and Ulrych, 2002; Rickett, 2006, 2007), and in tomographic frameworks (Quan and Harris, 1997; Brzostowski and McMechan, 1992). They have been applied in reflection and cross-well/tomographic settings, e.g., (White, 1992). These methods have in common the fact that they make use of the evolution of the amplitude spectra of events vs. propagation distance or time as their main input. We make particular note of the difference between the formalism we describe, which makes use of angle-dependent reflection information, and this standard style of Q-estimation.

1.3 The imprint of Q on the reflection coefficient

In seismic studies Q is predominantly discussed as a mechanism for loss of resolution, the spreading out and decaying in time of the event as it propagates. Interrogation of this behavior is the most

obvious, and robust, means for estimating Q. However, A-D reflection and transmission coefficients apply additional amplitude and phase alterations to the measured events. It is these that drive the inverse formalism we wish to describe. Born and Wolf (1999) discuss such alterations to the optical response of an absorbing target, noting that a complex index of refraction leads to a frequency independent phase change upon reflection. A similar consideration within the reflection seismic framework led Kjartansson (1979a) to point out the consequences to the amplitude and phase of a pulse reflecting from an A-D contrast; more recently, Lam et al. (2004) and de Hoop et al. (2005) have presented time domain expressions for the acoustic response, from a planar absorptive and dispersive boundary, to an incident spherical wave.

Driving an inversion procedure with such information is not common, no doubt in part due to the nuanced changes A-D contrasts cause in the data. For instance, in a numerical study involving picking in the space-time domain (Samec and Blangy, 1992), an inability to detect specific AVO behavior deriving from contrasts in an isotropic standard linear solid model is reported. Nevertheless, the information is in principle there to be interpreted. A linear inverse procedure for depth-profiles of $Q(z)$ given the wavespeed profile $c(z)$ as prior information has been posed (Carrion and VerWest, 1987), as has a non-linear indirect inversion procedure for layered anelastic media (Dahl and Ursin, 1992) , which cites specific use of AVO information (although a data misfit function will draw from the propagation effects of Q as much as it does AVO information). In earlier incarnations of the research in this paper (Innanen, 2003; Innanen and Weglein, 2004), the separability of the linear components of arbitrarily varying wavespeed and Q perturbations in depth has been demonstrated, provided data with offset. More recently, the use of offset data for the determination of the absorptive and dispersive properties of a plane target has been advocated (de Hoop et al., 2005). The methodology we present is an attempt to do precisely that, to multidimensional distributions of wavespeed and Q.

2 Basic scattering expressions

We define wave propagation in the actual medium as satisfying a straightforward two parameter A-D wave model, in which the Green's function satisfies

$$\left[\nabla^2 + K^2\right] G(\mathbf{x}|\mathbf{x_s}; K) = \delta(\mathbf{x} - \mathbf{x_s}), \tag{1}$$

where

$$K \equiv \frac{\omega}{c(\mathbf{x})}\left[1 + \frac{F(\omega)}{Q(\mathbf{x})}\right], \tag{2}$$

and, importantly, where we have specifically extracted the function

$$F(\omega) = \frac{i}{2} - \frac{1}{\pi}\ln\left(\frac{\omega}{\omega_r}\right). \tag{3}$$

The reference frequency ω_r is a component of the A-D model, which in our numerical studies we assume is the highest frequency in a given experiment. The model embodied in equations (2) and

(3) is consistent with those described by Aki and Richards (2002), and with that of Kjartansson (1979b) over a reasonable seismic bandwidth. The function $F(\omega)$ has two terms, one imaginary and one real and frequency-dependent; the former instills absorptive effects (i.e., attenuation proper) in the expression for a propagating wavefield, while the latter instills dispersive effects. Notice that the form of the A-D model has permitted us to separate out the space dependence of $Q(\mathbf{x})$ from the frequency-dependence produced by the dispersion, which we have placed in the function $F(\omega)$. The former will be treated as an unknown in the inverse scattering problem, and the latter as known.

Continuing in operator form (e.g., Weglein et al. (2003)), the reference wave equation and the actual wave equation, both based on equation (1) may be expressed as

$$\mathbf{L_0 G_0} = \mathbf{I}, \qquad \mathbf{LG} = \mathbf{I}, \tag{4}$$

respectively. We then define perturbation and scattered field quantities as

$$\mathbf{V} = \mathbf{L_0} - \mathbf{L}, \qquad \psi = \mathbf{G} - \mathbf{G_0}, \tag{5}$$

respectively, after which the Scattering equation and forward scattering series,

$$\begin{aligned} \psi &= \mathbf{G_0 V G}, \\ &= \mathbf{G_0 V G_0} + \mathbf{G_0 V G_0 V G_0} + \mathbf{G_0 V G_0 V G_0 V G_0} + ..., \end{aligned} \tag{6}$$

are inverted by defining the inverse scattering series as an infinite series $\mathbf{V} = \mathbf{V_1} + \mathbf{V_2} + \mathbf{V_3} + ...$ in orders of measured values of the scattered field, and solving for $\mathbf{V_n}$ through

$$\begin{aligned} \psi &= \mathbf{G_0 V_1 G_0}, \\ 0 &= \mathbf{G_0 V_2 G_0} + \mathbf{G_0 V_1 G_0 V_1 G_0}, \\ 0 &= \mathbf{G_0 V_3 G_0} + \mathbf{G_0 V_1 G_0 V_2 G_0} + \mathbf{G_0 V_2 G_0 V_1 G_0} \\ &\quad + \mathbf{G_0 V_1 G_0 V_1 G_0 V_1 G_0}, \end{aligned} \tag{7}$$

etc. Solving the first equation in (7) for $\mathbf{V_1}$ corresponds to direct linear inversion, our current aim. Specifically, we define the current problem as solving for $\mathbf{V_1}$ given the A-D model and reference medium choices made above. The perturbation operator $\mathbf{V}$ is the difference between two wave operators of the type in equation (1), a reference and an actual, namely:

$$\begin{aligned} \mathbf{V} &= \mathbf{L_0} - \mathbf{L} \\ &= \left[\nabla^2 + K_0^2\right] - \left[\nabla^2 + K^2\right] \\ &= \frac{\omega^2}{c_0^2(\mathbf{x})}\left[1 + \frac{F(\omega)}{Q_0(\mathbf{x})}\right]^2 - \frac{\omega^2}{c^2(\mathbf{x})}\left[1 + \frac{F(\omega)}{Q(\mathbf{x})}\right]^2 \\ &\approx \left(\frac{\omega}{c_0(\mathbf{x})}\right)^2 \left[\alpha(\mathbf{x}) + 2F(\omega)\beta(\mathbf{x})\right], \end{aligned} \tag{8}$$

where we have defined the two central perturbation quantities of the scattering expression to be

$$\begin{aligned} \alpha(\mathbf{x}) &= 1 - \frac{c_0^2(\mathbf{x})}{c^2(\mathbf{x})}, \\ \beta(\mathbf{x}) &= \frac{1}{Q_0(\mathbf{x})} - \frac{1}{Q(\mathbf{x})}. \end{aligned} \tag{9}$$

The final approximation in equation (8) assumes (1) that the product $\alpha\beta$ is small, and (2) that $F(\omega)\beta(\mathbf{x}) << 1$, which amounts to assuming the same thing about $Q^{-1}\ln(\omega/\omega_r)$. This assumption has already been made during the development of the Q model of equation (2), so we have introduced no new restrictions.

In this paper, as we have said, we are interested in a special form of equation (9), in which the reference medium is (1) homogeneous, such that $c_0(\mathbf{x}) = c_0$, and (2) non-attenuating, such that $Q_0(\mathbf{x}) \to \infty$, in which case we re-define β as $1/Q(\mathbf{x})$. Making these changes in the form for the full perturbation, the mathematical form for the part of this $\mathbf{V}$ that is linear in the measured data, simplifies to $\mathbf{V_1}$, where

$$\mathbf{V_1} = \left(\frac{\omega}{c_0}\right)^2 \left[\alpha_1(\mathbf{x}) - 2F(\omega)\beta_1(\mathbf{x})\right]. \tag{10}$$

The direct linear inverse problem is to determine the spatial distributions of $\alpha_1(\mathbf{x})$ and $\beta_1(\mathbf{x})$ from measured values of the scattered field. With homogeneous non-attenuating reference media, we have the following Green's functions:

$$\begin{aligned} G_0(x_g, z_g|x, z; \omega) &= \frac{1}{2\pi}\int_{-\infty}^{\infty} dk'_x e^{ik'_x(x_g - x')}\frac{e^{iq'|z_g - z'|}}{i2q'} \\ G_0(x, z|x_s, z_s; \omega) &= \frac{1}{2\pi}\int_{-\infty}^{\infty} dk'_x e^{ik'_x(x' - x_s)}\frac{e^{iq'|z' - z_s|}}{i2q'}, \end{aligned} \tag{11}$$

where $q'^2 = \omega^2/c_0^2 - k'^2_x$. Finally, Fourier transforming over x_g and x_s within $G_0(x_g, z_g|x, z; \omega)$ and $G_0(x, z|x_s, z_s; \omega)$ respectively produces the useful form:

$$\begin{aligned} G_0(k_g, z_g|x, z; \omega) &= e^{-ik_g x}\frac{e^{iq_g|z_g - z|}}{i2q_g}, \\ G_0(x, z|k_s, z_s; \omega) &= e^{ik_s x}\frac{e^{iq_s|z - z_s|}}{i2q_s}. \end{aligned} \tag{12}$$

3 Linear inversion over a vertically and laterally varying medium

We apply the general approach and parametrization of Clayton and Stolt (1981) to the absorptive-dispersive scattering problem, finding that arbitrary 2D variation in the two A-D parameters may be determined, in a linear approximation, from a data set involving reflected primaries measured over multiple shot records. The extension of the 2D problem to the 3D problem is immediate. The basic linear 2D data equations are

$$D''(k_g, k_s, \omega) = S(\omega)\int_{-\infty}^{\infty} d\mathbf{x}' G_0(k_g, z_g|\mathbf{x}'; \omega)V_1(\mathbf{x}')G_0(\mathbf{x}'|k_s, z_s; \omega), \tag{13}$$

where $\mathbf{x}' = (x', z')$, $S(\omega)$ is the source wavelet, and D'' are the measured data, expressed in Fourier coordinates conjugate to x_g, x_s, and t respectively. Upon substitution of the reference

Green's functions and the A-D form of the linear perturbation, from equations (11)-(12) and (10) respectively, we have

$$D'(k_g,k_s,\omega) = -\frac{\omega^2}{4c_0^2 q_g q_s}\left[\alpha_1(k_g-k_s,-q_g-q_s) \right. \\ \left. -2F(\omega)\beta_1(k_g-k_s,-q_g-q_s)\right], \tag{14}$$

where we have incurred the first of two slight changes to the data:

$$D'(k_g,k_s,\omega) = e^{i(q_g z_g + q_s z_s)}\frac{D''(k_g,k_s,\omega)}{S(\omega)}, \tag{15}$$

that is, we have corrected for the depths of the source and receiver planes, and deconvolved the source wavelet across the bandwidth of the experiment (which means we have assumed both that it is known, and that it has not suppressed any intervals of the temporal frequency spectrum of interest to us). We next change variables to the midpoint and offset conjugate wavenumbers $k_m = k_g - k_s$ and $k_h = k_g + k_s$, and the depth wavenumber $q_z = -q_g - q_s$, following Clayton and Stolt (1981), who provide expressions for ω, q_g and q_s in terms of the new three variables:

$$\begin{aligned} q_g(k_m,k_h,q_z) &= -\frac{q_z}{2}\left(1-\frac{k_m k_h}{q_z^2}\right) \\ q_s(k_m,k_h,q_z) &= -\frac{q_z}{2}\left(1+\frac{k_m k_h}{q_z^2}\right) \\ \omega(k_m,k_h,q_z) &= -\frac{c_0 q_z}{2}\sqrt{\left(1+\frac{k_m^2}{q_z^2}\right)\left(1+\frac{k_h^2}{q_z^2}\right)}, \end{aligned} \tag{16}$$

such that equation (14) may be re-written entirely in their terms. Doing so in the A-D equations and re-arranging, we have

$$\alpha_1(k_m,q_z) - 2F(k_m,k_h,q_z)\beta_1(k_m,q_z) = D(k_m,k_h,q_z), \tag{17}$$

where, combining equations (3) and (16),

$$F(k_m,k_h,q_z) = \frac{i}{2} - \frac{1}{\pi}\ln\left(\frac{\omega(k_m,k_h,q_z)}{\omega_r}\right), \tag{18}$$

and the second change to the data has now been invoked, such that the factor due to the change of variables is absorbed into the new 'data':

$$D(k_m,k_h,q_z) = -4\frac{q_z^4 - k_m^2 k_h^2}{(q_z^2+k_m^2)(q_z^2+k_h^2)}D'(k_m,k_h,q_z). \tag{19}$$

Equation (17) contains the basic linear inversion equations. To carry out the inversion, the wavenumber spectra of α_1 and β_1 must be filled in, i.e., we must solve a linear problem for each pair (k_m, q_z). That leaves k_h, or the offset-conjugate wavenumber, free to vary. Assuming a measured

datum exists for each of a set of $N > 2$ discrete k_h values, we may express instances of equation (17) at each of these values with the matrix equation

$$\mathbf{W_h}(k_m, q_z) \begin{bmatrix} \alpha_1(k_m, q_z) \\ \beta_1(k_m, q_z) \end{bmatrix} = \mathbf{d}(k_m, q_z), \tag{20}$$

where

$$\mathbf{W_h}(k_m, q_z) = \begin{bmatrix} 1 & -2F(k_m, k_{h_1}, q_z) \\ 1 & -2F(k_m, k_{h_2}, q_z) \\ \vdots & \vdots \\ 1 & -2F(k_m, k_{h_N}, q_z) \end{bmatrix}, \tag{21}$$

and

$$\mathbf{d}(k_m, q_z) = \begin{bmatrix} D(k_m, k_{h_1}, q_z) \\ D(k_m, k_{h_2}, q_z) \\ \vdots \\ D(k_m, k_{h_N}, q_z) \end{bmatrix}. \tag{22}$$

One sensible option is to attempt a least-squares solution to this problem:

$$\begin{bmatrix} \alpha_1 \\ \beta_1 \end{bmatrix}_{lsq} = \left(\mathbf{W_h}^T \mathbf{W_h}\right)^{-1} \mathbf{W_h}^T \mathbf{d}. \tag{23}$$

The matrix $\mathbf{W_h}^T \mathbf{W_h}$ is invertible if the columns of $\mathbf{W_h}$ are linearly independent. Since the first column is constant, the requirement, at each pair of wavenumbers k_m, q_z for which we wish to construct α_1 and β_1, is then simply that the second column – the function $F(k_m, k_h, q_z)$ – must not be; it must vary sufficiently over the available k_h range. It does so by definition, hence the linear A-D inversion problem is well-posed for an arbitrary distribution of $c(x, z)$ and $Q(x, z)$ given multiple shot records of input data.

4 Acknowledgments

Kris Innanen and Art Weglein were supported by the DOE Basic Energy Sciences award DE-FG02-05ER15697; Art Weglein was supported by the NSF-CMG award DMS-0327778. The support of the M-OSRP sponsors is also gratefully acknowledged.

References

Aki, K. and P. G. Richards. *Quantitative Seismology.* 2nd edition. University Science Books, 2002.

Beylkin, G. "Imaging of discontinuities in the inverse scattering problem by inversion of a causal generalized Radon transform." *J. Math. Phys.* 26 (1985): 99–108.

Bleistein, N. "Velocity inversion procedure for acoustic waves." *Geophysics* 44 (1979): 1077–1087.

Bleistein, N. "On the imaging of reflectors in the earth." *Geophysics* 52 (1987): 931–942.

Born, M. and E. Wolf. *Principles of optics*. 7th edition. Cambridge University Press, 1999.

Brzostowski, M. A. and G. A. McMechan. "3-D tomographic imaging of near-surface seismic velocity and attenuation." *Geophysics* 57 (1992): 396–403.

Carrion, P. M. and B. VerWest. "A procedure for inverting seismic data to obtain Q-profiles." *Inverse Problems* (1987): 65–71.

Clayton, R. W. and R. H. Stolt. "A Born-WKBJ inversion method for acoustic reflection data." *Geophysics* 46 (1981): 1559–1567.

Cohen, J. K. and N. Bleistein. "An inverse method for determining small variations in propagation speed." *SIAM Journal of Applied Math* 32 (1977): 784–799.

Dahl, T. and B. Ursin. "Non-linear AVO inversion for a stack of anelastic layers." *Geophysical Prospecting* 40 (1992): 243.

Hoop, A. T.de , C. H. Lam, and B. J. Kooij. "Parametrization of acoustic boundary absorption and dispersion properties in time domain source/receiver reflection measurement." *J. Acoust. Soc. Am.* 118 (2005): 654–660.

Innanen, K. A. *Methods for the treatment of acoustic and absorptive/dispersive wave field measurements*. PhD thesis, University of British Columbia, 2003.

Innanen, K. A. "Two non-linear forward and inverse approximations for wave fields in the presence of sustained medium perturbations." *Proceedings of the 75th Annual Meeting of the Society of Exploration Geophysicists, Houston, TX.* . SEG, 2005.

Innanen, K. A. and A. B. Weglein. "Construction of absorptive/dispersive wave fields with the forward scattering series." *Journal of Seismic Exploration* 12 (2003): 259–282.

Innanen, K. A. and A. B. Weglein. "Linear inversion for absorptive/dispersive medium parameters." *Proceedings of the 74th Annual Meeting of the Society of Exploration Geophysicists, Denver, CO.* . SEG, 2004.

Innanen, K. A. and A. B. Weglein. "Towards non-linear construction of a Q-compensation operator directly from reflection seismic data." *Proceedings of the 75th Annual Meeting of the Society of Exploration Geophysicists, Houston, TX.* . SEG, 2005.

Kjartansson, E. *Attenuation of seismic waves in rocks and applications in energy exploration*. PhD thesis, Stanford University, 1979.

Kjartansson, E. "Constant-Q Wave Propagation and Attenuation." *Journal of Geophysical Research* 84 (1979): 4737–4748.

Lam, C. H., B. J. Kooij, and A. T. de Hoop. "Impulsive sound reflection from an absorptive and dispersive planar boundary." *J. Acoust. Soc. Am.* 116 (2004): 677–685.

Liu, F., A. B. Weglein, K. A. Innanen, and B. G. Nita. "Multi-dimensional seismic imaging using the inverse scattering series." *Proceedings of the 76th Annual Meeting of the Society of Exploration Geophysicists, New Orleans, LA.* . Soc. Expl. Geop., 2006.

Liu, F., A.B. Weglein, K.A. Innanen, and B.G Nita. "Extension of the non-linear depth imaging capability of the inverse scattering series to multidimensional media: strategies and numerical results." 2005.

Quan, Y. and J. M. Harris. "Seismic attenuation tomography using the frequency shift method." *Geophysics* 62 (1997): 895–905.

Raz, S. "Direct reconstruction of velocity and density profiles from scattered field data." *Geophysics* 46 (1981): 832.

Rickett, J. "Integrated estimation of interval-attenuation profiles." *Geophysics* 71 (2006): A19.

Rickett, J. "Estimating attenuation and the relative information content of amplitude and phase spectra." *Geophysics* 72 (2007): R19.

Samec, P. and J. P. Blangy. "Viscoelastic attenuation, anisotropy, and AVO." *Geophysics* 57 (1992): 441.

Shaw, S. A. *An inverse scattering series algorithm for depth imaging of reflection data from a layered acoustic medium with an unknown velocity model*. PhD thesis, University of Houston, 2005.

Shaw, S. A., A. B. Weglein, D. J. Foster, K. H. Matson, and R. G. Keys. "Isolation of a leading order depth imaging series and analysis of its convergence properties." *Journal of Seismic Exploration* 2 (November 2004): 157–195.

Stolt, R. H. and A. B. Weglein. "Migration and inversion of seismic data." *Geophysics* 50 (1985): 2458–2472.

Tonn, R. "The Determination of the Seismic Quality Factor Q from VSP Data: a Comparison of Different Computational Methods." *Geophysical Prospecting* 39 (1991): 1–27.

Weglein, A. B., D. J. Foster, K. H. Matson, S. A. Shaw, P. M. Carvalho, and D. Corrigan. "An inverse-scattering sub-series for predicting the spatial location of reflectors without the precise reference medium and wave velocity." *71st Annual Internat. Mtg., Soc. Expl. Geophys., Expanded Abstracts*. . Soc. Expl. Geophys., 2001. 2108–2111.

Weglein, A. B. and R. H. Stolt. "Migration-Inversion Revisited." *The Leading Edge* Aug (1999): 950.

Weglein, Arthur B., Fernanda V. Araújo, Paulo M. Carvalho, Robert H. Stolt, Kenneth H. Matson, Richard T. Coats, Dennis Corrigan, Douglas J. Foster, Simon A. Shaw, and Haiyan Zhang. "Inverse Scattering Series and Seismic Exploration." *Inverse Problems* (2003): R27–R83.

White, J. E. "The accuracy of estimating Q from seismic data." *Geophysics* 57 (1992): 1508–1511.

Zhang, C. and T. J. Ulrych. "Estimation of Quality Factors from CMP Records." *Geophysics* 67 (2002): 1542.

Zhang, H. and A. B. Weglein. "The inverse scattering series for tasks associated with primaries: depth imaging and direct non-linear inversion of 1D variable velocity and density acoustic media." *Proceedings of the 75th Annual Meeting of the Society of Exploration Geophysicists, Houston, TX.* . Soc. Expl. Geop., 2006.

Zhang, H. and A. B. Weglein. "The inverse scattering series for tasks associated with primaries: direct non-linear inversion of 1D elastic media." *Proceedings of the 76th Annual Meeting of the Society of Exploration Geophysicists, New Orleans, LA.* . Soc. Expl. Geop., 2006.

Imaging diffractive targets within an unknown 1D overburden: progressing theory towards collapsing diffractions without the velocity model

K. A. Innanen

Abstract

There are closed-form forward scattering series approximations for scalar (acoustic constant density) primaries diffracting from a 2D target below a 1D overburden. By extending previous methods designed for purely 1D media, these primary approximations may be inverted order-by-order. The result is a set of direct non-linear formulas for the location and amplitude of a diffractive target beneath an unknown overburden. Under the 1D overburden assumption the forward mathematical forms are reminiscent of WKBJ- and eikonal approximations in a Born framework. The inverse forms are entirely in terms of data and the homogeneous reference medium properties. This work represents a partial capture of primary-processing capability of the inverse scattering series; we anticipate using the insight gained here to continue to extract further terms from the series, as a means to extend the types of imaging issues accommodated by current velocity independent imaging capture.

1 Introduction

Standard, linear depth-imaging methods correctly collapse diffractions when the velocity model is known. Non-linear direct imaging or imaging-inversion algorithms derived from the inverse scattering series bear a more difficult burden: to collapse diffractions in the absence of a velocity model, through non-linear data activity. We are working to capture sets of terms from the 2D/3D inverse scattering series accommodating of an increasingly complete set of wavefield/data phenomena, of which diffractions are an example, in their imaging capability. Liu et al. (2005) present a 2D imaging algorithm whose capture of imaging capability includes all aspects of the problem for which there is a 1D analog. Here we present an early stage candidate set of closed-form formulas derived directly from non-linear scattering theory for the location and amplitude of unknown diffractive targets in a subsurface with an unknown vertically-varying overburden.

We suspect that these formulas may prove to be of some value within their range of applicability: collapsing diffractions within unknown, extended overburdens that vary in depth. But as we focus on the details, the big picture should not be lost. The forward and inverse scattering series frameworks that underlie what is discussed below are not hindered by any such restricted range of medium variability. At any given time we may be, and are, attempting to extract computable portions of the full processing capability of the inverse scattering series. But we will in the end return to the underlying multidimensional framework, having gleaned the lessons of the 1D analysis, and launch into the more complex multidimensional world, extending and superseding the current extracted capability. All limitations of the effectiveness of any inverse scattering series formula to date (Carvalho, 1992; Araújo, 1994; Weglein et al., 1997, 2001, 2003; Shaw et al., 2004; Ramírez and

Weglein, 2005; Liu et al., 2005; Innanen, 2005; Zhang and Weglein, 2005, e.g.), whether signified by names like *leading order*, or *attenuator*, have been traced to partial, though powerful, capture of the full inverse scattering series capability. We study and implement the current subset of inverse scattering series terms, determine their strengths and limitations, and take what we have learned back to the full theory, to extract more. To be specific, why a 1D overburden? Two reasons. First, the best way to understand how the series works is to study it under the simplest conditions that permit the phenomenon of interest to exist. For diffractions, the entire medium cannot be 1D, because such media do not produce diffractions, but the overburden can—so long as the target is not. Second, we are also attracted to a non-fundamental aspect of inverse series algorithms: whether or not they are expressible in closed-form. If so, we achieve a very significant lessening of computational burden. The assumption of a 1D overburden also permits this.

That said, we turn to the details of the current problem. The derivation of the formulas follows a set of steps involving both the forward[1] and the inverse scattering series treatment of primaries. Let us begin with a survey of these steps. First, given a homogeneous acoustic reference medium and an actual medium that varies only in the vertical direction, a subset of terms of the forward scattering series can be extracted to approximate the primaries associated with this medium in a 1.5D reflected data set. This is reviewed in Appendix A. Second, this greatly reduced set of forward scattering series terms may be used to produce an inverse series that determines the depth-varying perturbation order-by-order in the reflected primary data. This is reviewed in Appendix B. These series are not fully task-separated, in that they work to determine the location and amplitude of the reflectors simultaneously, however they are straightforwardly derived, and reflect a particular and striking symmetry in the forward and inverse series.

Taking these developments as read, the questions of moment are (1) to what extent do these 1.5D developments transfer to multidimensional perturbations, and (2) to what extent can the computational efficiency of the 1.5D methods (which are expressible in closed-form) be maintained?

In the following section we first ask these questions of the forward scattering series, and answer by reviewing the diffraction expressions discussed in MOSRP-05 (Innanen, 2006), in which closed-form expressions for diffractions were shown to be derivable provided only the depth-varying component of the perturbation is large and/or extended. In particular, Appendix C illustrates more fully the two kinds of criteria for retention and rejection of forward series terms included in the diffracted primary approximation, which extends the results of Appendix A to media that can produce 2D wavefield phenomena.

The new research here is in Section 3, in which we apply the order-by-order inversion procedure of Appendix B to the diffracted primary approximation, generating candidate order-by-order formulas

[1]The forward scattering series is a formalism for the determination of wavefields that places no restrictions on the dimensionality of the medium or the rapidity of its variations. The inverse scattering series is a formalism which accomplishes all tasks of inversion with a similar lack of restriction. In MOSRP-05 (Innanen, 2006, 2007) we described a forward scattering series approximation of diffracted primaries that *assumed the perturbation to be large/extended in depth with small lateral variability.* In doing so, a mathematical form with the hallmarks of a Born approximation with eikonal-approximate Green's functions (Clayton and Stolt, 1981) for vertically heterogeneous media was produced (in a related matter, Amundsen et al. (2005) have derived data-driven imaging and inversion algorithms from a direct appeal to WKBJ-like forms). It is important to emphasize that these trappings are the consequence of the above medum assumptions, which may be jettisoned in favor of series forms.

for the location and amplitude of unknown diffractive targets given an unknown overburden, under the assumption that that overburden is vertically-varying.

2 Approximating primaries from a 2D target beneath/within a 1D overburden

We review the extension of the approximation of primaries that have reflected (and diffracted) from a medium consisting of (1) a homogeneous wholespace perturbed by (2) a large, extended 1D perturbation and a small, transient 2D perturbation underlying or embedded in the 1D structure. Assuming this type of medium (see Figure 1), in which the 2D component of the perturbation is adequately explicable as being linear in the wavefield, permits amongst other things closed form expressions for the reflected primaries to be generated. We develop the 2D case for convenience, but the 3D generalization is essentially immediate. The wave equations we begin with are

$$\begin{aligned}\left[\nabla_g^2 + \frac{\omega^2}{c^2(x_g, z_g)}\right] G(x_g, z_g, x_s, z_s, \omega) &= \delta(x_g - x_s)\delta(z_g - z_s)\\ \left[\nabla_g^2 + k^2\right] G_0(x_g, z_g, x_s, z_s, \omega) &= \delta(x_g - x_s)\delta(z_g - z_s)\end{aligned} \tag{1}$$

where $k = \omega/c_0$. Setting $\alpha(x, z) = 1 - c_0^2/c^2(x, z)$, and expressing the reference Green's function in three possible ways:

$$\begin{aligned}G_0(k_g, z_g, x_s, z_s, \omega) &= e^{-ik_g x_s} \frac{e^{iq_g|z_g - z_s|}}{i2q_g},\\ G_0(x_g, z_g, k_s, z_s, \omega) &= e^{ik_s x_g} \frac{e^{iq_s|z_s - z_g|}}{i2q_s},\\ G_0(x', z', x'', z'', \omega) &= \frac{1}{2\pi}\int dk' e^{ik'(x' - x'')} \frac{e^{iq'|z' - z''|}}{i2q'},\end{aligned} \tag{2}$$

where, e.g.,

$$q' = \frac{\omega}{c_0}\sqrt{1 - \frac{c_0^2 k'^2}{\omega^2}}, \tag{3}$$

by the usual means the resulting Born series is

$$\begin{aligned}G_s(k_g, z_g, k_s, z_s, \omega) &= G - G_0\\ &= G_1 + G_2 + G_3 + \ldots \ .\end{aligned} \tag{4}$$

We will evaluate and manipulate the low order terms of this series and identify patterns within. The terms have the general form

$$G_1(k_g, z_g, k_s, z_s, \omega) = \int dz' \int dx' G_0(k_g, z_g, x', z', \omega) k^2 \alpha(x', z') G_0(x', z', k_s, z_s, \omega), \tag{5}$$

then

$$\begin{aligned}G_2(k_g, z_g, k_s, z_s, \omega) = &\int dz' \int dx' G_0(k_g, z_g, x', z', \omega) k^2 \alpha(x', z')\\ &\times \int dz'' \int dx'' G_0(x', z', x'', z'', \omega) k^2 \alpha(x'', z'') G_0(x'', z'', k_s, z_s, \omega),\end{aligned} \tag{6}$$

etc. Now let us assume that although α is 2D, it is large and/or extended only in depth. That is, we may write it as

$$\alpha(x,z) = A(z) + B(x,z), \tag{7}$$

where $A(z)$ is large and extended and $B(x,z)$ is small and spatially transient, such that if it were alone perturbing the reference medium we would not hesitate to approximate it as being linear in the scattered field. Using this form for the perturbation, we will begin computing series terms.

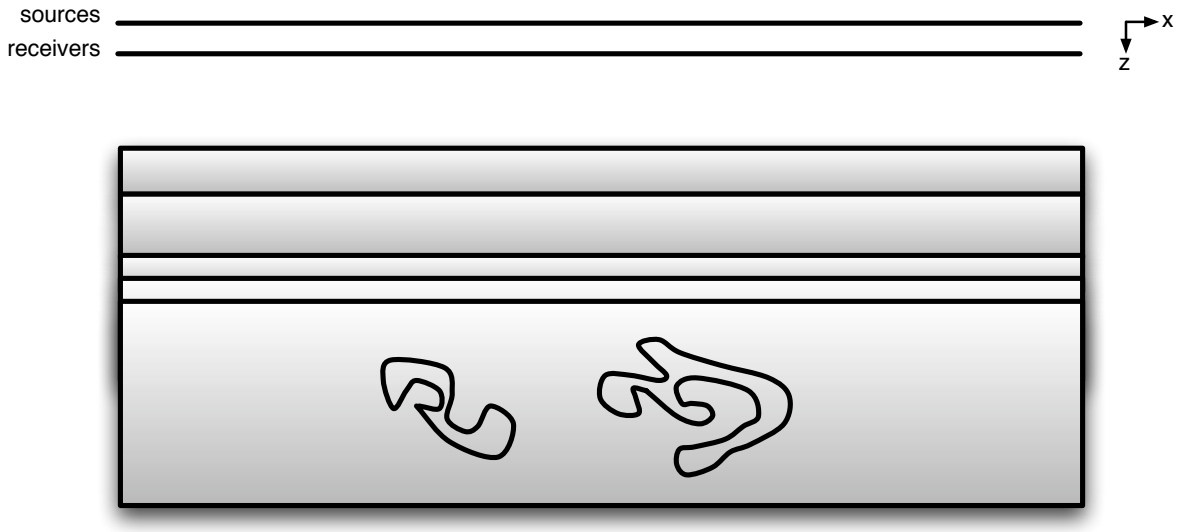

Figure 1: *Assume the perturbation has a 1D component that is large and extended, and a 2D component that is small and transient, but capable of generating, e.g., diffractions.*

At each order, we will retain or reject terms based on two criteria. First, scattering geometry will determine whether or not the term is contributing to a reflected primary (meaning either the primary due to specular reflection or the primary-like part of a diffraction) or, e.g., a multiple. Only those terms contributing to primaries are retained. Second, terms that are of a certain kind of non-linearity in α are to be retained: terms that are non-linear in A are kept, and terms that are non-linear in B are rejected. Every retained term will therefore take non-linear account of the (assumed) large and extended 1D overburden, and linear account of the 2D target as it constructs the primaries of the wavefield. See MOSRP-05 and/or Appendix A for more discussion.

Placing sources and receivers everywhere on the surfaces $z = z_s$ and $z = z_g$ respectively, the result is a series that forward models primary data:

$$R^P(k_g, z_g, k_s, z_s, \omega) = R_1^P + R_2^P + R_3^P + \ldots \ . \tag{8}$$

The linear term is the result of evaluating equation (5) with no rejection of any scattering contributions required:

$$R_1^P(k_g, z_g, k_s, z_s, \omega) = -\frac{e^{-iq_g z_g - iq_s z_s}}{4} \frac{k^2}{q_g q_s} \int dz' e^{i(q_g+q_s)z'} \alpha(k_g - k_s, z'). \tag{9}$$

The second order term requires no manipulation to reject non-primary contributions, however, it does require manipulation such that the retained terms are linear in B and non-linear in A. In appendix A we show that this results in

$$\begin{aligned} &R_2^P(k_g, z_g, k_s, z_s, \omega) \\ &\quad = -\frac{e^{-iq_g z_g - iq_s z_s}}{4}\frac{k^2}{q_g q_s}\int dz' e^{i(q_g+q_s)z'}\left(\frac{-iq_g}{2\cos^2\theta_g}\int_{z_g}^{z'} A(z'')dz''\right)\alpha(k_g-k_s,z') \\ &\quad - \frac{e^{-iq_g z_g - iq_s z_s}}{4}\frac{k^2}{q_g q_s}\int dz' e^{i(q_g+q_s)z'}\alpha(k_g-k_s,z')\left(\frac{-iq_s}{2\cos^2\theta_s}\int_{z_s}^{z'} A(z'')dz''\right), \end{aligned} \tag{10}$$

where $\cos\theta_g = q_g/k$ and $\cos\theta_s = q_s/k$. The third order term, after rejection of contributions to multiples and the same substitutions described in appendix C, is

$$\begin{aligned} &R_3^P(k_g, z_g, k_s, z_s, \omega) \\ &= -\frac{e^{-iq_g z_g - iq_s z_s}}{4}\frac{k^2}{q_g q_s}\int dz' e^{i(q_g+q_s)z'}\frac{1}{2}\left(\frac{-iq_g}{2\cos^2\theta_g}\int_{z_g}^{z'} A(z'')dz''\right)^2\alpha(k_g-k_s,z') \\ &\quad - \frac{e^{-iq_g z_g - iq_s z_s}}{4}\frac{k^2}{q_g q_s}\int dz' e^{i(q_g+q_s)z'}\left(\frac{-iq_g}{2\cos^2\theta_g}\int_{z_g}^{z'} A(z'')dz''\right)\alpha(k_g-k_s,z')\left(\frac{-iq_s}{2\cos^2\theta_s}\int_{z_g}^{z'} A(z'')dz''\right) \\ &\quad - \frac{e^{-iq_g z_g - iq_s z_s}}{4}\frac{k^2}{q_g q_s}\int dz' e^{i(q_g+q_s)z'}\alpha(k_g-k_s,z')\frac{1}{2}\left(\frac{-iq_s}{2\cos^2\theta_s}\int_{z_g}^{z'} A(z'')dz''\right)^2. \end{aligned} \tag{11}$$

The approximation is based on the sum of these types of retained terms over all orders, that is, the diffracted primaries are given by:

$$\begin{aligned} &R^P(k_g, z_g, k_s, z_s, \omega) \\ &\quad = R_1^P + R_2^P + R_3^P + ... \\ &\quad = -\frac{e^{-iq_g z_g - iq_s z_s}}{4}\frac{k^2}{q_g q_s}\int dz' e^{i(q_g+q_s)z'}\alpha(k_g-k_s,z') \\ &\qquad \times\left[1 + \left(\frac{-iq_g}{2\cos^2\theta_g}\int_{z_g}^{z'} A(z'')dz''\right) + \left(\frac{-iq_s}{2\cos^2\theta_s}\int_{z_s}^{z'} A(z'')dz''\right)\right. \\ &\qquad + \frac{1}{2!}\left(\frac{-iq_g}{2\cos^2\theta_g}\int_{z_g}^{z'} A(z'')dz''\right)^2 + \left(\frac{-iq_g}{2\cos^2\theta_g}\int_{z_g}^{z'} A(z'')dz''\right)\left(\frac{-iq_s}{2\cos^2\theta_s}\int_{z_s}^{z'} A(z'')dz''\right) \\ &\qquad \left. + \frac{1}{2!}\left(\frac{-iq_s}{2\cos^2\theta_s}\int_{z_s}^{z'} A(z'')dz''\right)^2 + ...\right]. \end{aligned} \tag{12}$$

The series in brackets is the product of two Taylor's series for exponential functions:

$$R^P(k_g, z_g, k_s, z_s, \omega) = \int dz' \frac{e^{iq_g\left[z'-z_g-\frac{1}{2\cos^2\theta_g}\int_{z_g}^{z'} A(z'')dz''\right]}}{i2q_g} k^2\alpha(k_g-k_s,z') \frac{e^{iq_g\left[z'-z_s-\frac{1}{2\cos^2\theta_s}\int_{z_s}^{z'} A(z'')dz''\right]}}{i2q_s}, \tag{13}$$

in which the non-linear influence of the 1D portion of the medium is seen to have been brought up into the arguments of "renormalized" Green's functions, whose form has many of the trappings of an eikonal approximation. The lessons of the high/low order approximations discussed in purely 1D case furthermore suggest that a scaling of these arguments is appropriate for larger contrasts in the 1D perturbation component:

$$R^{PM}(k_g, z_g, k_s, z_s, \omega) = \int dz' \frac{e^{iq_g[z'-z_g-Z_M(z_g,z',\theta_g,A)]}}{i2q_g} k^2\alpha(k_g-k_s,z') \frac{e^{iq_g[z'-z_s-Z_M(z_s,z',\theta_s,A)]}}{i2q_s}, \tag{14}$$

and

$$R^{PL}(k_g, z_g, k_s, z_s, \omega) = \int dz' \frac{e^{iq_g[z'-z_g-Z_L(z_g,z',\theta_g,A)]}}{i2q_g} k^2\alpha(k_g-k_s,z') \frac{e^{iq_g[z'-z_s-Z_L(z_s,z',\theta_s,A)]}}{i2q_s}, \tag{15}$$

where

$$\begin{aligned} Z_M(z,z',\theta,A) &= \frac{1}{2\cos^2\theta}\int_z^{z'} A(z'')dz'', \\ Z_L(z,z',\theta,A) &= \frac{1}{2\cos^2\theta}\int_z^{z'} \frac{A(z'')}{1-0.25A(z'')}dz'', \end{aligned} \tag{16}$$

contain the non-linear perturbation in a more compact form.

Let us illustrate the activity of this component of the forward scattering series with two numerical examples. Figures 2–3 illustrate two scenarios, the former of which involves a relatively simple boundary beneath a large extended overburden, and the latter of which involves a rugose boundary beneath a similar overburden. Figures 4a and c illustrate two shot records of the primaries from the scattering body in the absence of the perturbed overburden, i.e., assuming no overburden is present; Figures 4b and d illustrate the result of the non-linear scattering model in which the overburden is present in the perturbation. Similarly presented are the primaries from the second model in Figure 5. Notice in particular that although the linear and non-linear approximations responses have a similar aspect, the phase patterns–arrival times and move-out—are different.

3 Order-by-order inversion of the diffraction approximation

Part of the motivation for developing the forward scattering series approximation of primary diffractions within a large, extended perturbation is that there exist methods (previously developed in

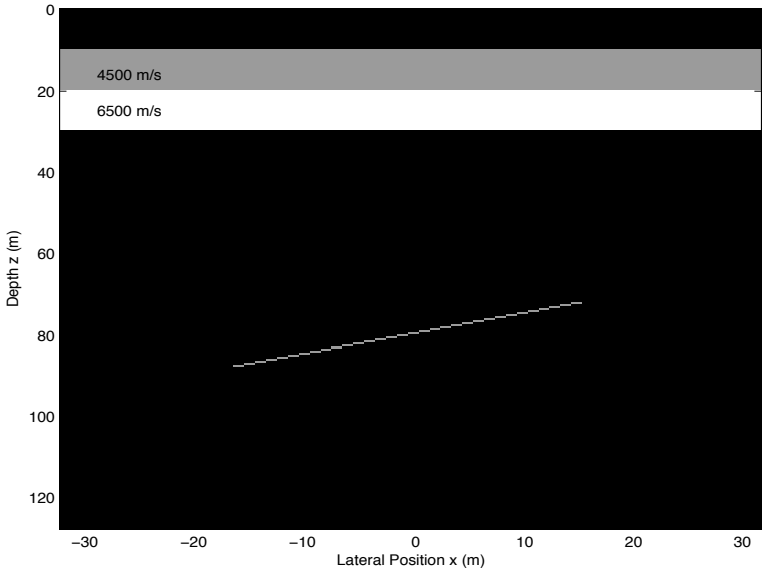

Figure 2: Model with a simple dipping boundary, overlain by a fast overburden.

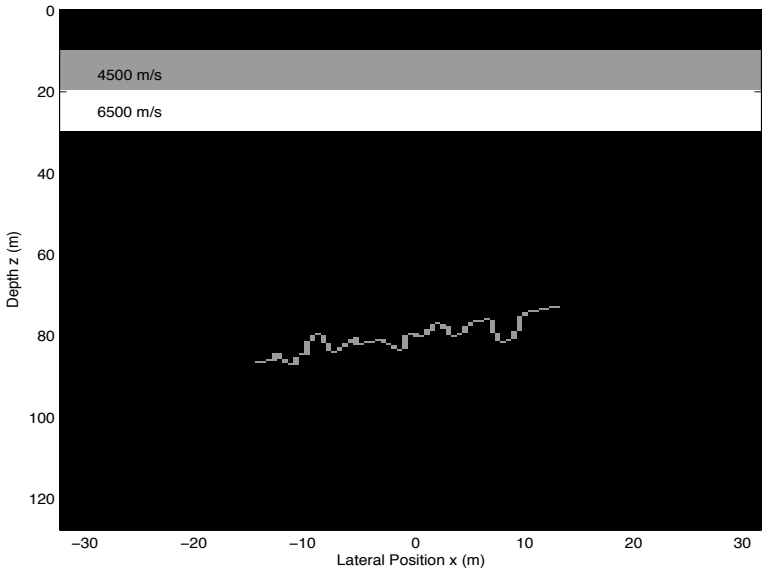

Figure 3: Model with a rugose dipping boundary, overlain by a fast overburden.

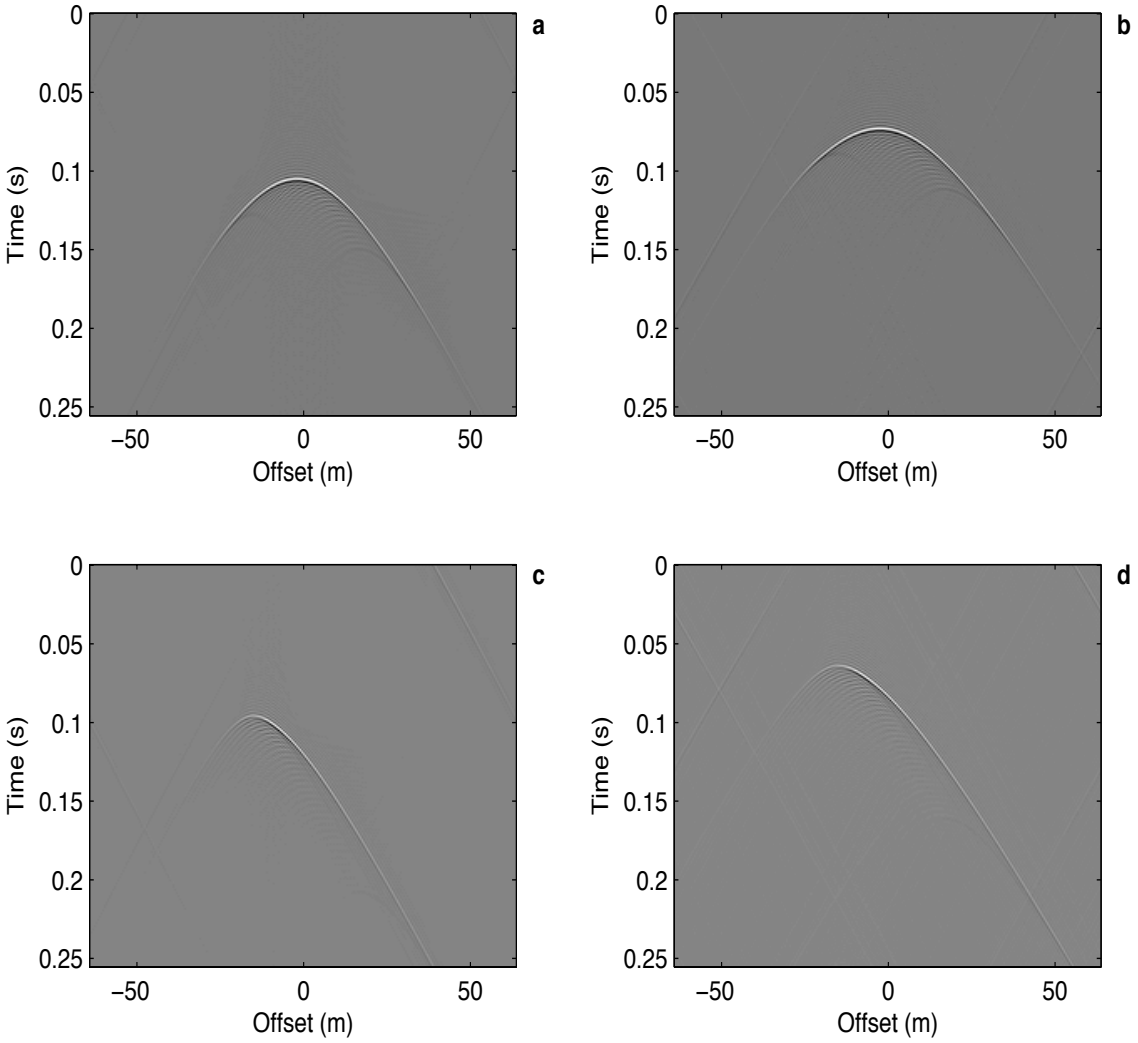

Figure 4: Scattering approximation results for the dipping boundary model: (a) shot record with centered shot location, no overburden; (b) shot record with centered shot location, overburden present; (c) shot record with offset shot location, no overburden; (d) shot record with offset shot location, overburden present.

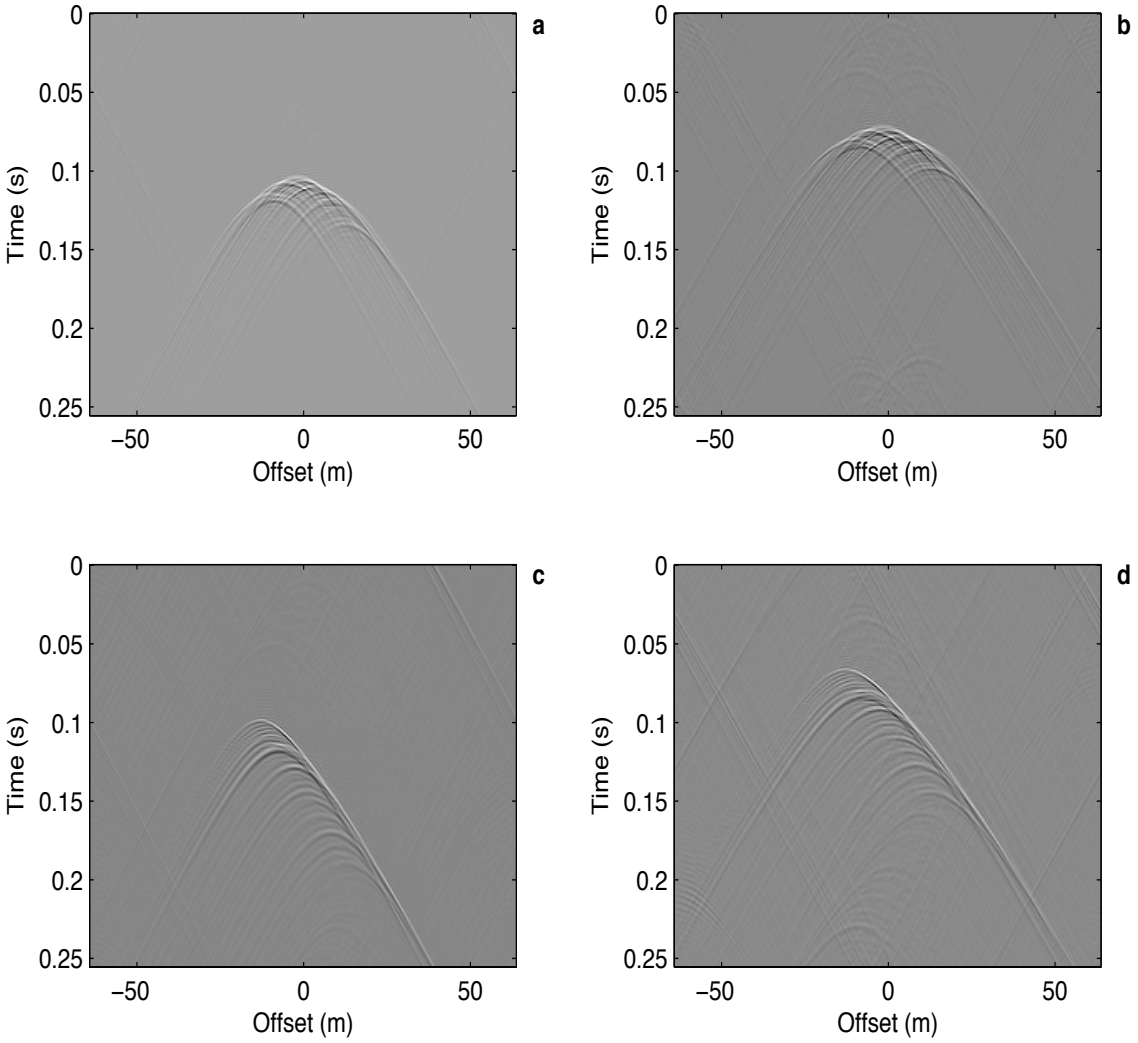

Figure 5: Scattering approximation results for the rugose boundary model: (a) shot record with centered shot location, no overburden; (b) shot record with centered shot location, overburden present; (c) shot record with offset shot location, no overburden; (d) shot record with offset shot location, overburden present.

the purely 1D case) for directly inverting such expressions, immediately producing algorithms for imaging/inversion directly and non-linearly in terms of measured data. In this section we extend those 1D inversion methods to this partial 2D case.

We begin with the series form of the diffracted primary approximation in equation (12). Although we loosely suggested that the primaries were evaluated on a fixed measurement surface in the previous section, it was not necessary to fix them as such. It is now. We define the data to be reflected primaries measured at a fixed depth z_s, due to sources at a fixed depth z_s:

$$\begin{aligned} &D(k_g, z_g, k_s, z_s, \omega) \\ &\equiv -\frac{e^{-iq_g z_g - iq_s z_s}}{4}\frac{k^2}{q_g q_s}\int dz' e^{i(q_g+q_s)z'}\alpha(k_g-k_s,z') \\ &\quad\times\left[1+\left(\frac{-iq_g}{2\cos^2\theta_g}\int_{z_g}^{z'}A(z'')dz''\right)+\left(\frac{-iq_s}{2\cos^2\theta_s}\int_{z_s}^{z'}A(z'')dz''\right)\right. \\ &\quad+\frac{1}{2!}\left(\frac{-iq_g}{2\cos^2\theta_g}\int_{z_g}^{z'}A(z'')dz''\right)^2+\left(\frac{-iq_g}{2\cos^2\theta_g}\int_{z_g}^{z'}A(z'')dz''\right)\left(\frac{-iq_s}{2\cos^2\theta_s}\int_{z_s}^{z'}A(z'')dz''\right) \\ &\quad\left.+\frac{1}{2!}\left(\frac{-iq_s}{2\cos^2\theta_s}\int_{z_s}^{z'}A(z'')dz''\right)^2+...\right]. \end{aligned} \tag{17}$$

We require a further approximation before proceeding. We have developed the series in equation (17) by assuming that the influence of $B(x,z)$ on the non-linear components of the series is small and can be neglected. Since the influence of B is by assumption small, we may now return it essentially without penalty. Hence we write:

$$\begin{aligned} &D(k_g, z_g, k_s, z_s, \omega) \\ &=-\frac{e^{-iq_g z_g - iq_s z_s}}{4c_0^2}\frac{\omega^2}{q_g q_s}\int dz' e^{i(q_g+q_s)z'}\alpha(k_g-k_s,z') \\ &\quad\times\left[1+\left(\frac{-iq_g}{2\cos^2\theta_g}\int_{z_g}^{z'}\alpha(k_g-k_s,z'')dz''\right)+\left(\frac{-iq_s}{2\cos^2\theta_s}\int_{z_s}^{z'}\alpha(k_g-k_s,z'')dz''\right)\right. \\ &\quad+\frac{1}{2!}\left(\frac{-iq_g}{2\cos^2\theta_g}\int_{z_g}^{z'}\alpha(k_g-k_s,z'')dz''\right)^2+\left(\frac{-iq_g}{2\cos^2\theta_g}\int_{z_g}^{z'}\alpha(k_g-k_s,z'')dz''\right) \\ &\quad\left.\times\left(\frac{-iq_s}{2\cos^2\theta_s}\int_{z_g}^{z'}\alpha(k_g-k_s,z'')dz''\right)+\frac{1}{2!}\left(\frac{-iq_s}{2\cos^2\theta_s}\int_{z_g}^{z'}\alpha(k_g-k_s,z'')dz''\right)^2+...\right]. \end{aligned} \tag{18}$$

To invert this directly, we express

$$\alpha(x,z)=\alpha_1(x,z)+\alpha_2(x,z)+\alpha_3(x,z)+..., \tag{19}$$

where α_n is n'th order in the *primary* data D, substitute this series into equation (17), equate like orders, and solve for each α_n. The first-order inverse equation is, after carrying out the integral

with respect to z',

$$D(k_g, z_g, k_s, z_s, \omega) = -\frac{e^{-iq_g z_g - iq_s z_s}}{4} \frac{k^2}{q_g q_s} \alpha_1(k_g - k_s, -q_g - q_s) \tag{20}$$

We next change variables to the midpoint and offset conjugate wavenumbers $k_m = k_g - k_s$ and $k_h = k_g + k_s$, and the depth wavenumber $k_z = -q_g - q_s$, following Clayton and Stolt (1981), who provide expressions for ω, q_g and q_s in terms of the new three variables:

$$\begin{aligned} q_g(k_m, k_h, k_z) &= -\frac{k_z}{2}\left(1 - \frac{k_m k_h}{k_z^2}\right) \\ q_s(k_m, k_h, k_z) &= -\frac{k_z}{2}\left(1 + \frac{k_m k_h}{k_z^2}\right) \\ \omega(k_m, k_h, k_z) &= -\frac{c_0 k_z}{2}\sqrt{\left(1 + \frac{k_m^2}{k_z^2}\right)\left(1 + \frac{k_h^2}{k_z^2}\right)}. \end{aligned} \tag{21}$$

Taking the dependence of the data on the source and receiver depths as read, we re-express equation (20) as

$$D(k_m, k_h, k_z) = -\frac{e^{-iq_g(k_m,k_h,k_z)z_g - iq_s(k_m,k_h,k_z)z_s}}{4c_0^2} \frac{\omega^2(k_m, k_h, k_z)}{q_g(k_m, k_h, k_z) q_s(k_m, k_h, k_z)} \alpha_1(k_m, k_z). \tag{22}$$

Since we are assuming the data are explainable through the variability of a single parameter, the P-wave velocity or acoustic wavespeed $c(x, z)$, each instance of the offset conjugate k_h produces a separate estimate of α_1:

$$\alpha_1(k_m, k_z | k_h) = -4c_0^2 C(k_m, k_h, k_z) D(k_m, k_h, k_z), \tag{23}$$

where

$$C(k_m, k_h, k_z) = e^{iq_g(k_m,k_h,k_z)z_g + iq_s(k_m,k_h,k_z)z_s} \frac{q_g(k_m, k_h, k_z) q_s(k_m, k_h, k_z)}{\omega^2(k_m, k_h, k_z)}, \tag{24}$$

and hence in the z domain we have

$$\alpha_1(k_m, z | k_h) = -\frac{2c_0^2}{\pi} \int dk_z e^{ik_z z} C(k_m, k_h, k_z) D(k_m, k_h, k_z). \tag{25}$$

Next we collect all second order terms that arise from substituting equation (19) into (18). After cancellation of several pre-factors and a Fourier transform on the LHS, we have

$$\begin{aligned} \alpha_2(k_m, k_z) = &\int dz' e^{i(q_g + q_s)z'} \alpha_1(k_m, z') \\ &\times \left[\left(\frac{iq_g}{2\cos^2\theta_g} \int_{z_g}^{z'} \alpha_1(k_m, z'') dz'' \right) + \left(\frac{iq_s}{2\cos^2\theta_s} \int_{z_s}^{z'} \alpha_1(k_m, z'') dz'' \right) \right]. \end{aligned} \tag{26}$$

But, from equation (25), we have an $\alpha_1(k_m, z)$ for every k_h value in the data, therefore we will likewise be able to compute a suite of second order functions $\alpha_2(k_m, z)$, one for each k_h:

$$\begin{aligned}\alpha_2(k_m, k_z|k_h) = &\int dz' e^{i(q_g+q_s)z'} \alpha_1(k_m, z'|k_h) \\ &\times \left[\left(\frac{iq_g}{2\cos^2\theta_g} \int_{z_g}^{z'} \alpha_1(k_m, z''|k_h) dz'' \right) + \left(\frac{iq_s}{2\cos^2\theta_s} \int_{z_s}^{z'} \alpha_1(k_m, z''|k_h) dz'' \right) \right],\end{aligned} \tag{27}$$

in which the functional dependences of q_g, q_s, ω, θ_g, and θ_s, on k_m, k_h, and k_z are all provided in equations (25).

As we continue this process at higher order, we produce a set of $\alpha_n(k_m, k_z|k_h)$ (left-hand side of each order), each of which is associated with (on the right-hand side) a sequence of operations on α_1 that closely mirrors the forward behavior, but without the alternating sign. The output we are interested is the sum of the left-hand side terms over all orders. This produces

$$\begin{aligned}\sum_{n=0}^{\infty} \alpha_{n+1}(k_m, k_z|k_h) = &\int dz' e^{i(q_g+q_s)z'} \alpha_1(k_m, z'|k_h) \\ &\times \left[\sum_{l=0}^{\infty} \frac{1}{l!} \left(\frac{iq_g}{2\cos^2\theta_g} \int_{z_g}^{z'} \alpha_1(k_m, z''|k_h) dz'' \right)^l \right] \left[\sum_{m=0}^{\infty} \frac{1}{m!} \left(\frac{iq_s}{2\cos^2\theta_s} \int_{z_s}^{z'} \alpha_1(k_m, z''|k_h) dz'' \right)^m \right].\end{aligned} \tag{28}$$

Defining $\alpha_{II} = \sum_n \alpha_{n+1}$, and recognizing again the product of Taylor's series, we finally have the moderate (which we derived) and large (which we presume based on experience) contrast algorithms

$$\alpha_{II}^M(k_m, k_z|k_h) = \int dz' e^{iq_g[z' + Z_M(z_g, z', \theta_g, \alpha_1)]} \alpha_1(k_m, z'|k_h) e^{iq_s[z' + Z_M(z_s, z', \theta_s, \alpha_1)]}, \tag{29}$$

and

$$\alpha_{II}^L(k_m, k_z|k_h) = \int dz' e^{iq_g[z' + Z_L(z_g, z', \theta_g, \alpha_1)]} \alpha_1(k_m, z'|k_h) e^{iq_s[z' + Z_L(z_s, z', \theta_s, \alpha_1)]}, \tag{30}$$

where

$$\begin{aligned}Z_M(z, z', \theta, \alpha_1) &= \frac{1}{2\cos^2\theta} \int_z^{z'} \alpha_1(k_m, z''|k_h) dz'', \\ Z_L(z, z', \theta, \alpha_1) &= \frac{1}{2\cos^2\theta} \int_z^{z'} \frac{\alpha_1(k_m, z''|k_h)}{1 - 0.25\alpha_1(k_m, z''|k_h)} dz'',\end{aligned} \tag{31}$$

and where (again) the functional dependences of q_g, q_s, ω, θ_g, and θ_s, on k_m, k_h, and k_z are all provided by the relations of Clayton and Stolt in equations (21).

The desired image in the spatial domain is then

$$\begin{aligned}\alpha_{II}^M(x, z|k_h) &= \left(\frac{1}{2\pi} \right)^2 \int dk_z \int dk_m e^{ik_z z} e^{ik_m x} \alpha_{II}^M(k_m, k_z|k_h) \\ \alpha_{II}^L(x, z|k_h) &= \left(\frac{1}{2\pi} \right)^2 \int dk_z \int dk_m e^{ik_z z} e^{ik_m x} \alpha_{II}^L(k_m, k_z|k_h).\end{aligned} \tag{32}$$

Provided the contrasts are within some reasonable range, the output α_{II} in equations (32) should be independent of k_h, i.e., the "gather" should have been "flattened".

The key equations here are (29) and (30). The resemblance to a linear form is misleading – notice that in the arguments of the exponentials are instances of the data, making this a highly non-linear activity. As with all task-separated inverse scattering series methods, the only inputs to this procedure are the homogeneous reference wavespeed (usually waterspeed), and the data.

4 Summary

There are closed-form forward scattering series approximations for scalar (acoustic constant density) primaries diffracting from a 2D target below a 1D overburden. By extending previous methods designed for purely 1D media, these primary approximations may be inverted order-by-order. The result is a set of direct non-linear formulas for the location and amplitude of a diffractive target beneath an unknown overburden. Under the 1D overburden assumption the forward mathematical forms are reminiscent of WKBJ- and eikonal approximations in a Born framework. The inverse forms are entirely in terms of data and the homogeneous reference medium properties.

5 Acknowledgments

Kris Innanen was supported by the DOE Basic Energy Sciences award DE-FG02-05ER15697. The support of the M-OSRP sponsors is also gratefully acknowledged.

References

Amundsen, L., A. Reitan, H. K. Helgesen, and B. Arntsen. "Data-driven inversion/depth imaging derived from approximations to one-dimensional inverse acoustic scattering." *Inverse Problems* 21 (2005): 1823–1850.

Araújo, F. V. *Linear and non-linear methods derived from scattering theory: backscattered tomography and internal multiple attenuation.* PhD thesis, Universidade Federal da Bahia, 1994.

Carvalho, P. M. *Free-surface multiple reflection elimination method based on nonlinear inversion of seismic data.* PhD thesis, Universidade Federal da Bahia, 1992.

Clayton, R. W. and R. H. Stolt. "A Born-WKBJ inversion method for acoustic reflection data." *Geophysics* 46 (1981): 1559–1567.

Innanen, K. A. "Two non-linear forward and inverse approximations for wave fields in the presence of sustained medium perturbations." *Proceedings of the 75th Annual Meeting of the Society of Exploration Geophysicists, Houston, TX.* . Soc. Expl. Geophys., 2005.

Innanen, K. A. "The forward scattering series and diffractions: non-linear series and closed-form expressions for wavefields reflecting from 2D medium structure." *MOSRP-05 Annual Report.* . 2006.

Innanen, K. A. "A non-linear scattering model of scalar wavefield events." *Submitted to Geophys. J. Int.* (2007).

Liu, F., A.B. Weglein, K.A. Innanen, and B.G Nita. "Extension of the non-linear depth imaging capability of the inverse scattering series to multidimensional media: strategies and numerical results." 2005.

Ramírez, A. C. and A.B. Weglein. "Progressing the analysis of the phase and amplitude prediction properties of the inverse scattering internal multiple attenuation algorithm.." *J. of Seismic Expl.* 13 (2005): 283–301.

Shaw, S. A., A. B. Weglein, D. J. Foster, K. H. Matson, and R. G. Keys. "Isolation of a leading order depth imaging series and analysis of its convergence properties." *Journal of Seismic Exploration* 2 (November 2004): 157–195.

Weglein, A. B., F. V. Araújo, P. M. Carvalho, R. H. Stolt, K. H. Matson, R. T. Coates, D. Corrigan, D. J. Foster, S. A. Shaw, and H. Zhang. "Inverse Scattering Series and Seismic Exploration." *Inverse Problems* (2003): R27–R83.

Weglein, A. B., D. J. Foster, K. H. Matson, S. A. Shaw, P. M. Carvalho, and D. Corrigan. "An inverse-scattering sub-series for predicting the spatial location of reflectors without the precise reference medium and wave velocity." *71st Annual Internat. Mtg., Soc. Expl. Geophys., Expanded Abstracts.* . Soc. Expl. Geophys., 2001. 2108–2111.

Weglein, A. B., F. A. Gasparotto, P. M. Carvalho, and R. H. Stolt. "An Inverse-Scattering Series Method for Attenuating Multiples in Seismic Reflection Data." *Geophysics* 62 (November-December 1997): 1975–1989.

Zhang, H. and A.B. Weglein. "The inverse scattering series for tasks associated with primaries: depth imaging and direct non-linear inversion of 1D variable velocity and density acoustic media." *SEG Technical Program Expanded Abstracts.* 2005, 1705–1708.

Appendix A: scattering approximation of primaries in 1.5D

In this appendix we demonstrate the approximation of primary reflections from the forward scattering series via a program of retention/rejection of certain relative scattering geometries in depth. We begin with two wave equations Weglein et al. (2003), involving differential operators $\mathbf{L}$, $\mathbf{L_0}$, and Green's operators $\mathbf{G}$, and $\mathbf{G_0}$:

$$\begin{aligned} \mathbf{LG} &= \mathbf{I}, \\ \mathbf{L_0 G_0} &= \mathbf{I}, \end{aligned} \tag{33}$$

whose elements are related through the Lippmann-Schwinger equation:

$$\mathbf{G} - \mathbf{G_0} = \mathbf{G_0}(\mathbf{L_0} - \mathbf{L})\mathbf{G}. \tag{34}$$

Calling these differences $\mathbf{\Psi} = \mathbf{G} - \mathbf{G_0}$ and $\mathbf{V} = \mathbf{L_0} - \mathbf{L}$, and eliminating $\mathbf{G}$ on the right-hand side by an iterating substitution, we have

$$\mathbf{\Psi} = \sum_{n=1}^{\infty} \mathbf{G_0}(\mathbf{V G_0})^n. \tag{35}$$

Equation (35) may be interpreted as an infinite series expansion of the "scattered" portion of the wave field associated with $\mathbf{G}$, namely $\mathbf{\Psi}$, in orders of the other Green's operator, $\mathbf{G_0}$, and $\mathbf{V}$, which is referred to as the perturbation operator. For the purposes of this paper, a 1.5D acoustic, constant density medium (i.e., scalar waves) is assumed in which all perturbations, or deviations from the reference medium, are in the wavespeed parameter. Under these circumstances, equation (34) becomes

$$\begin{aligned} \psi(x_g, z_g|k_s, z_s; k) = &\int_{-\infty}^{\infty} dz' \int_{-\infty}^{\infty} dx' G_0(x_g, z_g|x', z', k) \\ &\times V(z') G(x', z'|k_s, z_s; k), \end{aligned} \tag{36}$$

where $k = \omega/c_0$. Representing the forward scattering series in equation (35) as $\psi = \psi_1 + \psi_2 + ...$, the linear term is

$$\begin{aligned} \psi_1(x_g, z_g|k_s, z_s; k) = &\int_{-\infty}^{\infty} dz' \int_{-\infty}^{\infty} dx' G_0(x_g, z_g|x', z', k) \\ &\times V(z') G_0(x', z'|k_s, z_s; k), \end{aligned} \tag{37}$$

the quadratic term is

$$\begin{aligned} \psi_2(x_g, z_g|k_s, z_s; k) = &\int_{-\infty}^{\infty} dz' \int_{-\infty}^{\infty} dx' G_0(x_g, z_g|x', z', k) V(z') \\ &\times \int_{-\infty}^{\infty} dz'' \int_{-\infty}^{\infty} dx'' G_0(x', z'|x'', z'', k) V(z'') \\ &\times G_0(x'', z''|k_s, z_s; k), \end{aligned} \tag{38}$$

and so forth. In equations (37), (38) and beyond, the wave field is evaluated at a fixed receiver point (x_g, z_g) and source depth z_s, but is due to a suite of laterally-varying sources such that the wave field may be expressed in the x_s-conjugate domain k_s (i.e., source plane wave components are dealt with individually). Green's functions for 2D homogeneous acoustic media are

$$G_0(x_g, z_g|x', z', k) = \frac{1}{2\pi}\int_{-\infty}^{\infty} dk_g e^{ik_g(x_g-x')}\frac{e^{iq_g|z_g-z'|}}{i2q_g}, \tag{39}$$

and

$$G_0(x', z'|k_s, z_s, k) = e^{ik_s x'}\frac{e^{iq_s|z'-z_s|}}{i2q_s}, \tag{40}$$

where $q_g^2 = k^2 - k_g^2$ and $q_s^2 = k^2 - k_s^2$. These are used if the reference medium is chosen to be a homogeneous acoustic wholespace, fully characterized by a reference wavespeed c_0, in which case the perturbation is a measure of the disturbance of the actual medium away from c_0:

$$V(z) = k^2\left(1 - \frac{c_0^2}{c^2(z)}\right) \equiv k^2\alpha(z), \tag{41}$$

where the perturbation has been permitted to vary in depth (z) only. Assuming that $V(z) \neq 0$ for $z > 0$ only, and parametrizing in terms of the source plane wave angle $\theta = \cos^{-1}(q_s/k)$, the FSS expression for ψ becomes, after the solution of a sequence of Fourier integrals,

$$\psi(x_g|k_s, q_s, \theta) = \psi_1(x_g|k_s, q_s, \theta) + \psi_2(x_g|k_s, q_s, \theta) + ..., \tag{42}$$

where

$$\psi_1(x_g|k_s, q_s, \theta) = -\frac{1}{4\cos^2\theta}e^{ik_s x_g}e^{-iq_s(z_g+z_s)}\int_{-\infty}^{\infty} e^{i2q_s z'}\alpha(z')dz', \tag{43}$$

$$\begin{aligned}\psi_2(x_g|k_s, q_s, \theta) = \frac{i2q_s}{16\cos^4\theta}e^{ik_s x_g}e^{-iq_s(z_g+z_s)}&\int_{-\infty}^{\infty} e^{iq_s z'}\alpha(z') \\ &\times \int_{-\infty}^{\infty} e^{iq_s|z'-z''|}\alpha(z'')e^{iq_s z''}dz''dz',\end{aligned} \tag{44}$$

$$\begin{aligned}\psi_3(x_g|k_s, q_s, \theta) = -\frac{(i2q_s)^2}{64\cos^6\theta}e^{ik_s x_g}e^{-iq_s(z_g+z_s)}&\int_{-\infty}^{\infty} e^{iq_s z'}\alpha(z') \\ &\times \int_{-\infty}^{\infty} e^{iq_s|z'-z''|}\alpha(z'') \\ &\times \int_{-\infty}^{\infty} e^{iq_s|z''-z'''|}\alpha(z''')e^{iq_s z'''}dz'''dz''dz',\end{aligned} \tag{45}$$

etc. The computation and summation of a large number of these terms (assuming convergence) produces the full reflected wavefield associated with $\alpha(z)$.

Notice in equations (43) that the "down-and-back" nature of the linear term leads to a Fourier integral, with a depth of $2z$ in the kernel (one z from the "down", one from the "back"). To be

evaluated, each non-linear scattering term must be broken up into a set of sub-terms, or cases, based on the relative geometry of its scattering interactions. For instance, ψ_3 will be divided into four calculable parts, for the cases (1) $z' > z''$, $z'' > z'''$, (2) $z' > z''$, $z'' < z'''$, (3) $z' < z''$, $z'' > z'''$, and (4) $z' < z''$, $z'' < z'''$. To illustrate, consider further the third order term from equation (**??**) for three different cases of relative scattering geometry. Writing the third order term as

$$\psi_3(x_g|k_s, q_s, \theta) = -\frac{(i2q_s)^2}{64\cos^6\theta} e^{ik_s x_g} e^{-iq_s(z_g+z_s)} I_3, \tag{46}$$

and dividing I_3 into its four cases $I_{31} + I_{32} + I_{33} + I_{34}$, we can instructively examine three of those four.

Case 1: $z' > z''$ and $z'' > z'''$.

This portion of the integral in the expression for ψ_3 becomes

$$I_{31} = \int_{-\infty}^{\infty} e^{i2q_s z'} \alpha(z') \int_{-\infty}^{z'} \alpha(z'') \int_{-\infty}^{z''} \alpha(z''') dz''' dz'' dz'. \tag{47}$$

Notice that although this is third-order in α, i.e., it is no longer part of a single scattering approximation, the restrictions on relative scattering depths result in an integral with some strong similarities to that of ψ_1. The same Fourier kernel is generated, involving non-linear contributions that yet maintain the down-and-back geometry totaling a distance of $2z'$.

Case 2: $z' > z''$ and $z'' < z'''$.

This portion becomes

$$\begin{aligned} I_{32} &= \int_{-\infty}^{\infty} \alpha(z') \int_{-\infty}^{z'} e^{i2q_s z''} \alpha(z'') \int_{z''}^{\infty} \alpha(z''') dz''' dz'' dz' \\ &= \int_{-\infty}^{\infty} e^{i2q_s z'} \alpha(z') \left(\int_{-\infty}^{z'} \alpha(z'') dz'' \right)^2 dz'. \end{aligned} \tag{48}$$

The second line is derivable from the first by a switching of integration variables. Again, although the integrand has changed, the Fourier integral remains, as does the down-and-back geometry .

Case 3: $z' < z''$ and $z'' > z'''$.

This portion becomes

$$I_{33} = \int_{-\infty}^{\infty} e^{i2q_s z'} \alpha(z') \int_{-\infty}^{z'} e^{-i2q_s z''} \alpha(z'') \int_{z''}^{\infty} e^{i2q_s z'''} \alpha(z''') dz''' dz'' dz'. \tag{49}$$

The situation has changed slightly here; no general association with a "down and back" propagation distance of $2z'$ is possible. The form insists on reference medium propagation from 0 down to z''', from z''' up to z'', from z'' down to z', and from z' up to 0, a total distance usually in excess of $2z'$. However, the Fourier form occasionally recurs during integration: e.g., when $z''' = z''$, $z'' = z'$, and $z''' = z'' = z'$.

Since a certain subset of high order terms share the same Fourier integral form as the linear term, and the linear term approximates primaries only, we begin with the assumption that these high order terms also work to construct primaries, and primaries only. This seems to be supported by the argument from geometry for why the linear term itself approximates primaries: the "down-and-back" propagation path of wave energy mimics that of a primary. Here we peremptorily define a primary to be *the summation of all portions of the forward scattering series with the above Fourier form.* (This will include all instances similar to cases 1 and 2, and the special instances of case 3.)

Beyond deciding that a certain set of terms is worth computing, the key issue is collecting and calculating them in a reasonably efficient way. Although similar in scattering geometry, the terms to be summed are apparently different in their mathematical detail (compare cases 1 and 2 above). This suggests that computation of a high-order approximation with such a subset of terms, even if desirable, will be lengthy and involved. Fortunately, patterns exist that allow the reproduction of large (although incomplete) subsets of these terms. For instance, setting $z_g = z_s = 0$, successive application of integration by parts of each term shows that the expression

$$R_M(k_s, q_s, \theta) = -\frac{e^{ik_s x_g}}{4\cos^2\theta}\int_{-\infty}^{\infty} e^{i2q_s z'} \times \left\{\sum_{n=0}^{\infty} C_n^+ \left[\alpha(z')\left(\int_0^{z'} \alpha(z'')dz''\right)^n\right]^{(n)}\right\} dz', \tag{50}$$

where superscript (n) denotes the n'th derivative with respect to z' and $C_n^+ = \frac{(1/2)^n}{n!\cos^{2n}\theta}$, captures these terms exactly up to second order and closely but approximately thereafter, and

$$R_L(k_s, q_s, \theta) = -\frac{e^{ik_s x_g}}{4\cos^2\theta}\int_{-\infty}^{\infty} dz' e^{i2q_s z'} \times \left\{\sum_{n=0}^{\infty} C_n^+ \left[\alpha(z)\left(\sum_{k=1}^{\infty}\frac{1}{4^{k-1}}\int_0^{z} dz'\alpha^k(z')\right)^n\right]^{(n)}\right\} \tag{51}$$

captures them almost exactly up to third order and closely but approximately thereafter. Equation (51) incorporates all the terms of equation (50) and more, and hence subsumes it.

Appendix B: Order-by-order inversion of the 1.5D primary approximation

The inverse scattering series, a multi-dimensional multi-parameter inverse formalism, is here considered for a medium that allows vertical variations in wavespeed only. Following Carvalho (1992);

Weglein et al. (2003), consider the Born series:

$$\begin{aligned}\mathbf{\Psi} &= \sum_{n=1}^{\infty} \mathbf{G_0}(\mathbf{V}\mathbf{G_0})^n \\ &= \mathbf{G_0}\mathbf{V}\mathbf{G_0} + \mathbf{G_0}\mathbf{V}\mathbf{G_0}\mathbf{V}\mathbf{G_0} + \mathbf{G_0}\mathbf{V}\mathbf{G_0}\mathbf{V}\mathbf{G_0}\mathbf{V}\mathbf{G_0} + ...\end{aligned} \tag{52}$$

The relationship is inverted by representing $\mathbf{V}$ as an infinite series in orders of the wave field $\mathbf{\Psi}$ evaluated on a measurement surface: $\mathbf{V} = \mathbf{V_1} + \mathbf{V_2} + \mathbf{V_3} + ...$ Substituting this into equation (52), projecting the scattered field onto a given measurement surface, and equating like orders, a prescription for the term-by-term solution for $\mathbf{V}$ is created:

$$\begin{aligned}\mathbf{\Psi}_s =& \mathbf{G_0}\mathbf{V_1}\mathbf{G_0}, \\ 0 =& \mathbf{G_0}\mathbf{V_2}\mathbf{G_0} + \mathbf{G_0}\mathbf{V_1}\mathbf{G_0}\mathbf{V_1}\mathbf{G_0}, \\ 0 =& \mathbf{G_0}\mathbf{V_3}\mathbf{G_0} + \mathbf{G_0}\mathbf{V_2}\mathbf{G_0}\mathbf{V_1}\mathbf{G_0} + \mathbf{G_0}\mathbf{V_1}\mathbf{G_0}\mathbf{V_2}\mathbf{G_0} \\ &+ \mathbf{G_0}\mathbf{V_1}\mathbf{G_0}\mathbf{V_1}\mathbf{G_0}\mathbf{V_1}\mathbf{G_0}, \\ &...\end{aligned} \tag{53}$$

etc. Specifying to the single-parameter problem, the perturbation α is represented as $\alpha = \alpha_1 + \alpha_2 + \alpha_3 + ...$, in which α_n is n'th order in the data $D(k_s, \theta)$; let us assume these data are due to sources and receivers at depths $z_g = z_s = 0$. These choices produce a specific form of equations (53), in which α_n are solved for order by order in this measured data set. The linear relation

$$D(k_s, \theta) = -\frac{e^{ik_s x_g}}{4\cos^2\theta} \int_{-\infty}^{\infty} e^{i2q_s z'} \alpha_1(z') dz' \tag{54}$$

is solved for α_1, then this α_1 is used in

$$\begin{aligned}0 =& -\frac{e^{ik_s x_g}}{4\cos^2\theta} \int_{-\infty}^{\infty} e^{i2q_s z'} \alpha_2(z') dz' \\ &- \frac{i2q_s}{16\cos^4\theta} e^{ik_s x_g} \int_{-\infty}^{\infty} e^{iq_s z'} \alpha_1(z') \int_{-\infty}^{\infty} e^{iq_s|z'-z''|} \alpha_1(z'') e^{iq_s z''} dz'' dz',\end{aligned} \tag{55}$$

to solve for α_2, then

$$\begin{aligned}0 =& -\frac{e^{ik_s x_g}}{4\cos^2\theta} \int_{-\infty}^{\infty} e^{i2q_s z'} \alpha_3(z') dz' \\ &- \frac{i2q_s}{16\cos^4\theta} e^{ik_s x_g} \int_{-\infty}^{\infty} e^{iq_s z'} \alpha_1(z') \int_{-\infty}^{\infty} e^{iq_s|z'-z''|} \alpha_2(z'') e^{iq_s z''} dz'' dz' \\ &- \frac{i2q_s}{16\cos^4\theta} e^{ik_s x_g} \int_{-\infty}^{\infty} e^{iq_s z'} \alpha_2(z') \int_{-\infty}^{\infty} e^{iq_s|z'-z''|} \alpha_1(z'') e^{iq_s z''} dz'' dz' \\ &- \frac{(i2q_s)^2}{64\cos^6\theta} e^{ik_s x_g} \int_{-\infty}^{\infty} e^{iq_s z'} \alpha_1(z') \int_{-\infty}^{\infty} e^{iq_s|z'-z''|} \alpha_1(z'') \\ &\times \int_{-\infty}^{\infty} e^{iq_s|z''-z'''|} \alpha_1(z''') e^{iq_s z'''} dz''' dz'' dz',\end{aligned} \tag{56}$$

for α_3 and so on. We will treat this inverse problem in a slightly novel way in the next section; first, it is worth making a few statements in regards to this formalism as it is usually studied, some of which will carry over.

Consider equation (54). Taking the Fourier transform on the right hand side and re-arranging we have

$$\alpha_1(-2q_s) = -4\cos^2\theta \; D(x_g|k_s;\theta)e^{-ik_s x_g}. \tag{57}$$

We can reconstruct $\alpha_1(-2q_s)$, supplying it with all its required wavenumber components (to the extent that they are available from the wave field measurements) by, for instance, holding θ fixed and varying k_s:

$$\alpha_1(-2q_s)|_{\theta_0} = -4\cos^2\theta_0 \; D(x_g|k_s;\theta_0)e^{-ik_s x_g}. \tag{58}$$

When the reference medium is very close to the actual medium, and α_1 is therefore a good approximation of α, the model constructed in equation (58) is very close to being independent of θ_0, so given more than one angle, an average or least-squares best estimate could be chosen (Clayton and Stolt, 1981) to create a 1D model, or profile, from the 2D data. However, in the case of current interest, in which the reference and actual media are significantly different, both the location and amplitude of the discontinuities of α_1 must be expected to be functions of the incident plane wave angle. As a result, in its raw form, α_1 retains the same dimensionality as the data, i.e., $\alpha_1 = \alpha_1(q_s, \theta_0)$.

After the determination of this data-like $\alpha_1(q_s, \theta_0)$, the task-specific ISS strategy (Weglein et al., 2001, 2003; Shaw et al., 2004) departs into equations (55) and (56) and beyond. Supposing that portions of the full ISS that are involved with the processing and inversion of primaries are of interest, through integration-by-parts and various interchanges of integration variables, subseries of the full inverse scattering series are identified, separated, and used to form primary processing algorithms. In the following, we deviate from that approach, beginning instead with the FSS primaries approximations of Appendix A.

We generate primary processing algorithms, deriving them by means that, while closely related to the task-separated inverse scattering series, are distinct in a number of ways. Let us clarify this with a brief description of each method.

1. Task-separated inverse scattering series.

The full forward scattering series generates the full scattered wavefield, including all primaries and multiples. The full inverse scattering series is an order-by-order inversion of measurements of this full scattered field. The task-separated inverse scattering series is a framework for deriving algorithms from the extraction of portions of the full inverse series that are deemed to operate on (for instance) primaries only.

2. Direct inversion of non-linear primary approximations.

The full forward scattering series is altered such that only portions that construct primaries are retained. A series in orders of the measured primaries (*not* the full measured wavefield) is substituted for the perturbation in this portion of the forward scattering series, and the perturbation is solved for order-by-order. With no further intervention this produces algorithms for the direct determination of the location and strength of reflectors.

Let us assume that the primary data is well-modeled by $D_P(k_s,\theta) = R_M(k_s,\theta)|_{z_g,z_s=0}$, the scattered primary wavefield for moderate contrasts described in the previous section, here evaluated with fixed source and measurement depths. If so, we may express the data using equation (50),

$$\begin{aligned} D_P(k_s,\theta) = &-\frac{e^{ik_s x_g}}{4\cos^2\theta}\int_{-\infty}^{\infty} e^{i2q_s z'} \\ &\times\left\{\sum_{n=0}^{\infty}\frac{(1/2)^n}{n!\cos^{2n}\theta}\left[\alpha(z')\left(\int_0^{z'}\alpha(z'')dz''\right)^n\right]^{(n)}\right\}dz'. \end{aligned} \tag{59}$$

Expanding it as far as third order in the perturbation, we have

$$\begin{aligned} D_P(k_s,\theta) = &-\frac{e^{ik_s x_g}}{4\cos^2\theta}\int_{-\infty}^{\infty} e^{i2q_s z'}\left[\alpha(z') + \frac{\alpha'(z')}{2\cos^2\theta}\int_0^{z'}\alpha(z'')dz''\right. \\ &+\frac{\alpha^2(z')}{2\cos^2\theta} + \frac{\alpha''(z')}{8\cos^4\theta}\left(\int_0^{z'}\alpha(z'')dz''\right)^2 \\ &\left.+\frac{\alpha^3(z')}{4\cos^4\theta} + \frac{3\alpha'(z')}{4\cos^4\theta}\alpha(z')\int_0^{z'}\alpha(z'')dz'' + ...\right]dz', \end{aligned} \tag{60}$$

where primes indicate derivatives with respect to z'. We next invert this portion of the Born series order-by-order. Substituting $\alpha = \alpha_1 + \alpha_2 + \alpha_3 + ...$ into equation (60) and equating like orders, we have the prescription

$$\begin{aligned} D_P(k_s,\theta) &= -\frac{e^{ik_s x_g}}{4\cos^2\theta}\int_{-\infty}^{\infty} e^{i2q_s z'}\alpha_1(z')dz', \\ 0 &= \int_{-\infty}^{\infty} e^{i2q_s z'}\left[\alpha_2(z') + \frac{\alpha_1'(z')}{2\cos^2\theta}\int_0^{z'}\alpha_1(z'')dz'' + \frac{\alpha_1^2(z')}{2\cos^2\theta}\right]dz', \\ 0 &= \int_{-\infty}^{\infty} e^{i2q_s z'}\left[\alpha_3(z') + \frac{\alpha_1''(z')}{8\cos^4\theta}\left(\int_0^{z'}\alpha_1(z'')dz''\right)^2 + \frac{\alpha_1^3(z')}{4\cos^4\theta}\right. \\ &+\frac{\alpha_1'(z')}{2\cos^2\theta}\int_0^{z'}\alpha_2(z'')dz'' + \frac{\alpha_2'(z')}{2\cos^2\theta}\int_0^{z'}\alpha_1(z'')dz'' \\ &\left.+\frac{3}{4\cos^4\theta}\alpha_1'(z')\alpha_1(z')\int_0^{z'}\alpha_1(z'')dz''\right]dz', \end{aligned} \tag{61}$$

etc. The right-hand side of the linear term relating the measured part of the reflected primaries of the wave field and α_1 is mathematically identical to that of the full inverse scattering series discussed previously. A spectrum $\alpha_1(-2q_s, \theta)$ is estimated for each θ by fixing this angle and varying k_s in the primary data D_P. Inverse Fourier transforming over $-2q_s$ then produces a profile $\alpha_1(z, \theta)$ for each angle.

With these linear terms assumed to be in hand, we may move on to the higher orders. In the expressions equating second- and higher-order terms, cases of interest arise only when all $[\cdot]$-bracketed terms are equal to nil. Hence α_2 may be solved for as

$$\alpha_2(z,\theta) = -\frac{\alpha_1'(z',\theta)}{2\cos^2\theta}\int_0^{z'} \alpha_1(z'',\theta)dz'' - \frac{1}{2\cos^2\theta}\alpha_1^2(z',\theta). \tag{62}$$

Notice that since there is a profile $\alpha_1(z, \theta)$ for each angle, there is also a second-order profile $\alpha_2(z, \theta)$ for each angle.

Given α_1 and α_2, the third equation may be used to compute α_3:

$$\begin{aligned}\alpha_3(z,\theta) = &-\frac{\alpha_1''(z,\theta)}{8\cos^2\theta}\left(\int_0^z \alpha_1(z'',\theta)dz''\right)^2 \\ &-\frac{3\alpha_1'(z,\theta)}{4\cos^4\theta}\alpha_1(z',\theta)\int_0^z \alpha_1(z'',\theta)dz'' \\ &-\frac{\alpha_1^3(z,\theta)}{4\cos^4\theta} - \frac{\alpha_1'(z,\theta)}{2\cos^2\theta}\int_0^z \alpha_2(z'',\theta)dz'' \\ &-\frac{\alpha_2'(z,\theta)}{2\cos^2\theta}\int_0^z \alpha_1(z'',\theta)dz'' - \frac{\alpha_1(z,\theta)}{\cos^2\theta}\alpha_2(z,\theta).\end{aligned} \tag{63}$$

By substituting equation (62) for α_2 in equation (63), we may express α_3 entirely in terms of α_1:

$$\begin{aligned}\alpha_3(z,\theta) = &-\frac{1}{8\cos^2\theta}\alpha_1''(z,\theta)\left(\int_0^z \alpha_1(z'',\theta)dz''\right)^2 \\ &-\frac{3}{4\cos^4\theta}\alpha_1'(z,\theta)\alpha_1(z',\theta)\int_0^z \alpha_1(z'',\theta)dz'' \\ &-\frac{1}{4\cos^4\theta}\alpha_1^3(z,\theta) + \frac{1}{4\cos^2\theta}\alpha_1''(z,\theta)\left(\int_0^z \alpha_1(z'',\theta)dz''\right)^2 \\ &+\frac{3}{2\cos^4\theta}\alpha_1'(z,\theta)\alpha_1(z',\theta)\int_0^z \alpha_1(z'',\theta)dz'' \\ &+\frac{1}{2\cos^4\theta}\alpha_1^3(z,\theta).\end{aligned} \tag{64}$$

Notice that the terms that were in both α_1 and α_2 (the last three) are twice the negative of the

terms in α_1 only (the first three), hence we finally have

$$\begin{aligned}\alpha_3(z,\theta) =& \frac{1}{8\cos^2\theta}\alpha_1''(z,\theta)\left(\int_0^z \alpha_1(z'',\theta)dz''\right)^2 \\ &+ \frac{3}{4\cos^4\theta}\alpha_1'(z,\theta)\alpha_1(z',\theta)\int_0^z \alpha_1(z'',\theta)dz'' \\ &+ \frac{1}{4\cos^4\theta}\alpha_1^3(z,\theta).\end{aligned} \tag{65}$$

With little further brute computation, the behavior of this direct inversion becomes clear: the sum $\alpha_1+\alpha_2+\alpha_3+...$ is a series essentially identical to that of the forward primary approximation, but (*i*) in α_1 rather than α, and (*ii*) with an alternating sign, an attribute that we have seen is provided by terms of "mixed order", e.g., in α_1 and α_2 in equation (63). Calling this series $\alpha_M(z)$, we have

$$\alpha_M(z,\theta) = \sum_{n=0}^{\infty} C_n^- \left[\alpha_1(z,\theta)\left(\int_0^z \alpha_1(z',\theta)dz'\right)^n\right]^{(n)}, \tag{66}$$

where again superscript (n) denotes the n'th derivative with respect to z' and $C_n^- = \frac{(-1/2)^n}{n!\cos^{2n}\theta}$. We may further construct the reflector location/amplitude approximation α_L:

$$\alpha_L(z,\theta) = \sum_{n=0}^{\infty} C_n^- \left[\alpha_1(z,\theta)\left(\sum_{k=1}^{\infty}\frac{1}{4^{k-1}}\int_0^z dz'\alpha_1(z',\theta)\right)^n\right]^{(n)}. \tag{67}$$

Equations (66)–(67) constitute formulas for the location and amplitude of reflectors in scalar (acoustic constant density) 1.5D media. Numerical illustrations of their behavior are beyond the scope of this appendix, but have been reported elsewhere (Innanen, 2005).

Appendix C: derivation of second-order diffractive primary

We show that applying the linear/non-linear criteria to the second order term. The raw second order term is

$$\begin{aligned}G_2(k_g,z_g,k_s,z_s,\omega) =& \int dz' \int dx' G_0(k_g,z_g,x',z',\omega)k^2\alpha(x',z') \\ &\times \int dz'' \int dx'' G_0(x',z',x'',z'',\omega)k^2\alpha(x'',z'')G_0(x'',z'',k_s,z_s,\omega).\end{aligned} \tag{68}$$

Substituting the explicit form for the Green's functions in equations (2) into equation (68), we have

$$\begin{aligned}
&G_2(k_g, z_g, k_s, z_s, \omega) \\
&\quad = -\frac{e^{-iq_g z_g - iq_s z_s}}{4}\frac{k^4}{q_g q_s}\int\int\int dx'dx''dk'\left(\frac{-i}{4\pi q'}\right)e^{-ik_g x'}e^{ik'(x'-x'')}e^{ik_s x''} \\
&\quad \times \int dz' e^{i(q_g+q')z'}\alpha(x',z')\int_{-\infty}^{z'} e^{i(q_s-q')z''}\alpha(x'',z'') \\
&\quad + -\frac{e^{-iq_g z_g - iq_s z_s}}{4}\frac{k^4}{q_g q_s}\int\int\int dx'dx''dk'\left(\frac{-i}{4\pi q'}\right)e^{-ik_g x'}e^{ik'(x'-x'')}e^{ik_s x''} \\
&\quad \int dz' e^{i(q_g-q')z'}\alpha(x',z')\int_{z'}^{\infty} e^{i(q'+q_s)z''}\alpha(x'',z'').
\end{aligned} \tag{69}$$

The criteria for linear/non-linear construction of the wavefield primaries calls for A to be considered non-linearly and B to be considered linearly; at second order that means replacing one of the two instances of $\alpha = A + B$ with $\alpha \approx A$. To properly do this requires us to make a further decision: in *which* of the instances of α in each portion of equation (68) do we make this substitution? The answer is: in any instance of α that contributes to *transmission* rather than *reflection*, i.e., where the sense of propagation (in z) does not change after a scattering interaction. Mathematically this corresponds to any instance of $\alpha \times$ [exponentials in the *difference* of two depth wavenumbers]. In equation (68) that situation occurs in the rightmost α in the first term and the leftmost α in the second term. Making this substitution on these α's gives us the basis for the approximation R_2^P:

$$\begin{aligned}
&R_2^P(k_g, z_g, k_s, z_s, \omega) \\
&\quad = -\frac{e^{-iq_g z_g - iq_s z_s}}{4}\frac{k^4}{q_g q_s}\int\int\int dx'dx''dk'\left(\frac{-i}{4\pi q'}\right)e^{-ik_g x'}e^{ik'(x'-x'')}e^{ik_s x''} \\
&\quad \times \int dz' e^{i(q_g+q')z'}\alpha(x',z')\int_{-\infty}^{z'} e^{i(q_s-q')z''}A(z'') \\
&\quad - \frac{e^{-iq_g z_g - iq_s z_s}}{4}\frac{k^4}{q_g q_s}\int\int\int dx'dx''dk'\left(\frac{-i}{4\pi q'}\right)e^{-ik_g x'}e^{ik'(x'-x'')}e^{ik_s x''} \\
&\quad \int dz' e^{i(q_g-q')z'}A(z')\int_{z'}^{\infty} e^{i(q'+q_s)z''}\alpha(x'',z'').
\end{aligned} \tag{70}$$

Hereafter the derivation is entirely mechanical. Noting that

$$\begin{aligned}
\int dx'' e^{i(k_s-k')x''} &= 2\pi\delta(k'-k_s), \\
\int dx' e^{i(k'-k_g)x'} &= 2\pi\delta(k_g-k'),
\end{aligned} \tag{71}$$

the x'' integral in the first term and the x' integral in the second term generate delta functions that then simplify the k' integrals via sifting:

$$\begin{aligned} &R_2^P(k_g, z_g, k_s, z_s, \omega) \\ &\quad = -\frac{e^{-iq_g z_g - iq_s z_s}}{4}\frac{k^4}{q_g q_s}\int dx' \left(\frac{1}{i2q_s}\right) e^{-i(k_g-k_s)x'} \int dz' e^{i(q_g+q_s)z'}\alpha(x', z') \int_{-\infty}^{z'} A(z'') \\ &\quad\quad -\frac{e^{-iq_g z_g - iq_s z_s}}{4}\frac{k^4}{q_g q_s}\int dx'' \left(\frac{1}{i2q_g}\right) e^{-i(k_g-k_s)x''} \int dz' A(z') \int_{z'}^{\infty} e^{i(q_g+q_s)z''}\alpha(x'', z''). \end{aligned} \tag{72}$$

The remaining x integrals, which are Fourier transforms, along with the replacement of the $-\infty$ integration limits with the source and receiver depths, leaves us with the desired result:

$$\begin{aligned} &R_2^P(k_g, z_g, k_s, z_s, \omega) \\ &\quad = -\frac{e^{-iq_g z_g - iq_s z_s}}{4}\frac{k^2}{q_g q_s}\int dz' e^{i(q_g+q_s)z'} \left(\frac{-iq_g}{2\cos^2\theta_g}\int_{z_g}^{z'} dz'' a(z'')\right)\alpha(k_g - k_s, z') \\ &\quad\quad -\frac{e^{-iq_g z_g - iq_s z_s}}{4}\frac{k^2}{q_g q_s}\int dz' e^{i(q_g+q_s)z'}\alpha(k_g - k_s, z') \left(\frac{-iq_s}{2\cos^2\theta_s}\int_{z_s}^{z'} dz'' a(z'')\right), \end{aligned} \tag{73}$$

where, e.g., $\cos\theta_g = q_g/k$.

A comprehensive strategy for removing multiples and depth imaging primaries without subsurface information: Direct horizontal common image gathers without the velocity or "ironing"

Fang Liu, Arthur B. Weglein*, Kristopher A. Innanen *, Bogdan G. Nita *†, Jingfeng Zhang*, * M-OSRP, Physics Dept., University of Houston, † Montclair State University*

SUMMARY

In AVO (Amplitude Variation with Offset) analysis, the amplitudes of reflected waves with different incident angles are studied to deduce lithology information beyond the structure map obtained by seismic imaging algorithms. The quantitative analysis of the amplitude, relies on common-image gathers being flat (or equivalently, at the same depth). But the waves with different incident angles will have different apparent velocities, resulting in different depths for the same image point at different angles, or non-flat common image gathers. In many scenarios, non-flat common-image gather was flattened by trim means at the cost of compromising zero-crossing and polarity-reversal information. This work presents a solution based on the seismic imaging subseries of the inverse scattering series (ISS) that flattens the common image gather without knowing or determining the subsurface velocity, and without any harmful amplitude consequencies.

INTRODUCTION

Inverse scattering series (ISS) is a comprehensive theory for processing primaries and multiples without the traditional need for a subsurface velocity. Several task-specific subseries of ISS (Weglein et al., 2003) had been identified. These subseries correspond to classical objectives of seismic data processing: (1) eliminating free-surface multiple (Carvalho et al., 1991; Carvalho, 1992), (2) eliminating the internal multiples (Weglein et al., 1997; Araújo, 1994; Matson, 1997; Ramírez and Weglein, 2005), (3) imaging reflectors at depth (Weglein et al., 2000, 2002; Shaw et al., 2003; Innanen, 2003; Shaw, 2005; Liu, 2006), (4) determining the parameter changes across the reflectors (Zhang, 2006). This article is specific to task (3): the image of the same reflector in the same lateral coordinate, flattened and migrated to the same (actual) depth without knowing or determining the subsurface reflector.

Description of the problem

For simplicity, consider an exploration problem in 2D where z_s (the elevation of the source) and z_g (the elevation of the receiver) are fixed. In this case, the seismic data is considered a function of three variables: x_s (the horizontal coordinate of the source), x_g (the horizaontal coordinates of the receivers), and t (time).

Physical properties at points in the subsurface, including reflector location in space, are not in any way dependent on the surface reflection data, or any subset of the data, used to determine or estimate those properties. That criteria is in used current leading-edge imaging as a necessary condition that an imaging algorithm with a correct velocity would satisfy. For example, images from different offset components of the data ought to locate at the same point in space if the velocity is correct. That concept is simple but in practice often not easy to realize. Methods to force or "iron" the common-image gather data flat and horizontal can have very serious and harmful consequences on subsequent analysis with lost polarity reversals and difficulty identifying class I and class II AVO anomalies.

In this paper we demonstrate that the higher-order velocity-independent imaging subseries automatically produces the flat common-image gather, as you would expect from an imaging algorithm that produces the image at the correct depth. Not only is there no velocity, but the flatness is achieved without damaging the offset dependent amplitude information in imaged the data.

This phenomena can be illustrated by the two experiments shown in Figure 1.

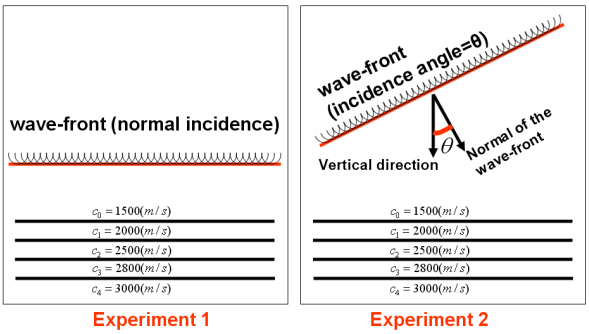

Figure 1: In Experiment 1 (left panel), a normal incident plane wave is used to study an earh without lateral variation. In Experiment 2 (right panel), a plane wave with non-zero incident angle θ is used to study the same earh as in Experiment 1.

Although Experiment 1 and Experiment 2 correspond to the same earh, their incident wavefields are different, and consequently the input data and seismic imaging result will be different, as illustrated in Figure 2.

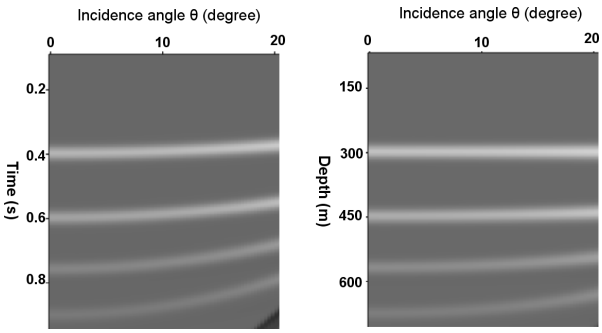

Figure 2: The left panel is the input data with different angles. The right panel is the corresponding common image gather (FK migration with homogeneous water velocity $c_0 = 1500m/s$) for different incident angles. It is obvious that no event in the input data is flat. In the common image gather, the first reflector (water bottom) is flattened, but the reflectors below are still curved.

The phenomena described above will compromise the AVO analysis, where the reflection event from the same reflection point should be flat. Flattened events are very desirable for quantitative estimation of the reflection strength. This phenomena had already been studied in Shaw (2005) for earh even without lateral variation and dealt with using the leading order imaging subseries.

THEORY

For a constant-density acoustic model, the mathematical description of the 2D wave-propagation is,

$$\left(\frac{\partial^2}{\partial x^2}+\frac{\partial^2}{\partial z^2}+\frac{\omega^2}{c^2(x,z)}\right)G(x,z,x_s,z_s\omega)=\delta(x-x_s)\delta(z-z_s), \quad (1)$$

where ω is the temporary frequency (the Fourier conjugate of time t), $G(x,z,x_s,z_s,\omega)$ is the wave-field, the function $c(x,z)$ is the velocity field.

Equation (1) can be systematically solved by the inverse scattering series (Weglein et al., 2003) with the help of a wave parapagation in a much simpler reference velocity c_0,

$$\left(\frac{\partial^2}{\partial x^2}+\frac{\partial^2}{\partial z^2}+\frac{\omega^2}{c_0^2}\right)G_0(x,z,x_s,z_s\omega)=\delta(x-x_s)\delta(z-z_s), \quad (2)$$

where $G_0(x,z,x_s,z_s\omega)$ is the reference wave-field.

In the inverse series, equation (1) is computed in an order-by-order fashion via the inverse scattering series (equation (11)$\sim$(13) of Weglein et al. (2003)) as,

$$G_0k^2\alpha_1G_0=D=G-G_0, \quad (3)$$

$$G_0k^2\alpha_2G_0=-G_0k^2\alpha_1G_0k^2\alpha_1G_0, \quad (4)$$

$$\begin{aligned}G_0k^2\alpha_3G_0=&-G_0k^2\alpha_1G_0k^2\alpha_2G_0-G_0k^2\alpha_2G_0k^2\alpha_1G_0\\&-G_0k^2\alpha_1G_0k^2\alpha_1G_0k^2\alpha_1G_0,\end{aligned} \quad (5)$$

where $k=\omega/c_0$; D in equation (3) is the input data for the inverse scattering series and is the difference between the actual wavefield G and the reference wavefield G_0; α_1, α_2, $\cdots$ are iteratively computed and can be used to construct $\alpha=\alpha_1+\alpha_2+\alpha_3+\cdots$, which is related to the subsurface geology via $\alpha=1-c_0^2/c^2(x,z)$. Equation (3) can be solved via Fourier transform. Following the notation in Clayton and Stolt (1981), we use k_z, k_g, k_s, k_m, and k_h to denote the Fourier conjugate of z, x_g, x_s, $x_m=0.5(x_g+x_s)$, and $x_h=x_g-x_s$ respectively. In the examples in this article, the reference velocity (the velocity actually used in migration) c_0 is chosen as whole-space constant water velocity. The detailed derivation of the equations in this article can be found in Liu (2006) and the final solution is summarized below.

The solution of the first term α_1

The data is chosen according to the following relation,

$$k_h=k_g+k_s=2\frac{\omega}{c_0}\sin(\theta) \qquad k_g-k_s=k_m \quad . \quad (6)$$

where the constant θ is the incident angle of synthesized plane wave by Radon transform defined in the CMP (common-mid point) gather (see equation (9)). With equation (6) as constraint, the temporary frequency ω can be expressed as a function of k_m and k_z,

$$\omega=\frac{c_0k_z}{2}\sqrt{\frac{k_z^2+k_m^2}{k_z^2\cos^2(\theta)-k_m^2\sin^2(\theta)}}. \quad (7)$$

With ω defined in equation (7), our generalized migration formulism can be expressed as,

$$\tilde{\tilde{\alpha}}_1(k_m,k_z)=-\frac{4q_gq_s}{\omega^2/c_0^2}\int_{-\infty}^{\infty}dx_me^{-ik_mx_m}\int_{-\infty}^{\infty}d\tau e^{i\omega\tau}D^{\tau p}(x_m,\tau). \quad (8)$$

where the double tidle signs in the equation above are used to denote the fact that the expression had been Fourier transformed twice from its original form in the spatial domain (x,z) to frequency-wavenumer domain (k_m,k_z), and $D^{\tau p}$ is computed via Radon transform,

$$D^{\tau p}(x_m,\tau)=\int_{-\infty}^{\infty}dx_hD\left(x_m+\frac{x_h}{2},x_m-\frac{x_h}{2},\tau+x_h\frac{\sin(\theta)}{c_0}\right). \quad (9)$$

Equation (6) of Liu et al. (2006) can be considered as a special case of equation (8) where the angle θ is chosen as zero.

Higher order imaging subseries

The higher-order imaging subseries (HOIS) in equation (11) of Liu et al. (2006) is generalized for non-zero θ as,

$$\alpha_{HOIS}\left(x,z+\frac{1}{2}\int_0^z\frac{\alpha_1(x,z')dz'}{\cos^2\theta-0.25\alpha_1(x,z')}\right)=\alpha_1(x,z) \quad (10)$$

Interested readers may refer to Liu (2006) for detailed derivation and discussion for equation (10).

NUMERICAL EXAMPLES

The synthetic data set (see examples in Figure 4) used in this article was generated upon a salt model shown in Figure 3.

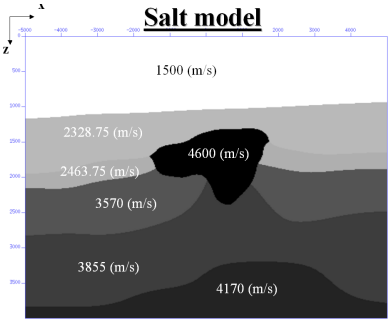

Figure 3: A salt model designed by Peter Traynin from ExxonMobil.

The linear images (α_1) of the inverse scattering series with different angles are calculated via equation (8) and the imaging results for two typical angles are shown in Figure 5 and Figure 6.

In order to consistently use the migration result in Figure 5 and Figure 6 in AVO analysis, it is very desirable that they share the same depth. But only the images of the water-bottom share the same depth, as indicated by the flat water-bottom in the common-image gather in Figure 7. The images of the reflectors below the water-bottom are not flat, as indicated by the bumpy refletors in Figure 7. Since the angles we studied in this example are very small (between 0° and 9°), the curvature of the non-flat events is not easily visible. For display purpose, we duplicate each imaging result for an angle 100 times. We

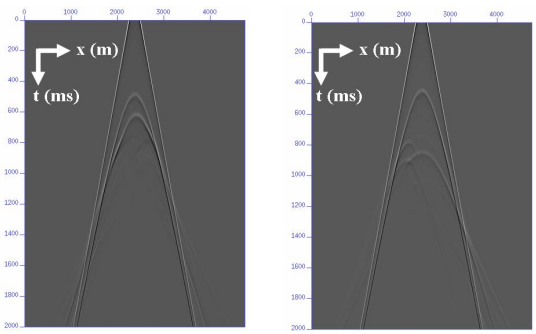

Figure 4: Two typical shot gathers extracted from the data set generated from the salt model in Figure 3.

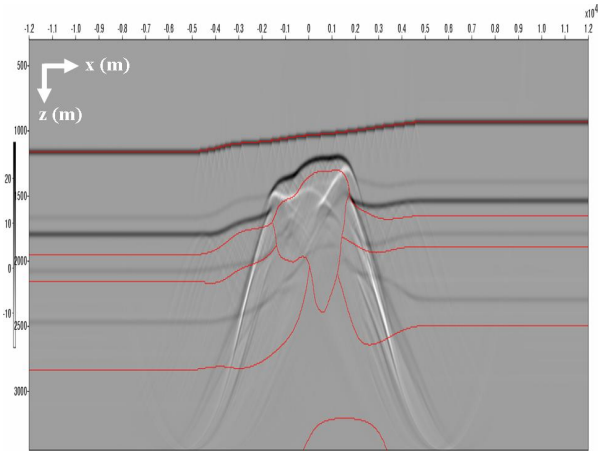

Figure 5: The linear image α_1 (see equation (8)) with $\theta = 0^\circ$. In this figure and Figure (6, 8, 9, 11), partial derivative over z operation $\partial/\partial z$ is taken before the display, and the red lines are bench-marks indicating the actual location of various reflectors

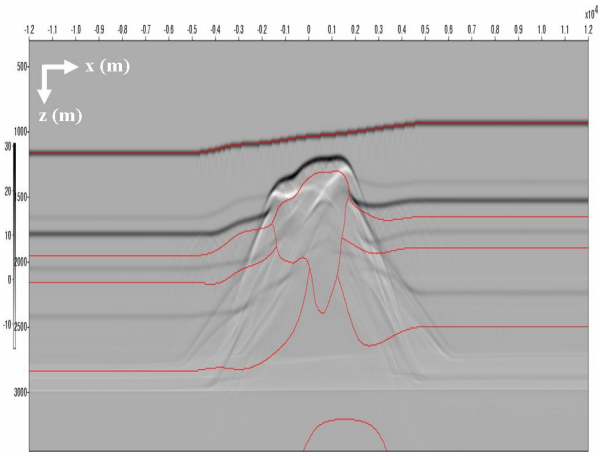

Figure 6: The linear image α_1 (see equation (8)) with $\theta = 9^\circ$. Due to the truncation artifacts (below 2500m) caused by unavailability of the data, $\theta = 9^\circ$ is the maximal angle we studied in this article.

then introduce 100 copy of imaging result for another angle θ, etc, $\cdots$. Since the imaging result for a specific angle is duplicated 100 times, this 100 identical traces will produce a smooth-looking background. In this manner, even the small changes between the imaging results of adjacent angles can be easily seen against the smooth background produced by trace duplication.

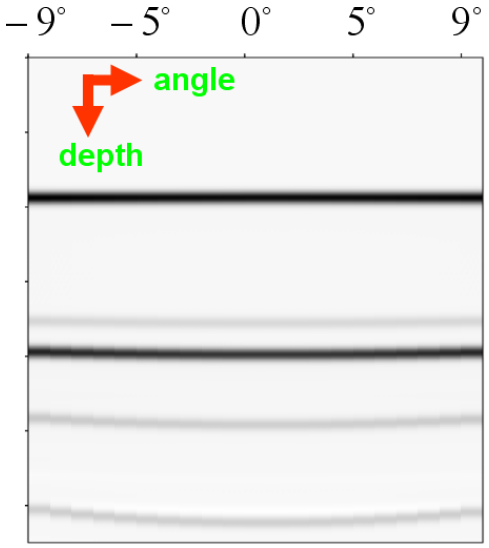

Figure 7: In this common-image gather taken from the left side of the linear image (α_1), only the water-bottom is flat. Although the curvature of the second reflect is still not very clear, the curvatures of the second, third, fourth, and fifth reflector are clearly shown again the smooth background produced by trace duplication.

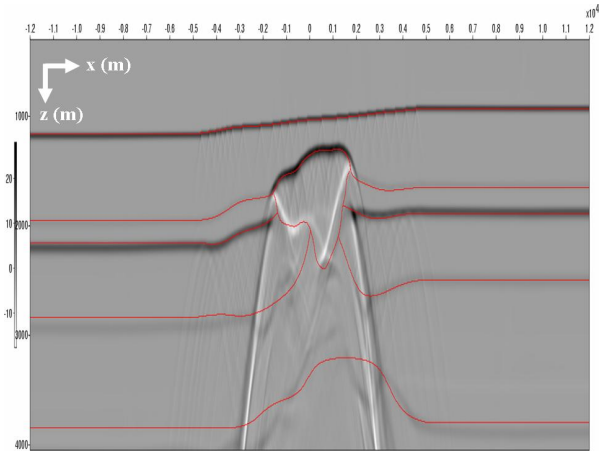

Figure 8: The higher-order imaging subseries (see equation (10)) with $\theta = 0^\circ$.

Since all the reflection events are imaged to the same location after applying the higher-order imaging subseries, it is reasonable to sum all the higher-order images together to have an improved image with better signal/noise ratio, as displayed in Figure 11.

CONCLUSIONS

In this paper, the efficacy of the higher order imaging subseries is further demonstrated by automatically and accurately producing common-

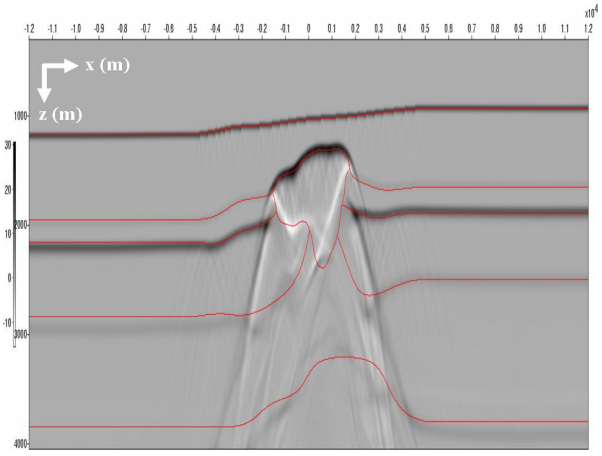

Figure 9: The higher-order imaging subseries (see equation (10)) with $\theta = 9^\circ$.

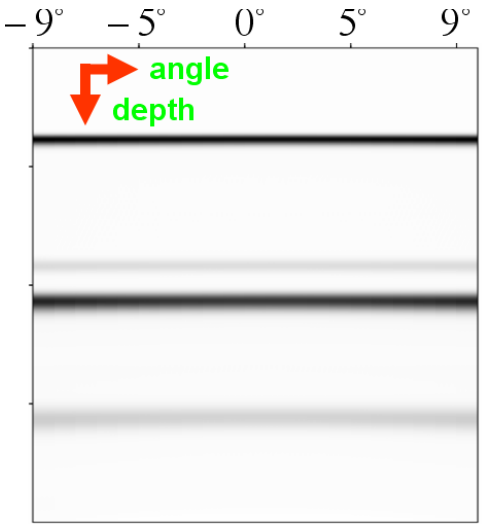

Figure 10: In this common-image gather taken from the left side of the the higher order imaging subseries, all the reflectors are flat. This demonstrates that the higher-order imaging subseries can be used to flatten events in the common-image gather.

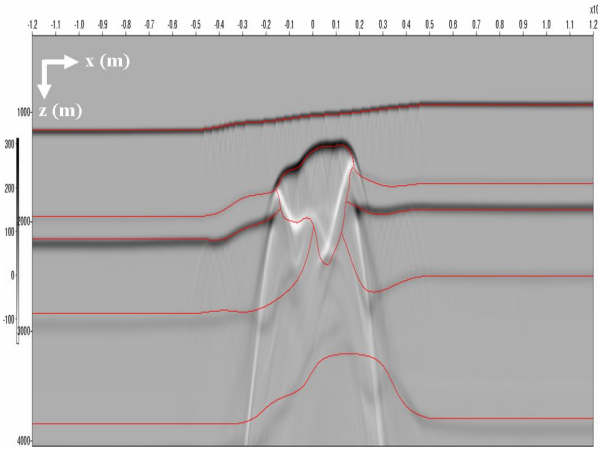

Figure 11: The sum of all the higher-order images. Since the reflection events are migrated to the same depth by the higher-order imaging subseries, they sum to each other constructively. But the residual diffractions are not migrated to the same depth, and hence they sum to each other destructively and become much weaker compared to the imaging result for any single fixed angle θ.

image gathers, without the velocity, and with amplitude intact and ready for subsequent AVO analysis.

ACKNOWLEDGMENTS

The authors would like to thank GX Technology for granting Fang 2006-2007 GXT fellowship, Peter Traynin from ExxonMobil for providing the salt model. We thank Simon Shaw and all M-OSRP members and sponsors. This work has been partially funded by NSF-CMG award DMS-0327778 and DOE Basic Science award DE-FG02-05ER15697.

The role of the direct wave and Green's Theorem in seismic interferometry and spurious multiples.

Adriana C. Ramírez and Arthur B. Weglein, M-OSRP University of Houston, Einar Otnes and Ketil Hokstad, Statoil Research Center*

SUMMARY

Techniques to estimate the Green's function between two measured points using wavefield correlations and/or crosscorrelations are classified as seismic interferometry. In this paper we provide a unifying framework for understanding a broad class of interferometric techniques using Green's theorem. This framework and foundation allows spurious multiples that occur in certain interferometric approaches to be anticipated and fully explain as a consequence of approximations and compromises made within Green's theorem. We also develop a set of more effective seismic interferometry methods, where fewer compromises effect in a better result.

Standard seismic interferometry is based on far-field and one-way approximations of the Green's theorem relating two wavefield measurements in the same volume. This method, when applied to surface seismic data, reconstructs the wavefield with a squared source signature and adds spurious multiples, whose amplitudes are comparable to the reconstructed primaries. The artefacts introduced, reduce the method's value. The spurious multiples come from the approximations made to avoid the need of the wavefield's normal derivative. We propose and examine various alternative approaches to seismic interferometry which overcome the appearance of spurious multiples and provides an improvement over traditional methods. One method uses Green's theorem relating a reference Green's function with the measured wavefield. The data are reconstructed without spurious multiples and with a wavelet due to a single source. A synthesized wavefield ought to have a single factor of the wavelet. Using an analytic reference Green's function, data can be extrapolated to positions where no receivers or sources were located. In addition, we provide another form of Green's theorem by imposing a two-surface Dirichlet boundary condition to the reference Green's function; this method only requires the total wavefield. The normal derivative of the field is not needed.

INTRODUCTION

Many approaches, papers and starting points for seismic interferometry have been proposed with different assumptions, approximations, pitfalls and benefits. Claerbout (1968) provided a formalism for wavefield reconstruction in horizontally layered media, which is considered the first formulation of seismic interferometry. Weglein et al. (2000) proposed to use Green's theorem to retrieve the total two-way wavefield anywhere above a typical towed streamer using measurements of only the pressure field along the cables and imposing Dirichlet boundary conditions on the reference Green's function. Lobkis and Weaver (2001) extended Claerbout's early theory to allow for a 3D heterogeneous media of nite extent (discrete frequency spectrum). Schuster (2001) gave the name *seismic interferometry* to all the processing tools that perform wave field reconstruction through correlation. Derode et al. (2003) and Roux and Fink (2003) proposed an alternative formulation for this technology using the principle of time reversal. Wapenaar et al. (2002) overcame the need for nite media with the one-way propagation representation theorem. Wapenaar (2004) and Weaver and Lobkis (2004) gave an equivalent formulation for seismic interferometry using high frequency approximations and the general representation theorem, which is a form of Green's Theorem and reciprocity.

Most of the approaches to seismic interferometry crosscorrelate the total wavefield recorded by two receivers and reconstruct the Green's function at one of the receivers as if the second receiver was a source (refer to Draganov et al. (2006); Wapenaar and Fokkema (2006) and references within). Using reciprocity, Otnes et al. (2006) crosscorrelated sources summing over all the receivers in a synthetic and a real WVSP experiment and retrieved the Green's function between the sources to effectively make a surface seismic experiment and derived a data-driven free surface demultiple algorithm for WVSP data. Vasconcelos and Snieder (2006) proposed deconvolution interferometry in which they derived a formalism that expands the wavefields into direct and scattered field in order to analyze its causal and acausal contributions to the synthesized data. It also performs a deconvolution of the reconstructed wavefield.

Green's theorem, a mathematical identity, is the corner stone of wave theory that incorporates boundary conditions to wavefield prediction. It provides a very general and comprehensive framework for analyzing interferometric methods. It allows us to place a very broad set of current approaches to seismic interferometry within a single unifying construct, and thereby better understand how each one represents some compromise to the exact wavefield prediction and, to anticipate artefacts and spurious multiples that are introduced by the approximations. The single encompassing framework facilitates comparisons between different approaches and a guide to more effectiveness with less assumptions.

GREEN'S THEOREM

Green's second identity has been widely used in seismic exploration for purposes as different as wavelet estimation (Weglein and Secrest, 1990; Osen et al., 1998; Tan, 1999), seismic interferometry (Weglein et al., 2000; Weaver and Lobkis, 2004; Bakulin and Calvert, 2004; Schuster and Zhou, 2006; Wapenaar and Fokkema, 2006; Ramírez et al., 2007) and deghosting (Amundsen et al., 2005; Zhang and Weglein, 2006), among several other topics. Green's second identity is a mathematical identity which originates from boundary value problems. It is an equation that relates a surface integral of two scalar functions and their derivatives with a volume integral of the same functions and their laplacian,

$$\int_V [u\nabla^2 v - u\nabla^2 v]d\mathbf{x} = \int_S [u\nabla v - v\nabla u]\cdot \mathbf{n} d\mathbf{s}, \tag{1}$$

where u and v are arbitrary scalar functions, $\mathbf{x}$ is a three dimensional vector (x_1, x_2, x_3) characterizing the volume V enclosed by the surface S, and $\mathbf{n}$ is the vector normal to this surface. In the following, we proceed to use this identity to relate two wavefields in a surface seismic experiment.

The acoustic wave equation for an inhomogeneous earth with constant density is

$$\left(\nabla^2 + \frac{\omega^2}{c^2(\mathbf{x})}\right) P(\mathbf{x}|\mathbf{x_a};\omega) = A(\omega)\delta(\mathbf{x}-\mathbf{x_a}), \tag{2}$$

where $c(\mathbf{x})$ is the velocity distribution, $A(\omega)$ is the source wavelet and the actual pressure field $P(\mathbf{x}|\mathbf{x_a};\omega) = A(\omega)G(\mathbf{x}|\mathbf{x_a};\omega)$, $G(\mathbf{x}|\mathbf{x_a};\omega)$ being the Green's function at point $\mathbf{x}$ and frequency ω due to a source at $\mathbf{x_a}$, excited at $t = 0$.

The solutions for equations 2 and 6 can be causal or anticausal with outgoing and ingoing boundary conditions, respectively. We denote the causal and anticausal waves by a $+$ and a $-$ superscript, respectively. The anticausal pressure field is then defined by

$$P^-(\mathbf{x}|\mathbf{x_b};\omega) = \int_{-\infty}^{\infty} e^{-i\omega t} P^+(\mathbf{x}|\mathbf{x_b};-t)dt. \tag{3}$$

Direct wave, Green's Theorem, seismic interferometry and spurious multiples.

Let's use the wavefield $P(\mathbf{x}|\mathbf{x_a};\omega)$ from equation 2 and a second field $P^-(\mathbf{x}|\mathbf{x_b};\omega)$ satisfying the same equation but with a different source position, $\mathbf{x_b}$, and source wavelet $B(\omega)$ in equation 1 as u and v; and, define an arbitrary volume, V, enclosed by a closed surface, S. to obtain

$$\int_V (P(\mathbf{x}|\mathbf{x_a};\omega)[-\frac{\omega^2}{c^2(\mathbf{x})}P^-(\mathbf{x}|\mathbf{x_b};\omega)+B(\omega)\delta(\mathbf{x}-\mathbf{x_b})]$$
$$-P^-(\mathbf{x}|\mathbf{x_b};\omega)[-\frac{\omega^2}{c^2(\mathbf{x})}P(\mathbf{x}|\mathbf{x_a};\omega)+A(\omega)\delta(\mathbf{x}-\mathbf{x_a})])\,d\mathbf{x}$$
$$=\oint_S [P(\mathbf{x}|\mathbf{x_a};\omega)\nabla P^-(\mathbf{x}|\mathbf{x_b};\omega)-P^-(\mathbf{x}|\mathbf{x_b};\omega)\nabla P(\mathbf{x}|\mathbf{x_a};\omega)]\cdot\mathbf{n}\,d\mathbf{s}. \tag{4}$$

This is Green's theorem applied to exploration seismology. It is a mathematical identity that relates two different wavefields, measured at the same surface, due to independent sources into a single equation. The need for both measurements (wavefield and its normal derivative) arises from the two-way nature of the wavefield.

Depending on the choice of volume and the surface surrounding it, the evaluation of the integrals in equation 4 leads to powerful, and sometimes rather simple, algorithms that aim to solve problems like wavefield retrieval, wavelet estimation, deghosting and demultiple.

Choosing a closed surface of sources to generate two wavefields measured by two receiver positions inside the volume, V; using them as u and v in equation 4 and, approximating the normal derivatives with a far-field and one-way wave approximations, we obtain the common seismic interferometry equation (Wapenaar and Fokkema, 2006):

$$2iA(\omega)\Im\left[P(\mathbf{x_b}|\mathbf{x_a};t)\right]\approx\frac{-2i\omega}{c(\mathbf{x})}\oint_S P(\mathbf{x_a}|\mathbf{x};t)P(\mathbf{x_b}|\mathbf{x};-t)\,d\mathbf{x}, \tag{5}$$

where $\mathbf{x_a}$ and $\mathbf{x_b}$ are two receiver positions inside the volume, the variable $\mathbf{x}$ corresponds to source positions which form a closed surface, S, and it is assumed that the source signatures are equal. Equation 5 is a compromised form of Green's theorem and, hence, gives rise to spurious multiples. The normal derivatives information required by Green's theorem, avoided by using far field approximations, would have combined nonlinearly to cancel the so called spurious multiples by using differences in sign that identify opposite directions of the wavefield. The directionality information is part of the wavefield's normal derivative. Furthermore, using two measured wavefields to construct new data instead of a measured wavefield and a Green's function, introduces an extra factor of the source wavelet multiplying the reconstructed data. If we had used a Green's function instead of the anticausal wavefield, $P^-(\mathbf{x}|\mathbf{x_b};\omega)$, we would not have an extra source signature (Wapenaar, 2004; Wapenaar and Fokkema, 2006). In equation 5, we are only able to reconstruct wavefield at the source and receiver locations.

There are several ways to improve the output of equation 5: 1) Ignore the fact that approximations were made, attempt an understanding of this interferometric approach and find methods to fix its weaknesses; this approach is taken by *e.g.* Vasconcelos and Snieder (2006), who derived a theory for seismic interferometry that also deconvolves the source wavelet, and Snieder et al. (2006), who studied the appearance of spurious multiples in traditional seismic interferometry and proposed types of sources and acquisition geometries that would help diminish its appearance. 2) Understand that spurious multiples and the extra source signature multiplying the synthesized wavefield are an effect of the assumptions applied to satisfy Green's theorem as well as the functions used in its derivation. Anticipating the consequences due to the compromises made, allow us to go back to our framework and ask ourselves for better ways to meet its requirements. An example of this approach is direct wave interferometry.

Direct wave interferometry

Using reciprocity and Green's theorem, Ramírez et al. (2007) have derived a more complete method based on the crosscorrelation of the reference Green's function and the total measured wave field that circumvents the appearance of spurious events and the squaring of the source signature. It also allows to extrapolate wavefield to positions where no sources or receivers exist. We now provide the formalism behind direct wave seismic interferometry.

Select the reference medium to be a homogeneous whole space, with constant reference velocity c_0, satisfying the wave equation,

$$\left(\nabla^2+\frac{\omega^2}{c_0^2}\right)G_0(\mathbf{x}|\mathbf{x_b};\omega)=\delta(\mathbf{x}-\mathbf{x_b}), \tag{6}$$

where $G_0(\mathbf{x}|\mathbf{x_b};\omega)$ is the free space or reference Green's function for a source at $\mathbf{x_b}$ excited at $t=0$. This Green's function represents the deconvolved direct wave from a seismic experiment.

Define an arbitrary volume, V, enclosed by a closed surface, S. Use

$$\frac{1}{c(\mathbf{x})^2}=\frac{1}{c_0^2}\left(1-\alpha(\mathbf{x})\right) \tag{7}$$

in equation 2 (α is the relative difference between the reference and the actual medium, Weglein and Secrest (1990)) and substitute the wavefield $P(\mathbf{x}|\mathbf{x_a};\omega)$ and the anticausal direct wave $G_0^-(\mathbf{x}|\mathbf{x_b};\omega)$ into equation 1 as u and v, to obtain,

$$\int_V (P(\mathbf{x}|\mathbf{x_a};\omega)[-\frac{\omega^2}{c_0^2}G_0^-(\mathbf{x}|\mathbf{x_b};\omega)+\delta(\mathbf{x}-\mathbf{x_b})]$$
$$-G_0^-(\mathbf{x}|\mathbf{x_b};\omega)[-\frac{\omega^2}{c_0^2}(1-\alpha(\mathbf{x}))P(\mathbf{x}|\mathbf{x_a};\omega)+A(\omega)\delta(\mathbf{x}-\mathbf{x_a})])\,d\mathbf{x}$$
$$=\oint_S [P(\mathbf{x}|\mathbf{x_a};\omega)\nabla G_0^-(\mathbf{x}|\mathbf{x_b};\omega)-G_0^-(\mathbf{x}|\mathbf{x_b};\omega)\nabla P(\mathbf{x}|\mathbf{x_a};\omega)]\cdot\mathbf{n}\,d\mathbf{s}. \tag{8}$$

To account for the free surface, use a background medium with a half space of water and a half space of air and a volume V bounded by the free surface and the measurement surface. The wave equation is expressed using a real source at $\mathbf{x_b}=(x_{1b},x_{2b},x_{3b})$ and an image source at $-\boldsymbol{\chi_b}=(x_{1b},x_{2b},-x_{3b})$, where x_3 is the vertical direction and $\mathbf{x_i}$ is zero at the free surface. The anticausal reference Green's function now includes the conjugate of the wave that propagates directly from the real source to the receiver, $\mathscr{G}_0^{d-}$, and the conjugate of the wave that propagates directly from the image source to the receiver, $\mathscr{G}_0^{d'-}$. Consider $\mathscr{G}_0^-(\mathbf{x}|\mathbf{x_b};\omega)=\mathscr{G}_0^{d-}(\mathbf{x}|\mathbf{x_b};\omega)+\mathscr{G}_0^{d'-}(\mathbf{x}|-\boldsymbol{\chi_b};\omega)$, and evaluate both sources inside V (image source outside) in equation 8. Hence,

$$P(\mathbf{x_a}|\mathbf{x_b};\omega)-A(\omega)\mathscr{G}_0^-(\mathbf{x_a}|\mathbf{x_b};\omega)=$$
$$\oint_S [P(\mathbf{x}|\mathbf{x_a};\omega)\nabla\mathscr{G}_0^-(\mathbf{x}|\mathbf{x_b};\omega)-\mathscr{G}_0^-(\mathbf{x}|\mathbf{x_b};\omega)\nabla P(\mathbf{x}|\mathbf{x_a};\omega)]\cdot\mathbf{n}\,d\mathbf{s}. \tag{9}$$

Calculating $\mathscr{G}_0^-(\mathbf{x}|\mathbf{x_b};\omega)$ and its normal derivative for the receiver positions in the data and for real sources at the desired output location, we can regularize and extrapolate the scattered wavefield. This form of Green's theorem was first derived by Weglein and Secrest (1990). It describes how to compute the scattered field between the measurement surface and the free surface, given a cable (or in 3D, a surface) where both the pressure and its normal derivative are measured.

To understand the output of the integral in equation 9, we use the definition

$$P(\mathbf{x_a}|\mathbf{x_b};\omega)=A(\omega)\mathscr{G}_0^+(\mathbf{x_a}|\mathbf{x_b};\omega)+P^s(\mathbf{x_a}|\mathbf{x_b};\omega), \tag{10}$$

where P^s is the scattered field. Introducing this expansion into the left hand side of equation 9, we obtain

$$P^s(\mathbf{x_a}|\mathbf{x_b};\omega)+A(\omega)\left[\mathscr{G}_0^+(\mathbf{x_a}|\mathbf{x_b};\omega)-\mathscr{G}_0^-(\mathbf{x_a}|\mathbf{x_b};\omega)\right]$$
$$=P^s(\mathbf{x_a}|\mathbf{x_b};\omega)+2\,A(\omega)\,\Im\left[\mathscr{G}_0^+(\mathbf{x_a}|\mathbf{x_b};\omega)\right]. \tag{11}$$

Thus, in equation 9 the total scattered field for a source at $\mathbf{x_b}$ and a receiver at $\mathbf{x_a}$ is reconstructed as well as the imaginary part of the direct wave.

The wave field and its normal derivative are required in the theory presented here. In a standard towed streamer acquisition, the normal derivative of the wave field is not recorded, and it is difficult to calculate. Hence, we apply a far field approximation for the actual wavefield's normal derivative (Wapenaar and Fokkema, 2006),

$$\nabla P(\mathbf{x}|\mathbf{x_a};\omega)]\cdot\mathbf{n} \approx ikP(\mathbf{x}|\mathbf{x_a};\omega) \tag{12}$$

where $k=\frac{\omega}{c_0}$. With this approximation and simple mathematical manipulation, we can reduce the integrand of equation 9 to a single term

$$P(\mathbf{x_a}|\mathbf{x_b};\omega) \approx 2\oint_S [P(\mathbf{x}|\mathbf{x_a};\omega)\nabla\mathscr{G}_0^-(\mathbf{x}|\mathbf{x_b};\omega)]\cdot\mathbf{n}\,d\mathbf{s}, \tag{13}$$

and analytically calculate the normal derivative of the reference field or, choose to compute the more complete form

$$P(\mathbf{x_a}|\mathbf{x_b};\omega) \approx \oint_S [P(\mathbf{x}|\mathbf{x_a};\omega)\nabla\mathscr{G}_0^-(\mathbf{x}|\mathbf{x_b};\omega) - ikP(\mathbf{x}|\mathbf{x_a};\omega)\mathscr{G}_0^-(\mathbf{x}|\mathbf{x_b};\omega)]\cdot\mathbf{n}\,d\mathbf{s}, \tag{14}$$

and use an analytical reference Green's function and its normal derivative. Note that the compromise introduced by approximating the normal derivative of the measured field is more forgiving than approximating twice, which was done to obtain equation 5. We anticipate a small error due to the single far-field approximation and an effect on the synthesized direct wave according to equation 11.

The characteristics of this method are: 1) the analytic reference Green's function is used; 2) the total scattered field is reconstructed (in contrast to only reconstructing the imaginary or real part of the wavefield, and calculating the complement via the Hilbert transform, Wapenaar and Fokkema (2006)); 3) the output data don't have spurious multiples nor an extra wavelet; 4) a far-field approximation is used to calculate the normal derivative of the actual field; 5) the normal derivative of the reference field is calculated analytically; and, 6) the wavefield can be reconstructed anywhere between the measurement surface and the free surface, allowing for applications like interpolation, extrapolation and regularization.

Thus, direct wave interferometry provides an improvement over traditional approaches to seismic interferometry. However, the method still uses one far-field approximation which affects the accuracy of the approach. In order to move the current technology towards its promised capability, we will examine another alternative method that formally eliminates the need of the measured wavefield's normal derivative using two-surface Dirichlet boundary conditions.

Direct wave interferometry with Dirichlet boundary conditions

In principle, it is not possible to compute the total two-way propagating pressure field above a cable from measurements of only the pressure field on a single typical towed streamer. In direct wave seismic interferometry, we used an analytic reference Green's function, $\mathscr{G}_0^-$, which is the anticausal impulse response for a half-space of water bounded by a free surface at the air-water boundary and approximated the vertical derivative of the actual pressure field.

Tan (1992) and Osen et al. (1998) were interested in eliminating the data requirement of the normal derivative for source wavelet estimation purposes. They achieved this by choosing a Green's function (in Green's theorem) that vanishes on both the free and the measurement surfaces. This boundary condition can be fulfilled by the source image method. The two-surface Dirichlet Green's function now includes the conjugate of the wave that propagates directly from the real source to the receiver and the conjugate of the wave that propagates directly from each image source to the receiver. Let $\mathscr{G}_0^D(\mathbf{x}|\mathbf{x_b};\omega)$ denote this two-surface Dirichlet Green's function and evaluate both real sources inside the volume (all the image sources are outside) in equation 8. We then obtain,

$$P(\mathbf{x_a}|\mathbf{x_b};\omega) - A(\omega)\mathscr{G}_0^D(\mathbf{x_a}|\mathbf{x_b};\omega) = \oint_S [P(\mathbf{x}|\mathbf{x_a};\omega)\nabla\mathscr{G}_0^D(\mathbf{x}|\mathbf{x_b};\omega) - \mathscr{G}_0^D(\mathbf{x}|\mathbf{x_b};\omega)\nabla P(\mathbf{x}|\mathbf{x_a};\omega)]\cdot\mathbf{n}d\mathbf{s}, \tag{15}$$

and,

$$P(\mathbf{x_a}|\mathbf{x_b};\omega) - A(\omega)\mathscr{G}_0^D(\mathbf{x_a}|\mathbf{x_b};\omega) = \oint_S P(\mathbf{x}|\mathbf{x_a};\omega)\nabla\mathscr{G}_0^D(\mathbf{x}|\mathbf{x_b};\omega)\cdot\mathbf{n}\,d\mathbf{s}, \tag{16}$$

since $\mathscr{G}_0^D = 0$ at the measurement surface. This equation shows how the wavefield above the measurement surface and below the free surface can be determined from measured pressure on a typical surface acquisition plus an estimate of the source wavelet. Tan (1992, 1999) and Weglein et al. (2000) proposed to assume that the contribution of $A(\omega)\mathscr{G}_0^D(\mathbf{x_a}|\mathbf{x_b};\omega)$ could be small and hence ignored to avoid the requirement of a source wavelet and compute the pressure field directly in terms of the measured wavefield,

$$P(\mathbf{x_a}|\mathbf{x_b};\omega) \approx \oint_S P(\mathbf{x}|\mathbf{x_a};\omega)\nabla\mathscr{G}_0^D(\mathbf{x}|\mathbf{x_b};\omega)\cdot\mathbf{n}\,d\mathbf{s}. \tag{17}$$

If an estimate of the wavelet is available, or obtainable, we encourage to use direct wave interferometry with Dirichlet boundary conditions as stated in equation 16, since this is an exact equation and its output is the exact wavefield at a point between the measurement and the air-water surface. The same Green's theorem framework, with all its flavors, has been successfully used to estimate the source wavelet (Weglein and Secrest, 1990; Osen et al., 1998; Tan, 1999; Guo et al., 2005). Any of these source signature estimation methods could help fulfilling the requirements in equation 16.

When the wavelet is not available and it is possible to separate the direct wave from the scattered field (*e.g.* in a deep water experiment) we can find an exact equation for reconstructing scattered field that does not need the source wavelet. Substitute $P^s(\mathbf{x_a}|\mathbf{x_b};\omega)$, the scattered field into Green's theorem instead of the total wavefield and use the two surface Dirichlet Green's function as the second function, to obtain

$$P^s(\mathbf{x_a}|\mathbf{x_b};\omega) = \oint_S P^s(\mathbf{x}|\mathbf{x_a};\omega)\nabla\mathscr{G}_0^D(\mathbf{x}|\mathbf{x_b};\omega)\cdot\mathbf{n}\,d\mathbf{s}. \tag{18}$$

This is possible because the scattered field obeys the wave equation without a source function,

$$\left(\nabla^2 + \frac{\omega^2}{c^2(\mathbf{x})}\right)P^s(\mathbf{x}|\mathbf{x_a};\omega) = 0. \tag{19}$$

This form of Green's theorem has no approximations and do not require the normal derivative of the pressure field, nor the source signature. It only asks for the scattered field and an analytic Green's function that vanishes at the measurement and air-water surface. Tests of this formulation will be shown at the SEG presentation.

NUMERICAL EXAMPLES

We used finite difference 3D surface seismic data in a model consisting of 3 layers, a free surface, and a set of random point diffractors. The modeled data consist of 10 source lines with 12 shots per line. The source and receiver spacing in the numerical modeling was 25 m in

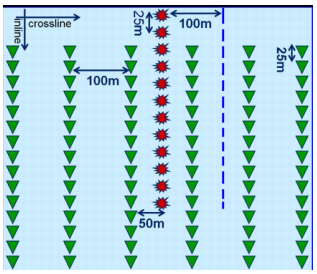

Figure 1: Configuration.

both (inline and crossline) directions. The configuration is shown in figure 1.

We applied direct wave seismic interferometry to 20 receiver lines with 121 receivers per line, 25 m inline separation and 100 m crossline separation. A simulated source line (12 sources) with 25 m source interval overlay each receiver line, as illustrated in figure 1 (sources are marked by red stars and receivers by green triangles). The minimum distance to the receivers in both inline and crossline direction is 50 m in the selected shot gathers. This data subset was put into equation 14 with an analytic anticausal reference Green's function. This Green's function was calculated for 12 sources in a line with 25 m source interval and located at 100 m crossline offset away from the source line in the input data. Our goal is to reconstruct the receiver line 100 meter away from the source line in the crossline direction marked by the dashed line in figure 1. The retrieved Green's function corresponds to a line of 12 sources at zero crossline offset, sources from the input data, and 12 receivers in a line at 100 m crossline offset (dashed line in figure 1).

Figure 1 shows the extrapolated data using direct wave seismic interferometry on the right. The modeled data is shown on the left hand side of figure 1 for comparison. We see that the output of direct wave seismic interferometry has all the events correctly predicted and there are no spurious multiples in the predicted data. The difference between the modeled data and the direct wave seismic interferometry result is due to the high frequency approximation and a bandlimited reference Green's function used in the calculations. Also remember that this algorithm has an effect on the output of the direct wave, as discussed in the previous sections.

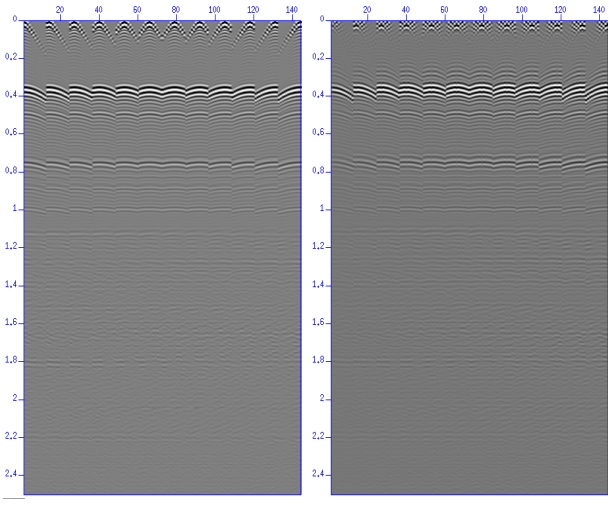

Figure 2: Modeled data and direct wave interferometry prediction.

We also show a 2D example. The data were modeled with finite differences for a receiver line with 200 receivers separated 12.5 m from each other and 20 sources with a 25m separation. In figure3 the output of seismic interferometry and direct wave interferometry as well as the modeled data are shown.

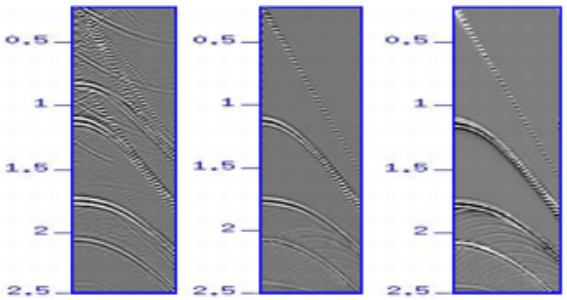

Figure 3: 2D data example. The figure on the left is data reconstructed with standard seismic interferometry. The innermost figure shows data reconstructed with direct wave interferometry. The figure on the right shows modeled data for comparison.

CONCLUSIONS

The foundations of seismic interferometry are in Green's theorem. While this theorem gives exact equations for wavefield retrieval within a volume, the far-field approximations made by some interferometry methods compromise its effectiveness. Within Green's theorem framework, spurious multiples are anticipated and fully explain as a consequence of the approximations. Hence, there is no need to attempt a physical understanding of these artefacts. Instead, we can provide an improvement and move the current technology towards its promised capability by: 1) trying to better provide the ingredients needed by the theorem, or 2) examining alternative approaches to eliminate the need of the normal derivatives of the measured field. An example of the first idea is direct wave interferometry (Ramírez et al., 2007), an approach based on using an analytical reference Green's function and the total measured wavefield in Green's theorem. The reference Green's function and its normal derivative can be analytically calculated for arbitrary source and receiver positions in the reference medium; and a far-field approximation is used only once to overcome the need of the measured wavefield's normal derivative. It is an improvement (no spurious multiples, no extra wavelet and the posibility to reconstruct wavefield in new positions) over other methods since the rest of Green's theorem requirements (reference Green's function, its normal derivative, and the measured pressure field) are fulfilled. An example of the second idea is to impose Dirichlet boundary conditions at the measurement and air-water surfaces to the reference Green's function (Weglein et al., 2000). The retrieval is then made by correlating the analytic normal derivative of this Green's function with the measured wavefield. This is an exact approach that does not require the vertical derivative of the measured field.

ACKNOWLEDGMENTS

Authors thank Statoil for permission to publish this work. The support of M-OSRP sponsors and personnel is gratefully acknowledged. A.C. Ramírez appreciates the internship opportunity she had at Statoil Research Center; the excellent environment, support and encouragement provided by Statoil made this research possible.

REFERENCES

Amundsen, L., T. R. Sten, J. O. A. Robertsson, and E. Kragh, 2005, Rough-sea deghosting of streamer data using pressure gradient approximations: Geophysics, **50**, 1–9.

Bakulin, A. and R. Calvert, 2004, Virtual source: new method for imaging and 4d below complex overburden: SEG Expanded Abstracts.

Claerbout, J., 1968, Synthesis of a layered medium from its acoustic transmission response.: Geophysics, **33**, 264–269.

Derode, A., E. Larose, M. Tanter, J. de Rosny, a. Tourin, M. Campillo, and M. Fink, 2003, Recovering the green's function for a heterogeneous medium between two passive sensors? application to acoustic waves: Applied Physics Letter, **83**, 3054–3056.

Draganov, D., K. A. Wapenaar, and J. Thorbecke, 2006, Seismic interferometry: Reconstructing the earth's reflection response: Geophysics, **71**, S161–S170.

Guo, Z., A. B. Weglein, and T. H. Tan, 2005, Using pressure data on the cable to estimate the seismic wavelet: SEG Technical Program Expanded Abstracts.

Lobkis, O. I. and R. L. Weaver, 2001, On the emergence of the green's function in the crosscorrelations of a diffuse field: Journal of the Acoustic Society of America, **110**, 3011–3017.

Osen, A., B. Secrest, L. Amundsen, and A. Reitan, 1998, Wavelet estimation from marine pressure measurements: Geophysics, **63**, 2108–2119.

Otnes, E., K. Hokstad, G. Rønholt, and S.-K. Foss, 2006, Data-driven surface related multiple elimination on walkaway VSP data: Extended Abstracts of the 68th Annual International Meeting of the EAGE.

Ramírez, A. C., K. Hokstad, and E. Otnes, 2007, Data driven regularization/extrapolation: EAGE 69^{th} Conference & Exhibition London, UK.

Roux, P. and Fink, 2003, Green's function estimation using secondary sources in a shallow water environment: Journal of the Acoustic Society of America, **113**, 1406–1416.

Schuster, G. T., 2001, Theory of daylight/interferometric imaging: tutorial: Extended Abstracts of the 63rd Annual Meeting Conference and Exhibition, EAGE, **A32**.

Schuster, G. T. and M. Zhou, 2006, A theoretical overview of model-based and correlation-based redatuming methods: Geophysics, **4**, SI103–SI110.

Snieder, R., K. Wapenaar, and K. Larner, 2006, Spurious multiples in seismic interferometry of primaries: Geophysics, **71**, SI111–SI124.

Tan, T. H., 1992, Source signature estimation: Presented at the Internat. Conf. and Expo. of Expl. and Development Geophys., Moscow, Russia.

———, 1999, Wavelet spectrum estimation: Geophysics, **64**, 1836–1846.

Vasconcelos, I. and R. Snieder, 2006, Interferometric imaging by deconvolution: Theory and numerical examples: SEG Technical Program Expanded Abstracts, 2416–2420.

Wapenaar, K., 2004, Retrieving the elastodynamic green's function of an arbitrary inhomogeneous medium by cross correlation: Phys. Rev. Lett., **93(25)**, 254301–1 –254301–4.

Wapenaar, K., D. Draganov, J. Thorbecke, and J. Fokkema, 2002, Theory of acoustic daylight imaging revisited: 72nd Annual International Meeting, SEG, Expanded Abstracts, 2269–2272.

Wapenaar, K. and J. Fokkema, 2006, Green's function representations for seismic interferometry: Geophysics, **71**, SI33–SI46.

Weaver, R. L. and O. I. Lobkis, 2004, Diffuse fields in open systems and the emergence of the green's function: Journal of the Acoustic Society of America, **116**, 2731–2734.

Weglein, A. B. and B. Secrest, 1990, Wavelet estimation for a multidimensional acoustic or elastic earth: Geophysics, **55**, 1975–1989.

Weglein, A. B., T. H. Tan, S. A. Shaw, K. H. Matson, and D. J. Foster, 2000, Prediction of the wavefield anywhere above an ordinary towed streamer: application to source waveform estimation, demultiple, deghosting, data reconstruction and imaging: SEG Expanded Abstracts.

Zhang, J. and A. B. Weglein, 2006, Application of extinction theorem deghosting method on ocean bottom data: Presented at the SEG/New Orleans 2006 Expanded Abstracts, SEG.

"Data-driven regularization/extrapolation using interferometry with the direct wave"

by A. C. Ramírez Pérez* (M-OSRP, University of Houston), K. Hokstad (Statoil R&D, Trondheim, Norway) & E. Otnes (Statoil R&D, Trondheim, Norway)

Abstract

We present a method to extrapolate and regularize data. The procedure is based on crosscorrelation of the measured field with the direct wave, and it is independent of earth properties. The method is derived from Green's theorem and, in principle, requires the total field and its normal derivative at the receiver locations. In order to apply the method to towed streamer data, certain approximations are introduced to compensate for the missing normal derivative of the field.

Introduction

Seismic interferometry refers to reconstruction through correlation (Schuster, 2001). Traditional seismic interferometry crosscorrelates wave fields recorded by two receivers and reconstructs the Green's function at one of the receivers as if the second receiver was a source (Wapenaar and Fokkema, 2006). Those methods assume that these receivers are surrounded by sources forming a closed surface. Using reciprocity, we can crosscorrelate two sources surrounded by a closed surface of receivers and retrieve the Green's function between the sources (Otnes et al., 2006). In practice, data are never acquired on a closed surface. Hence, only the kinematic part of the reconstructed Green's functions is predicted correctly. Snieder. et al. (2006) showed that the method also predicts spurious events with magnitudes comparable to the reconstructed primaries.

We have derived a new method based on the crosscorrelation of the direct wave (or reference Green's function) and the total wave field that circumvents the appearance of spurious events. If we crosscorrelate a source ignited in the reference medium with another ignited in the actual medium and sum over coincident receivers, we can retrieve the actual Green's function between the two source locations. The reference source position can be analytically calculated for any position in the reference medium; and, hence the data can be extrapolated to new locations. This theory accurately retrieves the total wave field in the new locations.

Theory

Green's second identity has been widely used in seismic exploration, *e.g.* Weglein and Secrest (1990). It relates a surface integral with a volume integral,

$$\int_V [u\nabla^2\nu - u\nabla^2\nu]d\boldsymbol{x} = \int_S [u\boldsymbol{\nabla}\nu - \nu\boldsymbol{\nabla}u]\cdot\boldsymbol{n}d\boldsymbol{s}, \tag{1}$$

where u and ν are scalar functions, $\boldsymbol{x}$ is a three dimensional vector characterizing the volume V enclosed by the surface S, and $\boldsymbol{n}$ is the vector normal to the surface S. The acoustic wave equation for an inhomogeneous earth with a velocity distribution $c(\boldsymbol{x})$ and constant density is

$$\left(\nabla^2 + \frac{\omega^2}{c^2(\boldsymbol{x})}\right) P(\boldsymbol{x}|\boldsymbol{x_a};\omega) = A(\omega)\delta(\boldsymbol{x}-\boldsymbol{x_a}), \tag{2}$$

where $A(\omega)$ is the source wavelet and $P(\boldsymbol{x}|\boldsymbol{x_a};\omega)$ is the actual pressure field at point $\boldsymbol{x}$ and frequency ω due to a source at $\boldsymbol{x_a}$ excited at $t=0$.

Choose the reference medium to be a homogeneous whole space satisfying the wave equation,

$$\nabla^2 G_0(\boldsymbol{x}|\boldsymbol{x_b};\omega) = -\frac{\omega^2}{c_0^2}G_0(\boldsymbol{x}|\boldsymbol{x_b};\omega) + \delta(\boldsymbol{x}-\boldsymbol{x_b}), \tag{3}$$

where $G_0(\boldsymbol{x}|\boldsymbol{x_b};\omega)$ is free space or reference Green's function for a source at $\mathbf{x_b}$ excited at $t=0$, and it represents the deconvolved direct wave from a seismic experiment. It can be causal (G_0^+) or anticausal (G_0^-) with outgoing and ingoing boundary conditions, respectively. We choose the anticausal Green's function defined by

$$G_0^-(\boldsymbol{x}|\boldsymbol{x_b};\omega) = \int_{-\infty}^{\infty} e^{-i\omega t}G_0^+(\boldsymbol{x}|\boldsymbol{x_b};-t)dt. \tag{4}$$

Consider a volume V within the reference medium, with boundary S and enclosing the source at $\mathbf{x_b}$. Introduce $\frac{1}{c(\boldsymbol{x})^2} = \frac{1}{c_0^2}\left(1-\alpha(\boldsymbol{x})\right),\ \alpha(\boldsymbol{x}) = 0\ \forall \boldsymbol{x}\ \in\ V$ into equation 2, where α is the relative difference between reference and actual medium (Weglein and Secrest, 1990). Hence,

$$\nabla^2 P(\boldsymbol{x}|\boldsymbol{x_a};\omega) = -\frac{\omega^2}{c_0^2}P(\boldsymbol{x}|\boldsymbol{x_a};\omega) + \frac{\omega^2}{c_0^2}\alpha(\boldsymbol{x})P(\boldsymbol{x}|\boldsymbol{x_a};\omega) + A(\omega)\delta(\boldsymbol{x}-\boldsymbol{x_a}). \tag{5}$$

Substituting the wavefield $P(\boldsymbol{x}|\boldsymbol{x_a};\omega)$ and the anticausal direct wave $G_0^-(\boldsymbol{x}|\boldsymbol{x_b};\omega)$ into equation 1 as u and ν, and using equations 3 and 5 in the volume integral, we obtain,

$$\begin{aligned}
&\int_V (P(\boldsymbol{x}|\boldsymbol{x_a};\omega)[-\frac{\omega^2}{c_0^2}G_0^-(\boldsymbol{x}|\boldsymbol{x_b};\omega) + \delta(\boldsymbol{x}-\boldsymbol{x_b})] \\
&-G_0^-(\boldsymbol{x}|\boldsymbol{x_b};\omega)[-\frac{\omega^2}{c_0^2}P(\boldsymbol{x}|\boldsymbol{x_a};\omega) + \frac{\omega^2}{c_0^2}\alpha(\boldsymbol{x})P(\boldsymbol{x}|\boldsymbol{x_a};\omega) + A(\omega)\delta(\boldsymbol{x}-\boldsymbol{x_a})])d\boldsymbol{x} \\
&\quad = \oint_S [P(\boldsymbol{x}|\boldsymbol{x_a};\omega)\boldsymbol{\nabla}G_0^-(\boldsymbol{x}|\boldsymbol{x_b};\omega) - G_0^-(\boldsymbol{x}|\boldsymbol{x_b};\omega)\boldsymbol{\nabla}P(\boldsymbol{x}|\boldsymbol{x_a};\omega)] \cdot \boldsymbol{n}\, d\boldsymbol{s}. \qquad (6)
\end{aligned}$$

Let $\boldsymbol{x}$ be within the volume and $\boldsymbol{x_a}$ outside the volume to obtain

$$P(\boldsymbol{x_a}|\boldsymbol{x_b};\omega) = \oint_S \quad [P(\boldsymbol{x}|\boldsymbol{x_a};\omega)\boldsymbol{\nabla}G_0^-(\boldsymbol{x}|\boldsymbol{x_b};\omega) - G_0^-(\boldsymbol{x}|\boldsymbol{x_b};\omega)\boldsymbol{\nabla}P(\boldsymbol{x}|\boldsymbol{x_a};\omega)] \cdot \boldsymbol{n}\, d\boldsymbol{s}. \quad (7)$$

Thus, if we measure the wavefield and its normal derivative at S for a source at $\boldsymbol{x_a}$ outside V, and measure/calculate the anticausal direct wave and its normal derivative at S for a source at $\boldsymbol{x_b}$ within V, equation 7 retrieves the wavefield produced by a source at $\boldsymbol{x_b}$ and measured at $\boldsymbol{x_a}$. Note that the anticausal direct wave is simply the complex conjugate of the causal one.

To account for the free surface, we use a background medium with a half space of water and a half space of air and a volume V bound by the free surface and the measurement surface. The wave equation is expressed using a real source at $\boldsymbol{x_b} = (\boldsymbol{x_{1b}}, \boldsymbol{x_{2b}}, \boldsymbol{x_{3b}})$ and an image source at $-\boldsymbol{\chi_b} = (\boldsymbol{x_{1b}}, \boldsymbol{x_{2b}}, -\boldsymbol{x_{3b}})$, where $\boldsymbol{x_3}$ is the vertical direction and $\boldsymbol{x}$ is zero at the free surface. The anticausal reference Green's function now includes the conjugate of the wave that propagates directly from the real source to the receiver, $\mathcal{G}_0^{d-}$, and the conjugate of the wave that propagates directly from the image source to the receiver, $\mathcal{G}_0^{d'-}$. Consider $\mathcal{G}_0^-(\boldsymbol{x}|\boldsymbol{x_b};\omega) = \mathcal{G}_0^{d-}(\boldsymbol{x}|\boldsymbol{x_b};\omega) + \mathcal{G}_0^{d'-}(\boldsymbol{x}|-\boldsymbol{\chi_b};\omega)$, and evaluate both sources inside V (image source outside) in equation 6. Hence,

$$\begin{aligned}
&P(\boldsymbol{x_a}|\boldsymbol{x_b};\omega) - A(\omega)\mathcal{G}_0^-(\boldsymbol{x_a}|\boldsymbol{x_b};\omega) = \\
&\qquad \oint_S [P(\boldsymbol{x}|\boldsymbol{x_a};\omega)\boldsymbol{\nabla}\mathcal{G}_0^-(\boldsymbol{x}|\boldsymbol{x_b};\omega) - \mathcal{G}_0^-(\boldsymbol{x}|\boldsymbol{x_b};\omega)\boldsymbol{\nabla}P(\boldsymbol{x}|\boldsymbol{x_a};\omega)] \cdot \boldsymbol{n}\, d\boldsymbol{s}. \qquad (8)
\end{aligned}$$

Introduce $P(\boldsymbol{x_a}|\boldsymbol{x_b};\omega) = A(\omega)\mathcal{G}_0^+(\boldsymbol{x_a}|\boldsymbol{x_b};\omega) + P^s(\boldsymbol{x_a}|\boldsymbol{x_b};\omega)$, where P^s is the scattered field, and use it on the left hand side of equation 8,

$$\begin{aligned}
&P^s(\boldsymbol{x_a}|\boldsymbol{x_b};\omega) + A(\omega)\left[\mathcal{G}_0^+(\boldsymbol{x_a}|\boldsymbol{x_b};\omega) - \mathcal{G}_0^-(\boldsymbol{x_a}|\boldsymbol{x_b};\omega)\right] \\
&\qquad = P^s(\boldsymbol{x_a}|\boldsymbol{x_b};\omega) + 2\,\Im\left[A(\omega)\mathcal{G}_0^+(\boldsymbol{x_a}|\boldsymbol{x_b};\omega)\right]. \qquad (9)
\end{aligned}$$

In equation 8, the total scattered field for a source at $\boldsymbol{x_b}$ and a receiver at $\boldsymbol{x_a}$ is reconstructed as well as the imaginary part of the direct wave. Calculating $\mathcal{G}_0^-(\boldsymbol{x}|\boldsymbol{x_b};\omega)$ for the receiver positions in the data and for real sources at the desired output location, we can regularize and extrapolate the scattered wavefield.

Towed Streamer Data

The wave field and its normal derivative are required in the theory presented here. There are new acquisition methods that measure the field at two parallel surfaces, so the gradient of the field is known and the normal derivative can be obtained. In a standard towed streamer acquisition, the normal derivative of the wave field is not recorded, and is difficult to calculate. Hence, we apply a high frequency approximation (Wapenaar and Fokkema, 2006) to reduce the integrand of equations 7 and 8 to a single term by assuming that the medium at the surface is homogeneous

and the local angle between the *ray* approximation of the wavefield and the vector normal to the surface is zero.

With these assumptions, we obtain

$$P(\boldsymbol{x_a}|\boldsymbol{x_b};\omega) \approx 2 \oint_S [P(\boldsymbol{x}|\boldsymbol{x_a};\omega) \boldsymbol{\nabla} G_0^-(\boldsymbol{x}|\boldsymbol{x_b};\omega)] \cdot \boldsymbol{n}\, d\boldsymbol{s}. \tag{10}$$

For an acoustic background medium without a free surface, the result is

$$P(\boldsymbol{x_a}|\boldsymbol{x_b};\omega) \approx 2 \oint_S P(\boldsymbol{x}|\boldsymbol{x_a};\omega) \left(\frac{i\omega(x_3 - x_{3b})}{c_0|\boldsymbol{x} - \boldsymbol{x_b}|} - \frac{(x_3 - x_{3b})}{c_0(\boldsymbol{x} - \boldsymbol{x_b})^2} \right) G_0^-(\boldsymbol{x}|\boldsymbol{x_b};\omega)\, d\boldsymbol{s}, \tag{11}$$

or, with a free surface,

$$\begin{aligned} P(\boldsymbol{x_a}|\boldsymbol{x_b};\omega) \approx 2 \oint_S P(\boldsymbol{x}|\boldsymbol{x_a};\omega) \, [\, & \left(\frac{i\omega(x_3 - x_{3b})}{c_0|\boldsymbol{x} - \boldsymbol{x_b}|} - \frac{(x_3 - x_{3b})}{c_0(\boldsymbol{x} - \boldsymbol{x_b})^2} \right) \mathcal{G}_0^{d-}(\boldsymbol{x}|\boldsymbol{x_b};\omega) \\ & + \left(\frac{i\omega(x_3 + \chi_{3b})}{c_0(\boldsymbol{x} + \boldsymbol{\chi_b})} - \frac{(x_3 + \chi_{3b})}{c_0(\boldsymbol{x} + \boldsymbol{\chi_b})^2} \right) \mathcal{G}_0^{d'-}(\boldsymbol{x}|\boldsymbol{\chi_b};\omega) \,] \, d\boldsymbol{s}. \end{aligned} \tag{12}$$

This method is different from the one in Wapenaar and Fokkema (2006) in three ways: 1) the direct wave is used instead of a second wave field, 2) the total wavefield or scattered field is reconstructed (in contrast to only reconstructing the imaginary or real part of the wavefield, and calculating the complement via the Hilbert transform), and 3) the output data don't have spurious events nor an extra wavelet, it is the crosscorrelation of a bandlimited delta function (direct wave) and a medium's response with a wavelet (actual field).

We used finite difference 3D surface seismic data in a model consisting of 3 layers, a free surface, and a set of random point diffractors. The modeled data consist of 10 source lines with 12 shots per line. The source and receiver spacing in the numerical modeling was 25 m in both (inline and crossline) directions. We applied direct wave seismic interferometry to 20 receiver lines with 121 receivers per line, 25 m inline separation and 100 m crossline separation. A simulated source line (12 sources) with 25 m source interval overlay each receiver line, as illustrated in figure 1 (sources are marked by red stars and receivers by green triangles). The minimum distance to the receivers in both inline and crossline direction is 50 m in the selected shot gathers. This data subset was put into equation 12, with an analytic anticausal direct wave calculated for 12 sources in a line with 25 m source interval and located at 100 m crossline offset away from the source line in the input data. Our goal is to reconstruct the receiver line 100 meter away from the source line in the crossline direction marked by the dashed line in figure 1. The retrieved Greens function corresponds to a line of 12 sources at zero crossline offset, sources from the input data, and 12 receivers in a line at 100 m crossline offset (dashed line in figure 1). Figure 1 shows the extrapolated data on the right and the modeled data on the left, for comparison. We see that

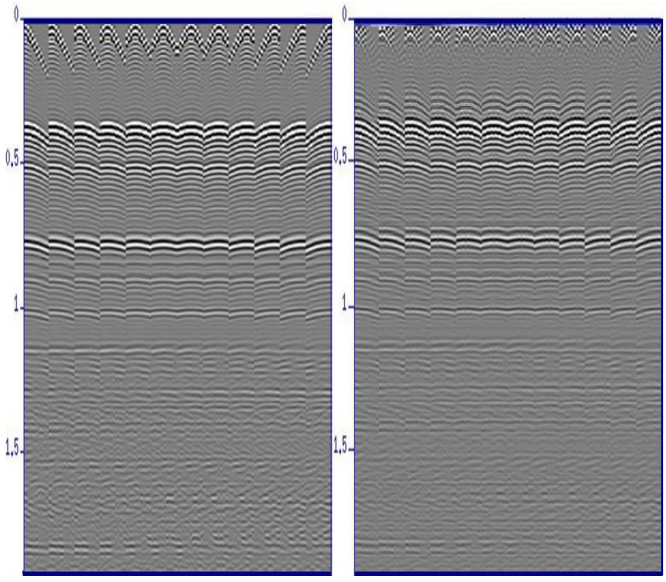

Figure 1: Modeled and reconstructed data.

all events are correctly predicted and there are no spurious events in the predicted data. The difference between the modeled data and the direct wave seismic interferometry result are due to the high frequency approximation and a bandlimited reference Green's function used in the calculations.

Conclusions

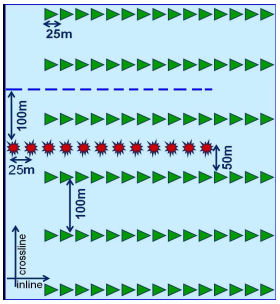

Figure 2: Configuration.

We have shown that using the direct wave in seismic interferometry where we don't have acquired data on a closed surface, improves standard seismic interferometry where only the real or imaginary field is obtained at source and receiver locations defined by the physical experiment. In addition, standard seismic interferometry introduces spurious events in the predicted data since the prerequisites of the method are not fulfilled.

We showed the mathematical derivation of a new method for seismic interferometry using the direct wave. This is an exact method that retrieves the total scattered field in new locations when its requirements are satisfied. One of the assumptions of the method is that the normal derivative of the wavefield is measured, which does not comply with current standard acquisition. Hence a high frequency approximation is applied to avoid the need of this derivative and the result depends only on the measured wave field and the derivative of the anticausal deconvolved direct wave, which can be obtained analytically.

This new theory has given encouraging results in 1D as well as multidimensional surface seismic synthetic data, where the total wavefield has been retrieved. The theory without the high frequency approximation is well suited for OBS data. Further analysis is necessary to implement the method on VSP data.

Acknowledgements

Authors thank Statoil for permission to publish this work. The support of Arthur B. Weglein is gratefully acknowledged.

References

Otnes, E., Hokstad, K., Ronholt, G., and Foss, S.-K., 2006, Data-driven surface related multiple elimination on walkaway vsp data: Extended Abstracts of the 68th Annual International Meeting of the EAGE.

Schuster, G. T., 2001, Theory of daylight/interferometric imaging: tutorial: Extended Abstracts of the 63rd Annual Meeting Conference and Exhibition, EAGE, **A32**.

Snieder., R., Wapenaar, K., and Larner, K., 2006, Spurious multiples in seismic interferometry of primaries: Geophysics, **71**, SI111–SI124.

Wapenaar, K., and Fokkema, J., 2006, Green's function representations for seismic interferometry: Geophysics, **71**, SI33–SI46.

Weglein, A. B., and Secrest, B., 1990, Wavelet estimation for a multidimensional acoustic or elastic earth: Geophysics, **55**, no. 6, 1975–1989.

Inverse scattering internal multiple attenuation algorithm: an analysis of the pseudo-depth and time monotonicity requirements

*Bogdan G. Nita *, Montclair State University and Arthur B. Weglein, University of Houston*

SUMMARY

Pseudo-depth monotonicity condition is an important assumption of the inverse scattering internal multiple attenuation algorithm. Analysis reveals that this condition is equivalent to a vertical-time monotonicity condition which is different than the total traveltime monotonicity suggested in recent literature/discussions. For certain complex media, the monotonicity condition can be too restrictive and, as a result, some multiples will not be predicted by the algorithm. Those cases have to be analyzed in the forward scattering series to determine how the multiples are modeled and to establish if an analogy between the forward and the inverse process would be useful to expand the algorithm to address these kind of events.

INTRODUCTION

The inverse scattering series provides a complete framework for processing primaries and multiples directly in terms of an inadequate velocity model, without updating or in any other way determining the accurate velocity configuration. Algorithms for eliminating free surface and attenuating internal multiples, identified as subseries in the full scattering series, have long been known and applied by the petroleum industry. Here we discuss the multi-dimensional inverse scattering internal multiple attenuation algorithm focusing our attention on the prediction mechanisms. Roughly speaking, the algorithm combines amplitude and phase information of three different arrivals (sub-events) in the data set to exactly predict the time and well approximate the amplitude of interbed multiples.

The inverse scattering internal multiple attenuation algorithm was found through a combination of simple one-dimensional models testing/evaluation and certain similarities between the way the data is constructed by the forward scattering series and the way arrivals in the data are processed by the inverse scattering series. This connection between the forward and the inverse series was analyzed and described in Matson (1996), Matson (1997), Weglein et al. (1997), and Weglein et al. (2003). Specifically, they showed that an internal multiple in the forward scattering series is constructed by summing certain types of scattering interactions which appear starting with the third order in the series. The piece of this term representing the first order approximation to an internal multiple is exactly the one for which the point scatterers satisfy a certain lower-higher-lower relationship in actual depth. Summing over all interactions of this type in the actual medium results in constructing the first order approximation to an internal multiple. By analogy, it was inferred that the first term in the subseries for eliminating the internal multiples would be one constructed from events satisfying the same lower-higher-lower relationship in pseudo-depth. The assumption that the ordering of the actual and the pseudo depths of two sub-events is preserved, i.e.

$$z_1^{actual} < z_2^{actual} \iff z_1^{pseudo} < z_2^{pseudo}, \qquad (1)$$

has been subsequently called "the pseudo-depth monotonicity condition".

In this paper we further analyze this relation and show that it is equivalent to a vertical or intercept time (here denoted by τ) monotonicity condition

$$z_1^{actual} < z_2^{actual} \iff \tau_1 < \tau_2, \qquad (2)$$

for any two sub-events. We also look at the differences between the time monotonicity condition in vertical or intercept time and total travel time. The latter was pointed out by a different algorithm derived from the inverse scattering series in ten Kroode (2002) and further described in Malcolm and de Hoop (2005). We show a 2D example which satisfies the former (and hence is predicted by the original algorithm) but not the latter. Finally we discuss one case in which the monotonicity condition is not satisfied by the sub-events of an internal multiple in either vertical or total travel time and consequently the multiple will not be predicted by either one of the two algorithms. For these cases, the monotonicity condition turns out to be too restrictive and we discuss ways of lowering these restrictions and hence expanding the algorithm to address these types of multiples.

THE INVERSE SCATTERING INTERNAL MULTIPLE ATTENUATION ALGORITHM

The first term in the inverse scattering subseries for internal multiple elimination is (see e.g. Weglein et al. (2003))

$$\begin{aligned} b_3 &= \frac{1}{(2\pi)^2}\int_{-\infty}^{\infty}\int_{-\infty}^{\infty} dk_1 e^{-iq_1(\varepsilon_g-\varepsilon_s)} dk_2 e^{iq_2(\varepsilon_g-\varepsilon_s)} \\ &\times \int_{-\infty}^{\infty} dz_1 e^{i(q_g+q_1)z_1} b_1(k_g,k_1,z_1) \\ &\times \int_{-\infty}^{z_1} dz_2 e^{i(-q_1-q_2)z_2} b_1(k_1,k_2,z_2) \\ &\times \int_{z_2}^{\infty} dz_3 e^{i(q_2+q_s)z_3} b_1(k_2,k_s,z_3) \end{aligned} \qquad (3)$$

where $z_1 > z_2$ and $z_2 < z_3$ and b_1 is defined in terms of the original pre-stack data with free surface multiples eliminated, D', to be

$$D'(k_g,k_s,\omega) = (-2iq_s)^{-1} B(\omega) b_1(k_g,k_s,q_g+q_s) \qquad (4)$$

with $B(\omega)$ being the source signature. Here k_s and k_g are horizontal wavenumbers, for source and receiver coordinates x_s

and x_g, and q_g and q_s are the vertical wavenumbers associated with them. The b_3 on the left hand side represents the first order prediction of the internal multiples. An internal multiple in b_3 is constructed through the following procedure.

The deconvolved data without free-surface multiples in the space-time domain, $D(x_s,x_g,t)$ can be described as a sum of Dirac delta functions

$$D(x_s,x_g,t)=\sum_a R_a\delta(t-t_a) \tag{5}$$

representing different arrivals (primaries and internal multiples). Here R_a represents the amplitude of each arrival and it is a function of source and receiver position x_s and x_g and frequency ω. When transformed to the frequency domain the transformed function $D(x_s,x_g,\omega)$ is a sum

$$\tilde{D}(x_s,x_g,\omega)=\sum_a \tilde{R}_a e^{-i\omega t_a}. \tag{6}$$

Here t_a is the total traveltime for each arrival and it can be thought of as a sum of horizontal and vertical times $t_a=\tau_a+t_{xa}$ (see e.g. Diebold and Stoffa (1981)), where t_{xa} is a function of x_g and x_s. After Fourier transforming over x_s and x_g, the data is $\tilde{D}(k_s,k_g,\omega)$. The transforms act on the amplitude as well as on the phase of the data and transform the part of the phase which is described by the horizontal time t_{xa}. Hence $D(k_s,k_g,\omega)$ can now be thought of as a sum of terms containing $e^{i\omega\tau_a}$ with τ_a being the vertical or intercept time of each arrival

$$\tilde{D}(k_s,k_g,\omega)=\sum_a \tilde{R'}_a e^{-i\omega\tau_a} \tag{7}$$

and where $\tilde{R'}_a$ is the double Fourier transform over x_g and x_s of $\tilde{R}_a e^{-i\omega t_{xa}}$. The multiplication by the obliquity factor, $2iq_s$, changes the amplitude of the plane wave components without affecting the phase; hence $b_1(k_s,k_g,\omega)$ represents an effective plane wave decomposed data and is given by

$$b_1(k_s,k_g,\omega)=\sum_a \tilde{R''}_a e^{-i\omega\tau_a} \tag{8}$$

where $\tilde{R''}_a=2iq_s\tilde{R'}_a$ and whose phase, $e^{i\omega\tau_a}$, contains information only about the recorded *actual* vertical or intercept time.

Notice that for each planewave component of fixed k_s, k_g and ω we have

$$\omega\tau_a=k_z^{actual}z_a^{actual} \tag{9}$$

where k_z^{actual} is the actual, velocity dependent, vertical wavenumber and z_a^{actual} is the actual depth of the turning point of the planewave. Since the velocity of the actual medium is assumed to be unkown, this relationship is written in terms of the reference velocity as

$$\omega\tau_a=k_z z_a \tag{10}$$

where k_z is the vertical wavenumber of the planewave in the reference medium, $k_z=\sqrt{\frac{\omega}{c_0}-k_s}+\sqrt{\frac{\omega}{c_0}-k_g}$, and z_a is the pseudo-depth of the turning point. This implicit operation in the algorithm is performed by denoting $b_1(k_s,k_g,\omega)=b_1(k_s,k_g,k_z)$ with the latter having the expression

$$b_1(k_s,k_g,k_z)=\sum_a \tilde{R''}_a e^{-ik_z z_a}. \tag{11}$$

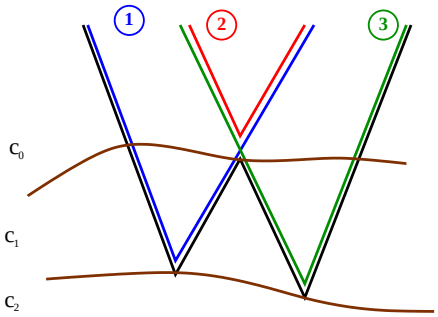

Figure 1: *The sub-events of an internal multiple: the green, blue and red are arrivals in the data which satisfy the lower-higher-lower relationship in pseudo-depths z. The algorithm will construct the phase of the internal multiple shown in black by adding the phases of the green and the blue primaries and subtract the one of the red primary.*

The next step is to Inverse Fourier Transform over the reference k_z hence obtaining

$$b_1(k_s,k_g,z)=\int_{-\infty}^{\infty} e^{ik_z z}b_1(k_s,k_g,k_z)dk_z. \tag{12}$$

Putting together equations (11) and (12)) we find

$$b_1(k_s,k_g,z)=\sum_a\int_{-\infty}^{\infty}\tilde{R''}_a e^{ik_z(z-z_a)}dk_z \tag{13}$$

which represents a sum of delta-like events placed at pseudo-depths z_a and hence the b_1 from the last equation is actually $b_1(k_s,k_g,z_a)$. This last step can also be interpreted as a downward continuation on both source and receiver sides, with the reference velocity c_0, and an imaging with $\tau=0$, or, in other words, an un-collapsed F-K migration (see e.g. Stolt (1978)). A discussion of differences in imaging with τ and with t was given in Nita and Weglein (2004). Each internal multiple is constructed by considering three effective data sets b_1 and searching, in the horizontal-wavenumber–pseudo-depth domain, for three arrivals which satisfy the lower-higher-lower relationship in their pseudo-depths, i.e. $z_1>z_2<z_3$, (see Figure 1 for an example of three such primary events). Having found such three arrivals in the data, the algorithm combines their amplitudes and phases to construct a multiple by adding the phases of the two pseudo-deeper events and subtracting the one of the pseudo-shallower one and by multiplying their amplitudes. One can then see (see e.g. Weglein et al. (2003)) that the time of arrival of an internal multiple is exactly predicted and its amplitude is well approximated by this procedure.

As pointed out in the first section, the lower-higher-lower restriction was inferred from the analogy with the forward scattering series description of internal multiples: the first order approximation to an internal multiple (which occurs in the third term of the series) is built up by summing over all

scattering interactions which satisfy a lower-higher-lower relationship in actual depth. The assumption that this relationship is preserved in going from actual depth to pseudo-depth is called "the pseudo-depth monotonicity condition". (Recall that a monotonic function $f(x)$ satisfies $f(x_1) < f(x_2) \iff x_1 < x_2$; here, we regard the pseudo-depth as a function of actual depth). Notice that the lower-higher-lower relationship in pseudo-depth can be translated, from equation (10), in a similar longer-shorter-longer relationship in the vertical or intercept time of the three events. Accordingly, the pseudo-depth monotonicity is also translated in a vertical time monotonicity condition. Notice that this is different from the total time monotonicity assumed by the algorithm introduced in ten Kroode (2002). The latter is employing asymptotic evaluations of certain Fourier integrals which result in an algorithm in the space domain, having a ray theory assumption and the less inclusive total time monotonicity requirement. The justification for this approach was the attempt to attenuate a first order approximation to an internal multiple built by the forward scattering series. In contrast, the original algorithm is aimed at predicting and attenuating the actual multiples in the data and hence it takes into consideration the full wavefield, with no asymptotic compromises, and results in a more inclusive vertical time monotonicity condition.

In the following section we discuss a 2D example in which the geometry of the subsurface leads to the existence of a multiple which satisfies the pseudo-depth/vertical-time but not the total time monotonicity condition.

VERTICAL TIME AND TOTAL TRAVEL TIME MONOTONICITY: A TWO DIMENSIONAL EXAMPLE

Consider the earth model shown in Figure 2. For simplicity we assume that only the density ρ varies at the interface and it has the value ρ_0 in the reference medium and ρ_1 in the actual medium. The velocity is constant c_0. The actual internal multiple is shown in black and the sub-events composing the multiple are shown in green, blue and red. First, notice that the total traveltime of the shallower reflection (the red event) is bigger than both deeper reflection (green and blue) due to the large offsets needed to record such an event. This implies that the longer-shorter-longer relationship is not satisfied by these particular sub-events in the total traveltime.

Next we calculate the vertical times for individual sub-events. The vertical time for the red event along the left leg is (see Figure 2)

$$\tau^1_{red} = z_1 \frac{\cos\theta_{in}}{c_0} \tag{14}$$

and along the right leg is

$$\tau^2_{red} = z_1 \frac{\cos\theta_{out}}{c_0}. \tag{15}$$

Summing the two legs we find the total vertical time along the red event to be

$$\tau_{red} = \frac{z_1}{c_0}\left(\cos\theta_{in} + \cos\theta_{out}\right). \tag{16}$$

Similarly, for the green event we have

$$\tau_{green} = \frac{z_2}{c_0}\left(\cos\phi_{in} + \cos\phi_{out}\right). \tag{17}$$

Since the velocity is constant, $\theta_{out} = \phi_{out}$; we also have that $\phi_{in} < \theta_{in}$, and hence $\cos\phi_{in} > \cos\theta_{in}$, and $z_2 > z_1$ which results in

$$\tau_{green} > \tau_{red}. \tag{18}$$

It is not difficult to see that similarly, for this example, we have

$$\tau_{blue} > \tau_{red} \tag{19}$$

where τ_{blue} is the vertical time of the blue primary in Figure 2. The conclusion is that for this model and particular internal multiple, the longer-shorter-longer relationship is satisfied by the vertical or intercept times of the three sub-events but not by their total traveltimes. According to equation (10), this relation translates into the lower-higher-lower relationship between the pseudo-depths of the sub-events and hence the internal multiple depicted in Figure 2 will be predicted by the inverse scattering internal multiple attenuation algorithm in Equation (3).

In the next section we discuss an earth model and a particular internal multiple in which the longer-shorter-longer relationship in vertical and total travel time is not satisfied.

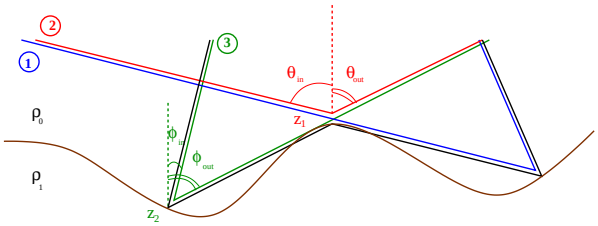

Figure 2: *A two dimensional earth model with an internal multiple satisfying the time monotonicity in vertical time but not in total travel time*

BREAKING THE TIME MONOTONICITY: A TWO DIMENSIONAL EXAMPLE

Consider the earth model shown in Figure 3 where $c_0 < c_1$ (a similar example was discussed in ten Kroode (2002)). A high velocity zone, in which the propagation speed is c_3 much higher than c_0, intersects one leg of the internal multiple and hence one leg of one of its sub-events (the blue primary in Figure 3). Due to this high velocity zone and the fact that $c_0 < c_1$, one can easily imagine a situation in which both the total and the vertical time of the blue primary are shorter than the total and vertical times respectively of the red primary (for example when the measurement surface is sufficiently far from the interface) . In this case the lower-higher-lower relationship between the pseudo-depths of the sub-events is not satisfied and hence the internal multiple shown in the picture will not be predicted. The monotonicity is in consequence broken, since even though the actual depths still satisfy a lower-higher-lower

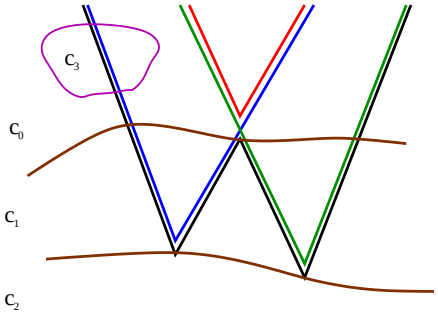

Figure 3: *A two dimensional earth model with an internal multiple containing sub-events which do not satisfy the time monotonicity in either total traveltime or vertical time.*

relationship, the pseudo-depths, vertical times or total times of the sub-events do not.

To better understand the multiples which do not satisfy the pseudo-depth / vertical-time monotonicity condition and to expand the algorithm to address them, one has to study their creation in the forward scattering series. As indicated in Matson (1996), Matson (1997) and Weglein et al. (2003) the lower-higher-lower relationship in pseudo-depth z was pointed to by the forward scattering series: the first order approximation to an internal multiple is constructed in the forward scattering series from interactions with point scatterers which satisfy the lower-higher-lower relationship in actual depth. It would be interesting to analyze how a multiple that breaks the monotonicity assumption is constructed by the forward series and to determine if an analogy between the forward and the inverse process would be useful to expand the algorithm to address these kind of events. This particular issue and others will be the subject of future research.

CONCLUSIONS

In this paper we presented an analytic analysis of the inverse scattering internal multiple attenuation algorithm for multi dimensional media. We particularly focused on the mechanism of predicting amplitude and phase properties of interbed multiples. We have discussed in detail the pseudo-depth/vertical-time monotonicity condition and compared it with a similar total traveltime relation. Furthermore, we showed that this restriction on the sub-events can be too strong and could prevent the prediction of some complex internal multiples.

This research is an important step forward in better understanding the inverse scattering series and the internal multiple attenuation algorithm derived from it. The analytic analysis presented, targets internal multiples which occur in complex multi-dimensional media. Having a better understanding of the structure and definition of such internal multiples opens up new possibilities of identifying, predicting and subtracting them from the collected data. The inverse scattering series is presently the only tool that can achieve these objectives without any knowledge about the actual medium.

ACKNOWLEDGMENTS

This work was partially supported by NSF-CMG 0327778 and DOE Basic Sciences DE-FG02-05ER15697. M-OSRP support is gratefully acknowledged. Adriana C. Ramírez is thanked for providing the earth model in Figure 2. Jon Sheiman, Einar Otnes and Fons ten Kroode are acknowledged for their useful comments and insights on this work.

REFERENCES

Diebold, J. and P. Stoffa, 1981, The traveltime equation, tau-p mapping, and inversion of common midpoint data: Geophysics, **46**, 238–254.

Malcolm, A. E. and M. V. de Hoop, 2005, A method for inverse scattering based on the generalized bremmer coupling series: Inverse Problems, **21**, 1137–1167.

Matson, K. H., 1996, The relationship between scattering theory and the primaries and multiples of reflection seismic data: Journal of Seismic Exploration, **5**, 63–78.

———, 1997, An inverse scattering series method for attenuating elastic multiples from multicomponent land and ocean bottom seismic data: PhD thesis, University of British Columbia, Vancouver, BC, Canada.

Nita, B. G. and A. B. Weglein, 2004, Imaging with $\tau = 0$ versus $t = 0$: implications for the inverse scattering internal multiple attenuation algorithm: 74th Annual International Meeting, SEG, Expanded Abstracts, 1289–1292.

Stolt, R. H., 1978, Migration by fourier transform: Geophysics, **43**, 23–48.

ten Kroode, A. P. E., 2002, Prediction of internal multiples: Wave Motion, **35**, 315–338.

Weglein, A. B., F. V. Araújo, P. M. Carvalho, R. H. Stolt, K. H. Matson, R. T. Coats, D. Corrigan, D. J. Foster, S. A. Shaw, and H. Zhang, 2003, Inverse scattering series and seismic exploration: Inverse Problems, R27–R83.

Weglein, A. B., F. A. Gasparotto, P. M. Carvalho, and R. H. Stolt, 1997, An inverse-scattering series method for attenuating multiples in seismic reflection data: Geophysics, **62**, 1975–1989.

Comprehending and analyzing the leading order and higher order imaging closed forms derived from inverse scattering series

Jingfeng Zhang, Fang Liu, Kristopher Innanen and Arthur B. Weglein, M-OSRP, University of Houston*

SUMMARY

All current leading-edge migration/imaging locates the depth of the subsurface reflectors using the phase in the reflected data and the velocity above the reflector. The subseries for imaging without the velocity (Weglein et al., 2003) is part of the whole inverse scattering series (ISS) has the capability of directly producing the image of the Earth using the data only. The imaging subseries is a cascaded series in the sense that the coefficient of each term is again an infinite series (Shaw, 2005). Part of this cascaded series was captured and called leading-order imaging series (LOIS) (Shaw et al., 2003). Then, more imaging terms were identified and *added* to the LOIS. This more capable series is called higher order imaging series (HOIS) (Liu, 2006). It is worth mentioning that the HOIS has not capture all of the terms for imaging. Both LOIS and HOIS have closed forms.

The closed form HOIS was developed by Liu (2006) using an intuitive leap and the conviction that only shallower events in the linear approximate image (α_1) should help, through nonlinear multiplications, any particular event to determine its correct location. The HOIS is an implicit function that does not immediately lend itself to understanding in terms of a translated interface as a shift from the incorrect to the correct depth. The central purpose of this paper is to provide precisely that insight, understanding and comprehension of what resides behind the implicit function nature of the HOIS.

INTRODUCTION

Migration/Imaging is the process of locating reflectors at depth using reflected seismic data. It is of no surprise that this process needs the arrival time of the signal and the wave velocity of the medium through which the signal traveled. This is exactly the case for most of the current imaging algorithm which utilize the arrival time information of the data and the velocity information obtained from another procedure, velocity analysis. So the idea of performing imaging without the velocity sounds so contradictory that most people would reasonably ask: how could it be possible? We would like to answer this question by first, asking a question: where does the velocity information come from? It comes from nowhere but the data. So essentially all information come from the data. Then, second, we would argue that it is possible there is such an algorithm that could *directly* produce the image of the subsurface, without a separate velocity analysis step. Third, the imaging without the velocity algorithm derived from inverse scattering series (ISS) is capable of using the amplitude information of the data as well as the arrival time. The significance of this capability is explained below. Figure 1 illustrates the two primaries for 1D nomal incidence case. The arrival times of the two primaries are t_a and t_b respectively. Assuming the wave speed in the medium between the source and the first interface is c_0 (which is called reference medium velocity), the water bottom is easy to locate: $z_a = t_a * c_0/2$. The second interface is not difficult either if the velocity of the medium between the two interfaces is known. However, note that the first signal contains more information than just the arrival time. Its amplitude directly relates to the property contrast across the first interface: $R = \frac{c_1 - c_0}{c_1 + c_0}$. So the velocity below the first interface can be obtained as long as we know the amplitude of the signal and the reference medium velocity. The question is whether or not we can find out an algorithm that can directly extract all of the necessary information from the data to perform imaing without finding the velocity through a separate step. The imaging without the velocity algorithm derived from ISS is one of those methods that have this kind of capability.

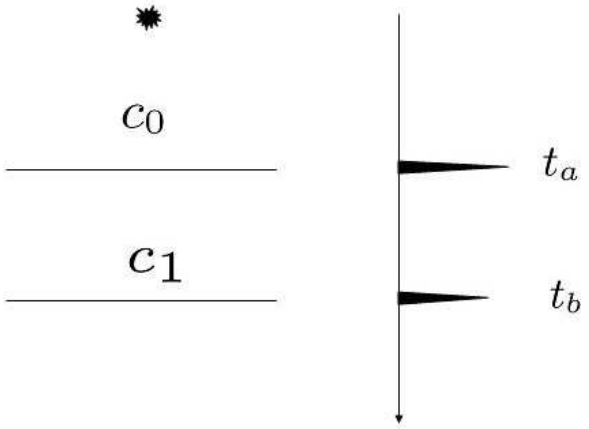

Figure 1: 1D normal incidence two primaries. Depth of the first and second interfaces are z_a and z_b respectively.

The framework and logic about the inverse scattering series are discussed in (Weglein et al., 2003). It mentioned that the whole inverse scattering series has very limited applications due to convergence issues (Carvalho et al., 1991; Carvalho, 1992). So, certain terms are identified and grouped together to perform one task only (multiple removal, imaging or inversion) and act like no other task exists at all. These subseries might have better convergence properties than the whole series. This is the idea of isolated task-specific subseries. In other words, it is the human intervene that makes the inverse series much more useful.

The first step of performing imaging without the velocity is to obtain $\alpha_1(z)$ which is very close to the Stolt migration result using reference medium velocity. Secondly, more terms of the inverse scattering series are identified to improve the locations of the reflectors in α_1, without changing their amplitude/properties. To date, two closed forms of the imaging sub-series have been identified and are known in the literature as the leading order imaging series (LOIS) and the higher order imaging series (HOIS) Shaw et al. (2003); Liu et al. (2006). In this note, through analysis of those closed forms and the work of Innanen (2005), we analyze their performance and show our understandings of these closed forms.

THEORY

The leading-order closed-form (LOIS) imaging series is

$$\alpha^{LOIS}(z) = \alpha_1\Big(z - \frac{1}{2}\int_0^z \alpha_1(z')dz'\Big); \tag{1}$$

and the high-order closed-form imaging series (HOIS) is and

$$\alpha^{HOIS}\Big(z + \frac{1}{2}\int_0^z \frac{\alpha_1(z')}{1 - \frac{1}{4}\alpha_1(z')}dz'\Big) = \alpha_1(z). \tag{2}$$

The functions $\alpha^{LOIS}(z)$ and $\alpha^{HOIS}(z)$ provide better reflector locations compared to α_1. One may notice that in Equation.1, the argument of α^{LOIS} is very simple and that of α_1 is relatively complicated, while

in Equation.2, it is α^{HOIS} that has the relative complicated argument. Why this transfer of complexity? What kind of difference will it make? What is the performance of these closed forms? We will try to answer these questions, without becoming too involved in the math or diagrams of the inverse scattering series.

Interpretation the closed forms

There are several ways to interpret Equation 1:

1. The value of α^{LOIS} at z equals to the value of α_1 at $z-\frac{1}{2}\int_0^z \alpha_1(z')dz' = z'_b$; or,
2. The value of α^{LOIS} at $z = z'_b + \frac{1}{2}\int_0^z \alpha_1(z')dz'$ equals to the value of α_1 at z'_b; or reversely,
3. The value of α_1 at z'_b equals to the value of α^{LOIS} at $z = z'_b + \frac{1}{2}\int_0^z \alpha_1(z')dz'$.

Imagine that there is an interface at z'_b in α_1. Then based on the third interpretation, this interface will be moved to another depth z, and the distance to be moved is determined by: $\frac{1}{2}\int_0^z \alpha_1(z')dz'$, which is an integration to depth z, *not* z'_b. So, if z is bigger than z'_b, then α_1 values from greater depths contribute to the moving of this shallower interface. This conclusion is actually a little strange since the diagram analysis only permit shallower events helping the locations of deeper events. Even from physical instincts, it seems strange that the moving of shallower events care about deeper events. What is going on here?

Actually, the higher order form for reflector location was first incorporated as part of a coupled imaging-inversion algorithm (Innanen, 2005). Through a "natural" isolation operation, the imaging part of this algorithm would seem to be

$$\alpha^{HOIS}(z) = \alpha_1\Big(z - \frac{1}{2}\int_0^z \frac{\alpha_1(z')}{1-\frac{1}{4}\alpha_1(z')}dz'\Big), \tag{3}$$

which is very similar to Equation 2 except where the complicated argument stays.

Equation 3 was tested and found that the results were poor. Then from physical intuition, Liu intuitively moved the argument to the left hand side and obtained Equation 2 which provided very good results (Liu et al., 2004). To understand this move, let's apply the same operation to Equation 1:

$$\alpha^{SLOIS}\Big(z + \frac{1}{2}\int_0^z \alpha_1(z')dz'\Big) = \alpha_1(z), \tag{4}$$

where SLOIS denotes "Shifted LOIS". Let's analyze its meaning in a similar way:

1. The value of α^{SLOIS} at $z+\frac{1}{2}\int_0^z \alpha_1(z')dz'$ equals to the value of α_1 at z; or, reversely,
2. The value of α_1 at z equals to the value of α^{SLOIS} at $z+\frac{1}{2}\int_0^z \alpha_1(z')dz'$; so,
3. The value of α_1 at z'_b equals to the value of α^{SLOIS} at $z'_b + \frac{1}{2}\int_0^{z'_b} \alpha_1(z')dz'$.

Clearly, if it happens that there is an interface at z'_b in α_1 then it will be moved to depth z and the distance to move is determined by an integration to depth z'_b. No deeper events will possibly contribute to the movement of shallower ones. So it seems that Equation 4 might be more reasonable compared to Equation 1, just like Equation 2 compared to Equation 3.

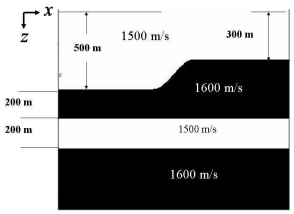

(a) model

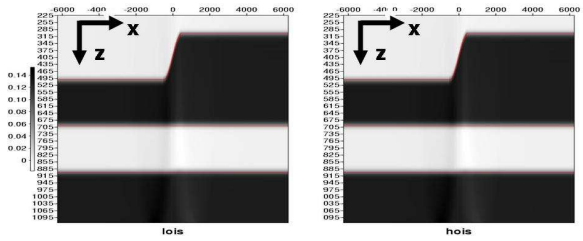

(b) LOIS and HOIS

Figure 2: Small constrast model

Performance of the closed forms

Although neither of the two closed forms has the full imaging capability of the imaging subseries, for many cases they can provide very promising results. For example, in Figure 2, for a relatively small contrast model, both LOIS and HOIS result is very satisfactory (Liu, 2006). While in Figure 3, for a large contrast model, HOIS gives much better result compared to LOIS (Liu, 2006).

One might still want to know how well can HOIS locate the interface? In the following, through a simple analytic example, we would demonstrate analytically that the HOIS can correctly locate the first interface below water bottom.

In Figure 4, we assume the depth of the water bottom is z_a and the interface below the water bottom is at z_b. The velocities are c_0 and c_1 for medium at $z < z_a$ and $z_a < z < z_b$ respectively. Using the reference medium velocity c_0, the interface z_a will be located correctly in α_1 since the reference medium is the correct velocity. But the interface at z_b will be located at $z'_b = z_a + \frac{c_0}{c_1}(z_b - z_a)$ which will be shallower than the correct depth. The objective of the imaging subseries is to shift the interface at z'_b to its correct location z_b. Let's evaluate the performance of the HOIS. From Equation 2, we know that the interface at z'_b in α_1 will be shifted to a deeper depth (in this case) by the amount of

$$\begin{aligned} \delta z &= \frac{1}{2}\int_0^{z'} \frac{\alpha_1(z'')}{1-\frac{1}{4}\alpha_1(z'')}dz'' \\ &= (z'_b - z_a)\frac{2R}{1-R} \\ &= z_b - z'_b, \end{aligned} \tag{5}$$

where we have used $\alpha_1 = 4RH(z-z_a)$ and $R = \frac{c_1-c_0}{c_1+c_0}$ (Shaw et al., 2003). So the correct amount of shifting has been performed by the HOIS for the first interface below water bottom. Deeper interfaces in general will not be shifted accurately to the correct place by the HOIS.

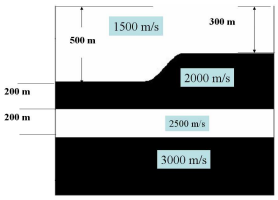

(a) model

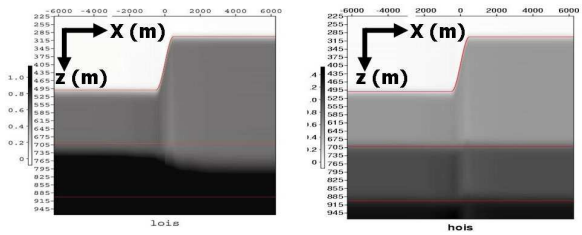

(b) LOIS and HOIS

Figure 3: Big constrast model

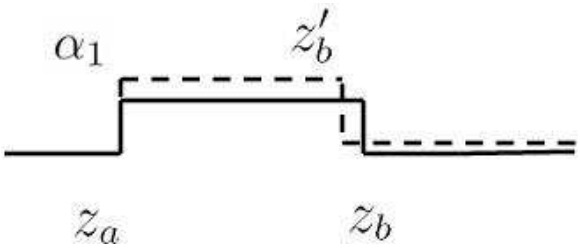

Figure 4: 1D normal incidence α and α_1.

DISCUSSIONS

The original LOIS has a readily explainable understanding in terms of shifting. The HOIS did not lend itself to that simple understanding of its action and purposefulness. Through a detailed analysis of the action of the LOIS and HOIS on an analytic two interface problem, a rational and reasonableness to the nature of the HOIS algorithm has been provided to go along with its effectiveness and speed.

ACKNOWLEDGEMENTS

We wish to thank Simon Shaw for his helpful discussions. The support of M-OSRP sponsors are appreciated. This work has been partially funded by NSF-CMG award DMS-0327778 and DOE Basic Sciences award DE-FG02-05ER15697. Jingfeng Zhang appreciates support as the 2006-2007 ConocoPhillips fellow. Fang Liu appreciates support as the 2006-2007 GXT fellowship.

REFERENCES

Carvalho, P. M., 1992, Free-surface multiple reflection elimination method based on nonlinear inversion of seismic data: PhD thesis, Universidade Federal da Bahia.

Carvalho, P. M., A. B. Weglein, and R. H. Stolt, 1991, Examples of a nonlinear inversion method based on the T-matrix of scattering theory: Application to multiple suppression, *in* 61st Ann. Internat. Mtg: Soc. of Expl. Geophys., Expanded Abstracts, 1319–1322, Soc. Expl. Geophys.

Innanen, K. A., 2005, Reflector location using high-order inverse scattering series terms: M-OSRP Annual Report, **4**, 264–270.

Liu, F., 2006, Multi-dimensional depth imaging without an adequate velocity model: PhD thesis, University of Houston.

Liu, F., B. G. Nita, A. B. Weglein, and K. A. Innanen, 2004, Inverse scattering series in the presence of lateral variations: M-OSRP Annual Report, **3**.

Liu, F., A. B. Weglein, K. A. Innanen, and B. G. Nita, 2006, Multi-dimensional seismic imaging using the inverse scattering series, *in* 76th Annual Internat. Mtg., Soc. Expl. Geophys., Expanded Abstracts, 937–940, Soc. Expl. Geophys.

Shaw, S. A., 2005, An inverse scattering series algorithm for depth imaging of reflection data from a layered acoustic medium with an unknown velocity model: PhD thesis, University of Houston.

Shaw, S. A., A. B. Weglein, D. J. Foster, K. H. Matson, and R. G. Keys, 2003, Convergence properties of a leading order depth imaging series, *in* 73rd Annual Internat. Mtg., Soc. Expl. Geophys., Expanded Abstracts, 937–940, Soc. Expl. Geophys.

Weglein, A. B., F. V. Araújo, P. M. Carvalho, R. H. Stolt, K. H. Matson, R. T. Coates, D. Corrigan, D. J. Foster, S. A. Shaw, and H. Zhang, 2003, Inverse scattering series and seismic exploration: Inverse Problems, **19**, R27–R83.

Estimating plane-wave transmission loss with the inverse scattering internal multiple attenuation algorithm: concept and an application to Q estimation

J. E. Lira, K. A. Innanen, A. B. Weglein and A. C. Ramirez, Univ. Houston, M-OSRP

SUMMARY

The inverse scattering series internal multiple attenuation algorithm suppresses internal multiples to within an amplitude error that is determined by plane wave transmission losses down to, and across, the reflector acting as the multiple generator (the reflector at which the shallowest downward reflection of the multiple takes place). In this paper we propose that this be exploited to address the problem of estimating and removing overburden effects on reflected primaries, to the benefit of current leading edge imaging and inversion algorithms. For instance, if an overburden is absorptive, the difference between the predicted and actual multiple spectra may be related to the integral of its Q profile. Furthermore, within a specific Q model, this estimation can be made insensitive to any scalar error in the multiple prediction arising from, e.g., numerical implementation. Early-stage synthetic examples provide evidence that extraction and calculation of the predicted and actual multiples' spectra, using straightforward FFT methods, stably provides estimates of the integrated Q profile. Research is ongoing on fundamental/analytic and practical/numerical aspects of this potential algorithm.

INTRODUCTION

A primary is a recorded seismic event with one upward reflection. These events are considered the source of subsurface information for structural mapping, parameter estimation, and, ultimately, petroleum delineation at the target. In all current leading-edge processing of primaries the ability to infer useful information at depth critically depends upon the ability to estimate and to remove the impact of the overburden on the character of the wave, during propagation from the source down to the reflector and from the reflector up to the receiver. The ability to effectively estimate (and remove) the effects of the down and up propagation legs determines the level of realistic ambition in subsequent processing of primaries. In this paper we propose a new method to estimate overburden effects, turning a deficiency of the internal multiple attenuation into an asset—an indirect source of this important overburden information.

The inverse scattering series has provided a set of algorithms for the removal of all orders of free-surface and internal multiples (Weglein et al., 1997, 2003). Within the overall class of events referred to as internal multiples, events are further catalogued by order, meaning the number of downward reflections experienced. The algorithm of Araújo (1994) and Weglein et al. (1997) is a series for the attenuation of all orders of internal multiples, the first term of which attenuates the first-order event. It is to this first term that we direct our current attention. In practice, this component of the full algorithm has often been fully adequate; however, there are occasions when an elimination rather than attenuation algorithm would provide distinct added value. Ramírez and Weglein (2005a) have provided a closed-form *elimination* algorithm for the first-order internal multiple to fill this requirement. The key here is that the two above algorithms, attenuation and elimination, and the understood properties of the former (Weglein et al., 1997; Weglein and Matson, 1998; Ramírez and Weglein, 2005b), may be exploited to provide seismic information at depth. The value of this information and the applicability of this idea is of moment as the algorithm is refined (Nita and Weglein, 2004) and implemented in multiple dimensions for large data sets (Kaplan et al., 2005).

The amplitude discrepancy between the actual first-order internal multiple and the attenuator described above is a direct expression of plane wave amplitude loss down to a particular reflector. We propose that this be exploited to address the problem of estimating and removing overburden effects on reflected primaries, to the benefit of current leading edge imaging and inversion algorithms. The ambitious goal of separation and extraction of a well-located and accurate angle dependent reflection coefficient at depth is typically hindered by the experience of the primary wavefield as it propagates through an unknown overburden, which cloaks the event with spurious amplitude changes. Contemporary methodologies to counter these effects are generally inconsistent with wave theoretic processing, and rarely go forward without a well-tie. The information provided by the internal multiple algorithm is a direct, immediate correcting factor for the cloaked primary.

Practical motivation for use of this amplitude information is severalfold. First, the information is a by-product of an existing part of the wave-theoretic processing flow–the demultiple phase–and comes at no additional cost. Second, this occurs at a convenient point during processing, just prior to its likely use in primary processing/inversion. Third, it is consistent with wave-theoretic processing. Fourth, it is not restricted to a production setting, but is also applicable in reconnaissance and exploration settings. Fifth, in addition to its potential value for current high-bar imaging and inversion/AVO processing, it would act to make the non-linear inverse scattering target identification series (Zhang and Weglein, 2005) an exploration as well as production tool, again by eliminating the requirement for a well-tie.

In this paper we present a simple, early stage study and example of such information extraction. By our previous statements, if a medium or target overburden is characterized by non-negligible Q, which will tend to dominate transmission effects, the difference between the predicted and actual spectra of the multiple event will bear interpretable information about the Q values in the overburden. We present basic theory and examples illustrating the use of internal multiple prediction as a means for Q estimation. In the first section we review the mathematical form of the internal multiple attenuation algorithm in 1D, its behavior in terms of the data sub-events, and the provenance of the amplitude error in the prediction. In the second section we review the influence of a well-known model for absorptive-dispersive wave propagation on the effective transmission coefficients present in reflection seismic data. In the third section, by generalizing the predicted internal multiple error to accommodate the above Q-type transmission coefficients, we demonstrate that the spectral ratio of the predicted and actual interbed multiples may be used to invert for the cumulative (integral) Q value down to and across the multiple generator. In the fourth section we carry this out on a layered medium model. We comment on the potential for extension of such methods to multiple dimensions and other avenues of research.

Determination of general attenuation vs. elimination properties

As a brief aside, let us comment on how the properties of the attenuation vs. elimination algorithms may be understood and thereafter exploited. It is known in principle (via the downward continuation/interface removal idea) that given complete medium information down to and across an interface acting as the downward reflector for a first-order internal multiple, that multiple may be precisely eliminated. This corresponds, then, to the information that would be required for brute transformation of the attenuated multiple into an eliminated multiple. Although the elimination series (Ramírez and Weglein, 2005a) does this task in the absence of such information, we then note that the brute division of the attenuated multiple by the actual multiple must correspond to the accumulation of the aforementioned overburden information.

Transmission loss via analysis of internal multiples: application to Q-estimation

IMA AND PREDICTED VS. ACTUAL AMPLITUDES

The full multiple attenuation algorithm is a series of terms that attenuate sequentially higher orders of multiples in fully 3D pre-stack reflection data (Weglein et al., 2003). For the purposes of this paper, reducing the algorithm to its 1D form for normal incidence data with a plane wave source, and considering the first term only, we have the predicted multiple algorithm (Weglein and Matson, 1998):

$$b_{3IM}(k_z) = \int_{-\infty}^{\infty} dz_1' b_1(z_1') e^{ik_z z_1'} \times \int_{-\infty}^{z_1'-\varepsilon} dz_2' b_1(z_2') e^{-ik_z z_2'} \int_{z_2'+\varepsilon}^{\infty} dz_3' b_1(z_3') e^{ik_z z_3'}, \quad (1)$$

where ε is a small constant determined by the approximate length of the wavelet. In implementing the algorithm, our first job is to transform the data into the input term $b_1(z)$. This required form can be obtained (Weglein et al., 1997) by (*i*) taking the surface recorded data $D(t)$, Fourier transforming over time to produce $D(\omega)$; (*ii*) performing a change of variables to the pseudo-depth conjugate variable $k_z = 2(\omega/c_0)$, where c_0 is waterspeed, and calling the data expressed in this variable $b_1(k_z)$; and (*iii*) performing an inverse Fourier transform over k_z to generate the pseudo-depth quantity $b_1(z)$. Each of these steps occurs entirely in terms of the measured data and a homogeneous background medium with wavespeed c_0.

The algorithm itself may then be applied. Using $b_1(z)$ as input, equation (1) searches for sub-events that obey the geometry dictated by the limits of the three integrals. Roughly speaking, the search proceeds as follows: via the outermost integral an event anywhere in $b_1(z)$, i.e., on $z = (-\infty, \infty)$, is sought. When an event is located, others are then sought at shallower pseudo-depths via the middle integral. Finally, if one or more shallower events are found a multiple is predicted by the final integral for any deeper event (including but not exclusive to the first). With the search over, eqn (1) essentially convolves the two deeper events, and then cross-correlates the result with the shallower event. This sums the travel-times of the deeper events and subtracts the travel-time of the shallower event, the correct time of the multiple is predicted (Figure 1). This second step, and hence the entire algorithm, also occurs entirely in terms of the data (via b_1) and the wavespeed c_0 (in the integral kernels).

Importantly for our current purposes, the predicted amplitudes are scaled by a factor that is related to the transmission coefficients of the interfaces above the *generator*, the reflector at which the downward reflection of the multiple takes place. See again Figure 1 and the Introduction. The discrepancy is a direct expression of *any* cumulative transmission losses above the generator. Hence, a correction of these losses could proceed with no assumptions made about their cause. Alternatively, if we are comfortable assuming a certain mechanism dominates the transmission loss, this information can also be used to derive specific estimates of overburden medium parameters, as well as thereafter providing corrections. Let us pursue this second route by assuming an absorptive/dispersive overburden.

TRANSMISSION COEFFICIENTS IN ABSORBING MEDIA

To do this, we must select an appropriate (quantitative) description of the influence of absorption on transmission above a multiple generator. *Intrinsic attenuation* describes amplitude and phase alterations in a wave due to friction. These alterations are modeled by a generalization of the (nominally real) wavefield phase velocity to a complex, frequency-dependent quantity, often parametrized in terms of Q, a measure of wave amplitude or energy lost per cycle. A reasonably well-accepted Q model (Aki and Richards, 2002; Kjartansson, 1979) alters the wavenumber describing propagation in a scalar medium,

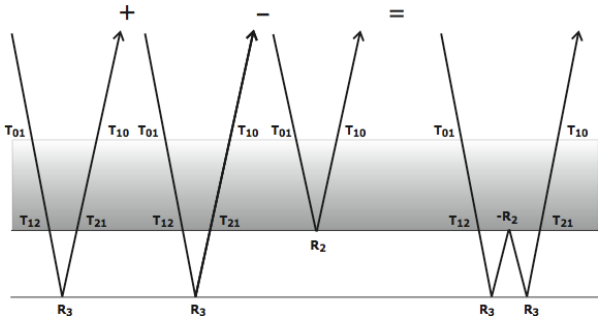

Figure 1: *Sub-events and amplitudes in the IMA algorithm.*

$k = \omega/c(z)$, to

$$K = \frac{\omega}{c(z)}\left[1 + \frac{F(\omega)}{Q(z)}\right], \quad (2)$$

where $F(\omega) = \frac{i}{2} - \frac{1}{\pi}\log(\omega/\omega_0)$. The reference frequency ω_0, at which the wave propagates with speed c, may be considered a parameter to be estimated, or assumed to be the largest frequency available to a given experiment. Notice that the model divides propagation up into three parts: a propagation component, an attenuation component, and a dispersion component.

Consider a plane wave of unit amplitude, normally-incident on a single layer (with interface depths z_1 and z_2) embedded in a homogeneous whole-space of wavespeed c_0, having departed from a source/receiver plane at depth $z = 0$ at $t = 0$. If the layer is acoustic with wavespeed c_1, amongst other components of the reflected field, the primary from the deeper interface (at z_2) may be written:

$$PR(\omega) = e^{i\frac{\omega}{c_0}z_1} T_{10} e^{i\frac{\omega}{c_1}(z_2-z_1)} R_2 e^{i\frac{\omega}{c_1}(z_2-z_1)} T_{01} e^{i\frac{\omega}{c_0}z_1}, \quad (3)$$

where $T_{10} = 2c_0/(c_0+c_1)$ and $T_{01} = 2c_1/(c_0+c_1)$, and R_2 is the reflection coefficient of the z_2 interface. If the layer is instead absorptive such that it obeys eqn (2), with parameters c_1 and Q_1, the primary may instead be written as

$$PR_Q(\omega) = e^{i\frac{\omega}{c_0}z_1} \mathscr{T}_{10} e^{i\frac{\omega}{c_1}(z_2-z_1)} R_2 e^{i\frac{\omega}{c_1}(z_2-z_1)} \mathscr{T}_{01} e^{i\frac{\omega}{c_0}z_1}, \quad (4)$$

where the transmission coefficients are generalized:

$$\mathscr{T}_{01} = \frac{2c_1[1+F(\omega)/Q_1]^{-1}}{c_0 + c_1[1+F(\omega)/Q_1]^{-1}} \exp\left[i\frac{\omega}{c_1}\frac{F(\omega)}{Q_1}(z_2-z_1)\right], \quad (5)$$

and

$$\mathscr{T}_{10} = \frac{2c_0}{c_0 + c_1[1+F(\omega)/Q_1]^{-1}} \exp\left[i\frac{\omega}{c_1}\frac{F(\omega)}{Q_1}(z_2-z_1)\right]. \quad (6)$$

The transmission has been altered in two ways. First, the wave amplitude/phase is altered as it crosses the boundary at z_1 going down and coming up; this small but potentially informative filtering operation on the field also has an impact on reflection coefficients (Lam et al., 2004), in our case R_2. Much more important, however, are the new exponential terms, sensitive to the properties and extent of the absorbing medium above the reflection point; this operator decays the amplitudes in accordance with the attenuation law. Separating out the components of eqns (5)–(6) that do not contribute to this (dominant) exponential amplitude attenuation into a multiplicative factor W, the combined effective transmission coefficients due to the absorbing overburden may be expressed as

$$\mathscr{T}_{01}\mathscr{T}_{10}(z_2) = W \exp\left[-\omega\frac{1}{c_1 Q_1}(z_2-z_1)\right]. \quad (7)$$

Generalizing to an arbitrary $c(z)$, $Q(z)$ profile above a reflector at depth z, and considering only the amplitude, we have

$$|\mathscr{T}_{01}\mathscr{T}_{10}(z)| \approx \exp\left[-\omega\int_0^z \frac{dz'}{c(z')Q(z')}\right]. \quad (8)$$

ESTIMATING THE INTEGRATED Q-PROFILE

The internal multiple attenuation algorithm requires no knowledge of nor assumptions about the medium giving rise to the data (Weglein et al., 1997). What we are proposing is the use of the error in the algorithm in an *ad hoc* estimation scheme whose assumptions and requirements are independent of those of the algorithm. With that in mind, let us consider that a number of circumstances are in place. First, we have measured data above a reflector of interest; second, this reflector acts as the generator of an internal multiple; third, that the multiple is sufficiently separable within the data set (and the prediction) that its local spectrum may be estimated.

Weglein and Matson (1998) show analytically in a single layer acoustic case that the predicted internal multiple amplitude PRED and the actual internal multiple amplitude MULT are related by

$$\text{PRED} = T_{01}T_{10}\ \text{MULT}, \quad (9)$$

where the transmission coefficients are as defined in the previous section. To determine the transmission loss down to and across the generator requires the ratio of the predicted and actual multiples to be calculated, viz.

$$T_{01}T_{10} = \frac{\text{PRED}}{\text{MULT}}. \quad (10)$$

In the case of an attenuating overburden, the transmission down to and across a given reflector has been generalized and approximated in equation (8). That is, upon estimating the spectra of the actual and predicted multiple, we surmise their ratio is related to Q by

$$\left|\frac{\text{PRED}(\omega)}{\text{MULT}(\omega)}\right| \approx \exp\left[-\omega\int_0^z \frac{dz'}{c(z')Q(z')}\right]. \quad (11)$$

This allows us access to the integrated effect of Q down to the generator. Calling

$$\text{QC} \equiv \int_0^z \frac{dz'}{c(z')Q(z')}, \quad (12)$$

we have

$$\text{QC} \approx -\frac{1}{\omega}\log\left|\frac{\text{PRED}(\omega)}{\text{MULT}(\omega)}\right|. \quad (13)$$

Notice that QC is independent of ω and hence may be estimated at any available frequency; or, all available frequencies may be used in (say) a least-squares estimation procedure. This situation is of course contingent on the particular Q model we have chosen.

Dealing with additional scalar error in the prediction

As a practical matter (that may occur when, e.g., using packaged FFT algorithms) when computing the internal multiple prediction, we may further wish to guard against the case in which the multiple prediction is modified by an unknown scalar factor, that is, in which the relation

$$A\left|\frac{\text{PRED}(\omega)}{\text{MULT}(\omega)}\right| \approx e^{-\omega\text{QC}}, \quad (14)$$

with A unknown, holds. In the absence of attenuation there is no recourse, but the frequency-dependence (spectral shape) arising in the attenuation case provides an alternate route. Consider two frequencies in the spectrum, ω_1 and ω_2; since each provides a valid estimate of QC, we may calculate equation (14) with each, and divide, canceling out the scalar error and leaving

$$\left|\frac{\text{PRED}(\omega_1)\text{MULT}(\omega_2)}{\text{MULT}(\omega_1)\text{PRED}(\omega_2)}\right| \approx e^{-(\omega_1-\omega_2)\text{QC}}, \quad (15)$$

which leads to a further slightly altered estimation

$$\text{QC}(\omega_1,\omega_2) \approx -\frac{1}{\omega_1-\omega_2}\log\left|\frac{\text{PRED}(\omega_1)\text{MULT}(\omega_2)}{\text{MULT}(\omega_1)\text{PRED}(\omega_2)}\right|. \quad (16)$$

For further robustness, QC can be averaged thus over all available pairs of frequencies in the experiment.

SYNTHETIC EXAMPLE

In this section we demonstrate early-stage numerical/synthetic testing of the estimation procedure proposed in the previous section. A layered absorptive Earth model is chosen (see Table 1); and numerical reflection data corresponding to the multiple *and the necessary subevents only* is computed with plane wave incident field (Figure 2a).

Layer depths (m)	c (m/s)	Q
000-300	1500	∞
300-480	2200	300
480-855	2800	150
855-∞	3300	75

Table 1. *Two-layer Earth model.*

The internal multiple algorithm of eqn (1) is applied to this data, predicting the polarity-reversed internal multiple (Figure 2b). The spectra of the predicted and actual multiples are computed and compared (Figure 3a). Per the developments of the previous section, within the chosen Q model we may estimate QC (the integrated $Q(z)$, $c(z)$ profile down to the internal multiple generator) either with the absolute amplitudes of the spectra (Figure 3a), or with their relative shape (Figure 3b). The latter of these is here illustrated by shifting the actual spectrum such that the lowest frequency matches that of the predicted spectrum. Noting that the actual integral of the c/Q profile is approximately QC$= 2.70\times10^{-4}$, we find estimates from various pairs of frequencies (using eqn 16) ranging from QC$\approx 2.47\times10^{-4} - 1.52\times10^{-4}$. We have chosen a particular Earth model for which attenuation has not reduced the data amplitudes by a large amount, but for which therefore the Q value is large; the impact of this is a reduced spectral variability between predicted and actual. We are investigating this as a source of the variability. A larger suite of models and more accurate approximations of the transmission coefficients are also being considered at present.

CONCLUSIONS

We have proposed that a discrepancy between a certain version of the inverse scattering series internal multiple attenuation algorithm be exploited to address the problem of estimating and removing overburden effects on reflected primaries. This includes, for instance, characterizing a Q profile down to and across an isolated internal multiple generator.

We anticipate that the information garnered from this specific application of the broad potential we are introducing, would be useful in two ways. First, it can be brought into a Q compensation operator and used to correct the primary in terms of resolution (as well as overall

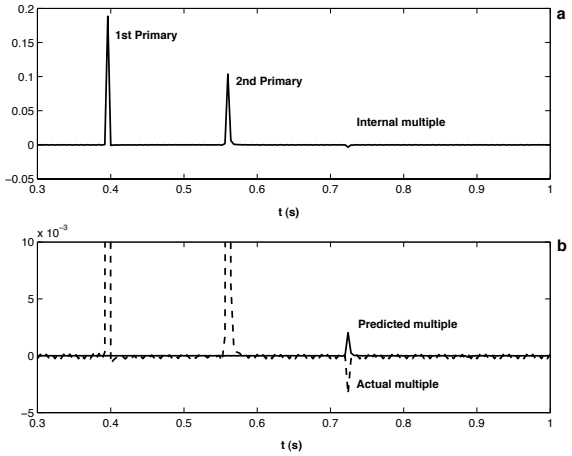

Figure 2: *Synthetic data. The requisite events in a normal incidence data set from a single absorptive layer are computed (***a***); the internal multiple is then predicted (***b***) using equation (1).*

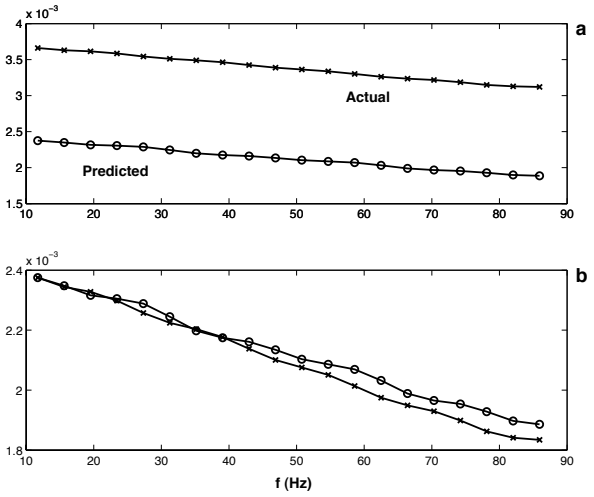

Figure 3: *Predicted vs. actual multiple spectra. The multiples may be compared in terms of (***a***) their absolute amplitudes, or (***b***) their relative spectral shape.*

amplitude/phase). Second, within a further set of assumptions, it can be used to estimate the Q profile itself. As part of this ongoing study we further anticipate examination of a number of extensions of the methodology. First, to layered media with offset data, and beyond to multidimensional subsurface structure. Second, to more complete descriptions of the overburden in addition to acceptable Q models, e.g., elastic, for whom the transmission error has already been studied and characterized (Weglein et al., 2003).

Finally, let us reiterate the broad beneficial aspects of the methodology we are developing: first, the information to be derived comes at no additional cost; second, it is derived at a convenient point during processing; third, it is consistent with wave-theoretic processing; fourth, it is applicable in reconnaissance and exploration as well as production settings; and fifth, it has the potential to transform the non-linear inverse scattering target identification series into an exploration tool, by eliminating the requirement for a well-tie.

ACKNOWLEDGEMENTS

We wish to thank the sponsors and personnel of M-OSRP. J. Lira was supported by Petrobras; A. Weglein and K. Innanen were supported by U.S. D.O.E. Grant No. DOE-De-FG02-05ER15697; A. Weglein was supported by NSF-CMG award DMS-0327778.

“A Hybrid Scattering Model of Scalar/Viscoacoustic Wavefield Events”

K.A. Innanen (M-OSRP, University of Houston)*

1. Introduction

Non-linear scattering theory permits direct inversion of reflected seismic data (Weglein et al., 2003). Here we consider its modelling aptitude. In particular, a non-linear, 3D, analytic, wave-theoretic scattering model of specific wavefield events, such as primaries, is discussed and further approximated. This is of some broad interest because full wave theory tends to resist such event-by-event separation, and of some detailed interest as a tool for analysis and, potentially, direct inverse procedures.

When the perturbation is large and extended, contributions from all orders of scattering are required to construct any specific event. For example, a primary, which experiences (1) transmission to a reflection point, (2) transmission from a reflection point, and (3) interaction at the reflection point, is highly non-linear in the (large, extended) perturbation in each of (1)—(3). Renormalization methods (de Wolf, 1971; Wu et al., 2006) based on a decomposition of the scatterer into forward- and backward-scattering elements have been studied as a way of approximating the non-linearity associated with (1) and (2). A different non-linear scattering event model (Innanen, 2006), based on decomposition of the pre- and post-scattering Green's function propagation, has been proposed to accommodate (1)—(3), i.e., to model non-linear (in the scattering sense) transmission *and* reflection phenomena within primaries and other events. In addition to its potential for modelling waves in complex heterogeneous media, this latter model is favourable to the casting of certain non-linear inverse scattering methods (Innanen, 2005). A suitable scattering description of scalar and visco-acoustic wavefields involves reference and actual wave equations:

$$\left(\nabla^2+\frac{\omega^2}{c_0^2}\right)G_0(\mathbf{x},\mathbf{x}_s,\omega)=\delta(\mathbf{x}-\mathrm{x}_s),\quad \left(\nabla^2+\frac{\omega^2}{c^2(\mathbf{x})}\right)G(\mathbf{x},\mathbf{x}_s,\omega)=\delta(\mathbf{x}-\mathrm{x}_s), \qquad (1)$$

respectively, where c_0 is assumed to be real but $c(\mathbf{x}) = c'(\mathbf{x})[1+i/2Q(\mathbf{x})]^{-1}$ may be complex such that a simple non-dispersive Q model is incorporated. The Born series is a computation of the actual field as an infinite series in the reference field and the perturbation $V=k^2\alpha(\mathbf{x})$, where $k=\omega/c_0$ and $\alpha(\mathbf{x})=1-c_0^2/c^2(\mathbf{x})$. In operator form:

$$\mathbf{G}=\mathbf{G_0}+\mathbf{G_0}\mathbf{V}\mathbf{G_0}+\mathbf{G_0}\mathbf{V}\mathbf{G_0}\mathbf{V}\mathbf{G_0}+\ldots\ . \qquad (2)$$

This series constructs the full Green's function, which includes all events, such as direct waves, primaries, multiples, etc. This is detrimental to math/physics interpretation, and (therefore) to its use as both a modelling tool, and a means for analysis.

2. A non-linear scattering model of reflected and transmitted events

Consider a Cartesian coordinate system with source/receiver planes normal to z (Figure 1). Constraints on scattering geometry in z (Figure 2), in the form of a retention/rejection of certain kinds of propagation occurring pre- and post-scatter (Innanen, 2006), permit the separate construction of reflected primaries, $R^P(\mathbf{k_g},z_g,\mathbf{k_s},z_s,\omega)$ and/or transmitted direct waves, $T^{DU}(\mathbf{k_g},z_g,\mathbf{k_s},z_s,\omega)$ and $T^{DD}(\mathbf{k_g},z_g,\mathbf{k_s},z_s,\omega)$ as in Fig. 2. These take the form of series, whose mathematical task is to approximate an event's amplitude and phase with polynomials in the spectral domain. For instance $T^{DD}(\mathbf{k_g},z_g,\mathbf{k_s},z_s,\omega)$ is recursively expressible as

$$T^{DD}(\mathbf{k_g},z_g,\mathbf{k_s},z_s,\omega)-G_0(\mathbf{k_g},z_g,\mathbf{k_s},z_s,\omega)=-\frac{e^{iq_gz_g-iq_sz_s}}{i2q_g}\sum_{n=1}^{\infty}\tilde{T}_n^{\ DD}(\mathbf{k_g},z_g,\mathbf{k_n},z_s,\omega), \qquad (3)$$

where

$$\tilde{T}_n^{\ DD}(\mathbf{k_g},z_g,\mathbf{k_n},z_s,\omega)=\frac{ik^2}{8\pi^2}\int_{z_s}^{z_g}dz'\int\frac{d\mathbf{k_1}}{q_1}e^{i(q_1-q_g)z'}\alpha(\mathbf{k_g}-\mathbf{k_1},z')\tilde{T}_{n-1}^{\ DD}(\mathbf{k_1},z_g,\mathbf{k_n},z_s,\omega), \qquad (4)$$

($\mathbf{k_n}$ in each term of eqn. (3), is interpreted as $\mathbf{k_s}$ for the convenience of the recursion), $q_g=(\omega^2/c_0^2 - k_{xg}^2 - k_{yg}^2)^{1/2}$, with the stopping criterion

$$\tilde{T}_0^{DD}(\mathbf{k}',z_g,\mathbf{k}',z_s,\omega)=\left(\frac{1}{2\pi}\right)^{-2}\delta(\mathbf{k}'-\mathbf{k}_s). \quad (5)$$

The upward transmitted field is expressible similarly, and the reflected primary approximation can be expressed as the sum of combinations of these:

$$R^P(\mathbf{k}_g,z_g,\mathbf{k}_s,z_s,\omega)=\sum_{N=1}^{\infty}R_N^P(\mathbf{k}_g,z_g,\mathbf{k}_n,z_s,\omega), \quad (6)$$

where

$$R_N{}^P(\mathbf{k}_g,z_g,\mathbf{k}_s,z_s,\omega)=\sum_{n=0}^{N-1}\int d\mathbf{x}T_n{}^{DU}(\mathbf{k}_g,z_g,\mathbf{x}',\omega)k^2\alpha(\mathbf{x}')T_{N-n-1}^{DD}(\mathbf{x}',\mathbf{k}_s,z_s,\omega). \quad (7)$$

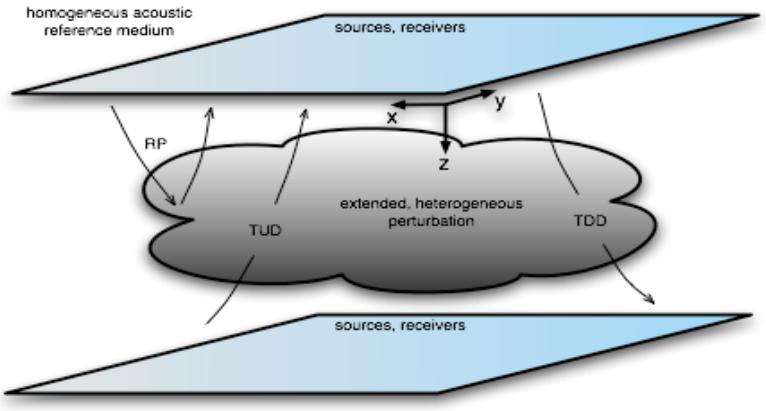

Figure 1: *Schematic illustration of scattering model of events. Transmitted direct upward and downward through a large/extended perturbation, and reflected from same.*

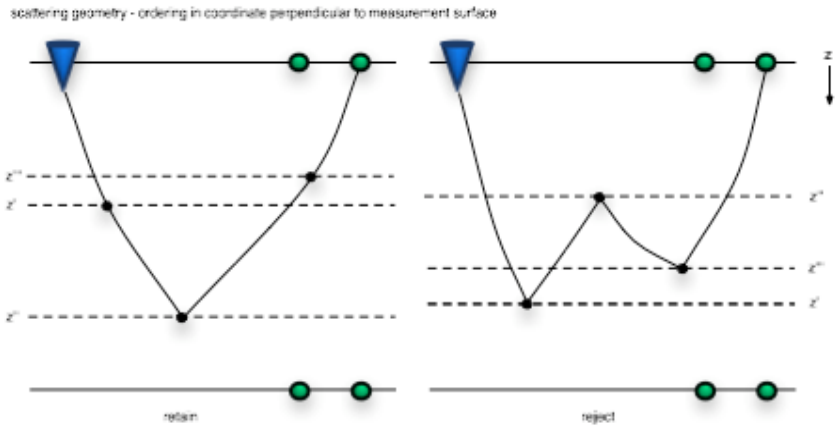

Figure 2: *Event model in eqns. (3)—(7) is generated by retention/rejection of propagation pre-and post-scattering. Reverberating elements are rejected, transmitted or single-turnaround elements are retained (Innanen, 2006).*

3. A hybrid linear target, non-linear overburden approximation

The event model of eqns. (3)-(7) represents an intensive computational problem, as a consequence of its support of a laterally/vertically heterogeneous medium. It has been shown that a much more efficient closed-form primary expression is available if the medium is depth-varying; however, we then lose the ability to model, e.g., diffractions. Considering the 2D case for simplicity, this problem may be addressed with a hybrid approximation, by

dividing the perturbation into two components, $\alpha(x,z)=A(z)+B(x,z)$. Since non-linear scattering operates in terms of increasing powers of V, or α (eqn. (2)), this division generates primary approximation terms that expand, schematically, as follows:

$$A+B$$
$$A^2 + AB + B^2$$
$$A^3 + A^2B + AB^2 + B^3$$
$$A^4 + A^3B + A^2B^2 + AB^3 + B^4,$$

etc. Notice that to retain only terms from the leftmost column, $A+A^2+A^3+\ldots = A(1+A+A^2+\ldots)$, would be to reduce to the depth-varying problem (for which closed forms are available). The series in brackets $(1+A+A^2+\ldots)$, *c.f.* the T terms in eqn. (7), operates non-linearly upon the extracted A (*c.f.* the α term in eqn. (7)) to create the primary. The proposed hybrid model instead extracts and computes the second-from-leftmost series: $B(1+A+A^2+\ldots)$, and hence has a dual nature: linear in B, the 2D part of the perturbation, and non-linear in A, the 1D part. Because the non-linearity is in the depth-varying component, closed-forms remain available and computation is straightforward, but because B is retained, wave phenomena such as diffractions may yet be modelled. This approximation is appropriate for, e.g., an extended vertically-varying overburden perturbation and a small, 2D target body (Figure 3). In particular, we have the hybrid primary expression:

$$R_h^P(k_g,k_s,\omega) = \int dz' T_h^U(k_g,\omega,z') k^2 B(k_g - k_s, z') T_h^D(k_s,\omega,z'), \tag{8}$$

where, for instance, the upward transmission leg is given by

$$T_h^U(k_g,\omega,z) = \frac{e^{iq_g z}}{i2q_g}\left[1 + \left(-\frac{iq_g\int_0^z A(z')dz'}{2\cos^2\theta_g}\right) + \frac{1}{2!}\left(-\frac{iq_g\int_0^z A(z')dz'}{2\cos^2\theta_g}\right)^2 + \ldots\right], \tag{9}$$

a series form that is non-linear in the perturbation, but that collapses in this case to

$$T_h^U(k_g,\omega,z) = \frac{1}{i2q_g}\exp\left[iq_g\left(z - \frac{iq_g\int_0^z A(z')dz'}{2\cos^2\theta_g}\right)\right]. \tag{10}$$

In precisely the same manner we have for the downward transmission leg:

$$T_h^D(k_s,\omega,z) = \frac{1}{i2q_s}\exp\left[iq_s\left(z - \frac{iq_s\int_0^z A(z')dz'}{2\cos^2\theta_s}\right)\right], \tag{11}$$

where, e.g., $\cos\theta_g = q_g/k$. In this closed form eqn. (8) can be straightforwardly computed, or potentially treated in an inverse procedure.

4. Numerical examples

The approximation accords us the flexibility to include or exclude a viscoacoustic perturbed overburden in the primary approximation. We demonstrate with the model illustrated in Figure 3. The left panel of Figure 4 shows the Born approximate primaries, and the right panel shows the non-linear approximation due to eqn. (8). In particular we note the temporal shift, move-out, and attenuation of the events.

5. Conclusions

The Born series permits direct analytic 3D modelling of scalar wavefield events, such as primaries. A hybrid scalar/viscoacoustic scattering model is proposed, in which non-linear account of transmission is taken through a 1D overburden perturbation, and linear account is taken of a 2D scattering body. This restricts the model, but produces straightforwardly-computable closed form expressions, is currently under study as the basis for a set of specific direct non-linear inverse procedures.

Acknowledgments

I am grateful for the commentary and advice of Art Weglein and Sam Kaplan. This work has been supported by M-OSRP, and D.O.E. Grant No. DOE-De-FG02-05ER15697.

References

de Wolf, D.A. (1971). Electromagnetic reflection from an extended turbulent medium: cumulative forward-scatter single back-scatter approximation. *IEEE Trans. Antennas and Propagations*, 19, 254—262.

Innanen, K.A. (2005). Two non-linear forward and inverse approximations for wave fields in the presence of sustained medium perturbations. *Proc. 75th Soc. Expl. Geophys. Ann. Mtg*., Houston, TX.

Innanen, K.A. (2006). A multidimensional acoustic forward scattering series model of reflected and transmitted wavefield events. *Proc. 76th Soc. Expl. Geophys. Ann. Mtg*., New Orleans, LA.

Weglein, A.B., Araujo, F.V., Carvalho, P.M., Stolt, R.H., Matson, K.H., Coates, R.T., Corrigan, D., Foster, D.J., Shaw, S.A. and Zhang, H. (2003). Topical review: inverse scattering series and seismic exploration. *Inverse Problems*, R27—R83.

Wu, R.S., Xie, X.B. and Wu, X.Y. (2006). One-way and one-return approximations (de Wolf approximation) for fast elastic modelling in complex media. In *Advances in Geophysics*, 48, 265, Elsevier.

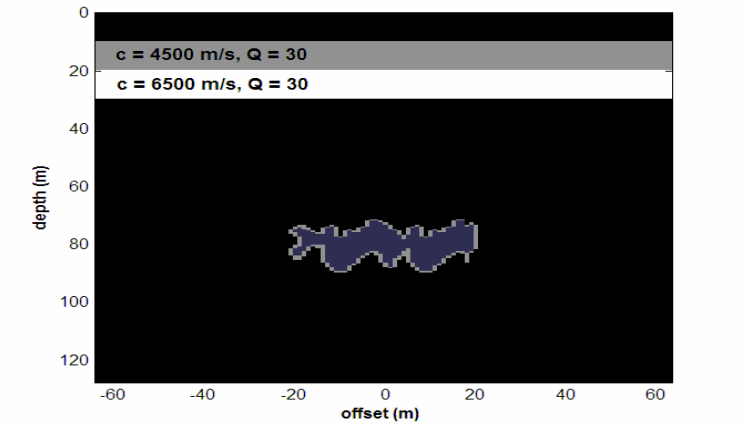

Figure 3: *Medium model. A scattering body c = 1600m/s in a homogeneous reference medium c_0 = 1500m/s, with a fast, 2-layer, attenuating overburden perturbation.*

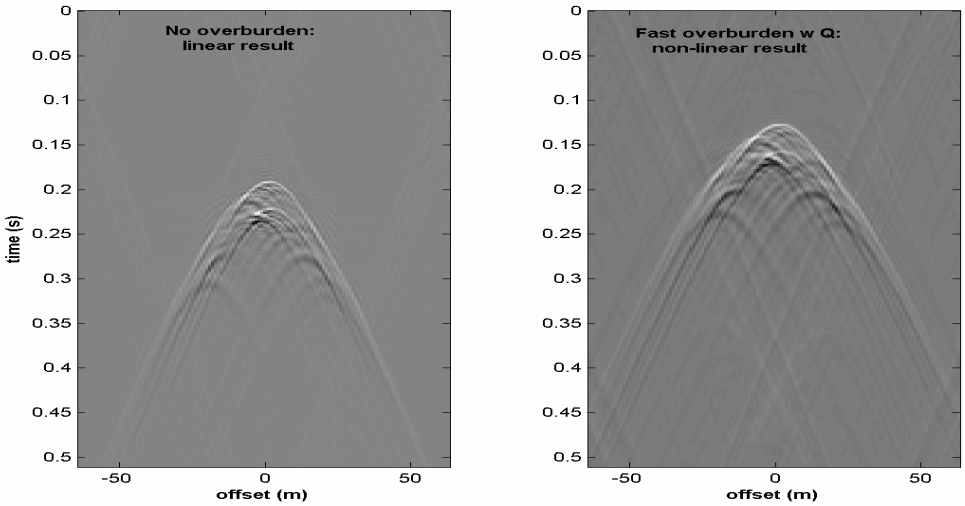

Figure 4: *Two shot records with shot at location 0 m (in Figure 3). Left panel is the linear primary approximation for the case with no overburden; right panel is the non-linear hybrid approximation for the fast attenuating overburden case.*

Inverse scattering sub-series direct removal of multiples and depth imaging and inversion of primaries without subsurface information: strategy and recent advances

A. B. Weglein[1]*, L. Amundsen*[2] *, F. Liu*[1]*, K. Innanen*[1]*, B. Nita*[3]*, J. Zhang*[1]*, A. Ramirez*[1] *and E. Otnes*[2]
[1]*Dept. of Physics, U. Houston, M-OSRP;* [2]*Statoil Research Center;* [3]*Dept. of Math, Montclair State University*

SUMMARY

This paper provides: (1) a review of the logic and promise behind the isolated task inverse-scattering sub-series concept for achieving all processing objectives directly in terms of data only, without knowing or determining or estimating the properties that govern wave propagation in the actual earth; (2) the recognition that an effective response to pressing seismic challenges requires understanding that those challenges arise when assumptions, and prerequisites behind current leading edge seismic processing are not satisfied and that those failures can be attributed to: (A) insufficient acquisition, and/or (B) compute power and (C) bumping into algorithmic limitations and assumptions, and (3) the status and plans of the inverse series campaign to address the fundamental algorithmic limitations of processing methods, that are not addressed by more complete acquisition and faster computers.

BACKGROUND

Scattering theory is a form of perturbation theory. It relates a perturbation in the properties of a medium to the concomitant perturbation in the wave field. $L_0G_0 = \delta$ and $LG = \delta$ represent the equations governing wave propagation in the unperturbed and perturbed media where L_0 and G_0, and L and G are the unperturbed and perturbed differential operators and Green's functions, respectively. $V = L_0 - L$ is the perturbation operator and $\psi = G - G_0$, is the scattered field, and is the difference between the unperturbed and perturbed medium's Green's functions. In our seismic application the unperturbed medium is called the reference medium, and will be chosen (in this paper) for the marine case to be water. The perturbed medium in our marine context is the actual earth and the domain of the perturbation, V, the difference between earth properties and water, begins at the water bottom.

Scattering equation

The relationship between G, G_0, and V is given by an operator identity called the scattering equation or the Lippmann-Schwinger (LS) equation (Goldberger and Watson, 2004; Taylor, 1972; Joachain, 1975, e.g.),

$$G = G_0 + G_0VG. \tag{1}$$

In general, the forward problem predicts the wave field from the properties of the medium, and the forward problem in scattering theory predicts the wave field from the medium in terms of L, not directly but in a perturbative sense, from L in terms of L_0 and V through G_0 and V.

Forward series

From (1) a forward scattering series can be written formally as

$$G = (1/(1-G_0V))G_0 = G_0 + G_0VG_0 + ..., \tag{2}$$

and using $\psi = G - G_0$, equation (2) becomes:

$$\psi = G_0VG_0 + G_0VG_0VG_0 + ... = \psi_1 + \psi_2 + \psi_3 + ..., \tag{3}$$

where ψ_n is the portion of ψ n'th order in V. In general, the inverse problem is to determine actual medium properties, contained in L, from measurements outside the support of the medium to be identified. The inverse problem in scattering theory assumes that the reference medium L_0 and Green's function G_0 are chosen and known; and, hence, the inverse problem is to determine L through determining V, the difference between L and L_0, from measurements of $\psi = G - G_0$ on a measurement surface outside the support of V. The measurements of $\psi = G - G_0$ constitute the data, D.

Inverse series

The inverse scattering series produces V in terms of D, through a series

$$V = V_1 + V_2 + V_3 + ..., \tag{4}$$

where V_n is the portion of V n'th order in the measured values of $\psi = D$. The equations for V_1, V_2, V_3, ... are derived in (Weglein et al., 1997, 2003,e.g.,):

$$\begin{aligned} &G_0V_1G_0 = D \\ &G_0V_2G_0 = -G_0V_1G_0V_1G_0 \\ &G_0V_3G_0 = -G_0V_1G_0V_1G_0V_1G_0 - G_0V_1G_0V_2G_0 - G_0V_2G_0V_1G_0, \end{aligned} \tag{5}$$

etc. It is worth noting that: (1) the inverse scattering series (equations (5)) provide a general direct formalism to solve the inverse problem explicitly in terms of data, D and the water speed Green's function; each V_n is explicitly and directly calculated from G_0 and D, (2) there is no updating of the reference nor claim that the reference is proximal to the actual nor any attempt nor need nor interest in moving it towards the actual, and hence the methodology is not e.g., in any way related to nor shares the properties of iterative linear inverse, and (3) the inverse series equations (5) do not in any sense represent the Born approximation, and e.g., the first equation in (5) is the exact equation for V_1, the second equation in (5) is the exact equation for V_2, and V_1 is never assumed to be an approximate to V, but rather the linear estimate to V, and the first equation in (5) is the exact relationship for the linear estimate and the data. Hence, equations (5) do not depend upon or launch from an assumption on the linear estimate, they in fact launch from the exact equation for the linear estimate; and hence the inverse series doesn't begin with an approximation; (4) at every term in equations (5) there is only a single and repeated inverse step of inverting G_0, on the left hand member, and in every step in the series, which for water speed and Fourier transforms becomes a simple multiplicative algebraic and stable operation, essentially a single Stolt FK prestack migration at water speed is the only inverse step; the complexity comes from multiplying factors involving the data, D, and the water speed Green's function on the right hand side of equation (5), and multiplying water speed Green's functions and data, is not comparable in terms of treacherous numerical and computational challenge, and stability issues to inverting an updated variable background Green's function, and (5) there is no optimization, no searching algorithm, no invariance such as flat common image gathers, no proxy or surrogate for the actual velocity, nor any other subsurface property, no optimal stacking nor searching for optimal weighted move-out patterns, but instead an explicit set of equations for V. It is multi-dimensional, fully non-linear and direct inversion. Equations (5) use the information in the data, D, the amplitude and phase of events in specific distinct task determined linear and non-linear combination, to achieve processing objectives where traditional linear processing methods required subsurface information, to then allow those goals to be realized without the traditional need for subsurface information.

In addition, the right hand sides of equation (5) provides a transparency and a unique window to look into the inner workings of the inverse

series and processing objectives, and the physical detail of inverse activity and to identify tasks achieved within the series and associated with inversion. Among tasks are: removing free surface multiples (Carvalho, 1992; Weglein et al., 1997), removing internal multiples (Araújo, 1994; Weglein et al., 1997; Matson, 1997; Nita and Weglein, 2004; Ramírez and Weglein, 2005b,a), depth imaging primaries (Weglein et al., 2001, 2002; Shaw et al., 2004; Innanen, 2003; Shaw, 2005; Liu et al., 2005, 2006), non-linear direct estimation of material property changes across those imaged reflectors (Zhang and Weglein, 2005), and Q-compensation (Innanen and Weglein, 2005). All of those separate tasks are being accomplished within the inverse series, and are performed directly in terms of water speed and the data. That is the unambiguous and unequivocal message and promise that derives from recognizing the properties of every term of the inverse scattering series, and hence the property shared by the entire series and every task specific sub-series. The way this is accomplished is clear from equations (5). The inverse scattering series states that to accomplish any inverse objective in terms of only water speed and measured data you will need to multiply the data or water speed imaged data by itself (V_1 times V_1) in various specific multiplicative combinations to accomplish different specific tasks. The free surface multiple algorithm is the very simplest example that derives from this thinking. While there are other methods that can derive the free surface multiple removal algorithm (Weglein and Dragoset, 2005, e.g.), there is no other methodology other than the inverse scattering series that derives the entire inverse problem, precisely as it accomplished free surface multiple removal, in this direct water speed and data manner, and all tasks associated with inversion including depth imaging and non-linear AVO in exactly the same single framework as free surface multiple removal and from the single set of equations (5). The evidence supporting the latter claim is that while others readily accepted and had their own derivations of the free surface multiple algorithm, there was vehement and repeated objections to even the possibility of removing internal multiples without subsurface information, from those with alternate derivations of the free surface multiple removal algorithm, and proofs were offered from those alternate perspectives to demonstrate that it was impossible. That of course has now changed, and the inverse scattering internal multiple methodology has now been widely accepted, including many of those who initially were skeptical, and it is used throughout the industry. Now that incredulity has largely shifted from multiples and there is now a struggle to grasp the possibility of the direct inverse scattering series depth imaging without the velocity algorithms, currently being developed and tested within M-OSRP. The inverse scattering series written in equations (5) has the same attitude towards all objectives associated with inversion: all multiple removal, depth imaging and non-linear AVO and Q compensation. The inverse scattering series is the ultimate, comprehensive and unique data-driven machine, for V, and hence for any task you associate with achieving that goal. Only data is input for any and every one of the seismic processing objectives associated with multiples or primaries.

The isolated task sub-series of multiple removal and depth imaging can be cast in a model type independent form (Weglein et al., 2003), and those isolated task sub-series each have less stringent bandwidth conditions than iterative linear inversion. Model-type independent means a single unchanged algorithm performs a task such as free surface multiple removal not only independent of subsurface properties, but independent of whether you assume the earth is acoustic, elastic, heterogeneous, anisotropic or inelastic: one single unchanged algorithm accommodates all and requires absolutely no alteration when applied and no information about model type or parameters within that model. The distinct isolated task sub-series to-date provide: (1) free surface multiple removal, (2) internal multiple attenuation, (3) internal multiple removal, for a set of internal multiples of a given order; (4) depth imaging, one dimensional -leading order; (5) direct non-linear target parameter identification, and (6) depth imaging, two dimensional - leading order, higher order, partial multi-D imaging capture. References are listed that provide background, detail and examples. ten Kroode (2002) has provided a more formal mathematical description and an insightful and useful analysis and discussion of the velocity independent inverse scattering internal multiple attenuator, and Amundsen et al. (2005) have contributed fundamental new understandings, concepts and significant new perspective to the velocity independent processing of primaries.

Many people have a hard time distinguishing what is needed for a specific algorithm to achieve a goal, and assume that all algorithms must assume the same conditions and prerequisies as the algorithm they are familiar with and have experienced. As an example: the Morley/Claerbout/Wiggins (MCW) method (Morley and Claerbout, 1983; Wiggins, 1999) for removing water column multiples requires modeling the source, water bottom and free surface, whereas free surface multiple removal methods do not require water bottom or any subsurface information to remove all free surface multiples including those removed by the MCW method. The MCW method requires modeling the entire multiple history, and is linear in the data, whereas the free surface multiple requires no subsurface information but requires data multiplied by data, D times D through V_1 times V_1 as in equation (5). Both algorithms are absolutely correct, and useful and different and have different assumptions and need for subsurface information and use data and the information about amplitude and phase of events in a different way. Multiplicative combination of the amplitude and phase information in different events, that is realized in the data times data, D times D, starting in the second term of equation (5), allows all processing objectives that require subsurface information, and require providing the history of the multiple or primary, to be lifted in exactly the same way that the conditions on the linear MCW were lifted in free surface multiple removal methods. MCW relates to free surface multiple removal in precisely the same way that all current leading edge imaging methods (e.g., finite difference, phase shift, phase screen, plane wave, FK, Beam, Kirchhoff, and Reversed Time) relates to inverse scattering depth imaging algorithms. We have become familiar with that property of not needing or requiring subsurface information for free surface multiple removal, but it remains odd and incredulous to many when we say that same message derives from the same equations for imaging primaries. And from the inverse scattering series viewpoint they are not in any way different and both derive from precisely the same thinking and the same set of equations (5) and use data, and information in the same manner to achieve their goals. If there is any mystery here, then there is only one mystery and that is in understanding the simple but profound message the inverse scattering series, equation (5) is communicating. If you understand how the free surface algorithm works, you have the key to understanding how internal multiples are removable and primaries are able to be depth imaged without the velocity, since the inverse scattering series treats all of these activities in an identical manner, and with a single framework and footing. It is the only methodology today that treats all processing objectives as it treats free surface multiple removal.

DIRECT FREE SURFACE MULTIPLE REMOVAL WITHOUT THE VELOCITY

Let us begin with some discussion of how the free surface multiple algorithms works. Consider Figures 1 and 2. $R_f(\omega)$ is the single frequency component of the data with a free surface and consists of deghosted primaries, internal multiples and free surface multiples. $R(\omega)$ is the single frequency of the data without a free surface, and consists of primaries and internal multiples. The free surface multiple algorithm inputs $R_f(\omega)$ and outputs $R(\omega)$. A derivation is found in e.g., Weglein et al. (2003) although that formula has a long history (Ware and Aki, 1969, e.g.)

$$R_f(\omega) = \frac{R(\omega)}{1+R(\omega)} \tag{6}$$

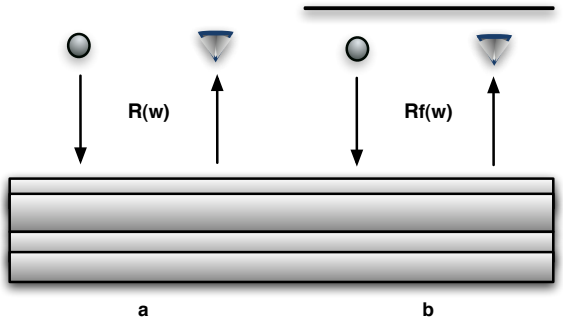

Figure 1: *Data without (a) and with (b) a free-surface.*

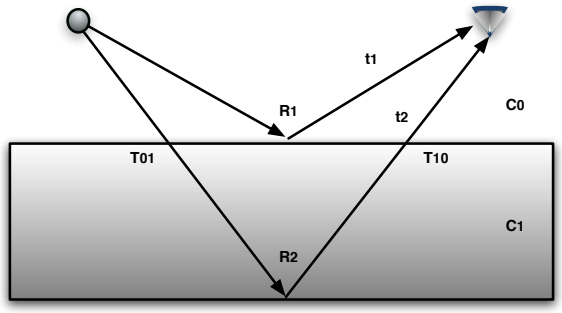

Figure 2: *Reflected primary events from a two reflector model.*

$$R(\omega) = \frac{R_f(\omega)}{1 - R_f(\omega)} \tag{7}$$

$$R(\omega) = R_f(\omega) + R_f^2(\omega) + R_f^3(\omega) + ... \tag{8}$$

Let us consider the two reflector example in Figure (2). R_1 and R_2' are the amplitude of the two primaries, and R_2' is $T_{01}R_2T_{10}$. A single multiple is exactly predicted with R_1 and R_2' and times t_1 and t_2 and without the velocity, and with data with a single frequency predicting precisely the free surface multiples at that single frequency. The data with the free surface is:

$$\begin{aligned} R_f(t) =& R_1\delta(t-t_1) + R_2'\delta(t-t_2) - R_1^2\delta(t-2t_1) - R_2'^2\delta(t-2t_2) \\ & - 2R_1R_2'\delta(t-(t_1+t_2)) + ... \end{aligned} \tag{9}$$

and in the frequency domain becomes

$$R_f(\omega) = R_1e^{i\omega t_1} + R_2'e^{i\omega t_2} - R_1^2e^{i\omega 2t_1} - R_2'^2e^{i\omega 2t_2} - 2R_1R_2'e^{i\omega(t_1+t_2)}... \tag{10}$$

Now evaluating the second term on the right hand side of equation (8)

$$R_f^2(\omega) = R_1^2e^{i\omega 2t_1} + R_2'^2e^{i\omega 2t_2} + 2R_1R_2'e^{i\omega(t_1+t_2)} + ...; \tag{11}$$

the free surface multiples are precisely and uniquely predicted, in amplitude and phase, and when R_f is added to R_f^2 squared they are exactly removed from an input consisting of a single frequency in the measured marine data, $R_f(\omega)$. We now follow this same two reflector problem for the imaging task.

DIRECT DEPTH IMAGING WITHOUT THE VELOCITY

Now consider the inverse scattering subseries for imaging without the velocity. Consider the same one dimensional medium in Figure 2. The free surface multiple removal algorithm and the first term in the depth imaging use precisely the same information in the data in a non-linear process to achieve different processing objectives, both derived from equations (5). In 1D we have

$$\left[\frac{d^2}{dz^2} + \frac{\omega^2}{c_0^2}\right]P_0(z,\omega) = 0, \quad \left[\frac{d^2}{dz^2} + \frac{\omega^2}{c^2(z)}\right]P(z,\omega) = 0, \tag{12}$$

hence $V = \frac{\omega^2}{c_0^2} - \frac{\omega^2}{c^2(z)}$, and we introduce the perturbation parameter alpha:

$$\frac{1}{c^2(z)} = \frac{1}{c_0^2}[1 - \alpha(z)]. \tag{13}$$

Therefore the inverse series in terms of alpha is

$$\alpha(z) = \alpha_1(z) + \alpha_2(z) + \alpha_3(z) + ..., \tag{14}$$

and the linear term is derivable from the data in pseudo-depth by

$$\alpha_1(z) = 4\int_0^z R(z')dz'. \tag{15}$$

The second-order term may be written

$$\alpha_2(z) = -\frac{1}{2}\left(\alpha_1^2(z) + \alpha_1'(z)\int_0^z \alpha_1(z')dz'\right). \tag{16}$$

The portion of α_2 that addresses mislocated images is:

$$-\frac{1}{2}\alpha_1'(z)\int_0^z \alpha_1(z')dz' = -8R_1T_{01}R_2T_{10}(b'-a)\delta(z-b'); \tag{17}$$

the right-hand side is the two-reflector case in Figure 2. Note that $b'-a = (c_0/2)(t_2-t_1)$. The free surface multiple removal algorithm multiplies the amplitude of two events and adds the phases , equation(11) , third term on the right hand side, to predict the free surface multiple and the first term in the imaging series starts the correction process of erroneously imaged reflectors with the same multiplicative communication, but now the amplitudes of the two primaries multiply and the phases subtract, equation(18). The sum of the phases in the former multiple case is the phase of the predicted multiple while the difference in the phases in the imaging algorithm gives a sense of the duration of the imaging mis-location problem it is addressing. Both the multiple removal and imaging algorithm from the inverse scattering series multiplicatively combine events and their amplitudes and phases, but they never use those amplitudes, in either case, to determine medium properties. R_1 is input but not used to determine or estimate c_1. R_1 could be used to estimate c_1 and that would be the iterative inverse route, R_1 in the inverse scattering series de- multiple and imaging algorithm is not used to linearly and non- linearly estimate c_1. What matters is not what R_1 could be used for but what R_1 is being used for in these demultiple and imaging algorithms. Each task is entirely data-driven and doesn't require, need or determine the velocity model, or any other subsurface information. In the example above illustrating the task of free surface multiple removal a single frequency of the data precisely and uniquely predicts the amplitude and phase of all free surface multiples at that frequency. That single frequency of data cannot locate the water bottom let alone invert it for anything sub-water bottom. Never-the- less that single frequency of the data can exactly and uniquely predict all free surface multiples at that frequency.

We sometimes hear "That's all wonderful, and very interesting, but please just don't tell us it is possible to directly depth image without

the velocity. OK?" One of the favorite and persistent offered arguments goes as follows: Consider a one dimensional layered earth and a normal incident wave. If the incident wave is band limited, and in particular has missing low frequency, then a linear inverse for parameter estimation, and subsequent linear iterates, would all suffer a uniqueness problem where an infinite number of different earth models with different low frequency data could satisfy the data within your bandwidth. Hence, with bandlimited data there are no uniquely inverted earth models, and no unique velocities, and no unique reflector locations, and no unique multiples. Therefore, the entire set of tasks starting with free surface multiple removal is as challenged and unattainable as the bandlimited linear inverse is in terms of a nonunique solution. This is a great argument and has tremendous appeal and traction and we have heard this for at least the past 16 years. It is entirely self consistent and entirely rigorous and also entirely irrelevant as regards task specific subseries of the inverse scattering series, starting with the free surface multiple case. The inverse scattering series and all of its isolated task specific sub-series never seek to determine the earth properties on their path to accomplish their task. It no more needs nor cares about determining the velocity in the case of free surface multiples, internal multiples or depth imaging. If that argument held, it would shut down the free surface case. As we noted in the analytic example above the free surface algorithm works at one temporal frequency at a time, and with that single frequency of the data precisely and uniquely predicts amplitude and time of all free surface multiples. Not a set of possible multiples. One unique and precise prediction. What would linear or iterative linear inverse be able to determine about the earth with one frequency of data, not even the location of the water bottom. That argument is equally misplaced and irrelevant for every task specific inverse scattering sub-series that removes free surface or internal multiples or depth images primaries. What the inverse scattering series applications require is a unique data within the bandwidth, and cares not in the least what linear and iterative linear inverse could or couldn't predict uniquely about earth properties from that band- limited data. The latter is not a step or stage in the former and hence the former doesn't depend upon or have any interest in satisfying the latter's requirements. All tasks within the inverse scattering series act according to the same template, whether the task is time to time, as in multiple removal, or time to depth as in depth imaging. The central flaw and fallacy is attributing to all methods the failings and limitations of one method. Assumptions are algorithm dependent. Again, MCW is to free surface multiple removal what all current velocity dependent linear imaging methods are to inverse scattering task specific imaging algorithms.

RECENT VELOCITY INDEPENDENT IMAGING RESULTS

In Figure 3 is the FK migration of the pre-stack data generated from the salt model shown. In Figure 4 is the result of the inverse scattering series imaging algorithm of Liu et al. (2006). No velocity is input and the entire process is 1.3 times the compute cost of a single water speed FK migration. This is a very encouraging result. This algorithm captures part of the terms that address imaging challenges within the multi- dimensional inverse series.

REMARKS

An effective response to pressing seismic E & P challenges starts by recognizing that there are three distinct sources of obstacles and hurdles: (1) acquisition, (2) compute, and (3)algorithmic limitations with perfect acquisition and compute resources. It is easy to show that there are simple but important 2D acoustic models where you can avail yourself of essentially perfect acquisition and fully adequate compute power and you cannot find an adequate velocity and/or you can provide a perfect velocity model and your imaging algorithm cannot image beneath it. A simple combination of variable dip and lateral velocity can

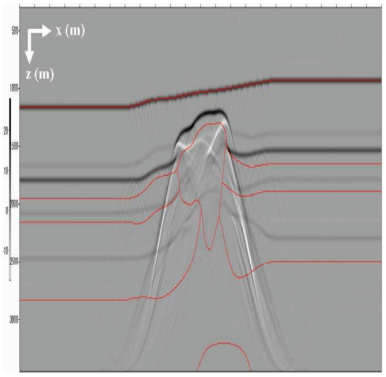

Figure 3: *FK imaging with waterspeed.*

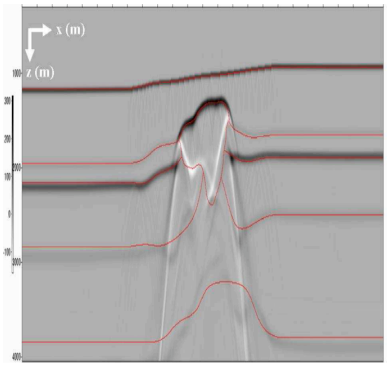

Figure 4: *Inverse scattering series based imaging (Liu et al., 2006)*

provide imaging challenges. We often hear the response to pressing seismic challenges defined as composed of only having a compute and acquisition strategy. And there are circumstances when that approach is indicated and adequate. There are also numerous and significant examples where that two pronged approach alone (ignoring intrinsic algorithmic limitations) will not represent an effective response, and will not meet the challenge. A comprehensive response to the pressing seismic challenges would recognize and simultaneously progress these three components. The inverse scattering series is a direct response to the algorithmic limitation component of pressing seismic challenges. In the area of multiple removal it has already provided the most comprehensive and effective algorithms, which show their mettle in the most complex and difficult to process and challenging conditions. Our goal in these ongoing research efforts, for capturing imaging capability within the inverse series, is to move from noise to signal and match the level of effectiveness already realized for removing multiples and extend that to extraction of subsurface information from primaries. The potential and promise are clear for these new imaging concepts and algorithms derived from the inverse scattering series. Within M-OSRP, we are progressing capturing further imaging capability, extending our algorithms to model-type independence and pursuing plans and tests for field data evaluation.

ACKNOWLEDGEMENTS

The authors are grateful to the sponsors of M-OSRP and the NSF-CMG and DOE-BES for encouragement and support. L. Amundsen and E. Otnes thank Statoil for permission to publish.